Microfluidic graphenised-paper electroanalytical devices (µGPED) for adsorptive cathodic stripping voltammetric detection of metal contaminants

UNIVERSITY *of the*
WESTERN CAPE

KEAGAN WILLIAM POKPAS
MSc Nanoscience (UWC)

A thesis is submitted in the fulfilment of the requirement for the degree of

Doctor Philosophiae

in the Department of Chemistry, Faculty of Science

University of the Western Cape

Supervisor:

Prof. Nazeem Jahed

Co-Supervisor:

Prof. Emmanuel Iwuoha

2017

Microfluidic graphenised-paper electroanalytical devices (µGPED) for adsorptive cathodic stripping voltammetric detection of metal contaminants

Keagan Pokpas

KEY WORDS:

Trace Metal Analysis

Paper-based Microfluidics

Square-wave Adsorptive Stripping Voltammetry

Graphene

Electrochemical Reduction

Nanocomposite

Gold Nanoparticles

Chemical Sensor

Inkjet Printing

Wax Patterning

ABSTRACT

The need for clean, non-toxic drinking water supplies, free of pollutants and metal contamination is vital in impoverished areas and the developing world alike. With this in mind, the development of accurate, inexpensive, portable and simple devices for remote sensing applications is therefore pivotal for early detection and the prevention of illnesses. Over the last two decades, adsorptive stripping voltammetry (AdSV) has emerged as a superior detection method over common analytical techniques due to its low-cost instrumentation, unskilled labour and ability to detect a wide range of analytes. The technique is based on the non-electrolytic accumulation (adsorption) of the analyte followed by a cathodic reduction scan measurement. Moreover, recent progress in paper-based microfluidics coupled to electrochemical approaches for analysis have shown tremendous promise as platforms for providing simple, portable and quantitative detection. Herein, a variety of novel paper-based electrochemical platforms are developed for the detection of metal contaminants, such as Ni^{2+} in drinking water with low-volume sample introduction in the presence of dimethylglyoxime as chelating agent. For the first time, paper-based microfluidics is combined with electrochemical AdSV in conjunction with conventional three-electrode systems to produce microfluidic paper-based electroanalytical devices (µPEDs) which function as one-step, low-cost electroanalytical sensors for the detection of Ni^{2+} in tap water samples. The study is based on two simple and unique fabrication approaches: (i) dry reagent infusion techniques in the development of novel pre-stored (infused) µPEDs and (ii) inkjet and screen printing techniques for production of integrated paper-based electrode systems. The pre-stored µPEDs with a novel single-step accumulation and deposition demonstrated highly selective detection of Ni^{2+} in the presence of metallic interferents (Zn^{2+}, Cd^{2+}, Pb^{2+}, Co^{2+} and In^{2+}) up to 100 times metal analyte concentration. A limit of detection of 6.27 ± 1.32 µg L^{-1} was established for Ni^{2+} detection over a dynamic linear range of 15 – 120 µg L^{-1} with sensitivity of 7.08 µA L $µg^{-1}$ for three replications at 90 s analysis times. The lower sensitivities normally associated with µPEDs was addressed by the incorporation of graphene, carbon black, gold nanoparticles or ionic liquids (1-methylimidazole) within the cellulose fibre structure. Microfluidic graphenised-paper electroanalytical devices (µGPEDs) demonstrated ability to improve electron transfer kinetics and enhance electroactive surface area within the fibrous cellulose structure at high graphene content (> 10 weight %). In addition, µPEDs prepared from

gold nanoparticles and 1-methylimidazole improved the electroactivity and sensitivity of AuNP-IL-μPEDs up to 3 times over unmodified counterparts with a uniform decoration of ~ 90 nm gold nanoparticles within the cellulose structure. A limit of detection of 5.13 ± 3.74 μg L^{-1} was recorded for Ni^{2+} detection over a dynamic linear range of 30 – 150 μg L^{-1} (n = 3). Further, integrated paper-based three-electrode systems based on inkjet printing were fabricated with high conductivity (< 50 Ω) from silver nanoparticle (AgNP) and graphene-based inks. Gold nanoparticle decorated electrochemically reduced graphene oxide (AuNP-ERGO) and carbon black, dimethylglyoxime (CB-DMG) modified paper-based electroanalytical devices (PEDs) yielded limits of detection of 32.19 ± 9.61 and 48.01 ± 12.24 μg L^{-1}, respectively, for Ni^{2+} detection at 90 s accumulation times over a dynamic linear range of 50 – 500 μg L^{-1} Ni^{2+}. Relative standard deviations (RSD %) for $[Ni(dmgH)_2]$ reduction were found to be within a 2 – 7 % error. For real sample analysis, the nanoparticle-enhanced voltammetric paper-based devices proved to be suitable for the detection and quantitation of Ni^{2+} below the United State Environmental Protection Agency (US EPA) and World Health Organization (WHO) prescribed limit (0.1 mg L^{-1} or 0.1 ppm) and South African Drinking Water Guidelines limit (0.15 mg L^{-1}) for drinking water.

PLAGIARISM DECLARATION

I declare that the study **"Microfluidic graphenised-paper electroanalytical devices (µGPED) for adsorptive cathodic stripping voltammetric detection of metal contaminants"** is my own work. It has not been submitted for any degree or examination in any university, and all the resources I have used or quoted have been indicated and acknowledged by complete references.

Keagan Pokpas May 2017

Signed……..

ACKNOWLEDGEMENTS

Firstly, I would like to thank God the Almighty for providing me with endless opportunities, strength and encouragement. Thank you for being my pillar.

To my supervisor, Prof. Nazeem Jahed, I wish to extend my sincerest gratitude. Thank you for your guidance, endless insight, encouragement and continuous support.

I would like to extend my gratitude to Prof. Emmanuel Iwuoha and Prof. Priscilla Baker, the leader and Co-leader of SensorLab, respectively as well as the entire staff of the Department of Chemistry. Thank you for the opportunity and trust placed in me. Thank you for your continuous support.

Sincere thanks to all SensorLab members and staff. Thank you for the endless discussions and laughs shared. Your support means a great deal to me.

A special thanks to the Department of Science and Technology (DST) and the National Research Foundation (NRF) for financial support.

Lastly, to my family and friends; thank you for all the sacrifices, support and good times. A special mention should be made to Larry and Crystal Pokpas, my mother and father, thank you for the encouragement in difficult times. Without you this would not be possible. Words cannot express what it has and continues to mean to me.

LIST OF PUBLICATIONS

CONFERENCE PROCEEDINGS

Poster presentations

- K. Pokpas, N. Jahed, P. Baker, E.I. Iwuoha, Detection of Nickel (II) at a Metal-Free Graphene-Chelate Probe in the Presence of Cobalt and Zinc by Adsorptive Stripping Voltammetry, in: 67th Annu. Meet. Int. Soc. Electrochem., The Hague, Netherlands, 2016.
- K. Pokpas, M.N. Jahed, P.G. Baker, E.I. Iwuoha, Detection of Nickel (II) at a Metal-Free Graphene-Chelate Probe in the Presence of Cobalt and Zinc by Adsorptive Stripping Voltammetry, in: Nanosci. Symp., Bellville, Western Cape, South Africa, 2016.

LIST OF ABBREVIATIONS

2D	Two Dimensional
3D	Three Dimensional
AAS	Atomic Adsorption Spectroscopy
ABS	Acetate Buffer Solution
AdSV	Adsorptive stripping voltammetry
AdCSV	Adsorptive Cathodic Stripping Voltammetry
AE	Auxiliary Electrode
AFM	Atomic Force Microscopy
ASV	Anodic Stripping Voltammetry
ATR	Attenuated Total Reflectance
BiE	Bismuth Film Electrode
BiF	Bismuth Film
CB-DMG	Carbon Black Dimethylglyoxime
CE	Counter Electrode
CNT	Carbon Nanotube
CSV	Cathodic Stripping Voltammetry
CV	Cyclic Voltammetry
CVD	Chemical Vapor Deposition
DL	Detection Limit
DMF	N,N-Dimethylformamide
DMG	Dimethylglyoxime
DNA	Deoxyribonucleic Acid

DPP	Differential Pulse Polarography
DPV	Differential Pulse Voltammetry
DPSV	Differential Pulse Stripping Voltammetry
EC	Electrochemical
EDS	Energy Dispersive X-Ray Spectroscopy
EG	Electrodeposited Graphene
EPA	Environmental Protective Agency
ERGO	Electrochemically Reduced Graphene Oxide
Eqn.	Equation
FAAS	Flame Atomic Absorption Spectrophotometry
FET	Field-Effect Transistor
FT-IR	Fourier Transformed Infrared
GCE	Glassy Carbon Electrode
GE	Gold Electrode
AuNP	Gold Nanoparticle
GFAAS	Graphite Furnace Atomic Absorption Spectroscopy
GO	Graphene Oxide
Gr-PG-BiE	Graphene Pencil Graphite Bismuth Film Electrode
HgFE	Mercury Film Electrode
HMDE	Hanging Mercury Drop Electrode
HRSEM	High Resolution Scanning Electron Microscopy
HRTEM	High Resolution Transmission Electron Microscopy
ICP	Inductively Coupled Plasma Spectroscopy

ICP-MS	Inductively Coupled Plasma Mass Spectroscopy
ICP-OES	Inductively Coupled Plasma Optical Emission Spectroscopy
IL	Ionic Liquid
LOD	Limit of Detection
LOQ	Limit of Quantitation
MCL	Maximum Contamination Level
MFE	Mercury Film Electrode
µPED	Microfluidic Paper-based Electroanalytical Device
NGr	Nafion-graphene
NGr-DMG	Nafion-graphene Dimethylglyoxime
NPV	Normal Pulse Voltammetry
PEC	Paper-based Electrochemical Cell
PG	Pencil Graphite
PGE	Pencil Graphite Electrode
POC	Point of Care
ppb	Parts Per Billion
ppm	Parts Per Million
PPPE	Printed Photographic Paper Electrode
RE	Reference Electrode
RGO	Reduced Graphene Oxide
RNA	Ribonucleic Acid
RSD	Relative Standard Deviation
SECM	Scanning Electrochemical Microscopy

SV	Stripping Voltammetry
SW	Square Wave
SWASV	Square Wave Anodic Stripping Voltammetry
AgNP	Silver Nanoparticle
SWCNT	Single Walled Carbon Nanotube
SWV	Square Wave Voltammetry
US	United States
USEPA	United States Environmental Protection Agency
WDS	Windows Deployment Services
WE	Working Electrode
WHO	World Health Organization
XRD	X-Ray Diffraction

Table of Contents

KEY WORDS: ii

ABSTRACT iii

PLAGIARISM DECLARATION v

ACKNOWLEDGEMENTS vi

LIST OF PUBLICATIONS vii

LIST OF ABBREVIATIONS viii

Chapter 1 : 1

Microfluidic graphenised-paper electroanalytical devices (µGPED) for adsorptive cathodic stripping voltammetric detection of metal contaminants: 1

An Introduction 1

Abstract 1

1.1. Background to the Study 2

1.2. Problem Identification 5

1.3. Rationale and Motivation 6

1.4. Objectives 9

1.5. Research Questions 11

1.6. Research Hypothesis 11

1.7. Research Approach 12

1.8. Scope and Delimitations 13

1.9. Thesis Structure 15

References 18

Chapter 2 : 22

Recent Advances in Electrochemical Stripping Analysis at Graphene-Derivatives: 22

A review 22

Abstract 22

Highlights 22

Keywords 23

Graphical Abstract 23

2.1. Introduction 23

2.2. Preparation of Graphene 26

2.2.1. Mechanical Methods 26

2.2.1.1. Mechanical and Solution based Exfoliation Methods 26

2.2.1.2. Electrochemical Exfoliation Methods 31

2.2.1.3. Laser Exfoliation Methods 31

2.2.2. Ball-milling Methods 32

2.2.3. Chemical Oxidation and Reduction 33

2.3. Electronic and Electrochemical Properties of Graphene 35

2.4. Recent Advances in Stripping Analysis at Graphene-based Electrochemical Systems . 39

2.4.1. Simple Graphene Derivatives 40

2.4.2. Graphene-derivatives based on Biomaterials 43

2.4.3. Polymer and Ionic Liquid assisted Graphenes 45

2.4.4. Graphene nanocomposites with Metallic and Other Nanoparticles 48

2.5. Conclusions and Future Work 50

References 52

Chapter 3 : 67

Metal Analysis at Paper-based Microfluidic Devices: 67

A review 67

Abstract 67

Keywords 67

Highlights 67

Graphical Abstract 68

3.1. Introduction 68

3.2. Toxicology of Heavy Metals 69

3.3. Conventional Detection Methods 71

3.4. Paper-based Microfluidic Design 72

3.4.1. Paper Choice 72

3.4.2. Patterning of Hydrophobic Barriers 73

3.4.3. Printing Techniques 74

3.4.4. Basic Theory 75

3.5. Quantitative Analytical Metal Analysis 77

3.5.1. Colorimetric Detection 77

3.5.2. Fluorescence Detection 79

3.5.3. Electrochemical Detection 81

3.5.4. Other Detection Methods 83

3.6. Conclusions and Future Work 84

References 85

Chapter 4 : 95

Structural and Morphological Characterisation of Prepared Reduced Graphene Oxide, Graphene Oxide and Gold Nanoparticles 95

Abstract 95

Keywords 95

Highlights 96

Graphical Abstract..... 96

4.1. Introduction..... 96

4.2. Experimental Methods..... 98

4.2.1. Chemicals and Reagents..... 98

4.2.2. Apparatus..... 98

4.2.3. Preparation of Graphene Oxide..... 99

4.2.4. Reduced Graphene Oxide Preparation..... 100

4.3. Results and Discussion..... 101

4.3.1. Structural and Morphological Characterization of Prepared Graphene Oxide and Reduced Graphene Oxide..... 101

4.3.1.1. GO and RGO dispersion in suitable solvents..... 101

4.3.1.2. Fourier-transform Infrared Spectroscopy (FT-IR)..... 102

4.3.1.3. High Resolution Scanning Electron Microscopy (HRSEM)..... 104

4.3.1.4. High Resolution Transmission Electron Microscopy (HRTEM)..... 105

4.3.1.5. X-ray Diffraction (XRD)..... 107

4.3.1.6. Raman Spectroscopy..... 108

4.3.1.7. Atomic Force Microscopy (AFM)..... 110

4.3.1.8. Ultraviolet Visible (UV-vis) Spectroscopy..... 111

4.3.2. Structural and Morphological Characterization of Commercial Gold Nanoparticles ……112

4.3.2.1. High Resolution Electron Microscopy..... 112

4.3.2.2. Ultraviolet Visible (UV-vis) Spectroscopy 113

4.4. Conclusions and Future Work 114

References 115

Chapter 5 : 120

Graphene-modified Pencil Graphite, In-situ Plated Mercury Film Electrodes (Gr-PG-MFEs) for the Ultratrace Determination of Nickel by Adsorptive Cathodic Stripping Voltammetry (AdCSV) 120

Abstract 120

Keywords: 121

Highlights: 121

Graphical Abstract 121

5.1. Introduction 122

5.2. Experimental Section 123

5.2.1. Reagents 123

5.2.2. Apparatus 124

5.2.3. Synthesis of graphene oxide(GO) 124

5.2.4. Preparation of electrochemically reduced grapheme oxide pencil graphite electrode (ERGO-PGE) 125

5.2.5. Electrode cleaning 125

5.2.6. Procedure for square wave anodic stripping voltammetry (SWASV) analysis 126

5.2.7. Sample Preparation 126

5.3. Results and Discussion 126

5.3.1. Electrochemical reduction of graphene oxide 126

5.3.2. Characteristic oxidation potential of Ni^{2+} 129

5.3.3. Microscopic characterization of electrochemically reduced graphene oxide modified pencil-graphite electrode (ERGO-PGE) 131

5.3.4. Effects of electrochemically reduced graphene oxide on the stripping peaks currents 132

5.3.5. Film stability and reproducibility 133

5.3.6. Optimization of instrumental parameters 134

5.3.7. Analytical performances of the electrochemically reduced graphene oxide modified pencil graphite mercury film electrode 137

5.3.8. Recoveries Studies of ERGO-PG-MFE 140

5.3.9. Application to tape water samples 141

5.3.10. Interferences 142

5.4. Conclusion 142

References 143

Chapter 6 : 146

Complexation based Detection of Nickel (II) at a Graphene-Chelate Probe In the Presence of Cobalt and Zinc by Adsorptive Stripping Voltammetry 146

Keywords: 147

Highlights: 147

Graphical Abstract: 147

6.1. Introduction: 148

6.2. Experimental Procedure: 150

6.2.1. Chemicals and Reagents 150

6.2.2. Apparatus 151

6.2.3. Preparation of the Nafion-Graphene Dimethylglyoxime Suspension (NGr-DMG) 151

6.2.4. Preparation of Nafion-Graphene Dimethylglyoxime Modified Glassy Carbon Electrode (NGr-DMG-GCE) 152

6.2.5. Procedure for Square Wave Adsorptive Cathodic Stripping Voltammetric (AdCSV) Analysis 152

6.2.6. Sample Preparation 152

6.3. Results and Discussion 153

6.3.1. Fourier Transform Infrared Spectroscopy (FT-IR) of DMG 153

6.3.2. Nickel Dimethylglyoxime ($Ni(DMG)_2$) Complex Formation and Electrochemical Stripping Reduction 154

6.3.3. Morphological Characterization of Modified Electrode 156

6.3.4. Electrochemical Characterization of the Nafion-Graphene Dimethylglyoxime Modified Glassy Carbon Electrode (NGr-DMG-GCE) 158

6.3.5. Electrochemical Behaviour of the NGr-DMG-GCE 160

6.3.6. Electrochemical Impedance Spectroscopy (EIS) Analysis of the NGr-DMG-GCE 161

6.3.7. Further electrochemical characterization of the NGr-DMG-GCE 163

6.3.8. Effect of the NGr-DMG-GCE on the stripping response of Ni^{2+} 164

6.3.9. Influence of Dimethylglyoxime Concentration 165

6.3.10. Optimization of Instrumental Parameters 167

6.3.11. Influence of Electrolyte pH 168

6.3.12. Influence of Oxygen Removal 169

6.3.13. Electrode Reproducibility and Interference Studies 171

6.3.14. Analytical Performance of the NGr-DMG-GCE 173

6.3.15. Application of the NGr-DMG-GCE to real water samples 176

6.4. Conclusion 178

References 179

Chapter 7 : 186

Electroanalytical Complexation-based Detection at Low-cost, Stored, Micro-volume, Paper-based Electrochemical Cells (µPECs) 186

Abstract: 186

Keywords: 187

Highlights: 187

Graphical Abstract: 188

7.1. Introduction: 188

7.2. Experimental Section: 189

7.2.1. Apparatus and Reagents 189

7.2.2. Pre-stored Paper-based Electrochemical Cell (PPEC) Preparation 190

7.2.3. Graphene-derivative Infused Paper-based Electrochemical Cell (PEC) Preparation 191

7.2.4. Square-wave Adsorptive Cathodic Stripping Voltammetric Detection of Ni 191

7.3. Results and Discussion: 192

7.3.1. Water sorption in the porous PEC 192

7.3.2. Characteristic quantitative detection of Ni(II) 193

7.3.3. Macro- vs. Micro-liter detection of Ni(II) 196

7.3.4. Development of pre-stored paper-based electrochemical cells (PPECs) 198

7.3.5. Effect of Reagent Storage on the Electrochemical Detection at PPECs 202

7.3.6. Influence of dimethylglyoxime (DMG) ligand concentration and storage 204

7.3.7. Effect of Hg concentration on Ni^{2+} stripping peak current 206

7.3.8. Instrumental parameter optimization 207

7.3.9. PPEC reproducibility and stability 209

7.3.10. Interference Studies of the PPECs 210

7.3.11. Quantitative Analytical Performance of the fabricated PPECs 212

7.3.12. Recovery studies of PPECs 216

7.3.13. Effect of Chelating Agent on Ni^{2+} Detection at PPECs 217

7.3.14. Graphene infused pre-stored paper-based electrochemical cells 219

7.3.15. µPECs with Integrated Graphene WE 224

7.4. Conclusions and Future Work 226

References 227

Chapter 8 : 230

Fabrication of Gold Nanoparticle, Ionic liquid (1-Methylimidazole) enhanced Microfluidic Paper-based Electroanalytical Devices (µPEDs) towards the detection of Cu(II) and Ni(II) by Stripping Voltammetric Techniques 230

Abstract 230

Keywords 230

Highlights 231

Graphical Abstract 231

8.1. Introduction 231

8.2. Experimental Section 234

8.2.1. Chemicals and Reagents 234

8.2.2. Apparatus 234

8.2.3. Gold Nanoparticle, Ionic Liquid, Microfluidic Paper-based Electrochemical Device (AuNP-IL-µPED) Fabrication 234

8.2.4. Procedure for Square-wave Anodic Stripping Voltammetry (SW-ASV)..... 236

8.2.5. Procedure for Square-wave Adsorptive Cathodic Stripping Voltammetry (SW-AdCSV). 237

8.2.6. Real Tap Water Sample Preparation..... 237

8.3. Results and Discussion..... 237

8.3.1. Wax Patterning of Hydrophobic Barriers 237

8.3.1.1. Visual Analysis of Wax Melting 237

8.3.1.2. Greyscale Testing of Hydrophobic Barriers..... 238

8.3.1.3. Optimisation of Melting Parameters..... 239

8.3.1.4. Leak Tests of Printed Hydrophobic Barriers..... 241

8.3.2. Characterization of Prepared AuNP-IL-µPED 243

8.3.2.1. High Resolution Electron Microscopy (HRSEM) of Modified µPEDs 243

8.3.3. Electrochemical application of AuNP-IL-µPED towards Cu^{2+} detection by ASV ……245

8.3.3.1. Characteristic oxidation potential of Cu^{2+} at AuNP-IL- µPED..... 245

8.3.3.2. Current responses of Cu^{2+} at AuNP-IL-µPED 247

8.3.3.3. Influence of Hg ion concentration..... 248

8.3.3.4. Optimisation of Instrumental Parameters 249

8.3.3.5. Quantitative Analytical Detection of Cu^{2+} at AuNP-IL- µPED 251

8.3.3.6. Real Sample analysis of Cu^{2+} at AuNP-IL- µPED 254

8.3.4. Detection of Ni^{2+} by AdCSV at AuNP-IL-µPED 255

8.3.4.1. Characteristic reduction potential of Ni^{2+} at AuNP-IL- µPED 255

8.3.4.2. Current responses of Ni^{2+} at AuNP-IL-µPED 256

8.3.4.3. Influence of DMG concentration on Ni^{2+} detection at AuNP-IL-µPED 257

8.3.4.5. Effect of Hg ion concentration on Ni^{2+} stripping response 259

8.3.4.6. Instrumental parameter optimisation 260

8.3.4.7. Analytical performance of the AuNP-IL-µPED 261

8.3.4.8. Real Sample analysis of Ni^{2+} at AuNP-IL- µPED 265

8.4. Conclusions and Future Work 266

References 266

Chapter 9 : 272

Graphene-enhanced Inkjet-printed Silver and Graphene Electrodes for the Detection of Nickel(II)-dimethylglyoxime [Ni($dmgH_2$)] complexes by Adsorptive Cathodic Stripping Voltammetry (AdCSV) 272

Abstract: 272

Keywords: 273

Highlights: 273

Graphical Abstract: 273

9.1. Introduction 274

9.2. Materials and Apparatus 275

9.2.1. Apparatus 275

9.2.2. Chemicals and Reagents 275

9.3. Experimental Methods 276

9.3.1. Fabrication of Inkjet-Printed Electrodes 276

9.3.2. Preparation of Electrochemically Reduced Graphene Oxide, Gold Nanoparticle, Carbon-coated Silver Printed Paper-based Electrodes (ERGO-AuNP-CC-Ag-PPE) 278

9.3.3. Preparation of Nafion, Dimethylglyoxime, Carbon Black, Silver Printed Paper-based Electrodes (N-DMG-CB-Ag-PPE) 278

9.3.4. Procedure for SW-AdCSV analysis of Ni^{2+} 279

9.4. Results and Discussion 279

9.4.1. Inkjet Printing of Paper-based Electrodes 279

9.4.1.1. Droplet Formation of Commercial Graphene Ink 279

9.4.1.2. Electrical Characterization of Printed Inks 280

9.4.1.3. Topographical Characterization of Printed Patterns 283

9.4.2. Preliminary Testing of Ag-printed Electrodes 287

9.4.3. Electrochemically Reduced Graphene Oxide – Gold Nanoparticle, Silver Printed Paper-based Electrodes (ERGO-AuNP-CC-Ag-PPE) 288

9.4.3.1. Electrochemical reduction of Graphene oxide and gold nanoparticles 288

9.4.3.2. Electrochemical stripping performance of ERGO-AuNP-CC-Ag-PPE towards Ni^{2+} detection 292

9.4.3.3. Morphological Characterization of ERGO-AuNP-CC-Ag-PPPE 294

9.4.3.4. Analytical performance of ERGO-AuNP-CC-Ag-PPPE 296

9.4.3.5. Effect of Chelating Agent Concentration at ERGO-AuNP-CC-Ag-PPPE.... 297

9.4.3.6. Effect of Hg Ion Concentration at ERGO-AuNP-CC-Ag-PPPE..... 298

9.4.3.7. Optimization of ERGO-AuNP-CC-Ag-PPPE Instrumental Parameters 300

9.4.3.8. Calibration Studies at ERGO-AuNP-CC-Ag-PPPE 301

9.4.3.9. Application to Tap Water Samples of the ERGO-AuNP-CC-Ag-PPPE..... 304

9.4.3.10. Application of the ERGO-AuNP-CC-Ag-PPPE Towards Co^{2+} Detection ... 306

9.4.4. Carbon Black, Dimethylglyoxime Silver Printed Paper-based Electrodes (CB-DMG-CC-Ag-PPE) 307

9.4.4.1. Ni^{2+} Detection at the CB-DMG-Ag-PPPE..... 307

9.4.4.2. Influence of Chelating Agent Concentration in CB-DMG Ink 309

9.4.4.3. Morphological Characterization of CB-DMG-Ag-PPPE 311

9.4.4.4. CB-DMG-Ag-PPPE Instrumental Parameter Optimization 311

9.4.4.5. Quantitative Analytical Performance of the CB-DMG-Ag-PPPE 313

9.4.4.6. Analysis of Tap Water Samples at the CB-DMG-Ag-PPPE..... 315

9.5. Conclusions and Future Work..... 320

References 320

Chapter 10 : 325

Microfluidic graphenised-paper electroanalytical devices (µGPED) for adsorptive cathodic stripping voltammetric detection of metal contaminants.... 325

Conclusions and Future Work 325

List of Figures

Figure 1.1: Geographic location of water sampling region under investigation in the study.. 14

Figure 2.1: Schematic representation of various carbon allotropes [3] 25

Figure 2.2: (a) Pristine graphite, (b) dry ice (solid phase CO_2), (c) edge-carboxylated graphite (ECG) prepared by ball milling for 48 h, (d) a schematic representation of physical cracking and edge-carboxylation of graphite by ball milling in the presence of dry ice, and protonation through subsequent exposure to air moisture [29]. 33

Figure 2.3: (a) The hexagonal lattice of graphene has a basis of two carbon atoms (A, B) per unit cell, (b) The π and π* bands in graphene and (c) The linear dispersion and the band structure at the Dirac point [59,60]..... 36

Figure 2.4: SEM images of (a) bare GCE, (b) GS/GCE and (c) GS/ 42

Figure 2.5: Schematic of the synthesis procedure of β-CD-RGO hybrid nanosheets and the interaction between β-CD-RGO and the heavy metal ions (Pb2+, Cd2+) [101]. . 45

Figure 2.6: A schematic representation of the thymidine functionalized AuNP-rGO biosensor for Hg^{2+} detection [120]. 49

Figure 3.1: (a) Schematic representation of the contact-printing method for fabricating mPADs with PDMS as hydrophobic barriers. (b) Paper-based electrochemical device (PED) with pencil-drawn electrodes utilized in cyclic voltammetry experiments. (c) PED with fluidic channel with pencil-drawn electrodes utilized in flow injection analysis with amperometric detection [31]. 74

Figure 3.2: Conceptual design of the multi-layer paper-based electrochemical sensor showing (a) the various materials and layers and (b) the complete sensor prepared by inkjet printing in the work by Smith *et al*. [45]..... 75

Figure 3.3: Schematic presentation of the mechanisms of water transport in a solid contributing to the overall water movement [47]. 77

Figure 3.4: A schematic illustration of the proposed Hg^{2+} sensing strategy by Chen *et al.* [54]. 79

Figure 3.5: Schematic of the paper-based microfluidic device for multiplex chemical contaminants detection using ssDNA-functionalized GO sensors. (a) Paper-based microfluidic chip design. (b and c) Illustrate the principle of the metal ions detection based on the interaction among GO, ssDNA and heavy metal ions. The fluorescence was quenched when Cy5-labeled ssDNA adsorbed on the GO surface (b, fluorescence OFF). In the presence of the metal ions, they caused the ssDNA spontaneously liberating from the GO surface and finally resulted in fluorescence recovery (c, fluorescence ON). (d) and (e) illustrate the principle of the antibiotic detection based on the interaction among GO, ssDNA and antibiotics. The fluorescence was partly quenched when Cy5-labeled ssDNA adsorbed with low GO concentration (d, fluorescence ON). In the presence of the aminoglycoside antibiotic, the antibiotic-probe duplex increased the bind effection between the duplex and GO surface through amide coupling, resulted in fluorescence intensity decreasing (e, fluorescence OFF) [61]. 81

Figure 3.6: Schematic drawing of (a) the preparation of the G/PANI nanocomposite, (b) electrochemical sensor fabrication on plastic film or paper and (c) drop-casting and electrospraying processes [72]. 83

Figure 4.1: Schematic depicting the chemical synthesis of graphene oxide from bulk commercial graphite. 100

Figure 4.2: Graphic representation of reduction of graphene oxide (GO) to form graphene powder. 101

Figure 4.3: Image of 0.25 mg mL^{-1} (a) reduced graphene oxide [black] and (b) graphene oxide [brown] dispersions in ethanol and water respectively, prepared via the chemical synthesis approach above. 102

Figure 4.4: FTIR spectra recorded for (a) graphite, graphene oxide (GO) and reduced graphene oxide (RGO), (b) magnified spectra of graphite and (c) a comparison of GO prepared by a Hummer's and Tour method. 103

Figure 4.5: HRSEM images of (a) graphite, (b) graphitic oxide, (c and d) reduced graphene oxide at 10 kX and 20 kX magnification. 105

Figure 4.6: HRTEM images of (a) graphite, (b) graphene oxide, (c and d) reduced graphene oxide at varying magnifications. 107

Figure 4.7: XRD patterns of (a) graphite, (b) graphene oxide, (c and d) reduced graphene oxide. 108

Figure 4.8: Raman spectra of (a) graphite, (b) graphene oxide, (c and d) reduced graphene oxide. 110

Figure 4.9: Tapping mode AFM image and corresponding cross-sectional view of prepared reduced graphene oxide. 111

Figure 4.10: UV-vis spectra of (a) graphene oxide and (b) reduced graphene oxide dispersed in water. Inset: UV-vis spectra of reduced graphene oxide. 112

Figure 4.11: (a) HRSEM image and HRTEM images at (b) low and (c) high magnification of 50 nm AuNPs. 113

Figure 4.12: UV-vis absorption spectra of (a) 1:10, (b) 1:5 and (c) 1:1 dilution of commercially bought 50 nm AuNPs in phosphate buffer solution (pH 7.1). Inset: Image of 50 nm AuNPs in PBS buffer solution. 114

Figure 5.1: Cyclic voltammograms depicting the electrochemical reduction of 0.5 mg mL^{-1} GO in acetate buffer solution (0.1 M, pH 4.6) at the PGE using the following instrumental parameters: scan rate (0.1V s^{-1}), deposition time (120 s); frequency (20 Hz); amplitude (0.04 V) and voltage step (0.005 V). 127

Figure 5.2: Cyclic voltammograms of (a) a bare PGE and (b) an ERGO-PGE in ammonium buffer solution (0.1 M, pH 9.4) at the following instrumental parameters: scan rate (10 mV s−1), deposition time (120 s), frequency (50 Hz), amplitude (0.04 V) and voltage step (0.004 V). 128

Figure 5.3: Cyclic voltammograms of bare-PGE (a) and ERGO-PGE (b) in 0.1mM $K_3Fe(CN)_6$ solution containing 0,1 M KCl. 129

Figure 5.4: Schematic representation of the AdCSV detection of metal cations in the presence of chelating agent and metallic film 130

Figure 5.5: Cathodic stripping voltammogram of characteristic oxidation stripping potential of 20μg.L^{-1} Ni^{2+}(-1.10 V) in 0.1 M ammonium buffer solution (pH 9.4) at the ERGO-PGE under the optimized parameters. 131

Figure 5.6: HRSEM images of bare-PGE (left) and ERGO-PGE (right) at 500 times magnification. 132

Figure 5.7: SWASV of 20 μgL^{-1} at (a) bare-PG-MFE, (b) ERGO-PGE and (c) ERGO- PG-MFE. Supporting electrolyte (0.1 M ammonium chloride ammonium hydroxide buffer solution, pH 9.4), deposition potential (-0.7 V), deposition time (120 s), frequency (50 Hz), amplitude (0.05 V) and voltage step (0.005 V). 133

Figure 5.8: The effect of (a) deposition time, (b) rotation speed, (c) amplitude, (d) deposition potential, (e) cleaning time and (f) frequency on the stripping peak of Ni^{2+} at electrochemically reduced graphene oxide pencil graphite mercury film electrode (ERGO-PG-MFE) in 0.1M ammonium hydroxide ammonium chloride buffer solution (pH = 9.4) containing 5 μg L^{-1} of Ni in 5 mg L^{-1} of Hg^{2+}. 136

Figure 5.9: SWAdCSV and corresponding calibration curve for the individual analysis of Ni^{2+} obtained at ERGO-PG-MFE between the concentration of 2 ppb – 16 ppb. The supporting electrolyte used was ammonium hydroxide ammonium chloride buffer solution (0.1M, pH 9.4), deposition time (210 s), deposition potential (- 0.7 V),

rotational speed (800 rpm), frequency (50 Hz), amplitude (0.05 V) and sweep rate (0.2 V s^{-1})..... 138

Figure 5.10: Calibration curve from a standard addition method for the determination of Ni^{2+} at ERGO-PG-MFE in test solutions..... 141

Figure 5.11: Square wave voltammograms (a) and standard addition calibration curve of Ni^{2+} for the analysis of tap water (pH = 9.4) spiked with 5 µg L^{-1} of Ni ions at deposition time of 240 s..... 142

Figure 6.1: Fourier Transform Infrared Spectrometry of Dimethylglyoxime as a KBr Pellet. Inset: Schematic Representation of the Dimethylglyoxime Structure. 154

Figure 6.2: Schematic Illustration of the Metal-Chelate Complex Formation [46]..... 155

Figure 6.3: High Resolution Scanning Electron Microscope (HRSEM) image of (a and c) Bare SPCE and (b and d) NGr-DMG-SPCE at 1.00 k X and 20.00 k X magnification. 157

Figure 6.4: Energy Dispersive Spectroscopy (EDS) Results obtained from HRSEM at the (a) Bare SPCE and (b) NGr-DMG-SPCE..... 157

Figure 6.5: Electrochemical Characterisation of N-DMG-GCE in 5 mM $Fe(CN)_6^{3-/4-}$ at scan rate of 10-100 mV s^{-1} in supporting electrolyte (1 M KCl). 159

Figure 6.6: Electrochemical Characterisation of NGr-DMG-GCE in 5 mM $Fe(CN)_6^{3-/4-}$ at scan rate of 10-100 mV s^{-1} in supporting electrolyte (1 M KCl). 160

Figure 6.7: Cyclic voltammograms of 5 mM $Fe(CN)_6^{3-/4-}$ at (a) N-DMG-GCE and (b) NGr-DMG-GCE in supporting electrolyte of 1 M KCl at scan rate 50 mV s^{-1}..... 161

Figure 6.8: Nyquist plots at (a) GCE, (b) DMG-GCE, (c) N-DMG-GCE and (d) NGr-DMG-GCE in 5 mM $Fe(CN)_6^{3-/4-}$ containing 1 M KCl. Inset is the magnified Nyquist plot between 0 and 12 kΩ. The frequency range is from 0.1 Hz to 100 kHz..... 163

Figure 6.9: Cyclic voltammograms of (a) N-DMG-GCE and (b) NGr-DMG-GCE. Supporting electrolyte 0.1 M NH_3/NH_4Cl Buffer (pH 9.3), scan rate (10 mV s^{-1}), deposition time (120 s), frequency (20 Hz), amplitude (0.02 V) and voltage step (0.005 V). 164

Figure 6.10: SW-AdCSV of 20 µg L^{-1} Ni^{2+} at (a) N-DMG-GCE and (b) NGr-DMG-GCE with a characteristic reduction stripping potential of -1.09 V. Supporting electrolyte (0.1 M NH_3/NH_4Cl Buffer (pH 9.3)), deposition potential (- 0.7 V), deposition time (120 s), frequency (20 Hz), amplitude (0.02 V) and voltage step (0.005 V)..... 165

Figure 6.11: Influence of Dimethylglyoxime Concentration (0 – 0.1 M) on the stripping peak currents of Ni^{2+} at the NGr-DMG-GCEs in 0.1 M NH_3/NH_4Cl Buffer (pH 9.3).166

Figure 6.12: Effect of Instrumental Parameters; (a) Deposition Potential, (b) Deposition Time, (c) Frequency and (d) Amplitude on the stripping peak current of 10 µg L^{-1} Ni^{2+} at NGr-DMG-GCE. Supporting electrolyte (0.1 M NH_3/NH_4Cl Buffer (pH 9.3)). 168

Figure 6.13: Dependence of Electrolyte pH on the stripping peak currents of Ni^{2+} at the NGr-DMG-GCEs in 0.1 M NH_3/NH_4Cl Buffer as electrolyte solution. 169

Figure 6.14: Square-Wave Voltammogram of 4 µg L^{-1} Ni^{2+} at a NGr-DMG-GCE (a) before deoxygenation and (b) after deoxygenation. Supporting electrolyte (0.1 M NH_3/NH_4Cl Buffer (pH 9.3)), deposition potential (- 0.7 V), deposition time (120 s), frequency (20 Hz), amplitude (0.02 V) and voltage step (0.005 V)..... 170

Figure 6.15: Square-Wave Voltammograms of (a) 0 µg L^{-1} metal cations, (b) 200 µg L^{-1} Co^{2+} and Zn^{2+}, (c) 20 µg L^{-1} Ni^{2+} and (d) 20 µg L^{-1} Ni^{2+} in the presence of 200 µg L^{-1} Co^{2+} and Zn^{2+} at a NGr-DMG-GCE. Supporting electrolyte (0.1 M NH_3/NH_4Cl Buffer (pH 9.3)), deposition potential (- 0.7 V), deposition time (120 s), frequency (20 Hz), amplitude (0.02 V) and voltage step (0.005 V). 172

Figure 6.16: SWAdSV and corresponding calibration plot of the individual analysis of Ni^{2+} in the presence of Co^{2+} and Zn^{2+} obtained at a NGr-DMG-GCE over 2 – 20 µg L^{-1}. Supporting electrolyte (0.1 M NH_3/NH_4Cl Buffer (pH 9.3)), deposition potential (-

0.7 V), deposition time (120 s), frequency (20 Hz), amplitude (0.02 V) and voltage step (0.005 V). 175

Figure 6.17: SWAdSV and corresponding standard addition calibration plot of the individual analysis of Ni^{2+} in the presence of Co^{2+} and Zn^{2+} obtained at a NGr-DMG-GCE in real tap water samples. Supporting electrolyte (0.1 M NH_3/NH_4Cl Buffer (pH 9.3)), deposition potential (- 0.7 V), deposition time (120 s), frequency (20 Hz), amplitude (0.02 V) and voltage step (0.005 V). 178

Figure 7.1: HRSEM image of the entangled cellulose fiber structure of unmodified PEC at 100 X magnification. 193

Figure 7.2: Square wave adsorptive cathodic stripping voltammogram (SWAdCSV) of 50 µg L^{-1} Ni^{2+} in 0.1 M NH_3/NH_4Cl buffer (pH 9.4) as supporting electrolyte containing 2 mM DMG and 10 mg L^{-1} Hg at a SPCE. SWV parameters: E_{acc} = - 0.7 V, t_{acc} = 90 s, amplitude = 35 mV and f = 20 Hz. 195

Figure 7.3: Square wave adsorptive cathodic stripping voltammograms (SWAdCSVs) of (a) 0.0 µg L^{-1} Ni^{2+}, (b) 5.0 µg L^{-1} Ni(II), (c) 15 µg L^{-1} Ni^{2+} and (d) 20 µg L^{-1} Ni(II) at screen printed carbon electrodes in 0.1 M NH_3/NH_4Cl buffer (pH 9.4) as supporting electrolyte containing 2 mM DMG and 10 mg L^{-1} Hg. SWV parameters: E_{acc} = - 0.7 V, t_{acc} = 90 s, amplitude = 35 mV and f = 20 Hz. 196

Figure 7.4: Square wave adsorptive cathodic stripping voltammograms (SWAdCSVs) of 50 µg L^{-1} Ni^{2+} at (a) SPCE immersed in 10 mL of 50 µg L^{-1} Ni^{2+} [Solution], (b) SPCE with 100 µL sample of 50 µg L^{-1} Ni^{2+} dropped directly onto the three electrode system [droplet] and (c) SPCE with PEC covering the three electrode system. 20 µL solution of 50 µg L^{-1} Ni^{2+} [paper disk]. 0.1 M NH_3/NH_4Cl buffer as supporting electrolyte containing 2 mM DMG and 10 mg L^{-1} Hg was used. SWV parameters: E_{acc} = - 0.7 V, t_{acc} = 90 s, amplitude = 35 mV and f = 20 Hz..... 198

Figure 7.5: Square wave adsorptive cathodic stripping voltammograms (SWAdCSVs) of 50 µg L^{-1} Ni^{2+} at: (a) SPCE with PEC covering the three electrode system. A 20 µL solution comprised of 0.1 M NH_3/NH_4Cl buffer as supporting electrolyte containing

2 mM DMG and 10 mg L^{-1} Hg was used and (b) SPCE with PEC pre-stored with a 20 µL solution containing 2 mM DMG and 10 mg L^{-1} Hg in 0.1 M NH_3/NH_4Cl buffer as supporting electrolyte. SWV parameters: E_{acc} = - 0.7 V, t_{acc} = 90 s, amplitude = 35 mV and f = 20 Hz. 200

Figure 7.6: Square wave adsorptive cathodic stripping voltammograms (SWAdCSVs) of 5 - 60 µg L^{-1} Ni^{2+} at a SPCE with PEC covering the three electrode system. A 20 µL solution comprised of metal analyte in 0.1 M NH_3/NH_4Cl buffer as supporting electrolyte containing 2 mM DMG and 10 mg L^{-1} Hg. SWV parameters: E_{acc} = - 0.7 V, t_{acc} = 90 s, amplitude = 35 mV and f = 20 Hz. 201

Figure 7.7: Square wave adsorptive cathodic stripping voltammograms (SWAdCSVs) of 10 - 60 µg L^{-1} Ni^{2+} at SPCE with PEC pre-stored with a 20 µL solution containing 2 mM DMG and 10 mg L^{-1} Hg in 0.1 M NH_3/NH_4Cl buffer as supporting electrolyte. SWV parameters: E_{acc} = - 0.7 V, t_{acc} = 90 s, amplitude = 35 mV and f = 20 Hz. 202

Figure 7.8: Square wave adsorptive cathodic stripping voltammograms (SWAdCSVs) of 20 µL sample of 50 µg L^{-1} Ni^{2+} at (a) SPCE with PEC pre-stored with ammonia buffer, (b) SPCE with PEC pre-stored with a 20 µL solution containing 10 mg L^{-1} Hg, (c) SPCE with PEC pre-stored with a 20 µL solution containing 2 mM DMG and (d) SPCE with PEC pre-stored with a 20 µL solution containing 2 mM DMG and 10 mg L^{-1} Hg. 0.1 M NH_3/NH_4Cl buffer was used as supporting electrolyte. SWV parameters: E_{acc} = - 0.7 V, t_{acc} = 90 s, amplitude = 35 mV and f = 20 Hz. 204

Figure 7.9: Dependence of the square wave stripping peak current of 50 µg L^{-1} Ni^{2+} reduction from the $[Ni(dmgH)_2]$ complex on the pre-stored PEC dimethylglyoxime concentration (mM) between 0 - 5 mM. Supporting electrolyte: 0.1 M NH_3/NH_4Cl buffer as supporting electrolyte. 206

Figure 7.10: Effect of Hg concentration (mg L^{-1}) on the adsorptive cathodic stripping peak current of Ni^{2+} detection in 0.1 M NH_3/NH_4Cl buffer as supporting electrolyte. 207

Figure 7.11: The influence of (a) accumulation potential (E_{acc}), (b) accumulation time (t_{acc}), (c) amplitude and (d) frequency on Ni^{2+} peak currents. Sample composition: 30 µg L^{-1} Ni, 2 mM DMG, 10 mg L^{-1} Hg(II), 0.1 M NH_3/NH_4Cl buffer. 209

Figure 7.12: Four consecutive square-wave voltammograms (SWV) obtained from PPEC in conjunction with SPCE in solution containing 30 µg L^{-1} Ni, 2 mM DMG, 10 mg L^{-1} Hg^{2+}, 0.1 M NH_3/NH_4Cl buffer, indicating the reproducibility of the PPECs. Inset: Ni^{2+} peak currents vs. consecutive runs. SWV parameters: E_{acc} = - 0.7 V, t_{acc} = 90 s, amplitude = 35 mV and f = 20 Hz (n = 4). 210

Figure 7.13: (a) Square-wave adsorptive cathodic stripping voltammograms (SW-AdCSV) and (b) corresponding $[Ni(dmgH)_2]$ stripping peak current vs. consecutive runs of 20 µL 30 µg L^{-1} Ni^{2+} in the presence of 100 µg L^{-1} Zn^{2+}, Cd^{2+}, Pb^{2+}, Co^{2+} and In^{2+} at PPECs in conjunction with commercial SPCEs..... 212

Figure 7.14: Square-wave adsorptive cathodic stripping voltammograms of PPECs in conjunction with SPCEs and corresponding calibration plots recorded with 20 µL volumes of (a) 300 – 2100, (b) 30 – 210 and (c) 15 - 120 µg L^{-1} $[Ni(dmgH)_2]$ in 0.1 M NH_3/NH_4Cl buffer. SWV parameters: E_{acc} = - 0.7 V, t_{acc} = 90 s, amplitude = 35 mV and f = 20 Hz, (n = 3). 213

Figure 7.15: Probable Ni(II)-chelate structures formed with (a) dimethylglyoxime, (b) nioxime and (c) morin hydrate 218

Figure 7.16: Square wave adsorptive cathodic stripping voltammograms (SW-AdCSVs) obtained from 20 µL sample of 50 µg L^{-1} Ni^{2+} at (a) SPCE with PEC pre-stored with a 20 µL solution containing 2 mM DMG and 10 mg L^{-1} Hg, (b) SPCE with PEC pre-stored with a 20 µL solution containing 2 mM Nioxime and 10 mg L^{-1} Hg and (c) SPCE with PEC pre-stored with a 20 µL solution containing 2 mM Morin hydrate and 10 mg L^{-1} Hg. 0.1 M NH_3/NH_4Cl buffer was used as supporting electrolyte. SWV parameters: E_{acc} = - 0.7 V, t_{acc} = 90 s, amplitude = 35 mV and f = 20 Hz. 219

Figure 7.17: CVs of (a) unmodified, (b) GO-infused and (c) ERGO PEC with 20 µL 5 mM $Fe(CN)_6^{3-/4}$ and 1 M KCl as supporting electrolyte at a SPCE and a scan rate of 100 mV s^{-1}. Inset: GO-infused PEC prior to electrochemical reduction. 221

Figure 7.18: CVs of (a) unmodified and (b) NGr-infused with 20 µL 5 mM $Fe(CN)_6^{3-/4}$ and 1 M KCl as supporting electrolyte at a SPCE and a scan rate of 100 mV s^{-1}. Inset: GO-infused PEC prior to electrochemical reduction. 222

Figure 7.19: Square-wave voltammograms (SWV) obtained from (a) unmodified and (b) NGr-infused PPEC in conjunction with SPCE in solution containing 30 µg L^{-1} Ni, 2 mM DMG, 10 mg L^{-1} Hg^{2+}, 0.1 M NH_3/NH_4Cl buffer, indicating the reproducibility of the PPECs. Inset: Ni^{2+} peak currents vs. consecutive runs. SWV parameters: E_{acc} = - 0.7 V, t_{acc} = 90 s, amplitude = 35 mV and f = 20 Hz. 223

Figure 7.20: Square-wave voltammograms (SWV) of NGr-infused PPEC in conjunction with SPCE for 0 - 100 µg L^{-1} Ni^{2+}, 2 mM DMG, 10 mg L^{-1} Hg^{2+}, 0.1 M NH_3/NH_4Cl buffer, indicating the reproducibility of the PPECs. Inset: Ni^{2+} peak currents vs. consecutive runs. SWV parameters: E_{acc} = - 0.7 V, t_{acc} = 90 s, amplitude = 35 mV and f = 20 Hz. 224

Figure 7.21: HRSEM image of the (a) unmodified PEC, (b) GO-PEC and (c) RGO-PEC at 100 X magnification 225

Figure 7.22: CV of filtered Gr-paper electrode with 20 µL 5 mM $Fe(CN)_6^{3-/4}$ and 1 M KCl as supporting electrolyte at a scan rate of 100 mV s^{-1}. 226

Figure 8.1: Schematic illustration of the AuNP-IL-µPED preparation and its subsequent application towards metal analysis in water samples by electrochemical stripping analysis 236

Figure 8.2: Array of wax lines (0.1 – 1 mm) patterned on Whatman No.1 chromatographic paper, before and after heating on a hot plate. 238

Figure 8.3: 8-bit Grey scale test studying the effect of wax line width on melting effectiveness. 239

Figure 8.4: Influence of melting temperature (50 – 250 °C) on effective boundary formation. 240

Figure 8.5: Influence of melting time on melting effectiveness at 200 °C. 241

Figure 8.6: Wax printed hydrophobic designs, before and after melting under optimised conditions: 3 min at 200 °C. 242

Figure 8.7: Effective leak test of (a) wax printed hydrophobic barriers and (b) µPED. Patterned stamps for contact printing made from (c) linoleum and (d) PDMS. 242

Figure 8.8: HRSEM image of (a) patterned chromatography paper showing clear distinction between hydrophobic and hydrophilic regions (20 X magnification) and (b) magnified image of unmodified cellulose structure (1000 X magnification). 243

Figure 8.9: HRSEM images of AuNP-µPED created from chromatography paper showing (a) back-scattered image of gold nanoparticle distribution in cellulose structure (5000 X magnification) and (b) magnified images of individual gold nanoparticles (100 kX magnification). 244

Figure 8.10: Energy dispersive spectra (EDS) of (a) chromatography paper and (b) AuNP-modified chromatography paper 245

Figure 8.11: Square-wave anodic stripping voltammogram (SW-ASV) of 40 µM Cu^{2+} detection in the presence of 2000 µM Hg^{3+} at the AuNP-IL-µPED. Supporting electrolyte: 0.1 M acetate buffer solution (pH 4.6), scan rate (10 mV s^{-1}), deposition time (120 s), frequency (50 Hz), amplitude (0.04 V) and voltage step (0.004 V)..... 246

Figure 8.12: Square-wave voltammograms recorded for 40 µM Cu^{2+} at SPCE in conjunction with µPEDs modified with 20 µL (a) electrolyte, (b) 1000 µM Hg^{3+} in electrolyte, (c) 1-methylimidazole and 1000 µM Hg^{3+} in electrolyte and (d) 0.05 µM AuNP, 1-methylimidazole and 1000 µM Hg^{3+} in electrolyte. Supporting electrolyte: 0.1 M acetate buffer solution (pH 4.6), scan rate (10 mV s^{-1}), deposition time (120 s), frequency (50 Hz), amplitude (0.04 V) and voltage step (0.004 V). 248

Figure 8.13: Influence of Hg ion concentration on the stripping peak current of 40 µM Cu^{2+} at AuNP-IL-µPEDs. 249

Figure 8.14: Influence of instrumental parameters: (a) deposition potential and (b) deposition time on the stripping peak response of 40 µM Cu^{2+} at AuNP-IL-µPEDs..... 250

Figure 8.15: SW-ASVs of 20 – 100 µM Cu^{2+} at AuNP-IL-µPED in conjunction with SPCE. Inset: Corresponding calibration plot. Supporting electrolyte: 0.1 M acetate buffer solution (pH 4.6), scan rate (10 mV s^{-1}), deposition time (120 s), frequency (50 Hz), amplitude (0.04 V) and voltage step (0.004 V). 252

Figure 8.16: SW-AdCSV of 60 µg L^{-1} Ni^{2+} in 0.1 M NH_3/NH_4Cl buffer (pH 9.4) as supporting electrolyte containing 2 mM DMG and 15 mg L^{-1} Hg at AuNP-IL-µPED in conjunction with SPCE. E_{acc} = - 0.7 V, t_{acc} = 90 s. 256

Figure 8.17: SW-AdCSVs of 60 µg L^{-1} Ni^{2+} in 0.1 M NH_3/NH_4Cl buffer (pH 9.4) as supporting electrolyte containing 2 mM DMG and 15 mg L^{-1} Hg at (a) µPED, (b) IL-µPED and (c) AuNP-IL-µPED in conjunction with SPCE. E_{acc} = - 0.7 V, t_{acc} = 90 s... 257

Figure 8.18: Influence of dimethylglyoxime concentration on the $[Ni(dmgH)_2]$ complex stripping response..... 259

Figure 8.19: Influence of Hg ion concentration on the $[Ni(dmgH)_2]$ complex stripping response. 260

Figure 8.20: Influence of instrumental parameters: (a) deposition potential and (b) deposition time on the stripping peak response of 60 µg L^{-1} Ni^{2+} at AuNP-IL-µPEDs in the presence of 2 mM DMG and 15 mg L^{-1} Hg. 261

Figure 8.21: SW-AdCSVs of 30 - 150 µg L^{-1} Ni^{2+} in 0.1 M NH_3/NH_4Cl buffer (pH 9.4) as supporting electrolyte containing 2 mM DMG and 15 mg L^{-1} Hg at AuNP-IL-µPED in conjunction with SPCE. E_{acc} = - 0.7 V, t_{acc} = 90 s. 263

Figure 9.1: Schematic representation of Inkjet-printed three-electrode system designs with (a) small and (b) large contacts for printing on a variety of paper substrates 277

Figure 9.2: HRSEM image of Inkjet printed silver WE on photographic paper and the three electrode system electrodes with carbon coated (b) CE and (c) WE and CE 278

Figure 9.3: Droplet formation sequence of inkjet printing of commercial graphene ink 280

Figure 9.4: Measured resistance of (a) Ag and (b) graphene ink tracks as a function of sintering temperature on photography paper..... 282

Figure 9.5: Measured resistance of three printed layers of (a) Ag and (b) graphene ink tracks as a function of sintering temperature on chromatography paper 282

Figure 9.6: Measured resistance as a function of curing at 1 and 3 printed layers on chromatography paper. Curing at 120 ^{o}C for 1 h. 283

Figure 9.7: Laser images of 0.5 mm (a) silver and (b) graphene features on photographic paper 284

Figure 9.8: Laser micrographs illustrating topography of 0.5 mm printed (a) graphene and (b) Ag features on photographic paper 285

Figure 9.9: Laser images of 0.5 mm (a) graphene, (b) Ag + graphene and (c) Ag features on chromatographic paper..... 286

Figure 9.10: Laser micrographs illustrating the topography of 0.5 mm printed (a) graphene, (b) Graphene on Ag and (c) Ag features on chromatography paper..... 286

Figure 9.11: Cyclic voltammograms Electrochemical Characterisation of (a) Ag-printed photo-paper electrode and (b) CC-Ag-printed photo-paper electrode in 5 mM $Fe(CN)_6^{3-/4-}$ at scan rate of 10-100 mV s^{-1} in supporting electrolyte (1 M KCl). 288

Figure 9.12: Cyclic voltammograms depicting the electrochemical reduction of 0.5 mg mL^{-1} GO and 15 mg L^{-1} Au^{3+} in acetate buffer solution (0.1 M, pH 4.6) at the CC-Ag-PPE under the following instrumental parameters: scan rate (10 mV s^{-1}), deposition time (120 s); frequency (50 Hz); amplitude (0.04 V) and voltage step (0.004 V)..... 290

Figure 9.13: Cyclic voltammograms recorded at the (a) CC-Ag-PPE, (b) ERGO-CC-Ag-PPE and (c) ERGO-AuNP-CC-Ag-PPE in acetate buffer solution (0.1 M, pH 4.6) under the following instrumental parameters: scan rate (10 mV s^{-1}), deposition time (120 s); frequency (50 Hz); amplitude (0.04 V) and voltage step (0.004 V). 291

Figure 9.14: SW-AdCSVs of 300 µg L^{-1} Ni^{2+} in the presence of 2 mM DMG and 10 mg L^{-1} Hg^{3+} at (a) CC-Ag-PPPE, (b) ERGO-CC-Ag-PPPE (5 cycles), (c) ERGO-CC-Ag-PPPE (30 cycles), (d) ERGO-CC-Ag-PPPE (50 cycles) and (e) ERGO-AuNP-CC-Ag-PPPE (30 cycles). Supporting electrolyte: 0.1 M NH_3/NH_4Cl buffer (pH 9.4). SWV instrumental parameters: E_{acc} = -0.7 V, t_{acc} = 120 s, f = 5 Hz and *Ampl* = 10 mV. 293

Figure 9.15: A comparison of stripping responses of 300 µg L^{-1} Ni^{2+} in the presence of 2 mM DMG and 10 mg L^{-1} Hg^{3+} at (a) CC-Ag-PPPE, (b) ERGO-CC-Ag-PPPE (5 cycles), (c) ERGO-CC-Ag-PPPE (30 cycles), (d) ERGO-CC-Ag-PPPE (50 cycles) and (e) ERGO-AuNP-CC-Ag-PPPE (30 cycles)..... 294

Figure 9.16: High resolution scanning electron microscope (HRSEM) images of (a) inkjet printed AgNP, (b) CC-AgNP, (c) ERGO-CC-AgNP and (d) AuNP-ERGO-CC-AgNP working electrodes on photographic paper at 5 kX magnification. 295

Figure 9.17: SW-AdCSVs of 300 µg L^{-1} Ni^{2+} at the ERGO-AuNP-CC-Ag-PPPE in the presence of (a) 0.1 M NH_3/NH_4Cl buffer, (b) 2 mM DMG, (c) 10 mg L^{-1} Hg^{3+} and (d) 2 mM DMG and 10 mg L^{-1} Hg^{3+}. Supporting electrolyte: 0.1 M NH_3/NH_4Cl buffer (pH 9.4). SWV instrumental parameters: E_{acc} = -0.7 V, t_{acc} = 120 s, f = 5 Hz and *Ampl* = 10 mV..... 297

Figure 9.18: Effect of 0 – 3 mM DMG concentration on the stripping peak current response of 300 µg L^{-1} Ni^{2+} at the ERGO-AuNP-CC-Ag-PPPE in the presence of 10 mg L^{-1} Hg^{3+}. Supporting electrolyte: 0.1 M NH_3/NH_4Cl buffer (pH 9.4). 298

Figure 9.19: Effect of Hg concentration (0 – 30 mg L^{-1}) on the stripping peak current response of 300 µg L^{-1} Ni^{2+} at the ERGO-AuNP-CC-Ag-PPPE in the presence of 2 mM DMG. Supporting electrolyte: 0.1 M NH_3/NH_4Cl buffer (pH 9.4)..... 299

Figure 9.20: The influence of (a) accumulation potential (E_{acc}), (b) accumulation time (t_{acc}), (c) amplitude and (d) frequency on Ni^{2+} peak currents. Sample composition: 300 µg L^{-1} Ni, 2 mM DMG, 10 mg L^{-1} Hg(II), 0.1 M NH_3/NH_4Cl buffer. 301

Figure 9.21: SWASV and corresponding calibration plot of individual analysis of Ni^{2+} obtained at ERGO-AuNP-CC-Ag-PPE over 50 – 500 µg L^{-1} range. Supporting electrolyte (0.1 NH_3/NH_4Cl Buffer, pH 9.4), deposition time (90 s), deposition potential (- 0.7 V), rotation speed (1000 rpm), frequency (5 Hz), amplitude (0.01 V). 303

Figure 9.22: Analysis of tap water (pH 9.4) spiked with 150 µg L^{-1} of metal ion in the presence of 2 mM DMG and 10 mg L^{-1} Hg^{3+}. (a) SW-AdSV and (b) Calibration plot. Supporting electrolyte: 0.1 M NH_3/NH_4Cl buffer (pH 9.4). SWV instrumental parameters: E_{acc} = -0.7 V, t_{acc} = 120 s, f = 5 Hz and Ampl = 10 mV..... 305

Figure 9.23: SW-AdCSV and corresponding calibration plot of Co^{2+} obtained at ERGO-AuNP-CC-Ag-PPE over 300 – 600 µg L^{-1} range. Supporting electrolyte (0.1 NH_3/NH_4Cl Buffer, pH 9.4), deposition time (90 s), deposition potential (- 0.7 V), rotation speed (1000 rpm), frequency (5 Hz), amplitude (0.01 V). 307

Figure 9.24: SW-AdCSV of 300 µg L^{-1} Ni^{2+}, obtained at the (a) CB-Ag-PPPE and (b) CB-DMG-Ag-PPPE. Supporting electrolyte (0.1 NH_3/NH_4Cl Buffer, pH 9.4), deposition time (90 s), deposition potential (- 0.7 V), rotation speed (1000 rpm), frequency (5 Hz), amplitude (0.1 V). 309

Figure 9.25: Influence of DMG loading within carbon black inks on the stripping peak current of 300 µg L^{-1} Ni^{2+}..... 310

Figure 9.26: High resolution scanning electron microscope images of (a) inkjet printed AgNPs, (b) CB-AgNP and (c) DMG-CB-AgNP working electrodes on photographic paper at 1 kX magnification. 311

Figure 9.27: The influence of (a) accumulation potential (E_{acc}), (b) accumulation time (t_{acc}), (c) frequency and (d) amplitude on Ni^{2+} peak currents at CB-DMG-Ag-PPPE. Sample composition: 300 µg L^{-1} Ni, 0.1 M NH_3/NH_4Cl buffer..... 313

Figure 9.28: SW-AdCSVs and corresponding calibration plot of individual analysis of Ni^{2+} obtained at CB-DMG-CC-Ag-PPE over a 50 – 500 µg L^{-1} range. Supporting electrolyte (0.1 NH_3/NH_4Cl Buffer, pH 9.4), deposition time (90 s), deposition potential (- 0.7 V), rotation speed (1000 rpm), frequency (5 Hz), amplitude (0.01 V)..... 314

Figure 9.29: Analysis of tap water (pH 9.4) spiked with 150 µg L^{-1} of metal ion in the presence of 2 mM DMG and 10 mg L^{-1} Hg^{3+}. (a) SW-AdSV and (b) Calibration plot. Supporting electrolyte: 0.1 M NH_3/NH_4Cl buffer (pH 9.4). SWV instrumental parameters: E_{acc} = -0.7 V, t_{acc} = 120 s, f = 5 Hz and *Ampl* = 10 mV. 317

Figure 9.30: A comparison of calibration plots of 50 – 500 µg L^{-1} Ni^{2+} at (a) ERGO-AuNP-CC-Ag-PPE and (b) CB-DMG-Ag-PPE 318

List of Tables

Table 2.1: A summary of electrical, optical, thermal and mechanical properties recorded for graphene in literature. 37

Table 3.1: A summary of commonly available heavy metal detection techniques 72

Table 4.1: A summary of characterization techniques used in the study and their corresponding uses. 99

Table 4.2: A summary of recorded stretching vibrations and corresponding functional groups found from FTIR analysis of Graphite, Graphene oxide and Reduced Graphene Oxide. 104

Table 5.1: Calibration data representation individual analysis of Ni^{2+} at ERGO-PG-MFE in 0.1M ammonium buffer solution (pH 9.4) under optimized parameters*. 139

Table 5.2: A summary of previously reported limits of detection (LOD) for Ni^{2+} detection in literature. 140

Table 6.1: Reproducibility and interference studies of the N-DMG-GCE and NGr-DMG-GCE*. 173

Table 6.2: A summary of selected previously reported (a) Chemically Modified DMG and (b) In-situ DMG Sensors for Adsorptive Stripping Voltammetric Detection of Ni^{2+}. 176

Table 6.3: Recovery studies of the NGr-DMG-GCE in test and tap water samples*. 178

Table 7.1: Analytical performance of the fabricated PPECs (n = 3) in the 15 – 120 µg L^{-1} Ni^{2+} concentration. 215

Table 7.2: A summary of previously reported detection limits for in-situ Ni^{2+} detection in water samples. 216

Table 7.3: Recovery studies for in-situ Ni^{2+} detection in test, contaminated and water samples*. 217

Table 8.1: Sensitivity, correlation coefficient (R^2), detection limit (LOD) and limit of quantitation (LOQ) recorded at AuNP-IL-µPED (n = 3)..... 253

Table 8.2: A summary of previously reported sensors and limits of detection (LOD) for Cu^{2+} detection by stripping voltammetric techniques..... 254

Table 8.3: Sensitivity, correlation coefficient (R^2), detection limit (LOD) and limit of quantitation (LOQ) recorded at AuNP-IL-µPED for Ni^{2+} detection*..... 264

Table 8.4: A summary of previously reported sensors and limits of detection (LOD) for Ni^{2+} detection by stripping voltammetric techniques..... 265

Table 9.1: A summary of recorded analytical data for the ERGO-AuNP-CC-Ag-PPE over the 50 – 500 µg L^{-1} range*. 304

Table 9.2: Recorded recovery percentages in both test and water samples*. 306

Table 9.3: A summary of recorded analytical data for the CB-DMG-Ag-PPE over the 50 – 500 µg L^{-1} range. 315

Table 9.4: Recorded recovery percentages in both test and water samples 317

Table 9.5: A summary of previously reported sensors and limits of detection (LOD) for Ni^{2+} detection by stripping voltammetric techniques..... 319

Chapter 1 :

Microfluidic graphenised-paper electroanalytical devices (µGPED) for adsorptive cathodic stripping voltammetric detection of metal contaminants:

An Introduction

Abstract

The need for clean, non-toxic drinking water supplies, free of pollutants and metal contamination is vital in impoverished areas and the developing world alike. With this in mind, the development of accurate, inexpensive, portable and simple devices for remote sensing applications is therefore pivotal for early detection and the prevention of illnesses. Over the last two decades, adsorptive stripping voltammetry (AdSV) has emerged as a superior detection method over common analytical techniques due to its low-cost instrumentation, unskilled labour and ability to detect a wide range of analytes. The technique is based on the non-electrolytic accumulation (adsorption) of the analyte followed by a cathodic reduction scan measurement. Moreover, recent progress in paper-based microfluidics coupled to electrochemical approaches for analysis have shown tremendous promise as platforms for providing simple, portable and quantitative detection. Herein, a variety of novel paper-based electrochemical platforms are developed for the detection of metal contaminants, such as Ni^{2+} in drinking water with low-volume sample introduction in the presence of dimethylglyoxime as chelating agent. For the first time, paper-based microfluidics is combined with electrochemical AdSV in conjunction with conventional three-electrode systems to produce microfluidic paper-based electroanalytical devices (µPEDs) which function as one-step, low-cost electroanalytical sensors for the detection of Ni^{2+} in tap water samples. The study is based on two simple and unique fabrication approaches: (i) dry reagent infusion techniques in the development of novel pre-stored (infused) µPEDs and

(ii) inkjet and screen printing techniques for production of integrated paper-based electrode systems. The pre-stored µPEDs with a novel single-step accumulation and deposition demonstrated highly selective detection of Ni^{2+} in the presence of metallic interferents (Zn^{2+}, Cd^{2+}, Pb^{2+}, Co^{2+} and In^{2+}) up to 100 times metal analyte concentration. A limit of detection of 6.27 ± 1.32 µg L^{-1} was established for Ni^{2+} detection over a dynamic linear range of 15 – 120 µg L^{-1} with sensitivity of 7.08 µA L $µg^{-1}$ for three replications at 90 s analysis times. The lower sensitivities normally associated with µPEDs was addressed by the incorporation of graphene, carbon black, gold nanoparticles or ionic liquids (1-methylimidazole) within the cellulose fibre structure. Microfluidic graphenised-paper electroanalytical devices (µGPEDs) demonstrated ability to improve electron transfer kinetics and enhance electroactive surface area within the fibrous cellulose structure at high graphene content percentages (> 10 weight %). In addition, µPEDs prepared from gold nanoparticles and 1-methylimidazole improved the electroactivity and sensitivity of AuNP-IL-µPEDs up to 3 times over unmodified counterparts with a uniform decoration of ~ 90 nm gold nanoparticles within the cellulose structure. A limit of detection of 5.13 ± 3.74 µg L^{-1} was recorded for Ni^{2+} detection over a dynamic linear range of 30 – 150 µg L^{-1} (n = 3). Further, integrated paper-based three-electrode systems based on inkjet printing were fabricated with high conductivity (< 50 Ω) from silver nanoparticle (AgNP) and graphene-based inks. Gold nanoparticle decorated electrochemically reduced graphene oxide (AuNP-ERGO) and carbon black, dimethylglyoxime (CB-DMG) modified paper-based electroanalytical devices (PEDs) yielded limits of detection of 32.19 ± 9.61 and 48.01 ± 12.24 µg L^{-1} respectively for Ni^{2+} detection at 90 s accumulation times over a dynamic linear range of 50 – 500 µg L^{-1} Ni^{2+}. Relative standard deviations (RSD %) for $[Ni(dmgH)_2]$ reduction were found to be within a 2 – 7 % error. For real sample analysis, the nanoparticle-enhanced voltammetric paper-based devices proved to be suitable for the detection and quantitation of Ni^{2+} below the United State Environmental Protection Agency (US EPA) and World Health Organization (WHO) prescribed limit (0.1 mg L^{-1} or 0.1 ppm) and South African Drinking Water Guidelines limit (0.15 mg L^{-1}) for drinking water.

1.1. Background to the Study

When conducting environmental monitoring or direct patient care in nontraditional settings, it is often necessary to ascertain measurements which are difficult to obtain outside of controlled settings. Rapid analysis of laboratory tests and data is essential in patient management and in

highly affected areas where pollution and outbreaks are experienced. External factors including electrolytes, pH and temperature can significantly impact treatment methods for patients and the output of certain industrial processes. The lack of this accurate information in a timely manner may have severe consequences on the prognosis and treatment of patients as well as adversely affect the policy decisions regarding various water quality and waste disposal methods in agricultural and industrial processes [1]. Laboratory grade testing is usually carried out by expensive instrumentation with the aid of skilled labor providing reliable, accurate results. These technologies are effective in first world countries but are unobtainable in developing countries where these facilities are not easily accessible [2]. Technological advancements have made laboratory testing possible at the point of exposure at industrial sites or natural water supplies as well as at the bedside in direct patient care.

Point-of-care testing, known by many names: near patient, bedside or extra laboratory testing is not new. A point-of-care device is a low cost, portable instrument defined as medical testing at or near the site of patient care. These are tests designed to be used at or near the site where the patient is located, that do not require permanent dedicated space, and that are performed outside the physical facilities of the clinical laboratories. Simple point-of-care (POC) testing has been in use since the 1970's when glucose was monitored through reagent strips [3]. Electrolyte monitoring of burn victims [4] and the detection of rapid changes in ionized calcium in liver transplant patients [5] triggered the drive to POC testing. Subsequent technological innovation led to the development of dip stick devices which evolved to self-contained lateral flow tests (e.g., for pregnancy, cardiac disease, and HIV-1) that require only the addition of small amounts of sample [6]. They have been developed to provide necessary improvement in convenience, patient care, and turnaround time. Important criteria for the acceptance of point-of-care systems are that they allow operators without technical training to perform assays easily and achieve accuracy and precision of measurement equivalent to that obtainable in the clinical laboratory, or for specific clinical purposes [7]**.** This is achieved by use of transportable, portable and handheld instruments and test kits. Recent developments in sensor technologies and applications have led to widespread use of accurate, reproducible POC testing. A major drawback of point-of-care diagnostics is the lack of accuracy as well as sensitivity of the low-cost devices.

Rapid, point-of-care (POC) testing may be used for a wide variety of reasons: Urinalysis, Environmental Monitoring, Bioterrorism, Food Safety, Veterinary Medicine and Immunoassays [8]. Environmental impact assessment is a formal process used to predict the environmental consequences of a plan, policy, program, or project prior to the implementation decision. It proposes measures to adjust impacts to acceptable levels or to investigate new technological solutions. Although it can lead to difficult economic decisions, strong political and social commitments, it aims to protect the environment. The purpose of the assessment is to ensure that decision makers consider the environmental impacts when deciding whether or not to proceed with a project. The assessment, with analytical detection will assist government and regulatory bodies develop and modify new and existing policies regarding contamination as well as evaluate exposure to contaminants for those working with metals on a regular basis. Diagnosis and point-of-care testing in the home is a critical part of disease management and is a growing area in the healthcare sector due to the rapidly increasing population. The results of these tests aid in determining the necessary treatment and associated costs and allow patients the opportunity to manage their own conditions. The effectiveness and efficiency of chelation therapy, a treatment to rid the body of high concentrations of heavy metals may also be determined. The benefits of patient self-testing include: (i) No need for patient travel, (ii) limited waiting time, (iii) reduction in materials and cost, (iv) increased patient freedom and (v) patient involvement is increased.

Determination of heavy metals has traditionally been carried out in laboratories, where time-consuming sampling, transportation, preparation and storage steps are employed. On site monitoring may reduce errors associated with contamination, losses and matrix changes along with time saved [9].

Heavy metals are natural components of the earth's crust and are defined as any metal that is toxic at low concentrations, with density greater than 0.5 g cm^{-3} [10]. These metals have become important in industrial applications and ubiquitous in the environment. Heavy metals pose a very distinguishable problem which set them apart from other known contaminants, owing to their non-biodegradable nature [11,12]. This feature leads to their bioaccumulation in vital organs and lead to the toxic nature of these metals. Of the large number of heavy metals in existence today, Lead, Cadmium, Mercury and Arsenic pose the most alarming concerns. Some of which have been known to lead to cancer, heart disease, anorexia, brain damage *etc*. [11]. In recent years, the

increase in heavy metal contamination has become widespread around the world in the form of pollution as well as food sources and drinking water [13]. Pollution in the environment may occur in different forms including anthropogenic activities such as mining and industrial processing [14]. Contaminated drinking water from lead pipes as well as pollution from the industrial sector are the most common sources in modern times [15].

Heavy metals can also appear in the form of inorganic and organic complexes. Appearance of different heavy metal chemical forms will depend also from chemical nature of a given heavy metal, conditions of environment, presence of complexation substances, colloid dispersion, etc. To what extent will heavy metals in water be mobile, depends from number of parameters: (i) pH of water; (ii) presence of carbonates and phosphates; (iii) hydrated oxides of iron and manages; (iv) content of organic matter; and (v) sulphide ions and pirite (significant for mobilization process of heavy metals in water environment.

In considering the ever growing concern for heavy metal contamination of drinking and ground water sources, it is wise to become acquainted with the toxicological effects of lead, cadmium and zinc on the environment and higher living organisms. Severe illnesses, caused by exposure to heavy metal contamination have been well documented in medical journals in recent years. On site monitoring, technology for continuous surveillance and automatic monitoring are important aspects of water policies and may lead to real time results which secure product quality and waste water treatment. The United States Environmental Protection Agency (US EPA) has set a maximum contamination limit by which all water treatment facilities need to abide. The maximum contamination levels (MCL) of zinc, cadmium and lead are 5 ppm, 5 ppb and 15 ppb respectively. While Ni contamination in water samples is no longer subject to stringent guidelines by the EPA, a set limit of 0.1 mg L^{-1} or 0.1 ppm has been set by the EPA and world health organization (WHO). This limit is comparable to the 0.15 mg L^{-1} set by the South African water guidelines (SAWG).

1.2. Problem Identification

In modern times, diagnostic testing is usually carried out by dedicated instruments performed by skilled operators. Techniques for analytes determination center around spectroscopic techniques like atomic absorption spectroscopy (AAS) and inductively coupled plasma mass

spectroscopy (ICP-MS) [16,17] which are sensitive and can perform a wide range of elemental analysis. The major drawbacks however, include complicated equipment, high costs which may only determine total concentrations. Speciation is possible by extraction and separation procedures but increases the risk of contamination [13]. Historically, electrochemical (EC) techniques have been at the forefront of analysis and have in certain instances been developed for this particular purpose. Stripping voltammetry (SV) is one such example. Inexpensive instrumentation and the possibility of metal speciation as well as accuracy in determination at the trace levels are advantages of electrochemical methods. Lately, screen testing kits has become common place for on-site monitoring of heavy metal ions in liquid samples. The screen testing kits make use of dithizone (diphenylthiocarbazone) which forms yellow, red, or violet complexes with more than dozen metals [10]. A color comparison chart is then used to compare the color obtained to the provided color band. The level of toxicity or concentration can then be determined in a certain range.

It has become increasingly important to explore a sensitive, rapid and simple analytical method for precise monitoring of metal contaminants in food, water and soil samples. The usual methods adopted for the concentration assessments of these inorganic and organic materials are mainly focused on the use of atomic absorption (AA) or inductively coupled plasma (ICP) atomic emission spectroscopy, ICP-mass spectrometry, screen testing and electrochemical (EC) techniques [17]. While extremely accurate, methods such as ICP and AA require expensive machinery as well as skilled labour which may result in long analysis times in laboratories. On-site or point-of-care analysis is an important criterion in highly infected areas and patients with history of heavy metal contamination and folic acid deficiency related illnesses. Screen test kits for heavy metal determination are unreliable due to intermetallic interferences, inaccurate measurements and quasi-analytical detection.

1.3. Rationale and Motivation

Paper is a thin material, discovered in the early 2nd century that is usually prepared by filtering a dilute (~ 1 wt. %) aqueous suspension of fibres, colloidal filler particles and soluble polymers such as cellulose pulp to form sheets [18]. The use of paper is well known stemming from its physical properties, which lend itself to a wide range of applications such as writing,

printing and packaging. Paper, generally made of cellulose, allows liquid to penetrate into its hydrophilic fiber and can be functionalized in order to change its properties such as permeability and reactivity. The use of paper substrates as sensor devices and other chemical applications has recently been discovered due to its versatility, low cost and high abundance [19]. Since its first use in 1956 [20], paper devices have moved from simple designs requiring lateral flow such as the pregnancy test [21] which were limited to providing only qualitative analysis to more advanced fabrication methods in order to obtain more accurate and quantitative results, sometimes at the detriment of cost and simplicity. These fabrication and patterning methods include photolithography [22], inkjet printing [23], etching [24], wax printing [25] and screen printing [26]. Paper choices depend on the required characteristics of the sensor and range from filter paper or wax paper to normal writing paper. Although there is great potential for paper substrates as electrochemical sensor devices improvements in fabrication and analysis techniques are still required to meet the standards set by other known substrates. The overall sensitivity of the device due to spreading of analytes, paper choices, utilization of lower power and portability analysis techniques and difficulty in multiplex analysis are challenges the paper substrate faces [27].

Paper offers many advantageous properties: (i) paper is very inexpensive and is manufactured locally in nearly every part of the world from renewable and recyclable resources; (ii) paper can be easily printed, coated, and impregnated with inks and chemical reagents; (iii) paper is a good filter; (iv) paper is biodegradable or easily disposed via burning; (v) the porous structure facilitates lateral-flow of fluids without the use of a pump or pipette; and (vi) is a biocompatible material resulting in more stable biomolecule probing. A dry filter paper can sorb more than its dry mass of aqueous solution when immersed in a bath. Removal of the paper and drying will leave all of the non-volatile components of the aqueous solution in the paper structure. Unspecific adsorbed components will fully distribute after subsequent exposure to water [28].

Electrochemistry is known to provide analytical techniques characterized by simplicity, low cost and portability. Electrochemical anodic stripping voltammetry (ASV) has, in recent years, been widely regarded as an extremely powerful technique for the determination of heavy metals while adsorptive stripping voltammetry (AdSV), commonly used for the determination of organic materials and detection of low solubility metals. Their high intrinsic advantageous features, such as its high sensitivity due to the built-in preconcentration step, good selectivity, inexpensive and

portable instrumentations and the ability of measuring four to six analytes in a sample simultaneously in the sub parts per billion (sub-ppb) ranges [29] make them good methods of detection.

The working electrode is characterized by its small surface area. Solid electrodes made of gold, carbon or platinum are commonly used. These carbon-based electrodes such as glassy carbon, screen-printed and pencil-graphite electrodes have been utilized in conjunction with metal films. Mercury electrodes show little to no background i.e. little interference as well as advantageous properties in the negative potential region but its toxicity as well as its use and disposal of its salts has put a limited life span on the use of these electrodes [2]. Bismuth, antimony and lead film electrodes show comparable results to that of Hg-film electrodes due to the formation of "fused" alloys or complexes with analytes compared to the amalgams formed with mercury [30]. These electrodes offer many attractive properties, including the simple preparation [31], high sensitivity, good stripping signal and excellent resolution of peaks [28].

Many techniques have been incorporated to improve the sensitivity for the analysis of metal ions including, chemically modified electrode. Modification of electrodes with nanoparticles, graphene, ligands and nafion has shown to greatly improve the electrode sensitivity as well as selectivity towards analytes. Nafion has shown to increase the detection sensitivity and alleviate the interference from the surfactants of bismuth film electrodes. It is a perfluorinated ionomer containing negatively charged sulfonic groups and has many applications as proton-conducting membrane material for fuel cells and other electrochemical applications. The Teflon like hydrophobic backbone and highly hydrophilic ionisable sulfonic groups are responsible for its excellent chemical stability and ionic conductivity. The unique ion- exchange, discriminative and biocompatibility properties have made Nafion- films useful for modification of electrode surfaces. The polar side chain of Nafion allows for CNTs and Graphene to be easily suspended in solutions of Nafion in phosphate buffer and alcohols.

Graphene, a 2D allotrope of carbon, is a very important material not only for fundamental research but also for device applications. It has its carbon atoms arranged in a honeycomb structure of hexagons with sp^2 hybridization [32]. Graphene has been attracting a lot of attention since it was first produced in 2004 and has shown to significantly improve the sensitivity in various

applications [33]. In addition to the possibility of low- power, high density, and high-speed switches, graphene- based devices may also be applied to other areas as a storm- thick membrane for sensing pressure as components in nano-electrochemical systems or in chemical sensing because of their high surface area. Synthesis of Graphene by the Hummers Method [34] produces good quality graphene.

Apart from electrode modification for improved sensitivity, improved selectivity and precision could also be achieved by selecting a suitable complexing agent (ligand) and electrolyte. Various ligands have been used including dimethylglyoxime, calcone and pyrroldine dithiocarbamate [35]. Calcone as ligand is a ketone formed by condensation reactions. Its role as complexing agent is supported by the free electron pair form hydroxyl group that may bind with metal ions in formation of complexes.

The proposed study seeks to investigate for the first-time the development of paper-based microfluidic sensing devices for the detection of heavy metals in water by electrochemical adsorptive stripping voltammetry. A dry reagent storage method for creating prestored reaction zones with electrolyte solution, chelating agent and nano-metal films was investigated towards the detection of metal cations, with Ni^{2+} being used for proof of concept. The pre-stored paper electrodes meet the requirements of point-of-care devices by providing an answer for direct analysis with a single sample introduction. Further, graphene nanocomposites, gold nanoparticle and ionic liquid modification of the paper-based sensors were employed to create novel electrode platforms with accurate, reproducible and ultrasensitive analyte detection as point-of-care devices on screen printed electrodes. The detection will be: one step, low cost, simple, highly sensitive and accurate with small amount of sample and easy to operate.

1.4. Objectives

The overall aim of the thesis is to develop paper-based sensors for the determination of metal ions in water samples by adsorptive cathodic stripping voltammetry (AdCSV) and investigate methods of improving its low-sensitivity by modification with reagents and nanoparticles alike.

The objectives of this work are to:

- Explore the synthesis of reagents used in the study by:

- Investigating the synthesis and characterisation of graphene oxide (GO) by a modified Hummers method and its subsequent reduction to graphene. Structural and morphological characterisation are performed using HRSEM, HRTEM, FTIR, AFM, XRD, Raman, UV-Vis and SECM.

- Investigating the development of graphene-chelate inks and electrochemically reduced platforms for surface modification to improve electrode sensitivity.

- The synthesis and characterisation of gold nanoparticles and comparison to bulk metal. Structural and morphological characterisation will be conducted by HRSEM, HRTEM, FTIR, AFM, XRD, Raman, UV-Vis and SECM.

- Develop a method for the adsorptive stripping voltammetric detection of metal cations in water based on a single accumulation and deposition step in the presence of suitable chelating agents and metallic films

- Investigate the ability to improve electrode sensitivity by electrode modification with graphene and gold nanoparticles

- Fabricate low-volume paper-based electroanalytical devices for the detection of Ni^{2+} by AdCSV

- Improve sensitivity of paper-based sensors by reagent storage with electrolyte, chelating agent and metallic films

- Further enhance sensitivity of the developed devices by modification with graphene, gold nanoparticles and ionic liquids

- Develop paper-based flow-systems based on patterning with hydrophobic materials

- Investigate the filtration, inkjet and screen printing techniques to create integrated electrode systems on paper substrates and apply them to the detection of metal ions by AdCSV

- Develop a method for the quantitative detection of metal ions in water based on the aforementioned devices.

1.5. Research Questions

- Is it possible to create a single deposition and accumulation step in AdCSV detection of Ni^{2+}?
- Can graphene and gold nanoparticles improve electrode sensitivity in AdCSV?
- Does pre-strorage of paper substrates result in low-cost POC devices for the detection of inorganic materials in aqueous solutions?
- Will the developed POC devices allow for accurate electroanalytical detection of simultaneous trace heavy metals?
- Do graphenated paper disks improve the detection of heavy metals?
- Is it possible to improve detection using a variety of metallic and nano-metallic films?
- Does ligand-metal complexes improve electrode sensitivity for the determination of heavy metals?
- Will chromatography and simple fluidic devices help in purification/filtration of 'dirty' aqueous samples and limit intermetallic interferences?
- Can wax patterning create simple fluidic channels for the continuous determination of metal ions?
- Will inkjet printing of conductive inks create low cost, flexible electrodes from paper and transparent plastics?

1.6. Research Hypothesis

Paper-based sensors offer a simple, low-cost method for detection capabilities in point-of-analysis testing. These detection capabilities may be further improved by coupling paper-devices with simple electrochemical stripping analysis to develop an ultra-sensitive technique for metal sensing. Impregnation of paper substrates with graphene, various ligands, buffer solution, metallic films and nanoparticles in conjunction with screen-printed carbon electrodes as well as simple

printing techniques for integrated devices may result in low-cost point-of-care devices. The pre-stored paper electrodes and printed paper sensors enhanced with graphene-based composites will offer numerous advantages: (i) it is one-step detection without additional external reagent(s); (ii) the paper disk with screen printed electrode is for single-use, low-cost and easy-to-fabricate; (iii) it has high sensitivity and accuracy with modifications; (iv) it requires only a small amount of sample (10 μL) for testing; and (v) it does not require professional personnel or complicated instruments.

1.7. Research Approach

A number of experiments will be designed in order to understand the effect of:

- Methods of graphene and gold nanoparticle synthesis and their electrochemical properties;
- Graphene-based nanocomposites to enhance electrode sensitivity for AdCSV detection of heavy metals
- Metal-free analysis of AdCSV detection of heavy metals;
- Impregnation techniques to develop integrated paper substrates with microfluidic channels;
- Pre-stored paper substrates for the determination of heavy metals in aqueous samples;
- Inkjet, wax and screen printing techniques for fabrication of paper-based devices;
- Standard addition and calibration methods on recovery studies of test solutions;
- Real sample analysis of graphene-based paper substrate chemical sensors.

In this study commercially bought Graphite powder, obtained from Sigma-Aldrich, simulated water as well as real water samples collected from tap water from the Bellville Municipality area in Cape Town, South Africa was used.

The chemistry involved during the synthesis of graphene was evaluated by analysis of solid, graphite-based structures, along the chemical synthesis process by morphological and structural

characterization techniques. These techniques included: FT-IR, EDS, Raman Spectroscopy, XRD, HRTEM, HRSEM and AFM

Square-wave adsorptive cathodic stripping voltammetry (SW-AdCSV) was utilized using a Autolab PGSTAT 101 to evaluate the viability of graphene-based composites as enhanced detection material towards the detection of trace metals in paper-based sensors. This was achieved by investigation of instrumental parameters, calibration data, test solution analysis and real water samples.

1.8. Scope and Delimitations

The scope and delimitations of the proposed study are discussed in this section. Briefly, areas of interest covered in the work found in this thesis are highlighted and special consideration given to relevant areas not covered by this work.

The study is descriptive and explorative in nature and focused on the development of sensitive, accurate and cost effective microfluidic paper-based electroanalytical devices (μPEDs) for the detection of metal contaminants belonging to the heavy metal class in drinking water samples below the acceptable maximum contamination level (MCL) as identified by the world health organization (WHO) and environmental protection agency (EPA). The research sample is composed solely of tap water samples collected from our laboratory in the Bellville municipal region in Cape Town, South Africa. *Figure 1.1,* represents an image of the sampling area used in the study. Contaminated water samples from rivers and lakes in the surrounding areas were eliminated for the purpose of the study and only drinking water samples were selected to prevent the need for further purification prior to analysis. The primary data gathering method used was experimental testing in our laboratory in order to answer particular research questions set above. This research used purposive and convenience sampling in order to demonstrate the developed devices for detection of metal ions by adsorptive stripping voltammetry. The gathered data were analyzed and compared to relevant literature to investigate its effectiveness as sensing device.

The research data was based on experimental approaches to study specific areas of interest in the development of enhanced paper-based sensors including electron transfer rates, fabrication

methods etc. It focused specifically on an electrochemical adsorptive stripping voltammetric approach, however anodic stripping voltammetry was also used for a comparative investigation.

Figure 1.1: Geographic location of water sampling region under investigation in the study.

Nickel detection is the most commonly used application of the adsorptive stripping voltammetric technique to date and is the leading method for its detection in water samples. As a result, the fabricated paper-based sensors will be applied to nickel detection to demonstrate their applicability in AdCSV.

The study is delimited to chromatographic paper of Grade 1 nature, due to its specific pore sizes allowing for liquid transport and Penguin photographic paper due to its ease of availability. Commercial paraffin wax was used in the hydrophobic barrier preparation.

In this research, metal cations were delimited to those readily found in water samples including Ni, Co, Zn, Cd, Pb, Cu, In, etc. identified by the WHO. All metal cations used for interference studies were selected due to their known interferences with Ni, reduction in the potential window under investigation and ready availability in our laboratory. All other metal interferents were eliminated from the study. Further, organic interferents were not investigated due to their low concentrations in drinking water.

The study was further delimited to graphene, gold nanoparticles and ionic liquids to enhance electrode sensitivity due to their ease of production. Chelating agents were limited to

dimethylglyoxime as a direct result of its widespread use in complexation with Ni. Lastly, mercury films were investigated due to their high sensitivity and affinity towards Ni-dmg detection.

1.9. Thesis Structure

The thesis to follow is comprised of ten chapters detailing the development of microfluidic graphene-enhanced paper-based electroanalytical devices (µGPEDs), based on the adsorptive stripping voltammetric determination of nickel-dimethylglyoxime [$Ni(dmgH)_2$] complexes in water samples. This section provides a general outline of work covered.

Chapter One: General Introduction

Chapter One provides a general introduction to the work covered in this study. This chapter specifically identifies and highlights the need for low-cost, accurate and sensitive detection of metal contaminants at disposable and portable devices for on-site analysis. A brief motivation of techniques and reagents used in the study is provided. Further, the proposed objectives and aims to be met within the scope and delimitations set for the study under investigation are listed.

Chapter Two: Recent Advances in Electrochemical Stripping Analysis at Graphene-Derivatives: A Review

A comprehensive outline of recent literature pertaining to the study is discussed in Chapter Two. The review focuses on the use of graphene-based materials and their possible applications in electrochemical stripping voltammetric analysis. A detailed summary of graphene synthesis methods and their effect on the achieved electrochemical properties of graphene are discussed. Reported general electrochemical properties achieved in literature are further highlighted in this chapter. The analytical performance of a variety of graphene materials in electrochemical analysis of metal contaminants and a range of organic materials are discussed.

Chapter Three: Metal analysis at Microfluidic Paper-based Analytical Devices (µPADs): A Review

In this chapter, the use of paper-based devices as substrate material for the analytical determination of metal contaminants are highlighted and discussed. A summary of fabrication methods, applications and procedures for enhancement are interrogated towards the detection of

heavy metals. A variety of common detection methods including: Colorimetric, fluorescent, electrochemical and nanoparticle methods are detailed.

Chapter Four: Morphological and Structural Characterization of Prepared Graphene Oxide, Graphene and Gold Nanoparticles

Chapter Four identifies the experimental procedure for the chemical synthesis of graphene oxide and graphene and gold nanoparticles used in the study. The chemistry involved in synthesis steps is reported and relevant findings are highlighted in the production of good-quality samples. Reference is made to relevant literature. Microscopic and spectroscopic techniques were used to scrutinize the morphology and structure of produced materials.

Chapter Five: Single-step, Adsorptive Cathodic Stripping Voltammetric Detection of Nickel in Tap Water Samples at Electrochemically Reduced Graphene Oxide, Pencil-graphite, Mercury-film Electrodes (ERGO-PG-MFE)

For the first-time the applicability of graphene-modification will be investigated towards adsorptive stripping voltammetric detection of Nickel in water samples. Chapter Five highlights the main trends and significant findings in the fabrication of electrochemically reduced graphene oxide, pencil graphite electrode (ERGO-PGE). Microscopic and electrochemical characterization of the prepared electrodes are provided. Further, quantitative analytical information is shown along with recovery and calibration studies to prove its applicability as sensor material. Real sample analysis as a real-world application is shown.

Chapter Six: Complexation based Detection of Nickel (II) at a Graphene-Chelate Probe in the Presence of Cobalt and Zinc by Adsorptive Stripping Voltammetry

Results and discussion of a nafion-graphene-dimethylglyoxime (NGr-DMG) complex, utilized as electrode modification towards the detection of Ni(II) by AdCSV in the absence of an electroplated metal film is provided in Chapter 6. Development of the NGr-DMG complex and its electrochemical properties are shown. Further, coating and instrumental parameters, optimization of chelating agent loading, as well as calibration, recovery and metallic interference studies are illustrated. Comparison is made between N-DMG-GCE and NGr-DMG-GCE and the analytical performance of graphene loading is highlighted. Relevant correlation is made to literature reported

values to indicate the effectiveness of the developed NGr-DMG-GCE sensor for selective detection of Ni(II) in the presence of common metallic cations.

Chapter Seven: Electroanalytical Complexation-based Detection at Low-cost, Stored, Micro-volume, Paper-based Electrochemical Cells (µPECs)

In Chapter Seven, the use of paper-based analytical devices will for the first time be applied to the adsorptive stripping voltammetric detection of Ni(II) in water samples. Relevant results and discussions outlining the first micro-volume detection of Ni(II) by AdCSV at paper-based electrochemical cells (paper-disks). Reagent loading, analytical parameters, interference studies and quantitative analysis are shown. Further, infusion of graphene to enhance electrode sensitivity was investigated and electrochemical sensitivity as a function of graphene loading shown. In addition, a graphene working electrode was investigated in the fabrication of a 3-D paper-based sensor.

Chapter Eight: Fabrication of Gold Nanoparticle, Ionic liquid Microfluidic Paper-based Electroanalytical Devices (µPEDs) towards the detection of Cu(II) and Ni(II) by Stripping Voltammetric Techniques

Building on the results obtained from Chapter 7, Chapter 8 discusses the possibility for fabrication of microfluidic paper-based electroanalytical devices (µPEDs) towards the detection of Cu(II) and Ni(II) by Stripping Voltammetric Technique. Methods to enhance electrode sensitivity other than graphene, namely Gold nanoparticles and conductive ionic liquids in the presence of chelating agents were investigated towards the detection of Copper and Nickel in a paper-based microfluidic device. The analytical performance of the developed sensor devices is shown and discussed in comparison to other reported sensors in literature.

Chapter Nine: Detection of Nickel at modified, Paper-based Ink-jet Printed Electrodes

In this chapter, ink-jet printing of silver and graphene conductive inks was used to fabricate 3-electrode systems on photographic paper. Simple screen printing techniques for carbon coating of working and counter electrodes are employed. Further, two-modification: (a) electrodeposited graphene and gold nanoparticles and (b) a carbon black – dimethylglyoxime inks were investigated. Instrumental parameters, nanomaterial loading, electrochemical properties of the

developed sensors are discussed. Quantitative detection of Ni(II) in water, calibration, recovery and interference studies are highlighted. Real sample analysis of the developed devices is shown.

Chapter Ten: Conclusions and Future Work

Chapter Ten summarizes the main findings of the work done and the hypothesis of the thesis is verified based on the results and discussions obtained in each of the previous chapters. Conclusions are drawn based on results obtained and areas for future interrogation are proposed based on any downfalls or significant findings arising from the work.

References

[1] T.E. Grissom, D. Lawlor, Point-of-Care Testing : Can It Be Adapted for the Field Environment ?, Aeromed. Support Issues Conting. Oper. (1997) 28:1-5.

[2] B. Claux, O. Vittori, Bismuth Film Electrode as an Alternative for Mercury Electrodes: Determination of Azo Dyes and Application for Detection in Food Stuffs, Electroanalysis. 19 (2007) 2243–2246. doi:10.1002/elan.200703978.

[3] B.D. Bennett, Blood glucose determination: point of care testing., South. Med. J. 90 (1997) 678–80. http://www.ncbi.nlm.nih.gov/pubmed/9225886 (accessed April 1, 2017).

[4] M.J. Stansell, S.J. Stansell, Portable self-powered system for the rapid measurement of blood electrolytes during aeromedical evacuation., Aerosp. Med. 41 (1970) 879–84. http://www.ncbi.nlm.nih.gov/pubmed/5431020 (accessed April 1, 2017).

[5] G.J. Kost, C. Hague, The current and future status of critical care testing and patient monitoring., Am. J. Clin. Pathol. 104 (1995) S2-17. http://www.ncbi.nlm.nih.gov/pubmed/7484945 (accessed April 1, 2017).

[6] K. a. Erickson, P. Wilding, Evaluation of a novel point-of-care system, the i-STAT Portable Clinical Analyzer, Clin. Chem. 39 (1993) 283–287.

[7] R. Pelton, Bioactive paper provides a low-cost platform for diagnostics, TrAC - Trends Anal. Chem. 28 (2009) 925–942. doi:10.1016/j.trac.2009.05.005.

[8] S.K. Sia, L.J. Kricka, Microfluidics and point-of-care testing., Lab Chip. 8 (2008) 1982–

1983. doi:10.1039/b817915h.

[9] J. Wang, B. Tian, J. Wang, J. Lu, C. Olsen, C. Yarnitzky, K. Olsen, D. Hammerstrom, W. Bennett, Stripping analysis into the 21st century: faster, smaller, cheaper, simpler and better, Anal. Chim. Acta. 385 (1999) 429–435. doi:10.1016/S0003-2670(98)00664-3.

[10] L. Sanità Di Toppi, R. Gabbrielli, Response to cadmium in higher plants, Environ. Exp. Bot. 41 (1999) 105–130. doi:10.1016/S0098-8472(98)00058-6.

[11] J. Wang, Stripping analysis: Principles, instrumentation, and applications, Deerf. Beach, FL, USA VCH Publ. Inc. (1985). https://scholar.google.com/scholar?q=J+Wang+1985&btnG=&hl=en&as_sdt=0%2C26#1 (accessed August 4, 2015).

[12] Heavy Metals, Lentech. (n.d.). http://www.lentech.com/heavymetals.htm (accessed January 10, 2014).

[13] J. Buffle, M.-L. Tercier-Waeber, Voltammetric environmental trace-metal analysis and speciation: from laboratory to in situ measurements, TrAC Trends Anal. Chem. 24 (2005) 172–191. doi:10.1016/j.trac.2004.11.013.

[14] X. Wang, T. Sato, B. Xing, S. Tao, Health risks of heavy metals to the general public in Tianjin, China via consumption of vegetables and fish., Sci. Total Environ. 350 (2005) 28–37. doi:10.1016/j.scitotenv.2004.09.044.

[15] C.M. Willemse, K. Tlhomelang, N. Jahed, P.G. Baker, E.I. Iwuoha, Metallo-Graphene nanocomposite electrocatalytic platform for the determination of toxic metal ions, Sensors. 11 (2011) 3970–3987. doi:10.3390/s110403970.

[16] M.A. Janusa, J.N. Beck, RECENT APPLICATIONS OF FLAME ATOMIC ABSORPTION SPECTROMETRY TO ENVIRONMENTAL MEASUREMENTS, Appl. Spectrosc. Rev. 37 (2002) 137–186. doi:10.1081/ASR-120006043.

[17] T. Inaba, E. Kobayashi, Y. Suwazono, M. Uetani, M. Oishi, H. Nakagawa, K. Nogawa, Estimation of cumulative cadmium intake causing Itai-itai disease., Toxicol. Lett. 159 (2005) 192–201. doi:10.1016/j.toxlet.2005.05.011.

[18] A.W. Martinez, S.T. Phillips, G.M. Whitesides, E. Carrilho, Diagnostics for the developing world: Microfluidic paper-based analytical devices, Anal. Chem. 82 (2010) 3–10. doi:10.1021/ac9013989.

[19] J. Comer, Semiquantitative specific test paper for glucose in urine, Anal. Chem. 28 (1956) 1748–1750.

[20] P. Von Lode, Point-of-care immunotesting: Approaching the analytical performance of central laboratory methods, Clin. Biochem. 38 (2005) 591–606.

[21] A.W. Martinez, S.T. Phillips, M.J. Butte, G.M. Whitesides, Patterned Paper as a Platform for Inexpensive, Low-Volume, Portable Bioassays, Angew. Chemie Int. Ed. 46 (2007) 1318–1320. doi:10.1002/anie.200603817.

[22] X. Li, D.R. Ballerini, W. Shen, A perspective on paper-based microfluidics: Current status and future trends, Biomicrofluidics. 6 (2012) 11301. doi:10.1063/1.3687398.

[23] X. Li, J. Tian, W. Shen, Progress in patterned paper sizing for fabrication of paper-based microfluidic sensors, Cellulose. 17 (2010) 649–659. doi:10.1007/s10570-010-9401-2.

[24] R. Lu, W. Shi, L. Jiang, J. Qin, B. Lin, Rapid prototyping of paper-based microfluidics with wax for low-cost, portable bioassay, Electrophoresis. 30 (2009) 1497–1500. doi:10.1002/elps.200800563.

[25] W. Dungchai, O. Chailapakul, C.S. Henry, A low-cost, simple, and rapid fabrication method for paper-based microfluidics using wax screen-printing., Analyst. 136 (2011) 77–82. doi:10.1039/c0an00406e.

[26] D.D. Liana, B. Raguse, J. Justin Gooding, E. Chow, J.J. Gooding, E. Chow, Recent advances in paper-based sensors, Sensors (Switzerland). 12 (2012) 11505–11526. doi:10.3390/s120911505.

[27] S.N. Tan, L. Ge, W. Wang, Paper disk on screen printed electrode for one-step sensing with an internal standard, Anal. Chem. 82 (2010) 8844–8847. doi:10.1021/ac1015062.

[28] A. Ala, A.P. Walker, K. Ashkan, J.S. Dooley, M.L. Schilsky, Wilson's disease., Lancet (London, England). 369 (2007) 397–408. doi:10.1016/S0140-6736(07)60196-2.

[29] M.J. Goldcamp, M.N. Underwood, J.L. Cloud, S. Harshman, K. Ashley, An Environmentally Friendly, Cost-Effective Determination of Lead in Environmental Samples Using Anodic Stripping Voltammetry, J. Chem. Educ. 85 (2008) 976. doi:10.1021/ed085p976.

[30] G. Kefala, A. Economou, A. Voulgaropoulos, M. Sofoniou, A study of bismuth-film electrodes for the detection of trace metals by anodic stripping voltammetry and their application to the determination of Pb and Zn in tapwater and human hair, Talanta. 61 (2003) 603–610. doi:10.1016/S0039-9140(03)00350-3.

[31] H. Xu, L. Zeng, S. Xing, Y. Xian, G. Shi, L. Jin, Ultrasensitive Voltammetric Detection of Trace Lead(II) and Cadmium(II) Using MWCNTs-Nafion/Bismuth Composite Electrodes, Electroanalysis. 20 (2008) 2655–2662. doi:10.1002/elan.200804367.

[32] M.J. Allen, V.C. Tung, R.B. Kaner, Honeycomb carbon: A review of graphene, Chem. Rev. 110 (2010) 132–145. doi:10.1021/cr900070d.

[33] a K. Geim, K.S. Novoselov, The rise of graphene., Nat. Mater. 6 (2007) 183–191. doi:10.1038/nmat1849.

[34] J. William S. Hummers, R.E. Offeman, Preparation of Graphitic Oxide, J. Am. Chem. Soc. 80 (1958) 1339. doi:10.1021/ja01539a017.

[35] R.J.C. Brown, M.R. Roberts, D.J.L. Brett, Stripping voltammetry using sequential standard addition calibration with the analytes themselves acting as internal standards, Anal. Chim. Acta. 635 (2009) 1–5. doi:10.1016/j.aca.2009.01.014.

Chapter 2 :

Recent Advances in Electrochemical Stripping Analysis at Graphene-Derivatives:

A review

Abstract

The use of graphene oxide, reduced graphene oxides and graphene in electrochemical sensors owing to their unique and advantageous electronic and electrochemical properties have garnered widespread use by researchers over the last two decades. For the first-time, the role of the sp^2 hybridized carbon nanomaterial (graphene) in the success of electrochemical stripping voltammetric analysis is reviewed. In this focused review, a critical examination of the synthesis methods, structure and electrochemical properties of the graphene-derivatives is provided. Further, recent advances on their use in stripping voltammetric sensors is provided. The role and function of graphene-derivatives and composite materials such as biomaterials, polymers, ionic liquids, nanoparticles, etc. exploited in the development of graphene-based sensors are highlighted.

Highlights

- Methods for preparation of Graphene and Graphene-derivatives are reviewed and their effects on properties investigated
- The electronic and electrochemical properties of graphene for use in electrochemical stripping analysis is highlighted
- Advances in electrochemical stripping analysis at graphene-based materials are studied for their applications in metal analysis emphasised

Keywords

Graphene, Graphene Oxide, Reduced Graphene Oxide, Electrochemistry, Electrochemical Sensors, Stripping Voltammetry and Metal Analysis

Graphical Abstract

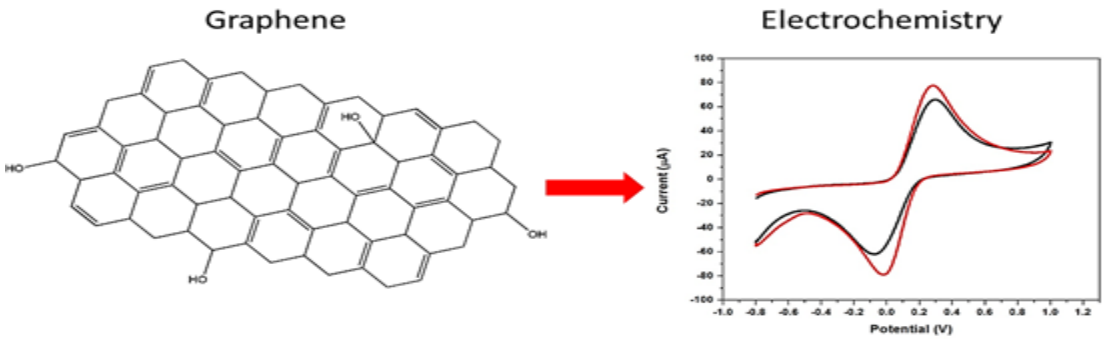

2.1. Introduction

Early detection of illnesses and environmental pollutants is at the heart of both the toxicology and health sectors, which pose a significant challenge to the global community at large. Electrochemistry, with applications in energy storage and creation, sensing abilities as well as purification methods, offers the possibility for widespread use in these particular fields. The sensing and biosensing by means of electrochemical techniques allow for, among others, interrogation of reaction mechanisms and kinetics in electron transport. This green approach involves the introduction of electricity through electrodes [1] and is characterized by cheap instrumentation, simultaneous detection and good sensitivity. Typically, mass transport and electron flow as a result of electroactive species changes at the electrode surface occurs as a function of concentration change. In turn, the availability of this electroactive species at the electrode interface is crucial in sensitive detection and a major limitation in commercialization of these devices.

For decades, preconcentration techniques have garnered significant traction in electrochemical sensing techniques to solve this particular problem. Electrochemical stripping analysis has for many years been at the forefront of this drive. Here, effective preconcentration coupled with advanced electrochemical methods and measurement make stripping voltammetry

(SV) the most sensitive electrochemical technique to date [2]. Accumulation and pre-concentration of the target analyte is achieved by amalgam or alloy formation at mercury, bismuth, antimony or lead based electrodes. This phenomenon is governed by the solubility of the material to be investigated within a metallic film, giving rise to classical anodic and cathodic stripping voltammetry (ASV and CSV). Ultra-trace determination of organic materials in the sub parts-per-billion (ppb) range has led to the introduction of adsorptive stripping voltammetry (AdSV) where electrolytic accumulation is based on adsorption of analyte, usually as a result of complex formation. An understanding of basic principles and definitions used in stripping analysis is required in order to fully understand any possible applications and electrode modifications which may be addressed in this review. A three step Faradaic reversible process governed by the Nernst equation is observed. Deposition and accumulation is achieved under fixed potential hydrodynamic conditions. Electroplating of metallic films generally precede adsorption or complex formation with analyte. The choice of accumulation potentials is highly dependent on the analyte under investigation. A rest period is employed to allow for even distribution of analyte concentration at the electrode surface and to prevent noise associated by hydrodynamic measurements. Anodic or cathodic potential sweeps allow for redox reactions of the target material, generating electron flow. The resulting voltammogram provides the analytical information required. The peak potential occurs at standard redox potentials of the metal ion. The stripping peak current for each individual metal is proportional to the concentration in the solution. Major advantages: (i) simultaneous detection, (ii) portable, simple instrumentation, (iii) analyte speciation and (iv) limited intermetallic interferences have been identified for stripping voltammetry, with few drawbacks.

Advancements and improvements of existing technologies and devices is ever changing stemming from the constant influx of new knowledge, ideas and advanced materials on a daily basis. Novel materials based on graphene-derivatives offer unlimited advantages in electrochemical stripping analysis. In this focused review, the electrochemical properties of graphene-based materials used in recent times will be identified and its applications towards stripping voltammetric analysis highlighted. Preparation methods of graphene will first be introduced and its effect on general and electrochemical properties highlighted. It is well documented that synthesis methods allow for introduction of impurities and defects within the graphene structure. Consequently, produced materials differ substantially in their electrochemical

properties. As such, detection capabilities as a result of these influenced properties will be discussed.

Carbon is ranked in the top five most abundant elements on earth and is present in large quantities in the earth's crust. It is essential to life and fundamental in all organic chemistry. Present in large deposits, allotropes of carbon (diamond, graphite, fullerenes, carbon nanotubes, or graphene) are readily accessible and easily applied to a host of applications.

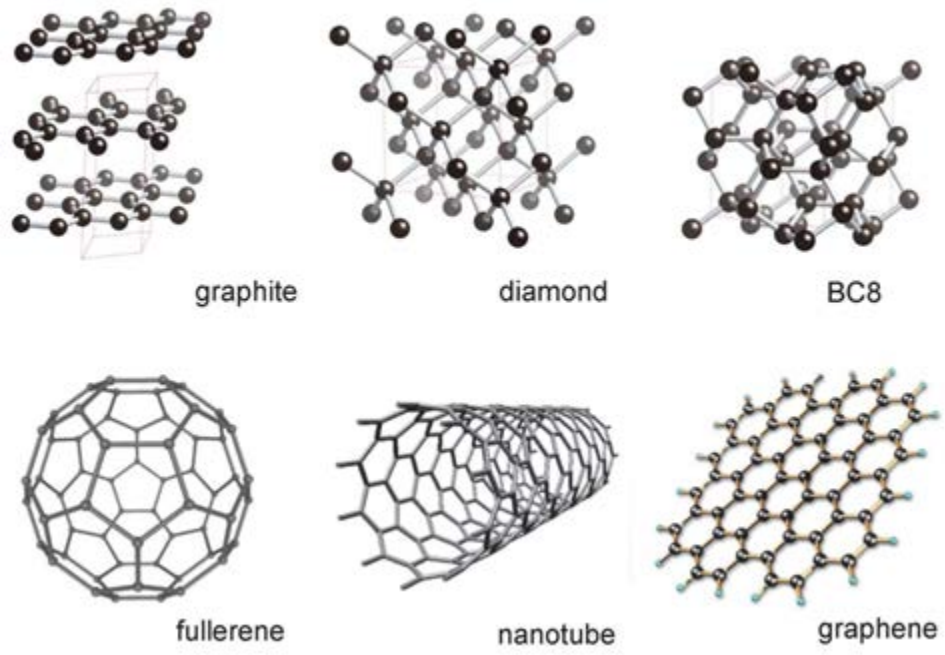

Figure 2.1: Schematic representation of various carbon allotropes [3]

Since its introduction less than two decades ago, the number of theoretical works performed on graphene have increased exponentially in order to fundamentally understand its properties. While definitions of graphene appearing in literature differ considerably, the 2-D allotrope of carbon with a sp^2 hybridized hexagonal configuration holds for all derivations. Quasi 2-D sheets of graphene with approximate C-C bond length of 0.142 nm sheets exist. While single layer graphene sheets offer the most interesting applications since its discovery in 2004, bi-layer and multi-layer graphene sheets too offer tunable and unique properties. It is possible to distinguish between single-, double- and few- (3 to < 10) layer graphene as three different types of 3D crystals. These bonds, electron configuration and flexible layered nature give rise to the extraordinary properties of graphene. Among others, a tunable band gap, quantum hall effect, high conductivity

in bulk samples ($0.96x10^6\ \Omega^{-1}cm^{-1}$), transparency, light weight (0.77 mg m^2), high mechanical strength, large surface area, high thermal conductivity and high elasticity have been reported.

2.2. Preparation of Graphene

A wide range of fabrication methods have been proposed to produce graphene. Its tunable properties and characteristics are largely dependent on their processing and scalability. Synthetic approaches for graphene production in research and commercialization fields rely on two fundamental approaches, i.e. top-down and bottom-up methods. The top-down approaches rely heavily on the steady destruction of bulk graphitic material into smaller derivatives. Exfoliation of graphite sheets by mechanical, chemical or electrochemical processes resulting in the weakening of the existing Van der Waal's forces. Conversely, bottom-up approaches are described by consecutive deposition of fundamental material building blocks on selected substrate materials. These processes yield graphene of excellent quality but rely on costly instrumentation. Thermal, chemical or catalytic approaches have been employed.

2.2.1. Mechanical Methods

Mechanical methods rely on a top-down approach to the synthesis of graphene. Layer by layer, graphite sheets with interlayer spacing of 3.35 Å and weak Van der Waal's forces are pulled apart by the application of mechanical forces. Exfoliation and fragmentation techniques are two common approaches to graphene approaches. This section aims to discuss the existing mechanical approaches to the fabrication of graphene.

2.2.1.1. Mechanical and Solution based Exfoliation Methods

Geim *et al*. first introduced a micromechanical cleavage method for the preparation of single layer graphene in 2004 [4]. This was not the first foray into graphene production but has to date been the most effective method for pristine graphene production. Highly ordered pyrolytic graphite (HOPG) was separated into thin single layer sheets of graphite by applying a simple scotch tape method. Repeated folding and unfolding of scotch tape applies a normal force to the surface layer of bulk HOPG which may be removed by mechanical cleavage. Successive removal of graphitic sheets results in thinning of the bulk material. The mechanics involved in this process limits the use of expensive instrumentation. The high purity graphene flakes with large area offer many

outstanding characteristics but are limited to research application due to labor intensive and expensive technique.

Few methods have expanded on the simple scotch tape approach as many researchers have found the method to be unsuitable for large scale production required to produce bulk, reproducible quantities needed for applications in electrochemistry. One such work however, was suggested by Jayasena *et al.* [5]. An automated mechanical cleavage approach was suggested, making use of an ultra-sharp diamond wedge to slice small fragments of HOPG embedded in a triangular shaped epoxy resin, with the aid of ultrasonic oscillations. Large area sheets could be determined but is confined to flakes with relative thickness unsuitable for applications in transparent or optical devices. While automation reduces the time consumed approach of 'Scotch tape method', the addition of expensive instrumentation as well as lack of control in creating single layer sheets are significant downfalls [6]. A sulfur assisted mechanical exfoliation approach was proposed in the work by Lin *et al.* [7] to develop low-defect graphene sheets. Sulfur electrostatically attaches to graphite flakes, overcoming weak Van der Waal's forces associated with π-π stacked graphene sheets making mechanical cleavage possible. This technique demonstrates a considerably high Hall mobility and good electrical conductivity. Another technique, arguably more closely based on the conventional approach developed by Geim *et al*. was developed by Chen *et al*. in 2012 [8]. Mechanical exfoliation is achieved using a three-roll mill machine coated in a polyvinyl chloride based adhesive. Continuous rolling through the three-roll system results in excellent exfoliation of graphite flakes. The addition of adhesive materials, replacing the scotch tape system makes for difficult transfer to additional substrates due to removal of the adhesive.

While mechanical exfoliation methods offer the ability for fabrication of pristine graphene sheets with minimal defects in the sp^2 hybridized structure, large scale, reproducible production is not easily performed. Liquid-phase exfoliation approaches in aqueous media were introduced for its application in bulk production. Ultrasound acts as the driving force behind the exfoliation in a liquid environment. Typically, three steps are involved in any solution-based exfoliation technique, according to Ciesielski *et al.*: (i) dispersion in a suitable solvent or surfactant, (2) exfoliation of layered sheets and (3) purification to remove contaminants and solvent [9]. The first such technique for graphene preparation was developed by Hernandez *et al.* [10], building on the expansive work in carbon nanotube preparation by the Coleman group. This technique was

designed as a means to perform solution-based exfoliation without the need for the introduction of water stabilizing functional groups which destroy the electronic structure. In summary, dispersion of graphite in N,N-dimethylformamide (DMF) or N-methylpyrrolidone (NMP), organic solvents able to overcome the Van der Waal's forces were performed and ultrasonication resulted in the formation and removal of bubbles acting on the material allowing for cleavage when energy loss was minimized. Characterization confirmed the production of monolayer graphene. Solvents with the surface energy capable of exfoliating graphite is required and gives reasonable quantities of produced graphene. This however is not an adequate measure of solvent quality [11]. Solvents used in these cases are expensive, often toxic and have high boiling points resulting in difficult removal or deposition on substrates [12]. Since its invention, many techniques have been sought out to improve the low concentration yield achieved by the Coleman group approach.

Surfactant, ionic liquid and polymer aided methods have also been investigated. The dispersion of graphite in a suitable solvent to produce small graphitic flakes with suitable surface energy to overcome Van der Waal's interactions in π-π stacking is the governing factor in all solution based exfoliation methods. The use of small molecules which may adhere to the edges of graphite structures and aid in the promotion of exfoliation have been introduced. Surfactants adhere to the basal plane of graphite and have surface energy greater than the weak interactions between graphene sheets. Adequate dispersion of graphite in aqueous media, including water is not possible due to the hydrophobic nature of sheets. Lotya *et al*. introduced a method to disperse and exfoliate graphite to form graphene in water by addition of surfactants [12]. Rapid ultrasonication allowed for good exfoliation of graphite flakes. Sodium dodecylbenzene sulfonate (SDBS) allowed for stable dispersions of exfoliated graphite in aqueous media by electrostatic repulsion between surfactant coated graphene flakes and prevented the re-aggregation of samples. Excellent optical and electrical properties were achieved by this method and transfer to substrates by spray deposition due to low boiling point temperatures was possible. The method still suffered from low concentration yields. The group further looked into production of high concentration yields with excellent stability [13]. Concentrations up to 0.3 mg mL^{-1} were observed with sheets between 1 – 10 stacked monolayers with high stability in water in the presence of sodium cholate as stabilizing agent. This was a significant improvement in yield achieved in liquid-phase production of graphene. Pyrene derivatives were further investigated as surfactant stabilized

method for graphene exfoliation. Palermo *et al*. [14] studied the mechanism involved in surface adsorption of pyrene dyes on graphite flake dispersion. The effect of sulfonic groups was studied and experimental models created. It was found that colloidal stabilization was achieved without the influence dipoles. Bourlinos *et al.* completed a study investigating the use of pyridine and a range of perfluorinated aromatic solvents (hexa-fluorobenzene (C_6F_6), octafluorotoluene ($C_6F_5CF_3$), penta-fluorobenzonitrile (C_6F_5CN), and pentafluoropyridine (C_5F_5N)) to produce graphene from graphite [15]. The latter produced stable colloidal suspensions between 0.05 and 0.1 mg mL^{-1} with yields between 1 % and 2 % following 1 hr sonication. The dispersions were found to contain up to 15 % pristine graphene sheets. Other aromatic and non-aromatic surfactants were also studied in recent years. The addition of organic salts to enhance graphene concentration yield was investigated by Singh *et al.* [16]. The sonochemical route in organic solvent ortho-dichlorobenzene (ODCB) showed large graphene sheets up to 1 µm. Addition of organic salts like EDTA disodium salts improved the graphene yield by up to 50 %. Guardia *et al*. suggested that reported concentrations for surfactant aided exfoliation methods are typically found on the order of ~ 0.01 mg mL^{-1} [17]. This group produced pristine graphene dispersions from graphite in water upon exfoliation in the presence of non-ionic surfactants. Yields up to 100 times greater than some reported values (1 mg mL^{-1}) were achieved. This is one of the highest yields reported to date. While the use of surfactant improves stabilization of graphene dispersions, the technique is marred by the formation of graphene-surfactant dispersions which limit electronic properties required for highly conductive materials. Removal of surfactants is often labor-intensive requiring many washing or purification steps.

Ionic liquids (ILs) are molten salts comprised of ions with high electrical conductivity, able to dissolve salts and have surface energies similar to graphene. The use of ionic liquid therefore offers the possibility for use in liquid phase exfoliation. The first such method made use of a tip sonication approach in the presence of 1-butyl-3-methyl-imidazolium bis(trifluoromethane sulfonyl) imide ([Bmim] [Tf_2N]) and was demonstrated by Wang *et al.* [18]. Here, sheets could be formed and concentrations close to 0.95 mg mL^{-1} achieved. Even today this is considered a considerably high yield. The produced sheets were 5 atomic units thick. Nuvoli *et al*. [19] reported yields up to 5 mg mL^{-1} graphene, never seen before. The method relied on the use of fluorinated imidazole compounds (1-hexyl-3-methyl-imidazo-lium hexafluorophosphate (HMIH)), commonly used in electrochemical applications due to high conductivity associated with its ionic

nature. The large flake thickness achieved has led to exclusion of this method in successive applications. A further study was conducted by Matsumoto *et al.* [20] in which oligomeric ionic liquids (IL_2PF_6 and IL_4PF_6) were used as solvent with microwave agitation replacing commonly used ultrasonication. The work yielded graphene products with excellent yield (93 wt. %), a high percentage of single layer graphene (95 %) and good I_D/I_G ratios from raman spectra at low exfoliation times. Najafabadi *et al.* [21] examined the use of a low IL load IL/acetonitrile electrolyte (~ 1:50 IL/acetonitrile vol. ratio) for graphite exfoliation to graphene. This method was able to lower costs associated with IL-assisted exfoliation, extended electrochemical stability in a non-aqueous electrolyte and provide high exfoliation yield (86 %) by effective anionic intercalation within the graphitic layers. Not many further works have been conducted on the use of ionic liquid aided exfoliation methods. The production of large scale sheets by exfoliation in IL is still a major concern of this process, however the possibility for applications in ionic solutions cannot be easily overlooked.

Lastly, upon the discovery of solution-based exfoliation in organic solvents and aqueous media, studies have been conducted for the exfoliation of graphite to form graphene in polymer solutions including polystyrene (PS), polyvinyl-chloride (PVC) and cellulose acetate (CA) [9]. The technique relies on the inclusion of monomers between the graphitic layers which upon polymerization force sheets apart breaking the interlayer attraction. May *et al*. [22], by theoretical modeling, theorized that a comparison of Hildebrand solubility parameters of polymer, solvent and graphene was an accurate measure to predict graphite exfoliation in any particular polymer aided solvent. In 2009, Bourlinos *et al.* [23] investigated the use of non-toxic, non-ionic polyvinylpyrrolidone (PVP) in a polymer assisted exfoliation of graphite. Fine graphite powder was dispersed in water and PVP by prolonged sonication. Stable dispersions of polymer coated graphene is achieved by steric stabilization of the hydrophobic polymer to form a colloidal model. Single layer graphene is achieved without any damage to its structural integrity. The produced polymer protected monolayers offer applications in sensing due to the ease of functionalization of the polymer layer. Removal of polymer however is a labor intensive process. Similarly, Wajid *et al*. prepared stable dispersions of graphene in PVP based solvents [24]. Single to multilayer graphene sheets could be produced.

2.2.1.2. Electrochemical Exfoliation Methods

Electrochemical exfoliation methods have made tremendous strides in graphene research in recent years. Offering many advantages over other exfoliation methods (environmentally friendly, tunable due to application of applied potentials and rapid) it is useful to understand its use even though control of particle size is difficult [1]. Mechanical exfoliation generally follows oxidation or reduction of the graphite electrode. A range of intercalation compounds have been interrogated over the years since its introduction in the late 1980s. Generally speaking, two common approaches for electrochemical exfoliation exist: anodic and cathodic approaches. In the anodic approach, oxidation of the graphite anode surface is achieved by application of an oxidative potential. Sulfonate ions form the most common anodic approach to date. Li *et al*. [25] used sodium dodecyl benzene sulfonate (SDBS) solution as electrolyte and a graphite rod as anode material. The anode graphite was corroded and deposited on the bottom of the beaker as a black precipitate. Single layer graphene was produced with thickness < 2 nm. The approach produces SDBS graphene. These products typically include some oxidative moieties due to oxidation of the surface or the presence of other impurities thus limiting the electronic properties of the produced material. Conversely, non-oxidative routes could be employed by making use of the cathode. Zhong and Swager [26] developed a two-step hyper expansion technique. Subsequent intercalation of small particle Li^+ ions and considerably larger tetra-n-butylammonium (TBA) between the graphite basal planes was performed. A liquid phase exfoliation approach based on the intercalation of expanded graphite (EG) was investigated by Zhou *et al.* [27]. The technique looked to improve exfoliation process in a water, DMF solution by addition of Li^+ ions between EG sheets which undergoes rapid hydrolysis. Small size EG flakes produced few layer graphene flakes in stable suspensions.

2.2.1.3. Laser Exfoliation Methods

Exfoliation by ultrasonication remains the most popular technique due to its simplistic nature and labor-free process. Laser exfoliation offers a simple, fast approach but too is limited to low yields when conducted in vacuum chambers. Qian *et al*. [28] introduced a liquid phase pulsed laser exfoliation method for preparation of graphene. Dispersions of HOPG in NMP or sodium dodecylbenzene sulfonate/water (SDBS/water) were pulsed with a laser fluence of 1.0 J/cm^2 over a period of 2 hrs. Stable graphene suspensions were collected. Few layer graphene sheets with ~ 1 nm thickness and low micrometer sizes were recorded. Among others the technique offers an

alternative approach to lengthy analysis times of ultrasonication and avoids contamination based on tape and adhesive methods.

2.2.2. Ball-milling Methods

Effective mechanical exfoliation of graphite to graphene occurs via both external normal and shear force application. While ultrasonication techniques dominate the large scale fabrication process for graphene preparation, shear force applications still hold significant advantages. Ball milling techniques produce shear forces and upon fragmentation allow for exfoliation to single sheets. Both wet and dry approaches have been looked at. Jeon *et al*. [29] has proposed a method to prepare edge-carboxylated graphene nanosheets (ECG) by a simple ball milling method in the presence of dry ice. Pristine graphite, in the presence of solid form of carbon dioxide, was introduced into a planetary ball-mill machine. Carboxylation of the graphite precursor is achieved by ball milling after 48 hrs. The prepared hydrophilic ECG could then be protonated in air moisture to form H-ECG. The procedure is conducted in solid state without the use of hazardous chemicals required in liquid phase methods. Here, ECG could further be dispersed in a range of polar solvents and graphene sheets with high electrical conductivity could be fabricated on a large scale. Wet ball milling approaches have been interrogated to improve the exfoliation of graphite prior to mechanical exfoliation associated with milling techniques. A schematic representation of the ball milling process is illustrated in *Figure 2.2*. Colloidal dispersions of single- and few-layer graphene sheets were prepared in the work by Zhao *et al.* [30] using a wet ball milling technique. In the work, graphite was exfoliated in a two-step process. Pristine graphite was first dispersed in solutions of ethanol and water by ultrasonication methods. Upon drying, the prepared graphite nanosheets were dispersed in a range of organic solvents and passed through a ball milling process by mechanical stirring. The dominant shearing stress exerted on the particles allows for further cleavage of the graphite layers. Stable, homogenous dispersions were produced with particle thickness in the 0.8 to 1.8 nm range. A good yield of ~ 0.096 mg mL^{-1} was observed in DMF. While, these techniques are beneficial in the mass production of graphene sheets with good electrical conductivity by non-destructive oxidation methods, long milling times are a significant drawback of the technique. Further, expensive instrumentation is required to undergo milling techniques.

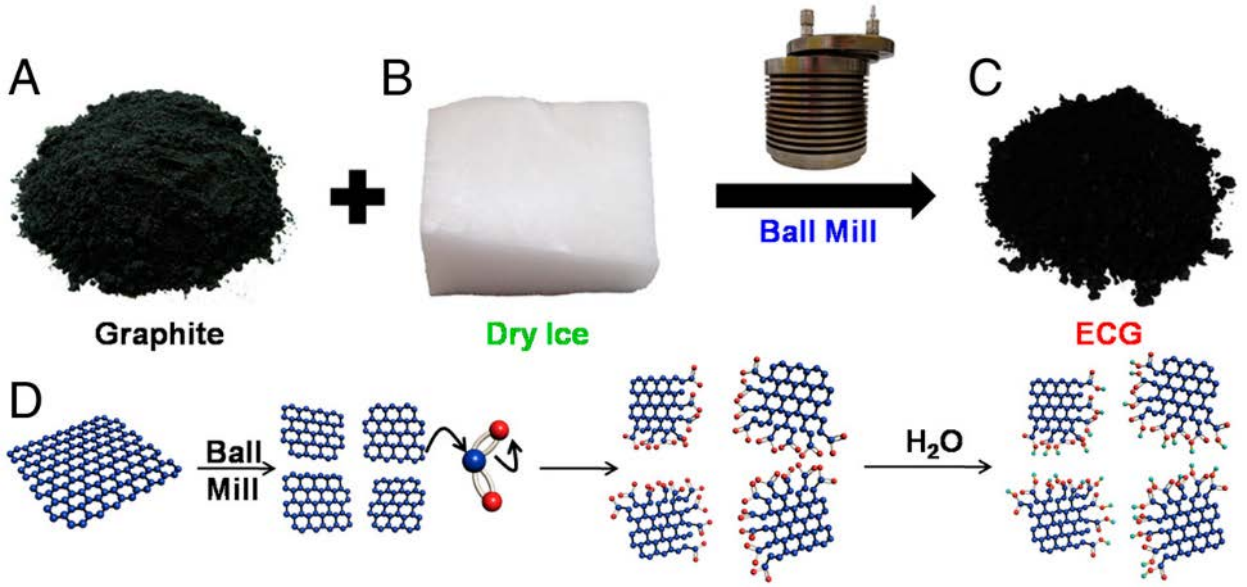

Figure 2.2: (a) Pristine graphite, (b) dry ice (solid phase CO_2), (c) edge-carboxylated graphite (ECG) prepared by ball milling for 48 h, (d) a schematic representation of physical cracking and edge-carboxylation of graphite by ball milling in the presence of dry ice, and protonation through subsequent exposure to air moisture [29].

2.2.3. Chemical Oxidation and Reduction

To date, micromechanical exfoliation of graphite to produce graphene still remains the most effective technique for the production of pristine single-layer graphene with little to no defects. This technique relies solely on the cleavage of layers by means of an adhesive tape able to overcome the intermetallic forces between graphene layers. Further mechanical techniques have been suggested to overcome the low yield produced, as previously introduced. Chemical synthesis approaches are common place in laboratory scale applications due to their ability to produce large scale products with minimal defects. Intercalation techniques, which allows for the insertion of small molecules between graphitic layers is one such approach. Oxidative intercalation has gained the most attention in this field due to its simplicity and low-cost chemicals. Typically, strong oxidizing agents like potassium permanganate in the presence of sulfuric and nitric acid are used for insertion of oxygen molecules between layers of graphite as starting material. Brodie [31] offered the first known chemical oxidation approach to the production of graphitic oxide. Potassium chlorate was used as the oxidizing agent in this process. A variety of variations to the

technique was introduced in the works by both Staudenmaier *et al*. [32] and Hoffman *et al*. [33]. These procedures produce explosive ClO_2 gas as harmful byproduct and are no longer used in practice today. Hummers *et al*., [34] and Tour *et al*. [35] have since replaced these techniques by replacing the oxidizing agent with potassium permanganate ($KMnO_4$). Studies of the produced graphitic oxide materials have been performed by Szabo *et al*. [36] and Cai *et al*. [37] respectively. Oxygen functional groups including hydroxyl, carboxyl, carbonyl and epoxy groups are deposited on the basal planes and edges of the graphitic layers. A resultant weakening of the observed Van der Waal's forces and shift to hydrophilic nature of the produced GO is achieved resulting in exfoliation in aqueous media. Single layer graphene oxide sheets are achieved, with oxygen moieties offering a variety of chemical properties and electron mobility associated with insulating materials. Functionalization of the produced GO at the basal plane has been studied in a wide range of works.

The use of GO in many sensor applications is not particularly useful due to its low conductivity, however the graphitic network can be substantially restored by thermal annealing or chemical reduction etc. [38]. The produced GO is subsequently reduced to graphene via many routes. Chemical reduction using sodium borohydride [39,40] or hydrazine [41,42], thermal reduction [43], photo reduction, electrochemical reduction [44,45] among others are commonly used. The formation of defects or voids in the graphene structure due to inclusion and removal of oxygen moieties is a major drawback of this technique and limits the excellent properties attributed with graphene. Various studies have reported on the extent of graphene reduction for a variety of applications and the influence of oxygen content on the desired application reported [46,47]. Chemical reduction approaches for the reduction of GO still remains the most useful means for production of RGO, making use of commonly used reducing agents. Alternative and green reduction approaches have also been studied [48].

Typically, exfoliation methods are very useful in lab setups due to their ability to produce pure graphene. However, they are limited to producing randomly scattered flakes of graphene across a surface leaving large areas uncovered. For a large number of applications of graphene this is not ideal. Continuous film production is therefore required. A common approach for graphene growth is epitaxial growth. In this method single sheets of carbon are deposited on a metallic substrate from a silicon carbide (SiC) source. The SiC source may be heated allowing silicon to

sublimate, leaving a layer of carbon behind. In another approach, a graphene filament is heated in a high-vacuum, carbon sublimates forming a beam which is deposited on a metallic substrate [49].

Chemical vapor deposition (CVD) is the most promising growth method to produce graphene. The CVD methods results in high quality single graphene sheets on a large scale, without the need for further treatment. As a result, the method is one of the cheapest graphene synthesis methods in use to date. The CVD method can be employed to grow single sheets of graphene on arbitrary surfaces using transition metal catalysts. Hydrogen catalyzes methane gas in a furnace forming carbon atoms which can be deposited on a substrate by chemical adsorption. Graphene may contain impurities and contain wrinkles attributed with improper annealing. Transferring the formed graphene can pose some further challenges.

2.3. Electronic and Electrochemical Properties of Graphene

The rise of graphene over the last thirteen years has thrilled scientists in all spheres of research, owing to its outstanding properties: high tensile and mechanical strength [50–52], excellent thermal conductivity [39,53], superior surface area [54,55], electron mobility associated with its sp^2 hybridized carbon structure [10,56], quantum Hall effect [52,57], current density [58] etc. In order to effectively discuss the applications of graphene-derivatives in electrochemical stripping analysis, a basic working knowledge of the electronic and electrochemical properties common to all graphene-based sensors is required. Many reviews to date have been performed on the theoretical properties attributed to pristine and few layer graphenes. As such, only the electrochemical and briefly electronic properties will be studied in this review.

The excellent electronic properties of graphene may be attributed to the nature of its sp^2 hybridization. Carbon, with a ground state electron configuration of $1s^2 2s^2 2p^2$ involves six associated electrons in its hybridization and is important as it is the main constituent of graphene. Bonding of carbon in graphene is initiated by its four valence electron orbitals with sp^2 hybridization, formed by the mixing of the 2*s* orbital and two 2*p* orbitals. The hexagonal structure occurs as each of the three sp^2 orbitals forms a strong covalent carbon-carbon σ bond, with bond length of 0.142 nm with three neighboring carbon atoms on the 2D plane [59]. A two atom unit cell is therefore derived for graphene as showing in *Figure 2.3 (a)*. The sp^2 orbitals of neighboring carbon atoms causes spreading of the formed lobes and interactions of the 2*pz* orbitals creates

movement of electrons across the graphene sheets as delocalization of the π electrons is possible. *Figure 2.3 (b)* represents the formed delocalized π (bonding) and π^* (antibonding) bands. These formed valence and conduction bands (VB and CB) were shown to be represented as smooth sided cones, meeting at a point (k), known as the Dirac point at low energies associated with electron transport (*Figure 2.3 (c)*). Since the VB and CB touch, graphene has a zero bandgap and known as a zero-gap semiconductor.

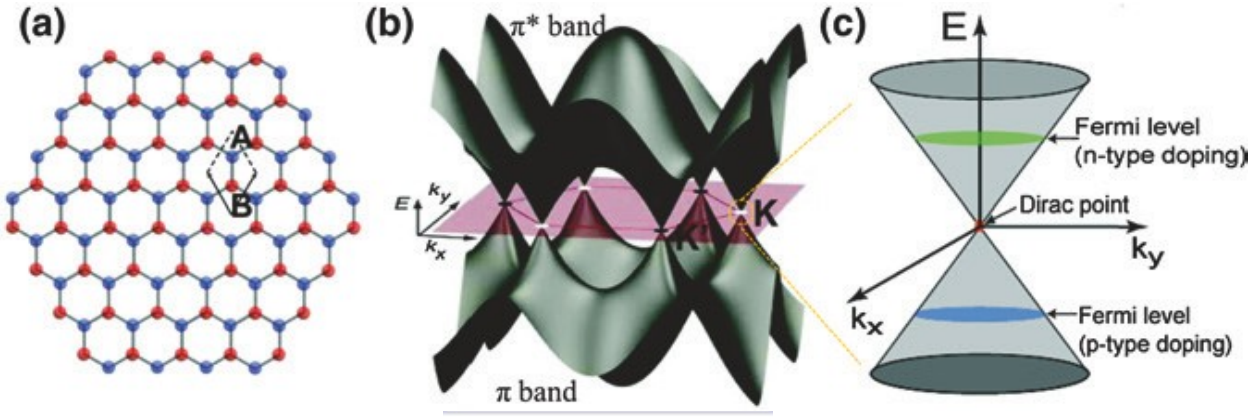

Figure 2.3: (a) The hexagonal lattice of graphene has a basis of two carbon atoms (A, B) per unit cell, (b) The π and π* bands in graphene and (c) The linear dispersion and the band structure at the Dirac point [59,60].

A summary of previously reported properties of graphene is provided in *Table 2.1* in order to accurately convey the excellent properties of graphene.

Table 2.1: A summary of electrical, optical, thermal and mechanical properties recorded for graphene in literature.

Property	*Value*	*Reference*
Bulk Conductivity	*0.96 x 10^6 Ω^{-1} cm^{-1}*	[61]
Electron Mobility	*> 15 000 cm^2 $V^{-1}s^{-1}$* *200 000 cm^2 $V^{-1}s^{-1}$, limited by acoustic phonons*	[4,62] [63]
Resistivity	*10^{-6} Ω cm (7,8)*	[64]
Density	*0.77 mg m^{-2}*	[60]
Thermal Conductivity	*5 x 10^3 W $m^{-1}K^{-1}$ (20)*	[65]
Elastic Modulus	*1.0 TPa (27)*	[66]
Coefficient of Thermal Expansion	*-6 x 10^{-6} K^{-1}*	[67]
Tensile Strength	*130 GPa (27)*	[66]

Graphite, with covalent bonds between carbon atoms forming a co-planar trigonal geometry forms the basis of any discussion on graphene electronic properties. The interaction of delocalized π-electrons between graphene layers are responsible for weak interlayer bonding. This was previously discussed as the driving factor in mechanical cleavage of graphite. This free electron cloud allows for graphite to have semi-metal behavior with high electrical and thermal conductivity. Further localized densities of electrons occur at pockets and electron holes due to degenerate Fermi energy bands. Graphite edges facilitate electron transfer and show activity toward redox changes owing to portability of electrons. Lastly, the inclusion of impurities in the graphitic structure limits electron transfer and also facilitate adsorption based on the inclusion of

functional groups [68]. These electronic and electrochemical properties are often indiscriminate from graphene properties arising from multi-layer graphene.

Intrinsic electrochemical properties associated with carbon-based electrodes, beneficial for the application in electrochemical stripping analysis would be ideal for graphene-derivative based stripping voltammetry. Since oxidative procedures to synthesis graphene via graphene oxides are extremely popular, let's first look at the properties of GO derivatives. The high electron mobility and high specific surface area of GO allows for electron transfer at the electrode surface [69]. Zou *et al*. [56] studied the electron transfer of proteins in the presence of GO. Efficient, rapid electron transfer was facilitated by GO at glassy carbon electrodes. Wen *et al*. [70] further reported the unusual electron donor properties of GO in a gold nanocluster-graphene oxide nanocomposite (AuNC-GO). Electrons are excited from the GO into the highest occupied molecular orbital (HOMO) of the AuNC. It has been found that GO exhibits good electrocatalytic properties in a wide range of applications. Basirun *et al.* [71] showed good electrocatalytic activity towards oxygen reduction at a GO coated MnO_2 cathode. Xu *et al*. [72] expanded on this work by demonstrating sulfur and nitrogen co-doped few-layer graphene oxide could further improve the catalytic effects of graphene oxide. The presence of oxygen at the edges of graphene sheets allows for easy functionalization of graphenes by simple covalent bonding.

A wide electrochemical potential window, enhanced electron transfer rates and redox active sites are crucial in sensor development. The determined active electrochemical potential window of any particular electrode material is pivotal to possibility for many applications. Similar to carbon-based electrodes, a wide electrochemical potential window was found for graphene prepared by a chemically reduced graphene oxide by Zhou *et al.* [73]. A 2.5 V potential window is shown in aqueous electrolyte solutions. Our research group reported similar results at pencil-graphite electrodes modified with electrochemically reduced graphene oxide. In addition to wide potential windows, an increase in capacitive current is observed for the graphene electrodes over bulk electrode material [74].

Electrochemical applications rely heavily on macro-scale electrodes with a large area modified with graphene. An understanding of bulk graphene electrochemical properties can therefore only be determined. Graphite-like properties of multilayer or graphene flakes provide a

suitable introduction to bulk properties. A study on the electrochemical properties of multilayer graphene flakes was performed by Shang *et al.* [26]. A catalyst-free approach relying on a microwave CVD was used to prepare multilayer graphene on a variety of substrates. The edged structure provides multiple sites of activity which are available to the electrolyte solution. Excellent electrochemical oxidation and reduction peaks are demonstrated in the presence of a $Fe(CN)_6^{3/4}{}_{(aq)}$ redox probe with peak-to-peak separation similar to that of graphite electrodes obtained. Fast electron transfer kinetics is thus achieved at multilayer graphene flakes. Pumera *et al*. [75] reported a clear distinction between the edge plane and basal plane electron transfer-rate constants (k_e *and* k_b). Goh *et al*. [76] further reported that the electrochemistry between single and multilayer graphene is therefore indiscernible from one another. Many more studies were performed to study the electron transfer behavior of graphene in the presence of redox probes. Well defined redox peaks and an increase in peak currents indicate the enhanced electron transfer kinetics. Velicky *et al*. [77] however, reported findings contrary to those previously stated, suggesting that both edge and basal planes are active. They studied the electron transfer kinetics of mono- and multilayer graphene in the presence of three redox probes; namely ferricyanide, hexaammineruthenium, and hexachloroiridate ($Fe(CN)_6^{3-}$, $Ru(NH_3)_6^{3+}$, and $IrCl_5^{2-}$, respectively). A change in electron transfer is recorded across a single basal plane crystal. Brownson *et al.* [78] reported that quasi-graphene (~ 4 layers) exhibited a better response to the redox probes with heterogeneous electron transfer greater than for monolayer graphene. It is clear that optimum graphene loading at the electrode surface is therefore required for improved electrochemical performance. Diffusion control of analyte towards the graphene surface is observed by the linear relationship to the square root of scan rate.

2.4. Recent Advances in Stripping Analysis at Graphene-based Electrochemical Systems

Owing to its relative ease of production, handling and intrinsic electronic and electrochemical properties, it is no wonder that graphene oxides (GO), reduced graphene oxides (RGOs) and graphenes (G) have been used in electrochemical bio- and chemical sensing applications. Numerous reviews have been conducted on their use in electrochemical sensors over the past decade [1,54,68,69,75,79–83]. While the properties of these graphene-derivatives are unique, their use as ‘stand-alone’ materials in electrochemical sensing is quite limited.

Functionalized, doped or composite forms with polymers, nanoparticles etc. have been studied to improve electrode sensitivity or selectivity in a range of applications. To date no study, has been performed focusing on the use of graphene-derivatives in electrochemical stripping analysis. As is well documented, stripping voltammetry (SV) is the leading electrochemical technique for metal analysis due to its ability to accurately detect at low concentrations, however it has also been applied to other analytes. Consequently, in order to place special emphasis on the role of graphene-derivatives in electrochemical stripping voltammetric sensors, the work will group common functionalization or composite approaches rather than target analyte. A similar approach was performed in the work by Ratinac *et al.* [68]. This study will focus on recent progress in the filed only.

2.4.1. Simple Graphene Derivatives

A great demand for electrochemical sensor designs based on simple materials is of great interest to researchers worldwide in order to simplify the chemistry involved and reduce cost and times associated with production on a large scale. The most straightforward designs therefore rely on the use of GO, RGO and graphene without modification by simple coating techniques.

Very few studies have been performed on the use of GO in electrochemical stripping analysis without further modification, mainly due to its slow electron transfer processes. Ruengpirasiri *et al.* [84] proposed the use of a chemically modified electrode based on graphene oxide prepared by a Hummer's method for the detection of Cd^{2+}, Pb^{2+}, Cu^{2+} and Hg^{2+} in the presence of an Sb-film by anodic stripping voltammetry (ASV). The sensor design is based on a simple screen printing technique with a GO-carbon ink to create the working electrode. The GO working electrode was found to have synergistic effects which is capable of increasing the electrode surface area and increase the metal ion adsorption. Further, the work surmised that GO was used for its higher electrical conductivity, which is contrary to previous findings on its insulating behavior. Increased loading above 1 wt.% showed to significantly inhibit the electron transfer and decrease the electrode sensitivity. In a separate study Kablan *et al.* [85] investigated the electrochemical behavior of a GO-modified glassy carbon electrode (GCE) towards the electrochemical oxidation of Cefuroxime Axetil (CEFA), an oral prodrug formulation of the injectable antibiotic cefuroxime. Similarly, the GO-GCE showed improved electrode sensitivity toward CEFA due to increased

surface area and high electrical conductivity associated with the inclusion of GO. While both of these works make mention of the high electron conductivity of GO as means to improve electrode sensitivity, it is well established that GO is an insulating material and can therefore only be used in low quantities, for improved electrode surface area. Smarzewska *et al*. [86] for the first time investigated the ability of GO and RGO to influence carbon paste electrode (CPE) properties for thioguanine detection by ASV. GO modification of the CPE resulted in a lowering of electrode resistance and background currents, while increasing the electroactive surface area and improving the electrode sensitivity towards thioguanine oxidation due to the presence of oxygen-containing functional groups. Simple GO-derivatives are therefore not particularly useful in electrochemical stripping analysis where enhanced electron transfer rates associated with electrolytic conversion is required.

The reduced graphene oxide counterparts have been studied more extensively in stripping analysis due to its ability to facilitate electron transfer at the electrode surface. Commercial multilayer graphene was for the first time applied to the detection of Pb^{2+} in soy beans by ASV on a screen printed carbon electrode (SPCE) [87]. The non-ideal behavior of SPCEs are improved by modification with the ordered graphene material. In addition, it could be inferred that the porous nature of the graphene-SPCE could absorb more Pb ions. Detection capabilities were improved to the trace level. Wang *et al.* [88] further reported on the use of graphene nanosheets prepared by a chemical exfoliation method for the detection of Cd^{2+} and Pb^{2+} by ASV. An increase in number of active sites associated with larger surface area showed improved detection capabilities towards the metal cations. SEM images of the GNS modified electrode is shown in *Figure 2.4*. A shift to bulk graphite was seen with increasing GS concentration lowering the peak currents. Shan *et al.* [89] made use of a graphene-modified GCE for the indirect detection of ciprofloxacin in the presence of Cd^{2+}. The peak current of Cd^{2+} was remarkably enhanced due to the large specific area and the ability of negatively charged graphene to improve absorption of metal cations. Moreover, graphene-based sensors prepared by screen printing techniques were also applied to the simultaneous detection of pesticides using ASV [90]. Here, the improved sensitivity towards isoproturon and carbendazim were attributed to enhanced electron transfer properties of the graphene working electrode. Sys *et al*. [91] further performed a comparative study of GCE, CPE, MWCNT-CPE and single layer graphene-CPE for the adsorptive stripping voltammetry (AdSV) of retinol. It was concluded that despite its high surface area, graphene variants were not able to

enhance electrode performance in AdSV applications. This finding is uniquely interesting and may be interesting for further exploration. It was also discovered that restoration of the modified electrode surface was not possible and single analysis was required.

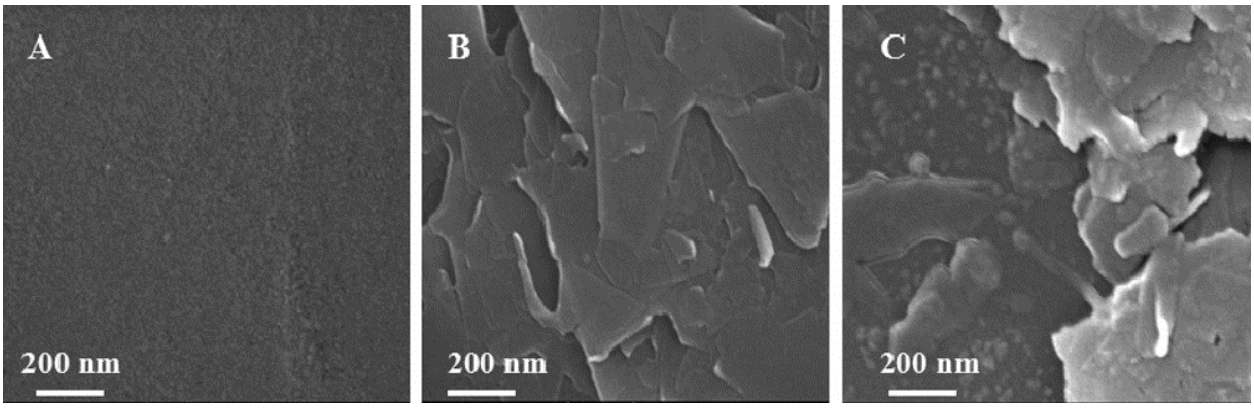

Figure 2.4: SEM images of (a) bare GCE, (b) GS/GCE and (c) GS/ GCE after being reduced in the presence of 300 mgL¢1 Bi3+ [88].

Electrochemically reduced graphene oxides (ERGO) provide a one-step approach for modification of electrode surface without the need for lengthy solvent evaporation times. Our group performed a study on the detection of Zn^{2+}, Cd^{2+} and Pb^{2+} in water samples by ASV in the presence of a Bi-film at pencil graphite electrodes (PGE) [74]. Electrode modification by simple solvent evaporation methods was not possible and electrochemical deposition provided a simple coating procedure. The enhanced peak currents were observed due to a combination of enhanced surface-area-to-volume ratio and improved electron transfer kinetics of the ERGO structure. Detection capabilities in the low μg L^{-1} was achieved. Similar results were recorded in studies for the detection of taxifolin [92] and carbofuran and carbendazim [93] as a result of restoration of electron configuration by electrochemical reduction of oxygen moieties.

Chemical doping of graphenes with nitrogen, boron and sulfur introduces the possibility for tailoring the unique properties, electronic behavior and surface chemistry of the 2D-carbon material [94,95]. Only a few studies have reported the use of Nitrogen-doped graphenes (NG) for use in stripping voltammetry applications to date. Wen *et al*. [94] first studied the role of NG towards the stripping voltammetric detection of Pb^{2+}. The presence of NG at the GCE surface facilitated the deposition of Pb ions by an increase in effective active sites, showed characteristic

high conductivity, large surface area and catalytic activity. The NG-sensor exhibited detection limits in the low micro-molar range for metal cation detection. Similarly, NG was applied in the fabrication of a nanocarbon paste electrode for the detection of Cd^{2+} and Pb^{2+} by ASV [96]. While these works show excellent sensitivity towards metal analysis, extra modification steps required for doping make it a tedious process. To the best of our knowledge no work has been performed on doped-graphenes for detection of organic materials by adsorptive stripping voltammetric techniques.

2.4.2. Graphene-derivatives based on Biomaterials

Chitosan (Ch), a biocompatible polymer derived from alkaline deacetylation of chitin has gained tremendous use in sensing application due to its biocompatible nature and widespread availability. Chitosan-based sensors have been utilized in electrochemical stripping analysis of metal cations by ASV due to its ability to electrostatically interact with ions. Studies have combined the binding ability of chitosan with graphene-derivatives. One such study was performed by Magerusan *et al.* in 2017 [97], based on a chitosan nanocomposite formed with Nitrogen-doped graphene for the detection of Pb^{2+} ions by ASV. The chitosan provided dual functionality in the modified sensor. Owing to its excellent water permeability, improved dispersion of the N-Gr into aqueous solutions was achieved. It further acted as binding agent allowing for adherence of the doped graphene to the metallic electrode surface and allowed improved metal ion adsorption with observed functional groups due to presence of primary amines in its backbone. The Ch-N-Gr showed improved sensitivity and selectivity towards Pb^{2+} detection over the bare gold electrode. A similar sensor was reported by Chen *et al.*, based on a RGO-carboxymethyl chitosan composite for the detection of Cu^{2+} by stripping analysis [98]. Here, the role of chitosan was exploited to improve dispersion of RGO in aqueous samples similar to that performed by Magerusan *et al.*

The role of L-cysteine (L-cys), the widely available amino acid with electroactive mercapto groups have also been investigated towards metal ion detection by ASV. Its ability to form a stable polymer film in conjunction with graphene was utilized in the study by Zhou *et al*. for detection of Cd^{2+} and Pb^{2+} at a GCE [99]. Induced growth of the L-cys polymer on the graphene support was achieved. Electrical conductivity of the prepared L-cys/GR–CS/GCE showed and overall increase in conductivity of the prepared sensor due to inclusion of graphene. It was found however that a

slight weakening in redox current studied at the $[Fe(CN)_6]^{3-/4-}$ couple as a direct result of the poor conductivity of the polymer. The net enhancement in stripping peak currents of Cd^{2+} and Pb^{2+} occurred as a result of improved conductivity and catalytic effect of the graphene to facilitate electron transfer and also due the coordination of metal cations with sulfur, nitrogen and oxygen atoms present in the cysteine structure. Similar studies were reported in the work by Cheng *et al*. [100] in conjunction with gold nanoparticles and nitrogen-doped graphene with functionalized cysteine for detection of Pb^{2+}. Improve electron transfer kinetics associated with graphene and synergistic effects of the metal ligand receptor was shown.

Three studies have recently reported works on the use of starch-derived cyclodextrins for the stripping voltammetric detection of metallic cations. β-cyclodextrin (β-CD), a cyclic oligosaccharides composing of seven glucose units joined by glycosidic bonds was used in all three studies due to its hydrophilic exterior structure and ability to incorporate organic, inorganic or biological molecules within its cavity to form stable complexes [101,102]. Lv *et al*. [101] reported on the use of a β-CD-RGO hybrid material in the presence of an electroplated Bi-film for the detection of Cd^{2+} and Pb^{2+} by ASV. The hydrophilic nature of β-CD, was used to improve the dispersibility of RGO in water. The prepared β-CD-RGO hybrid material showed improved peak currents for both metal cations and occurred as a result of synergistic effects of β-CD and large surface area and conductivity of RGO. The hybrid material further showed the ability to regenerate the electrode surface. The schematic representation of the β-CD-RGO hybrid nanosheets synthesis is demonstrated in *Figure 2.5*. Similarly, detection of Cu^{2+} was performed by Huang *et al*. [103] in the presence of amino-functionalized reduced graphene oxide (NH_2-RGO). The β-CD prevented aggregation associated with the NH_2-RGO material and improved the stability of the formed complex. In addition, its ability to facilitate accumulation of Cu^{2+} was investigated. Lastly, Zhan *et al*. [102] reported its use in adsorptive stripping voltammetric detection of Pb^{2+} in the form of a composite material with RGO. Here, β-CD improved the water solubility of the graphene-derivative. Further, the strong absorption ability of β-CD towards Pb^{2+}, confirmed the host-guest recognition and multiple-site adsorption properties.

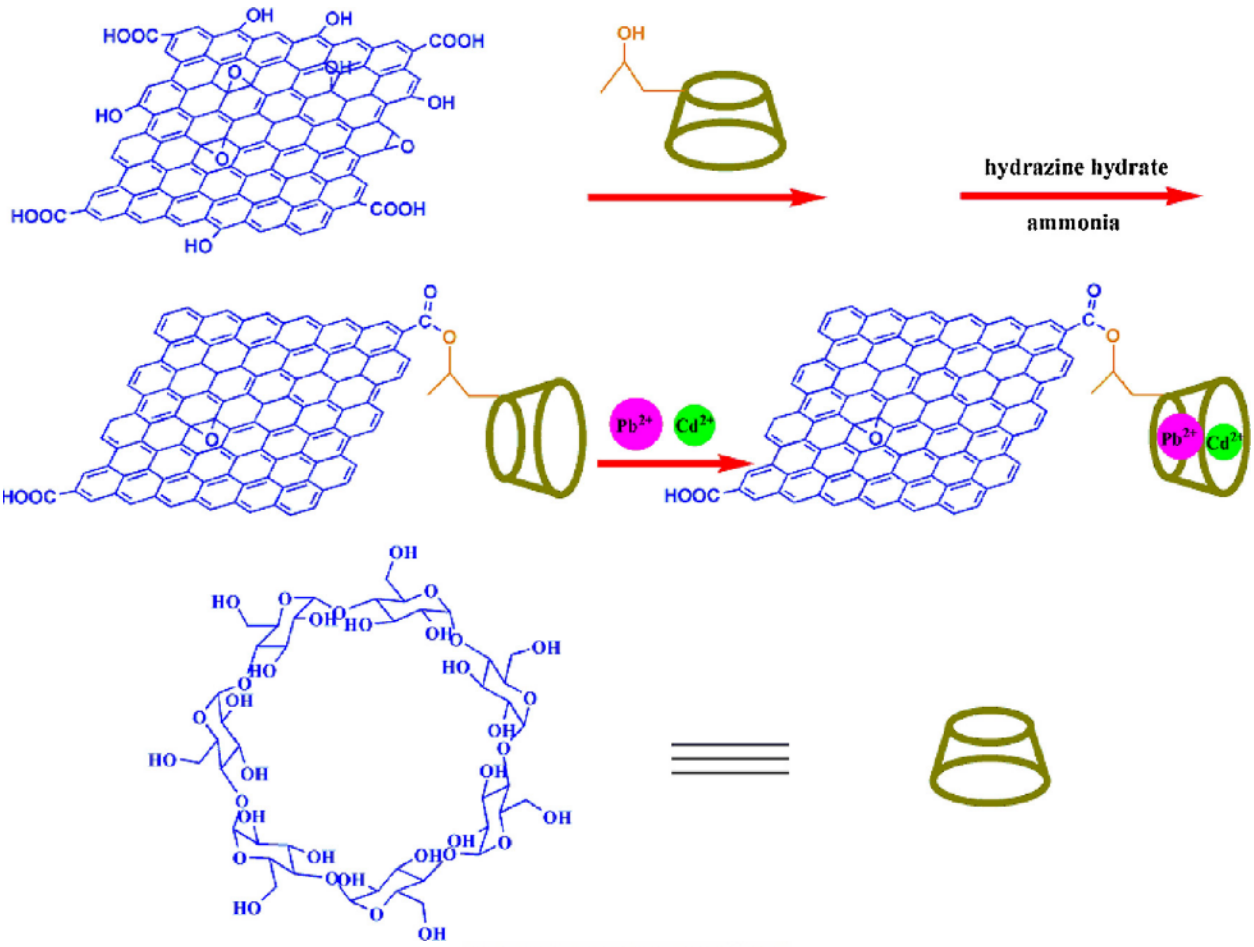

Figure 2.5: Schematic of the synthesis procedure of β-CD-RGO hybrid nanosheets and the interaction between β-CD-RGO and the heavy metal ions (Pb2+, Cd2+) [101].

Razmi *et al*. [104] reported the use of eggshell membrane protein, the cheap, green biopolymer, doped with reduced graphene oxide as sorbent material for the preconcentration and detection of Hg^{2+}. Its complex framework composed of insoluble fibers, chemical stability, high area and surface functionalized groups make it an attractive material for absorption purposes. The bio-sorbent material showed excellent extraction of metal ions while the presence of RGO significantly improved the electron transfer and stripping peak currents.

2.4.3. Polymer and Ionic Liquid assisted Graphenes

Biomaterials and biopolymers offer unique dispersing, binding and adsorption properties for the detection of metal cations and organic materials by stripping voltammetric techniques and consequently enhance the electrode performance in graphene-based sensing, as discussed in the

previous section. Many researchers however, have examined the use of synthetic or conducting polymers derived from suitable monomers and ionic liquids to replace the use of biomaterials. Recently, Ruecha *et al.* [105] exploited the high compatibility of a graphene-polyaniline (G-PANI) composite material for electrode preparation and intrinsic conductive nature of the polymer for modification on paper and plastic substrates. The nanoparticle preparation was performed by a chemical synthesis approach in the presence of a capping agent to prevent particle aggregation and a monodispersed solution of particle size 371 nm created. An increase in effective surface-area-to-volume ratio was achieved. It was found that both graphene and PANI, conducting polymer improves electron pathways and as a result electron transfer kinetics of the electrode. The sensor was applied to the detection of Zn^{2+}, Cd^{2+} and Pb^{2+} by ASV. The ability of conducting polymers to complex with metal cations was further studied in the work by Nguyen *et al.* [106]. Poly(diaminonaphthalene), poly-(DAN) a common conducting polymer was used for its ability as complexing agent in the detection of Pb^{2+} due to free amine groups in its structure. However, the low electron conductivity and compact structure limits diffusion. A hybrid with RGO was prepared by an electropolymerization technique to counter this downfall for sensing ability. The sensor showed improved performance over its counterparts due to enhanced electron transfer processes associated with RGO and the ability of polymer to chelate Pb^{2+} via free amine sites. Molecular imprinting techniques were further utilized based on the creation of recognition properties into synthetic materials using suitable templates. Bai *et al.* [44] utilized a two-step process for the fabrication of a Pd(II)-ion imprinted sensor: Electrodeposition of RGO followed by polymerization using allyluread (NAU) as a functional monomer, ethylene glycol dimethacrylate (EGDMA) as a cross-linking agent, and azobisisobutyronitrile (AIBN) as an initiator. $PdCl_2$ was used as the template material. The graphene increased electrode specific area and electrical conductivity improving the sensor sensitivity while the ion imprinted polymer drastically improved electrode selectivity and acted as preconcentrator. A similar study was performed for the detection of organic streptomycin based on poly(pyrrole-3-carboxy acid) by Wen *et al*. [107]. Further works were also performed making use of graphene-polymer complexes [42,108,109].

Nafion, a perfluorosulphonate polymer has been used as flexible binding material in many studies on electrochemical sensors to date. Its use has been based on its intrinsic antifouling behavior and ability to maintain the hydrophobicity of graphene. Er *et al.* [110] utilized the nafion to form stable suspension of graphene in water due to the interaction with oxygen functional groups

on the graphene surface. The Nafion-graphene composite material was applied to the detection of the nebivolol, beta blocker drug. Lee *et al.* [111] exploited the unique nafion properties for use in a metallic sensor based on the ASV detection of Zn^{2+}, Cd^{2+} and Pb^{2+}. The nafion acts as an effective solubilizing agent for activated graphene and anti-fouling coating to reduce the influence of surface-active macromolecules. Further, the negative charges associated with its structure shows electrostatic attraction towards the metal cations. Improved stripping peak currents were therefore achieved. A similar study for the use of nafion to bind graphene to a non-flat pencil graphite electrode was performed by our research group [112]. Increasing the oxygen content of the electrode surface by electrolytic processes allowed for adsorption of graphene materials onto the PGE surface form nafion-graphene suspensions. The nafion further facilitated adsorption of the metal cations onto the electrode surface in the preconcentration step. Wu *et al*. [113] reported the use of a nafion-graphene modified bismuth film electrode for the detection of Cd^{2+}.

Incorporation of ionic liquids (IL) into electrochemical sensor designs has steadily increased as a shift from traditional organic binders to ionic binders is made. Numerous groups have examined the role of ionic liquids when combined with graphene derivatives for electrochemical stripping analysis. Bagheri *et al*. [114] made use of graphene with 1-n-octylpyridinum hexafluorophosphate (OPFP) for the detection of Tl^{+}, Pb^{2+} and Hg^{2+}. High conductivity and sensitivity, fast electron transfer and good antifouling ability is characterized by the IL modified electrodes towards metal cations. Moreover, the same IL was applied to the detection of Cd^{2+} in soil by a portable device [115]. Liu *et al*. [116] investigated the use of 1-butyl-3-methyl-imid-azole hexafluorophosphate [BMIM]PF_6 to form a composite material with graphene and selenium doped carbon paste electrode for the determination of Cu^{2+} and Sb^{3+}. The IL-GN-Se-CPE showed improved sensitivity and selectivity towards Cu^{2+} and Sb^{3+}. The IL not only showed improved stability of the graphene based composite over other non-conductive binders but also increased the effective surface area of the electrode by filling pores in the paste structure. The surface morphology of the electrode upon inclusion of IL showed a smooth surface. The high ionic conductivity of the [BMIM]PF_6 IL was also confirmed by an increase in stripping peak current associated with IL inclusion. This increased electron transfer kinetics was further improved by graphene inclusion. Chaiyo *et al*. [117] reported the use of a nafion-IL-graphene composite on a SPCE for the simultaneous detection of Zn^{2+}, Cd^{2+} and Pb^{2+}. Here, 1-butyl-2,3-

dimethylimidazolium tetrafluoroborate with high electric conductivity and good stability was used. Consequently, the IL improved the negative effects associated with the nafion binder.

2.4.4. Graphene nanocomposites with Metallic and Other Nanoparticles

The inclusion of metallic nanoparticles, like graphene in research application in all spheres of life has dramatically increased since the discovery of their unique properties. The small size, quantum confinement, good electrical conductivity and increased surface-area-to volume ratio have been exploited. Of the ever-growing list of prepared nanoparticles, gold nanoparticles (AuNPs) have been used in most applications due to the ease of preparation. It is no wonder, that numerous studies have been performed on their use in conjunction with graphene-derivatives for stripping voltammetry applications. Lee *et al*. [118] examined its use in the formation of a Gr-AuNP composite material for Pb^{2+} detection by a an electrochemical reduction process. The inclusion of the graphene in the electrodeposition step helped disperse the AuNPs (its primary function) on the electrode surface. The AuNPs were used for their high electrical conductivity. An increased electrode surface area and absorption ability for Pb^{2+} was also recognized. Sanghavi *et al*. [119] further reported the use of AuNPs in a graphene paste electrode (GPE) for As^{3+} detection. The AuNPs further improved the high conductivity and surface area associated with the GPE while also showing strong ability to form stable intermetallic complexes with As^{3+}. In addition, thiacrown ether was used as a complexing agent due to presence of sulfur groups to form complex with the metal cation. A recent study on a functionalized AuNP, RGO composite for detection of Hg^{2+} was used by Wang *et al*. [120]. The ability of amine groups of cysteamine capped AuNPs to react with carboxylic groups of thymine-1-acetic acid covalently was utilized. The graphene substrate along with AuNPs provided a highly conductive platform with high surface area, while the AuNPs provided a platform for immobilization of the complexing agent. Stable complexes with Hg cations could therefore be achieved in the preconcentration step. Detection of organic materials at graphene-AuNP composites have also been observed. A schematic representation of the thymidine functionalized biosensor is shown in *Figure 2.6*. Er *et al*. [110] reported its use in conjunction with graphene and nafion for silodosin detection as previously discussed. In a separate study the use of AuNPs in conjunction with graphene nanosheets (GNS) were used to enhance the adsorptive stripping voltammetric performance of a carbon paste electrode for rivastigmine (RIV) detection [121]. A simultaneous reduction of GO and $AuCl_4$ in the presence of $NaBH_4$ was used.

Uniform deposition of a large amount of AuNPs on the graphene sheets was achieved. It was found that adsorption of RIV was able to adsorb onto the gold surface which in conjunction with GNS improved electron transfer rate and surface area. Other nanoparticles were also investigated along with graphene in electrochemical stripping analysis: Tin nanoparticles (SnNPs) for detection of Pb^{2+}, Cu^{2+} and Hg^{2+} [53], Platinum nanoparticles (PtNPs) for metoprolol detection [122] and Silver nanoparticles (AgNPs) for Hg^{2+} detection.

Figure 2.6: A schematic representation of the thymidine functionalized AuNP-rGO biosensor for Hg^{2+} detection [120].

Graphene quantum dots (GQDs), a derivative of the carbon dot family, have recently showed great interest in electrochemical sensing owing to their large specific surface area, hypotoxicity and biocompatibility. In addition, the small size was found to accelerate electron transfer over bulk graphenes. Three studies have recently been conducted on their use in stripping analysis. Huang *et al*. [108] reported the detection of levofloxacin at a poly(o-aminophenol) and GQD modified GCE. The GQDs adsorbed on the polymer by π-stacking interactions and enhanced electronic transfer efficiency associated with the sensor. The incorporation of GQDs further enhanced the active surface area of the electrode by 1.3 times over its polymer counterpart. Another study reported the use of GQDs in conjunction with polyaniline by an electropolymerization technique for the stripping voltammetric reduction of Cr^{6+} using an automated system [123]. The PANI-GQD showed improved sensitivity to the detection of Cr^{6+}. Coagulation/aggregation of the GQDs at increased volumes affects the surface area. A steep dependence on GQD concentration was not established. Both studies made use of a polymer support for the GQDs. Ting *et al*. [124] however,

reported the functionalization of cysteamine-capped gold nanoparticles (AuNPs) with GQDs for the detection of Hg^{2+} and Cu^{2+}. To the best of our knowledge this was the first such work reported for electrochemical stripping analysis. Reactions between the carboxyl groups on GQDs with amine groups on capped AuNPs is responsible for the functionalization of the material. Weak signals are observed for metal cation detection at GQD electrodes due to insufficient binding of the material onto the working electrode. In the presence of the composite material, adsorption of the metal ions onto the electrode and enhanced electron transfer and increased active surface area associated the functionalized material is achieved.

2.5. Conclusions and Future Work

Since its discovery, a wide range of approaches have been suggested for the production of graphene-based materials. Simple designs, scalability, expensive instrumentation, yield, etc. are all important variables in the choice of technique. Arguably the most notable feature in selection of a preparation technique is the tenability of the intrinsic properties associated with the various techniques. While, micromechanical exfoliation approaches remain the most useful technique for production of pristine graphene sheets, low yield is a distinct limiting factor in its use. Chemical synthesis approaches remain the most widely used in the research fields owing to distinct defects and therefore unique properties. While a large number of studies have been employed for the use of graphene-based materials in electrochemical approaches, only a few characteristic electrochemical properties of graphenes are exploited. Wide potential windows, improved electron transfer rates, improved surface area and synergistic effects of graphene materials have been utilized.

A growing shift to simplify electrode designs in electrochemical sensing has been observed in recent times. Consequently, the drive to create sensors based on GO, RGO or just graphene has been shown. It was found that not too many works have been demonstrated on the use of simple graphene-derivatives in stripping voltammetric sensing to take advantage of the high electronic conductivity and large surface-area-to-volume ratio or synergistic effects of oxygen containing functional groups without the additional of other materials. Most works have been based on composite formation with biomaterials, polymers, ionic liquids, nanoparticles etc. to create dual functionality at the electrode surface. Synergistic effects in metal adsorption of graphenes are

further achieved. Further studies may thus be conducted to more accurately demonstrate the intrinsic effects of graphenes (GO, RGO) in the stripping voltammetric detection. Techniques for electrode modification with graphene materials have relied mainly on simple drop casting techniques to date. However, a rise in the number of studies performed based on alternative fabrication techniques has significantly improved. Electrochemical reduction, deposition, screen-printing and inkjet printing techniques have all been investigated and offer promising potentials in stripping voltammetric detection. These techniques offer a more controllable approach to amount and concentration of graphene-based materials at the electrode surface, adjust graphene film thickness and as a result control electron transfer through the modification and further allow for simultaneous deposition of active materials. Further, the ability to create disposable, reproducible approaches and scalability is possible. Functionalization of graphene-derivatives in stripping voltammetric detection has shown to be an exciting approach. Here, inclusion of active sites at the electrode surface for particular detection was achieved. Covalent and non-covalent approaches for functionalization of materials onto graphene sheets dominate the synthesis approaches. This opens the door to a wide range of possibilities and complexes to be formed for graphene materials. Complexation with analyte as well as electrochemical properties of graphene are demonstrated. Most work demonstrated for electrochemical stripping analysis at graphene-based electrodes have centered on the detection of organic materials, however a growing number of studies have been introduced for detection of metal ions. The organic approaches have relied on anodic, cathodic and adsorptive stripping voltammetric approaches while metal analysis was limited to anodic stripping voltammetry where catalytic reduction of metal ions in a preconcentration step was employed. An interesting finding is that no work has been conducted on the use of graphene based materials towards the adsorptive stripping voltammetric detection of metal ions. Solid, conventional substrates have also been highlighted in all the works investigated in this study, however no significant work on alternative substrate materials suggested. Further, the use of graphene materials in paper sensing for stripping voltammetric applications has not yet been introduced.

All of the above findings lead to a conclusion that great potential exists for the use of graphene in electrochemical stripping analysis. Further works on direct fabrication of unique devices and electrode systems may show a dramatic rise in production in part due to improved printing technologies. In addition, low-cost substrates may be looked into. A dramatic rise in

complexation based detection should also be investigated for analytes unable to easily undergo electrolytic redox processes.

References

[1] A. Ambrosi, C.K. Chua, A. Bonanni, M. Pumera, Electrochemistry of graphene and related materials, Chem. Rev. (2014). doi:10.1021/cr500023c.

[2] J. Wang, Stripping analysis at bismuth electrodes: A review, Electroanalysis. 17 (2005) 1341–1346. doi:10.1002/elan.200403270.

[3] Definition of Allotropy of Carbon, (n.d.). http://www.icoachmath.com/chemistry/definition-of-allotropy-of-carbon.html# (accessed April 28, 2017).

[4] K.S. Noveslov, A.K. Geim, S.V. Morozov, D. Jiang, Y. Zhang, S.V. Dubonos, I.V. Grigorieva, A.A. Firsov, Electric Field Effect in Atomically Thin Carbon Films, Science (80-.). 306 (2004) 666–669.

[5] B. Jayasena, S. Subbiah, A novel mechanical cleavage method for synthesizing few-layer graphenes., Nanoscale Res. Lett. 6 (2011) 95. doi:10.1186/1556-276X-6-95.

[6] M. Yi, Z. Shen, A review on mechanical exfoliation for the scalable production of graphene, J. Mater. Chem. A. 3 (2015) 11700–11715. doi:10.1039/C5TA00252D.

[7] T. Lin, Y. Tang, Y. Wang, H. Bi, Z. Liu, F. Huang, X. Xie, M. Jiang, G.L.C. Paulus, N.F. Reuel, Q.H. Wang, D. Blankschtein, M.S. Strano, Scotch-tape-like exfoliation of graphite assisted with elemental sulfur and graphene–sulfur composites for high-performance lithium-sulfur batteries, Energy Environ. Sci. 6 (2013) 1283. doi:10.1039/c3ee24324a.

[8] J. Chen, M. Duan, G. Chen, H.T. Jung, M. Lazzeri, F. Mauri, S. Piscanec, D. Jiang, K.S. Novoselov, S. Roth, A.K. Geim, J.N. Coleman, G. Duesberg, S. Krishnamurthy, R. Goodhue, J. Hutchison, V. Scardaci, A.C. Ferrari, J.N. Coleman, Continuous mechanical exfoliation of graphene sheets via three-roll mill, J. Mater. Chem. 22 (2012) 19625. doi:10.1039/c2jm33740a.

[9] A. Ciesielski, P. Samorì, Grapheneviasonication assisted liquid-phase exfoliation, Chem. Soc. Rev. 43 (2014) 381–398. doi:10.1039/C3CS60217F.

[10] Y. Hernandez, V. Nicolosi, M. Lotya, F.M. Blighe, Z. Sun, S. De, I.T. McGovern, B. Holland, M. Byrne, Y.K. Gun'Ko, J.J. Boland, P. Niraj, G. Duesberg, S. Krishnamurthy, R. Goodhue, J. Hutchison, V. Scardaci, A.C. Ferrari, J.N. Coleman, High-yield production of graphene by liquid-phase exfoliation of graphite., Nat. Nanotechnol. 3 (2008) 563–568. doi:10.1038/nnano.2008.215.

[11] J.N. Coleman, Liquid exfoliation of defect-free graphene, Acc. Chem. Res. 46 (2013) 14–22. doi:10.1021/ar300009f.

[12] M. Lotya, Y. Hernandez, P.J. King, R.J. Smith, V. Nicolosi, L.S. Karlsson, M. Blighe, S. De, Z. Wang, I.T. Mcgovern, G.S. Duesberg, J.N. Coleman, F.M. Blighe, Liquid Phase Production of Graphene by Exfoliation of Graphite in Surfactant / Water Solutions Liquid Phase Production of Graphene by Exfoliation of Graphite in Surfactant / Water Solutions, (2009) 3611–3620. doi:10.1021/ja807449u.

[13] M. Lotya, P.J. King, U. Khan, S. De, J.N. Coleman, High-concentration, surfactant-stabilized graphene dispersions, ACS Nano. 4 (2010) 3155–3162. doi:10.1021/nn1005304.

[14] A. Schlierf, H. Yang, E. Gebremedhn, E. Treossi, L. Ortolani, L. Chen, A. Minoia, V. Morandi, P. Samorì, C. Casiraghi, D. Beljonne, V. Palermo, Nanoscale insight into the exfoliation mechanism of graphene with organic dyes: effect of charge, dipole and molecular structure, Nanoscale. 5 (2013) 4205. doi:10.1039/c3nr00258f.

[15] A.B. Bourlinos, V. Georgakilas, R. Zboril, T.A. Steriotis, A.K. Stubos, Liquid - Phase Exfoliation of Graphite Towards Solubilized Graphenes * *, (n.d.). doi:10.1002/smll.200900242.

[16] R. Singh, D. Kumar, C.C. Tripathi, Concentration Enhancement of Liquid Phase Exfoliated Graphene with Addition of Organic Salts, Procedia Comput. Sci. 70 (2015) 565–571. doi:10.1016/j.procs.2015.10.024.

[17] L. Guardia, M.J. Fernández-Merino, J.I. Paredes, P. Solís-Fernández, S. Villar-Rodil, A. Martínez-Alonso, J.M.D. Tascón, High-throughput production of pristine graphene in an aqueous dispersion assisted by non-ionic surfactants, Carbon N. Y. 49 (2011) 1653–1662. doi:10.1016/j.carbon.2010.12.049.

[18] X. Wang, P.F. Fulvio, G.A. Baker, G.M. Veith, R.R. Unocic, S.M. Mahurin, M. Chi, S. Dai, K.S. Novoselov, S. Roth, A.K. Geim, J.N. Coleman, G. Duesberg, S. Krishnamurthy, R. Goodhue, J. Hutchison, V. Scardaci, A.C. Ferrari, J.N. Coleman, Direct exfoliation of natural graphite into micrometre size few layers graphene sheets using ionic liquids, Chem. Commun. 46 (2010) 4487. doi:10.1039/c0cc00799d.

[19] D. Nuvoli, L. Valentini, V. Alzari, S. Scognamillo, S.B. Bon, M. Piccinini, J. Illescas, A. Mariani, A.C. Ferrari, S. Roth, A.K. Geim, Y. Talmon, J.M. Tour, M. Pasquali, R. Goodhue, J.H. Hutchison, V. Scardaci, A.C. Ferrari, J.N. Coleman, High concentration few-layer graphene sheets obtained by liquid phase exfoliation of graphite in ionic liquid, J. Mater. Chem. 21 (2011) 3428–3431. doi:10.1039/C0JM02461A.

[20] M. Matsumoto, Y. Saito, C. Park, T. Fukushima, T. Aida, Ultrahigh-throughput exfoliation of graphite into pristine "single-layer" graphene using microwaves and molecularly engineered ionic liquids, Nat. Chem. 7 (2015) 730–736. doi:10.1038/nchem.2315.

[21] A.T. Najafabadi, E. Gyenge, High-yield graphene production by electrochemical exfoliation of graphite: Novel ionic liquid (IL)-acetonitrile electrolyte with low IL content, Carbon N. Y. 71 (2014) 58–69. doi:10.1016/j.carbon.2014.01.012.

[22] P. May, U. Khan, J.M. Hughes, J.N. Coleman, Role of Solubility Parameters in Understanding the Steric Stabilization of Exfoliated Two-Dimensional Nanosheets by Adsorbed Polymers, (n.d.). doi:10.1021/jp302365w.

[23] A.B. Bourlinos, V. Georgakilas, R. Zboril, T.A. Steriotis, A.K. Stubos, C. Trapalis, P. Sheng, Aqueous-phase exfoliation of graphite in the presence of polyvinylpyrrolidone for the production of water-soluble graphenes, Solid State Commun. 149 (2009) 2172–2176. doi:10.1016/j.ssc.2009.09.018.

[24] A.S. Wajid, S. Das, F. Irin, H.S.T. Ahmed, J.L. Shelburne, D. Parviz, R.J. Fullerton, A.F. Jankowski, R.C. Hedden, M.J. Green, Polymer-stabilized graphene dispersions at high concentrations in organic solvents for composite production, Carbon N. Y. 50 (2012) 526–534. doi:10.1016/j.carbon.2011.09.008.

[25] P. Li, S.H. Bae, Q.Y. Zan, N.H. Kim, J.H. Lee, One-Step Process for the Exfoliation and

Surface Modification of Graphene by Electrochemical Method, Adv. Mater. Res. 123–125 (2010) 743–746. doi:10.4028/www.scientific.net/AMR.123-125.743.

[26] Y.L. Zhong, T.M. Swager, Enhanced Electrochemical Expansion of Graphite for in Situ Electrochemical Functionalization, (n.d.). doi:10.1021/ja309023f.

[27] K. Zhou, Y. Shi, S. Jiang, L. Song, Y. Hu, Z. Gui, A facile liquid phase exfoliation method to prepare graphene sheets with different sizes expandable graphite, Mater. Res. Bull. 48 (2013) 2985–2992. doi:10.1016/j.materresbull.2013.04.016.

[28] M. Qian, Y.S. Zhou, Y. Gao, T. Feng, Z. Sun, L. Jiang, Y.F. Lu, Production of few-layer graphene through liquid-phase pulsed laser exfoliation of highly ordered pyrolytic graphite, Appl. Surf. Sci. 258 (2012) 9092–9095. doi:10.1016/j.apsusc.2012.06.006.

[29] I.-Y. Jeon, Y.-R. Shin, G.-J. Sohn, H.-J. Choi, S.-Y. Bae, J. Mahmood, S.-M. Jung, J.-M. Seo, M.-J. Kim, D.W. Chang, L. Dai, J.-B. Baek, Edge-carboxylated graphene nanosheets via ball milling, (n.d.). http://www.pnas.org/content/109/15/5588.full.pdf (accessed March 30, 2017).

[30] W. Zhao, F. Wu, H. Wu, G. Chen, Preparation of Colloidal Dispersions of Graphene Sheets in Organic Solvents by Using Ball Milling, J. Nanomater. 5 (2010). doi:10.1155/2010/528235.

[31] B. Brodie, Sur le poids atomique du graphite, Ann. Chim. Phys. 59 (1860) 466–472.

[32] L. Staudenmaier, Verfahren zur Darstellung der Graphitsäure, Berichte Der Dtsch. Chem. Gesellschaft. 31 (1898) 1481–1487. doi:10.1002/cber.18980310237.

[33] U. Hofmann, E. König, Untersuchungen über Graphitoxyd, Zeitschrift Für Anorg. Und Allg. Chemie. 234 (1937) 311–336. doi:10.1002/zaac.19372340405.

[34] J. William S. Hummers, R.E. Offeman, Preparation of Graphitic Oxide, J. Am. Chem. Soc. 80 (1958) 1339. doi:10.1021/ja01539a017.

[35] D.C. Marcano, D. V. Kosynkin, J.M. Berlin, A. Sinitskii, Z. Sun, A. Slesarev, L.B. Alemany, W. Lu, J.M. Tour, Improved synthesis of graphene oxide, ACS Nano. 4 (2010) 4806–4814. doi:10.1021/nn1006368.

[36] T. Szabó, O. Berkesi, P. Forgó, K. Josepovits, Y. Sanakis, A. Dimitris Petridis, Imre

Dékány, Evolution of Surface Functional Groups in a Series of Progressively Oxidized Graphite Oxides, (2006). doi:10.1021/CM060258+.

[37] W. Cai, R.D. Piner, F.J. Stadermann, S. Park, M.A. Shaibat, Y. Ishii, D. Yang, A. Velamakanni, S.J. An, M. Stoller, J. An, D. Chen, R.S. Ruoff, Synthesis and solid-state NMR structural characterization of 13C-labeled graphite oxide., Science. 321 (2008) 1815–7. doi:10.1126/science.1162369.

[38] G. Jo, M. Choe, S. Lee, W. Park, Y.H. Kahng, T. Lee, The application of graphene as electrodes in electrical and optical devices, Nanotechnology. 23 (2012) 112001. doi:10.1088/0957-4484/23/11/112001.

[39] S. Cinti, F. Arduini, Graphene-based screen-printed electrochemical (bio)sensors and their applications: Efforts and criticisms, Biosens. Bioelectron. 89 (2017) 107–122. doi:10.1016/j.bios.2016.07.005.

[40] Y. Si, E.T. Samulski, Synthesis of water soluble graphene, Nano Lett. 8 (2008) 1679–82. doi:10.1021/nl080604h.

[41] M.-Q. Xu, J.-F. Wu, G.-C. Zhao, Direct Electrochemistry of Hemoglobin at a Graphene Gold Nanoparticle Composite Film for Nitric Oxide Biosensing, Sensors. 13 (2013) 7492–7504. doi:10.3390/s130607492.

[42] P. Deng, Z. Xu, R. Zeng, C. Ding, Electrochemical behavior and voltammetric determination of vanillin based on an acetylene black paste electrode modified with graphene-polyvinylpyrrolidone composite film, Food Chem. 180 (2015) 156–163. doi:10.1016/j.foodchem.2015.02.035.

[43] L. Huang, Y. Huang, J. Liang, X. Wan, Y. Chen, Graphene-based conducting inks for direct inkjet printing of flexible conductive patterns and their applications in electric circuits and chemical sensors, Nano Res. 4 (2011) 675–684. doi:10.1007/s12274-011-0123-z.

[44] H. Bai, S. Wang, P. Liu, C. Xiong, K. Zhang, Q. Cao, Electrochemical sensor based on in situ polymerized ion-imprinted membranes at graphene modified electrode for palladium determination, J. Electroanal. Chem. 771 (2016) 29–36. doi:10.1016/j.jelechem.2016.04.013.

[45] B.B. Prasad, R. Singh, A. Kumar, Development of imprinted polyneutral red / electrochemically reduced graphene oxide composite for ultra-trace sensing of 6-thioguanine, Carbon N. Y. 102 (2016) 86–96. doi:10.1016/j.carbon.2016.02.031.

[46] W. Gao, C. Ran, M. Wang, L. Li, Z. Sun, X. Yao, I.T.K. Joo, T.H. Lau, Z.L. Dong, Z. Chen, J.P. Wang, M.H. Whangbo, The role of reduction extent of graphene oxide in the photocatalytic performance of Ag/AgX (X = Cl, Br)/rGO composites and the pseudo-second-order kinetics reaction nature of the Ag/AgBr system, Phys. Chem. Chem. Phys. 18 (2016) 18219–18226. doi:10.1039/C6CP03110B.

[47] L. Shao, J. Li, Y. Zhang, S. Gong, H. Zhang, Y. Wang, S.H. Chan, J. Zhao, S. Yang, S.J. Ding, D.W. Zhang, W.A. de Heer, P.E. Sheehan, E. Riedo, The effect of the reduction extent on the performance of graphene/poly(vinyl alcohol) composites, J. Mater. Chem. A. 2 (2014) 14173. doi:10.1039/C4TA02833C.

[48] V. León, A.M. Rodriguez, P. Prieto, M. Prato, E. Vázquez, Exfoliation of Graphite with Triazine Derivatives under Ball-Milling Conditions: Preparation of Few-Layer Graphene *via* Selective Noncovalent Interactions, ACS Nano. 8 (2014) 563–571. doi:10.1021/nn405148t.

[49] B. Pollard, Growing Graphene via Chemical Vapor Deposition, Ph. D. Thesis. (2011) 1–47. http://scholar.google.com/scholar?hl=en&btnG=Search&q=intitle:Growing+Graphene+via+Chemical+Vapor+Deposition#9.

[50] J.M. Malho, P. Laaksonen, A. Walther, O. Ikkala, M.B. Linder, Facile method for stiff, tough, and strong nanocomposites by direct exfoliation of multilayered graphene into native nanocellulose matrix, Biomacromolecules. 13 (2012) 1093–1099. doi:10.1021/bm2018189.

[51] M. Allen, Honeycomb carbon -- A study of graphene, (2009) 184. http://proquest.umi.com/pqdweb?did=2056360521&Fmt=7&clientId=7961&RQT=309&VName=PQD.

[52] S. Pei, H.M. Cheng, The reduction of graphene oxide, Carbon N. Y. 50 (2012) 3210–3228. doi:10.1016/j.carbon.2011.11.010.

[53] P.M. Lee, Z. Chen, L. Li, E. Liu, Reduced graphene oxide decorated with tin nanoparticles through electrodeposition for simultaneous determination of trace heavy metals, Electrochim. Acta. 174 (2015) 207–214. doi:10.1016/j.electacta.2015.05.092.

[54] H. Ma, D. Wu, Z. Cui, Y. Li, Y. Zhang, B. Du, Q. Wei, Graphene-Based Optical and Electrochemical Biosensors: A Review, Anal. Lett. 46 (2013) 1–17. doi:10.1080/00032719.2012.706850.

[55] H. Zhu, Y. Cao, J. Zhang, W. Zhang, Y. Xu, J. Guo, W. Yang, J. Liu, One-step preparation of graphene nanosheets via ball milling of graphite and the application in lithium-ion batteries, J. Mater. Sci. 51 (2016) 3675–3683. doi:10.1007/s10853-015-9655-z.

[56] X. Zuo, S. He, D. Li, C. Peng, Q. Huang, S. Song, C. Fan, Graphene oxide-facilitated electron transfer of metalloproteins at electrode surfaces, Langmuir. 26 (2010) 1936–1939. doi:10.1021/la902496u.

[57] K.S. Kim, Y. Zhao, H. Jang, S.Y. Lee, J.M. Kim, K.S. Kim, J.-H. Ahn, P. Kim, J.-Y. Choi, B.H. Hong, Large-scale pattern growth of graphene films for stretchable transparent electrodes., Nature. 457 (2009) 706–710. doi:10.1038/nature07719.

[58] L.Y. Xu, G.Y. Yang, H.Y. Jing, J. Wei, Y.D. Han, Ag-graphene hybrid conductive ink for writing electronics., Nanotechnology. 25 (2014) 55201. doi:10.1088/0957-4484/25/5/055201.

[59] P. Avouris, Graphene: Electronic and Photonic Properties and Devices, Nano Lett. 10 (2010) 4285–4294. doi:10.1021/nl102824h.

[60] J. Chen, Z. Bo, G. Lu, The Properties of Vertically-Oriented Graphene, in: Vertically-Oriented Graphene, Springer International Publishing, Cham, 2015: pp. 11–18. doi:10.1007/978-3-319-15302-5_2.

[61] O. V. Roussak, H.D. Gesser, Applied chemistry : a textbook for engineers and technologists, Springer, 2012. https://books.google.co.za/books/about/Applied_Chemistry.html?id=L4QH3_bqWJ4C&source=kp_cover&redir_esc=y (accessed April 29, 2017).

[62] a K. Geim, K.S. Novoselov, The rise of graphene., Nat. Mater. 6 (2007) 183–191.

doi:10.1038/nmat1849.

[63] K.I. Bolotin, K.J. Sikes, Z. Jiang, M. Klima, G. Fudenberg, J. Hone, P. Kim, H.L. Stormer, Ultrahigh electron mobility in suspended graphene, Solid State Commun. 146 (2008) 351–355. doi:10.1016/j.ssc.2008.02.024.

[64] S. V. Morozov, K.S. Novoselov, M.I. Katsnelson, F. Schedin, D.C. Elias, J.A. Jaszczak, A.K. Geim, Giant intrinsic carrier mobilities in graphene and its bilayer, Phys. Rev. Lett. 100 (2008) 11–14. doi:10.1103/PhysRevLett.100.016602.

[65] A.A. Balandin, S. Ghosh, W. Bao, I. Calizo, D. Teweldebrhan, F. Miao, C.N. Lau, Superior Thermal Conductivity of Single-Layer Graphene, Nano Lett. 8 (2008) 902–907. doi:10.1021/nl0731872.

[66] C. Lee, X. Wei, J.W. Kysar, J. Hone, Measurement of the elastic properties and intrinsic strength of monolayer graphene., Science. 321 (2008) 385–388. doi:10.1126/science.1157996.

[67] W. Bao, F. Miao, Z. Chen, H. Zhang, W. Jang, C. Dames, C.N. Lau, Controlled ripple texturing of suspended graphene and ultrathin graphite membranes, Nat. Nanotechnol. 4 (2009) 562–566. doi:10.1038/nnano.2009.191.

[68] K.R. Ratinac, W. Yang, J.J. Gooding, P. Thordarson, F. Braet, Graphene and related materials in electrochemical sensing, Electroanalysis. 23 (2011) 803–826. doi:10.1002/elan.201000545.

[69] D. Chen, H. Feng, J. Li, Graphene oxide: Preparation, functionalization, and electrochemical applications, Chem. Rev. 112 (2012) 6027–6053. doi:10.1021/cr300115g.

[70] X. Wen, P. Yu, Y.-R. Toh, Y.-C. Lee, K.-Y. Huang, S. Huang, S. Shrestha, G. Conibeer, J. Tang, B. Yang, H.-B. Sun, Ultrafast electron transfer in the nanocomposite of the graphene oxide–Au nanocluster with graphene oxide as a donor, J. Mater. Chem. C. 2 (2014) 3826. doi:10.1039/c3tc32376e.

[71] W.J. Basirun, M. Sookhakian, S. Baradaran, Z. Endut, M.R. Mahmoudian, M. Ebadi, R. Yousefi, H. Ghadimi, S. Ahmed, Graphene oxide electrocatalyst on MnO 2 air cathode as an efficient electron pump for enhanced oxygen reduction in alkaline solution, (n.d.). doi:10.1038/srep09108.

[72] J. Xu, G. Dong, C. Jin, M. Huang, L. Guan, Sulfur and Nitrogen Co-Doped, Few-Layered Graphene Oxide as a Highly Efficient Electrocatalyst for the Oxygen-Reduction Reaction, ChemSusChem. 6 (2013) 493–499. doi:10.1002/cssc.201200564.

[73] M. Zhou, Y. Zhai, S. Dong, Electrochemical Sensing and Biosensing Platform Based on Chemically Reduced Graphene Oxide, Chem. Rev. Chem. Commun. Electrochem. Commun. Anal. Chem. Anal. Chem. J. Anal. Chem. I. V.; Firsov, A. A. Sci. Serv. R. F. Sci. J. Sci. Anal. Chem. 108 (2008) 2646–2687. doi:10.1021/ac900136z.

[74] K. Pokpas, S. Zbeda, N. Jahed, N. Mohamed, P.G. Baker, E.I. Iwuoha, E.I.I. Sensorlab, Electrochemically reduced graphene oxide pencil-graphite in situ plated bismuth-film electrode for the determination of trace metals by anodic stripping voltammetry, Int. J. Electrochem. Sci. 9 (2014) 736–759. www.electrochemsci.org (accessed April 3, 2017).

[75] M. Pumera, A. Ambrosi, A. Bonanni, E. Lay, K. Chng, H.L. Poh, E.L.K. Chng, H.L. Poh, Graphene for electrochemical sensing and biosensing, TrAC - Trends Anal. Chem. 29 (2010) 954–965. doi:10.1016/j.trac.2010.05.011.

[76] M.S. Goh, M. Pumera, The Electrochemical Response of Graphene Sheets is Independent of the Number of Layers from a Single Graphene Sheet to Multilayer Stacked Graphene Platelets, Chem. - An Asian J. 5 (2010) 2355–2357. doi:10.1002/asia.201000437.

[77] M. Ej Velick, D.F. Bradley, A.J. Cooper, E.W. Hill, I.A. Kinloch, A. Mishchenko, K.S. Novoselov, H. V Patten, P.S. Toth, A.T. Valota, S.D. Worrall, R.A.W. Dryfe, Electron Transfer Kinetics on Mono-and Multilayer Graphene, 8 (1008). doi:10.1021/nn504298r.

[78] D.A.C. Brownson, S.A. Varey, F. Hussain, S.J. Haigh, C.E. Banks, Electrochemical properties of CVD grown pristine graphene: monolayer-vs. quasi-graphene, (n.d.). doi:10.1039/c3nr05643k.

[79] D.A.C. Brownson, C.E. Banks, Graphene electrochemistry: an overview of potential applications., Analyst. 135 (2010) 2768–2778. doi:10.1039/c0an00590h.

[80] Y. Shao, J. Wang, H. Wu, J. Liu, I.A. Aksay, Y. Lin, Graphene based electrochemical sensors and biosensors: A review, Electroanalysis. 22 (2010) 1027–1036. doi:10.1002/elan.200900571.

[81] S. Wu, Q. He, C. Tan, Y. Wang, H. Zhang, Graphene - Based Electrochemical Sensors,

(n.d.). doi:10.1002/smll.201202896.

[82] F. Ban, S. Majid, Graphene oxide and its electrochemical performance, Inter. J.Electrochem. Sci. 7 (2012) 4345–4351.

[83] M. Pumera, Electrochemistry of graphene, graphene oxide and other graphenoids: Review, Electrochem. Commun. 36 (2013) 14–18. doi:10.1016/j.elecom.2013.08.028.

[84] P. Ruengpirasiri, E. Punrat, O. Chailapakul, S. Chuanuwatanakul, Graphene Oxide-Modified Electrode Coated with *in-situ* Antimony Film for the Simultaneous Determination of Heavy Metals by Sequential Injection-Anodic Stripping Voltammetry, Electroanalysis. (2016) 1–10. doi:10.1002/elan.201600568.

[85] S.E. Kablan, N. Özaltın, Investigation of electrochemical behaviour of cefuroxime axetil using hanging mercury drop electrode and graphene oxide modified glassy carbon electrode, J. Electroanal. Chem. 785 (2017) 144–151. doi:10.1016/j.jelechem.2016.12.030.

[86] S. Smarzewska, J. Pokora, A. Leniart, N. Festinger, W. Ciesielski, Carbon Paste Electrodes Modified with Graphene Oxides - Comparative Electrochemical Studies of Thioguanine, Electroanalysis. (2016) n/a-n/a. doi:10.1002/elan.201501101.

[87] Y. Teng, T. Chen, F. Xu, W. Zhao, W. Liu, Screen-printed Carbon Electrode Modified with Commercial Multilayer Graphene for Lead Detection in Soybean Sauces by Differential Pulse Stripping Voltammetry, Int. J. Electrochem. Sci. 11 (2016) 1907–1917. www.electrochemsci.org (accessed April 3, 2017).

[88] J. Wang, X. Chen, K. Wu, M. Zhang, W. Huang, Highly-sensitive electrochemical sensor for Cd^{2+} and Pb^{2+} based on the synergistic enhancement of exfoliated graphene nanosheets and bismuth, Electroanalysis. (2015) n/a-n/a. doi:10.1002/elan.201500447.

[89] J. Shan, Y. Liu, R. Li, C. Wu, L. Zhu, J. Zhang, Indirect electrochemical determination of ciprofloxacin by anodic stripping voltammetry of Cd(II) on graphene-modified electrode, J. Electroanal. Chem. 738 (2015) 123–129. doi:10.1016/j.jelechem.2014.11.031.

[90] P. Noyrod, O. Chailapakul, W. Wonsawat, S. Chuanuwatanakul, The simultaneous determination of isoproturon and carbendazim pesticides by single drop analysis using a graphene-based electrochemical sensor, J. Electroanal. Chem. 719 (2014) 54–59.

doi:10.1016/j.jelechem.2014.02.001.

[91] M. Sys, S. Zabcikova, L. Cervenka, K. Vytras, Comparison of Adsorptive with Extractive Stripping Voltammetry in Electrochemical Determination of Retinol, Slovak J. Food Sci. 11 (2017) 96–105.

[92] F. Wang, Y. Wu, K. Lu, B. Ye, A sensitive voltammetric sensor for taxifolin based on graphene nanosheets with certain orientation modified glassy carbon electrode, Sensors Actuators, B Chem. 208 (2015) 188–194. doi:10.1016/j.snb.2014.11.008.

[93] N. Akkarachanchainon, P. Rattanawaleedirojn, O. Chailapakul, N. Rodthongkum, Hydrophilic graphene surface prepared by electrochemically reduced micellar graphene oxide as a platform for electrochemical sensor, Talanta. 165 (2017) 692–701. doi:10.1016/j.talanta.2016.12.092.

[94] Z. Wen, X. Niu, L. Yan, Y. Niu, D. Wang, W. Sun, Z. Shi, L. Dong, Nitrogen-doped Graphene Modified Glassy Carbon Electrode for Anodic Stripping Voltammetric Detection of Lead Ion, Int. J. Electrochem. Sci. 11 (2016) 6648–6654. doi:10.20964/2016.08.23.

[95] X. Li, H. Zhao, L. Shi, X. Zhu, M. Lan, Q. Zhang, Z.H. Fan, Electrochemical sensing of nicotine using screen-printed carbon electrodes modi fi ed with nitrogen-doped graphene sheets, JEAC. 784 (2017) 77–84. doi:10.1016/j.jelechem.2016.12.009.

[96] X. Liu, Z. Li, R. Ding, B. Ren, Y. Li, A nanocarbon paste electrode modified with nitrogen-doped graphene for square wave anodic stripping voltammetric determination of trace lead and cadmium, Microchim. Acta. 183 (2016) 709–714. doi:10.1007/s00604-015-1713-3.

[97] L. Magerusan, C. Socaci, M. Coros, F. Pogacean, Electrochemical platform based on nitrogen- doped graphene / chitosan nanocomposite for selective Pb 2 + detection, (n.d.).

[98] S. Chen, R. Ding, X. Ma, L. Xue, X. Lin, X. Fan, Z. Luo, Preparation of highly dispersed reduced graphene oxide modified with carboxymethyl chitosan for highly sensitive detection of trace Cu(II) in water, Polymers (Basel). 8 (2016). doi:10.3390/polym8040078.

[99] W. Zhou, C. Li, C. Sun, X. Yang, Simultaneously determination of trace Cd2+ and Pb2+

based on l-cysteine/graphene modified glassy carbon electrode, Food Chem. 192 (2016) 351–357. doi:10.1016/j.foodchem.2015.07.042.

[100] Y. Cheng, H. Fa, W. Yin, C. Hou, D. Huo, F. Liu, Y. Zhang, C. Chen, A sensitive electrochemical sensor for lead based on gold nanoparticles/nitrogen-doped graphene composites functionalized with l-cysteine-modified electrode, J. Solid State Electrochem. 20 (2016) 327–335. doi:10.1007/s10008-015-3043-0.

[101] M. Lv, X. Wang, J. Li, X. Yang, C. Zhang, J. Yang, H. Hu, Cyclodextrin-reduced graphene oxide hybrid nanosheets for the simultaneous determination of lead(II) and cadmium(II) using square wave anodic stripping voltammetry, Electrochim. Acta. (2013). doi:10.1016/j.electacta.2013.06.099.

[102] F. Zhan, F. Gao, X. Wang, L. Xie, F. Gao, Q. Wang, Determination of lead(II) by adsorptive stripping voltammetry using a glassy carbon electrode modified with β-cyclodextrin and chemically reduced graphene oxide composite, Microchim. Acta. 183 (2016) 1169–1176. doi:10.1007/s00604-016-1754-2.

[103] S. Huang, S. Lu, C. Huang, J. Sheng, W. Su, L. Zhang, Q. Xiao, Sensitive and selective stripping voltammetric determination of copper(II) using a glassy carbon electrode modified with amino-reduced graphene oxide and β-cyclodextrin, Microchim. Acta. 182 (2015) 2529–2539. doi:10.1007/s00604-015-1627-0.

[104] H. Razmi, S.J. Musevi, R. Mohammad-Rezaei, Solid phase extraction of mercury(II) using soluble eggshell membrane protein doped with reduced graphene oxide, and its quantitation by anodic stripping voltammetry, Microchim. Acta. 183 (2016) 555–562. doi:10.1007/s00604-015-1665-7.

[105] N. Ruecha, N. Rodthongkum, D.M. Cate, J. Volckens, O. Chailapakul, C.S. Henry, Sensitive electrochemical sensor using a graphene-polyaniline nanocomposite for simultaneous detection of Zn(II), Cd(II), and Pb(II), Anal. Chim. Acta. 874 (2015) 40–48. doi:10.1016/j.aca.2015.02.064.

[106] T.D. Nguyen, T.T.H. Dang, H. Thai, L.H. Nguyen, D.L. Tran, B. Piro, M.C. Pham, One-step Electrosynthesis of Poly(1,5-diaminonaphthalene)/Graphene Nanocomposite as Platform for Lead Detection in Water, Electroanalysis. (2016) n/a-n/a.

doi:10.1002/elan.201501075.

[107] Y. Wen, X. Liao, C. Deng, G. Liu, Q. Yan, L. Li, X. Wang, Imprinted voltammetric streptomycin sensor based on a glassy carbon electrode modified with electropolymerized poly(pyrrole-3-carboxy acid) and electrochemically reduced graphene oxide, Microchim. Acta. (2017) 1–7. doi:10.1007/s00604-017-2089-3.

[108] J.-Y. Huang, T. Bao, T.-X. Hu, W. Wen, X.-H. Zhang, S.-F. Wang, Voltammetric determination of levofloxacin using a glassy carbon electrode modified with poly(o-aminophenol) and graphene quantum dots, Microchim. Acta. 184 (2017) 127–135. doi:10.1007/s00604-016-1982-5.

[109] A. Özcan, S. Ilkbaş, Poly(pyrrole-3-carboxylic acid)-modified pencil graphite electrode for the determination of serotonin in biological samples by adsorptive stripping voltammetry, Sensors Actuators, B Chem. 215 (2015) 518–524. doi:10.1016/j.snb.2015.03.100.

[110] E. Er, H. Çelikkan, N. Erk, Highly sensitive and selective electrochemical sensor based on high-quality graphene/nafion nanocomposite for voltammetric determination of nebivolol, Sensors Actuators B Chem. 224 (2016) 170–177. doi:10.1016/j.snb.2015.10.028.

[111] S. Lee, S. Bong, J. Ha, M. Kwak, S.K. Park, Y. Piao, Electrochemical deposition of bismuth on activated graphene-nafion composite for anodic stripping voltammetric determination of trace heavy metals, Sensors Actuators, B Chem. 215 (2015) 62–69. doi:10.1016/j.snb.2015.03.032.

[112] K. Pokpas, N. Jahed, O. Tovide, P.G. Baker, E.I. Iwuoha, Nafion-graphene nanocomposite in situ plated bismuth-film electrodes on pencil graphite substrates for the determination of trace heavy metals by anodic stripping voltammetry, Int. J. Electrochem. Sci. 9 (2014) 5092–5115.

[113] S. Wu, X. Huang, Y. Wu, L. Luo, Y. Jin, Q. Li, Differential pulse anodic stripping voltammetry detection of cadmium with nafion-graphene modified bismuth film electrode, Int. J. Electrochem. Sci. 10 (2015) 8255–8262. www.electrochemsci.org (accessed April 3, 2017).

[114] H. Bagheri, A. Afkhami, H. Khoshsafar, M. Rezaei, S.J. Sabounchei, M. Sarlakifar,

Simultaneous electrochemical sensing of thallium, lead and mercury using a novel ionic liquid/graphene modified electrode, Anal. Chim. Acta. 870 (2014) 56–66. doi:10.1016/j.aca.2015.03.004.

[115] G. Zhao, Y. Si, H. Wang, G. Liu, A Portable Electrochemical Detection System based on Graphene/Ionic Liquid Modified Screen-printed Electrode for the Detection of Cadmium in Soil by Square Wave Anodic Stripping Voltammetry, Int. J. Electrochem. Sci. Int. J. Electrochem. Sci. 11 (2016) 54–64. www.electrochemsci.org (accessed April 3, 2017).

[116] R. Liu, C. Lei, T. Zhong, L. Long, Z. Wu, S. Huan, Q. Zhang, A graphene/ionic liquid modified selenium-doped carbon paste electrode for determination of copper and antimony, Anal. Methods. 8 (2016) 1120–1126. doi:10.1039/C5AY02945G.

[117] S. Chaiyo, E. Mehmeti, K. Žagar, W. Siangproh, O. Chailapakul, K. Kalcher, Electrochemical sensors for the simultaneous determination of zinc, cadmium and lead using a Nafion/ionic liquid/graphene composite modified screen-printed carbon electrode, Anal. Chim. Acta. 918 (2016) 26–34. doi:10.1016/j.aca.2016.03.026.

[118] P.M. Lee, Z. Wang, X. Liu, Z. Chen, E. Liu, Glassy carbon electrode modified by graphene-gold nanocomposite coating for detection of trace lead ions in acetate buffer solution, Thin Solid Films. 584 (2015) 85–89. doi:10.1016/j.tsf.2015.03.017.

[119] B.J. Sanghavi, N.S. Gadhari, P.K. Kalambate, S.P. Karna, A.K. Srivastava, Potentiometric stripping analysis of arsenic using a graphene paste electrode modified with a thiacrown ether and gold nanoparticles, Microchim. Acta. 182 (2015) 1473–1481. doi:10.1007/s00604-015-1470-3.

[120] N. Wang, M. Lin, H. Dai, H. Ma, Functionalized gold nanoparticles/reduced graphene oxide nanocomposites for ultrasensitive electrochemical sensing of mercury ions based on thymine-mercury-thymine structure, Biosens. Bioelectron. 79 (2016) 320–326. doi:10.1016/j.bios.2015.12.056.

[121] P.K. Kalambate, M.R. Biradar, S.P. Karna, A.K. Srivastava, Adsorptive stripping differential pulse voltammetry determination of rivastigmine at graphene nanosheet-gold nanoparticle/carbon paste electrode, J. Electroanal. Chem. 757 (2015) 150–158. doi:10.1016/j.jelechem.2015.09.027.

[122] E. Er, H. ??elikkan, N. Erk, A novel electrochemical nano-platform based on graphene/platinum nanoparticles/nafion composites for the electrochemical sensing of metoprolol, Sensors Actuators, B Chem. 238 (2017) 779–787. doi:10.1016/j.snb.2016.07.108.

[123] E. Punrat, C. Maksuk, S. Chuanuwatanakul, W. Wonsawat, O. Chailapakul, Polyaniline/graphene quantum dot-modified screen-printed carbon electrode for the rapid determination of Cr(VI) using stopped-flow analysis coupled with voltammetric technique, Talanta. 150 (2016) 198–205. doi:10.1016/j.talanta.2015.12.016.

[124] S.L. Ting, S.J. Ee, A. Ananthanarayanan, K.C. Leong, P. Chen, Graphene quantum dots functionalized gold nanoparticles for sensitive electrochemical detection of heavy metal ions, Electrochim. Acta. 172 (2015) 7–11. doi:10.1016/j.electacta.2015.01.026.

Chapter 3 :

Metal Analysis at Paper-based Microfluidic Devices:

A review

Abstract

The prevalence of metal contamination in the environment due to increased technological advancement in modern society has resulted in significant overexposure for prolonged periods of time. As a result, bioaccumulation in the organs of the human body have led to detrimental toxicological effects on humans and have been linked to a variety of illnesses. Early and rapid detection methods are therefore being sought out. Microfluidic paper-based analytical devices (μPADs) have been identified as possible solution due to their low cost, sensitivity, disposable nature and simplistic design. In this review, recent progress in paper-based devices for metal analysis will be investigated. The toxicology of common metal contaminants and existing methods of detection are highlighted to provide a basis for the development of paper-based devices. Paper substrate choices and fabrication methods are then identified and discussed. A comparative discussion on recent techniques and methods utilized for metal analysis at paper-based devices including colorimetric, fluorescence and electrochemical methods are identified. A brief discussion on future trends is then provided in light of the findings from this work.

Keywords

Paper-based microfluidics, metal analysis, colorimetric, fluorescence, electrochemistry, nanoparticles

Highlights

- Metal toxicology and existing methods of detection are discussed

- Paper-based sensor fabrication methods are identified
- Recent advances in metal analysis at μPADs are provided

Graphical Abstract

3.1. Introduction

Microfluidic devices have emerged as a leading technology in the field of diagnostics over the last two decades as a direct result of their ability to offer portable, cost efficient and simplistic expertise for use in developing countries where access to skilled labor, expensive instrumentation and reliable infrastructure is lacking [1]. Microfluidics, involves the simple and robust manipulation of small volumes of fluids within micro-sized channels [2] and has garnered attention in biomedical and environmental studies at large. The most common microfluidic devices in use to date are based on glass, silicon or polymer materials, such as polydimethylsiloxane (PDMS) where etching of microfluidic channels is possible. However, expensive and dedicated instrumentation is often required for their fabrication. Paper has since drawn much interest as alternative substrate material in microfluidic devices for a wide range of sensing applications due to its flexibility, versatility, disposable nature and low cost. The first use of paper in analytical applications were derived from their use in paper chromatography [3,4] and have since spread to semi-quantitative detection of glucose [5] and immunoassays like the pregnancy test [6]. Due to

technological advancements, a shift from simple designs to more advanced systems where by fabrication and patterning techniques as well as coupled systems have been created. From these, analytical applications based on colorimetric detection methods have been well established but there remains opportunity for expansion into other detection modes such as fluorescence and electrochemistry [7]. The underlying principle of paper-based microfluidics is the ability to create distinct regions of hydrophilicity and hydrophobicity within the cellulose fiber matrix to control liquid transport in designated areas by capillary forces in place of external pumps [8].

An ever-growing increase in technological advancement in all spheres of life have led to a significant escalation in associated environmental concerns. Pollution in the form of toxic gas, raw sewage, industrial waste, radiation and biological contamination etc. are prevalent as a result. Heavy metal contamination is one of the most damaging forms owing to its non-biodegradable nature. As byproducts from mining and industrial process, leaching from packaging, contamination from lead pipes and coating materials and gaseous pollution, heavy metals enter the environment and affect drinking water in more rural areas. Heavy metals enter the human body by infecting drinking water, food sources and pollution and result in bioaccumulation in organic organisms. As a consequence, detrimental health concerns are demonstrated and show adverse effects on humans and animals alike. A growing need for accurate, sensitive and rapid monitoring of these health concerns are thus required. Many techniques have been suggested for metal determination in laboratories including atomic absorption spectroscopy (AAS), inductively coupled plasma mass spectroscopy (ICP-MS), electrochemical methods, X-ray fluorescence (XRF), etc. Laboratory testing making use of sampling, storage, expensive instrumentation and skilled labor are thus employed and a growing demand for portable, low cost detection methods has arisen. Paper-based microfluidics has gained significant traction to address this problem.

3.2. Toxicology of Heavy Metals

A general understanding of the toxicological effects of metal pollution in the environment is thus required to provide context for the aforementioned mounting demand for clean drinking water. Heavy metals, with density greater than 0.5 g cm^{-3} such as zinc (Zn), cadmium (Cd), lead (Pb), mercury (Hg), nickel (Ni), cobalt (Co) etc. will be addressed in this section. Although significant consequences of Zn deficiency have been well documented over the years due to its

ability to promote efficient metabolism in children and adults alike, toxicological effects associated with overexposure has also been recognized. Nausea, vomiting, epigastric pain, lethargy, and fatigue are all common side effects due to prolonged exposure to zinc at high concentrations [9]. Poisoning by zinc has further been shown to result in damage to the pancreas and causes harmful symptoms in unborn children. The environmental protection agency (EPA) has therefore set a maximum contamination level (MCL) of 5 mg mL^{-1} or 5 ppm for Zn contamination in drinking water [10]. Lead, Pb as a metal has been in existence in human activities for centuries where its use in utensils, decorations, paints, plumbing, fuel and more have been exploited. While exposure in occupational settings has observed a dramatic decline, and blood levels significantly diminished, lead exposure is still of great concern and seen in demolition and cleaning industries [11]. Exposure to lead has shown to lead to hypertension, renal failure [11], inhibition of enzyme function, memory loss, kidney failure, constipation, abortions and miscarriages [12]. In addition, it has led to damage to brain, heart, kidneys, and reproductive organs [13]. The EPA has set a MCL of 15 ppb for Pb contamination. Cadmium is prevalent in soil, water and the atmosphere through heating systems, factory byproducts etc. and is considered a class 1 human carcinogen [14]. It enters the body through dietary sources and inhalation [15]. Prolonged exposure to Cd has been linked to kidney failure and a decrease in bone mineral density [15]. Chronic exposure may result in renal and testicular injury and cancer [16] as well as lesions on the prostate and hypertension [17]. EPA standards of 5 ppb have been set for Cd contamination. Nickel is another metal of great importance in industrial applications, metallurgy and electroplating and alloy production [18]. Skin allergies, lung fibrosis, variable degrees of kidney and cardiovascular system poisoning and stimulation of neoplastic transformation are all possible health effects associated with Ni contamination [19]. Drinking water generally contains Ni concentration less than 10 µg L^{-1} [20]. While Ni contamination in water samples is no longer subject to stringent guidelines by the EPA, a set limit of 0.1 mg L^{-1} or 0.1 ppm has been set by the EPA and world health organization (WHO) [21]. This limit is comparable to the 0.15 mg L^{-1} set by the South African water guidelines (SAWG) [22]. Cobalt forms part of an essential class of pollutant due to its constituency in vitamin B_{12} [23] and may have many advantageous effects [24]. Cobalt overexposure may lead to asthma, skin allergies, thyroid gland problems etc. [24]. Due to the significant side effects associated of heavy metals, methods of early and accurate detection are required.

3.3. Conventional Detection Methods

Detection of metal contamination in laboratory scale applications rely heavily on the use of optical detection methods for analysis. Graphite furnace atomic absorption spectroscopy (GFAAS) is the most commonly used method of detection. Typically, samples are atomized in a furnace at extreme temperatures for short analysis times in order to concentrate the available atoms and as a result improve sensitivity. Analysis is performed by measuring sample absorption at characteristic wavelengths and low limits of detection and small sample volumes are achieved. Small sample volumes comparable to other techniques are compensated however by long light path times. The need for sample injection systems, expensive lamps and low reproducibility are important factors which limit the GFAAS method. In addition to this, large volumes of inert gasses such as argon are utilized in the analysis process, often at large costs. Another important technique for metal detection is the Inductively Coupled Plasma Optical Emission Spectrophotometry (ICP-OES) which offers the benefit of having low detection limits but more notably its applicability to a large number of elements. Here, simultaneous analysis is possible with fewer interferences over other conventional methods. Both these techniques are time consuming, requiring strenuous sample preparation and expensive instrumentation. Further, analysis is limited to optical techniques and also samples in the liquid state. Electrochemical techniques such as stripping voltammetry have made great strides in laboratory research and miniaturized devices however, its use in analytical testing has not yet been exploited. Simultaneous analysis, speciation, low cost and low detection limits are a few of its advantageous properties. This method unlike GFAAS and ICP-OES, makes use of redox processes for detection and can therefore be applied to any material which undergoes redox processes. In other methods, fluorescence based detection has also gained significant traction but is highly dependent on materials which undergo fluorescence.

Table 3.1: A summary of commonly available heavy metal detection techniques

Analysis Method	Advantages	Disadvantages
GFAAS	• Detection limits in the ng L^{-1} • Short atomisation time • Increased sensitivity • Small sample volumes	• Large number of lamps • Automated sample and injection system • Expensive • Wasteful of inert gas
ICP-OES	• Large number of samples • Detection limits in µg L^{-1} • Simultaneous analysis	• Wasteful of inert gas • Expensive • Time consuming
SV	• 4-6 trace metals simultaneously • Detection limits in µg L^{-1} • Inexpensive • Low power demand • Species characterisation	• Intermetallic interferences • Analysis limited to 6 metals simultaneously • Electrode modification often limits choice of analytes

3.4. Paper-based Microfluidic Design

3.4.1. Paper Choice

Since its discovery in the early 2nd century paper has been utilized in a variety of applications. Prepared by simple filtration of suspended fibers, fillers and cellulose polymers to form sheets, paper offers the basis of paper-based microfluidic devices. Owing to voids in the fibrous matrix, penetration of the substrate can be achieved and the properties tuned to the desired application. A wide range of paper types with varying properties are in existence today. Wax, photo, filter, glossy, chromatography, transparency, tissue are all common paper types being used today with varying textures, thicknesses, pore sizes etc. Filter and chromatography paper are most commonly utilized in paper-based microfluidic applications for metal analysis. Its wicking ability is of significant importance. Nitrocellulose membranes, photographic paper, transparency paper and glassy paper have also garnered interest and showed good applicability in paper-based microfluidics.

3.4.2. Patterning of Hydrophobic Barriers

Patterning of paper substrates with hydrophobic materials provides the basis for fabrication of microfluidic channels in paper-based substrates. Paper as substrate material in paper microfluidics was first introduced by the Whiteside's research group for rapid diagnostics [25] using a photoresist and organic polymer. While photolithography is widely used in the fabrication of devices on a large scale [25,26], the technique is characterized by expensive instrumentation and skilled labor. Alternative methods have been developed based on commercial molten paraffin (PF) wax and hydrophobic polymethylsiloxane (PDMS) to alleviate costs and time required in fabrication steps. Wax printing using Xerox wax printers have made tremendous strides in the field of paper-based microfluidics due to its ability to easily pattern a wide range of patterns with little modification. However, this technique still makes use of designated instrumentation. Simpler methods have been developed. These techniques include: crayon or wax screen printing [26–28], one-step plotting using permanent markers [29], wax-dipping relying on a magnetic field [30] and vinyl templates, contact printing using rubber [31] and metallic [32,33] stamps, soldering iron, Parafilm pressing [34], embossing and simple cut-and-stick methods [35,36]. Yamada *et al.* [37] made use of a conventional EPSON inkjet printing technique for the fabrication of a paper-based analytical device. Printing of a UV curable ink based on octadecyl acrylate and 1,10- decanediol diacrylate resulted in hydrophobic barriers patterned directly on paper substrates.

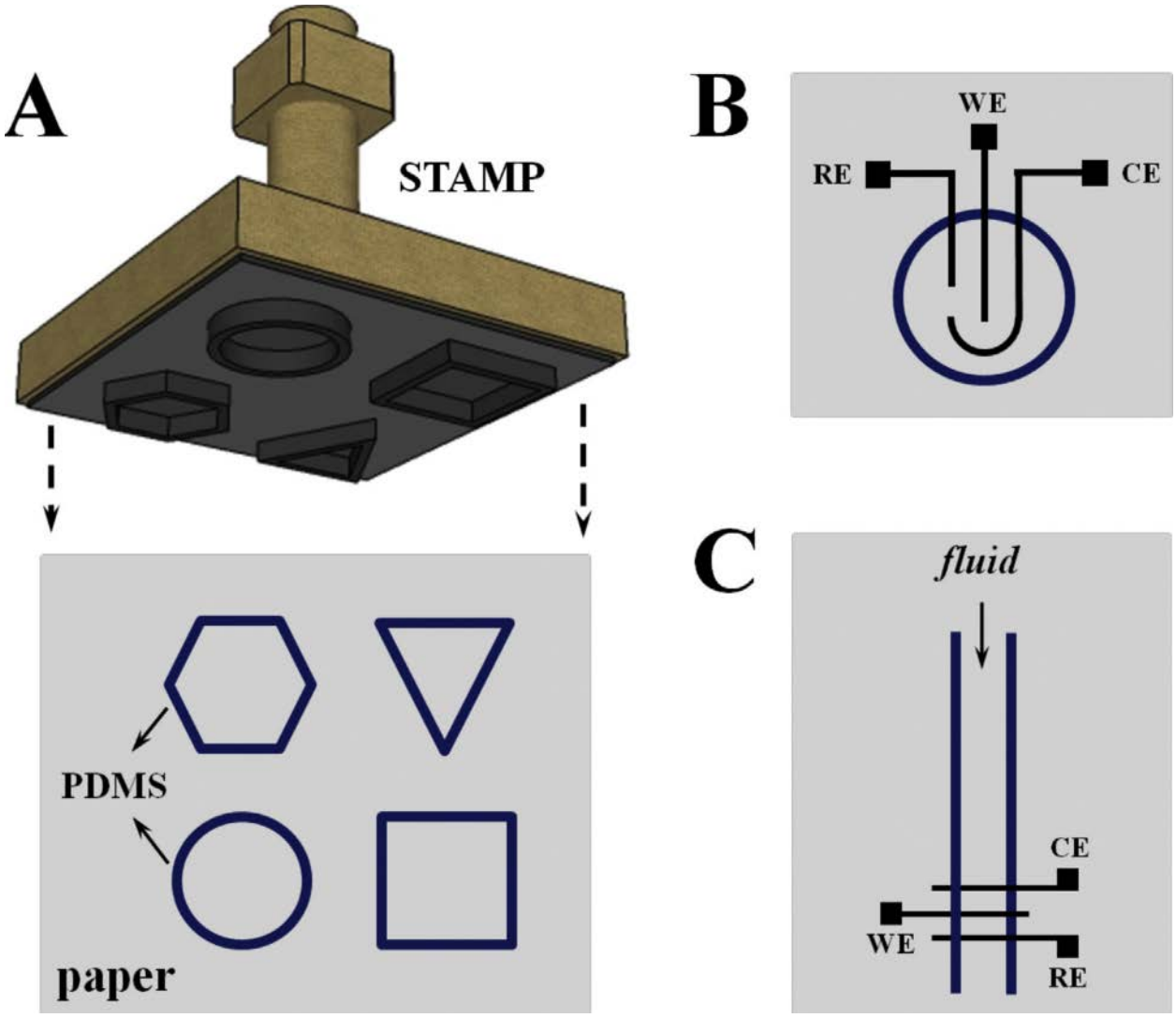

Figure 3.1: (a) Schematic representation of the contact-printing method for fabricating mPADs with PDMS as hydrophobic barriers. (b) Paper-based electrochemical device (PED) with pencil-drawn electrodes utilized in cyclic voltammetry experiments. (c) PED with fluidic channel with pencil-drawn electrodes utilized in flow injection analysis with amperometric detection [31].

3.4.3. Printing Techniques

Patterning of paper devices with integrated electrode systems is also of great importance in the development of paper-based sensors with integrated sensing capabilities. Printing techniques and techniques relying of the use of a photoresist are common place in these fabrication steps. Screen printing technology is the most useful in creating low-cost and easily modified three electrode systems. Dungchai *et al.* [38], Kit-Anan *et al.* [39] and Rattanarat *et al.* [40] have all

made use of a 'homemade' screen printing approach. Inkjet printing on paper substrates has also been deemed as an effective and efficient method of patterning paper substrates due to low cost, speed, little spreading and accurate patterning [41–44]. Smith *et al.* [45] made use of a Fujifilm Dimatix inkjet printer for the fabrication of a Ag-nanoparticle three-electrode system on photographic paper. The printed paper-device was then applied to the stripping voltammetric detection of heavy metals following modification with an onion-like bismuth ink. Dossi *et al.* [46] introduced a hand-drawn patterning technique based on pencil graphite to create three-electrode systems. The system was applied towards the detection of lactoferrin. These methods all provide accurate and precise patterning of the paper substrates with little to no lateral spreading. However, these techniques are costly due to the need for expensive instrumentation and often large sample volumes.

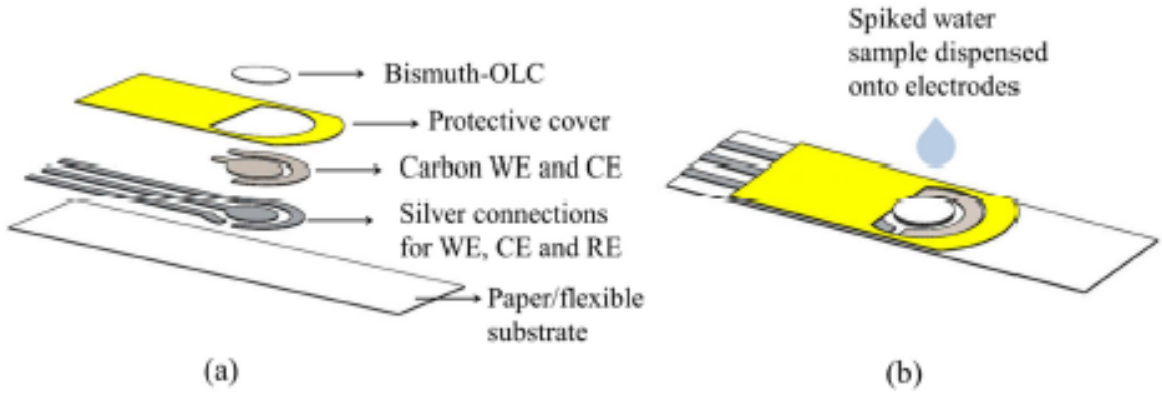

Figure 3.2: Conceptual design of the multi-layer paper-based electrochemical sensor showing (a) the various materials and layers and (b) the complete sensor prepared by inkjet printing in the work by Smith *et al*. [45].

3.4.4. Basic Theory

The movement of water within solid or porous materials is complex and may be explained by modeling of different mechanisms, including molecular diffusion due to a concentration gradient, liquid movement due to capillary flow, liquid movement due to gravity, vapor diffusion and surface diffusion [47]. To accurately describe the flow of motion of water in porous medium such as paper a mechanism of its permeation is first required. Fluid penetration in the paper substrate is controlled by capillary driven flow in a simple wicking process. Wicking is the

transport of liquid through a porous media in the absence of external pressure [48]. The driving pressure of water permeation is governed by the Young-Laplace equation (*3.1*), describing the capillary pressure differences (ΔP) across the interface between water and air within the porous structure due to surface tension. When adhesion is greater than cohesion motion occurs along the porous wall.

$$\Delta P = \frac{2 \cdot \gamma \cdot cos\theta}{R} \qquad \textit{(Equation 3.1)}$$

Where, γ is the surface tension, θ is the contact angle of the liquid with the material and R is the mean pore radius. Acting in opposition to the capillary pressure is the viscous drag, based on the viscosity of the fluid, wettability of the substrate and geometry of the pores [48]. This effect of the capillary pressure is to produce fluid movement in the porous medium governed by Darcy's Law [8].

$$\frac{Q}{A} = \upsilon = \frac{K \cdot \Delta P}{\mu \cdot L} \qquad \textit{(Equation 3.2)}$$

Where, υ is the fluid velocity, κ is the permeability of the porous medium, ΔP is the pressure difference over the length L of the liquid-filled region and μ is the viscosity. The common unit of permeability is the darcy which is defined as the permeability such that one cubic centimeter of fluid, viscosity of one centipoise, flows one centimeter through one square centimeter of area in one second, when the pressure gradient is 1 atm cm^{-1}. A more complete definition of fluid permeation in paper substrates at negligible polymer swelling can thus be given by the Lucas-Washburn equation:

$$TLV = \varepsilon \sqrt{\frac{R \cdot \gamma \cdot cos\theta \cdot t}{2 \cdot \mu}} \qquad (\textit{Equation 3.3})$$

Where, TLV is the total liquid volume absorbed per unit area, ε is the void fraction, R is pore radius, γ is fluid surface tension, θ is the contact angle established between the liquid and the inner

wall of the pore, t is penetrating time and μ is fluid viscosity. It predicts that flow velocity diminishes with the increase of time and provides a model of a rectangular strip.

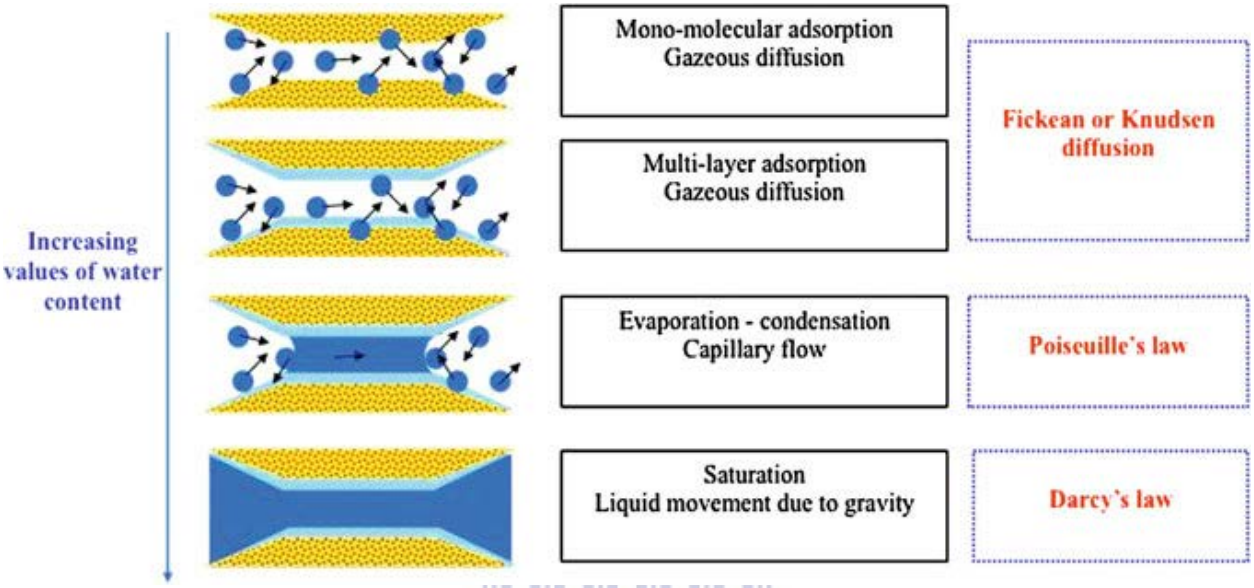

Figure 3.3: Schematic presentation of the mechanisms of water transport in a solid contributing to the overall water movement [47].

3.5. Quantitative Analytical Metal Analysis

Sensing of heavy metals at paper-based microfluidic sensors alleviates the cost associated with traditional modes of detection while offering simplistic, scalable and portable means. However, paper merely offers the substrate material required for these applications but does not present the analytical method of detection. As such, the addition of transducers such as electrochemical methods are required [3]. Additional reagents, electrolytes, materials and instrumentation is therefore required. Colorimetric, fluorescence, electro- and chemiluminescence, electrochemical and hybrid detection methods have all been investigated. While these fields have been expanded for a range of analytes, metal analysis at μPADs is still quite new [8].

3.5.1. Colorimetric Detection

In light of developing of simplistic devices without the need for expensive instrumentation and skilled labor, the simplest method for metal detection is colorimetric detection. Interaction of the metal analyte with an enzyme or chemical results in a color change which is easily observable

by the human eye [25]. These techniques provide a simple means of identifying the presence of a certain analyte or the semi-quantitative analysis. A bulk of the work performed on metal analysis at paper-based sensors rely on colorimetric detection. Chaiyo *et al.* [49] proposed a method for the determination of Cu^{2+} in a paper-based sensor based on the catalytic etching of silver nanoplates (AgNPl) by thiosulfate (S_2O_3) in the presence of Cu^{2+}. Reaction zones were modified with S_2O_3/CTAB/AgNPl prior to analysis. A color change from violet-red to colorless with increasing Cu^{2+}. After reduction, the S_2O_3/CTAB/AgNPl would be oxidized and etched into solution. A semi-quantitative analysis could be achieved by digitizing the associated color change. Satarpai *et al.* [50] more recently reported a study whereby preconcentration of Pb^{2+} onto fabricated filter paper modified with zirconium silicate was achieved. The adsorbed Pb filter paper was then used in colorimetric detection based on a simple paper-based valve system. Opening the valve allowed for flow of the sodium rhodizonate reagent over the pre-concentrated paper disk and a chemical reaction with lead took place to from a pink color. A grey scale intensity was used to study the extent of color change; detection in the low µg L^{-1} range was observed. The on/off technique offered a unique approach. Many other methods based on simple imaging or scanning procedures were studied [51–54]. In the work by Chen *et al.* [55] a fiber optic device provided the readout by measuring the blue color intensity obtained over the other imaging software approaches for Hg^{2+} detection. Here, Hg^{2+} interacts with platinum nanoparticles and inhibits its ability to oxidize the 3,3,5,5-tetramethylbenzidine (TMB) substrate. Wang *et al.* [56] further introduced an anion intercalation approach towards the detection of a variety of metal ions. Metal cations formed precipitates with sandwiched $[Fe(CN)_6]^{4-}$ to form a colorful $M_2[Fe(CN)_6]_m$ precipitate. The intensity of color change then provided information as to the metal concentration. While colorimetric sensing provides simple chemistry by interaction with a chemical reagent, the major drawback of colorimetric detection is the need for visual analysis of color changes to provide semi-quantitative responses, but still offers the best possibility for simple designs. The low sensitivity of these devices are still of great concern.

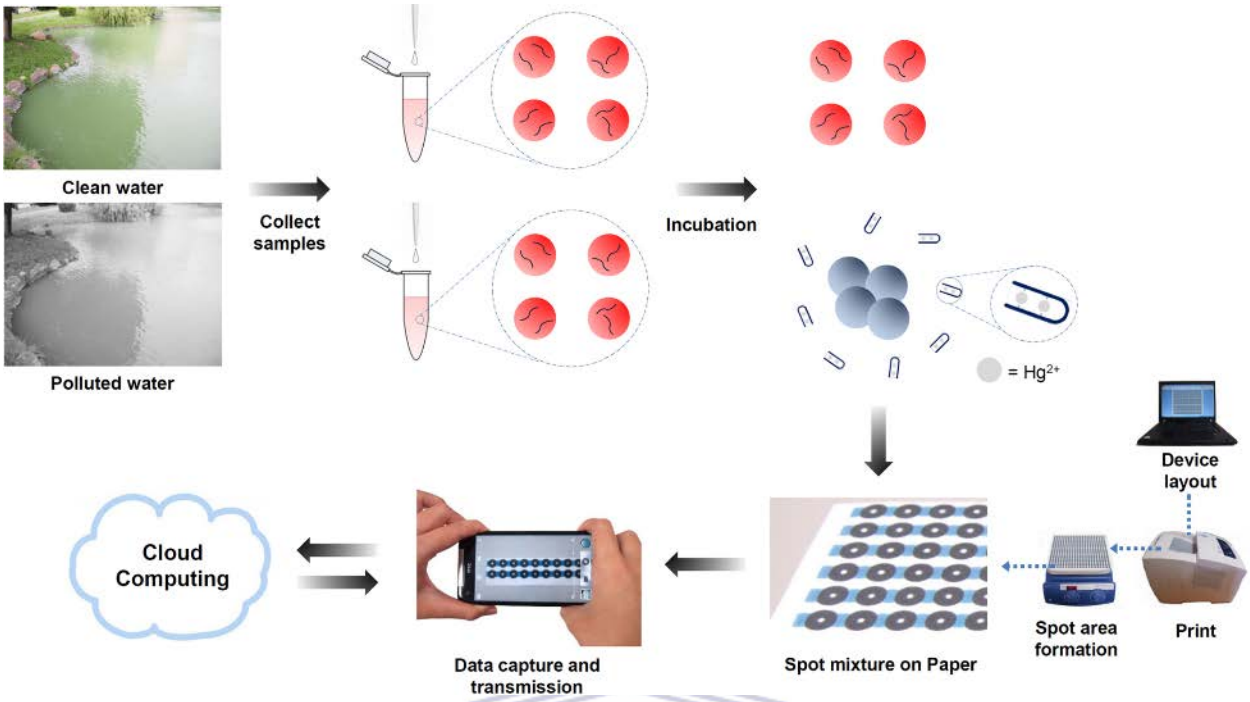

Figure 3.4: A schematic illustration of the proposed Hg^{2+} sensing strategy by Chen *et al.* [54].

3.5.2. Fluorescence Detection

As a direct answer to the low sensitivities associated with colorimetric detection, fluorescence based methods have been studied as an alternative means of detection. Largely, interactions of the target metal analytes with receptor molecules, modified with fluorophores or fluorescence labeled materials is crucial in providing accurate detection [8]. Enhancement or quenching of the fluorescence signal is achieved in the presence of the target analyte and forms the basis of its detection [57]. Typically, the metal ions do not have the desired optical properties and labelling is therefore required [58]. A variety of fluorescence probes have been investigated for metal detection [59] but only a handful of studies have been performed on paper-based sensing. Kim *et al.* [60] proposed a metal ion detection method based on rhodamine molecules covalently coupled to carbon nanodots (C-dots) in modified filter paper for detection of Al^{3+}. A Forster resonance energy transfer (FRET) mechanism is utilized for metal ion detection where the C-dots act as an energy donor and the rhodamine moiety as an energy acceptor. Blue emission is seen at unopened rhodamine due to its inability to absorb energy from C-dots. Complex formation of the metal ion with rhodamine molecules shifts to a yellow emission as rhodamine moieties are opened allowing for energy accepting. An enrichment approach was employed in the work by Zhang *et*

al. [61] for Ag^{+} and Hg^{2+} detection. In this work, single stranded DNA (ssDNA) is labelled with a Cy5 fluorescence label in conjunction with GO. The fluorescence was quenched when Cy5-labeled ssDNA was adsorbed on the GO surface. However, in the presence of target metal ions, coordination chemistry allows for the spontaneous liberation of the ssDNA resulting in fluorescence recovery. This is an interesting approach due to the on switch ultimately enriching the achieved fluorescence. A highly sensitive and selective method was achieved and could be further applied to multi-analyte detection. Feng *et al*. [62] proposed a multi-array sensor for a range of metal ions based on BODIPY (4,4-difluoro-4-bora-3a,4a-diaza-s-indacene)-based fluorescent indicators. Further studies for metal detection were recently performed based on similar techniques [37,63–66]. High sensitivity and selectivity is achieved in all these sensors, however Wang *et al*. [67] reported high fluorescence background associated with laminate coating in fluorescence-based paper sensors. As a means to combat this polymer-based composite films were used to sandwich the device effectively eliminating fluorescence background towards Cu^{2+}.

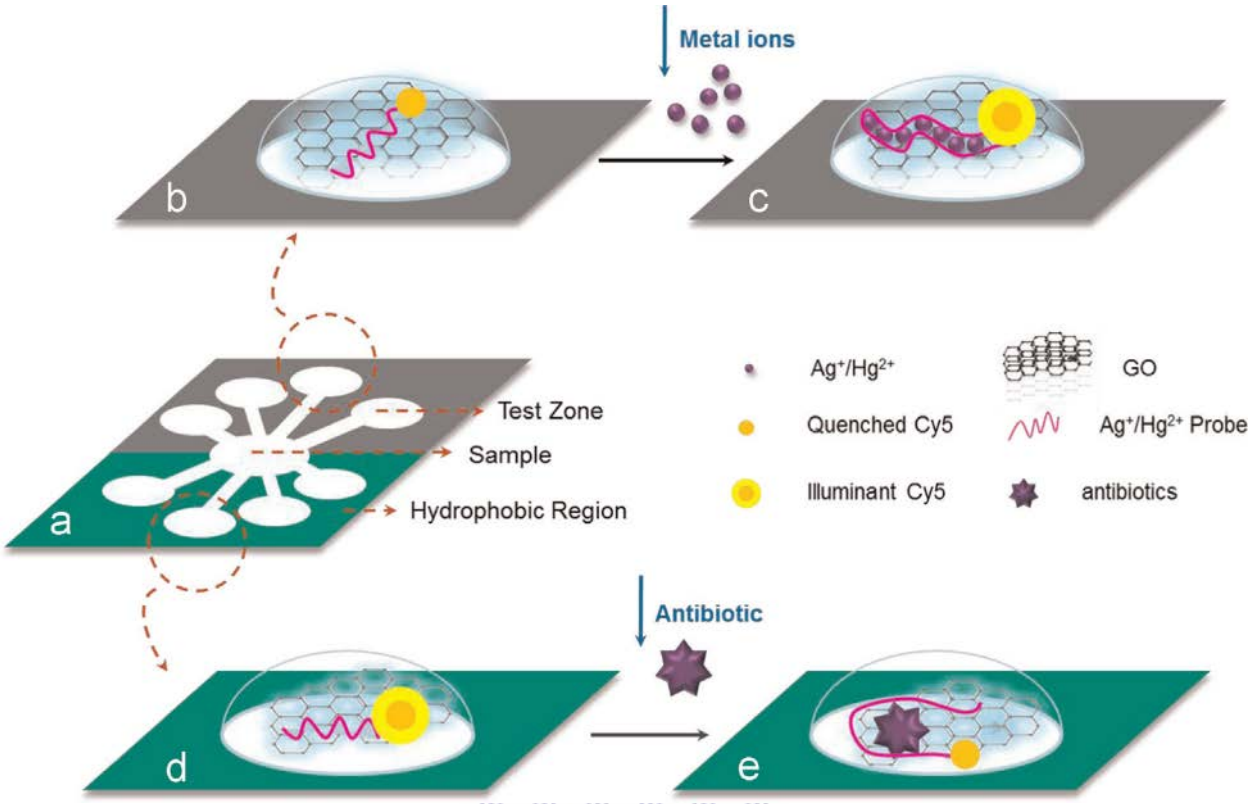

Figure 3.5: Schematic of the paper-based microfluidic device for multiplex chemical contaminants detection using ssDNA-functionalized GO sensors. (a) Paper-based microfluidic chip design. (b and c) Illustrate the principle of the metal ions detection based on the interaction among GO, ssDNA and heavy metal ions. The fluorescence was quenched when Cy5-labeled ssDNA adsorbed on the GO surface (b, fluorescence OFF). In the presence of the metal ions, they caused the ssDNA spontaneously liberating from the GO surface and finally resulted in fluorescence recovery (c, fluorescence ON). (d) and (e) illustrate the principle of the antibiotic detection based on the interaction among GO, ssDNA and antibiotics. The fluorescence was partly quenched when Cy5-labeled ssDNA adsorbed with low GO concentration (d, fluorescence ON). In the presence of the aminoglycoside antibiotic, the antibiotic-probe duplex increased the bind effection between the duplex and GO surface through amide coupling, resulted in fluorescence intensity decreasing (e, fluorescence OFF) [61].

3.5.3. Electrochemical Detection

Electrochemical approaches towards the detection of metal ions in water samples has rapidly become one of the most effective methods for metal analysis to date. Combining three electrode

systems with electroactive species allows for rapid, accurate and highly quantitative results. The three electrode systems make use of working, counter and reference electrodes. Detection usually involves a chemical reaction. Recently a growing number of studies have been conducted on paper-based sensor for metal analysis but is still in the very early stages. Shi *et al.* [68] successfully implemented a method for direct quantification of Pb^{2+} and Cd^{2+} in water samples by means of paper-based analytical devices. In this work, filter paper strips in conjunction with commercial screen printed electrodes was used in the construction of portable microfluidic paper-based analytical devices. Capillary driven flow allowed for liquid transport from a sample reservoir over the external three electrode system. The paper acted as carrier material bringing fresh sample to the electrode surface and also allowed for filtration of contaminants. Tan *et al.* [69] further built on this work by creating paper disks with prestored reagents in conjunction with external SPCE for the detection of Pb^{2+}. A dry reagent storage method for modifying the paper with electrolyte, metallic film and internal standard was achieved without the need for sample pretreatment prior to analysis. The method further allowed for only 10 µL sample volumes to be used. High accuracy was demonstrated by use of a Zn^{2+} internal standard. Both of these works made use of external three electrode systems to simplify fabrication steps and reduce associated costs. However, most studies rely on integrated electrode systems prepared by printing techniques. Apilux *et al.* [70] reported a screen printing technique to create a carbon working electrode on paper and applied it to the detection of Au^{3+} and Fe^{3+}. Rattanarat *et al.* [40] created a three-electrode system on transparency paper and utilized it for the detection of Cd^{2+} and Pb^{2+} in an origami design folded paper-based device. Nie *et al.* [71] proposed a fabrication method for a microfluidic paper-based electrochemical device based on photolithography patterned paper-based channel flowing over screen printed three electrode system. In a separate study Ruecha *et al.* [72] also reported a conventional screen printing approach for the fabrication of three electrode systems. The electrodes were further modified with a graphene-polyaniline (G/PANi) composite to improve electrode sensitivity towards the detection of Zn^{2+}, Cd^{2+} and Pb^{2+}. Other works on paper-based electrochemical detection of metal ions was also conducted [45,73]. All of these works made use of electrochemical anodic stripping voltammetry (ASV) for their detection of metal cations in water sample due to its simplicity, sensitivity and possibility for speciation. No works performed for electrochemical detection of metal ions have made use on an adsorptive stripping voltammetric (AdSV) approach. Further, only the one study made use of graphene and conductive polymers to

enhance electrode sensitivity in paper-based sensing, a technique that is readily used in solid electrode applications.

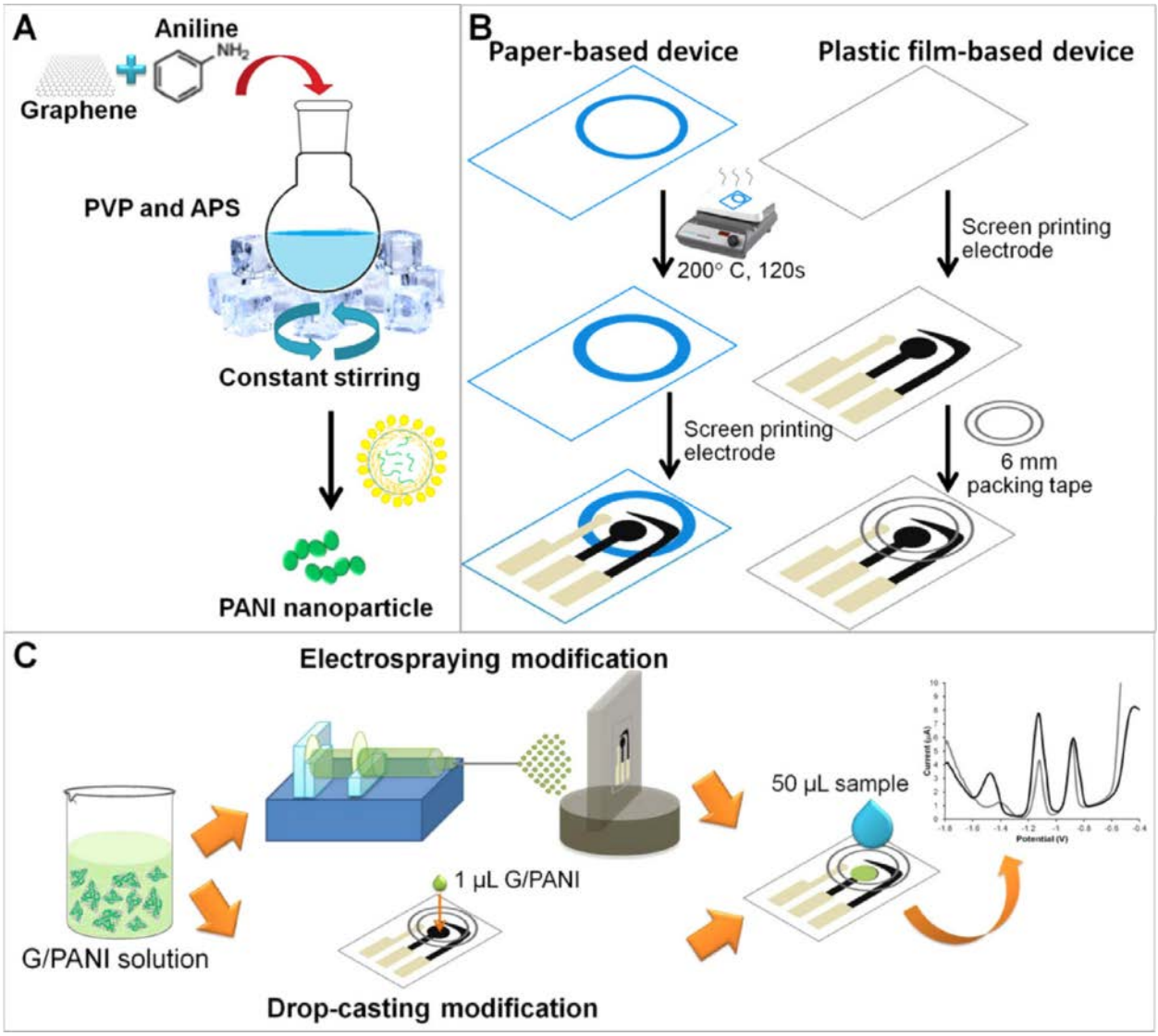

Figure 3.6: Schematic drawing of (a) the preparation of the G/PANI nanocomposite, (b) electrochemical sensor fabrication on plastic film or paper and (c) drop-casting and electrospraying processes [72].

3.5.4. Other Detection Methods

While colorimetric, fluorescence and electrochemical detection methods have proved to be the most popular methods of detection in paper-based microfluidic devices owing to their

simplistic design, inexpensive instrumentation and sensitive and accurate semi to quantitative analysis other methods of detection have also been suggested for metal analysis in paper-based sensors. The low sensitivity associated with colorimetric detection and high background scattering of fluorescence based detection methods offer considerable drawbacks to these methods. Chemiluminescence (CL), like fluorescence involves the production of light as the method of detection, however in here light is generated by chemical interactions under catalyst or excited intermediates instead of fluorescence [8]. Therefore, CL is considered an attractive alternative due to its high sensitivity, wide linear range, simple instrumentation, and no background scattering light interference [74]. Liu *et al.* proposed an aptamer based method for Hg^{2+} detection. Carboxylated phenylene-ethynylene referred to as P-acid was used as CL reagent, while single stranded DNA was used as aptamer to capture Hg^{2+} ions. The CL intensity is dependent on Hg ion concentration due to its ability to improve conjugation in the aptamer [74]. To further improve sensitivity of the CL technique, electrochemiluminescence (ECL) was suggested. Here, luminescence was generated by electrochemical reactions instead of chemical interactions. A three dimensional paper-based device was suggested for the simultaneous detection of Pb^{2+} and Hg^{2+} based on electrochemiluminescence by Zhang *et al.* [75]. In the study simultaneous detection of the metal cations were achieved by selective interactions with carbon nanocrystal capped silica nanoparticles and $Ru(bpy)_3^{2+}$-gold nanoparticles (AuNPs) aggregates respectively. Folded structures are formed upon interaction with the metal cations and luminescence is generated. A scanometric approach for Pb^{2+} detection was investigated by Vijitvarasan *et al.* [76]. In the study, AuNPs and magnetic beads are bound together by the ends of GR5-DNAzyme to form a MB-DNAzyme-AuNP complex. In the presence of Pb^{2+} the GR5-DNAzyme is activated and the s-strand is cleaved. A AuNP-Ps strand is then detached from the MB and dispersed in solution which can then be collected and reacted with silver particles. Silver coated gold nanoparticles are dotted on paper and a grey color appears directly proportional to the Pb^{2+} ion concentration. This method is tedious and requires sample pretreatment prior to detection. Cunningham *et al.* [77] further proposed a galvanic exchange electrochemical approach for detection of AgNP labels.

3.6. Conclusions and Future Work

Paper-based sensor development has shown a dramatic increase in the last decade, however metal analysis at paper-based microfluidic devices is still in its infancy. However, many studies

have been performed for detection of metal contaminants. Selection of paper substrates offers a wide range of properties and its choice is critical when deciding on possible applications. Further, fabrication methods for creating hydrophobic barriers have been developed in order to lower cost and simplify patterning processes in existence today. Contact printing approaches appear to be the simplest and offer lowest cost, however precise and accurate patterning when developing nanometer scale features may suffer. In the development of integrated electrode systems, a variety of approaches have been investigated. Conventional screen printing still remains tenable to date due to limited restrictions on ink specifications but other methods provide good alternatives over photolithography which is still being used to date. Recent advances show good progress in sensitivity, selectivity, limited interferences, rapid analysis and low cost. While, colorimetric approaches still remain the most widely used technique, alternative methods to improve sensitivity have been investigated. Electrochemical detection offers the most quantitative analytical approach and allows for accurate speciation. All electrochemical approaches used to date rely on anodic stripping voltammetry. Possibility exists for expansion into other spheres including adsorptive stripping voltammetry. Low limits of detection have been found for all detection methods studied in this review and choice of technique relies mainly on preference. Overall, paper-based sensing towards metal analysis has shown great promise. Further studies to improve electrode sensitivity and accuracy can be employed.

References

[1] A.W. Martinez, S.T. Phillips, G.M. Whitesides, E. Carrilho, Diagnostics for the developing world: Microfluidic paper-based analytical devices, Anal. Chem. 82 (2010) 3–10. doi:10.1021/ac9013989.

[2] P. Lisowski, P.K. Zarzycki, Advances on paper- based analytical devices (µPADs) – literature review, Camera Separatoria. 4 (2012) 143–149.

[3] D.D. Liana, B. Raguse, J. Justin Gooding, E. Chow, J.J. Gooding, E. Chow, Recent advances in paper-based sensors, Sensors (Switzerland). 12 (2012) 11505–11526. doi:10.3390/s120911505.

[4] S. S. Dhote, L. Deshmukh, Heavy Metal Ions Separation on Thin Layer of Impregnated

Carbamide-Formaldehyde Polymer, J. Chromatogr. Sep. Tech. 3 (2012) 2–4. doi:10.4172/2157-7064.1000124.

[5] J.P. Comer, Semiquantitative specific test paper for glucose in urine, Anal. Chem. 28 (1956) 1748–1750. doi:10.1021/ac60119a030.

[6] P. Von Lode, Point-of-care immunotesting: Approaching the analytical performance of central laboratory methods, Clin. Biochem. 38 (2005) 591–606. doi:10.1016/j.clinbiochem.2005.03.008.

[7] E.J. Maxwell, A.D. Mazzeo, G.M. Whitesides, Paper-based electroanalytical devices for accessible diagnostic testing, MRS Bull. 38 (2013) 309–314. doi:10.1557/mrs.2013.56.

[8] Y. Lin, D. Gritsenko, S. Feng, Y.C. Teh, X. Lu, J. Xu, Detection of heavy metal by paper-based microfluidics, Biosens. Bioelectron. 83 (2016) 256–266. doi:10.1016/j.bios.2016.04.061.

[9] G.J. Fosmire, Zinc toxicity., Am. J. Clin. Nutr. 51 (1990) 225–7. http://www.ncbi.nlm.nih.gov/pubmed/2407097.

[10] Atsdr, TOXICOLOGICAL PROFILE FOR ZINC, (2005). https://www.atsdr.cdc.gov/toxprofiles/tp60.pdf (accessed April 23, 2017).

[11] D.A. Gidlow, IN-DEPTH REVIEW Lead toxicity, Occup. Med. (Chic. Ill). 54 (2004) 76–81. doi:10.1093/occmed/kqh019.

[12] N.C. Papanikolaou, E.G. Hatzidaki, S. Belivanis, G.N. Tzanakakis, A.M. Tsatsakis, Lead toxicity update. A brief review., Med. Sci. Monit. 11 (2005) RA329--A336. doi:3687 [pii].

[13] L. Patrick, Lead toxicity, a review of the literature. Part 1: Exposure, evaluation, and treatment., Altern. Med. Rev. 11 (2006) 2–22. http://www.ncbi.nlm.nih.gov/pubmed/16597190 (accessed April 1, 2017).

[14] S.M. Gallego, L.B. Pena, R.A. Barcia, C.E. Azpilicueta, M.F. Iannone, E.P. Rosales, M.S. Zawoznik, M.D. Groppa, M.P. Benavides, Unravelling cadmium toxicity and tolerance in

plants: Insight into regulatory mechanisms, Environ. Exp. Bot. 83 (2012) 33–46. doi:10.1016/j.envexpbot.2012.04.006.

[15] S. Satarug, M.R. Moore, Adverse health effects of chronic exposure to low-level cadmium in foodstuffs and cigarette smoke, Environ. Health Perspect. 112 (2004) 1099–1103. doi:10.1289/ehp.6751.

[16] C.D. Klaassen, J. Liu, S. Choudhuri, Metallothionein: an intracellular protein to protect against cadmium toxicity., Annu. Rev. Pharmacol. Toxicol. 39 (1999) 267–294. doi:10.1146/annurev.pharmtox.39.1.267.

[17] M.P. Waalkes, Cadmium carcinogenesis in review, J. Inorg. Biochem. 79 (2000) 241–244. doi:10.1016/S0162-0134(00)00009-X.

[18] K.K. Das, S.N. Das, S. Dhundasi, Nickel, its adverse health effects & oxidative stress., Indian J. Med. Res. 128 (2008) 412–425.

[19] E. Denkhaus, K. Salnikow, Nickel essentiality, toxicity, and carcinogenicity, Crit. Rev. Oncol. Hematol. 42 (2002) 35–56. doi:10.1016/S1040-8428(01)00214-1.

[20] M. Cempel, G. Nikel, Nickel: A review of its sources and environmental toxicology, Polish J. Environ. Stud. 15 (2006) 375–382. doi:10.1109/TUFFC.2008.827.

[21] WHO, Nickel in Drinking-water, Environ. Heal. (2005) 1–16.

[22] B.B. Mamba, L.C. Rietveld, J.Q.J.C. Verberk, SA drinking water standards under the microscope, Water Wheel. 7 (2008) 24–27. doi:www.sxc.hu.

[23] N. Gault, C. Sandre, J.-L. Poncy, C. Moulin, J.-L. Lefaix, C. Bresson, Cobalt toxicity: Chemical and radiological combined effects on HaCaT keratinocyte cell line, Toxicol. Vitr. 24 (2010) 92–98. doi:10.1016/j.tiv.2009.08.027.

[24] L.O. Simonsen, H. Harbak, P. Bennekou, Cobalt metabolism and toxicology-A brief update, Sci. Total Environ. 432 (2012) 210–215. doi:10.1016/j.scitotenv.2012.06.009.

[25] A.W. Martinez, S.T. Phillips, M.J. Butte, G.M. Whitesides, Patterned Paper as a Platform

for Inexpensive, Low-Volume, Portable Bioassays, Angew. Chemie Int. Ed. 46 (2007) 1318–1320. doi:10.1002/anie.200603817.

[26] W. Dungchai, O. Chailapakul, C.S. Henry, A low-cost, simple, and rapid fabrication method for paper-based microfluidics using wax screen-printing., Analyst. 136 (2011) 77–82. doi:10.1039/c0an00406e.

[27] R. Lu, W. Shi, L. Jiang, J. Qin, B. Lin, Rapid prototyping of paper-based microfluidics with wax for low-cost, portable bioassay, Electrophoresis. 30 (2009) 1497–1500. doi:10.1002/elps.200800563.

[28] M. Liu, C. Zhang, F. Liu, Understanding wax screen-printing: A novel patterning process for microfluidic cloth-based analytical devices, Anal. Chim. Acta. 891 (2015) 234–246. doi:10.1016/j.aca.2015.06.034.

[29] J. Nie, Y. Zhang, L. Lin, C. Zhou, S. Li, L. Zhang, J. Li, Low-Cost Fabrication of Paper-Based Micro fl uidic Devices by One- Step Plotting, Anal. Chem. 84 (2012) 6331–6335.

[30] T. Songjaroen, J. Noiphung, I. Hongwarittorrn, K. Talalak, W. Laiwattanapaisal, Assay time reduction and thermal stability improvement of a low- cost , wax-dipping paper-based microfluidic device, J. Chem. Pharm. Res. 6 (2014) 2895–2903.

[31] K.L. Dornelas, N. Dossi, E. Piccin, A simple method for patterning poly(dimethylsiloxane) barriers in paper using contact-printing with low-cost rubber stamps, Anal. Chim. Acta. 858 (2015) 82–90. doi:10.1016/j.aca.2014.11.025.

[32] P. de T. Garcia, T.M.G. Cardoso, C.D. Garcia, E. Carrilho, W.K.T. Coltro, A handheld stamping process to fabricate microfluidic paper-based analytical devices with chemically modified surface for clinical assays, RSC Adv. 4 (2014) 37637–37644. doi:10.1039/C4RA07112C.

[33] R.H. Muller, D.L. Clegg, Automatic Paper Chromatography, Anal. Chem. 21 (1949) 1123–1125. doi:10.1111/j.1749-6632.1951.tb48886.x.

[34] D. Delivery, P. Tip, P.M. Device, Chips and Tips, (2016) 3–6.

[35] M.M. Thuo, R. V Martinez, W. Lan, X. Liu, J. Barber, Fabrication of Low-Cost Paper-Based Micro fl uidic Devices by Embossing or Cut-and-Stack Methods, Chem. Mater. 26 (2014) 4230–4237.

[36] X. Fang, S. Wei, J. Kong, Paper-based microfluidics with high resolution, cut on a glass fiber membrane for bioassays., Lab Chip. 14 (2014) 911–5. doi:10.1039/c3lc51246k.

[37] D. Citterio, K. Suzuki, S.D. Citterio, K. Yamada, S. Takaki, N. Komuro, Showcasing research on inkjet-printed microfl uidic paper-based analytical devices (μPADs) from the team around Professor As featured in: An antibody-free microfluidic paper-based analytical device for the determination of tear fluid lactoferrin by fluore, (n.d.). www.rsc.org/analyst (accessed April 19, 2017).

[38] W. Dungchai, O. Chailapakul, C.S. Henry, Electrochemical detection for paper-based microfluidics, Anal. Chem. 81 (2009) 5821–5826. doi:10.1021/ac9007573.

[39] W. Kit-Anan, A. Olarnwanich, C. Sriprachuabwong, C. Karuwan, A. Tuantranont, A. Wisitsoraat, W. Srituravanich, A. Pimpin, Disposable paper-based electrochemical sensor utilizing inkjet-printed Polyaniline modified screen-printed carbon electrode for Ascorbic acid detection, J. Electroanal. Chem. 685 (2012) 72–78. doi:10.1016/j.jelechem.2012.08.039.

[40] P. Rattanarat, W. Dungchai, D. Cate, J. Volckens, O. Chailapakul, C.S. Henry, Multilayer paper-based device for colorimetric and electrochemical quantification of metals, Anal. Chem. 86 (2014) 3555–3562. doi:10.1021/ac5000224.

[41] P. Teengam, W. Siangproh, A. Tuantranont, C.S. Henry, T. Vilaivan, O. Chailapakul, Electrochemical paper-based peptide nucleic acid biosensor for detecting human papillomavirus, (2017). doi:10.1016/j.aca.2016.11.071.

[42] P. Sjöberg, A. Määttänen, U. Vanamo, M. Novell, P. Ihalainen, F.J. Andrade, J. Bobacka, J. Peltonen, Paper-based potentiometric ion sensors constructed on ink-jet printed gold electrodes, Sensors Actuators B. 224 (2016) 325–332. doi:10.1016/j.snb.2015.10.051.

[43] B.G. Expósito, Paper-based microfluidic sensing devices fabricated by inkjet printing

technology, (n.d.) 2–4.

[44] K. Abe, K. Kotera, K. Suzuki, D. Citterio, Inkjet-printed paperfluidic immuno-chemical sensing device, Anal. Bioanal. Chem. 398 (2010) 885–893. doi:10.1007/s00216-010-4011-2.

[45] S. Smith, P. Bezuidenhout, M. Mbanjwa, H. Zheng, M. Conning, N. Palaniyandy, K. Ozoemena, K. Land, Development of paper-based electrochemical sensors for water quality monitoring, 10036 (2017) 100360C. doi:10.1117/12.2244290.

[46] N. Dossi, R. Toniolo, A. Pizzariello, F. Impellizzieri, E. Piccin, G. Bontempelli, Pencil-drawn paper supported electrodes as simple electrochemical detectors for paper-based fluidic devices, Electrophoresis. 34 (2013) 2085–2091. doi:10.1002/elps.201200425.

[47] V. Guillard, C. Bourlieu, N. Gontard, Relationship Between Multiscale Food Structure and Moisture Transfer Properties, 2013. doi:10.1007/978-1-4614-6342-9.

[48] P. Mcdonald, Wicking in multi-ply paper strucutres with dissimilar plies, Georgia Institute of Technology, 2006.

[49] S. Chaiyo, W. Siangproh, A. Apilux, O. Chailapakul, Highly selective and sensitive paper-based colorimetric sensor using thiosulfate catalytic etching of silver nanoplates for trace determination of copper ions, Anal. Chim. Acta. 866 (2015) 75–83. doi:10.1016/j.aca.2015.01.042.

[50] T. Satarpai, J. Shiowatana, A. Siripinyanond, Paper-based analytical device for sampling, on-site preconcentration and detection of ppb lead in water, Talanta. 154 (2016) 504–510. doi:10.1016/j.talanta.2016.04.017.

[51] M.T. Koesdjojo, S. Pengpumkiat, Y. Wu, A. Boonloed, D. Huynh, T.P. Remcho, V.T. Remcho, Cost Effective Paper-Based Colorimetric Microfluidic Devices and Mobile Phone Camera Readers for the Classroom, J. Chem. Educ. 92 (2015) 737–741. doi:10.1021/ed500401d.

[52] L. Liu, H. Lin, Paper-Based Colorimetric Array Test Strip for Selective and

Semiquantitative Multi-Ion Analysis: Simultaneous Detection of Hg, Anal. Chem. 86 (2014) 8829–8834. doi:10.1021/ac5021886.

[53] D.M. Cate, P. Nanthasurasak, P. Riwkulkajorn, C. L'Orange, C.S. Henry, J. Volckens, Rapid detection of transition metals in welding fumes using paper-based analytical devices, Ann. Occup. Hyg. (2014). doi:10.1093/annhyg/met078.

[54] G.-H. Chen, W.-Y. Chen, Y.-C. Yen, C.-W. Wang, H.-T. Chang, C.-F. Chen, Detection of Mercury(II) Ions Using Colorimetric Gold Nanoparticles on Paper-Based Analytical Devices, (n.d.). doi:10.1021/ac5008688.

[55] W. Chen, X. Fang, H. Li, H. Cao, J. Kong, A Simple Paper-Based Colorimetric Device for Rapid Mercury(II) Assay, (2016). doi:10.1038/srep31948.

[56] N. Wang, J. Sun, H. Fan, S. Ai, Anion-intercalated layered double hydroxides modified test strips for detection of heavy metal ions, Talanta. 148 (2015) 301–307. doi:10.1016/j.talanta.2015.11.007.

[57] M. Formica, V. Fusi, L. Giorgi, M. Micheloni, New fluorescent chemosensors for metal ions in solution, Coord. Chem. Rev. 256 (2012) 170–192. doi:10.1016/j.ccr.2011.09.010.

[58] S.E. Andria, C.J. Sellskar, W.R. Heineman, Simultaneous detection of two analytes using a spectroelectrochemical sensor, Anal. Chem. 82 (2010) 1720–1726. doi:10.1021/ac902243u.

[59] J. Abolhasani, J. Hassanzadeh, E.S. Jalali, Ultrasensitive determination of lead and chromium contamination in well and dam water based on fluorescence quenching of CdS quantum dots, Int. Nano Lett. 4 (2014) 65–72. doi:10.1007/s40089-014-0120-9.

[60] Y. Kim, G. Jang, T.S. Lee, New Fluorescent Metal-Ion Detection Using a Paper-Based Sensor Strip Containing Tethered Rhodamine Carbon Nanodots, (n.d.). doi:10.1021/acsami.5b04724.

[61] Y. Zhang, P. Zuo, B.-C. Ye, A low-cost and simple paper-based microfluidic device for simulta- neous multiplex determination of different types of chemical con- taminants in

food, Biosens. Bioelectron. 68 (2016) 14–19. doi:10.1016/j.bios.2014.12.042.

[62] L. Feng, H. Li, L.-Y. Niu, Y.-S. Guan, C.-F. Duan, Y.-F. Guan, C.-H. Tung, Q.-Z. Yang, A fluorometric paper-based sensor array for the discrimination of heavy-metal ions, (2013). doi:10.1016/j.talanta.2013.02.073.

[63] X. Fang, Q. Zhao, H. Cao, J. Liu, M. Guan, J. Kong, P. Tabeling, Rapid detection of Cu^{2+} by a paper-based microfluidic device coated with bovine serum albumin (BSA)–Au nanoclusters, Analyst. 140 (2015) 7823–7826. doi:10.1039/C5AN01016K.

[64] N.K. Thom, G.G. Lewis, K. Yeung, S.T. Phillips, G.F. Busscher, A.E. Seelen, C. Albrecht, P. de Bruijn, H.W. Scheeren, G. Moeller, D.C.H. Burgess, Quantitative fluorescence assays using a self-powered paper-based microfluidic device and a camera-equipped cellular phone, RSC Adv. 4 (2014) 1334–1340. doi:10.1039/C3RA44717K.

[65] P. Nath, R.K. Arun, N. Chanda, C.Y. Hsu, J. Xi, K.J. Lin, X. Jiang, S. McAfee, B. Robinson, S. Banerjee, A.K. Singh, D. Senapati, P.C. Ray, A paper based microfluidic device for the detection of arsenic using a gold nanosensor, RSC Adv. 4 (2014) 59558–59561. doi:10.1039/C4RA12946F.

[66] M.G. Caglayan, S. Sheykhi, L. Mosca, P. Anzenbacher, C.P. McCoy, J.T. Rademacher, T.E. Rice, Y. Xu, M. Wu, G. Ouyang, Fluorescent zinc and copper complexes for detection of adrafinil in paper-based microfluidic devices, Chem. Commun. 52 (2016) 8279–8282. doi:10.1039/C6CC03640F.

[67] C.-M. Wang, C.-Y. Chen, W.-S. Liao, Paper-polymer composite devices with minimal fluorescence background, Anal. Chim. Acta. 963 (2017) 93–98. doi:10.1016/j.aca.2017.01.044.

[68] J. Shi, F. Tang, H. Xing, H. Zheng, L. Bi, W. Wang, Electrochemical detection of Pb and Cd in paper-based microfluidic devices, J. Braz. Chem. Soc. 23 (2012) 1124–1130. doi:10.1590/S0103-50532012000600018.

[69] S.N. Tan, L. Ge, W. Wang, Paper disk on screen printed electrode for one-step sensing with an internal standard, Anal. Chem. 82 (2010) 8844–8847. doi:10.1021/ac1015062.

[70] A. Apilux, W. Dungchai, W. Siangproh, N. Praphairaksit, C.S. Henry, O. Chailapakul, Lab-on-paper with dual electrochemical/ colorimetric detection for simultaneous determination of gold and iron, Anal. Chem. 82 (2010) 1727–1732. doi:10.1021/ac9022555.

[71] Z. Nie, C. a Nijhuis, J. Gong, X. Chen, A. Kumachev, A.W. Martinez, M. Narovlyansky, G.M. Whitesides, Electrochemical sensing in paper-based microfluidic devices., Lab Chip. 10 (2010) 477–483. doi:10.1039/b917150a.

[72] N. Ruecha, N. Rodthongkum, D.M. Cate, J. Volckens, O. Chailapakul, C.S. Henry, Sensitive electrochemical sensor using a graphene-polyaniline nanocomposite for simultaneous detection of Zn(II), Cd(II), and Pb(II), Anal. Chim. Acta. 874 (2015) 40–48. doi:10.1016/j.aca.2015.02.064.

[73] W.R. de Araujo, T.R.L.C. Paixão, A. Pizzariello, F. Impellizzieri, E. Piccin, G. Bontempelli, X.G. Shao, G.M. Whitesides, Fabrication of disposable electrochemical devices using silver ink and office paper, Analyst. 139 (2014) 2742. doi:10.1039/c4an00097h.

[74] F. Liu, S. Wang, M. Zhang, Y. Wang, S. Ge, J. Yu, M. Yan, Aptamer based test stripe for ultrasensitive detection of mercury(II) using a phenylene-ethynylene reagent on nanoporous silver as a chemiluminescence reagent, Microchim. Actaa. 181 (2014) 663–670. doi:doi:10.1007/s00604-014-1171-3.

[75] M. Zhang, L. Ge, S. Ge, M. Yan, J. Yu, J. Huang, S. Liu, Three-dimensional paper-based electrochemiluminescence device for simultaneous detection of Pb 2 þ and Hg 2 þ based on potential-control technique, Biosens. Bioelectron. 41 (2012) 544–550. doi:10.1016/j.bios.2012.09.022.

[76] P. Vijitvarasan, S. Oaew, W. Surareungchai, Paper-based scanometric assay for lead ion detection using DNAzyme, Anal. Chim. Acta. 896 (2015) 152–159. doi:10.1016/j.aca.2015.09.011.

[77] J.C. Cunningham, M.R. Kogan, Y.-J. Tsai, L. Luo, I. Richards, R.M. Crooks, Paper-Based

Sensor for Electrochemical Detection of Silver Nanoparticle Labels by Galvanic Exchange, ACS Sensors. 1 (2015) acssensors.5b00051. doi:10.1021/acssensors.5b00051.

Chapter 4 :

Structural and Morphological Characterisation of Prepared Reduced Graphene Oxide, Graphene Oxide and Gold Nanoparticles

Abstract

A simple, low-cost chemical synthesis approach based on a modified Hummer's method was utilized for the production of graphitic oxide, which was exfoliated upon ultrasonication processes to produce graphene oxide (GO) sheets. The produced GO was converted to reduced graphene oxide (RGO) in the presence of $NaBH_4$ as reducing agent. Commercial gold nanoparticles (AuNPs) purchased from Sigma Aldrich were also investigated. The structural, morphological and topographical properties of the synthesized and purchased materials were characterized by FTIR, HRSEM, HRTEM, XRD, Raman spectroscopy, AFM and UV-vis spectroscopy. The characterization procedure confirmed the inclusion and removal of oxygen-containing functional groups (hydroxyl, carboxyl and epoxy) within and from the graphitic structure yielding large quantities of produced material. Impurities associated with chemical reduction methods were limited and materials with few defects observed. Further, conversion from sp^3 hybridized carbon associated with bulk graphite to sp^2 hybridized carbon in RGO sheets was confirmed. Good quality RGO was produced with an average flake size of ~ 2 nm confirming the presence of few-layer RGO sheets of 5 individual layers. Restoration of the electronic structure associated with RGO was further established. Uniform, stable dispersions of GO and RGO in water and ethanol respectively were obtained for use in further experimentation. Gold nanoparticles were found to have and average particle size of ~ 57 nm from electron microscope images.

Keywords

Graphite, graphene oxide, reduced graphene oxide, gold nanoparticles, electron microscopy, x-ray diffraction, raman, ultraviolet-visible spectroscopy, infrared spectroscopy

Highlights

- High quality graphene oxide was prepared by a modified Hummer's method as previously reported
- A chemical synthesis approach was employed for the production of few-layer graphene sheets in the presence of $NaBH_4$
- Structural and morphological characterization of prepared graphene oxide, reduced graphene oxide and commercial gold nanoparticle dispersions was performed and found to produce good quality materials for use in electrochemical sensors

Graphical Abstract

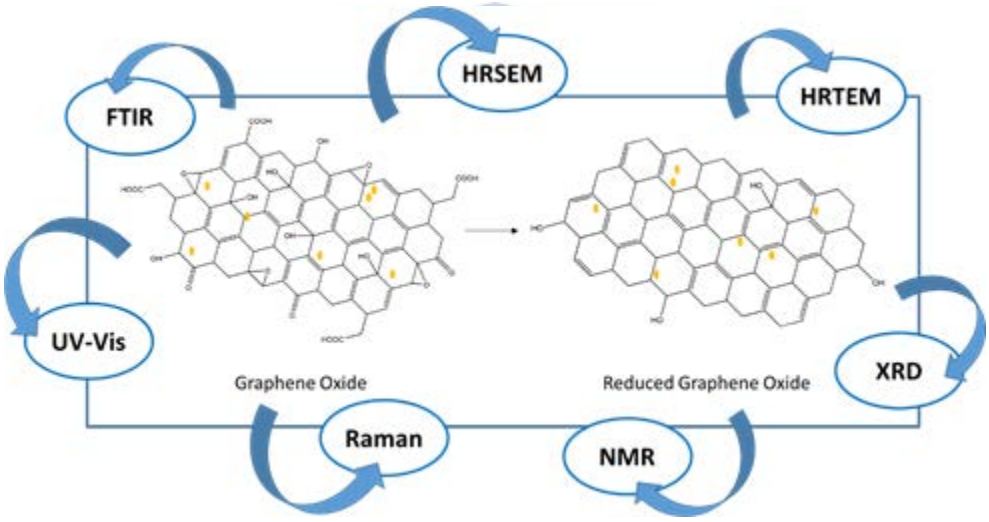

4.1. Introduction

Since its discovery in 2004 by a micromechanical exfoliation technique [1], the application of graphene and graphene derivatives by exploiting their various properties has skyrocketed. The fast electron transfer, high surface area and tensile strength make it an attractive material for use in a range of applications. To date, it has been used in a wide range of applications including, batteries [2–4], solar cells [5–7], sensors [8–10], light-emitting diodes [11,12], filtration [13,14], super capacitors [15,16] etc. Fine-tuning of these specific properties may be performed by simply altering the method of synthesis or preparation. As previously discussed, switching between

methods not only drastically affects the electrochemical properties of the material but also significantly influences the yield of high-quality prepared graphenes. As such, the selection of preparation technique is pivotal in the application of graphene-derivatives in electrochemical sensing devices.

Chemical synthesis approaches remain the most commonly employed route for graphene preparation via the oxidation of bulk commercial graphite, due to their many advantageous properties. Low-cost instrumentation, use of semi-skilled labor, environmentally friendly materials and mass production all characterize the chemical synthesis routes. To date, a variety of approaches have been suggested for the 'top-down' oxidation and exfoliation of graphitic layers. Typically, oxygen moieties are inserted between the individual sheets of graphite forcing layers apart to the extent of overcoming the existing Van der Waal's forces. This method was first introduced by Brodie *et al.* in 1859 [17]. Since its inception, more environmentally friendly approaches have been introduced to limit the toxic byproduct associated with the technique. The Hummer's method [18] has become the most popular choice due to its safe and timely approach. More recently however, the Tour group at Rice University, Texas have proposed a "one-pot" approach with minimal temperature dependence as an alternative to the Hummer's method [19].

The inclusion of oxygen functionalities within the carbon network disrupts the flow of electrons creating a material that is insulating in nature, limiting conductivity of the prepared graphitic oxide, making it a poor choice for electronic or electrochemical applications. The subsequent removal of the oxygen moieties restores the C-C lattice and improves the electron transfer kinetics. A range of techniques have been employed for the removal of the oxygen to produce single, few or multi-layer graphene sheets upon exfoliation. Chemical, thermal, flash, microwave, etc. are all commonly used techniques. Chemical reduction by means of reducing agents such as hydrazine and sodium borohydride ($NaBH_4$) have been most extensively studied.

In this section, a modified Hummer's method was employed for the production of graphitic oxide and its subsequent reduction and exfoliation to produce few-layer reduced graphene oxide. This work interrogates the structural and morphological characterization of the prepared materials via each synthesis step.

4.2. Experimental Methods

4.2.1. Chemicals and Reagents

All chemicals utilized in the study were of analytical grade and used as received without further modification or purification. Natural graphite powder (< 100 microns, mesh, microcrystal grade, 99.99 %), metal base with ultra "F" purity was purchased from Alfa Aesar (Massachusetts, United States) and used for the preparation of graphene oxide. Potassium permanganate ($KMnO_4$), sulfuric acid (H_2SO_4), nitric acid (HNO_3), hydrochloric acid (HCl) and ethanol (EtOH) were all purchased from Sigma Aldrich or Fluka. Ultrapure water was collected from a Millipore system and used for all dilutions where necessary.

4.2.2. Apparatus

Fourier Transform Infrared (FT-IR) spectra were recorded using a (Perkin Elmer Spectrum 100) coupled to an Attenuated Total Reflectance (ATR) sample holder. FT-IR was used to confirm the presence of oxime groups in the dimethylglyoxime structure. Appropriate quantities of ground KBr and samples were mixed and pressed in a handheld hydraulic press to prepare KBr pellets. High Resolution Scanning Electron Microscopy (HRSEM) measurements were performed using an Auriga HRSEM instrument equipped with Electronic Data System (EDS). The samples were dried in a vacuum oven and deposited on the silicon grid surface before HRSEM observations. High Resolution Transmission Electron Microscopy (HRTEM) measurements were carried out with a Tecnai G2 F20X-Twin MAT Field Emission Transmission Electron Microscope from FEI (Eindhoven, Netherlands) under an acceleration voltage of 200 kV. The samples were prepared by dropping a dilute suspension of graphene in ethanol onto copper grids followed by air drying at room temperature. Raman spectroscopy was obtained using a LabRam HR by Jobin-Yvon Horiba scientific Explora, France in conjunction with a Model BX41, Olympus microscope at 532 nm wavelength laser. Samples were prepared by drop coating graphene suspensions or thin graphene films onto glass slides and allowing to dry at room temperature. Zahner-Elektrik Electrochemical Workstation IM6e from Zahner-Elektrik GmbH & CoKG (Germany) was used for electrochemical impedance spectroscopy (EIS) measurements in 5 mM $K_3Fe(CN)_6$ in 1 M KCl as electrolyte solution.

Table 4.1: A summary of characterization techniques used in the study and their corresponding uses.

Technique	*Use*
FT-IR	*Structural Configuration*
XRD	*Structure/ Mineralogy*
TEM, SEM	*Morphology and Particle Size*
UV-vis	*Electronic transitions*
AFM	*Morphology*
Raman Spectroscopy	*Vibrational and Rotational Frequency modes/ Configuration*
Cyclic Voltammetry	*Electro activity*
NMR	*Molecular structure*

4.2.3. Preparation of Graphene Oxide

Both Hummer's [18] and Tour [19] methods were utilized for the synthesis of graphitic oxide with few modifications. In the Hummer's approach, 2 g graphite powder and 1 g sodium nitrite were dispersed in 50 mL of sulfuric acid in a dry 250 mL conical flask and mixed at room temperature for 30 min. A uniform dispersion and mixing of the reagents in order to facilitate the oxidation process was achieved. The resultant solution was cooled by subsequent mixing in an ice bath for approximately 20 min prior to the addition of the oxidizing agent. An adequate quantity of potassium permanganate (7 g) was slowly added over a 30 min period under constant stirring to avoid a sudden increase in the solution temperature. The solution was allowed to cool to room temperature. The cooled solution was then mixed at 35 ^{o}C for 2 h in a water bath before being returned to the ice bath to cool. Successive additions of 150 mL ultra-pure water and 5 mL hydrogen peroxide were performed until effervescence ceased. The flask was removed from the ice bath and allowed to stir at room temperature overnight and centrifuged for 20 min to allow large flakes to settle. Purification and removal of contaminants was performed by three successive

acid washes and one with ultra-pure water. The resulting product was the dried for 48 h under a vacuum. The prepared graphite oxide (10 mg) was exfoliated in 10 mL of ultra-pure water or Ethanol to give a 1.0 mg mL^{-1} GO solution.

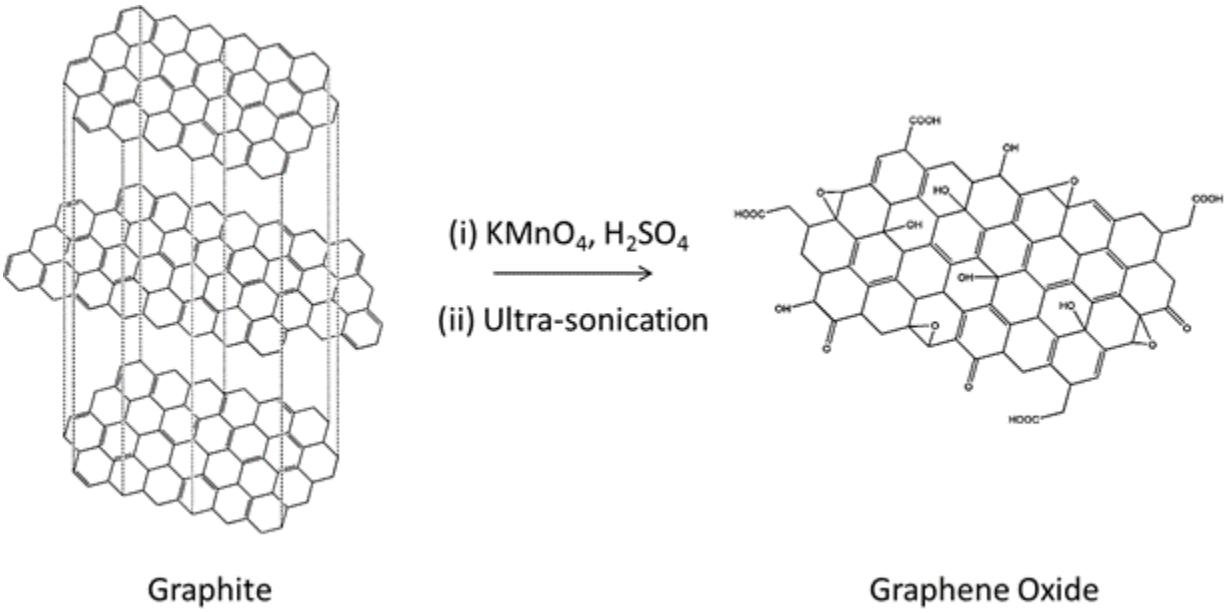

Figure 4.1: Schematic depicting the chemical synthesis of graphene oxide from bulk commercial graphite.

4.2.4. Reduced Graphene Oxide Preparation

A 1 mg mL^{-1} dispersion of the synthesised graphene oxide was prepared by dispersing 100 mg graphene oxide in a 100 mL portion of ultra-pure distilled water in a 250 mL round-bottom flask. The prepared GO dispersion was exfoliated by ultrasonication for 1 hr. Following the ultrasonication, 200 mg $NaBH_4$ was added in excess and stirred for at least 30 min before being allowed to cool to room temperature. The cooled solution was then heated to 135 ^oC for 3 hrs in a silicon oil bath under reflux conditions. The synthesis approach yields approximately 100 mL reduced graphene oxide in water. The resultant back solid was then separated from the aqueous layer centrifugation at 8000 rpm for 30 min. Further separation was performed by resting the solution overnight. The supernatant was then decanted and discarded. The graphene produced was dried at 60 ^oC for 3 days in a vacuum oven.

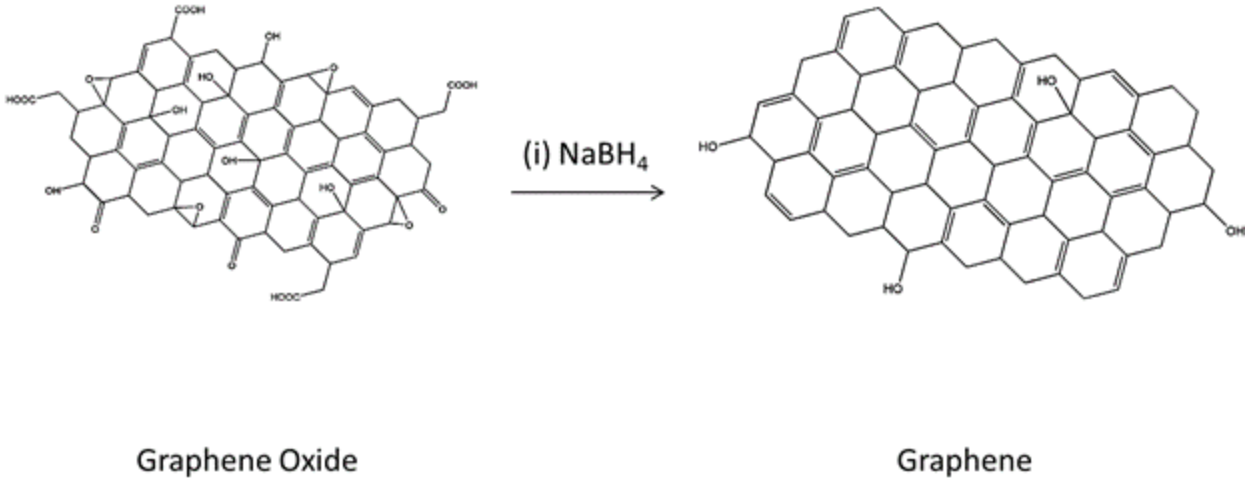

Figure 4.2: Graphic representation of reduction of graphene oxide (GO) to form graphene powder.

4.3. Results and Discussion

4.3.1. Structural and Morphological Characterization of Prepared Graphene Oxide and Reduced Graphene Oxide

4.3.1.1. GO and RGO dispersion in suitable solvents

The ability to form stable, uniform dispersion of graphene oxide and reduced graphene oxide in suitable solvents is vital for its use in a variety of applications. Dispersions prepared from the synthesised graphene-materials are shown in *Figure 4.3*. Clear brown and black solutions are recorded for graphene oxide and reduced graphene oxide in water and ethanol respectively following ultrasonication for 2 hrs. The hydrophilic nature of GO due to the presence of oxygen containing functional groups generated during the oxidation step allows for a colloidal suspension to be generated in water. The solution turns from yellowish to black upon reduction and may be easily dispersed in ethanol.

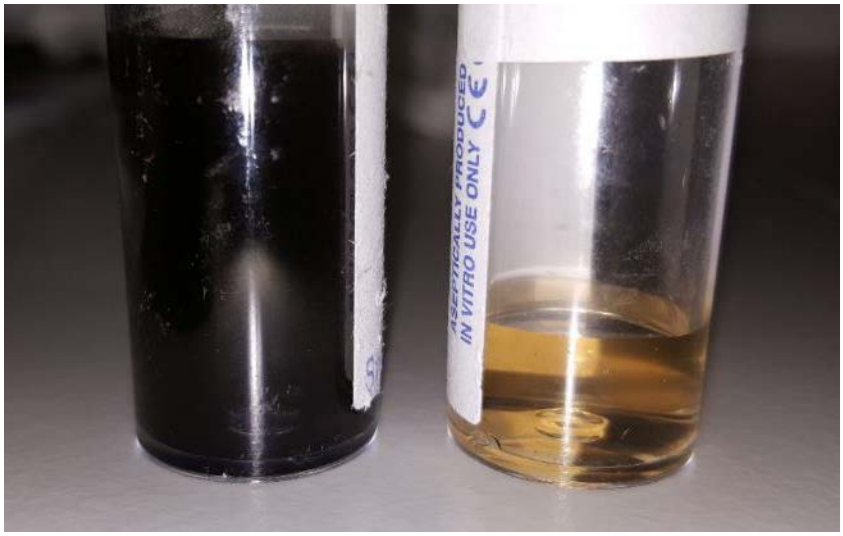

Figure 4.3: Image of 0.25 mg mL^{-1} (a) reduced graphene oxide [black] and (b) graphene oxide [brown] dispersions in ethanol and water respectively, prepared via the chemical synthesis approach above.

4.3.1.2. Fourier-transform Infrared Spectroscopy (FT-IR)

The preparation of graphene oxide (GO) and reduced graphene oxide (RGO) from natural graphite powder was performed by the insertion and subsequent removal of oxygen containing moieties within the graphitic structure. Fourier transform infrared spectroscopy (FT-IR) was used to study the variations in structural configuration via the chemical synthesis routes detailed in *Section 4.2 and 4.3. Figure 4.4 (a)* shows the FT-IR spectra of (a) graphite, (b) graphene oxide and (c) reduced graphene oxide recorded from KBr pellets between 400 and 4000 cm^{-1}. The FT-IR spectra of graphite (*Figure 4.4 (a and b)*) shows no significant IR features of notable intensity, attributed to the high purity carbon structure associated with graphite flakes, as expected. For GO however, large transmission bands can be seen and occur as a result of the inclusion of oxygen moieties within the ordered carbon structure. Hydroxyl, carboxyl and epoxy functional groups are reported in literature. Characteristic IR peaks associated with the following functional groups are shown: O-H stretching vibrations at 3353 and 2474 cm^{-1} attributed to the hydroxyl of –COOH and alcohols, the C=O stretching vibration at 1725 cm^{-1} and C=C stretching vibrations of aromatic rings at 1590 cm^{-1}. The weak band at 1374 cm^{-1} arises from O-H stretching vibrations as a result of deformation or bending of C-O-H. The peaks at 1167 and 1065 cm^{-1} are attributed to the C-O stretching vibrations of epoxides and alkoxides. Lastly, the C-H stretching vibrations arising from

aromatic rings can be seen. A summary of all observed stretching vibrations and corresponding functional groups are shown in *Table 4.2*. Upon reduction of GO in the presence of $NaBH_4$ as reducing agent, to form a RGO, a significant reduction or disappearance in peak intensities occurring due to the presence of oxygen functional groups can be seen. This result indicates the removal of a large percentage of oxygen from the graphitic structure. These findings are in agreement with literature reported results for the preparation of reduced graphene oxide [19–22]. A comparison of the FT-IR spectra obtained by a modified Hummer's method and Tour method is shown in *Figure 4.4 (c)*. Similar characteristic IR peaks are seen in both synthesis approaches resulting from the oxidation of natural graphite. The Hummer's method appears to have provided increased oxidation over the Tour method and was therefore selected for all further experimentation.

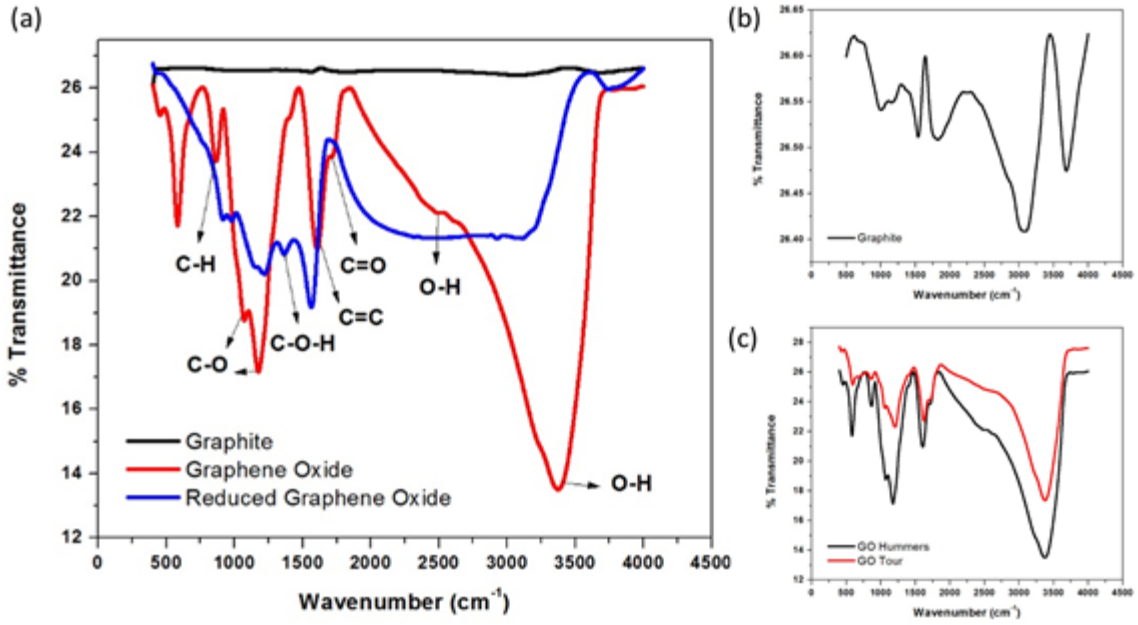

Figure 4.4: FTIR spectra recorded for (a) graphite, graphene oxide (GO) and reduced graphene oxide (RGO), (b) magnified spectra of graphite and (c) a comparison of GO prepared by a Hummer's and Tour method.

Table 4.2: A summary of recorded stretching vibrations and corresponding functional groups found from FTIR analysis of Graphite, Graphene oxide and Reduced Graphene Oxide.

Stretching Vibration (cm^{-1})	*Associated Functional Group*
857	*C-H (aromatic rings)*
1065	*C-O (alkoxy)*
1167	*C-O (epoxy)*
1374	*O-H (deformation of C-OH)*
1590	*C=C (aromatic)*
1725	*C=O (carboxyl)*
2474	*O-H*
3353	*O-H (hydroxyl of –COOH)*

4.3.1.3. High Resolution Scanning Electron Microscopy (HRSEM)

The structural surface morphologies of graphite, graphitic oxide and reduced graphene oxide flakes were studied by high resolution scanning electron microscopy (HRSEM) and recorded in *Figure 4.5*. The surface morphology of graphite (*Figure 5 (a)*) showed a feather-like structure with a crumpled paper nature and harsh edges attributed to the crystalline nature of graphite powder. Agglomeration and aggregation of particles is further observed and indicative of the stacking of graphene sheets to form the layered material. The HRSEM image of graphitic oxide in *Figure 4.5 (b)* indicates a similar uneven surface morphology of the graphitic oxide platelets. Agglomeration and stacking of sheets is still seen in the absence of a suitable exfoliation step. The preparation of reduced graphene oxide via a chemical synthesis approach produces large RGO sheets as seen in *Figure 4.5 (c)*. Thin, crumpled and wrinkled sheets with increasing transparency and significantly less harsh edges are observed for the reduced graphene oxide sheets. The stacking and exfoliation of individual layers is evident in *Figure 4.5 (d)* with an interplanar spacing of < 5 nm observed.

Elemental composition conducted by energy dispersive X-ray spectroscopy (EDS) shows 46 % and 14 % composition of oxygen in GO and RGO respectively confirming the inclusion and subsequent removal of oxygen.

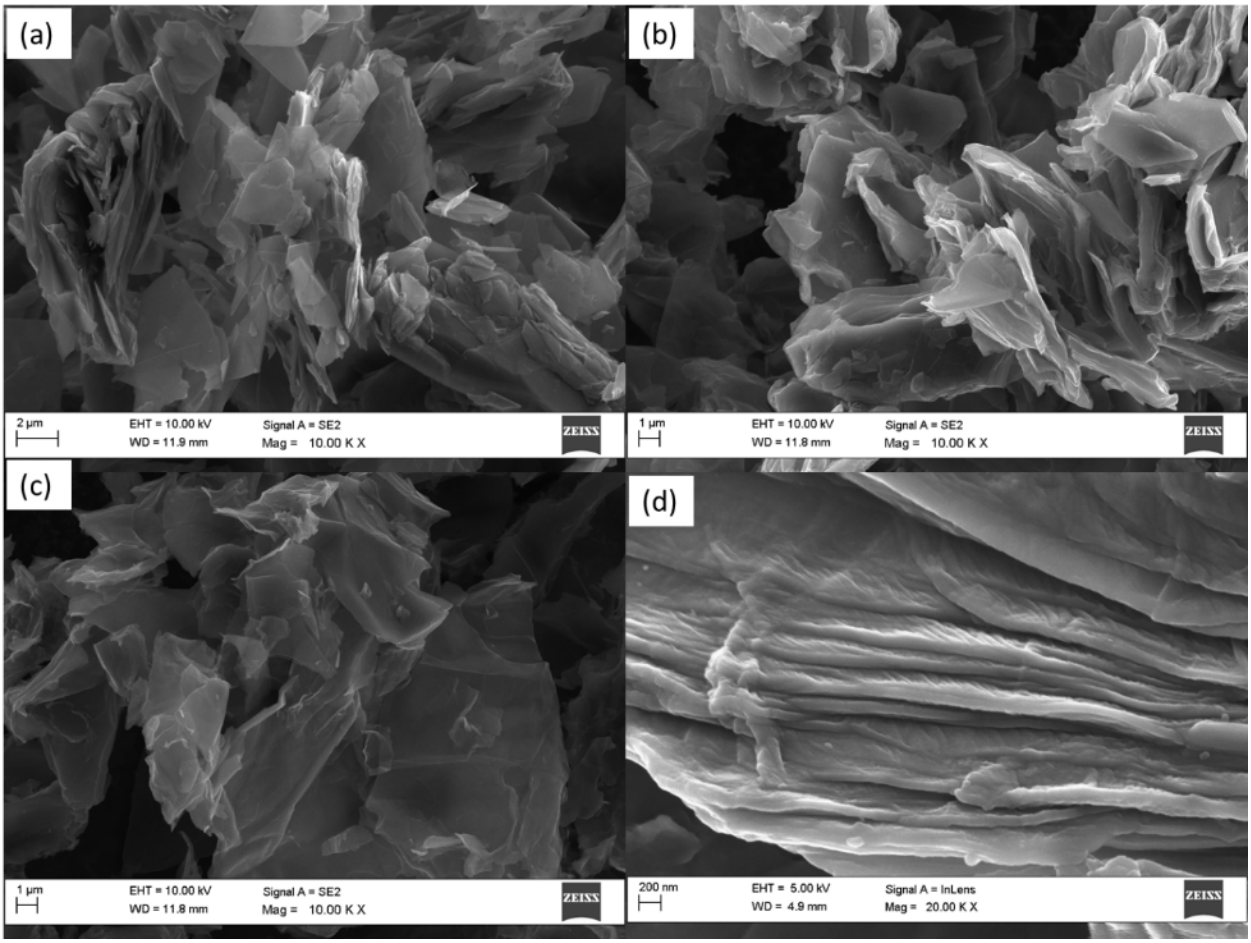

Figure 4.5: HRSEM images of (a) graphite, (b) graphitic oxide, (c and d) reduced graphene oxide at 10 kX and 20 kX magnification.

4.3.1.4. High Resolution Transmission Electron Microscopy (HRTEM)

High resolution transmission electron microscopy (HRTEM) analysis was performed to probe the structural changes in graphite, graphene oxide and reduced graphene oxide samples via the synthesis route. HRTEM analysis was conducted by drop casting prepared sample dispersion (0.5 mg mL^{-1}) in ethanol onto copper mesh grids following a 1 hr ultrasonication step. Characteristic HRTEM images are illustrated for graphite, graphene oxide and reduced graphene oxide in *Figure 6*. The HRTEM image of graphite (*Figure 4.6 (a)*) is portrayed as dark flakes with

stacked layers. Sharp and harsh edges as well presence of distinct lattice fringes in the graphite structure further demonstrate its high ordered crystalline nature. In contrast, the HRTEM image of GO, shown in *Figure 4.6 (b)* is seen as large flat silky transparent sheets. The wavy nature with thick folds and sections of entangles sheets is observed as a result of the large surface area associated with exfoliation. Areas of increased transparency, generally towards the edge of sheets indicates regions of monolayer graphene oxide. The slightly darker color is indicative of the incomplete exfoliation of GO in ethanol due to strong hydrogen bonding between oxygen functional groups of adjacent layers. *Figure 4.6 (c)* shows highly transparent, large sheets with wrinkles representing entangled layers and high surface area are observed for few-layer RGO. The increased transparency shows confinement of the sheet thickness into the low nanometer range. Suitable exfoliation and the crystalline nature of RGO at higher magnifications are demonstrated in *Figure 4.6 (d)*. Useful information of the quantum confinement and crystalline nature of the prepared materials were discovered. Similar to analysis by HRSEM, elemental composition of the prepared samples confirmed the inclusion and removal of oxygen along the synthesis route towards a reduced graphene oxide.

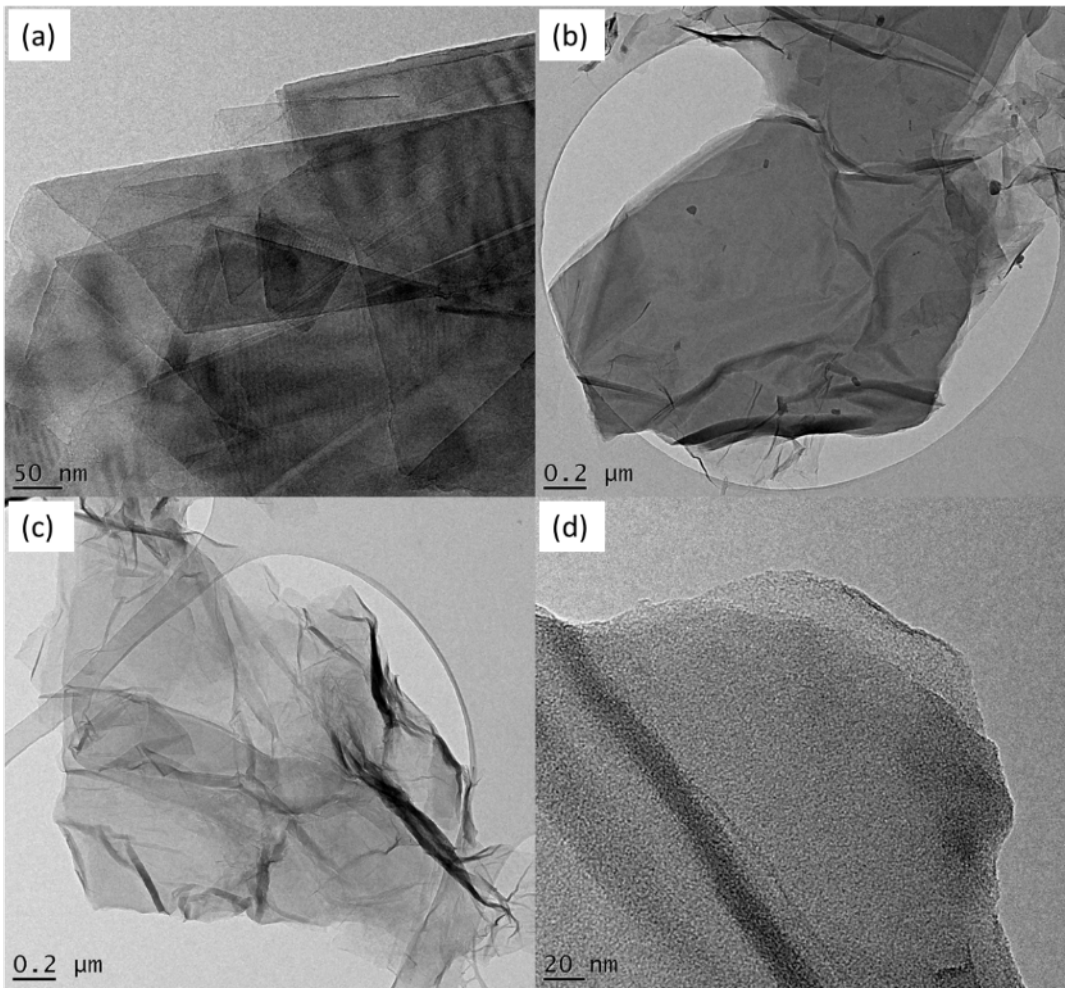

Figure 4.6: HRTEM images of (a) graphite, (b) graphene oxide, (c and d) reduced graphene oxide at varying magnifications.

4.3.1.5. X-ray Diffraction (XRD)

The diffraction patterns of graphite, graphene oxide and reduced graphene oxide are recorded in *Figure 4.7*. The XRD pattern of graphite demonstrates three distinct peaks at 26.5º, 44.6º and 54,6º attributed to the highly ordered crystalline carbon structure of the 002 plane, 100 plane and 004 plane respectively [23]. A distinct broadening of the peak at 26.5º is observed due to distortion of the carbon structure upon the inclusion of oxygen containing functional groups and moisture [24]. A shift to 9.8º corresponding to the diffraction of the 001 plane of graphene oxide is seen. The calculated interlayer spacing increases from 0.34 nm (graphite) to 0.7 nm and confirms the presence of the oxygen moieties [25]. Upon reduction of GO using $NaBH_4$, a broad diffraction

peak is seen at 22°. The observation confirms the removal of most of the oxygen to form a reduced graphene oxide and the restoration of the conjugate carbon structure. Similar results are reported in literature.

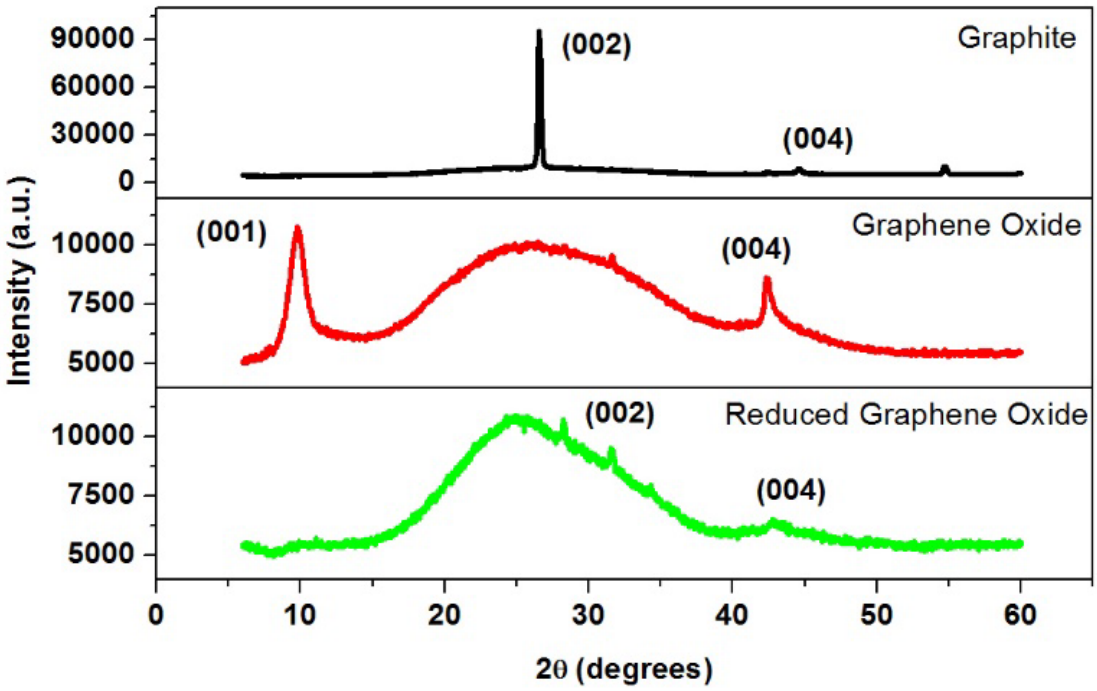

Figure 4.7: XRD patterns of (a) graphite, (b) graphene oxide, (c and d) reduced graphene oxide.

4.3.1.6. Raman Spectroscopy

Raman spectroscopy has proved to be a powerful tool for the analysis of graphene due to its intrinsic ability to probe structural changes in the graphitic structure along the synthesis process. Chemical and structural changes in commercial (a) graphite, (b) graphene oxide and (c) reduced graphene oxide were investigated by Raman spectroscopy between 0 and 3000 cm^{-1} and recorded in *Figure 4.8*. The raman spectra recorded for graphite consists of a sharp, strong band at 1560 cm^{-1}, a weak band at 1332 cm^{-1} and a moderate band at 2678 cm^{-1} attributed to characteristic G, D and 2 D bands of graphite respectively. The G-band, with highest intensity occurs as a result of symmetry allowed scattering of phonons of the E_{2g} mode arising from sp^3 hybridized carbon atoms [26]. The high intensity and sharp peak corresponds to an ordered structure of the graphitic

material. The weak D-band in contrast represents defects in the hexagonal carbon-carbon structure as a result of defects arising from vacancies, grain boundaries and deviations in the sp^3 hybridized carbon-carbon bonds [27]. The 2D band, occurring at double the energy of the G-band may be attributed to second order raman scattering processes of the multilayered structure. This corresponds to the morphological characterization of graphite found in previous techniques. The intensity of the calculated I_D/I_G ratio is 0.246 and provides evidence to the low degree of deviation from the graphitic structure. Further the intensity ratio, $I_{2D}/I_G = 0.26$ is calculated << 0.5 and occurs as a result of a multilayered structure.

Further interrogation of the Raman spectra of graphene oxide shows two distinct peaks with considerably lower intensities compared to graphite at 1590 cm^{-1} and 1349 cm^{-1} arising from G and D bands respectively. A lowering in peak intensities occurs due to an overall lowering of layers to produce phonons. The G-band here, occurs as a result of in-plane vibrations of the sp^2 carbon-carbon bonds while the large D-band confirms the deviation from the ordered graphitic structure due to the presence of oxygen containing functional groups within the carbon lattice. The 2D band is no longer present due to the presence of oxygen moieties and is characteristic of GO [10]. An I_D/I_G ratio of 0.94 confirms the highly disordered nature of the material due to oxidation processes.

The Raman spectra of reduced graphene oxide again shows characteristic G, D and 2D bands at 1594 cm^{-1}, 1341 cm^{-1} and 2866 cm^{-1} respectively. The D-band occurs due to the presence of defects or edge effects of the graphite structure upon removal of oxygen moieties. The G-band arises from vibration of sp^2 carbon-carbon atoms. An I_D/I_G ratio of 1.19 is increased over the recorded value for GO and graphite and is indicative of a shift to reduced graphene oxide [27]. Further the sharp 2D band shows a shift to high energies, generally associated with few-layer graphene and is confirmed by the $I_{2D}/I_G = 0.69$ corresponding to few-layer graphenes [28]. This confirms the reduction of graphene oxide to a reduced graphene oxide [26].

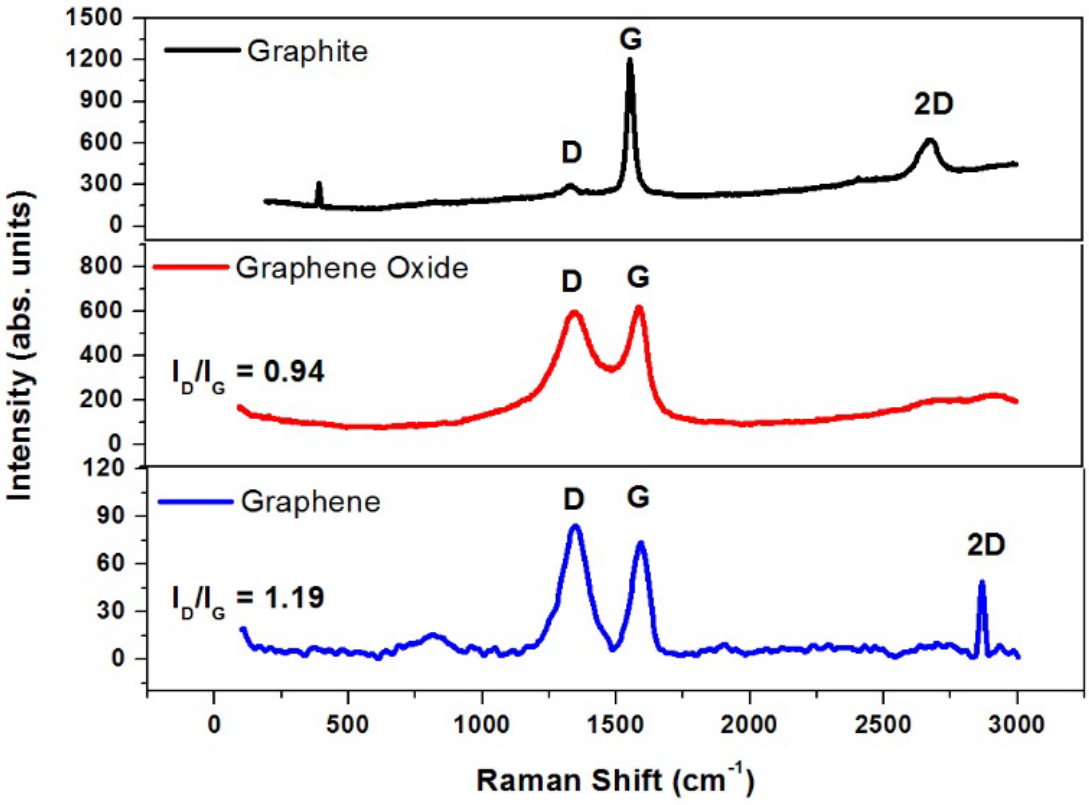

Figure 4.8: Raman spectra of (a) graphite, (b) graphene oxide, (c and d) reduced graphene oxide.

4.3.1.7. Atomic Force Microscopy (AFM)

Atomic force microscopy (AFM) was used to further evaluate the morphology of reduced graphene oxide (RGO). *Figure 4.9* shows a typical AFM image of a single RGO flake deposited from a 0.5 mg mL^{-1} RGO dispersion in Ethanol onto a silicon wafer. RGO flakes of non-uniform shape were observed on the silicon substrate with particle sizes ranging between 0.6 – 0.7 µm recorded from the observed cross-sectional view. An estimated vertical distance of ~ 2.0 nm was observed over 5 RGO flakes. Inter-planar distance for graphene of 0.35 nm has been reported in literature [29]. Few-layer RGO sheets with approximately 5 layers is therefore estimated. Similar results were reported in literature for graphene preparation.

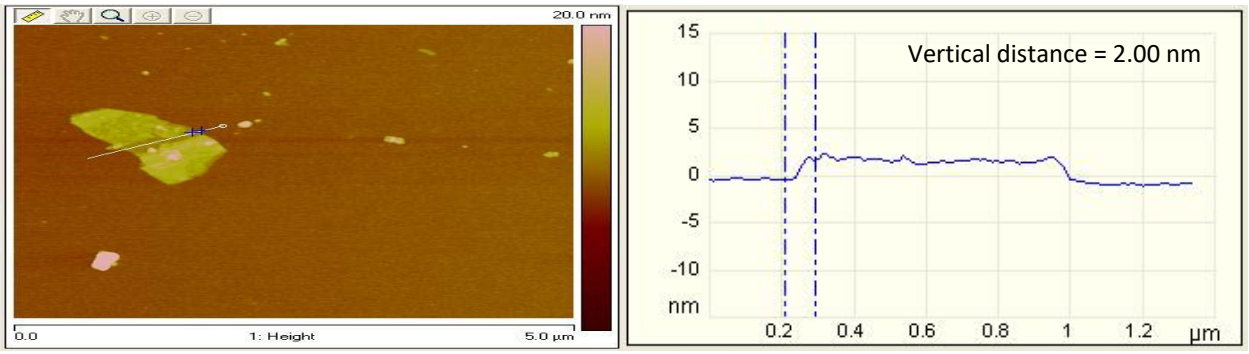

Figure 4.9: Tapping mode AFM image and corresponding cross-sectional view of prepared reduced graphene oxide.

4.3.1.8. Ultraviolet Visible (UV-vis) Spectroscopy

Ultraviolet visible (UV-vis) spectroscopy was used to study the electron transitions which occur as a result of oxygen functionalization and removal from the graphitic structure. The UV-vis spectra of graphene oxide (GO) prepared via a modified Hummer's method and reduced graphene oxide (RGO) using $NaBH_4$ as reducing agent between 200 and 800 nm is shown in *Figure 4.10*. GO shows two absorption peaks at 231 nm (i) and 303 nm (ii) respectively. The maximum absorption peak for GO occurring at 231 nm arises due to $\pi \rightarrow \pi^*$ transitions of the C-C bonds in the sp^2 hybridized structure, while the shoulder at 303 nm corresponds to the $n \rightarrow \pi^*$ transition of the C-O bonds [30]. Upon reduction of the GO, an overall lowering in absorbance is seen for reduced graphene oxide. A magnified image of the UV-vis spectra of RGO is shown in *Figure 4.10, inset*. A shift in peak position from 230 nm to 259 nm (iii), along with a lowering in peak intensity and broadening of the peak. The red shift indicates the removal of oxygen functionalities and a restoration of electronic configuration of the reduced graphene oxide sheets [26,31].

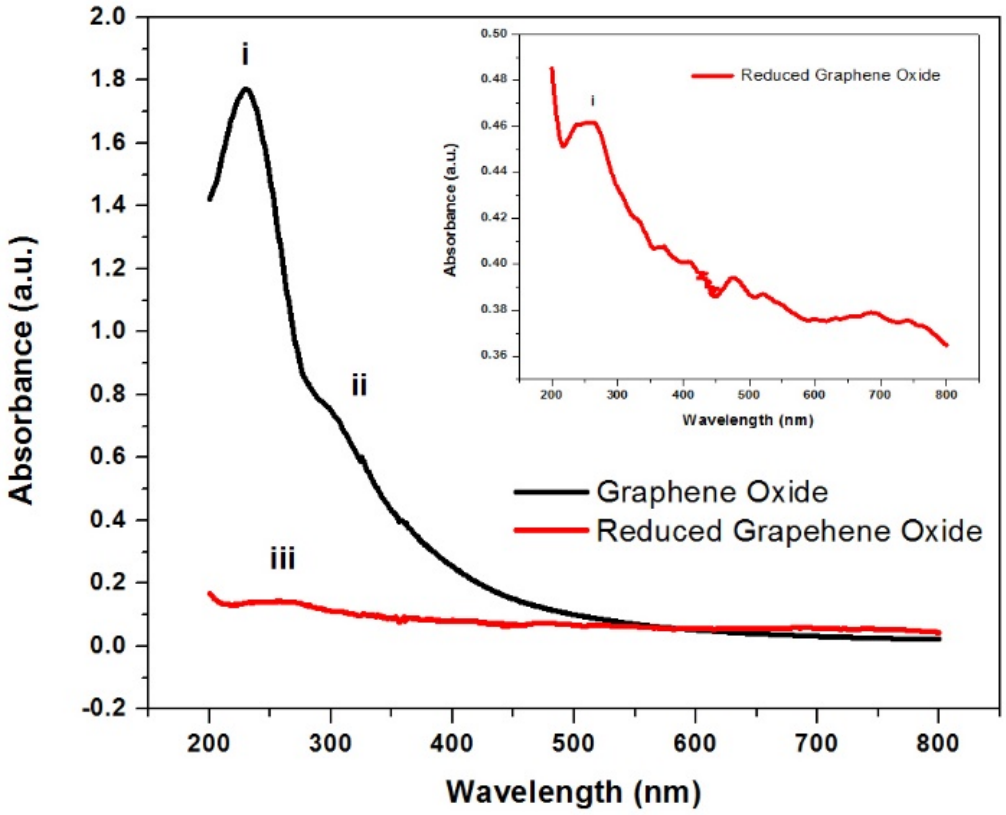

Figure 4.10: UV-vis spectra of (a) graphene oxide and (b) reduced graphene oxide dispersed in water. Inset: UV-vis spectra of reduced graphene oxide.

4.3.2. Structural and Morphological Characterization of Commercial Gold Nanoparticles

4.3.2.1. High Resolution Electron Microscopy

High resolution electron microscopy was used to study the morphological profile of the commercial gold nanoparticles to be used in the study. High resolution (a) scanning electron microscopy and (b and c) transmission electron microscopy images of the AuNPs are shown in *Figure 4.11*. The HRSEM image illustrated in *Figure 4.11 (a)* shows the morphological profile of a group of AuNPs deposited on a carbon substrate by a simple drop casting method at 100 kX magnification. Spherical particles are observed with relatively uniform size distribution. An

average particle size over 10 AuNPs of ~ 57 nm was recorded. Clusters of nanoparticles are observed with no significant agglomeration taking place. EDS confirmed the elemental composition of the observed nanoparticles to be that of AuNPs. While HRSEM, provided only surface characterization, HRTEM is able to probe the particles and provide information as to the shape and crystallinity of the material under investigation. *Figure 4.11 (b)*, shows HRTEM image of AuNPs decorated on a Cu-mesh grid. Similar to HRSEM, uniform spherical particles are seen decorated on the Cu-grid. An average particle size of ~ 50 nm in diameter was observed. Upon increased magnification (*Figure 4.11 (c)*), the highly crystalline nature and ordered structure of the nanoparticles can be seen.

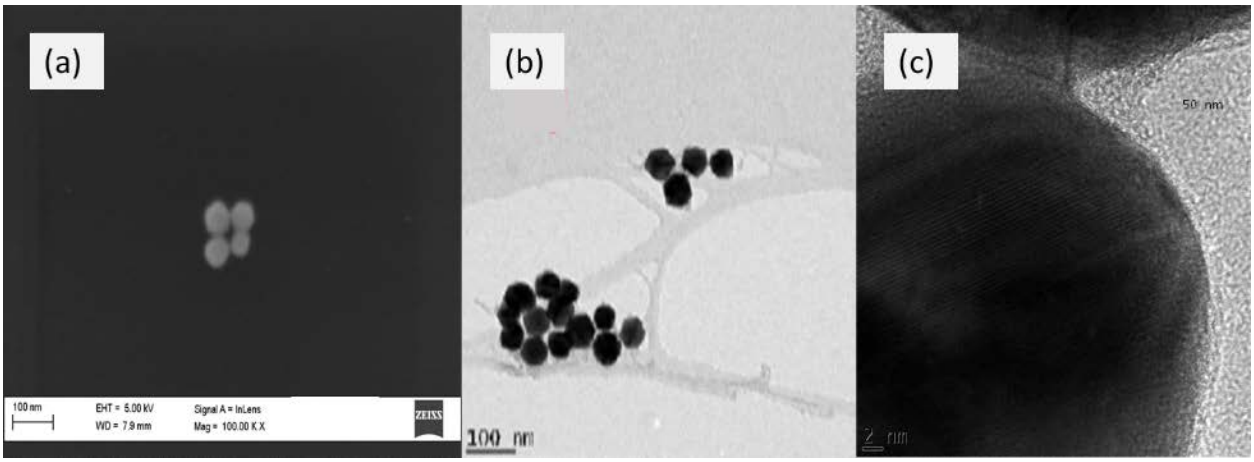

Figure 4.11: (a) HRSEM image and HRTEM images at (b) low and (c) high magnification of 50 nm AuNPs.

4.3.2.2. Ultraviolet Visible (UV-vis) Spectroscopy

The UV-vis absorption spectra of commercial gold nanoparticles at three dilutions: (a) 1:10, (b) 1:5 and (c) 1:1 between 400 and 800 nm is recorded in *Figure 4.12*. A single, sharp absorption band at 536 nm is shown for all three dilutions under investigation with no shift in absorption wavelength seen. The uniform peak wavelength indicates the formation of stable suspensions of AuNPs in ultrapure water. An increase in peak height is seen with increasing AuNP concentration showing a clear dependence of AuNP concentration on the observed absorbance. The peak at 536 nm corresponds to an approximate particle size of ~ 50 nm and is in agreement with the expected result found in electron microscope images. *Figure 4.12, inset* shows the commercial AuNP

suspension in phosphate buffer solution (pH 7.1). A pink color is seen and is generally an indication of particle sizes in the mid nanometer range. Similar results for UV-vis spectra of AuNPs were observed in literature [32–34].

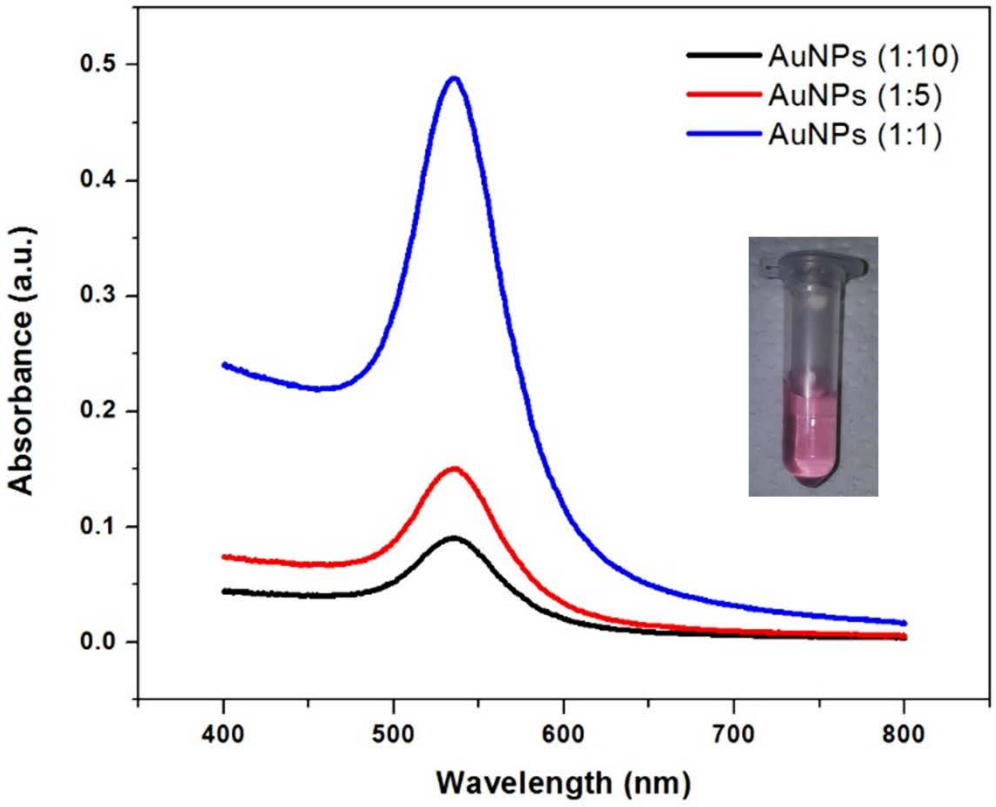

Figure 4.12: UV-vis absorption spectra of (a) 1:10, (b) 1:5 and (c) 1:1 dilution of commercially bought 50 nm AuNPs in phosphate buffer solution (pH 7.1). Inset: Image of 50 nm AuNPs in PBS buffer solution.

4.4. Conclusions and Future Work

The characterization of natural graphite powder, graphene oxide and reduced graphene oxide confirmed the oxidation and subsequent reduction of oxygen within the graphitic structure of the modified Hummer's process. The inclusion of oxygen moieties between graphene layers of graphite, forced the layers apart so as to overcome the weak Van der Waal's forces between layers.

Exfoliation of the oxidized material in ultrapure water resulted in adequate exfoliation to few layer structures. The reduction of GO using $NaBH_4$ was further confirmed. A large percentage of included oxygen functional groups were removed to produce RGO. Few-layer structures of approximately 5 layers were obtained. The removal of oxygen restored the electronic configuration of the produced material and large area sheets with high yields could be produces. The reported results matched those recorded in literature for GO and RGO production. Further, characterization of the purchased commercial AuNPs showed stable, uniform suspensions in buffer solutions. A uniform distribution of spherical NPs of average particles size of 57 nm were observed. The characterized materials were therefore of good quality for further use in the electrochemical sensors.

References

[1] K.S. Noveslov, A.K. Geim, S.V. Morozov, D. Jiang, Y. Zhang, S.V. Dubonos, I.V. Grigorieva, A.A. Firsov, Electric Field Effect in Atomically Thin Carbon Films, Science (80-.). 306 (2004) 666–669.

[2] Y. Li, J. Yang, J. Song, Nano energy system model and nanoscale effect of graphene battery in renewable energy electric vehicle, Renew. Sustain. Energy Rev. 69 (2017) 652–663. doi:10.1016/j.rser.2016.11.118.

[3] J. Song, Z. Yu, M.L. Gordin, D. Wang, Advanced Sulfur Cathode Enabled by Highly Crumpled Nitrogen- Doped Graphene Sheets for High-Energy-Density Lithium−Sulfur Batteries, (n.d.). doi:10.1021/acs.nanolett.5b03217.

[4] D. Li, L. Zhang, H. Chen, J. Wang, L.-X. Ding, S. Wang, P.J. Ashman, H. Wang, B. Dunn, J. Li, Graphene-based nitrogen-doped carbon sandwich nanosheets: a new capacitive process controlled anode material for high-performance sodium-ion batteries, J. Mater. Chem. A. 4 (2016) 8630–8635. doi:10.1039/C6TA02139E.

[5] L. Zhang, Z.C. Ding, T. Tong, J. Liu, Z.Y. Xie, L.X. Wang, J.H. Park, B.H. Hong, W.K. Choi, Y. Yic, J.Y. Hwang, D.I. Son, W. Haske, E. Najafabadi, T.M. Khan, H. Sojoudi, S. Barlow, S. Graham, J.L. Bredas, S.R. Marder, A. Kahn, B. Kippelen, Tuning the work functions of graphene quantum dot-modified electrodes for polymer solar cell

applications, Nanoscale. 9 (2017) 3524–3529. doi:10.1039/C7NR00136C.

[6] Z. Gao, L. Wang, J. Chang, X. Liu, D. Wu, F. Xu, Y. Guo, K. Jiang, Nitrogen doped porous graphene as counter electrode for efficient dye sensitized solar cell, Electrochim. Acta. 188 (2016) 441–449. doi:10.1016/j.electacta.2015.12.008.

[7] I.A. Sahito, K.C. Sun, A.A. Arbab, M.B. Qadir, Y.S. Choi, S.H. Jeong, Flexible and conductive cotton fabric counter electrode coated with graphene nanosheets for high efficiency dye sensitized solar cell, J. Power Sources. 319 (2016) 90–98. doi:10.1016/j.jpowsour.2016.04.025.

[8] T. Le, V. Lakafosis, Z. Lin, C.P. Wong, M.M. Tentzeris, Inkjet-printed graphene-based wireless gas sensor modules, Proc. - Electron. Components Technol. Conf. (2012) 1003–1008. doi:10.1109/ECTC.2012.6248958.

[9] E. Er, H. Çelikkan, N. Erk, Highly sensitive and selective electrochemical sensor based on high-quality graphene/nafion nanocomposite for voltammetric determination of nebivolol, Sensors Actuators B Chem. 224 (2016) 170–177. doi:10.1016/j.snb.2015.10.028.

[10] K. Pokpas, S. Zbeda, N. Jahed, N. Mohamed, P.G. Baker, E.I. Iwuoha, E.I.I. Sensorlab, Electrochemically reduced graphene oxide pencil-graphite in situ plated bismuth-film electrode for the determination of trace metals by anodic stripping voltammetry, Int. J. Electrochem. Sci. 9 (2014) 736–759. www.electrochemsci.org (accessed April 3, 2017).

[11] Y. Xu, X. Wei, C. Wang, J. Cao, Y. Chen, Z. Ma, Y. You, J. Wan, X. Fang, X. Chen, Silver Nanowires Modified with PEDOT: PSS and Graphene for Organic Light-Emitting Diodes Anode., Sci. Rep. 7 (2017) 45392. doi:10.1038/srep45392.

[12] Y. Xu, H. Yu, C. Wang, J. Cao, Y. Chen, Z. Ma, Y. You, J. Wan, X. Fang, X. Chen, Multilayer Graphene with Chemical Modification as Transparent Conducting Electrodes in Organic Light-Emitting Diode, Nanoscale Res. Lett. 12 (2017) 254. doi:10.1186/s11671-017-2009-9.

[13] K.M. Ang, L. Yeo, Y.M. Hung, M.K. Tan, Acoustially-Mediated Microfluidic Nanofiltration through Graphene Films, Nanoscale. (2017). doi:10.1039/C7NR01690E.

[14] D. Li, M.B. Müller, S. Gilje, R.B. Kaner, G.G. Wallace, R.B. Capaz, M.V.O. Moutinho, A. Lombardo, T.S. Kulmala, A.C. Ferrari, Processable aqueous dispersions of graphene nanosheets, Nat. Nanotechnol. 3 (2008) 101–105. doi:10.1038/nnano.2007.451.

[15] H. Li, Y. Tao, X. Zheng, J. Luo, F. Kang, H.-M. Cheng, Q.-H. Yang, P. Simon, M.W. Barsoum, Y. Gogotsi, D. Su, E.A. Stach, R.S. Ruoff, Ultra-thick graphene bulk supercapacitor electrodes for compact energy storage, Energy Environ. Sci. 9 (2016) 3135–3142. doi:10.1039/C6EE00941G.

[16] X. Xu, Y. Liu, M. Wang, C. Zhu, T. Lu, R. Zhao, L. Pan, Hierarchical hybrids with microporous carbon spheres decorated three-dimensional graphene frameworks for capacitive applications in supercapacitor and deionization, Electrochim. Acta. 193 (2016) 88–95. doi:10.1016/j.electacta.2016.02.049.

[17] B. Brodie, Sur le poids atomique du graphite, Ann. Chim. Phys. 59 (1860) 466–472.

[18] J. William S. Hummers, R.E. Offeman, Preparation of Graphitic Oxide, J. Am. Chem. Soc. 80 (1958) 1339. doi:10.1021/ja01539a017.

[19] D.C. Marcano, D. V. Kosynkin, J.M. Berlin, A. Sinitskii, Z. Sun, A. Slesarev, L.B. Alemany, W. Lu, J.M. Tour, Improved synthesis of graphene oxide, ACS Nano. 4 (2010) 4806–4814. doi:10.1021/nn1006368.

[20] A.B. Bourlinos, D. Gournis, D. Petridis, T. Szabo, A. Szeri, I. Dékány, Graphite Oxide : Chemical Reduction to Graphite and Surface Modification with Primary Aliphatic Amines and Amino Acids, Langmuir. 19 (2003) 6050–6055. doi:10.1021/la026525h.

[21] W. Chen, L. Yan, P.R. Bangal, I. Jung, D. Yang, A. Velamakanni, S.T. Nguyen, R.S. Ruoff, J. Hass, A.N. Marchenkov, E.H. Conrad, P.N. First, W.A. de Heer, Preparation of graphene by a low-temperature thermal reduction at atmosphere pressure, Nanoscale. 2 (2010) 559. doi:10.1039/b9nr00191c.

[22] Y. Wang, L. Tang, Z. Li, Y. Lin, J. Li, In situ simultaneous monitoring of ATP and GTP using a graphene oxide nanosheet-based sensing platform in living cells., Nat. Protoc. 9 (2014) 1944–55. doi:10.1038/nprot.2014.126.

[23] F. Ban, S. Majid, Graphene oxide and its electrochemical performance, InterJournal Electrochem. …Journal Electrochem. …. 7 (2012) 4345–4351.

[24] D. Pan, J. Zhang, Z. Li, M. Wu, Hydrothermal Route for Cutting Graphene Sheets into Blue-Luminescent Graphene Quantum Dots, Adv. Mater. 22 (2010) 734–738. doi:10.1002/adma.200902825.

[25] F.T. Thema, M.J. Moloto, E.D. Dikio, N.N. Nyangiwe, L. Kotsedi, M. Maaza, M. Khenfouch, Synthesis and characterization of graphene thin films by chemical reduction of exfoliated and intercalated graphite oxide, J. Chem. 3 (2013) 1–6. doi:10.1155/2013/150536.

[26] S. Stankovich, D. a. Dikin, R.D. Piner, K. a. Kohlhaas, A. Kleinhammes, Y. Jia, Y. Wu, S.T. Nguyen, R.S. Ruoff, Synthesis of graphene-based nanosheets via chemical reduction of exfoliated graphite oxide, Carbon N. Y. 45 (2007) 1558–1565. doi:10.1016/j.carbon.2007.02.034.

[27] S.-G. Kim, O.-K. Park, J.H. Lee, B.-C. Ku, Layer-by-layer assembled graphene oxide films and barrier properties of thermally reduced graphene oxide membranes, Carbon Lett. 14 (2013) 247–250. doi:10.5714/CL.2013.14.4.247.

[28] Raman of Graphene - InstaNANO, (n.d.). http://www.instanano.com/characterization/experimental/raman-graphene/ (accessed April 15, 2017).

[29] D. Chen, H. Feng, J. Li, Graphene oxide: Preparation, functionalization, and electrochemical applications, Chem. Rev. 112 (2012) 6027–6053. doi:10.1021/cr300115g.

[30] P. Khanra, T. Kuila, N.H. Kim, S.H. Bae, D. sheng Yu, J.H. Lee, Simultaneous bio-functionalization and reduction of graphene oxide by baker's yeast, Chem. Eng. J. 183 (2012) 526–533. doi:10.1016/j.cej.2011.12.075.

[31] Y. Gui, J. Yuan, W. Wang, J. Zhao, J. Tian, B. Xie, Facile Solvothermal Synthesis and Gas Sensitivity of Graphene/WO3 Nanocomposites, Materials (Basel). 7 (2014) 4587–4600. doi:10.3390/ma7064587.

[32] S.L. Ting, S.J. Ee, A. Ananthanarayanan, K.C. Leong, P. Chen, Graphene quantum dots functionalized gold nanoparticles for sensitive electrochemical detection of heavy metal ions, Electrochim. Acta. 172 (2015) 7–11. doi:10.1016/j.electacta.2015.01.026.

[33] P.K. Kalambate, M.R. Biradar, S.P. Karna, A.K. Srivastava, Adsorptive stripping differential pulse voltammetry determination of rivastigmine at graphene nanosheet-gold nanoparticle/carbon paste electrode, J. Electroanal. Chem. 757 (2015) 150–158. doi:10.1016/j.jelechem.2015.09.027.

[34] B. Zhang, Y. Zhang, W. Liang, B. Cui, J. Li, X. Yu, L. Huang, Nanogold-penetrated poly(amidoamine) dendrimer for enzyme-free electrochemical immunoassay of cardiac biomarker using cathodic stripping voltammetric method, Anal. Chim. Acta. 904 (2016) 51–57. doi:10.1016/j.aca.2015.11.025.

Chapter 5 :

Graphene-modified Pencil Graphite, In-situ Plated Mercury Film Electrodes (Gr-PG-MFEs) for the Ultratrace Determination of Nickel by Adsorptive Cathodic Stripping Voltammetry (AdCSV)

Abstract

Graphene, the 2-D allotrope of carbon has previously been employed in a variety of chemical sensing applications due to its ability to (i) enhance electron transfer kinetics and (ii) improve active surface area at electrode materials. Its application in metal analysis has been limited to use in anodic stripping voltammetry (ASV). Adsorptive stripping voltammetry (AdSV) offers a fast, simple, sensitive, low cost and green electroanalytical technique for the determination of trace concentrations of metal ions in water samples with low solubility in metallic films. Electrochemically reduced graphene oxide (ERGO), in conjunction with an electroplated mercury film was utilized to improve pencil graphite electrode (PGE) sensitivity towards the square-wave adsorptive cathodic stripping voltammetric (SW-AdCSV) determination of selected heavy metals (Ni^{2+} and Co^{2+}) in the presence of dimethylglyoxime as chelating agent. Simultaneous electroplating of Hg-films and accumulation of formed $[Ni(dmgH)_2]$ complexes were performed under a constant – 0.7 V accumulation potential for the first time. In addition, few-layer graphene sheets were successfully deposited on PGEs by cyclic voltammetry reduction from graphene oxide dispersions prior to analysis. The experimental parameters of the fabricated ERGO-PG-MFE (deposition potential, deposition time, rotation speed, frequency and amplitude) were optimized, and its applicability was investigated towards the individual and simultaneous determination of Ni^{2+} and Co^{2+} at the low concentration levels (µg L^{-1}) in 0.1 M ammonium buffer solution (pH 9.4) using square wave adsorptive cathodic stripping voltammetry (SW-AdCSV). The calculated detection limit for Ni^{2+} at 120 s accumulation time was found to be 0.120 ± 0.002 µg L^{-1} for individual analysis. Real sample analysis, of laboratory tap water was performed using the ERGO-

PG-MFEs. The developed electrode was found to exhibit sensitive detection of metal ions in the tap water samples at the 0.2 μg L^{-1} level.

Keywords:

Electrochemically reduced graphene oxide, pencil-graphite electrode, mercury-film, trace metals, cathodic stripping voltammetry

Highlights:

- A one-step, simultaneous electroplating of metallic film and accumulation of metal cation by adsorption is achieved in the AdCSV technique
- Electrochemically reduced graphene oxide modified pencil graphite electrodes (ERGO-PGE) is investigated towards the detection of Ni^{2+}
- Selective determination of Ni^{2+} in the presence of Co^{2+}

Graphical Abstract

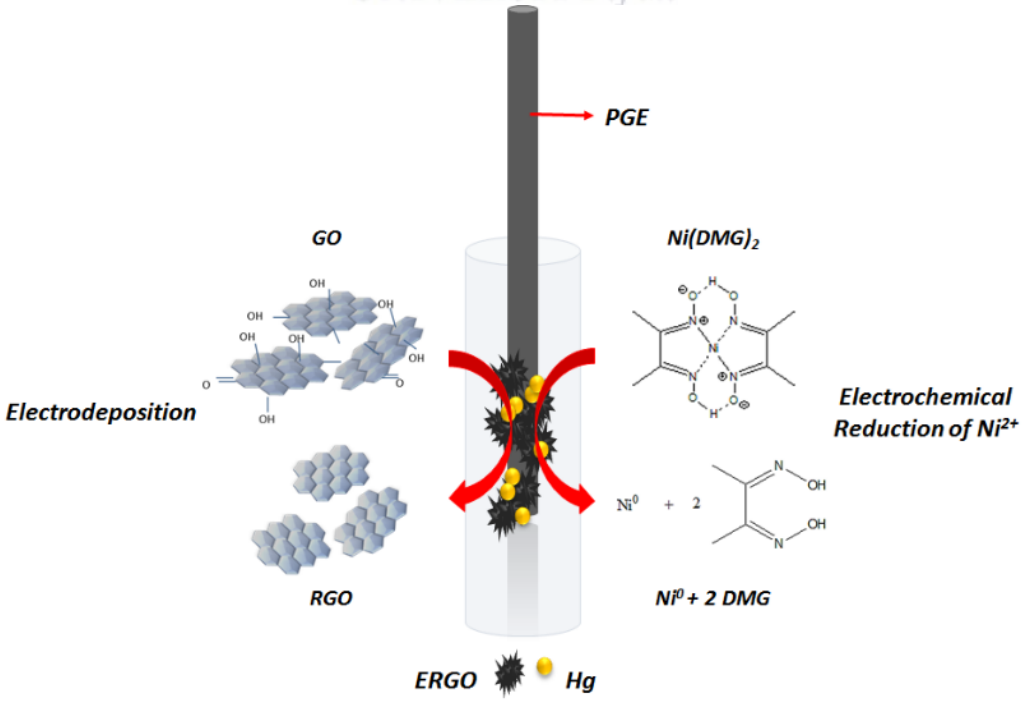

5.1. Introduction

Nickel is a toxic transition metal which has been linked to some serious health problems such as respiratory system cancer [1]. Nickel is noted as one of the most important transition metal ions in biological samples [2] and is both vital and toxic for biological systems. Nickel has been linked to skin allergies or dermatitis in regard to eyeglass frames, dental materials, and costume jewelry however, of the approximately 10 mg in the body, significant amounts of nickel are found in RNA and DNA where it interacts with these nucleic acids. Moreover, nickel is known to cause a skin disorder known as nickel-eczema [3]. The pollution by heavy metals is of growing concern globally and has been on the increase over this past few years. The main source of nickel pollution in water is nickel bearing pipes and fittings in contact with water and nickel ore containing rocks, and industrial activities such as electroplating, stainless steel and alloys [1]. In considering the aforementioned health benefits and toxicity of Ni, the determination of nickel (II) in drinking water is an important task.

The various analytical methods that have been developed and used for the determination of nickel includes flame atomic absorption spectrometry, FAAS, electrothermal atomic absorption spectrometry, ETAAS, neutron activation analysis, NAA, x-ray fluorescence spectrometry, XRF inductively coupled plasma atomic emission spectrometry, ICP-AES, spectrophotometry and Electroanalytical techniques. However, these spectroscopic methods are expensive, their availability is limited, and they are not well suited for *in situ* measurements and, require complicated instrumentation. For trace nickel (II) analysis, adsorptive stripping voltammetry has been the most popular electroanalytical technique because of its speed, good selectivity and sensitivity, and low instrumentation cost [4] compared to other techniques.

Electroanalysis of heavy metals with mercury electrodes have been around for many decades and are still very popular at present. The usefulness of mercury electrodes for the determination of nickel is due to their ability to form amalgams, allowing pre-concentration of metal ions prior to their determination by voltammetric stripping method. The other advantage of using mercury based electrodes is its association with high over-potential of hydrogen evolution [3], and it presents the possibility of a constantly renewable surface. This eliminates the possibility of electrode poisoning by pre-deposited mater. Mercury-modified electrodes coupled with stripping

techniques have been recognized as the most-sensitive method for the determination of heavy metals such as nickel [3].

The development and application of pencil graphite electrodes have received considerable attention in recent years for different application of stripping analysis. These kind of electrodes are inexpensive and possess many advantages such as a good conductor of electricity, needs almost no pretreatment, has low cost, readily available and has low background current [5]. All of these properties make it a good alternative to the well-known glassy-carbon and gold electrodes (GCE and GE) [4]. A number of studies on the use of pencil graphite electrodes for analytical determinations of different metal ions by stripping voltammetric measurements have been reported [4–7].

Due to its excellent electronic, thermal and mechanical properties graphene, is a single atomic layer of carbon atoms tightly packed in a two dimensional honeycomb lattice. This novel material is atomically thin, chemically inert, consists of light atoms, and possesses a high ordered structure [8]. Graphene is electrically and thermally conductive, and is the strongest material ever measured. These remarkable properties make graphene the ideal support film for graphite pencil. Since it was first produced in 2004, graphene has attracted many attentions and has shown to significantly improve the sensitivity in various applications due to rapid electron transfer [9] and high surface-to-volume ratio.

In this work, an electrochemically reduced graphene oxide pencil graphite electrode (ERGO-PG) was prepared from graphene oxide in acetate buffer solution in conjunction with in situ plated mercury film for the ultra-trace determination of nickel by Adsorptive Cathodic Stripping Voltammetry (AdCSV).

5.2. Experimental Section

5.2.1. Reagents

All chemicals used in this study were analytical reagent grade and used without further purification. Standard stock solutions (1,000 mg L^{-1}, atomic absorption standard solution) were obtained from Sigma-Aldrich and diluted as required.

Ammonium hydroxide ammonium chloride solution buffer (0.1 M, pH 9.35) was used as supporting electrolyte and prepared by mixing ammonium chloride and ammonium hydroxide followed by diluting the solution with ultra-pure distilled water (Millipore). A pH meter (Metrohm 827 pH lab.) was calibrated using pH 4, pH 7 and pH 9 calibration buffer solutions and, then used to verify the pH of the ammonia hydroxide-ammonium hydroxide buffer solution (supporting electrolyte) solution.

5.2.2. Apparatus

Square-wave anodic stripping voltammetric measurements were performed using a 797 VA COMPUTRACE instrument (Metrohm, Switzerland) controlled by a personal computer. A three electrode electrochemical system consisting of an electrochemically reduced graphene oxide pencil-graphite mercury-film electrode (ERGO-PG-MFE) served as the working electrode. An Ag/AgCl (saturated KCl) and platinum wire served as the reference and counter electrodes, respectively. All experiments were performed in a one compartment 20 mL voltammetric cell at room temperature.

Fourier Transform Infrared (FT-IR) spectra were recorded using a (Perkin Elmer Spectrum 100) coupled to an Attenuated Total Reflectance (ATR) sample holder. FT-IR was used to obtain information and confirmation on graphene oxide. The High Resolution Scanning Electron Microscopy (HR-SEM) images and information were obtained using a LEO 1450 SEM 30 kV instrument equipped with Electronic Data System (EDS) and Windows Deployment Services (WDS). High Resolution Transmission Electron Microscopy (HRTEM) measurements were carried out with a Tecnai G2 F20X-Twin MAT Field Emission Transmission Electron Microscope from FEI (Eindhoven, Netherlands) under an acceleration voltage of 200 kV.

5.2.3. Synthesis of graphene oxide(GO)

Graphite oxide was synthesized from graphite powder according to the Hummers' method with some modification. Graphite powder (2 g) and sodium nitrite (1 g) was mixed with sulfuric acid (50 mL) in a clean dry conical flask and stirred at room temperature for 30 min, followed by subsequent mixing in an ice bath for 20 min. Potassium permanganate (7 g) was added gradually over a 30 min period with constant stirring. The resulting solution was allowed to reach room

temperature by stirring for 2 h prior to being placed in a water bath set at 35 ºC. The flask was returned to the ice bath with constant stirring. Ultra-pure water, 150 mL, was added before the addition of approximately 5 mL hydrogen peroxide until effervescence ceased. The flask was removed from the ice bath and allowed to stir at room temperature overnight and centrifuged for 20 min. Three successive acid washes were performed followed by one with ultra-pure water. The resulting product was dried for 48 h in a vacuum oven.

5.2.4. Preparation of electrochemically reduced grapheme oxide pencil graphite electrode (ERGO-PGE)

The pencil-graphite rods (Pentel, HB of 0.5 mm in diameter and 6 cm in length) were purchased from the local bookstore. A plastic syringe served as a holder into which the pencil rod was inserted exposing 1 cm of the rod tip at one end of the syringe. In order to establish electrical connection with the potentiostat a copper wire was attached to the other end of the pencil rod and passed through the top of the syringe.

To make 100 mL of 0.5 mg mL^{-1} of graphene oxide solution, 50 mg of graphene oxide was exfoliated in 100 mL of 0.1 M acetate buffer solution (pH 4.6) by ultrasonication for 1.0 h to give 0.5 mg mL^{-1} GO solution. A 1 cm portion of the pencil rod tip was immersed in 20 mL of GO dispersion (0.5 mg mL^{-1}) and cyclic voltammetric reduction of GO was performed in the potential range between - 1.5 and + 0.3 V for five successive cycles. The instrumental parameters that were used for the electro-deposition procedure are as follows; deposition time (120 s), cleaning time (30 s), sweep rate (0.1 V) and voltage step (0.005 V).

5.2.5. Electrode cleaning

To achieve accurate and reproducible results in quantitative analysis impeccable electrode hygiene was applied. The pencil-graphite electrodes were thoroughly cleaned before their use and this was done by dipping a pencil graphite electrode in a small amount of ethanol for at least 60 s and the surface of the electrode was gently wiped using a tissue paper followed by thorough rinsing with ultra-pure water. Successive dipping of the PGE in a 3 M HNO_3 solution and rinsing with ultra-pure water followed. The electrodes were then allowed to dry in air for at least 10 min before use.

5.2.6. Procedure for square wave anodic stripping voltammetry (SWASV) analysis

The ERGO-PG electrode was placed into a 20 mL of NH_4OH-NH_4Cl buffer (0.1M, pH 9.2) solution containing 100 µL Hg (1000 ppm), 100 µL Dimethylglyoxime (0.1 M in ethanol) and 10 µL of 10 mg L^{-1} each of Ni^{2+} and Co^{2+} individually. A deposition potential of - 0.7 V was applied for 120 s using a pulse height of 20 mV, a frequency of 50 Hz and with constant stirring at 800 rpm. After an equilibration time of 10 s, a square wave waveform was applied from - 0.7 V to - 1.4 V followed by electrochemically cleaning of any target metals residues by applying a potential of + 30V for 120 s. Once development of the electrode and an understanding of this technique was achieved, tap water was collected and analyzed for the determination of Co^{2+} and Ni^{2+} using the new sensor developed above.

5.2.7. Sample Preparation

For the preparation of the water sample, tap water was collected from our research laboratory after being allowed to run for 1 min. An 18 mL aliquot of tap water and 2 mL of 1 M ammonium hydroxide ammonium chloride buffer solution was added to the compartment cell and the analysis of Ni^{2+} was carried out as describe in *Section 5.2.6* above.

5.3. Results and Discussion

5.3.1. Electrochemical reduction of graphene oxide

The electrochemical reduction of graphene oxide onto the PGE was performed by repetitive cyclic voltammetric scans from a graphene oxide (0.5 mg mL^{-1}) solution in acetate buffer. Two anodic (i and ii) and one cathodic (iii) peak is observed in the cyclic voltammograms shown in *Figure 5.1,* below. The exact nature of the small anodic peak at – 0.7 V is not clear to date, but its rapid reduction with successive cycling could be attributed to the deposition of ERGO at the electrode surface. The cyclic voltammogram further shows a very large anodic peak (ii) which is obtained after 1 cycle and attributed to the oxidation of the graphite electrode surface. The anodic peak current decreases with increasing scan number indicating the electrochemical deposition of ERGO sheets onto the electrode surface. Deposition of graphene sheets at the electrode surface inhibits available sites of the graphite electrode for oxidation. The cathodic peak (II) decreases with number of scans can be ascribed to some electrochemically active oxygen-containing groups

on the surface of GO which are too stable to reduce at more negative potentials [10] or due to the reduction of the irreversible surface oxygen groups since the reduction of water to hydrogen occurs at more negative potentials.

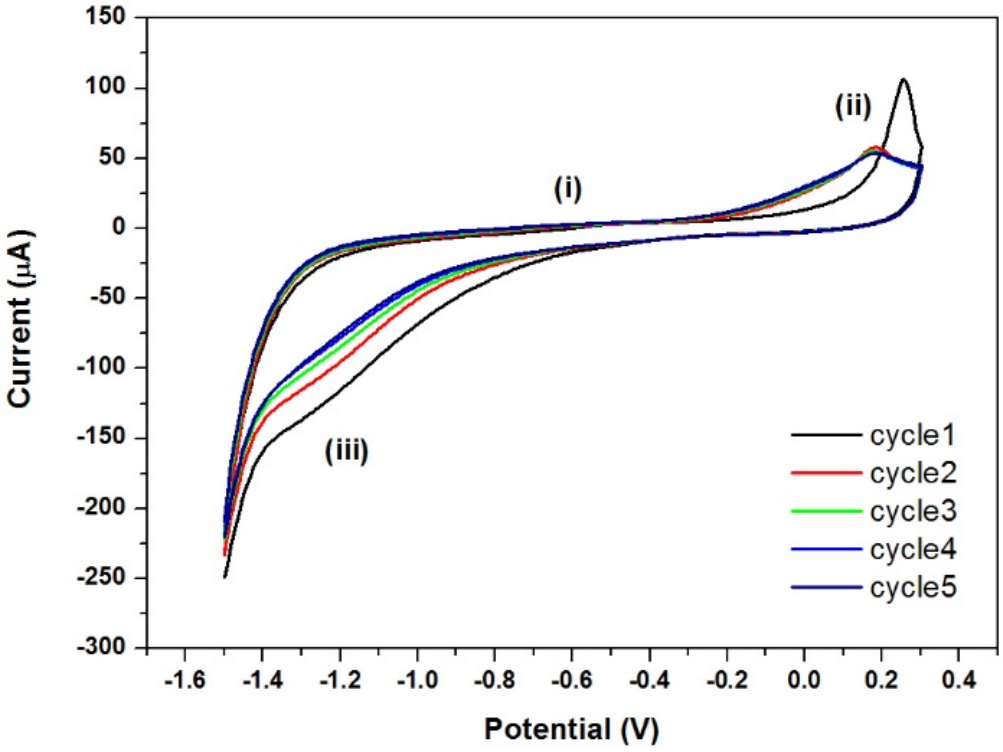

Figure 5.1: Cyclic voltammograms depicting the electrochemical reduction of 0.5 mg mL^{-1} GO in acetate buffer solution (0.1 M, pH 4.6) at the PGE using the following instrumental parameters: scan rate (0.1V s^{-1}), deposition time (120 s); frequency (20 Hz); amplitude (0.04 V) and voltage step (0.005 V).

Cyclic voltammograms for the bare PGE and ERGO-PGE recorded in 0.1 M ammonium buffer solution are shown in *Figure 5.2*. The voltammogram show the larger background current observed for the ERGO-PGE in comparison with the PGE indicate ERGO's capacity to enhance electron transfer and conductivity when immobilized at the electrode surface.

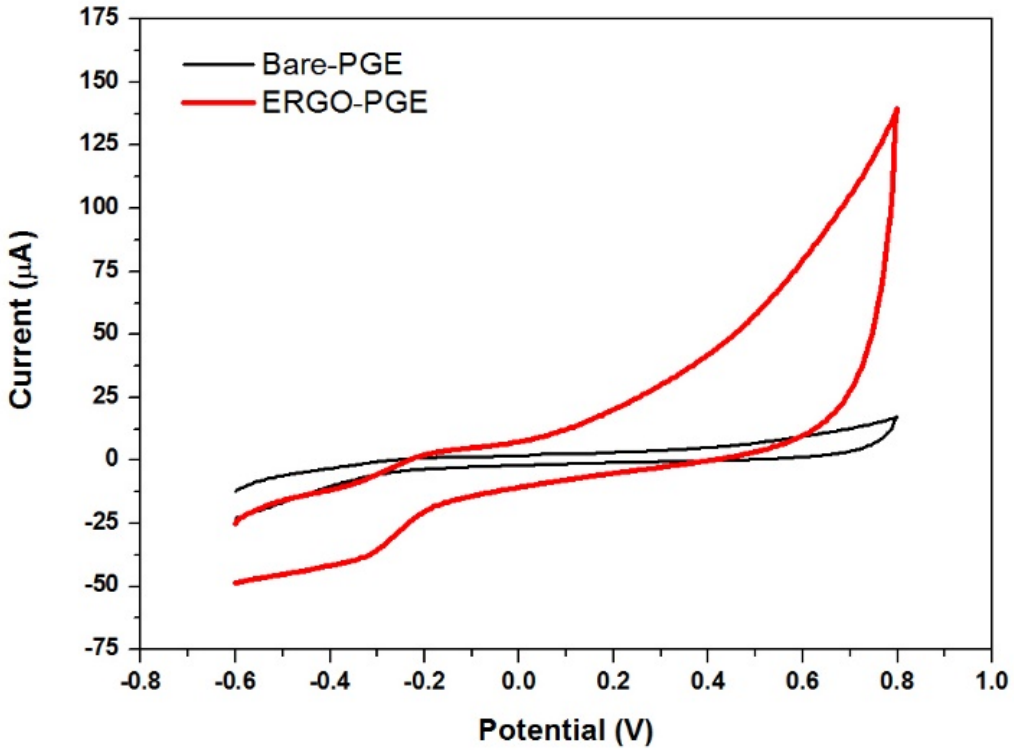

Figure 5.2: Cyclic voltammograms of (a) a bare PGE and (b) an ERGO-PGE in ammonium buffer solution (0.1 M, pH 9.4) at the following instrumental parameters: scan rate (10 mV s−1), deposition time (120 s), frequency (50 Hz), amplitude (0.04 V) and voltage step (0.004 V).

The redox couple of $K_3Fe(CN)_6$ solution is close to an ideal quasi-reversible system and it was used to characterize the properties and response of our bare and ERGO pencil graphite electrodes *Figure 5.3.* below. It is evident to see that the ERGO on a pencil graphite increase the anodic and redox peaks currents compared to those of bare electrodes indicating that the high electroactive graphene interface was formed, owing to the high conductivity of graphene. Further, a distinct narrowing in peak current separation (ΔE_p) is observed from 0.274 V to 0.06 V upon graphene inclusion at the electrode surface.

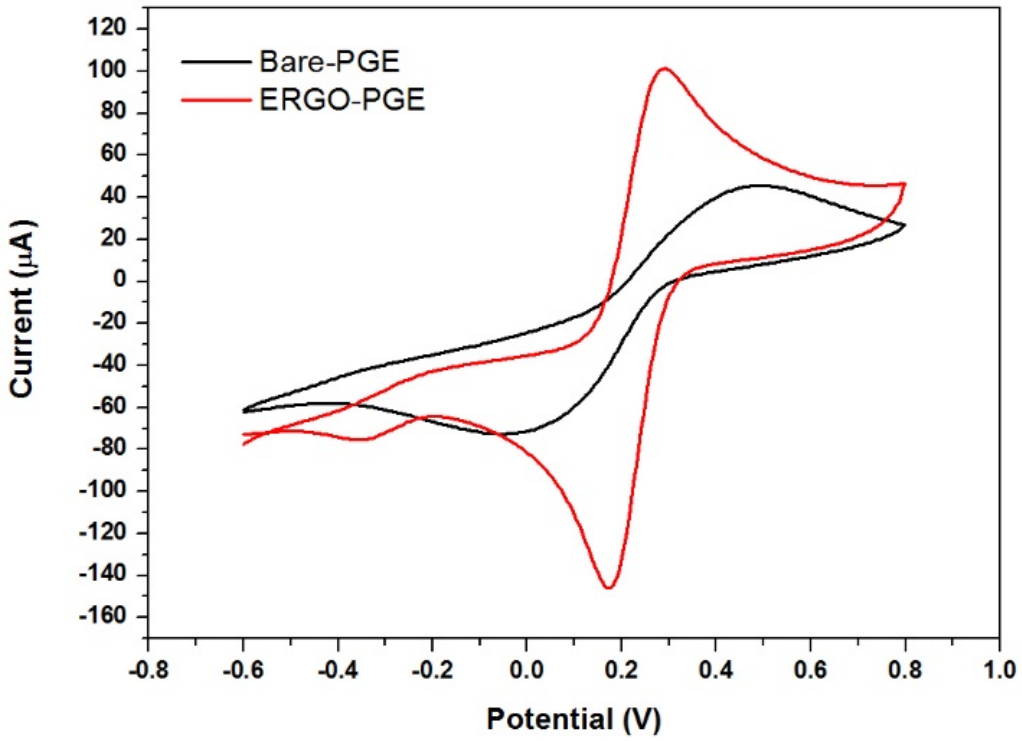

Figure 5.3: Cyclic voltammograms of bare-PGE (a) and ERGO-PGE (b) in 0.1mM $K_3Fe(CN)_6$ solution containing 0,1 M KCl.

5.3.2. Characteristic oxidation potential of Ni^{2+}

Figure 5.5, shows a well-resolved, symmetrical characteristic stripping reduction peak at –1.10 V for 20 μgL^{-1} of Ni^{2+} at the ERGO-PG-MFE in 0.1 M ammonium chloride, ammonium buffer solution (pH 9.4). The exact mechanism describing the reduction of metal cations by AdCSV is not well known and is quite ambiguous. Typically, metallo-chelate complex formation is formed in solution with suitable complexing agent under favorable conditions. The formed $[Ni(dmgH)_2]$ complex is then adsorbed at the electrode surface in the presence of an electroplated metal film. Subsequent reduction of the adsorbed metal cation complex from the electrode surface is achieved by application of a cathodic reduction potential scan. The general mechanism is illustrated in *Equations 5.1,5.2 and 5.3*, below.

$$Ni(II)\text{-}(dmgH)_2\ (solution) \rightarrow Ni(II)\text{-}(dmgH)_2\ (ads) \qquad (Equation\ 5.1)$$

$$Ni(II)\text{-}(dmgH)_2\ (ads) + ne^{-1} \rightarrow [Ni(II)\text{-}(dmgH)_2]\text{-}Hg^{n-}\ (ads) \qquad (Equation\ 5.2)$$

$$[Ni(II)\text{-}(dmgH)_2]\text{-}Hg^{n-}\ (ads) + 2e^- \rightarrow Ni(0) + DMG \qquad (Equation\ 5.3)$$

A schematic representation of the observed mechanism of the AdCSV procedure for the detection of Ni^{2+} is shown in *Figure 5.4*. A single step accumulation and complex formation of Ni^{2+} with dimethylglyoxime to form a stable metal-chelate complex precedes adsorption. A cathodic reduction scan measurement is then performed.

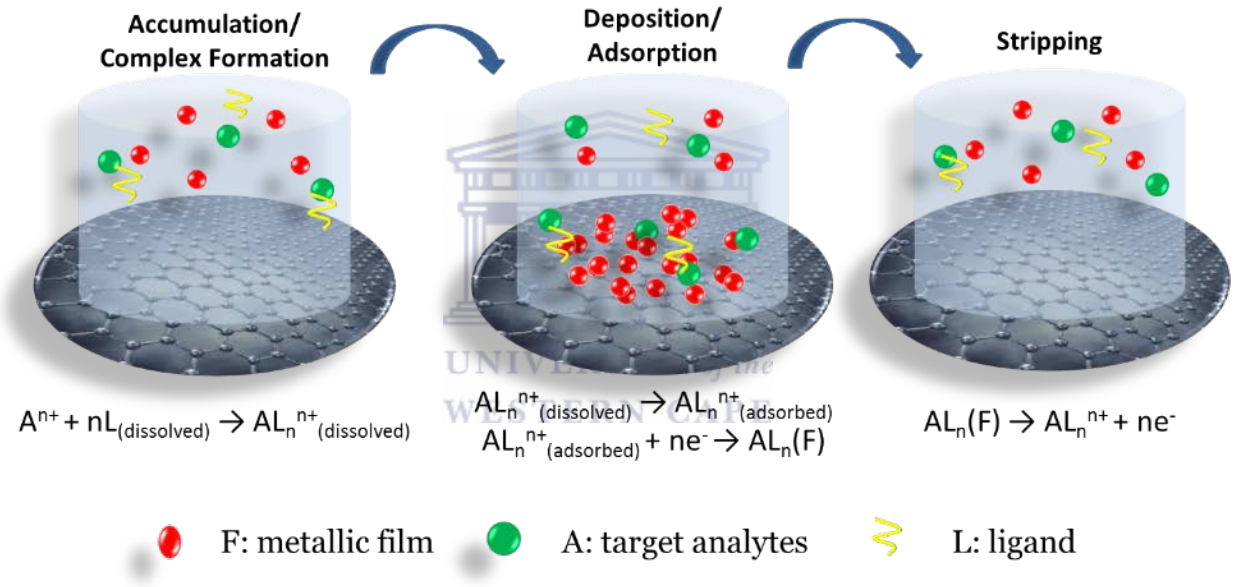

Figure 5.4: Schematic representation of the AdCSV detection of metal cations in the presence of chelating agent and metallic film

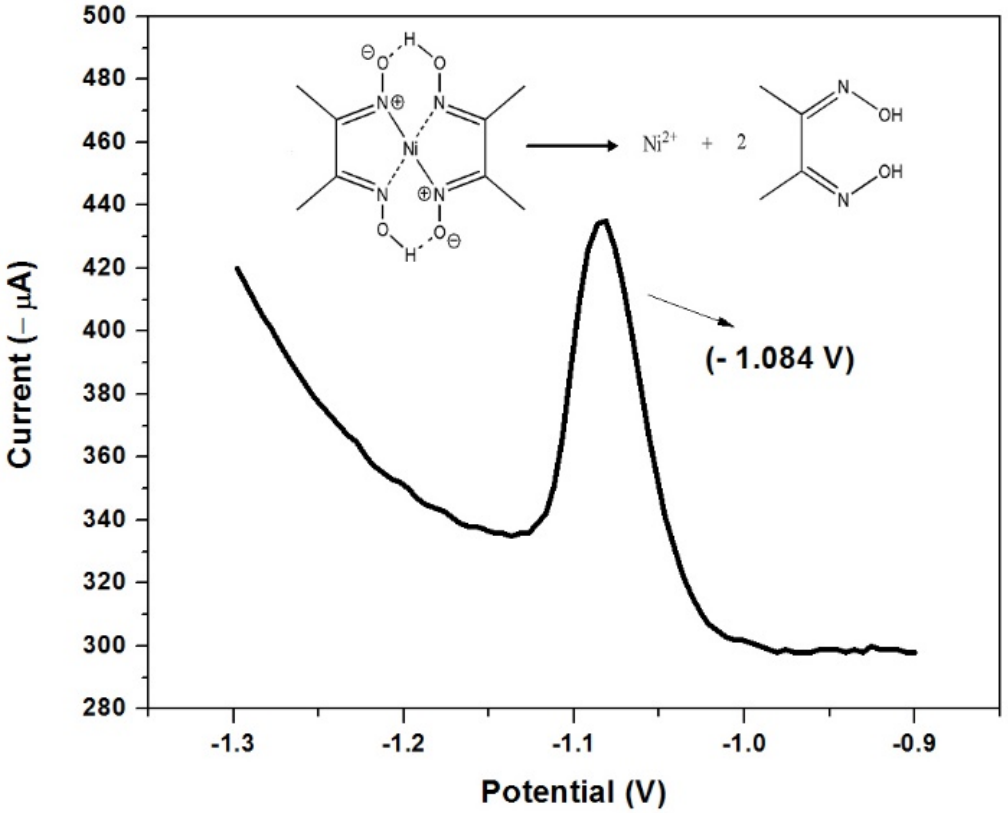

Figure 5.5: Cathodic stripping voltammogram of characteristic oxidation stripping potential of 20μg.L^{-1} Ni^{2+}(-1.10 V) in 0.1 M ammonium buffer solution (pH 9.4) at the ERGO-PGE under the optimized parameters.

5.3.3. Microscopic characterization of electrochemically reduced graphene oxide modified pencil-graphite electrode (ERGO-PGE)

The high resolution scanning electron microscopy (HRSEM) images of the bare PGE and ERGO-PGE surfaces are shown in *Figure 5.6*. Surface roughness with grooves on the surface along the direction of machining can be observed at the bare PGE surface. Following the electrochemical reduction of graphene oxide flakes of graphene sheets are observed at the ERGO-PGE surface.

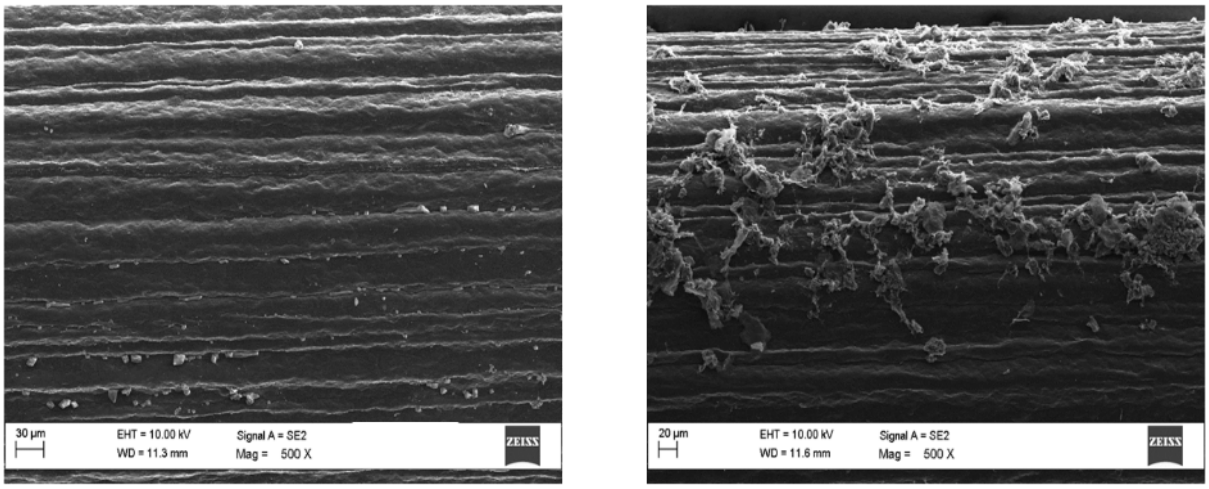

Figure 5.6: HRSEM images of bare-PGE (left) and ERGO-PGE (right) at 500 times magnification.

5.3.4. Effects of electrochemically reduced graphene oxide on the stripping peaks currents

The peak current responses of the bare-PG-MFE, ERGO-PGE and ERGO-PG-MFE platforms towards Ni^{2+} in 0.1 M ammonium chloride ammonium hydroxide buffer solution (pH 9.4) are compared in *Figure 5.7*. A considerable increase in peak current (three times) is observed at the ERGO-PGE in comparison to the bare-PG-MFE which is seen as a flat line indicating improved sensitivity towards the Ni ions. The higher surface area-to-volume ratio, enhanced electron transfers and conductivity due to quantum confinement of ERGO in the nanometer range (1-100 nm) all contribute towards the increase in stripping peak current. However, the enhancement in stripping peak current and peak symmetry from ERGO-PGE to ERGO- PG- MFE is evidence that the mercury film onto the electrode surface is contributes to the much improved selectivity and sensitivity of the Nickel stripping peak.

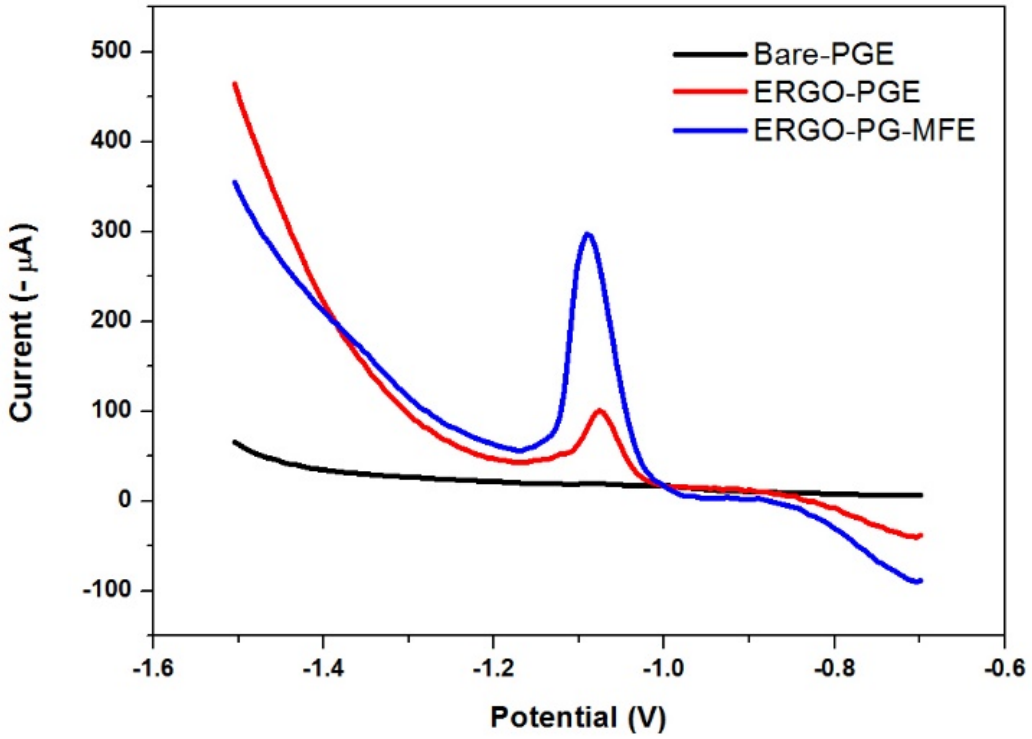

Figure 5.7: SWASV of 20 μgL^{-1} at (a) bare-PG-MFE, (b) ERGO-PGE and (c) ERGO- PG-MFE. Supporting electrolyte (0.1 M ammonium chloride ammonium hydroxide buffer solution, pH 9.4), deposition potential (-0.7 V), deposition time (120 s), frequency (50 Hz), amplitude (0.05 V) and voltage step (0.005 V).

5.3.5. Film stability and reproducibility

The stripping peak current of Ni^{2+} showed little or no change during the preparation of the modified electrodes as well as its application to the detection of 20 μg L^{-1} of target metal ions in 0.1 M of ammonium buffer (pH 9.4), at the same conditions. Relative standard deviation (RSD %) for the oxidation peaks were calculated to be in the range of 1 – 5 % for the target metal ion. The low standard deviation provides evidence as to the good reproducibility in preparing the ERGO-Hg-PGEs.

5.3.6. Optimization of instrumental parameters

Effect of instrumental parameters on the stripping peak currents of Ni^{2+}at the electrochemically reduced graphene oxide-pencil graphite mercury thin film electrode(ERGO-PG-MFE) were investigated. Among the square-wave parameters which were investigated which affect the analytical responses at the ERGO-PG-MFE are deposition time, deposition potential, cleaning time, frequency, amplitude and rotation speed.

Figure 5.8 (a) shows the effect of deposition time on the peak current of Ni^{2+} investigated over a time interval of 0 to 300 s. The peak current of Ni^{2+} increased with increase deposition time since more time is allowed for the analyte ions to undergo reduction and deposition at the ERGO-PG-MFE surface. At deposition time of more than 210 s the peak heights started decreasing as an indication of surface saturation of the electrode. For the subsequent experiments a deposition time of 120 s was chosen as it gives a much better enhanced peak current of Ni^{2+} while avoiding any possible saturation of the electrode surface.

The effect of the rotational speed on the peak current of Ni^{2+} from 200 to 2000rpm was investigated during the pre-concentration step as shown in *Figure 5.8 (b)*. The peak height of the detected target metal was found to be increasing with an increase in rotational speed until there was a steady and flat peak current at rotational speed above 1000 rpm. A rotational speed of 800 rpm was found to maximize/ fully spread the metals all around the supporting electrolyte to the electrode surface resulting in an enhanced peak current than the rest of the rotational speeds.

The amplitude in *Figure 5.8 (c)* was varied from 10 to 100 mV and showed an increase in stripping peak current of Ni^{2+} with increasing amplitude up to a maximum, followed by a gradually decrease. A 50 mV amplitude of was selected for subsequent experiments since the maximum enhancement of the stripping peak of Ni^{2+} is achieved at that amplitude and any further amplitude increase results in the decrease peak current.

The influence of deposition potential on the peak currents of Ni^{2+}at the ERGP-PG-MFE was investigated in the potential range from - 0.4 V to – 1.2 V, *Figure 5.8 (d)***.** At potential more negative than the oxidation potential of the Ni ion no stripping peaks were observed due the suppression of the reduction reaction responsible for the deposition of metal ion from the solution

onto the electrode surface. A sharp increase between - 1.1V and - 0.7 V can be observed followed by a sharp decrease from - 0.7 V to more positive potentials. A deposition potential of - 0.7 V was chosen for further experiments as the optimal deposition potential.

Figure 5.8 (e) shows the variation of cleaning time with peak height of Ni^{2+} applied over the cleaning time range of 0 – 210 s. The peak current of Ni^{2+} increased with increase cleaning time until maximum and started to gradually decrease. A cleaning time of 120 s was chosen for the rest of the experiment as it gives the maximum possible enhancement of the current peak of the Ni^{2+}. Peak currents of which the cleaning time is either less or more than 120 s gives less enhanced peak current compared to the cleaning time of 120 s.

In *Figure 5.8 (d)*, the change in frequency and its influence on the peak current of the target metal over the range of 0 to 100 Hz was investigated. The peak current of Ni increased as the frequency was increased and after a frequency of 50 Hz was applied the peak current of Ni started decreasing. An increase in the frequency results in an increase of the scan rate. A frequency of 50 Hz was chosen as the optimum frequency for this experiment since a maximum enhancement of the peak current is reach at that frequency.

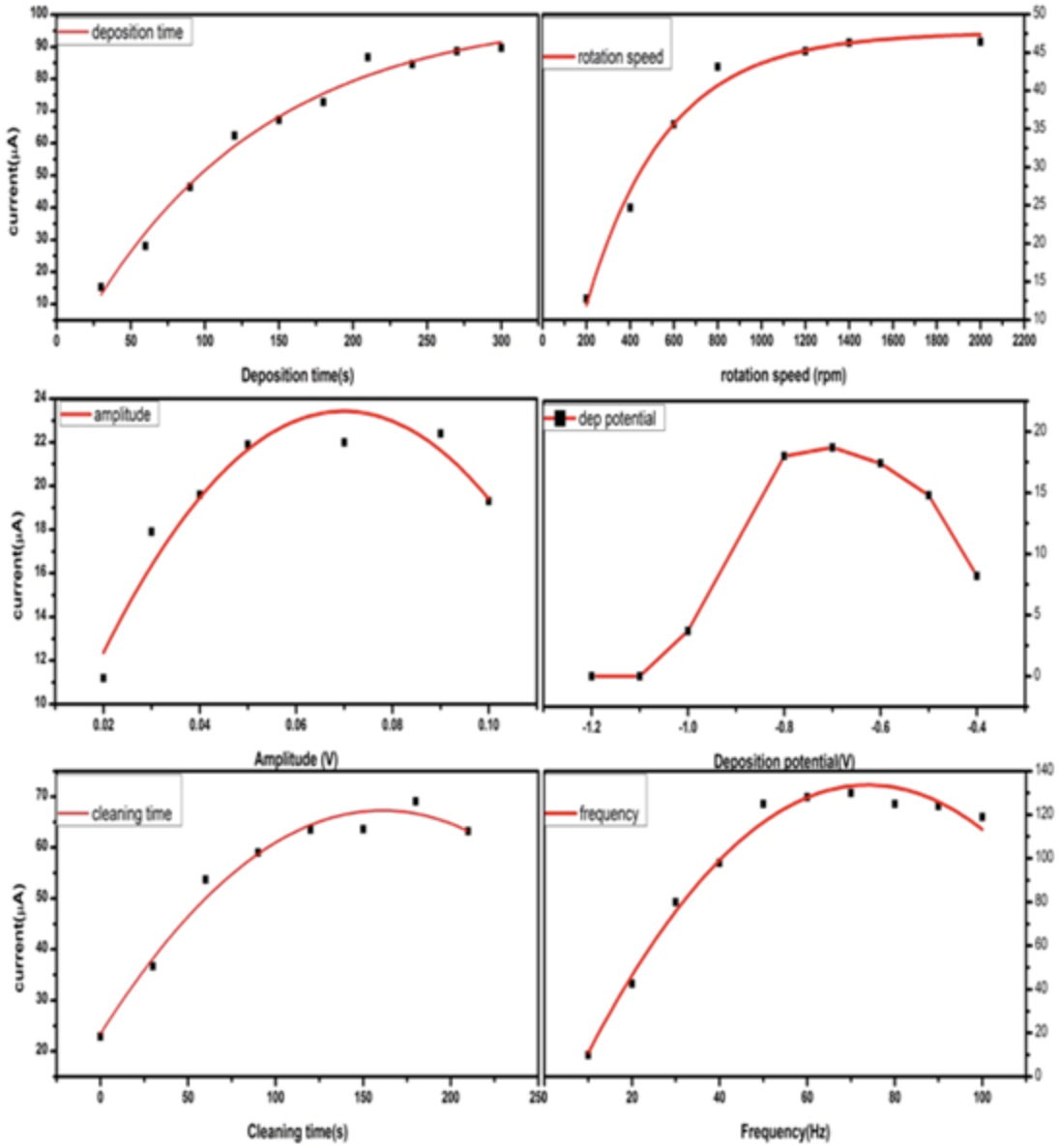

Figure 5.8: The effect of (a) deposition time, (b) rotation speed, (c) amplitude, (d) deposition potential, (e) cleaning time and (f) frequency on the stripping peak of Ni^{2+} at electrochemically reduced graphene oxide pencil graphite mercury film electrode (ERGO-PG-MFE) in 0.1M ammonium hydroxide ammonium chloride buffer solution (pH = 9.4) containing 5 μg L^{-1} of Ni in 5 mg L^{-1} of Hg^{2+}.

5.3.7. Analytical performances of the electrochemically reduced graphene oxide modified pencil graphite mercury film electrode

The analytical performance of the ERGO-PG-MFE was investigated by individual analysis of Ni^{2+} over the concentration range of 2 – 18 μg L^{-1}. The square wave cathodic stripping voltammetry and their corresponding calibration curve for the analysis of Ni^{2+} in 0,1 M ammonium chloride ammonium hydroxide solution (pH 9.4) at ERGO-PG-MFE is shown in *Figure 5.9,* below. Constant increases in peak currents is observed over the concentration range under investigation with no shifts in observed peak potentials. A linear increase in stripping peak currents is observed over the dynamic linear range of 2 and 16 μg L^{-1} before electrode saturation was observed. A recorded linear correlation coefficient (R^2) of 0.996 was determined with a sensitivity of 0.97 μAL μg^{-1}. The calibration plots, constructed from voltammogram data was used to calculate the limit of detection and quantitation according to *Equation 5.4.* and are presented in *Table 5.1.* Limits of detection and quantitation were found to 0.120 ± 0.002 μg L^{-1} and 0.401 ± 0.007 μg L^{-1}, respectively. The observed LOD is well below the prescribed EPA and WHO maximum contamination limit of 0.1 mg L^{-1} of Ni^{2+}.

$$\mathrm{LOD/LOQ} = \frac{F \times \sigma}{b} \quad (\textit{Equation 5.4})$$

Where

LOD: Limit of Detection

LOQ: Limit of Quantitation

F: Factor of 3.3 and 10 for LOD and LOQ, respectively

σ: Standard deviation of the blank, standard deviation of the ordinate intercept, or residual standard deviation of the linear regression

b: Slope of the regression line

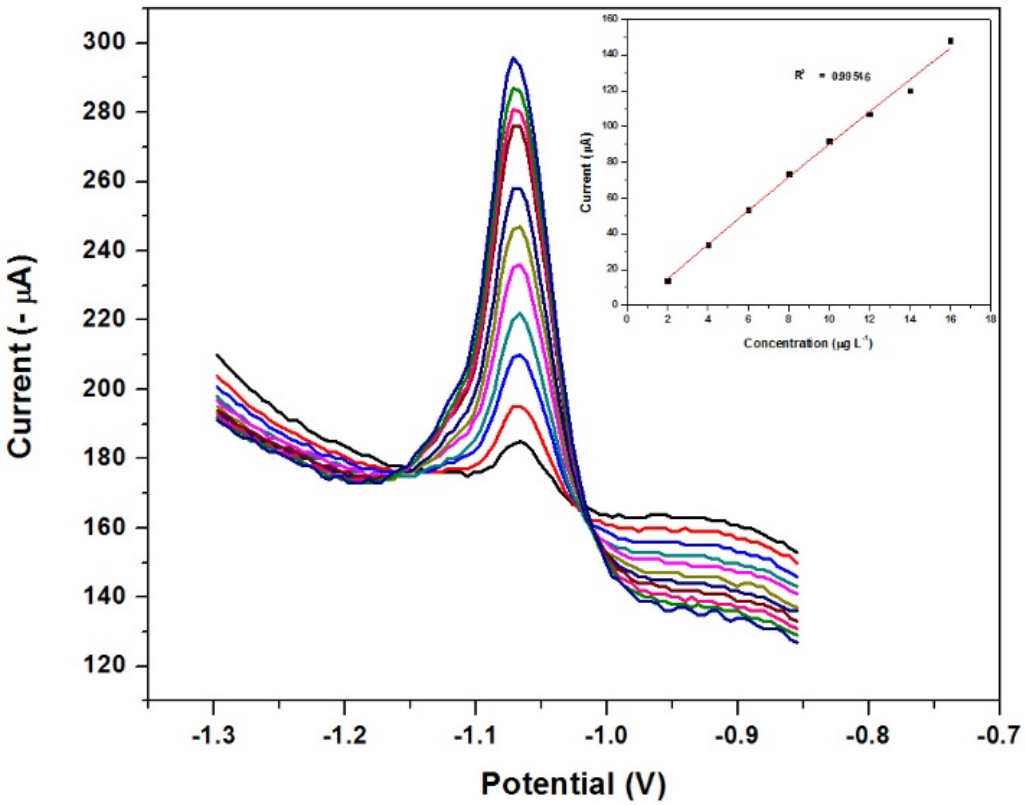

Figure 5.9: SWAdCSV and corresponding calibration curve for the individual analysis of Ni^{2+} obtained at ERGO-PG-MFE between the concentration of 2 ppb – 16 ppb. The supporting electrolyte used was ammonium hydroxide ammonium chloride buffer solution (0.1M, pH 9.4), deposition time (210 s), deposition potential (- 0.7 V), rotational speed (800 rpm), frequency (50 Hz), amplitude (0.05 V) and sweep rate (0.2 V s^{-1}).

Table 5.1: Calibration data representation individual analysis of Ni^{2+} at ERGO-PG-MFE in 0.1M ammonium buffer solution (pH 9.4) under optimized parameters*.

Analytical Parameter	*Analysis of Ni^{2+} (2-22 µg L^{-1})*
Sensitivity (µA L $µg^{-1}$)	9.71E-7
Correlation Coefficient (R^2)	0.997
Detection Limits (µg L^{-1})	0.120 ± 0.002
Limit of Quantification (µg L^{-1})	0,401 ± 0,007

*n = 3, where n is the number of replications.

The effectiveness of the developed ERGO-PG-MFE, to quantitatively detect Ni^{2+} metal cations in water samples was investigated by comparing the determined limits of detection (LOD) with recently reported literature values. *Table 5.2*, illustrates a summary of previously reported Ni^{2+} sensing techniques and its analytical performance. The developed sensor shows comparable results to other reported sensor technologies based on the adsorptive stripping voltammetric technique in the low µg L^{-1} range under short evaluation times.

Table 5.2: A summary of previously reported limits of detection (LOD) for Ni^{2+} detection in literature.

Metal Ions	Substrate	Technique	Accumulation Time (s)	Dynamic Linear Range ($\mu g\ L^{-1}$)	Detection Limit ($\mu g\ L^{-1}$)	Reference
Ni^{2+}	mpBiF-SPCE	AdCSV	180	1 - 10	0.027	[11]
Co^{2+}				1 - 10	0.094	
Ni^{2+}	RBiABE	DPAdSV	30	0.6 - 41	0.18	[12]
Co^{2+}				0.06 – 4.1	0.018	
Ni^{2+}	PbF-SPE	SWV	60	0.6 – 2.9	0.2	[13]
Co^{2+}				0.6 – 5.9	0.3	
Ni^{2+}	SBVE	SWAdCSV	30	0 - 10	0.6	[14]
Ni^{2+}	DMG-CPE	DPAdSV	120	80 - 600	27	[15]
Ni^{2+}	DMG-N-SPE	DPAdSV	120	60 - 500	30	[16]
Ni^{2+}	ERGO-PG-MFE	SWAdCSV	210	2 - 16	0.12	This Work

5.3.8. *Recoveries Studies of ERGO-PG-MFE*

The electrochemically reduced graphene oxide pencil graphite mercury film electrode (ERGO-PG-MFE) was used for the analysis of Ni^{2+} in test solutions for recoveries experiment. Known concentrations of target metal ions were used to spiked 20 mL portions of 0.1 M ammonium chloride ammonium hydroxide buffer solutions followed by their determination using the standard addition method for three replications. The voltammograms obtained during the analysis of target metal ions together with their corresponding standard addition curves is shown in *Figure 5.10.* Recovery percentages of the Ni ions from test solutions spiked with 5 μgL^{-1} Ni^{2+} yielded recovery of 94%.

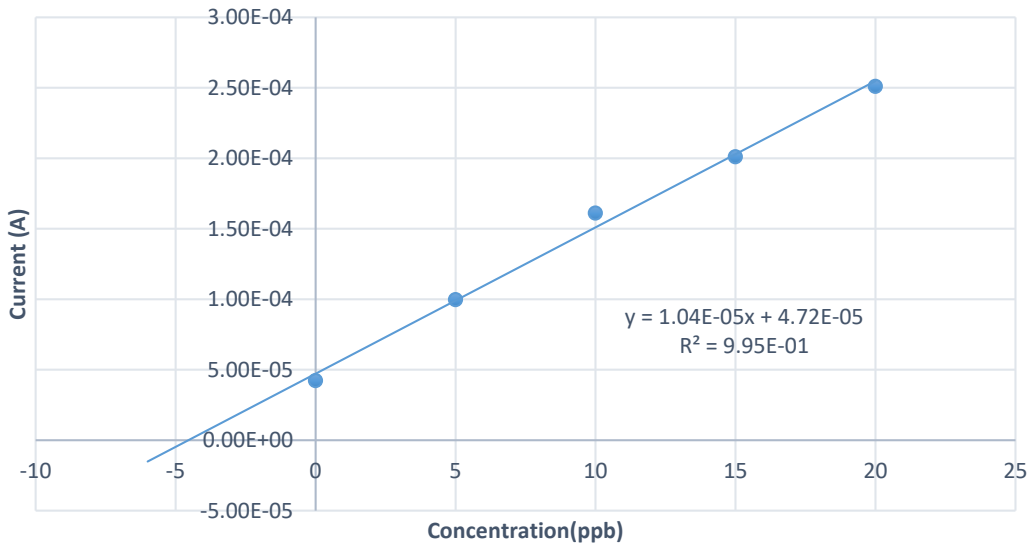

Figure 5.10: Calibration curve from a standard addition method for the determination of Ni^{2+} at ERGO-PG-MFE in test solutions.

5.3.9. Application to tape water samples

The ERGO-PG-MFE was applied to the analysis of Ni^{2+} in tap water samples, which was collected in our laboratory. An 18 mL sample of tap water was added to 2 mL of 1 M ammonium buffer (pH 9.4) to give a 0.1 M ammonium chloride ammonium hydroxide buffered tap water sample. SWCSV analyses were performed by in situ deposition of the metal film and target metal under the optimized parameters, using cleaning time = 0 s. due to the sensitivity of ERGO-PG-MFE during the analysis, a peak could be observed due to the nickel ion present in the water sample. The amount of metal ions present in the tap water sample was determined by the standard additions method as shown in the *Figure 5.11* below. In order to evaluate the accuracy of the method with the different electrodes, tap water samples were spiked with known amounts of target metal ions and then re-determined by applying the method of standards additions.

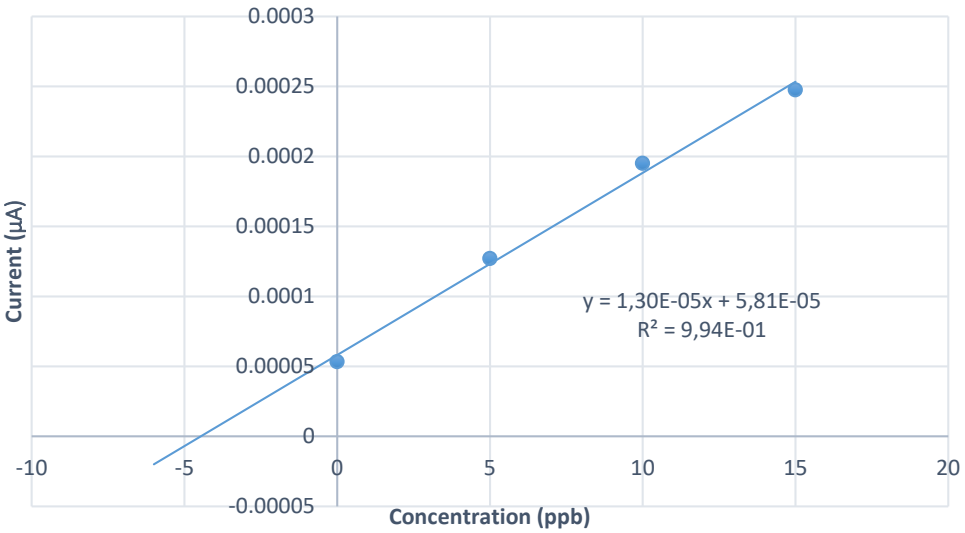

Figure 5.11: Square wave voltammograms (a) and standard addition calibration curve of Ni^{2+} for the analysis of tap water (pH = 9.4) spiked with 5 µg L^{-1} of Ni ions at deposition time of 240 s.

5.3.10. Interferences

Interferences by other metal ions found in water samples was investigated by a method of standard addition and spiking the solution test with a certain concentration of those that interfere with Ni ions. Metal ions interfere with the measurement by complexing competitively with DMG or by producing reduction peaks that overlap with, or even completely suppress, the Ni peak. The most potential intermetallic interferences to Ni peak were investigated using Zn^{2+}, Cd^{2+}, Co^{2+}, Pb^{2+} and Cu^{2+}. However, at five-fold excess Pd^{2+}, the peak current of Ni^{2+} decrease by 10 %. The rest of metals mentioned above were found not to be interfering with Ni^{2+}.

5.4. Conclusion

ERGO-PG-MFEs were successfully prepared by immobilizing the multilayer graphene nano-sheets on a pencil graphite electrode for the detection of ultratrace concentration of Ni^{2+} in the water by square-wave cathodic stripping voltammetry. A highly enhanced sensing platform was successfully obtained for the individual analysis of Ni^{2+} by square wave cathodic stripping voltammetry. The electrochemical reduced graphene oxide was found not only to act as the sensing platform with enhanced sensitivity towards Ni^{2+} but also as an antifouling coating to reduce the influence of intermetallic interferences.

The detection limits detected in water samples using ERGO-PG-MFE for individual analysis of Ni^{2+} were found to be 0.120 ± 0.002 µg L^{-1} which is way below the US EPA maximum contaminant level of 5 mg L^{-1} which makes this technique suitable for tap water analysis.

The electrochemically reduced graphene oxide pencil-graphite mercury- film electrode (ERGO-PG-MFE) showed larger currents and well-resolved stripping voltammetric peaks compared to BARE-PG-MFE electrodes reported in literature due to graphene's enhanced electron transfer rate and surface-to-volume ratio with sensitivity of 9.71E-7 µAL $µg^{-1}$.

References

[1] Ç. Büyükpınar, E. Maltepe, D.S. Chormey, N. San, S. Bakırdere, Determination of nickel in water and soil samples at trace levels using photochemical vapor generation-batch type ultrasonication assisted gas liquid separator-atomic absorption spectrometry, Microchem. J. 132 (2017) 167–171. doi:10.1016/j.microc.2017.01.024.

[2] B.N. Kumar, S. Kanchi, M.I. Sabela, K. Bisetty, N.V.V. Jyothi, Spectrophotometric determination of nickel (II) in waters and soils: Novel chelating agents and their biological applications supported by DFT method, Karbala Int. J. Mod. Sci. 2 (2016) 239–250. doi:10.1016/j.kijoms.2016.08.003.

[3] J. Kristiansen, J.M. Christensen, T. Henriksen, N.H. Nielsen, T. Menné, Determination of nickel in fingernails and forearm skin (stratum corneum), Anal. Chim. Acta. 403 (2000) 265–272. doi:10.1016/S0003-2670(99)00568-1.

[4] K. Pokpas, S. Zbeda, N. Jahed, N. Mohamed, P.G. Baker, E.I. Iwuoha, Electrochemically reduced graphene oxide pencil-graphite in situ plated bismuth-film electrode for the determination of trace metals by anodic stripping voltammetry, Int. J. Electrochem. Sci. 9 (2014) 736–759.

[5] J. Kariuki, E. Ervin, C. Olafson, Development of a novel, low-cost, disposable wooden pencil graphite electrode for use in the determination of antioxidants and other biological compounds, Sensors (Switzerland). 15 (2015) 18887–18900. doi:10.3390/s150818887.

[6] J. Wang, Stripping analysis at bismuth electrodes: A review, Electroanalysis. 17 (2005)

1341–1346. doi:10.1002/elan.200403270.

[7] F. Ahour, M.K. Ahsani, An electrochemical label-free and sensitive thrombin aptasensor based on graphene oxide modified pencil graphite electrode, Biosens. Bioelectron. 86 (2016) 764–769. doi:10.1016/j.bios.2016.07.053.

[8] S. Lee, S.K. Park, E. Choi, Y. Piao, Voltammetric determination of trace heavy metals using an electrochemically deposited graphene/bismuth nanocomposite film-modified glassy carbon electrode, J. Electroanal. Chem. 766 (2016) 120–127. doi:10.1016/j.jelechem.2016.02.003.

[9] K. Parvez, Z. Wu, R. Li, X. Liu, R. Graf, Exfoliation of Graphite into Graphene in Aqueous Solutions of Inorganic Salts, (2014). doi:10.1021/ja5017156.

[10] Z. Xue, B. Yin, M. Li, H. Rao, H. Wang, X. Zhou, X. Liu, X. Lu, Direct electrodeposition of well dispersed electrochemical reduction graphene oxide assembled with nickel oxide nanocomposite and its improved electrocatalytic activity toward 2, 4, 6-Trinitrophenol, Electrochim. Acta. 192 (2016) 512–520. doi:10.1016/j.electacta.2016.01.206.

[11] S. Dal Borgo, H. Sopha, S. Smarzewska, S.B. Hočevar, I. Švancara, R. Metelka, Macroporous Bismuth Film Screen-Printed Carbon Electrode for Simultaneous Determination of Ni(II) and Co(II), Electroanalysis. 27 (2015) 209–216. doi:10.1002/elan.201400422.

[12] B. Bas, K. Wegiel, K. Jedlinska, The renewable bismuth bulk annular band working electrode: Fabrication and application in the adsorptive stripping voltammetric determination of nickel(II) and cobalt(II), Anal. Chim. Acta. 881 (2015) 44–53. doi:10.1016/j.aca.2015.05.005.

[13] A. Bobrowski, A. Królicka, M. Maczuga, J. Zarębski, A novel screen-printed electrode modified with lead film for adsorptive stripping voltammetric determination of cobalt and nickel, Sensors Actuators, B Chem. 191 (2014) 291–297. doi:10.1016/j.snb.2013.10.006.

[14] G.M.S. Alves, J.M.C.S. Magalhães, H.M.V.M. Soares, Simultaneous Determination of Nickel and Cobalt Using a Solid Bismuth Vibrating Electrode by Adsorptive Cathodic Stripping Voltammetry, Electroanalysis. 25 (2013) 1247–1255.

doi:10.1002/elan.201200643.

[15] A. Ferancová, M.K. Hattuniemi, A.M. Sesay, J.P. Räty, V.T. Virtanen, Electrochemical Monitoring of Nickel(II) in Mine Water, Mine Water Environ. (2015). doi:10.1007/s10230-015-0357-1.

[16] A. Ferancová, M.K. Hattuniemi, A.M. Sesay, J.P. Räty, V.T. Virtanen, Rapid and direct electrochemical determination of Ni(II) in industrial discharge water, J. Hazard. Mater. 306 (2016) 50–57. doi:http://dx.doi.org/10.1016/j.jhazmat.2015.11.057.

Chapter 6 :

Complexation based Detection of Nickel (II) at a Graphene-Chelate Probe In the Presence of Cobalt and Zinc by Adsorptive Stripping Voltammetry

Abstract:

The adsorptive stripping voltammetric detection of nickel and cobalt in water samples at metal film electrodes has been extensively studied. In this work, a novel, environmentally friendly, metal-free electrochemical probe was constructed for the ultra-trace determination of Ni^{2+} in water samples by Adsorptive Cathodic Stripping Voltammetry (AdCSV). The electrochemical platform is based on the adsorptive accumulation of Ni^{2+} ions directly onto a glassy carbon electrode (GCE) modified with dimethylglyoxime (DMG) as chelating agent and a nafion-graphene (NGr) nanocomposite to enhance electrode sensitivity. The nafion-graphene dimethylglyoxime modified glassy carbon electrode (NGr-DMG-GCE) shows superior detection capabilities as a result of the improved surface-area-to-volume ratio and enhanced electron transfer kinetics following the incorporation of single layer graphene, while limiting the toxic effects of the sensor by removal of the more common mercury, bismuth and lead films. Furthermore, for the first time the NGr-DMG-GCE, in the presence of common interfering metal ions of Co^{2+} and Zn^{2+} demonstrates good selectivity and preferential binding towards the detection of Ni^{2+} in water samples. Structural and morphological characterisation of the synthesised single layer graphene sheets was conducted by Raman spectrometry, HRTEM and HRSEM analysis. The instrumental parameters associated with the electrochemical response, including accumulation potential and accumulation time were investigated and optimised in addition to the influence of DMG and graphene concentrations. The NGr-DMG-GCE demonstrated well resolved, reproducible peaks, with RSD (%) below 5 % and a detection limit of 1.5 µg L^{-1} for Ni^{2+} reduction at an accumulation time of 120 s, the prepared electrochemical sensor exhibited good detection and quantitation towards Ni^{2+} detection in tap

water samples, well below 0.1 mg L^{-1} set by the WHO and EPA standards [1]. This comparable to the South African drinking water guidelines of 0.15 mg L^{-1} [2].

Keywords:

Graphene, Trace Metal Analysis, Dimethylglyoxime, Adsorptive Stripping Voltammetry, Nickel Determination, Nafion

Highlights:

- A novel nafion graphene-dimethylglyoxime (NGr-DMG) nanocomposite is used in the preparation of chemically modified electrodes
- An environmentally friendly approach is developed for Ni^{2+} detection in drinking water samples in the absence of a 'toxic' electroplated metal film
- A nine-fold enhancement in Ni^{2+} stripping reduction peak current is observed
- Accurate, reproducible and selective detection of Ni^{2+} is achieved in the presence of Zn^{2+} and Co^{2+}

Graphical Abstract:

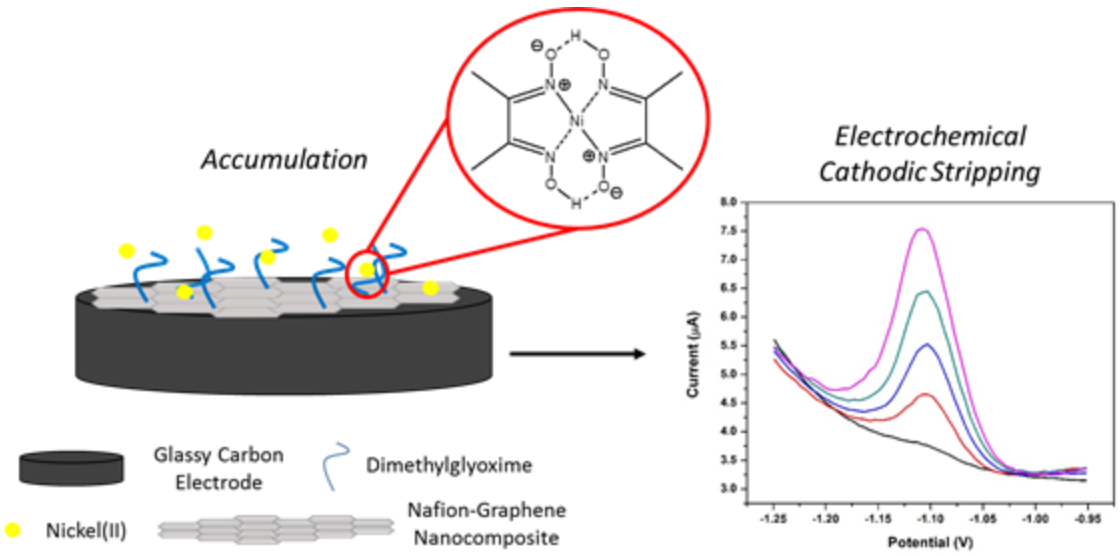

6.1. Introduction:

A considerable increase in technological advancement has led to a growing demand for accurate, analytical monitoring of trace levels of metal ions in drinking and wastewater samples. While nickel, cobalt and zinc, three common trace elements are essential to human health, they may exhibit toxic effects in humans as a result of their non-biodegradable nature and long biological half-life [3,4]. At high concentrations they have been linked to a range of illnesses including cardiovascular diseases, cancer and skin allergies such as dermatitis. Ni, Co and Zn are common place in water samples due to their use in alloys and the electroplating of materials for enhancement of mechanical properties and corrosion resistance. Dangerous exposures may be minimized by limiting common sources of exposure and accurate detection methods [5].

The use of stripping analysis has significantly increased over the last two decades and has proved to be a highly sensitive method for the ultra-trace determination of metal ions. The simplicity and rapidness of the electrochemical analytical techniques, ability for *in-situ* pre-concentration steps [6,7] and low cost and reliable nature [8] makes it an attractive alternative to the more common chromatographic and atomic absorption spectrometric methods. Anodic stripping voltammetry (ASV), cathodic stripping voltammetry (CSV) and adsorptive stripping voltammetry (AdSV) are three common examples of conventional stripping methods. Here, electrolytic deposition and stripping at metal-based electrodes are among the most sensitive electrochemical sensing techniques. AdSV, suitable for samples in which preconcentration cannot be controlled by electrolysis [9] has been shown to be a highly sensitive technique for the simultaneous and individual detection of Ni and Co. Commonly, the technique is based on the accumulation of analyte species, in the presence of a suitable complexing agent, on an electroplated metal film. In contrast to most metal ions, the detection of Ni is often complicated and associated with low electrochemical signals [10]. Complexation with organic ligands has shown to significantly enhance the sensitivity and selectivity of electrochemical sensors for Ni^{2+} determination. A wide range of complexing agents have been employed in stripping analysis and are highly dependent on the application. Dioximes such as, nioxime [11–13] and more popularly dimethylglyoxime (DMG) [8,10,14–24] have gained widespread attention.

Mercury film (MF) [25,26], lead film (LF) [11,15,27] and bismuth film (BF) [28–31] electrodes, prepared by *ex-situ* and *in-situ* plating techniques have been widely employed as alternatives to the highly toxic hanging mercury drop electrodes (HMDE) and their development for analytical applications is still of great interest. While more environmentally friendly and of lower toxic nature, the MFE, LFE and BFE still pose toxic effects in the environment, owing to their non-biodegradable nature. As a result, manufacturing of electrochemical platforms without the use of metal films may result in green, non-toxic sensing techniques for future applications.

The use of chemically modified electrodes (CME) has garnered tremendous interest among analytical chemists in recent times and is one such method that holds great potential for alleviating the use of metallic films. CME's have chemically selective functional groups attached to the electrode surface for improved selectivity and sensitivity [8]. The CMEs have particularly demonstrated usefulness in analytical systems in which detection at mercury or metal based electrodes by conventional stripping analysis is not possible. The analyte may be sparingly soluble in mercury or lack amalgam formation with the metal film reducing electrode sensitivity. A major advantage of CMEs is the ability to incorporate a wide range of chemical modifiers into the substrate system with little effort. CMEs for the detection of metal ions, in conjunction with metal films at drop coated GCE [19,22–24,32] and modified carbon paste electrodes (CPE) [18,20] have been demonstrated. The CMEs show improved electrode selectivity and improved resistance to surface active compounds and intermetallic interferences [24]. Zen *et al*. for the first time reported the use of a novel nafion-coated mercury film electrode (NCMFE) by incorporating chelating agents directly into the NCMFE to improve analyte sensitivity and selectivity for the detection of trace metals by SWASV [22]. The results showed to have limited organic interferents over common in-situ experiments. Presently, research has expanded to include mercury or metal-free sensors relying on CMEs. Bing *et al*. reported the use of a glassy carbon electrode modified with DMG- containing polymers as mercury-free sensor for detection of Ni^{2+} [8]. In the works by Gonzalez *et al*. and Tartarotti *el al.*, carbon paste electrodes modified with chelating agents were employed as alternatives to the modified electrodes previously suggested for the detection of Ni^{2+} in water and fuel ethanol samples respectively. These works exhibited for the first time the applicability of modified electrochemical sensors in the absence of metallic films for detection of metal ions by AdSV [18,20]. The results showed detection limits comparable to common metal-based transducers with longer detection times and therefore lower sensitivity. Ferancova *et al*.

further proposed the use of screen printed electrodes modified with nafion and DMG as a low cost, robust metal-free sensor for the detection of Ni^{2+} in industrial discharge water [16]. The metal-free CMEs have shown good selectivity and long-term stability compared to their metallic counterparts. The metal-free CMEs however, have one major drawback towards the detection of trace metals namely, their relatively low sensitivity at shorter analysis times.

Graphene, a 2-D allotrope of carbon has found tremendous application in electrochemical sensing technologies due to its ability to enhance electrode sensitivity in a range of applications since its discovery in 2004. Its large surface-area-to-volume ratio, enhanced electrocatalytic effects and enhanced electron transfer kinetics make it ideal for applications in electrochemical sensors [33][34]. Extensive research has been conducted in the use of graphene-based sensors for detection of trace metal ions by stripping voltammetric techniques [33,35–41]. To date however, no publications have been reported on the use of graphene for determination of trace Ni^{2+} at *in situ* or chemically modified DMG electrode by AdSV.

A Nafion semi-permeable membrane, has been employed as a binder in electrode coatings for a variety of sensing applications It assists in reducing the effects of adsorbed surfactants at the electrode surface by providing mechanical stability and utilizes its cation exchanger ability to exclude anion interference [16,22,32,35].

In this work we report, for the first time, a highly selective, voltammetric - chemically modified electrode for the determination of Ni^{2+} in water samples, in the presence of Co^{2+} and Zn^{2+}. The sensor is based on a glassy carbon electrode modified with dimethylglyoxime as chelating agent to enhance analyte selectivity and a nafion-graphene nanocomposite to enhance electrode sensitivity, in the absence of an electroplated metal film. To date no work has been reported on the use of a nafion-graphene-dimethylglyoxime nanocomposite CME for the detection of Ni^{2+} in water by AdCSV.

6.2. Experimental Procedure:

6.2.1. Chemicals and Reagents

All chemicals used in the study were of analytical reagent grade. Ultra-pure distilled water (Millipore) was used to prepare all solutions. Nafion perfluorinated resin solution 5 wt. % in lower

aliphatic alcohols and water and 2, 3-Butanedione-dioxime (Dimethylglyoxime) were purchased from Aldrich. Ni^{2+} standard stock solutions (1 000 mg L^{-1}, atomic absorption standard solution) and all other metal standards were obtained from Sigma-Aldrich and diluted as required. Natural graphite powder (microcrystal grade, 99.9995%) (Metal base) UCP1-M grade, Ultra "F" purity was purchased from Alfa-Aesar and used for the preparation of graphene oxide (GO) by a modified Hummers method.

Ammonia/Ammonium Chloride (NH_3/NH_4Cl) buffer solution (0.1 M, pH 9.3) was used as supporting electrolyte and prepared by mixing appropriate quantities of ammonia (NH_3) and ammonium chloride (NH_4Cl). A Metrohm 827 pH lab pH meter was calibrated using pH 4 and 7 calibration buffer solutions and then used to verify the pH of the prepared NH_3/NH_4Cl buffer solution

6.2.2. Apparatus

All electrochemical voltammetric experiments were performed with a Metrohm Autolab PGSTAT101 instrument, in combination with the Nova 1.11 Software and controlled by a personal computer. A conventional three-electrode electrochemical system, consisting of a nafion graphene modified dimethylglyoxime glassy carbon electrode (NGr-DMG-GCE) serving as working electrode was utilized for all electrochemical studies, unless stated otherwise. An Ag/AgCl (saturated with KCl) and platinum wire served as reference and counter electrodes, respectively. All experiments were performed in a one compartment 20 mL voltammetric cell at room temperature

6.2.3. Preparation of the Nafion-Graphene Dimethylglyoxime Suspension (NGr-DMG)

All graphene samples used in this work were prepared by chemical reduction of graphene oxide with sodium borohydride ($NaBH_4$) as reducing agent. Appropriate quantities of graphene oxide, prepared using a modified Hummer's method [42], sodium borohydride and distilled water were mixed for 30 min followed by heating to 135°C under reflux for 3 h. The resulting black precipitate was centrifuged, washed with water, ethanol and dried in a vacuum oven as described in the work by Shen *et al*. [35,43].

NGr-DMG suspensions were then prepared by mixing appropriate quantities of Nafion (5 wt %), prepared graphene and dimethylglyoxime powder in an ethanol solvent followed by ultrasonication for 1 h.

6.2.4. Preparation of Nafion-Graphene Dimethylglyoxime Modified Glassy Carbon Electrode (NGr-DMG-GCE)

Glassy carbon electrodes (BASi) with area of 0.071 cm^2 (3 mm diameter) was polished with slurries of alumina powder (1, 0.3 and 0.05 µm). The electrode was rinsed with ultra-pure distilled water, successively sonicated for 5 min in Ethanol and ultra-pure water respectively and dried at room temperature. The polished surface of the GCE was then coated with 4 µL of the prepared NGr-DMG suspension and allowed to dry at room temperature in order to allow the solvent to evaporate to form the NGr-DMG-GCE. No further electrode pre-treatment was required.

6.2.5. Procedure for Square Wave Adsorptive Cathodic Stripping Voltammetric (AdCSV) Analysis

The three-electrode system with NGr-DMG-GCE as working electrode was immersed into an electrochemical cell containing 20 mL NH_3/NH_4Cl buffer solution (0.1 M, pH 9.3), degassed with N_2 gas for 5 min, as supporting electrolyte. Appropriate volumes of 10 ppm Ni^{2+} stock solution was added prior to analysis. A reduction potential of – 0.7 V was applied to the working electrode, under constant stirring for 120 min to aid with accumulation of the metal ions at the electrode surface. After a brief rest period, the potential of the NGr-DMG-GCE was cathodically scanned between – 0.7 and –1.3 V by applying a square-wave waveform. No further electrochemical cleaning was required in between runs.

6.2.6. Sample Preparation

All tap water samples were collected from our laboratory at the University of the Western Cape, Bellville, South Africa after allowing the tap to run for 1 min. The tap water samples used for nickel detection were diluted for characterization by SWAdCSV by mixing a 9 mL sample of tap water and 1 mL of 1 M NH_3/NH_4Cl buffer. The prepared tap water samples were added to the electrochemical cell and the analysis was performed as described by the procedure in *Section 6.2.5*.

6.3. Results and Discussion

6.3.1. Fourier Transform Infrared Spectroscopy (FT-IR) of DMG

The presence of vibrational frequencies of functional groups in the chelating agent (dimethylglyoxime, DMG) was analysed using FT-IR spectra in the form of KBr (Potassium Bromide) pellets. The spectra of the DMG chelating agent, before adsorption was measured within the range of 4,000 to 450 cm^{-1} wave number and presented in *Figure 6.1*. The infrared spectra of the dimethylglyoxime exhibited distinct absorption bands at 3205, 1441, 1144, 979 and 716 cm^{-1} which are attributed to ν (OH), ν (C=C), ν (N-O), ν (C-H) aliphatic and ν (C=N-O) respectively. The FT-IR spectra confirm the presence of two oxime groups (NOH) on each molecule of dimethylglyoxime to facilitate complex formation, responsible for analyte adsorption on the electrode surface. A schematic representation of the dimethylglyoxime structure (*inset*), confirming the IR findings, is shown in the *Figure 1*. Similar results have been demonstrated in the work performed by Shaker *et al.* [44–46].

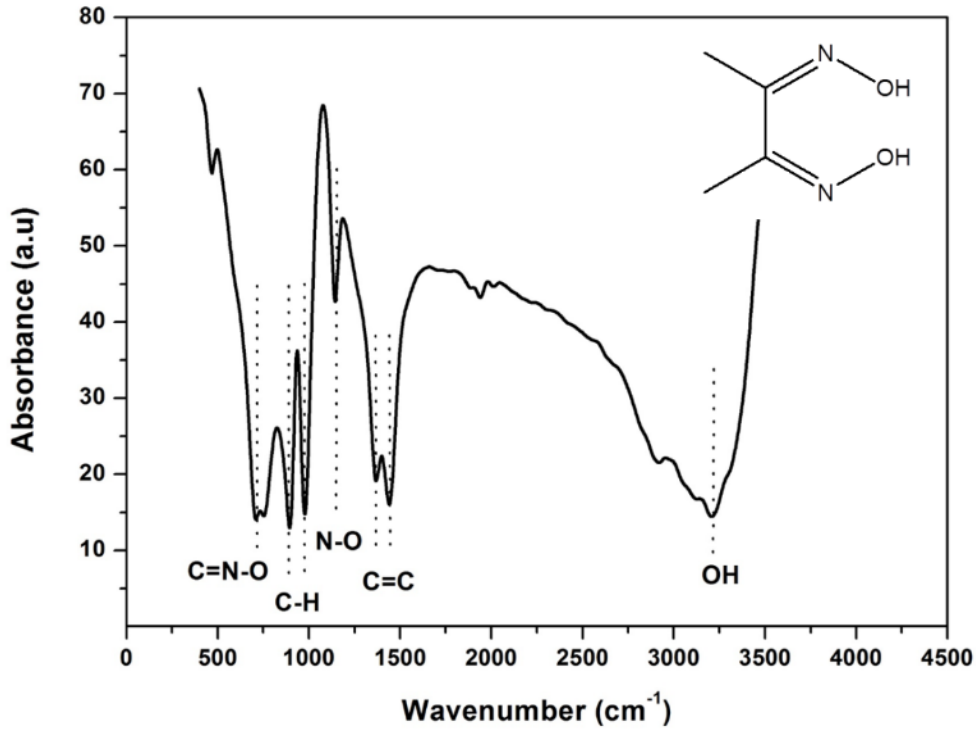

Figure 6.1: Fourier Transform Infrared Spectrometry of Dimethylglyoxime as a KBr Pellet. Inset: Schematic Representation of the Dimethylglyoxime Structure.

6.3.2. Nickel Dimethylglyoxime ($Ni(DMG)_2$) Complex Formation and Electrochemical Stripping Reduction

The complex formation of Ni, commonly present in the +2 oxidation state forms a 1:2 stoichiometric complex with the organic dimethylglyoxime, $C_4H_6(NOH)_2$ and has been extensively studied in the gravimetric and electrochemical determination of Nickel [47]. *Figure 6.2* shows the schematic representation of the above mentioned chelation reaction. Here, electron pairs are donated to the Ni^{2+} molecules by the four nitrogen atoms of the dimethylglyoxime and not the oxygen atoms as commonly expected. In addition, one proton is lost from one oxime group on each of the two molecules of dimethylglyoxime [48]. Addition of OH anions facilitates aids in metal-chelate complex formation [49] which occurs quantitatively in solutions in which the pH is buffered between 5 and 9. Ammonia or citrate buffer are required to facilitate the reaction by preventing the drop in pH below 5. At pH values lower than 5 a disturbance in the equilibria of

the reaction occurs, favouring the formation of Ni^{2+} and causing the dissolution of the $[Ni(dmgH)_2]$ complex. Previous research showed that the $[Ni(dmgH)_2]$ complex was found to have a square planar geometry [47][50] with Nitrogen atoms situated at the corners of a square in a single plane situated around a central Nickel atom [50].

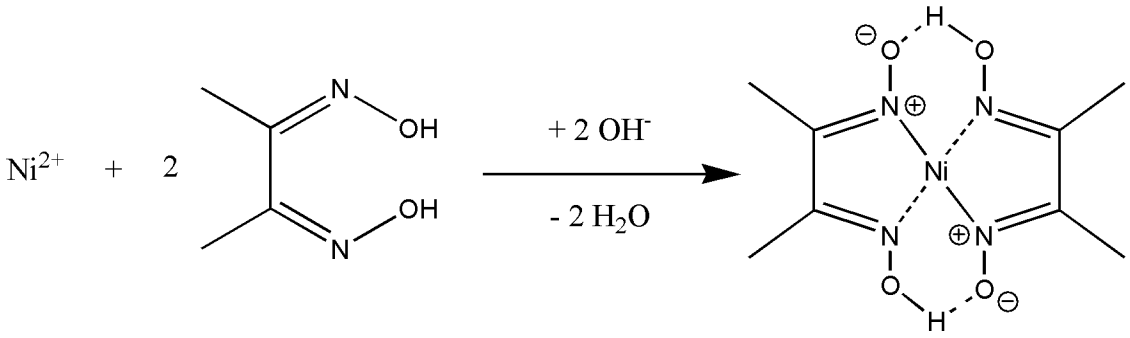

Figure 6.2: Schematic Illustration of the Metal-Chelate Complex Formation [46].

The exact nature of adsorptive stripping voltammetric adsorption and reduction of Ni(II) has been widely debated and remains a highly controversial topic. Traditionally complexation of Ni(II) with DMG occurs in solution, prior to its subsequent adsorption onto an electrochemically plated metal film. In the NGr-DMG-GCE sensor the adsorption process is significantly simplified. Pre-concentration of the electrode surface is achieved by adsorption of the dissolved Ni^{2+} ions onto the hydrophobic DMG ligand bound to the GCE surface in the form of NGr-DMG to form the $[Ni(dmgH)_2]$ complex (*Equation 6.1*) [51,52]. The subsequent electrochemical reduction of the $[Ni(dmgH)_2]$ complex is shown in *Equation 6.2*. It involves the overall reduction of both central metal atom and the surrounding ligands in an overall 10-electron reduction process giving rise to 2,3-bishydroxylaminebutane, a stable electrolysis product [51,52]. The reacted $[Ni(dmgH)_2]$ complex is reduced and subsequently moved away from the electrode surface. Unconverted DMG remains present for further complexation with metal cations.

$$Ni^{2+} + 2\ dmgH_2 + 2\ OH^- \rightarrow [Ni(dmgH)_2] + 2\ H_2O \quad \text{Pre-concentration Step} \quad (6.1)$$

$$[Ni(dmgH)_2] + 10\ e^- + 10\ H^+ \rightarrow Ni^{2+} + 2\ DHAB \quad \text{Stripping/reduction step} \quad (6.2)$$

6.3.3. Morphological Characterization of Modified Electrode

The surface morphology of the modified electrodes was studied using HRSEM analysis in conjunction with Energy dispersive spectroscopy (EDS) for confirming the presence of graphene and dimethylglyoxime at the electrode surface. High resolution scanning electron microscope images of bare screen printed carbon electrodes (SPCE) and nafion-graphene dimethylglyoxime modified screen printed electrodes (NGr-DMG-SPCE) are shown in *Figure 6.3* at 1000 X and 20 000 X magnification. Samples for HRSEM were prepared by drop coating 4 µL of NGr-DMG nanocomposite directly onto the cleaned SPCE and allowing it to dry at room temperature. Improved imaging is achieved by sputter coating of a Au-Pd film (≤ 5 nm) onto the dried SPCE surface to enhance surface conductivity. The bare SPCE (*Figure 6.3 (a and c)*) shows a rough, porous surface, typically associated with most carbon structures as a result of the printed carbon ink. No other significant features are observed. In contrast, *Figure 6.3 (b and d)*, demonstrate HRSEM images of the NGr-DMG-SPCE surface. A smooth, uniform, solid surface can be seen at both low and high magnifications. This may be attributed to the presence of a film at the electrode surface, characteristic due to the incorporation of Nafion. Furthermore, flake-like features, associated with the presence of graphene at the electrode surface can be seen. The changes in surface morphology of the electrode surface due to the electrode modification confirm the presence of the nafion-graphene dimethylglyoxime film on the SPCE. Elemental analysis of the bare and modified SPCE surface was performed by energy dispersive spectroscopy (EDS). *Figure 6.4*, represents the recorded EDS data obtained from HRSEM analysis. The bare SPCE (*Figure 6.4 (a)*) shows the presence of C, O and Cl at 0.3, 0.5 and 2.6 keV, associated with the conductive carbon ink used to create the carbon electrode. Gold sputter coating was employed in the HRSEM analysis and can be seen at the electrode surface. Analysis of the modified NGr-DMG-GCE (*Figure 6.4 (b)*) shows the inclusion of N and F at 0.4 and 0.6 keV and an increase in the C and O elemental intensities compared to the bare SPCE. The presence of N and a significant increase in C and O at the electrode surface confirms the presence of both Nafion and DMG at the NGr-DMG-SPCE surface while fluorine is associated with the Nafion binder.

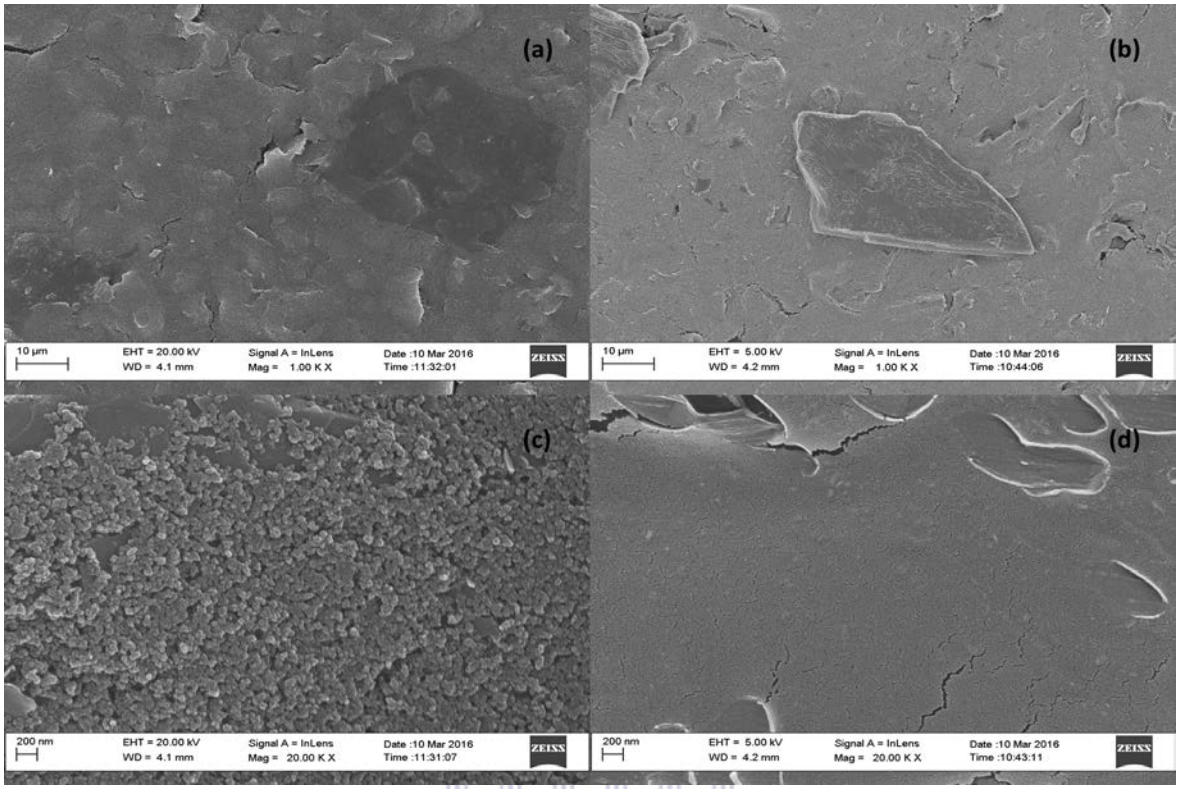

Figure 6.3: High Resolution Scanning Electron Microscope (HRSEM) image of (a and c) Bare SPCE and (b and d) NGr-DMG-SPCE at 1.00 k X and 20.00 k X magnification.

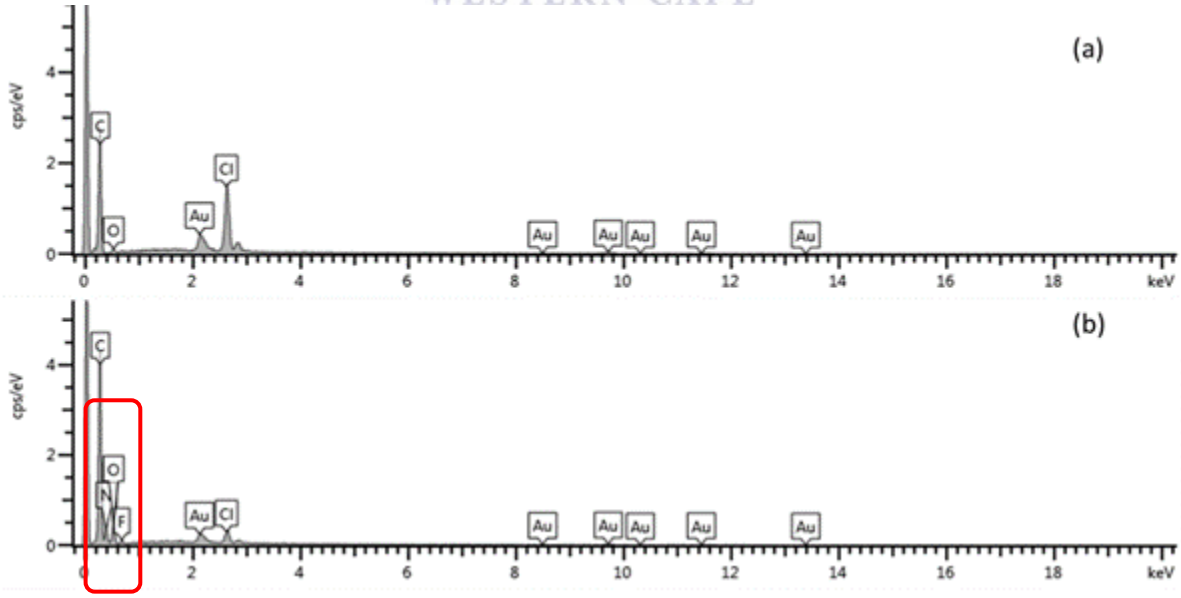

Figure 6.4: Energy Dispersive Spectroscopy (EDS) Results obtained from HRSEM at the (a) Bare SPCE and (b) NGr-DMG-SPCE.

6.3.4. Electrochemical Characterization of the Nafion-Graphene Dimethylglyoxime Modified Glassy Carbon Electrode (NGr-DMG-GCE)

The electrochemical properties related to the active surface area of the modified glassy carbon electrodes were characterized by cyclic voltammetry (CV). Since the NGr-DMG-GCE demonstrates no significant redox peaks in the potential window of interest, a ferro/ferricyanide ($Fe(CN)_6^{3-/4-}$) redox couple, giving rise to a reversible one electron system is used to further study the electrochemical electrode properties. Cyclic voltammograms obtained for the N-DMG-GCE and NGr-DMG-GCE at various scan rates were recorded in the presence of a 5 mM $K_3Fe(CN)_6$ solution and illustrated in *Figure 6.5 and 6.6* respectively. The CV for the NGr-DMG-GCE demonstrates single oxidation and reduction peaks in the potential range between – 1.0 and + 1.25 V. An increase in anodic and cathodic peak currents is observed with a slight shift to more positive and negative potentials respectively with increasing scan rates between 10 – 100 mV s^{-1}. Proportionality of the measured current was studied vs (a) scan rate and (b) scan rate$^{1/2}$ and recorded in *Figure 6.5 and 6.6, inset* respectively in order to differentiate between adsorption and diffusion controlled processes. Linear proportionality of peak currents with the square root of scan rates is observed at both modified electrodes and suggests a diffusion controlled process of reactants at both the N-DMG-GCE and NGr-DMG-GCE surfaces [53]. The diffusion coefficients (rate of diffusion through modified electrode surface) of the N-DMG-GCE and NGr-DMG-GCE's were determined by studying the cyclic voltammetric response of the reversible system using the Randles-Sevcik equation:

$$I_{pf} = (2.69 \times 10^5) n^{3/2} A D^{1/2} C^* v^{1/2} \qquad \text{(Equation 6.3)}$$

Where I_{pf} is peak current (A), n is the number of electrons transferred, A is the active area of the working electrode (cm^2), D is the diffusion coefficient ($cm^2\ s^{-1}$), C* is the bulk concentration of the electroactive species (mol cm^{-3}) and v is the potential scan rate (V s^{-1}).

The diffusion coefficients of the N-DMG-GCE and NGr-DMG-GCE were calculated as 4.88 x 10^{-8} and 1.13 x 10^{-6} cm^2s^{-1} respectively. A 23 times increase in diffusion rate is observed for the NGr-DMG-GCE over the N-DMG-GCE. This significant increase in diffusion of ferricyanide anions through the modification to the glassy carbon electrode surface is as a result of a significant increase in active surface area attributed to graphene loading [54].

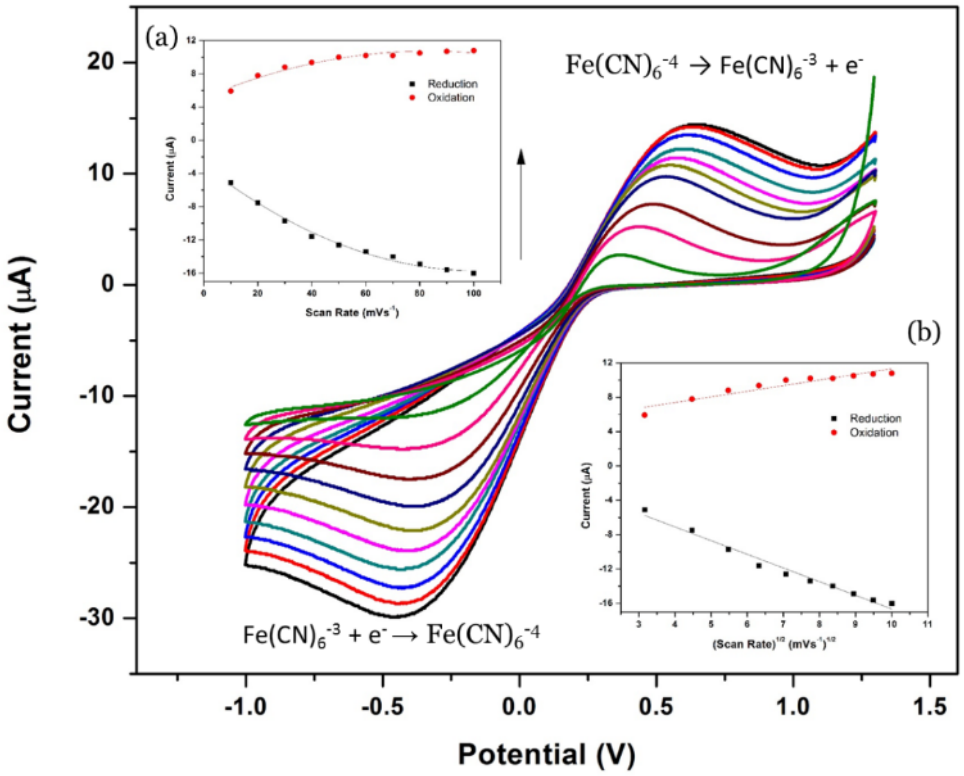

Figure 6.5: Electrochemical Characterisation of N-DMG-GCE in 5 mM $Fe(CN)_6^{3-/4-}$ at scan rate of 10-100 mV s^{-1} in supporting electrolyte (1 M KCl).

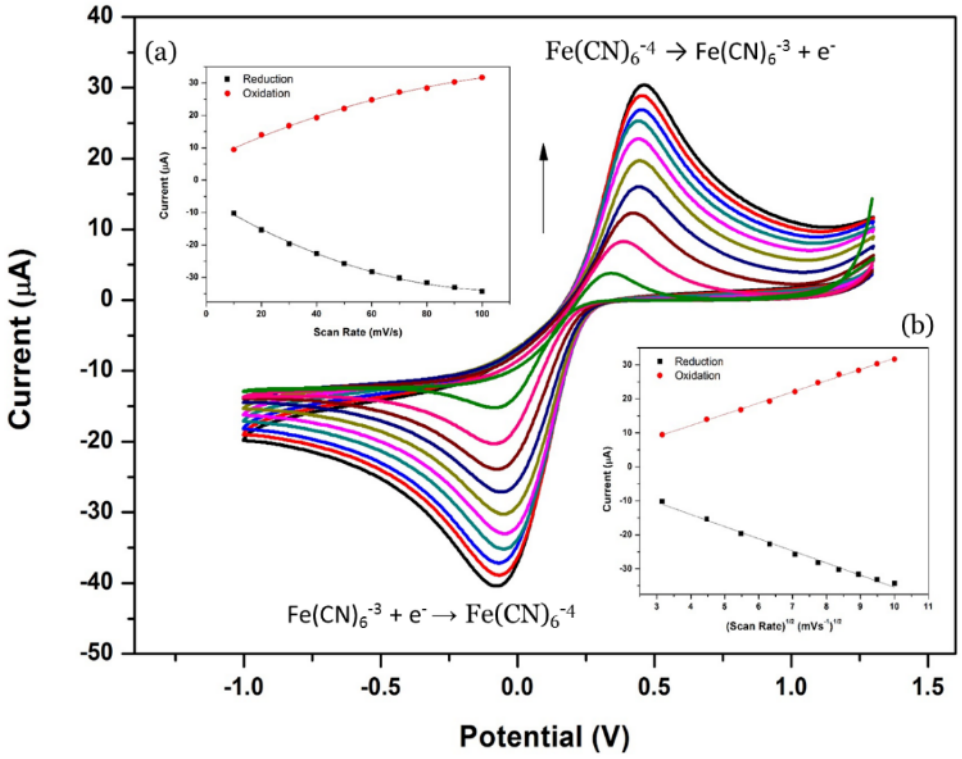

Figure 6.6: Electrochemical Characterisation of NGr-DMG-GCE in 5 mM $Fe(CN)_6^{3-/4-}$ at scan rate of 10-100 mV s^{-1} in supporting electrolyte (1 M KCl).

6.3.5. Electrochemical Behaviour of the NGr-DMG-GCE

Cyclic voltammograms of the N-DMG-GCE and NGr-DMG-GCE recorded in 5 mM $Fe(CN)_6^{3-/4-}$ solution with 1 M KCl as supporting electrolyte at a scan rate of 50 mV s^{-1} are shown in *Figure 6.7* below. A pair of distinct, well-defined redox couple peaks for $Fe(CN)_6^{3-/4-}$ are shown between -1.0 V and +1.25 V in a 1 M KCl solution. Two broad peaks are found at the N-DMG-GCE, with a large formal potential (ΔE_p) of 0.45 V. The large ΔE_p is as a result of diffusion controlled processes dominating over the electrochemical reduction of the $Fe(CN)_6^{3-/4-}$ couple. This is expected due to the organic nature of the DMG ligand deterring electron transfer [49]. A reduction of ΔE_p (0.25 V) for the NGr-DMG-GCE is demonstrated. The NGr-DMG-GCE shows a distinct increase in peak currents of the redox peaks as well as an observed narrowing in peak separation over the N-DMG-GCE, as observed by the lower *Ep* value. This is attributed to the

improved electrical properties of the graphene film as a result of the enhanced electron transfer processes. In addition the background current is also increased showing improvement of the non-electroactive surface area due to graphene modification [54]. This result favours the use of the NGr-DMG complex as a modifier for the electrochemical sensing application.

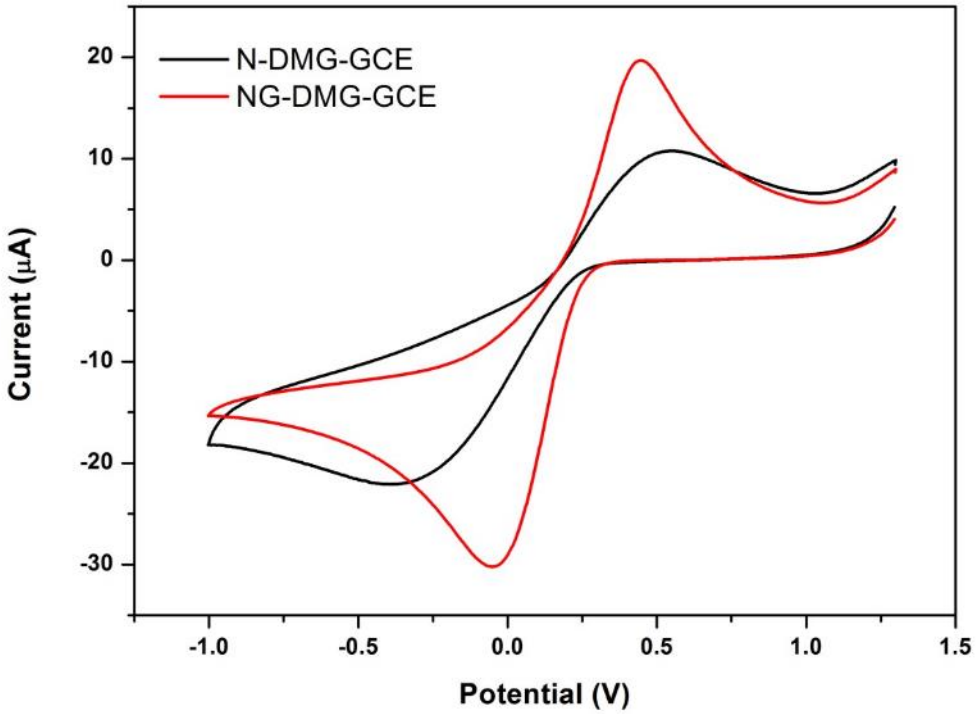

Figure 6.7: Cyclic voltammograms of 5 mM $Fe(CN)_6^{3-/4-}$ at (a) N-DMG-GCE and (b) NGr-DMG-GCE in supporting electrolyte of 1 M KCl at scan rate 50 mV s^{-1}.

6.3.6. Electrochemical Impedance Spectroscopy (EIS) Analysis of the NGr-DMG-GCE

Further investigation of the electron transfer properties of the bare and modified electrodes were performed by electrochemical AC impedance experiments. Here, impedance changes and interface properties during the surface modification processes of electrodes were observed and recorded in *Figure 6.8*. All electrochemical impedance spectroscopy (EIS) experiments were carried out in the presence of a 5 mM $Fe(CN)_6^{3-/4-}$ redox probe over the 1-10 000 Hz range. Typically, impedance spectra consist of semi-circular (electron transfer processes) and linear

(diffusion processes) regions at high and low frequencies respectively where the real and imaginary parts of the impedance were calculated from the overall impedance.

Figure 6.8, shows the associated Nyquist plots obtained by plotting Z' vs Z", from bare GCE, DMG-GCE, N-DMG-GCE and NGr-DMG-GCE. Considerable changes were observed in the semicircle diameter upon electrode modification. A large increase in charge transfer resistance (R_{ct}), was observed upon the inclusion of the non-conductive dimethylglyoxime chelating agent onto the GCE. The infinitely large semicircle implies very slow electron transfer processes and a resultant increase in the total impedance was observed. Incorporating both Nafion and Nafion-graphene nanocomposites results in an effective lowering of the recorded R_{ct} values. This demonstrates the higher electrochemical activity and enhanced electron transfer kinetics between the solution and the electrode surface of the NGr-DMG-GCE over the other modified electrodes, due to the subsequent inclusion of highly conductive graphene confirming its high electron transfer and improved surface area to volume ratio. This confirms the findings in *Figure 6.7* above. In general, the linear region in the Nyquist plot is linked to reactions where mass-transfer (Warburg Impedance) controls the reaction rate and electron transfer is fast. The absence of a linear diffusion region in the DMG-GCE and N-DMG-GCE may be attributed to the dominance of slow electron transfer over the diffusion controlled processes.

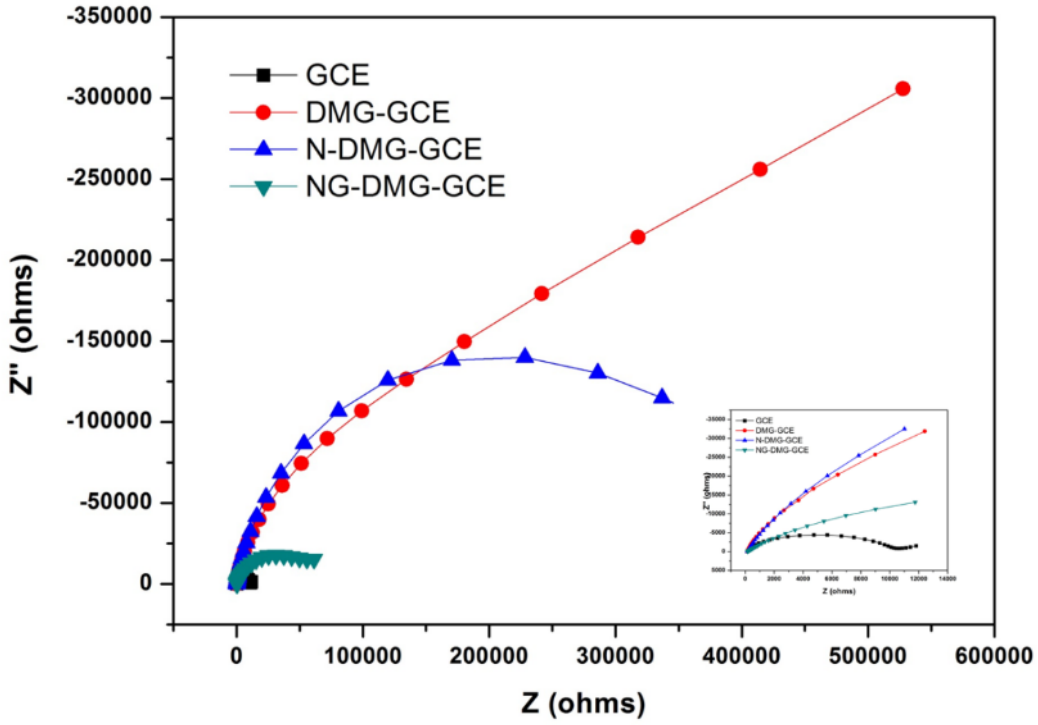

Figure 6.8: Nyquist plots at (a) GCE, (b) DMG-GCE, (c) N-DMG-GCE and (d) NGr-DMG-GCE in 5 mM $Fe(CN)_6^{3-/4-}$ containing 1 M KCl. Inset is the magnified Nyquist plot between 0 and 12 kΩ. The frequency range is from 0.1 Hz to 100 kHz.

6.3.7. Further electrochemical characterization of the NGr-DMG-GCE

The electrochemical properties of the N-DMG-GCE and NGr-DMG-GCE were further interrogated by cyclic voltammetry in a 0.1 M NH_3/NH_4Cl Buffer solution (pH 9.3) as supporting electrolyte and a scan rate of 10 mV s^{-1}. The resultant voltammograms are shown in *Figure 6.9* below. No observed redox peaks are present at either modified electrodes, indicating the lack of electrochemical activity of the DMG in the specified region as well as the complete reduction of GO to graphene. An increase in the background current and a lowering in potential value for oxygen evolution is evident in the voltammogram of the NGr-DMG-GCE can be seen over the N-DMG-GCE. This phenomenon indicates the increase of active surface area and conductivity of the modified electrode as a result of the graphene coating. No further significant peaks, due to the

reduction of dissolved oxygen can be seen. No interferences (peaks) from the modified platform were expected.

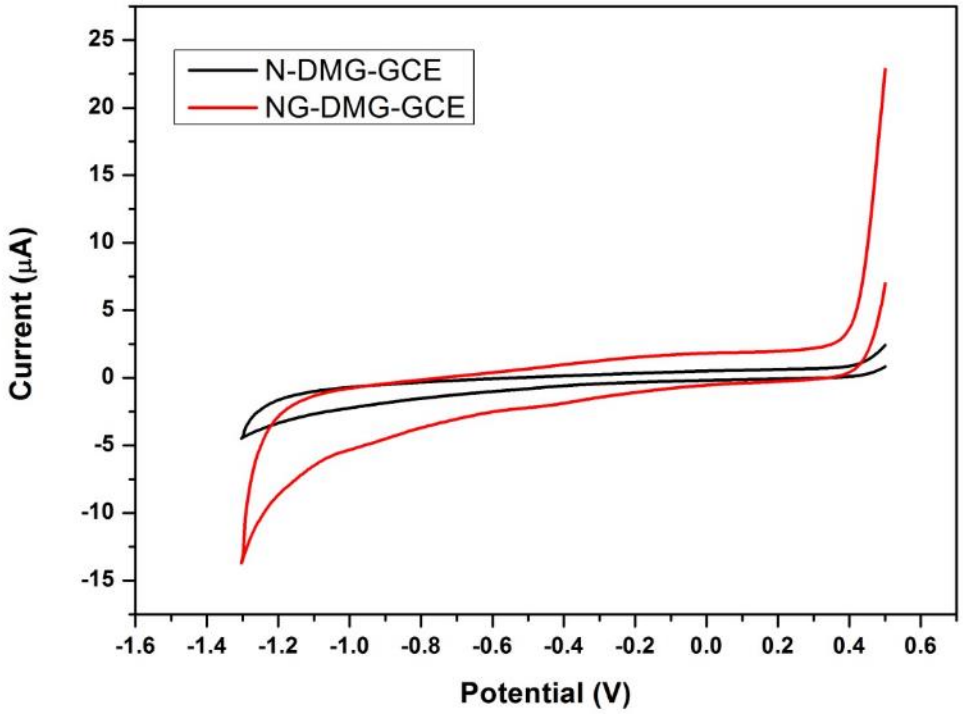

Figure 6.9: Cyclic voltammograms of (a) N-DMG-GCE and (b) NGr-DMG-GCE. Supporting electrolyte 0.1 M NH_3/NH_4Cl Buffer (pH 9.3), scan rate (10 mV s^{-1}), deposition time (120 s), frequency (20 Hz), amplitude (0.02 V) and voltage step (0.005 V).

6.3.8. Effect of the NGr-DMG-GCE on the stripping response of Ni^{2+}

Figure 6.10 represents the influence of graphene concentration in the NGr-DMG nanocomposite on the stripping response of Ni^{2+}. The N-DMG-GCE shows a broad, small peak at – 1.08 V in 0.1 M NH_3/NH_4Cl Buffer (pH 9.3) with deposition potential (- 0.7 V), deposition time (120 s), frequency (20 Hz), amplitude (0.02 V) and voltage step (0.005 V). In contrast, the NGr-DMG-GCE shows a sharp, well-resolved stripping peak at - 1.09 V for Ni^{2+} reduction from the $Ni(DMG)_2$ adsorption complex as demonstrated in *Equation 6.2*. A considerable increase (9 times) in stripping peak current is observed for the NGr-DMG-GCE over the N-DMG-GCE with no shift

in redox half-wave potential. This increase may be attributed to the increase in active surface area and quantum confinement of the electrode due to the incorporation of conductive, single layer graphene sheets as discussed in *Section 6.3.3*.

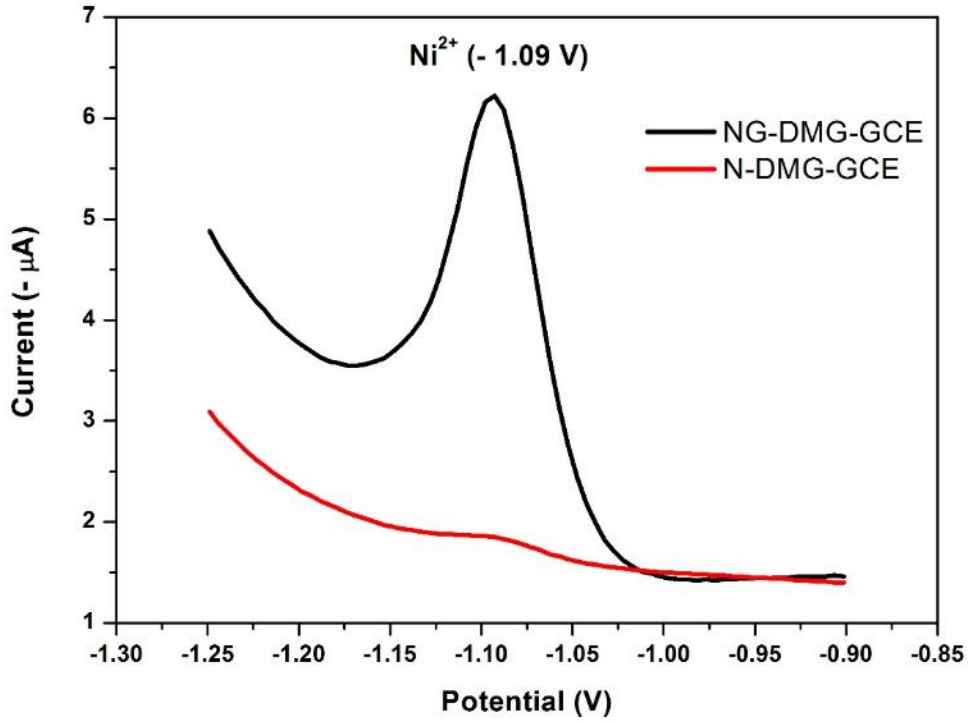

Figure 6.10: SW-AdCSV of 20 µg L^{-1} Ni^{2+} at (a) N-DMG-GCE and (b) NGr-DMG-GCE with a characteristic reduction stripping potential of -1.09 V. Supporting electrolyte (0.1 M NH_3/NH_4Cl Buffer (pH 9.3)), deposition potential (- 0.7 V), deposition time (120 s), frequency (20 Hz), amplitude (0.02 V) and voltage step (0.005 V).

6.3.9. Influence of Dimethylglyoxime Concentration

The reduction of Ni^{2+} from the electrochemical probe is dependent on two important criteria: (1) the adsorption of the metal ions onto the electrode surface (*equation 6.1*) and (*6.2*) the speed and ease of electron transfer through the chemical coating. The influence of chelating agent, dimethylglyoxime on the stripping peak current of Nickel (II) in the NGr-DMG suspension was investigated and recorded in *Figure 6.11*. The concentration of dimethylglyoxime was varied

between 0.0 M and 0.1 M (maximum concentration before saturation) by dissolving appropriate quantities of dimethylglyoxime into ethanol. The appropriate ratio of DMG was mixed with Nafion and graphene to form the NGr-DMG suspension before ultrasonication. No stripping peak current for Ni^{2+} was observed in the absence of DMG (0.0 M) in the 0.1 M NH_3/NH_4Cl buffer solution. A constant increase in stripping peak response is then observed with increasing dimethylglyoxime concentration in the coating solution between 0.0 and 0.075 M. Saturation of the electrode surface with the non-conductive DMG (*Section 6.3.6*) at DMG concentrations greater than 0.075 M is evident in a sharp decrease in the resultant stripping peak current. Here, saturation of the electrode surface with metal ions as well as blocking of electron transfer reactions through the chelating agent takes place. A concentration of 0.075 M dimethylglyoxime in the NGr-DMG suspension was utilized for all further experiments.

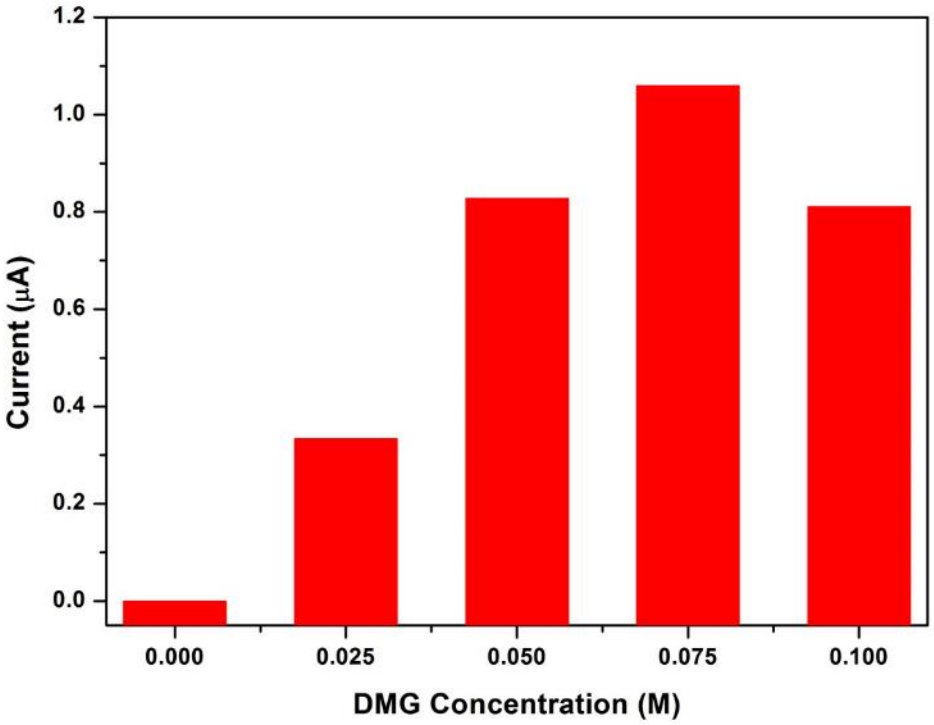

Figure 6.11: Influence of Dimethylglyoxime Concentration (0 – 0.1 M) on the stripping peak currents of Ni^{2+} at the NGr-DMG-GCEs in 0.1 M NH_3/NH_4Cl Buffer (pH 9.3).

6.3.10. Optimization of Instrumental Parameters

The square wave instrumental parameters affecting the analytical response of the NGr-DMG-GCE; namely deposition potential, deposition time, frequency and amplitude were optimized and illustrated in *Figure 6.12*.

The influence of deposition potential on the stripping response of Ni^{2+} at the NGr-DMG-GCE was interrogated in the potential range between 0.0 and – 1.0 V, more positive than the half-wave potential of Ni^{2+}, *Figure 6.12(a)*. The deposition potential is responsible for aiding in the accumulation of the analyte at the electrode surface. The stripping response increased to a maximum at – 0.4 V, due to the formation of the $Ni(DMG)_2$ adsorption complex. A gradual decrease is observed at potentials more negative than – 0.4 V as the Ni^{2+} half-wave potential is approached. A deposition potential of – 0.7 V was selected for all further experiments.

The effect of deposition/accumulation time on the Ni^{2+} stripping response was studied between 30 and 300 s. *Figure 6.12 (b)*, shows a rapid increase in the Ni^{2+} peak current with increasing accumulation time between 0 and 180 s confirming the increase in adsorption of the Ni^{2+} on the NGr-DMG-GCE surface. Saturation of the NGr-DMG-GCE takes place at accumulation times greater than 180 s and results in a decrease in stripping peak current. A deposition time of 120 s was selected for all analysis.

Figure 6.12 (c), shows the dependence of peak currents on the square wave frequency over the 5 to 70 Hz range. The peak current increases with increasing frequency to 60 Hz, before gradually decreasing. The increase in peak current is as a result of the increase in scan rate with increasing frequency. A frequency of 50 Hz was selected for further study.

The influence of amplitude on the stripping peak current of Ni^{2+} was studied between 5 and 100 mV and shown in *Figure 6.12 (d)*. The stripping peak current increases with increasing amplitude hence an amplitude of 40 mV was selected for all further experiments.

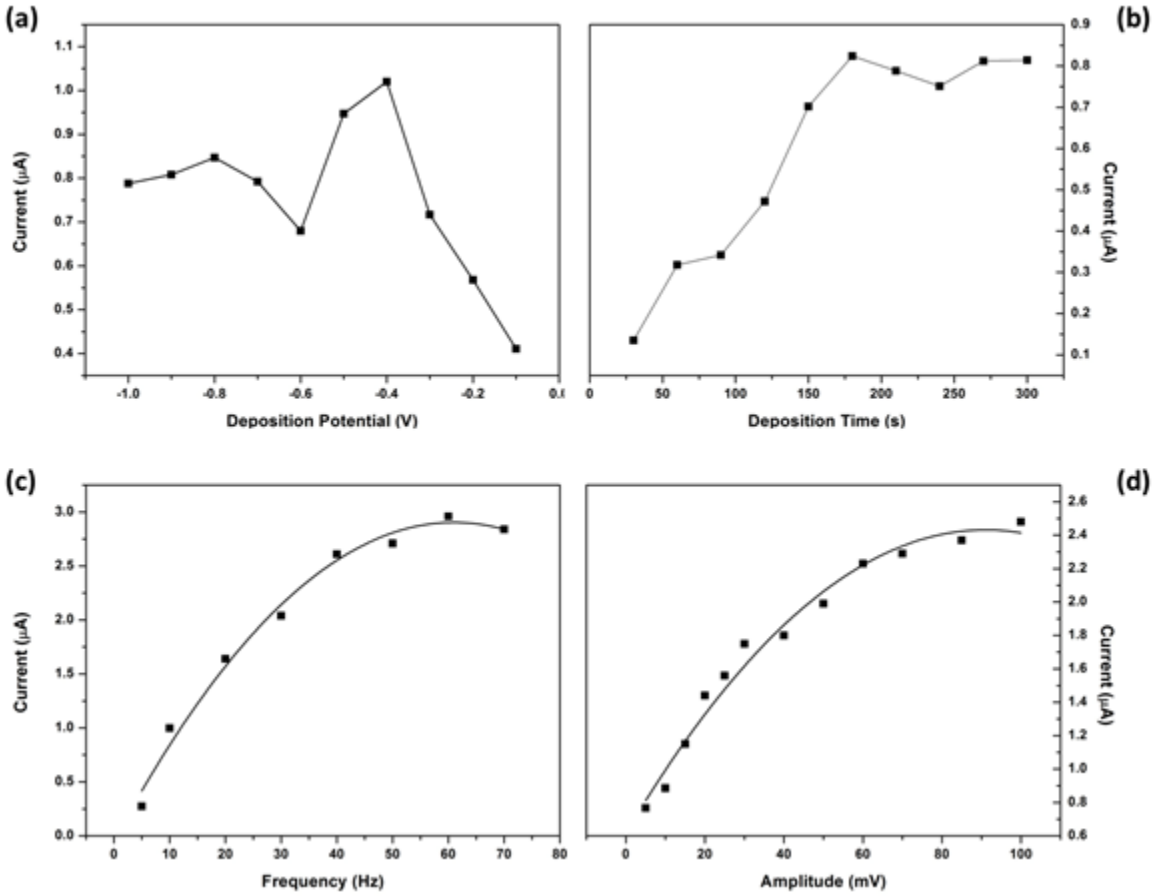

Figure 6.12: Effect of Instrumental Parameters; (a) Deposition Potential, (b) Deposition Time, (c) Frequency and (d) Amplitude on the stripping peak current of 10 µg L^{-1} Ni^{2+} at NGr-DMG-GCE. Supporting electrolyte (0.1 M NH_3/NH_4Cl Buffer (pH 9.3)).

6.3.11. Influence of Electrolyte pH

The accumulation of nickel cations at/onto the electrode surface, forming the $Ni(DMG)_2$ complex, is the determining step in Ni^{2+} detection by AdSV and is controlled by the electrolyte solution and its pH, as discussed in *Section 6.3.2*. The influence of electrolyte solution pH between 6 and 10 on the stripping peak current of Ni^{2+} was investigated in 0.1 M NH_3/NH_4Cl Buffer under optimum conditions and recorded in *Figure 6.13*. No significant stripping peak current was found at the NGr-DMG-GCE for pH values below 8 indicating very little complex formation took place. A drastic increase in peak currents between pH 8.5 and 10 can be seen as a result of increased complex formation. A minimum pH of 8.5 is therefore required to aid in the formation of the

$Ni(DMG)_2$ complex at the NGr-DMG-GCE surface. A pH of 9.2 was selected for all further experiments.

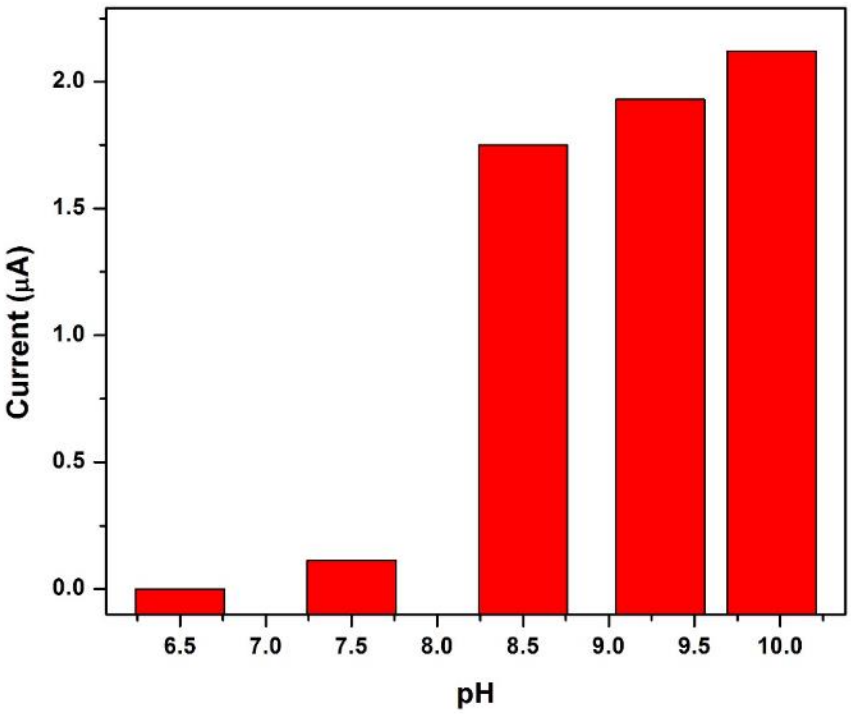

Figure 6.13: Dependence of Electrolyte pH on the stripping peak currents of Ni^{2+} at the NGr-DMG-GCEs in 0.1 M NH_3/NH_4Cl Buffer as electrolyte solution.

6.3.12. Influence of Oxygen Removal

Rapid analysis times of the square-wave waveform limits the effects of the irreversible oxygen reduction. As a result, removal of oxygen from the sample is not usually required. The effects of the cathodic stripping peak current of Ni^{2+} reduction at the NGr-DMG-GCE measured before and after deoxygenation of the sample are recorded in *Figure 6.14*. Deoxygenation was achieved by bubbling N_2 gas through the sample for 5 min. A large broad peak between - 0.7 and - 1.0 V is observed at the NGr-DMG-GCE before oxygen removal and may be attributed to the reduction of dissolved oxygen. Similar stripping peak currents of Ni^{2+} are observed before and after deoxygenation at low and high concentrations. The slight increase in response after oxygen

removal indicates a minute interference of oxygen on the measurement, owing to the cation reduction near the oxygen reduction wave. Similar results are obtained in the work by Zen *et al.* [23,24]. A slight shift in peak potential of the Ni^{2+} reduction peak from - 1.105 V to more positive oxidation potentials of - 1.092 V is observed after oxygen removal due to improved electron transfer processes. All samples were degassed under N_2 for 5 min prior to use in order to avoid any possible interference on the analysis.

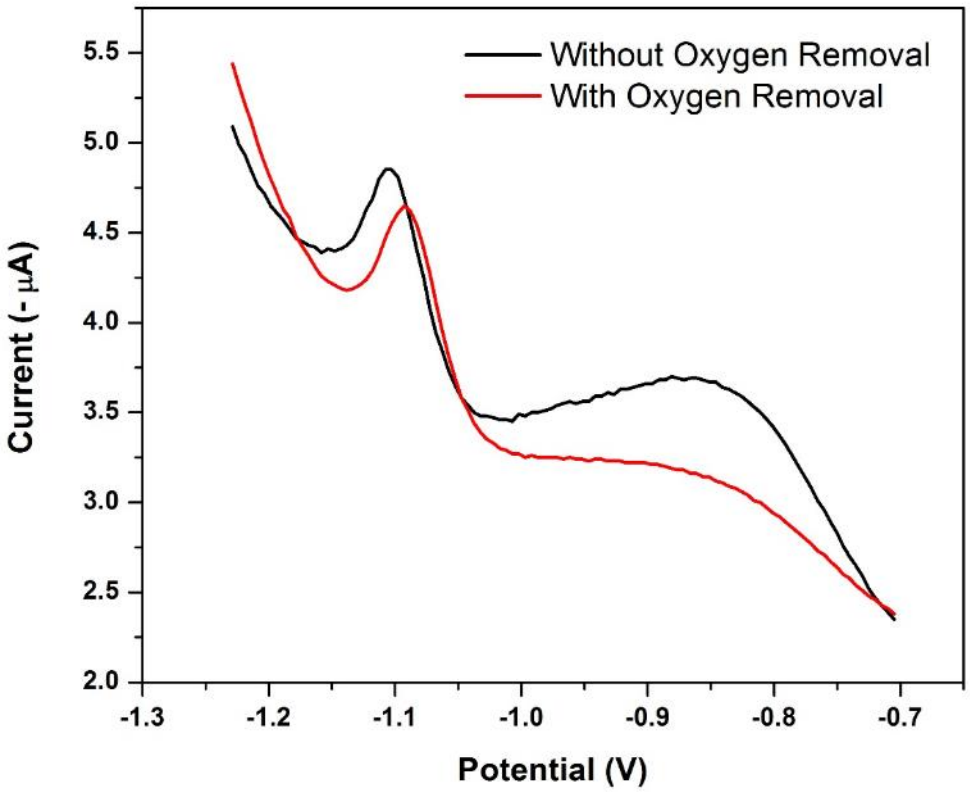

Figure 6.14: Square-Wave Voltammogram of 4 µg L^{-1} Ni^{2+} at a NGr-DMG-GCE (a) before deoxygenation and (b) after deoxygenation. Supporting electrolyte (0.1 M NH_3/NH_4Cl Buffer (pH 9.3)), deposition potential (- 0.7 V), deposition time (120 s), frequency (20 Hz), amplitude (0.02 V) and voltage step (0.005 V).

6.3.13. Electrode Reproducibility and Interference Studies

The selectivity of the proposed method was investigated by studying the effects of Co^{2+} and Zn^{2+} cations on the stripping voltammetric determination of 20 µg L^{-1} Ni^{2+}, under optimised conditions. Co^{2+} and Zn^{2+}, were selected as possible interferents due to the similar peak potentials compared to Ni^{2+} within the potential range under investigation. Further, Co^{2+} readily forms complexes with dimethylglyoxime under similar conditions. All other metallic cations were eliminated for interference studies. *Figure 6.15*, depicts the voltammograms recorded at the NGr-DMG-GCEs for (a) 0 µg L^{-1} metal cations, (b) 200 µg L^{-1} Co^{2+} and Zn^{2+}, (c) 20 µg L^{-1} Ni^{2+} and (d) 20 µg L^{-1} Ni^{2+} in the presence of 200 µg L^{-1} Co^{2+} and Zn^{2+}. No stripping peaks were found in the absence of metal cations between - 0.7 and - 1.3 V, as expected. Similarly, Co^{2+} and Zn^{2+} were also found to exhibit no reduction stripping peaks at the NGr-DMG-GCE between 0 and 200 µg L^{-1}. This result differs significantly from previous research on metal-based sensors where Co^{2+} has been detected in the presence of DMG and a metallic film, and could be attributed to the lack of metal film for Co^{2+}- and Zn^{2+}- chelate adsorption on the electrode surface. This is a significant finding in improving electrode selectivity towards Ni^{2+} detection. Determination of Ni^{2+} in 0.1 M NH_3/NH_4Cl Buffer (pH 9.3) as electrolyte solution, under optimum conditions shows a reproducible, well-defined stripping peak for Ni^{2+} reduction from the $Ni(dmgH)_2$ complex. $Ni(dmgH)_2$ detection is therefore independent of mercury or metallic film and relies solely on the metal-chelate complex formation. The sensor provides similar stripping peak currents for Ni detection in the presence of Co^{2+} or Zn^{2+}.

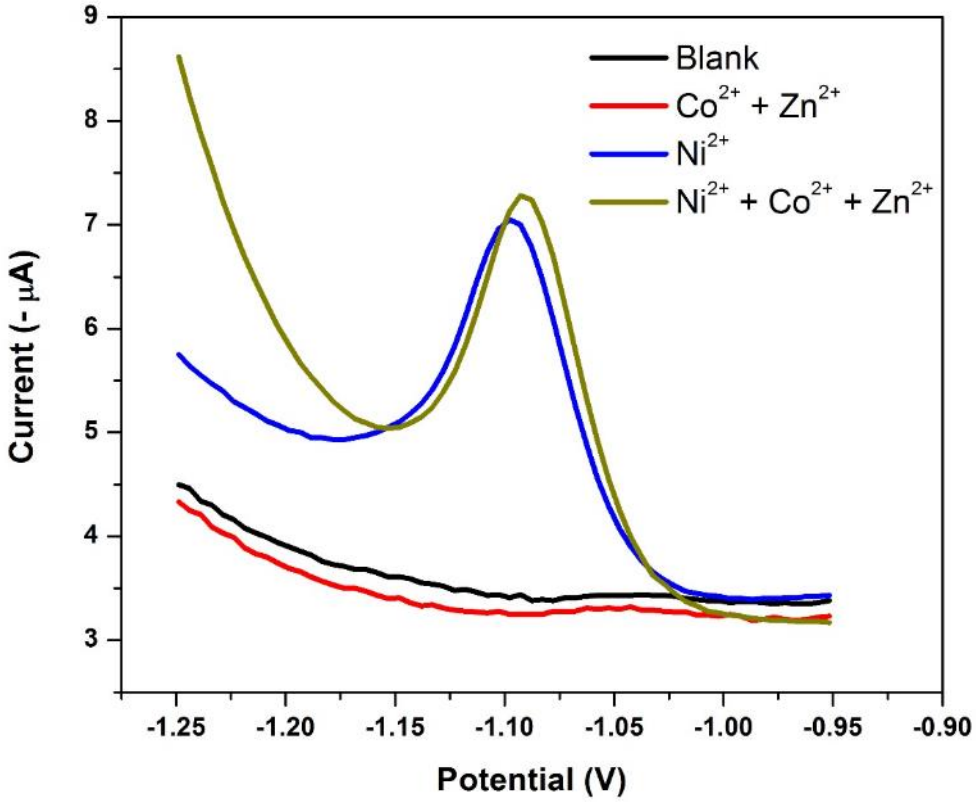

Figure 6.15: Square-Wave Voltammograms of (a) 0 µg L^{-1} metal cations, (b) 200 µg L^{-1} Co^{2+} and Zn^{2+}, (c) 20 µg L^{-1} Ni^{2+} and (d) 20 µg L^{-1} Ni^{2+} in the presence of 200 µg L^{-1} Co^{2+} and Zn^{2+} at a NGr-DMG-GCE. Supporting electrolyte (0.1 M NH_3/NH_4Cl Buffer (pH 9.3)), deposition potential (- 0.7 V), deposition time (120 s), frequency (20 Hz), amplitude (0.02 V) and voltage step (0.005 V).

The results are further summarized in *Table 6.1*. Cations with variation in stripping peak current greater than 5 - 10 % for three successive replicas (n = 3) was considered as interferent. The sensitivity of the NGr-DMG-GCE is shown to be 10 times greater than the N-DMG-GCE (further supporting the findings in *Section 3.9* above). The peak current for Ni^{2+} reduction remained constant each time 20 µg L^{-1} was detected, with a relative standard deviation (RSD) of 5.46 % confirming a highly reproducible system. The stripping peak currents of Ni^{2+} in the presence of excess Co^{2+} and Zn^{2+} up to 10 times Ni^{2+} concentration were investigated and a RSD (%) of 3.94 % was observed. The results indicate that the NGr-DMG-GCE sensor is highly

reproducible for Ni^{2+} determination and shows good stability. It further indicates no significant interference from Co^{2+} and Zn^{2+} on the Ni^{2+} determination up to concentrations 10 times the analyte concentration. The NGr-DMG-GCE sensor can therefore be applied for Ni^{2+} detection in complex samples.

Table 6.1: Reproducibility and interference studies of the N-DMG-GCE and NGr-DMG-GCE*.

Analyte	*Concentration ($\mu g\ L^{-1}$)*	*Peak Current (A)*	*Std. Dev. (A)*	*% Error*
N-DMG-GCE				
Co^{2+} and Zn^{2+}	200	N/D	N/D	N/D
Ni^{2+}	20	1.12E-07	1.12E-08	3.72
Ni^{2+} in the presence of Co^{2+} and Zn^{2+}	20	1.09E-07	1.63E-8	4.01
NGr-DMG-GCE				
Co^{2+} and Zn^{2+}	200	N/D	N/D	N/D
Ni^{2+}	20	1.94E-06	1.06E-07	5.46
Ni^{2+} in the presence of Co^{2+} and Zn^{2+}	20	1.87E-06	1.34E-07	3.94

* where, n = 3

6.3.14. Analytical Performance of the NGr-DMG-GCE

The analytical performance of the GCE sensor, modified with a dimethylglyoxime chelating agent and a nafion-graphene nanocomposite to enhance electrode sensitivity in the absence of an electroplated metal film was evaluated for Nickel detection in test samples under optimum conditions. The recorded square-wave stripping voltammograms and corresponding calibration plots for the analysis of Ni^{2+} in 0.1 M NH_3/NH_4Cl buffer solution (pH 9.3) containing Co^{2+} and Zn^{2+} at a NGr-DMG-GCE for 120 s are shown in *Figure 6.16*. The performance of the sensor was investigated in the 2-20 µg L^{-1} range. A linear increase in the Ni^{2+} reduction stripping

peak current is observed with increasing concentration of Ni^{2+}. The detection limit (DL) of the Ni^{2+} sensor in the presence of Co^{2+} and Zn^{2+} were determined according to *Equation 6.4*:

$$\mathrm{LOD/LOQ} = \frac{F \times \sigma}{b} \qquad (\textit{Equation 6.4})$$

Where

LOD: Limit of Detection

LOQ: Limit of Quantitation

F: Factor of 3.3 and 10 for LOD and LOQ, respectively

σ: Standard deviation of the blank, standard deviation of the ordinate intercept, or residual standard deviation of the linear regression

b: Slope of the regression line

The standard deviation of the blanks was determined from 10 replications of the NGr-DMG-GCE in 0.1 M NH_3/NH_4Cl Buffer (pH 9.3) in the presence of excess Co^{2+} and Zn^{2+}. A summary of previously reported electrochemical sensors for the detection of Ni^{2+} in water at: (a) chemically modified DMG electrodes and (b) In-situ deposited DMG electrodes as well as a summary of detection limits from this work are reported in *Table 6.2* below. It can be observed that the *in-situ* deposition of metal-DMG complexes onto metallic films provides more sensitive electrochemical sensors as seen by its significantly lower detection limits and faster analysis times compared to that of chemically modified DMG electrodes. This is to be expected due to the presence of excess chelating agent for complexation as well as the presence of metal film for adsorption of metal-chelate complexes. Further, the detection of Co^{2+} has been limited to in-situ DMG electrodes in the presence of electroplated metal films. The use of chemically modified DMG electrodes in the presence of mercury films still provide improved detection limits over the metal-free counterparts. The use of graphene in our study has significantly lowered the observed detection limits by improving electrode sensitivity over previous chemically modified DMG

metal-free sensors and has for the first time shown that Ni^{2+} detection can be observed in the presence of Co^{2+} and Zn^{2+}.

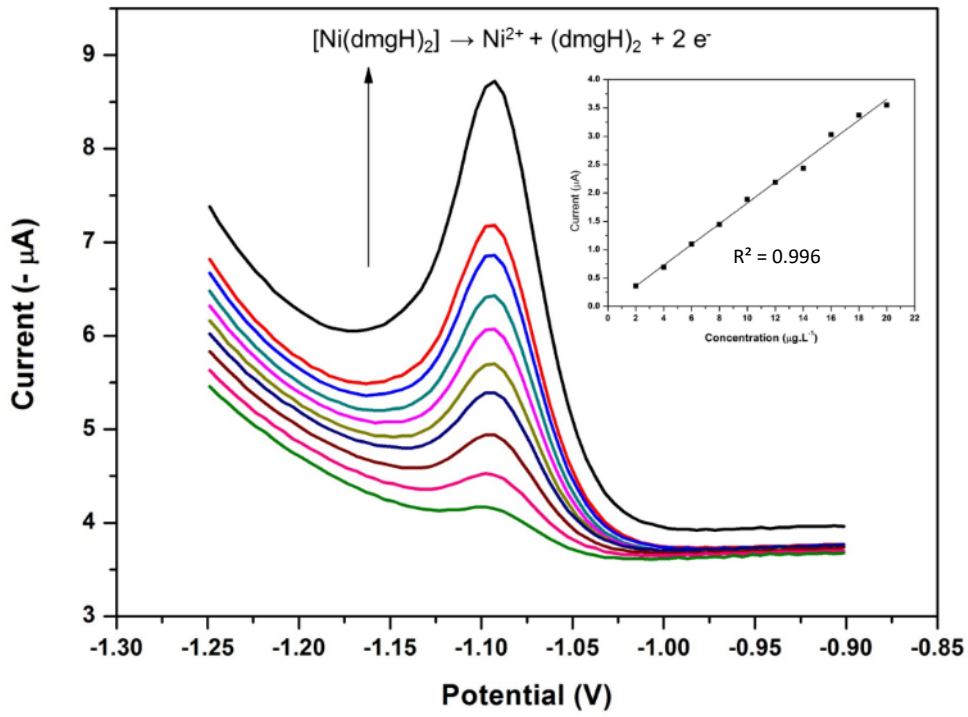

Figure 6.16: SWAdSV and corresponding calibration plot of the individual analysis of Ni^{2+} in the presence of Co^{2+} and Zn^{2+} obtained at a NGr-DMG-GCE over 2 – 20 µg L^{-1}. Supporting electrolyte (0.1 M NH_3/NH_4Cl Buffer (pH 9.3)), deposition potential (- 0.7 V), deposition time (120 s), frequency (20 Hz), amplitude (0.02 V) and voltage step (0.005 V).

Table 6.2: A summary of selected previously reported (a) Chemically Modified DMG and (b) In-situ DMG Sensors for Adsorptive Stripping Voltammetric Detection of Ni^{2+}.

	Metal Ions	Substrate	Technique	Accumulation Time (s)	Dynamic Linear Range ($\mu g\ L^{-1}$)	Detection Limit ($\mu g\ L^{-1}$)	Reference
In-situ DMG Electrodes	Ni^{2+}	mpBiF-SPCE	AdCSV	180	1 - 10	0.027	[28]
	Co^{2+}				1 - 10	0.094	
	Ni^{2+}	RBiABE	DPAdSV	30	0.6 - 41	0.18	[14]
	Co^{2+}				0.06 – 4.1	0.018	
	Ni^{2+}	PbF-SPE	SWV	60	0.6 – 2.9	0.2	[15]
	Co^{2+}				0.6 – 5.9	0.3	
	Ni^{2+}	SBVE	SW-AdCSV	30	0 - 10	0.6	[55]
Chemically Modified DMG Electrodes	Ni^{2+}	NC-DMG-MFE	SWASV	300	0.1 - 100	0.1	[22]
	Cu^{2+}				1.0 - 80	1.0	
	Ni^{2+}	MCPE	AAdSV	720	6 - 600	0.006	[18]
	Ni^{2+}	DMG-CPE	DPV	1500	80 - 600	27	[20]
	Ni^{2+}	DMG-N/SPE	DPV	120	60 - 500	30	[16]
	Ni^{2+}	PVC-PA-DMG-GCE	SWAdCSV	240	18 - 180	18	[8]
	Ni^{2+} i.p.o. Co^{2+} and Zn^{2+}	NGr-DMG-GCE	SWAdSV	120	2 - 20	1.5	This Work

* i.p.o. = in the presence of

6.3.15. *Application of the NGr-DMG-GCE to real water samples*

In order to further investigate the analytical performance and accuracy of the NGr-DMG-GCE sensor towards the detection of Ni^{2+} in the presence of excess Co^{2+} and Zn^{2+}, recovery studies were performed in both test and real water samples by a standard addition method. Tap water samples were collected from our laboratory and investigated for the detection of Ni^{2+}. The recorded voltammogram and associated calibration plot are illustrated in *Figure 6.17* and a summary of the recovery percentages obtained when performing analysis in tap water and electrolyte solutions is

shown in *Table 6.3*. No target metal ions (Ni^{2+}, Co^{2+} or Zn^{2+}) was detected in either electrolyte or real water samples at 120 s preconcentration time. This distinct lack of reduction peaks suggests that the concentration of metal ions was below the sensor limits of detection in the real samples. Known concentrations (3 µg L^{-1}) of Ni^{2+} were spiked in the water samples in the presence of Co^{2+} and Zn^{2+} and detected by performing consecutive additions of known concentration to the 'unknown' sample (standard addition method) from 3 – 12 µg L^{-1}. Ni^{2+} yielded accurate recovery percentages in both test and real water samples with errors within the acceptable sensor limits. The results verify the use of the sensor in water samples with low concentrations of Ni^{2+}.

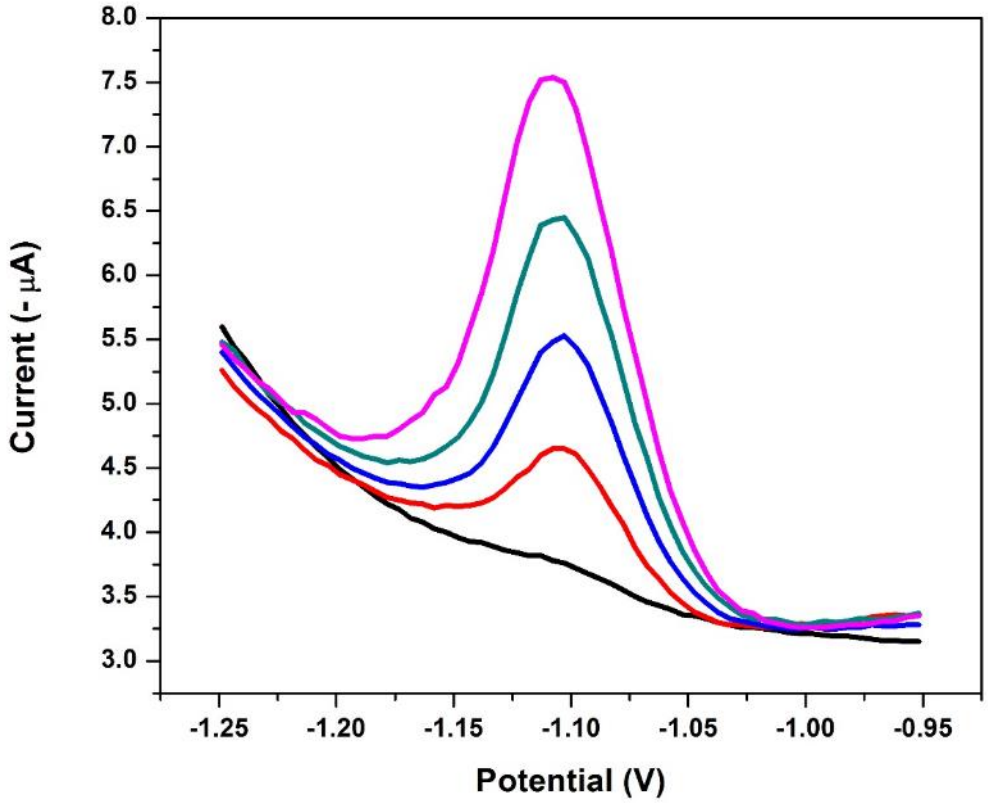

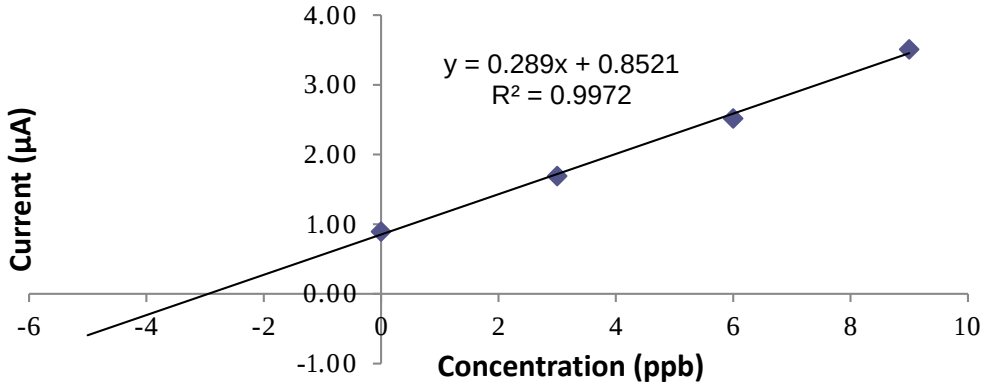

Figure 6.17: SWAdSV and corresponding standard addition calibration plot of the individual analysis of Ni^{2+} in the presence of Co^{2+} and Zn^{2+} obtained at a NGr-DMG-GCE in real tap water samples. Supporting electrolyte (0.1 M NH_3/NH_4Cl Buffer (pH 9.3)), deposition potential (- 0.7 V), deposition time (120 s), frequency (20 Hz), amplitude (0.02 V) and voltage step (0.005 V).

Table 6.3: Recovery studies of the NGr-DMG-GCE in test and tap water samples*.

Ni^{2+} Sample	*Original ($\mu g\ L^{-1}$)*	*Added ($\mu g\ L^{-1}$)*	*Found ($\mu g\ L^{-1}$)*	*RSD (%)*	*Recovery (%)*
Test Sample	*N/D*	*3.00*	*3.16*	*8.21*	*105*
Real Water Sample	*N/D*	*3.00*	*3.35*	*7.46*	*111*

* where, n = 3

6.4. Conclusion

For the first time a nafion-graphene dimethylglyoxime modified glassy carbon electrode was interrogated for the ultra-trace determination of Ni^{2+} in water samples. Fabrication of a DMG modified probe showed a green approach towards Ni^{2+} detection by eliminating the need for toxic metal films commonly used in metal analysis to date. Good quality graphene synthesised by a modified Hummer's method further showed good ability to enhance the electrode sensitivity towards Ni^{2+} detection by improving the electron transfer kinetics and active surface area of the electrode surface modified with DMG. The NGr-DMG-GCE probe further showed superior

sensitivity and selectivity towards detection of Ni^{2+} in the presence of common interferents such as Co^{2+} and Zn^{2+} ions. Detection limits in the low parts per billion range (1.5 µg L^{-1}), well below the USEPA and WHO maximum contamination limits were achieved at short pre-concentration times (120 s) confirming the improved sensitivity over common DMG-modified electrodes. The NGr-DMG-GCE was successfully applied to the detection of Ni^{2+} in real tap water samples with accurate recorded recoveries within 5-10 % error.

References

[1] WHO, Nickel in Drinking-water, Environ. Heal. (2005) 1–16.

[2] B.B. Mamba, L.C. Rietveld, J.Q.J.C. Verberk, SA drinking water standards under the microscope, Water Wheel. 7 (2008) 24–27. doi:www.sxc.hu.

[3] Z. Zou, A. Jang, E.T. MacKnight, P.-M. Wu, J. Do, J.S. Shim, P.L. Bishop, C.H. Ahn, An On-Site Heavy Metal Analyzer With Polymer Lab-on-a-Chips for Continuous Sampling and Monitoring, IEEE Sens. J. 9 (2009) 586–594. doi:10.1109/JSEN.2009.2018348.

[4] G. March, T. Nguyen, B. Piro, Modified Electrodes Used for Electrochemical Detection of Metal Ions in Environmental Analysis, Biosensors. 5 (2015) 241–275. doi:10.3390/bios5020241.

[5] D.E. Keil, J. Berger-Ritchie, G. a. McMillin, Testing for Toxic Elements: A Focus on Arsenic, Cadmium, Lead, and Mercury, Lab. Med. 42 (2011) 735–742. doi:10.1309/LMYKGU05BEPE7IAW.

[6] J.L.C.P. Christopher M. A. Brett, Ana Maria C. F. Oliveira Brett, 8-ASV-Electroanalysis.pdf, (1991).

[7] P. Wararattananurak, P. Chooto, P. Sherdshoopongse, C. Chuaynukool, C. Innuphat, Lead determination in canned food by square-wave adsorptive cathodic stripping voltammetry, ScienceAsia. 40 (2014) 355–361. doi:10.2306/scienceasia1513-1874.2014.40.355.

[8] C. Bing, Chemical accumulation and voltammetric determination of traces of nickel(II) at glassy carbon electrodes modified with dimethyl glyoxime containing polymer coatings,

Talanta. 49 (1999) 651–659. doi:10.1016/S0039-9140(99)00055-7.

[9] J. Wang, Stripping analysis: Principles, instrumentation, and applications, Deerf. Beach, FL, USA VCH Publ. Inc. (1985). https://scholar.google.com/scholar?q=J+Wang+1985&btnG=&hl=en&as_sdt=0%2C26#1 (accessed August 4, 2015).

[10] A. Ferancová, M.K. Hattuniemi, A.M. Sesay, J.P. Räty, V.T. Virtanen, Electrochemical Monitoring of Nickel(II) in Mine Water, Mine Water Environ. (2015). doi:10.1007/s10230-015-0357-1.

[11] A. Bobrowski, A. Krolicka, M. Maczuga, J. Zarebski, Highly Sensitive and Selective Adsorptive Stripping Voltammetric Method Employing a Lead Film Screen-printed Electrode for Determination of Cobalt as its Nioximate Complex, Electroanalysis. 28 (2016) 343–349. doi:10.1002/elan.201500362.

[12] L. Zhang, D. Pan, Y. Liu, Rapid and sensitive determination of cobalt by adsorptive cathodic stripping voltammetry using tin–bismuth alloy electrode, Ionics (Kiel). 22 (2016) 721–729. doi:10.1007/s11581-015-1596-7.

[13] K. Tyszczuk-Rotko, R. Metelka, K. Vytřas, M. Barczak, Lead Film Electrode Prepared with the Use of a Reversibly Deposited Mediator Metal in Adsorptive Stripping Voltammetry of Nickel, Electroanalysis. 26 (2014) 2049–2056. doi:10.1002/elan.201400263.

[14] B. Bas, K. Wegiel, K. Jedlinska, The renewable bismuth bulk annular band working electrode: Fabrication and application in the adsorptive stripping voltammetric determination of nickel(II) and cobalt(II), Anal. Chim. Acta. 881 (2015) 44–53. doi:10.1016/j.aca.2015.05.005.

[15] A. Bobrowski, A. Królicka, M. Maczuga, J. Zarębski, A novel screen-printed electrode modified with lead film for adsorptive stripping voltammetric determination of cobalt and nickel, Sensors Actuators, B Chem. 191 (2014) 291–297. doi:10.1016/j.snb.2013.10.006.

[16] A. Ferancová, M.K. Hattuniemi, A.M. Sesay, J.P. Räty, V.T. Virtanen, Rapid and direct

electrochemical determination of Ni(II) in industrial discharge water, J. Hazard. Mater. 306 (2016) 50–57. doi:http://dx.doi.org/10.1016/j.jhazmat.2015.11.057.

[17] A. Ferancová, M.K. Hattuniemi, A.M. Sesay, J.P. Räty, V.T. Virtanen, Complexation of Ni(II) by Dimethylglyoxime for Rapid Removal and Monitoring of Ni(II) in Water, Mine Water Environ. (2016). doi:10.1007/s10230-016-0402-8.

[18] P. González, V.A. Cortínez, C.A. Fontán, Determination of nickel by anodic adsorptive stripping voltammetry with a cation exchanger-modified carbon paste electrode, Talanta. 58 (2002) 679–690. doi:10.1016/S0039-9140(02)00381-8.

[19] B. Rezaei, E. Rezaei, Simultaneous determination of trace amounts of nickel, cobalt, and zinc in the wastewater of a galvanic workshop by using adsorptive cathodic stripping voltammetry, J. Anal. Chem. 61 (2006) 262–265. doi:10.1134/S1061934806030129.

[20] F.O. Tartarotti, M.F. De Oliveira, V.R. Balbo, N.R. Stradiotto, Determination of nickel in fuel ethanol using a carbon paste modified electrode containing dimethylglyoxime, Microchim. Acta. 155 (2006) 397–401. doi:10.1007/s00604-006-0638-2.

[21] K.N. Thomsen, L. Kryger, R.P. Baldwin, Voltammetric Determination of Traces of Nickel (I I) with a Medium Exchange Flow System and a Chemically Modified Carbon Paste Electrode Containing Dimet h ylg lyoxime, (1988) 151–155.

[22] H. Tien, The Application of Chelating Agent Incorporated Polymer Modified Electrodes in the Detection of Trace Metals, J. Chinese Chem. Soc. 45 (1998).

[23] J. Zen, N. Chi, F. Hsu, M. Chung, Sq uare-wave Voltam metric Determination of Copper(ii) With a Nafion-Dimethylglyoxime Mercu ry-f il m Electrode, Analyst. 120 (1995) 0–4.

[24] J. Zen, M. Lee, Determination of Traces of Nickel(, Society. (1993) 3238–3243.

[25] S.B. Adeloju, A. Hadjichari, Simultaneous Determination of Nickel and Cobalt in Natural Water and Sediment Samples on an in-situ Plated Mercury Film Electrode by Adsorptive Cathodic Stripping Voltammetry., Anal. Sci. 15 (1999) 95–100.

doi:10.2116/analsci.15.95.

[26] T.V. Nghit, H. Tho, P. Hung, V. Chu, X. Quangt, P. Dinh, ADSORPTIVE CATHODIC STRIPPING VOLTAMMETRIC DETERMINATION OF SEVERAL HEAVY METALS (Ni , Co ; Cu , Pb) IN NATURAL WATERS, (n.d.).

[27] M. Korolczuk, K. Tyszczuk, M. Grabarczyk, Adsorptive stripping voltammetry of nickel and cobalt at in situ plated lead film electrode, Electrochem. Commun. 7 (2005) 1185–1189. doi:10.1016/j.elecom.2005.08.022.

[28] S. Dal Borgo, H. Sopha, S. Smarzewska, S.B. Hočevar, I. Švancara, R. Metelka, Macroporous Bismuth Film Screen-Printed Carbon Electrode for Simultaneous Determination of Ni(II) and Co(II), Electroanalysis. 27 (2015) 209–216. doi:10.1002/elan.201400422.

[29] N. Gharib Naseri, S.J. Baldock, A. Economou, N.J. Goddard, P.R. Fielden, Disposable electrochemical flow cells for catalytic adsorptive stripping voltammetry (CAdSV) at a bismuth film electrode (BiFE), Anal. Bioanal. Chem. 391 (2008) 1283–1292. doi:10.1007/s00216-008-1948-5.

[30] E.A. Hutton, S.B. Hočevar, B. Ogorevc, M.R. Smyth, Bismuth film electrode for simultaneous adsorptive stripping analysis of trace cobalt and nickel using constant current chronopotentiometric and voltammetric protocol, Electrochem. Commun. 5 (2003) 765–769. doi:10.1016/S1388-2481(03)00177-2.

[31] R. Segura, M. Pradena, D. Pinto, F. Godoy, E. Nagles, V. Arancibia, Adsorptive stripping voltammetry of nickel with 1-nitroso-2-napthol using a bismuth film electrode, Talanta. 85 (2011) 2316–2319. doi:10.1016/j.talanta.2011.07.062.

[32] R.A. Segura, J.A. Pizarro, M.P. Oyarzun, A.D. Castillo, K.J. Díaz, A.B. Placencio, Determination of Lead and Cadmium in Water Samples by Adsorptive Stripping Voltammetry Using a Bismuth film / 1- Nitroso-2-Napthol / Nafion Modified Glassy Carbon Electrode, Int. J. Electrochem. Sci. 11 (2016) 1707–1719.

[33] K. Pokpas, S. Zbeda, N. Jahed, N. Mohamed, P.G. Baker, E.I. Iwuoha, E.I.I. Sensorlab,

Electrochemically reduced graphene oxide pencil-graphite in situ plated bismuth-film electrode for the determination of trace metals by anodic stripping voltammetry, Int. J. Electrochem. Sci. 9 (2014) 736–759. www.electrochemsci.org (accessed April 3, 2017).

[34] N.J. Walch, F. Davis, N. Langford, J.L. Holmes, S.D. Collyer, S.P.J. Higson, Enhancement of Electrode Performance by a Simple Casting Method Using Sonochemically Exfoliated Graphene, Anal. Chem. 87 (2015) 9273–9279. doi:10.1021/acs.analchem.5b01829.

[35] K. Pokpas, N. Jahed, O. Tovide, P.G. Baker, E.I. Iwuoha, Nafion-graphene nanocomposite in situ plated bismuth-film electrodes on pencil graphite substrates for the determination of trace heavy metals by anodic stripping voltammetry, Int. J. Electrochem. Sci. 9 (2014) 5092–5115.

[36] S. Zbeda, K. Pokpas, S. Titinchi, N. Jahed, P.G. Baker, E.I. Iwuoha, Few-layer binder free graphene modified mercury film electrode for trace metal analysis by square wave anodic stripping voltammetry, Int. J. Electrochem. Sci. 8 (2013) 11125–11141.

[37] S. Chaiyo, E. Mehmeti, K. Žagar, W. Siangproh, O. Chailapakul, K. Kalcher, Electrochemical sensors for the simultaneous determination of zinc, cadmium and lead using a Nafion/ionic liquid/graphene composite modified screen-printed carbon electrode, Anal. Chim. Acta. 918 (2016) 26–34. doi:10.1016/j.aca.2016.03.026.

[38] M. Ghanei-Motlagh, M.A. Taher, A. Heydari, R. Ghanei-Motlagh, V.K. Gupta, A novel voltammetric sensor for sensitive detection of mercury(II) ions using glassy carbon electrode modified with graphene-based ion imprinted polymer, Mater. Sci. Eng. C. 63 (2016) 367–375. doi:10.1016/j.msec.2016.03.005.

[39] R. Liu, C. Lei, T. Zhong, L. Long, Z. Wu, S. Huan, Q. Zhang, A graphene/ionic liquid modified selenium-doped carbon paste electrode for determination of copper and antimony, Anal. Methods. 8 (2016) 1120–1126. doi:10.1039/C5AY02945G.

[40] E. Punrat, C. Maksuk, S. Chuanuwatanakul, W. Wonsawat, O. Chailapakul, Polyaniline/graphene quantum dot-modified screen-printed carbon electrode for the rapid

determination of Cr(VI) using stopped-flow analysis coupled with voltammetric technique, Talanta. 150 (2016) 198–205. doi:10.1016/j.talanta.2015.12.016.

[41] Y. Teng, T. Chen, F. Xu, W. Zhao, W. Liu, Screen-printed Carbon Electrode Modified with Commercial Multilayer Graphene for Lead Detection in Soybean Sauces by Differential Pulse Stripping Voltammetry, Int. J. Electrochem. Sci. 11 (2016) 1907–1917. www.electrochemsci.org (accessed April 3, 2017).

[42] J. William S. Hummers, R.E. Offeman, Preparation of Graphitic Oxide, J. Am. Chem. Soc. 80 (1958) 1339. doi:10.1021/ja01539a017.

[43] J. Shen, Y. Hu, M. Shi, X. Lu, C. Qin, C. Li, M. Ye, Fast and facile preparation of graphene oxide and reduced graphene oxide nanoplatelets, Chem. Mater. 21 (2009) 3514–3520. doi:10.1021/cm901247t.

[44] U.T. Nasional, Preparation and Spectral Properties of Mixed-Ligand Complexes of VO (IV), Ni (II), Zn (II), Pd (II), Cd (II) and Pb (II) with Dimethylglyoxime and N - Acetylglycine, 7 (2010) 580–587.

[45] S. Jadhav, S. Kulkarni, S. Quadri, Ultrasound Assisted Synthesis and Physiochemical Investigation of Nickel – Dimethyl Glyoxime Complex, 5 (2015) 311–316.

[46] W.S. Cardoso, V.L.N. Dias, W.M. Costa, I. De Araujo Rodrigues, E.P. Marques, A.G. Sousa, J. Boaventura, C.W.B. Bezerra, C. Song, H. Liu, J. Zhang, A.L.B. Marques, Nickel-dimethylglyoxime complex modified graphite and carbon paste electrodes: Preparation and catalytic activity towards methanol/ethanol oxidation, J. Appl. Electrochem. 39 (2009) 55–64. doi:10.1007/s10800-008-9636-x.

[47] L.E. Godycki, R.E. Rundle, The structure of nickel dimethylglyoxime, Acta Cryst. 1953 (1953) 487–495. doi:10.1107/S0365110X5300137X.

[48] R.T. Bambenek, Mark A., Pflaum, The Reaction of Nickel with Dioximes, Inorg. Chem. 758 (1963) 24–27.

[49] F.O.G. Olorundare, D. Nkosi, O.A. Arotiba, Voltammetric determination of nitrophenols

at a nickel dimethylglyoxime complex - gold nanoparticle modified glassy carbon electrode, Int. J. Electrochem. Sci. 11 (2016) 7318–7332. doi:10.20964/2016.09.47.

[50] S. Anderson, Metal-metal bonds and physical properties of some nickel (II) -vic-dioxime complexes, Retrosp. Theses Diss. (1962) Paper 2035.

[51] L. Baxter, A. Bobrowski, M. Bond, G. Heath, R.L. Paul, R. Mrzljak, J. Zarebski, Electrochemical and spectroscopic investigation of the reduction of dimethylglyoxime at mercury electrodes in the presence of cobalt and nickel., Anal. Chem. 70 (1998) 1312–23. doi:10.1021/ac9703616.

[52] F. Scholz, Voltammetric techniques of analysis: the essentials, ChemTexts. 1 (2015) 17. doi:10.1007/s40828-015-0016-y.

[53] I. Taurino, S. Carrara, M. Giorcelli, A. Tagliaferro, G. De Micheli, Comparison of two different carbon nanotube-based surfaces with respect to potassium ferricyanide electrochemistry, Surf. Sci. 606 (2012) 156–160. doi:10.1016/j.susc.2011.09.001.

[54] R.C. Carvalho, C. Gouveia-caridade, C.M.A. Brett, Glassy carbon electrodes modified by multiwalled carbon nanotubes and poly (neutral red): A comparative study of different brands and application to electrocatalytic ascorbate determination, (2010) 1675–1685. doi:10.1007/s00216-010-3966-3.

[55] G.M.S. Alves, J.M.C.S. Magalhães, H.M.V.M. Soares, Simultaneous Determination of Nickel and Cobalt Using a Solid Bismuth Vibrating Electrode by Adsorptive Cathodic Stripping Voltammetry, Electroanalysis. 25 (2013) 1247–1255. doi:10.1002/elan.201200643.

Chapter 7 :

Electroanalytical Complexation-based Detection at Low-cost, Stored, Micro-volume, Paper-based Electrochemical Cells (µPECs)

Abstract:

The development of point-of-care (POC) devices offering disposable, low-cost and accurate detection of environmental contaminants and early monitoring in the health and food sectors has steadily grown in recent times. Real-time analysis offered by POCs are pivotal in developing areas where access to skilled labor is often lacking. Chelating agent based signal amplication methods have previously been employed in conjunction with electroplated metallic films to improve electrode sensitivity in trace metal analysis. Here, we describe a method for the dry storage of electrochemical reagents: ammonia/ammonium (NH_3/NH_4Cl) buffer as supporting electrolyte, dimethylglyoxime (DMG) as chelating agent and mercury in paper-based electrochemical cells (PECs), fabricated from commercial filter paper. The stored PECs were applied to the trace, micro-liter analysis of Nickel in water samples by Adsorptive cathodic stripping voltammetry (AdCSV) in conjunction with screen printed electrodes. The method relies on the single-step accumulation/adsorption of micro-volumes of metallic analyte onto stored DMG ligands to form $[Ni(dmgH)_2]$ complexes in the presence of mercury films. By integrating the AdCSV techniques with paper-based analytical devices, detection of Ni^{2+} in water samples with good resolution was achieved at 20 µL sample volumes in the low parts per billion range. Instrumental parameters of the PECs, accumulation time and deposition potential were optimized along with reagent storage introduction and concentrations. The prepared PPECs showed good reproducibility (4.36 %, n = 4) and no intermetallic interferences in the presence of 100 µg L^{-1} Zn^{2+}, Cd^{2+}, Pb^{2+}, Co^{2+} and In^{2+}. Detection and quantitation limits were calculated and recorded as 6.27 and 18.8 µg L^{-1} respectively for Ni^{2+} determination at 90 s accumulation time. The PPECs were then applied to the detection of Ni^{2+} in real tap water samples and showed good recovery values of ± 94 %. Further, the infusion

of PECs with GO, ERGO and NGr-nanocomposites showed no significant enhancement in electron transfer rate and a distinct lack of sensitivity towards Ni^{2+} detection by AdCSV. Further, integrated electrode systems prepared by filtration and screen printing were achieved with working electrode resistance of 324 Ω recorded. The developed paper 3-electrode system was applied to $Fe(CN)_6^{3-/4}$ and detection of Ni^{2+}.

Keywords:

Paper-based electroanalytical cells; Adsorptive stripping voltammetry; Nickel detection; Dimethylglyoxime

Highlights:

- Paper-based electrochemical cells (PECs) have for the first-time been employed as sensor technology in combination with AdCSV for Ni(II) detection
- PECs offer reagent loading and storage of electrolyte, chelating agent and metallic films within the cellulose structure
- Simple, microliter-volume sample introduction
- Graphene-infused PECs exhibit no noticeable enhancement in conductivity or response towards Ni^{2+} detection
- Integrated graphene-filtered Wes with screen printed CE and RE demonstrate promising future applications

Graphical Abstract:

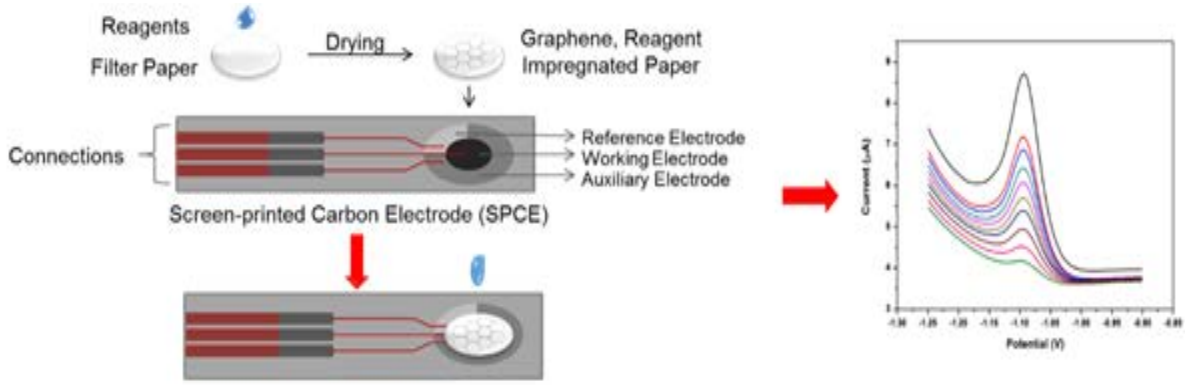

7.1. Introduction:

On-site analysis of environmental pollutants is crucial in impoverished areas where access to skilled labor and suitable instrumentation is often limited. The development of inexpensive sensor technologies, offering simple and rapid detection with short analysis times is of great importance and has significantly increased in recent years. Portable instrumentation, low-cost substrates, ease of modification, integrated battery and electrode systems, etc. have all been investigated with the aim of developing reliable point-of-care (POC) devices capable of early detection and accurate monitoring of illnesses and environmental issues in resource limited settings. The applicability of POC devices hinge on its cost, robustness, ease of use and accuracy. While dipstick and lateral flow devices have dominated rapid diagnostic sensing for decades, paper-based microfluidic sensors have garnered tremendous support in improving the ability for accurate POC devices. Simple sample introduction and reagent storage methods limit the widespread commercialization of POC devices. As such, reagent loaded plug in cartridges [1] and glass ampoules [2] have been investigated as possible reagent storage methods offering the possibility for automization in reagent delivery to microfluidic POCDs. These techniques were considered as alternative to simple inlet and outlet devices used in microfluidic devices to date. The rise of microfluidic devices has gained significant traction in the last two decades due to their ability for accurate mixing, separation of species and the possibility for low-volume analysis. However, high costs associated with the devices are based on the poly-dimethylsiloxane (PDMS) elastomer. Paper-based analytical devices (PADs) offer the most reliable reagent storage method for once-off use owing to its excellent sorption nature as a result of absorptive surface properties

of the porous cellulose structure [3]. Tan *et al.* proposed for the first time a simple reagent storage system by employing paper disks for a one-step detection of Pb^{2+} in water with an internal calibration technique [4].

To date, metal analysis at paper-based analytical devices, while still in their infancy stage, have been limited to colorimetric, electrochemical, fluorescent and nanoparticle complex based detection methods. These techniques generally rely on qualitative analysis represented by color changes, the first of which was investigated by Hossain *et al.* in 2011. Microfluidic paper-based electrochemical devices (μPEDs), introduced by the Whitesides' research group in 2007 combine the advantageous properties of paper substrates with ultra-sensitive electrochemical detection methods to develop disposable, low-cost and quantitative analytical techniques. Few studies have been investigated for application of μPEDs to metal analysis. These works have been limited to the anodic stripping voltammetric (ASV) detection of heavy metals such as Pb^{2+}, Cd^{2+}, Hg^{2+} etc. in water samples. Application of μPEDs have yet to be applied to simple complexation-based accumulation techniques demonstrated by adsorptive stripping voltammetry (AdSV).

This work describes a novel micro-volume analysis of Nickel in tap water samples at low-cost, disposable and pre-stored paper-based electrochemical cells (PECs). Herein pre-storage of electrolyte, chelating agents and metallic films within the cellulose structure of paper disks created from commercial filter paper, in conjunction with screen printed electrodes resulted in accurate, sensitive and quantitative systems for metal analysis by adsorptive cathodic stripping voltammetry (AdCSV). The work done expands on previously reported reagents storage systems for electrochemical detection by demonstrating for the first time the incorporation of microscale quantities of dimethylglyoxime (DMG) ligands within in the paper substrate in conjunction with electroplated mercury films. This storage allows for a one-step accumulation of the Ni^{2+} analyte within the paper-based cell pores by simple adsorption processes to form $[Ni(dmgH)_2]$ complexes.

7.2. Experimental Section:

7.2.1. Apparatus and Reagents

All voltammetric experiments were performed using a computer-controlled Nova 1.1 software on an Autolab PGSTAT101 potentiostat (Metrohm Autolab, The Netherlands). A three-

electrode SPCE system with carbon working electrode (4 mm diameter), carbon auxiliary electrode and Ag/AgCl reference electrode (DRP-C101), purchased from Dropsens, was employed without further modification or pretreatment. Conventional 20 mL voltammetric cells were replaced with pre-stored paper-based electrochemical cells (PPECs) for all analysis unless stated otherwise. All experiments were carried out at room temperature.

All reagents used in the study were purchased from Sigma-Aldrich chemical company (Missouri, USA) and were of analytical reagent grade. Ultra-pure water, collected from a Millipore Milli-Q system (Milford, MA, USA), was used to prepare all solutions. An ammonia buffer, used as supporting electrolyte was prepared from appropriate quantities of NH_3 (ammonia) and NH_4Cl (ammonium chloride), respectively and was obtained from Lasec. Hydrochloric (HCl) and nitric acid (HNO_3) were purchased from Lasec. Standard stock solutions of Ni^{2+} and Hg^{2+} were prepared by diluting the appropriate quantities of standard 10^3 mg L^{-1} Ni^{2+} and Hg^{2+} solutions (Sigma-Aldrich). Dimethylglyoxime (2,3-Butanedione dioxime, $C_4H_8N_2O_2$), Nioxime (1,2-Cycloheanedione, $C_6H_{10}N_2O_2$) and Morin hydrate (2,3,4,5,7-Pentahydroxyflavone, $C_{15}H_{12}O_8$), purchased form Sigma-Aldrich was dissolved in Ethanol, absolute 99.8 % (CH_3CH_2OH) to the desired concentration to prepare stock solutions and used as is without further modification. All stock solutions used in the study were prepared fresh once per week. All chemicals purchased were used as received without further treatment or modification unless stated otherwise. Graphene oxide and graphene samples were prepared as described in *Chapter 4*. Whatman No. 1 chromatography paper (200.0 mm × 200.0 mm, pure cellulose paper, GE Healthcare) was purchased from Sigma Aldrich.

7.2.2. Pre-stored Paper-based Electrochemical Cell (PPEC) Preparation

Paper-based electrochemical cells (PECs) were prepared by cutting 8 mm diameter disks (circles) out of Whatman filter paper No.1. Two successive additions of 10 µL portions of prepared solutions, containing the desired reagent concentrations (typically; 2 mM DMG and 10 mg L^{-1} Hg) in 0.1 M NH_3/NH_4Cl buffer (pH 9.4) were dropped onto the paper sheets and allowed to dry at room temperature (23 ^oC) for 30 min. Drop-casting of pre-prepared reagent samples provided superior sensitivity over successive additions of separate samples. Prior to analysis the prepared

pre-stored paper-based electrochemical cells (PPECs) were placed on the surface of commercially bought screen printed carbon electrodes (SPCE) so as to cover the entire three-electrode system.

7.2.3. Graphene-derivative Infused Paper-based Electrochemical Cell (PEC) Preparation

Prior to reagent storage, graphene oxide (GO) infused PECs were fabricated by drop-casting 20 µL aliquots of 0.5 mg mL^{-1} GO, dispersed in water following 1 hr ultrasonication onto the unmodified PEC. The GO infused PEC was allowed to dry at room temperature for 30 min to allow evaporation of solvent. Electrochemically reduced graphene oxide (ERGO) PECs were prepared by electrochemical reduction between - 1.4 and 0.3 V by cyclic voltammetry in 0.1 M acetate buffer solution (pH 4.6).

0.25 wt.% Nafion-graphene nanocomposites were prepared by mixing 0.2 % Nafion solution with appropriate amounts of graphene powder followed by ultrasonication for 1 h. 20 µL aliquots of the resultant solution was drop-cast onto the unmodified PEC and allowed to dry at room temperature.

7.2.4. Square-wave Adsorptive Cathodic Stripping Voltammetric Detection of Ni

A 20 µL aliquot of desired metal analyte concentration, prepared in supporting electrolyte was added to the PPEC prior to analysis. 20 µL was the desired sample volume to prevent floating of the PPEC and still allow for excellent contact with the working electrode. The sample, in aqueous media, through wicking wets the PPEC and allows for dissolution of the dried, stored reagents. Stripping voltammetry was performed by *in-situ* accumulation and deposition of formed $[Ni(dmgH)_2]$ complex onto an electroplated Hg film. Stripping voltammetric measurements were performed by square-wave adsorptive cathodic stripping voltammetry (SW-AdCSV) between - 0.7 and - 1.4 V, unless stated otherwise. A fixed accumulation potential of - 0.7 V was employed for 90 s during analysis, followed by a 10 s equilibration time. Square-wave instrumental parameters of 35 mV amplitude, 20 Hz frequency and 5 mV potential step was employed for all analysis.

7.3. Results and Discussion:

7.3.1. Water sorption in the porous PEC

Figure 7.1, shows an HRSEM image of the unmodified PEC at 100 X magnification. The porous nature of the chromatography paper within the entangled cellulose fiber structure is further observed. Slight artifacts are further seen between pores, which may arise from the carbon coating process required for conductive imaging in HRSEM analysis. These are attractive features in our application as it allows liquid to penetrate within the hydrophilic fiber matrix without need for an external pump source [5]. The fluid flow in the porous media is crucial in its ability to be used as electrochemical cell and also in dry reagent storage techniques. An understanding of the permeation mechanism is therefore required for a complete discussion on its use in µPECs. Fluid penetration in the PEC is governed by capillary-driven flow via simple wicking processes. While Young-Laplace equation (*Equation 7.1*) and Darcy's law (*Equation 7.2*) define the capillary pressure driving fluid flow through pores and laminar flow of fluids respectively, the Lucas-Washburn equation, shown in *Equation 7.3*, provides a more complete definition of fluid permeation in paper substrates at negligible polymer swelling. Further modifications of the Washburn equation have been developed to model swelling in the porous structure.

$$\Delta P = \frac{2 \cdot \gamma \cdot cos\theta}{R} \qquad Equation\ 7.1$$

$$\frac{Q}{A} = \upsilon = \frac{K \cdot \Delta P}{\mu \cdot L} \qquad Equation\ 7.2$$

$$TLV = \varepsilon \sqrt{\frac{R \cdot \gamma \cdot cos\theta \cdot t}{2 \cdot \mu}} \qquad Equation\ 7.3$$

Where, TLV is the total liquid volume absorbed per unit area, ε is the void fraction, R is pore radius, γ is fluid surface tension, θ is the contact angle established between the liquid and the inner wall of the pore, t is penetrating time and µ is fluid viscosity.

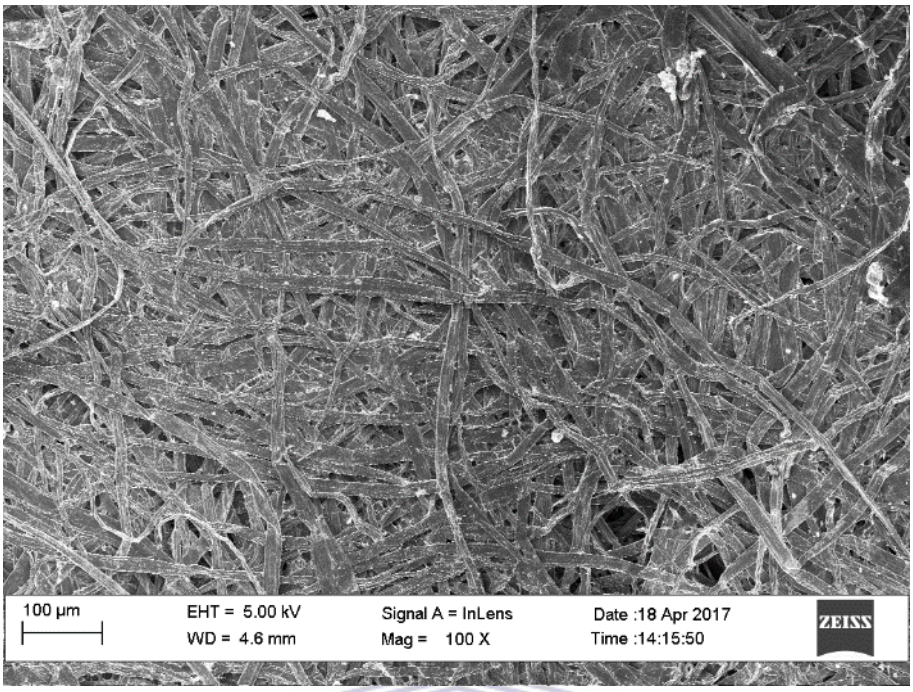

Figure 7.1: HRSEM image of the entangled cellulose fiber structure of unmodified PEC at 100 X magnification.

7.3.2. Characteristic quantitative detection of Ni(II)

The adsorptive cathodic stripping voltammetric reduction of Ni^{2+} occurs via a three-step process: (1) complex formation, (2) accumulation and (3) electrochemical stripping and reduction in basic electrolyte solutions. Adsorption of a formed $[Ni(dmgH)_2]$ complex onto an electroplated Hg film is required for pre-concentration/accumulation of metal species at the electrode surface. The subsequent reduction involves a 10 electron transfer reduction process of Ni(II) metal cation from the $[Ni(dmgH)_2]$ complex to Ni^0 along with the reduction of the DMG ligand to 2,3-bishydroxylaminebutane (DHAB). The overall reduction is summarized in *Equation 7.4,7.5 and 7.6* below, according to the work described by Baxter *et al.* [6].

$$Ni(II) + 2dmgH_2 \rightarrow [Ni(II)(dmgH)_2] + 2H^+ \qquad Equation\ 7.4$$

$$[Ni(II)(dmgH)_2] + Hg \rightarrow [Ni(II)(dmgH)_2]_{ads}Hg \qquad Equation\ 7.5$$

$$[Ni(II)(dmgH)_2]_{ads}Hg + 10e^- + 10H^+ \rightarrow Ni(Hg) + 2DHAB \qquad Equation\ 7.6$$

A typical square-wave voltammogram for Ni^{2+} detection at a bare screen printed carbon electrode (SPCE) in the presence of a DMG ligand and electroplated Hg film in a bulk solution of 0.1 M NH_3/NH_4Cl buffer (pH 9.4) as supporting electrolyte is shown in *Figure 7.2*. A single, well-resolved stripping peak is observed at – 1.032 V is observed. This is attributed to the characteristic cathodic two-electron electrochemical reduction of Ni^{2+} to Ni^0. Similar reduction potentials are observed in literature and *Chapters 5 and 6* respectively. An increase in background current is seen with progressive scanning to increasingly negative potentials (- 0.7 to – 1.3 V).

Figure 7.3 further demonstrates the dependence of the cathodic stripping peak current on the Ni^{2+} concentration between 0 and 20 μg L^{-1}. An increase in stripping peak current as well as a slight shift to more negative potentials (- 1.0 to - 1.05 V), is observed with increasing metal analyte concentration. This shift demonstrates the incomplete removal of material from the electrode surface between consecutive runs without an adequate cleaning step. The results obtained confirm the use of Nickel-dimethylglyoxime complexes as accurate method for detection of Ni^{2+} in water samples.

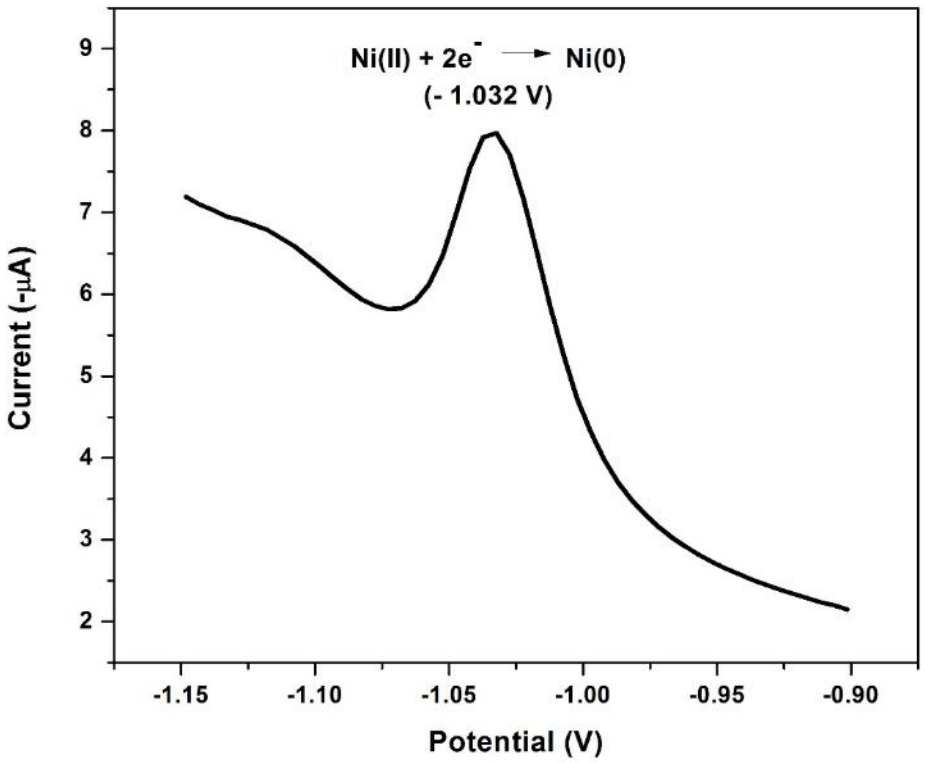

Figure 7.2: Square wave adsorptive cathodic stripping voltammogram (SWAdCSV) of 50 μg L^{-1} Ni^{2+} in 0.1 M NH_3/NH_4Cl buffer (pH 9.4) as supporting electrolyte containing 2 mM DMG and 10 mg L^{-1} Hg at a SPCE. SWV parameters: E_{acc} = - 0.7 V, t_{acc} = 90 s, amplitude = 35 mV and f = 20 Hz.

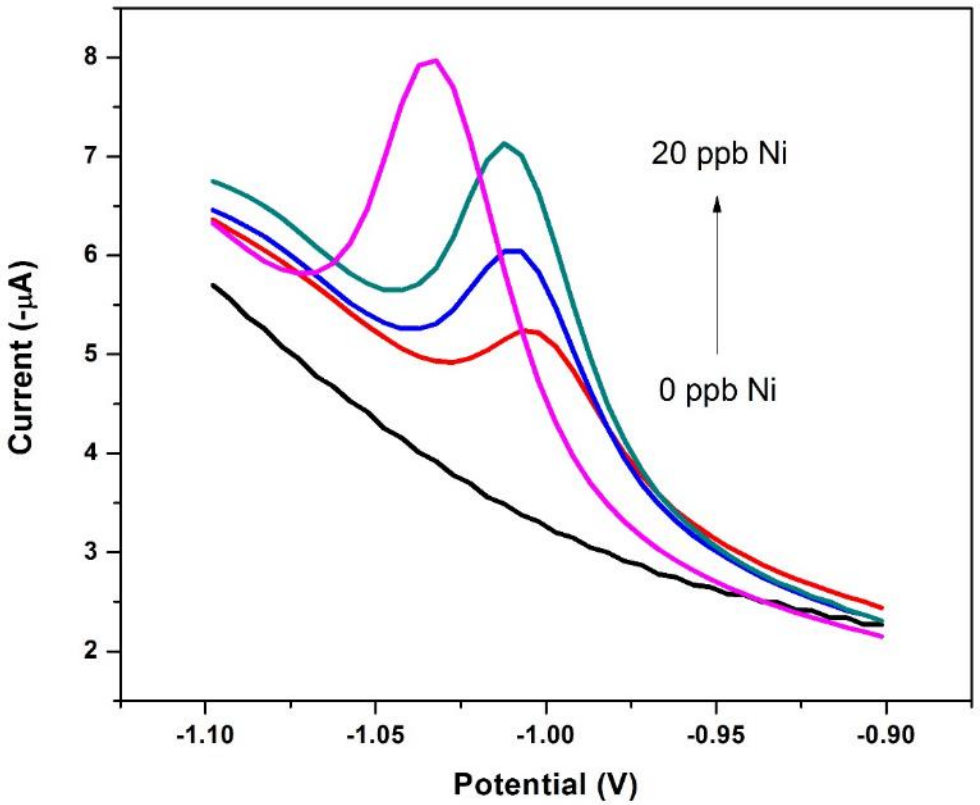

Figure 7.3: Square wave adsorptive cathodic stripping voltammograms (SWAdCSVs) of (a) 0.0 µg L^{-1} Ni^{2+}, (b) 5.0 µg L^{-1} Ni(II), (c) 15 µg L^{-1} Ni^{2+} and (d) 20 µg L^{-1} Ni(II) at screen printed carbon electrodes in 0.1 M NH_3/NH_4Cl buffer (pH 9.4) as supporting electrolyte containing 2 mM DMG and 10 mg L^{-1} Hg. SWV parameters: E_{acc} = - 0.7 V, t_{acc} = 90 s, amplitude = 35 mV and f = 20 Hz.

7.3.3. Macro- vs. Micro-liter detection of Ni(II)

The reported AdCSV technique demonstrated in literature has shown to offer a simple, sensitive analytical technique for the detection of Ni(II) in water samples. Large volumes of sample required for accurate detection make it a disadvantageous method for on-site analysis of real samples. The feasibility of the fabricated PECs was investigated by comparing its electrochemical detection in both bulk and microliter sample volumes. *Figure 7.4* shows the comparative SWAdCSVs of SPCEs (a) immersed in bulk solution, (b) with 100 µL droplet dropped directly

onto the three-electrode system and (c) with 20 µL sample volume dropped onto PEC covering the three-electrode area. Bulk solution analysis of a square-wave cathodic sweep in 0.1 M NH_3/NH_4Cl buffer (pH 9.4), shows three separate distinct peaks: A large, well-defined peak due at – 1.032 V and a significantly smaller peak at - 1.13 V due to the reduction of Ni(II) from the $[Ni(dmgH)_2]$ complex and a broad peak at more negative potentials (– 1.23 V) arising from reduction of dissolved oxygen. The main reduction peak is influenced by the migration and transport of excess metal ions to the electrode surface through stirring during the accumulation/pre-concentration step. Replacing bulk electrolyte solution with microliter volumes of metal analyte samples was investigated and recorded in *Figure 7.4*. 100 µL of Ni^{2+} sample provided the perfect volume for accurate wetting and spreading of the sample droplet across the three electrode system. Two well-resolved reduction peaks at – 1.09 V and – 1.18 V are observed. The calculated peak currents at 100 µL sample volumes (droplet) were significantly smaller than those observed in bulk metal samples. This is attributed to the fixed amount of metal cations available in the microliter sample volume during electrode preconcentration. The exact nature of the second reduction peak is not yet known and requires further testing. Utilizing the excellent sorption properties of the filter paper used in the fabrication of the PECs, microliter sample volumes were significantly reduced when using PECs in conjunction with the SPCE, as discussed in the introduction. 20 µL volumes of sample was found to be the maximum allowed volume to allow for good contact on the electrode surface so as to prevent floating of the PEC in the sample droplet. The porous structure of the PECs act as a three-dimensional scaffolding which holds low volume of samples. PECs were found to only exhibit a single cathodic reduction peak (- 1.18 V) due to the reduction of Ni^{2+} according to *Equation 7.6* in *Section 7.3.2* above. The position of the Ni(II) reduction is found at the second reduction peak position in larger sample volumes. This more negative reduction potential could be indicative of increasing difficulty to reduce metal cations due to lower sample volume. The results highlight the use of PECs to utilize low microliter volumes of sample while still offering good detection.

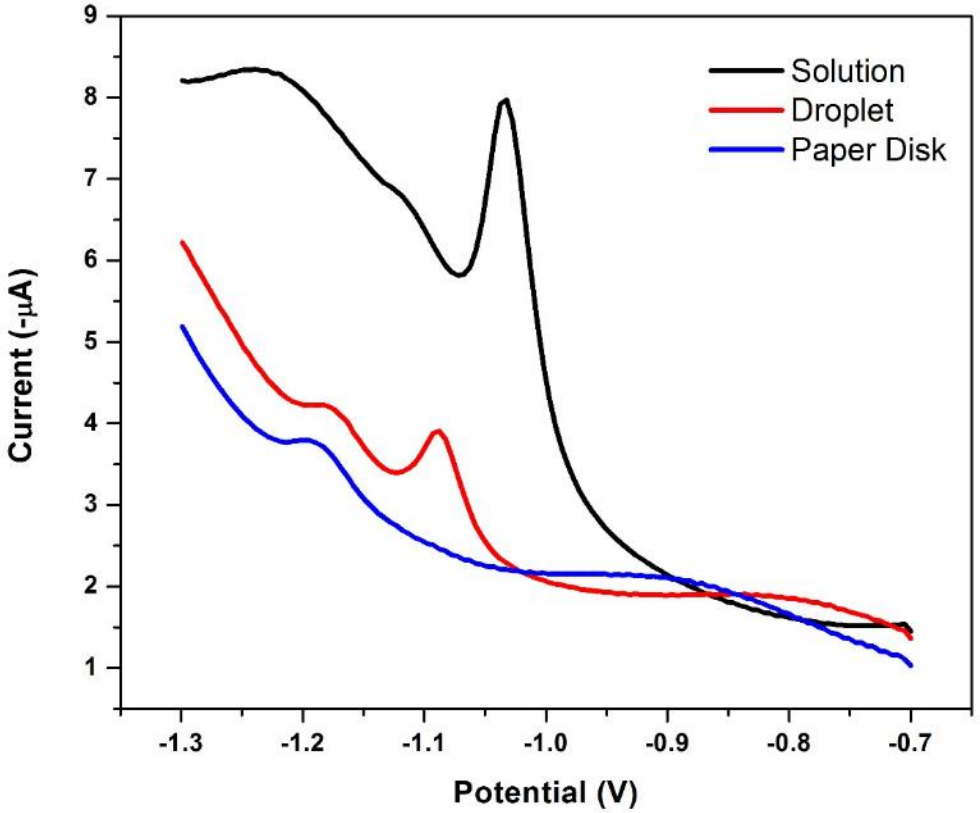

Figure 7.4: Square wave adsorptive cathodic stripping voltammograms (SWAdCSVs) of 50 µg L^{-1} Ni^{2+} at (a) SPCE immersed in 10 mL of 50 µg L^{-1} Ni^{2+} [Solution], (b) SPCE with 100 µL sample of 50 µg L^{-1} Ni^{2+} dropped directly onto the three electrode system [droplet] and (c) SPCE with PEC covering the three electrode system. 20 µL solution of 50 µg L^{-1} Ni^{2+} [paper disk]. 0.1 M NH_3/NH_4Cl buffer as supporting electrolyte containing 2 mM DMG and 10 mg L^{-1} Hg was used. SWV parameters: E_{acc} = - 0.7 V, t_{acc} = 90 s, amplitude = 35 mV and f = 20 Hz.

7.3.4. Development of pre-stored paper-based electrochemical cells (PPECs)

Reagent storage is crucial in developing effective POCs. The excellent sorption properties of the cellulose fiber structure make paper-based electrochemical cells (PECs) capable of not only acting as 3-D electrochemical cells to significantly reduce sample volume (*Section 7.3.3.*), but also allow for sorption of reagents prior to analysis. The dry reagent storage method was investigated in fabricating PPECs. Typically, 20 µL samples containing appropriate quantities of reagents in

preferred buffer solutions were drop cast onto PECs and allowed to dry at room temperature for 30 min. The reagents are absorbed within the porous cellulose structure. Prior to analysis, a definite volume of liquid analyte was dropped onto the PPEC, allowing for dissolution of the stored reagents in aqueous media.

Comparative voltammograms (*Figure 7.5*) of paper-based electrochemical cells on a three-electrode SPCE with (a) 20 µL of 50 µg L^{-1} Ni^{2+} solution containing 10 mg L^{-1} Hg and 2 mM DMG in 0.1 M NH_3/NH_4Cl buffer (pH 9.4) and (b) 20 µL of 50 µg L^{-1} Ni^{2+} solution. The PEC was previously impregnated or sorbed with 20 µL of solution containing 10 mg L^{-1} Hg and 2 mM DMG in 0.1 M NH_3/NH_4Cl buffer (pH 9.4). The square-wave voltammogram of paper-based electrochemical cells (PECs) in conjunction with SPCEs and samples containing reagents and target metal ions demonstrate a single, symmetrical reduction peak at – 1.20 V. Pre-mixing of analyte ions and reagents in suitable solvents prior to analysis resulted in improved sensitivities of the PEC. While offering accurate and sensitive detection, pre-mixing and pre-treatment of samples is tedious and time consuming. Similarly, a single stripping peak (- 1.198 V), attributed to the cathodic reduction of Ni^{2+} is observed for the PPECs with sorbed reagents (electrolyte, DMG and Hg). A steady increase in the background current at more negative potentials can be seen due to increased charge build-up at the electrode surface resulting in asymmetry due to the irreversible nature of the $[Ni(dmgH)_2]$ reduction reaction [7]. Comparison of the stripping reduction peaks of the un-stored and pre-stored PECs indicate similar peak heights (1.75 vs 1.51 µA respectively) for both PEC derivatives with minimum shifts in peak potential (± 2 mV). This result is in agreement with the chapter hypothesis and shows the applicability of PPECs towards the detection of metal analyte by AdCSV.

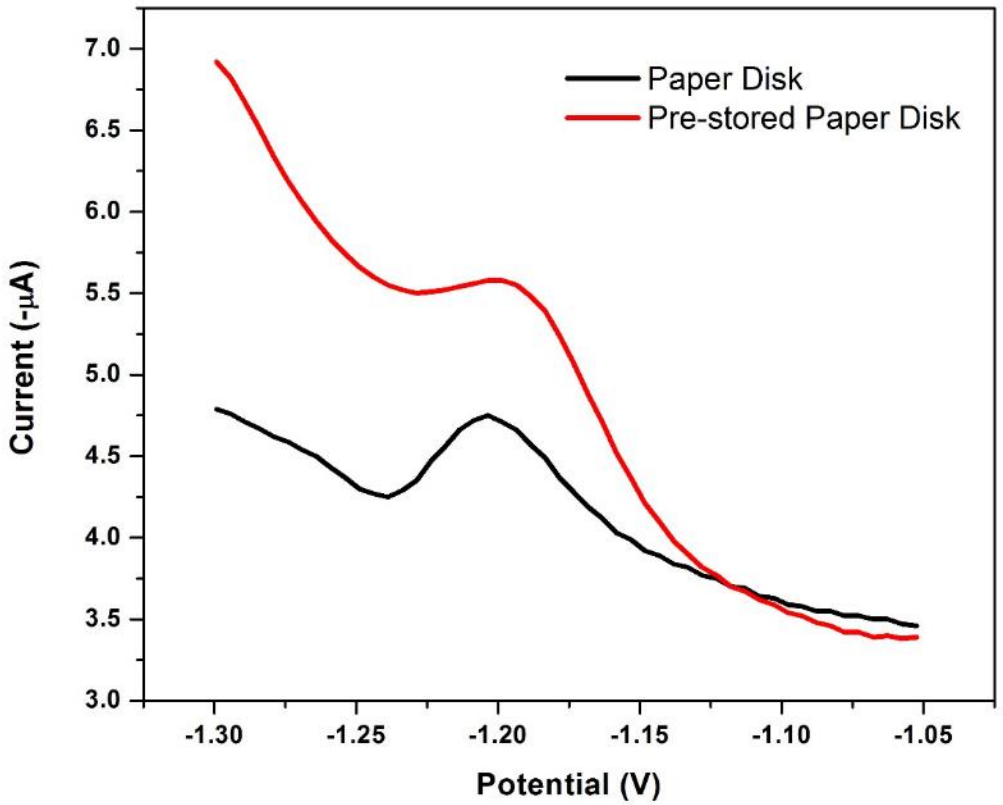

Figure 7.5: Square wave adsorptive cathodic stripping voltammograms (SWAdCSVs) of 50 µg L^{-1} Ni^{2+} at: (a) SPCE with PEC covering the three electrode system. A 20 µL solution comprised of 0.1 M NH_3/NH_4Cl buffer as supporting electrolyte containing 2 mM DMG and 10 mg L^{-1} Hg was used and (b) SPCE with PEC pre-stored with a 20 µL solution containing 2 mM DMG and 10 mg L^{-1} Hg in 0.1 M NH_3/NH_4Cl buffer as supporting electrolyte. SWV parameters: E_{acc} = -0.7 V, t_{acc} = 90 s, amplitude = 35 mV and f = 20 Hz.

Figure 7.6 and 7.7 show the recorded preliminary voltammograms and resulting calibration plots of the un-stored and pre-stored PECs. Nickel concentration between 0 and 60 µg L^{-1} Ni^{2+} concentrations were investigated for initial testing by SWAdCSV. Well-developed signals were recorded at low and high concentrations. A linear dependence of stripping peak current with increasing metal cation concentration for both stored and un-stored PECs are observed with no significant shift in reduction potential. Good regression of calibration plots associated with the

stored and un-stored PECs are shown in the low concentration ranges under analysis. The possibility towards quantitative analysis of the PPEC is demonstrated.

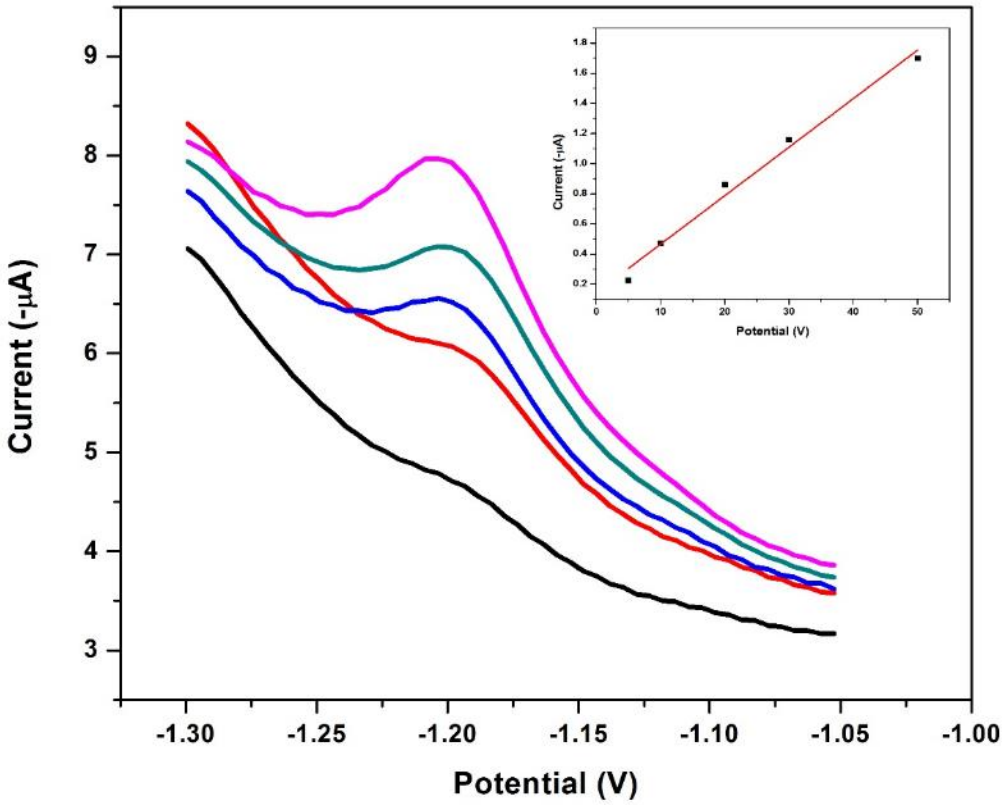

Figure 7.6: Square wave adsorptive cathodic stripping voltammograms (SWAdCSVs) of 5 - 60 µg L^{-1} Ni^{2+} at a SPCE with PEC covering the three electrode system. A 20 µL solution comprised of metal analyte in 0.1 M NH_3/NH_4Cl buffer as supporting electrolyte containing 2 mM DMG and 10 mg L^{-1} Hg. SWV parameters: E_{acc} = - 0.7 V, t_{acc} = 90 s, amplitude = 35 mV and f = 20 Hz.

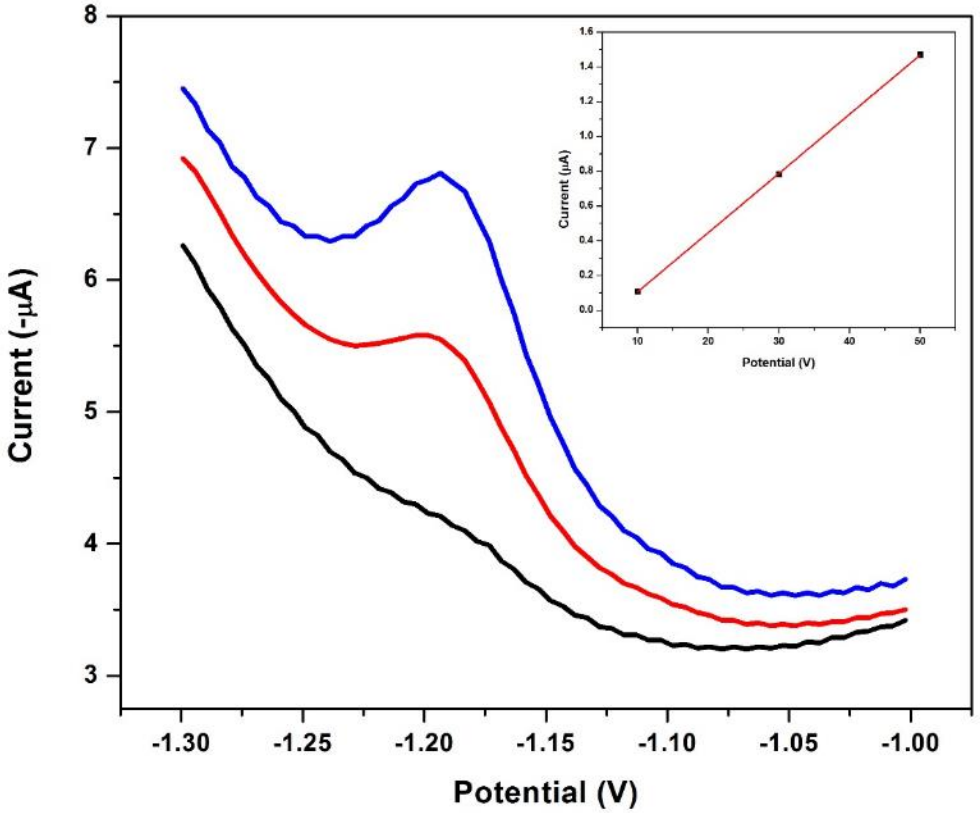

Figure 7.7: Square wave adsorptive cathodic stripping voltammograms (SWAdCSVs) of 10 - 60 µg L^{-1} Ni^{2+} at SPCE with PEC pre-stored with a 20 µL solution containing 2 mM DMG and 10 mg L^{-1} Hg in 0.1 M NH_3/NH_4Cl buffer as supporting electrolyte. SWV parameters: E_{acc} = - 0.7 V, t_{acc} = 90 s, amplitude = 35 mV and f = 20 Hz.

7.3.5. Effect of Reagent Storage on the Electrochemical Detection at PPECs

Reagent storage in PPECs is largely responsible for the simple sample introduction without a need for sample pre-treatment prior to analysis. Interrogation of a variety reagents; namely (a) NH_3/NH_4Cl buffer as supporting electrolyte, (b) Hg films for adsorption of target species in NH_3/NH_4Cl buffer, (c) DMG as chelating agent in NH_3/NH_4Cl buffer and (d) DMG and Hg in NH_3/NH_4Cl buffer on the stripping reduction peak of Ni^{2+} was performed and recorded in *Figure 7.8.* The square-wave voltammogram of the PPEC, pre-stored with only electrolyte, indicates the absence of any stripping peaks due to the reduction of Ni^{2+}. Pre-concentration of the electrode

surface with Ni^{2+} metallic cations was not possible by simple adsorption and the deposition/accumulation potentials were unsuitable for Ni^{2+} reduction and electrode pre-concentration. The low solubility of Ni^{2+} within an electroplated Hg film, reported in literature is evident upon sorption of the PEC with Hg cations prior to analysis. Extremely low sensitivity of the PEC towards Ni^{2+} detection is shown by an extremely small reduction peak for Ni^{2+} conversion to Ni^{0} at – 1.18 V. This supports literature findings of the AdCSV technique at a variety of carbon-based electrode substrates. Dry storage of the DMG ligand and 0.1 M NH_3/NH_4Cl buffer within the cellulose fiber structure produces a well-defined reduction peak at – 1.14 V upon dissolution in an aqueous solution containing 50 μg L^{-1} Ni^{2+}. Pre-concentration of the electrode surface results from $[Ni(dmgH)_2]$ complex formation within the PPEC by adsorption according to *Equation 1*. Ease of reduction is demonstrated over the Hg-PPEC by a 40 mV peak shift to a more positive reduction potential. A slight enhancement in stripping peak current is seen upon the impregnation of DMG along with Hg and a suitable electrolyte solution. Pre-storage of chelating agent and metallic film in suitable electrolyte solution shows accurate and sensitive detection of Ni^{2+} cations and confirms the incorporation of the hypothesized reagents within the PEC devices. Here, $[Ni(dmgH)_2]$ complexes adsorb onto the present Hg ions improving electrode sensitivity.

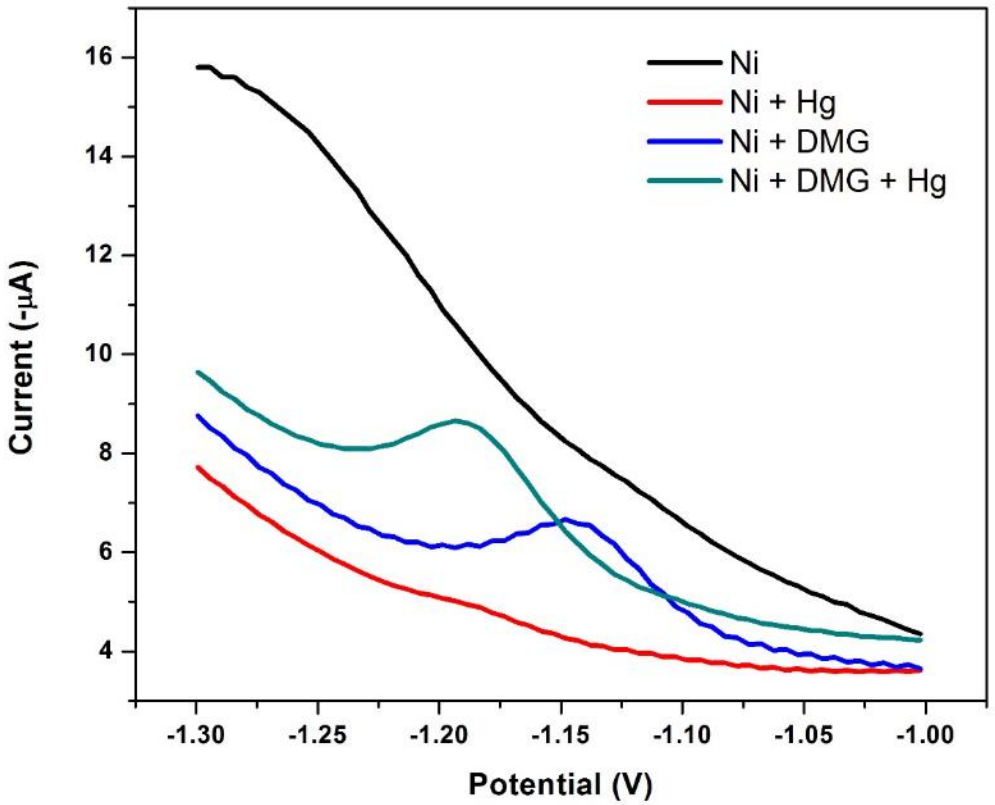

Figure 7.8: Square wave adsorptive cathodic stripping voltammograms (SWAdCSVs) of 20 µL sample of 50 µg L^{-1} Ni^{2+} at (a) SPCE with PEC pre-stored with ammonia buffer, (b) SPCE with PEC pre-stored with a 20 µL solution containing 10 mg L^{-1} Hg, (c) SPCE with PEC pre-stored with a 20 µL solution containing 2 mM DMG and (d) SPCE with PEC pre-stored with a 20 µL solution containing 2 mM DMG and 10 mg L^{-1} Hg. 0.1 M NH_3/NH_4Cl buffer was used as supporting electrolyte. SWV parameters: E_{acc} = - 0.7 V, t_{acc} = 90 s, amplitude = 35 mV and f = 20 Hz.

7.3.6. Influence of dimethylglyoxime (DMG) ligand concentration and storage

The presence of dimethylglyoxime within the PPEC is crucial towards the detection of Ni^{2+}, resulting in metal-ligand complex formation and electrode preconcentration by adsorption. The dependence of $[Ni(dmgH)_2]$ stripping peak current as a function of complexing agent concentration was investigated between 0 and 5 mM DMG-ligand concentrations (*Figure 7.9*).

This was achieved by drop casting fixed microliter volumes of sample containing the appropriate DMG-ligand concentrations onto developed PECs. The DMG ligand fills the pores in the cellulose structure by sorption methods creating a 3-D electrochemical cell in which metal-complex formation is possible. A constant, linear dependence and increase in stripping peak current is observed with increasing DMG concentration in the range under investigation. A further increase to 0.1 M, DMG concentration (not shown here), results in saturation of the electrode surface with non-conductive DMG ligands. Electron transfer kinetics through the adsorbed ligand-species is significantly hindered and stripping peak currents are adversely affected. A 2 mM DMG concentration was selected for all further experiments to lower reagent storage concentrations, providing a more environmentally friendly device.

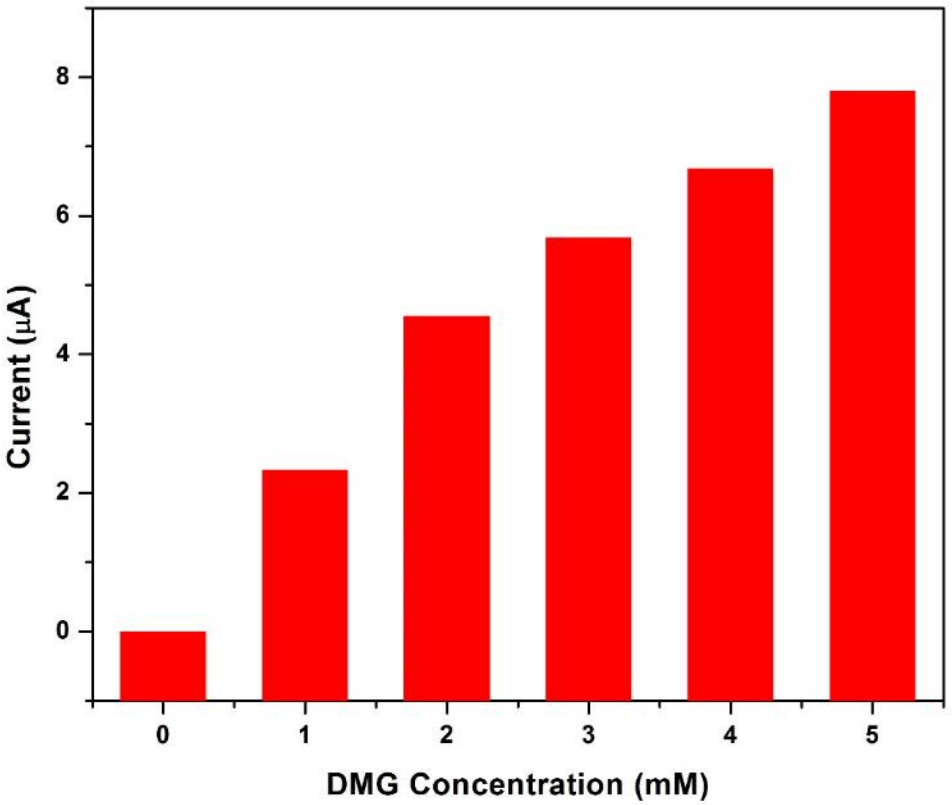

Figure 7.9: Dependence of the square wave stripping peak current of 50 μg L^{-1} Ni^{2+} reduction from the $[Ni(dmgH)_2]$ complex on the pre-stored PEC dimethylglyoxime concentration (mM) between 0 - 5 mM. Supporting electrolyte: 0.1 M NH_3/NH_4Cl buffer as supporting electrolyte.

7.3.7. Effect of Hg concentration on Ni^{2+} stripping peak current

It follows, from *Section 7.3.5,* a dependance of the $[Ni(dmgH)_2]$ stripping peak current on the Hg ion concentration in the fabricated PPEC exists. As such, optimal Hg concentrations for pre-strorage were investigated. *Figure 7.10* shows the effect of Hg concentration on the recorded stripping peak currents of Ni^{2+} reduction. An increase in peak currents up to 10 mg L^{-1} was observed. At concentrations greater than 10 mg L^{-1} electrode saturation occurs and a steady decrease in peak currents are recorded. Relatively low changes in stripping peak currents with increasing Hg concentrations show a weak dependance of the stripping peak currents on Hg ion

concentration. As a result Hg storage loosely affects the AdCSV reduction of [Ni(dmgH)$_2$]. Consequently, 10 mg L^{-1} Hg ion concentraion was selected for further analysis.

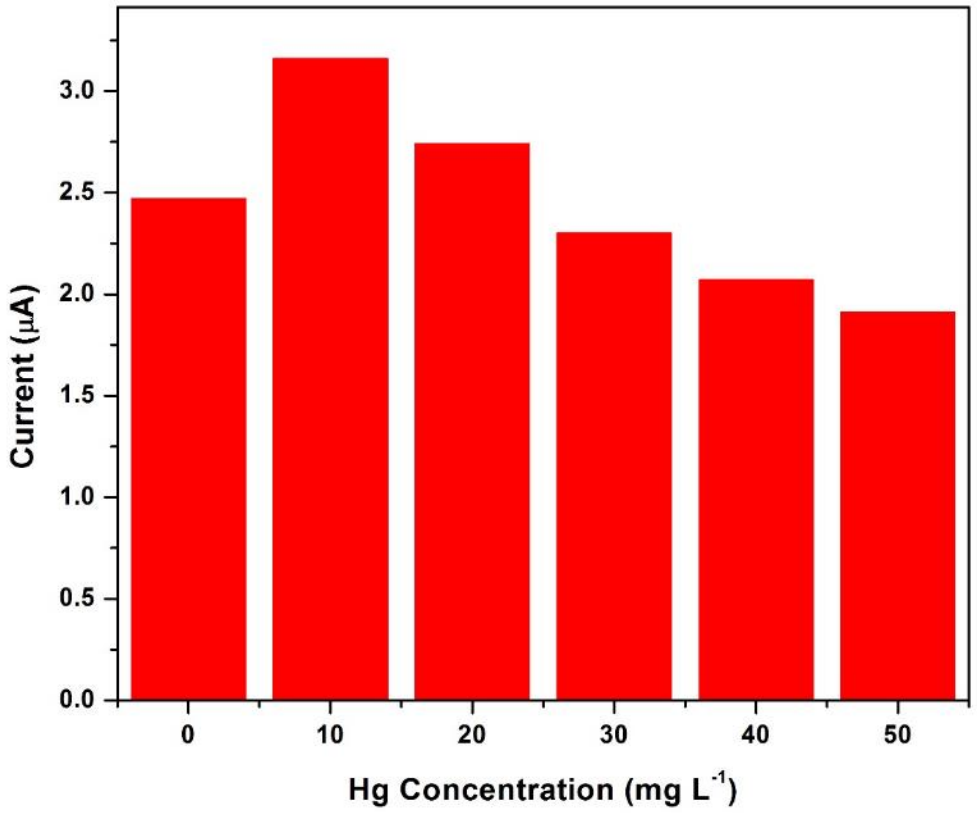

Figure 7.10: Effect of Hg concentration (mg L^{-1}) on the adsorptive cathodic stripping peak current of Ni^{2+} detection in 0.1 M NH_3/NH_4Cl buffer as supporting electrolyte.

7.3.8. Instrumental parameter optimization

Square-wave wave forms were selected for analysis of the pre-stored paper-based electrochemical cells (PPEC) over other commonly used wave-forms including; linear sweep voltammetry (LSV), differential pulse voltammetry (DPV) and cyclic voltammetry (CV) due to its high sensitivity towards metal characterization. Optimization of the instrumental parameters associated with the square-wave wave form was performed and recorded in *Figure 7.11*.

The effect of varying accumulation potentials in the range from 0.0 to – 1.0 V was performed in a basic solution containing 30 µg L^{-1} Ni(II) cations, 2 mM DMG and 10 mg L^{-1} Hg (*Figure 7.11 (a)*). The peak current associated with the reduction of $[Ni(dmgH)_2]$ showed an increase in peak sensitivity and up to E_{acc} = -0.75 V. At accumulation potentials more negative than – 0.75 V, the efficiency of Ni^{2+} preconcentration significantly declined. The observed phenomena indicated a distinct dependence of accumulation potential on stripping peak currents. An E_{acc} = - 0.75 V indicated the most effective accumulation potential towards detection of $[Ni(dmgH)_2]$ and was selected for future experiments.

Figure 7.11, (b) demonstrates the dependence of $[Ni(dmgH)_2]$ stripping peak current on the applied accumulation time. Accumulation times were investigated from 0 to 300 s. Pre-concentration of the electrode surface results in improved sensitivities. Prolonged accumulation times up to 120 s in 0.1 M NH_3/NH_4Cl buffer resulted in an increase in peak currents. Saturation of the electrode surface due to adsorption of $[Ni(dmgH)_2]$ occurred for voltammograms run between 150 and 300 s as seen by constant stripping peaks. An accumulation time of 120 s was chosen for further analysis.

The analysis of stripping peak currents recorded with instrumental parameters such as amplitude ranging between 5 – 50 mV is described in *Figure 7.11, (c)*. A constant increase in stripping reduction peak heights is shown between 5 and 35 mV, before a significant decrease at 50 mV. An amplitude of 35 mV provided the optimum conditions for Ni^{2+} detection by AdCSV.

Frequency changes between 5 and 65 Hz were investigated as means to improve the stripping peak current associated with $[Ni(dmgH)_2]$ reduction. The obtained results are summarized in *Figure 7.11, (d)*. Low frequency (5 – 20 Hz) changes showed the best electrode sensitivity. Increasing the frequency above 20 Hz indicated a decrease in $[Ni(dmgH)_2]$ stripping. A frequency of 20 Hz was selected for all further testing.

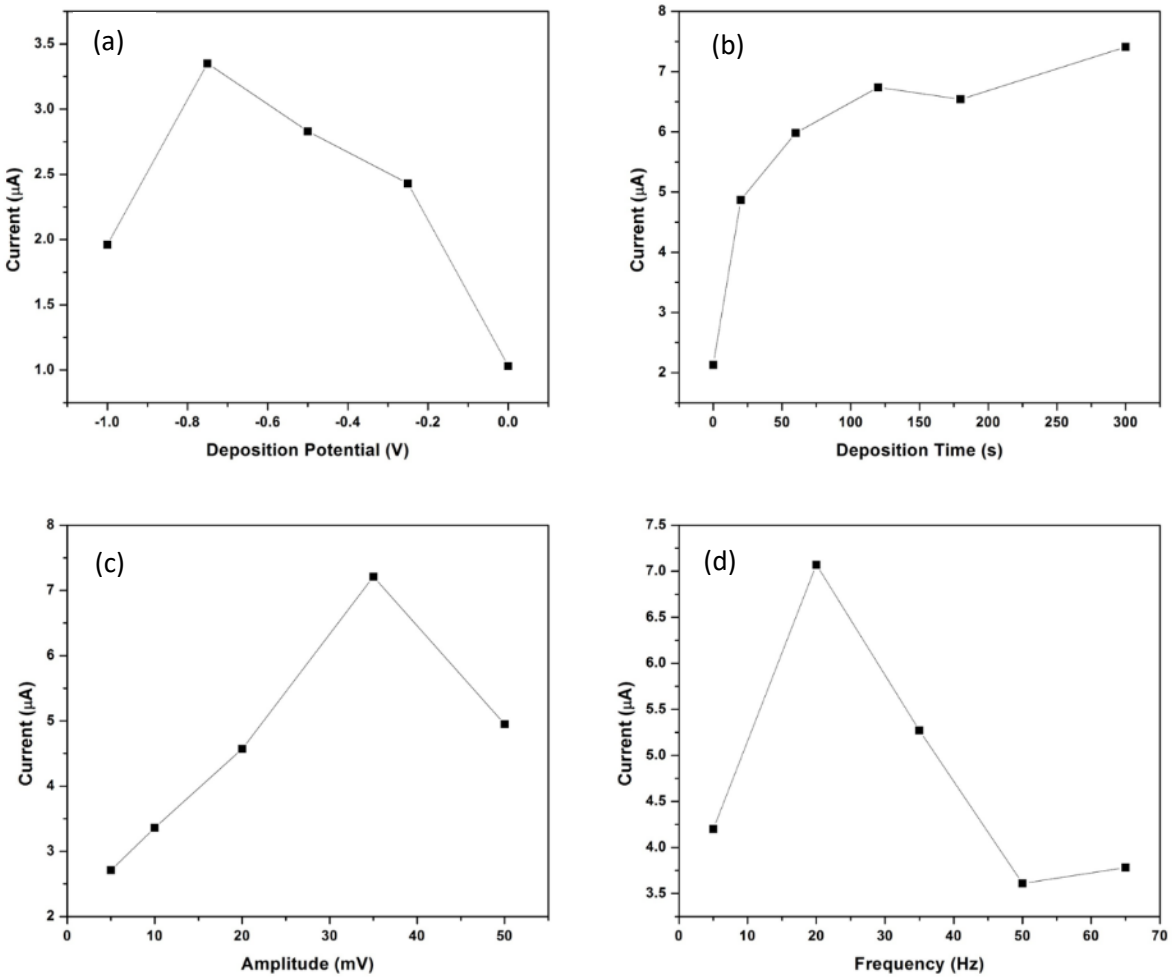

Figure 7.11: The influence of (a) accumulation potential (E_{acc}), (b) accumulation time (t_{acc}), (c) amplitude and (d) frequency on Ni^{2+} peak currents. Sample composition: 30 μg L^{-1} Ni, 2 mM DMG, 10 mg L^{-1} Hg(II), 0.1 M NH_3/NH_4Cl buffer.

7.3.9. PPEC reproducibility and stability

Stability and reproducibility of the developed PPECs towards $[Ni(dmgH)_2]$ detection was performed at SPCEs in conjunction with pre-stored PECs for 30 μg L^{-1} Ni^{2+} concentrations. Square-wave voltammograms, recorded on four identically fabricated PPECs on a single SPCE is illustrated in *Figure 7.12*. Single, well-defined and reproducible peaks were recorded at an average reduction potential of – 1.16 V with little deviation for $[Ni(dmgH)_2]$ reduction. An average stripping peak current of $3.93 \times 10^{-6} \pm 1.71 \times 10^{-7}$ A was reported for the four replications (n = 4).

A relative standard deviation (RSD %) of 4.36 % was calculated. The low calculated percentage error demonstrates excellent reproducibility in the fabrication of the PPEC system. Regeneration of the SPCE surface is observed without any further electrochemical cleaning steps.

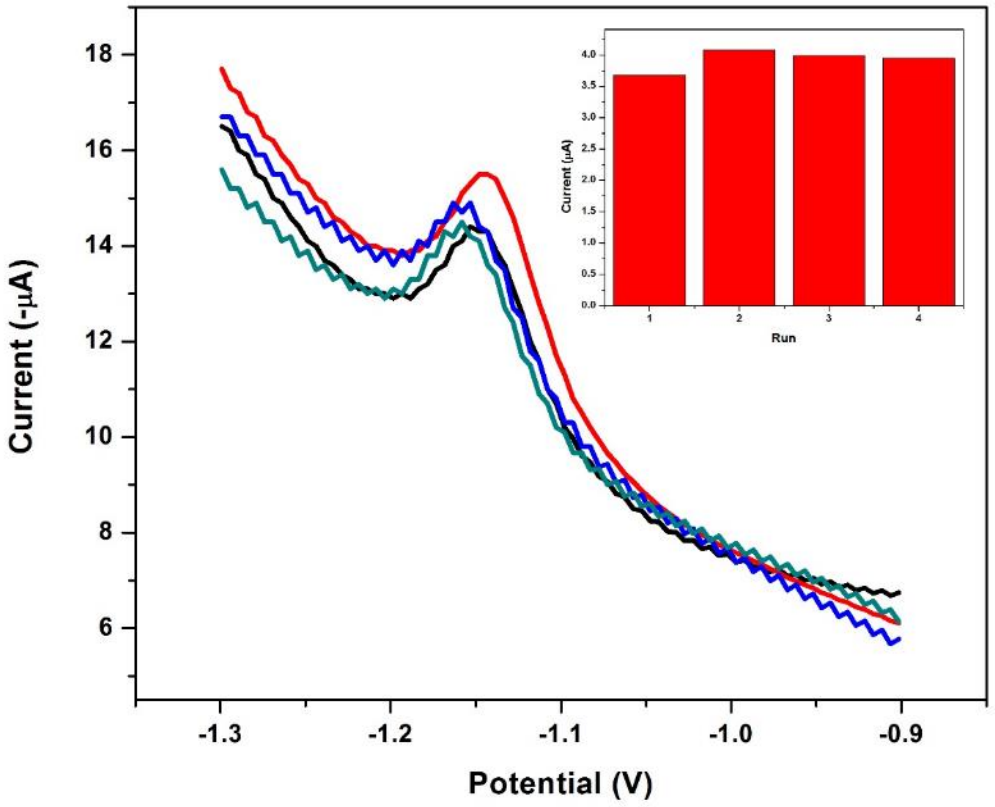

Figure 7.12: Four consecutive square-wave voltammograms (SWV) obtained from PPEC in conjunction with SPCE in solution containing 30 µg L^{-1} Ni, 2 mM DMG, 10 mg L^{-1} Hg^{2+}, 0.1 M NH_3/NH_4Cl buffer, indicating the reproducibility of the PPECs. Inset: Ni^{2+} peak currents vs. consecutive runs. SWV parameters: E_{acc} = - 0.7 V, t_{acc} = 90 s, amplitude = 35 mV and f = 20 Hz (n = 4).

7.3.10. Interference Studies of the PPECs

Accurate quantitative analysis is pivotal in the fabrication of POC devices for real sample analysis. Understanding the effects of common interferents present in tap water samples on the

stripping peak current obtained for $[Ni(dmgH)_2]$ complex detection is vital in the development of the PPECs. Commonly found metallic cations such as Zn^{2+}, Cd^{2+}, Pb^{2+}, Co^{2+} and In^{2+}, present in tap water samples and with redox potentials found in the potential window under investigation were interrogated as possible metallic interferents (*Figure 7.13*). Under optimized conditions, the effects of the metallic cations on the stripping reduction of 30 µg L^{-1} $[Ni(dmgH)_2]$ were investigated by SWV. The recorded SW-AdCSV of (a) 20 µL 100 µg L^{-1} Zn^{2+}, Cd^{2+}, Pb^{2+}, Co^{2+} and In^{2+} and (b) repeated runs of 20 µL 30 µg L^{-1} Ni^{2+} in the presence of 100 µg L^{-1} Zn^{2+}, Cd^{2+}, Pb^{2+}, Co^{2+} and In^{2+} are shown in *Figure 7.13, (a)*. The voltammograms show no distinct stripping reduction peaks for Zn^{2+}, Cd^{2+}, Pb^{2+}, Co^{2+} and In^{2+} up to 100 µg L^{-1} between - 0.7 V and - 1.4 V, E_{acc} = - 0.7 V, t_{acc} = 90 s. The stripping peak currents recorded for six replications of Ni^{2+} in the presence of metallic cations are demonstrated in *Figure 7.13, (b)*. The relative standard deviation (RSD %) was calculated for each metal cation. Any metal cation with calculated RSD % over 10 % was deemed to be an interferent. A recorded RSD % of 7.58 % was calculated in the presence of all metal cations (n = 6). The results show no interference of Zn^{2+}, Cd^{2+}, Pb^{2+}, Co^{2+} and In^{2+} up to 100 µg L^{-1} towards the AdCSV detection of $[Ni(dmgH)_2]$ and indicated the satisfactory analytical performance of the sensor.

(a) (b)

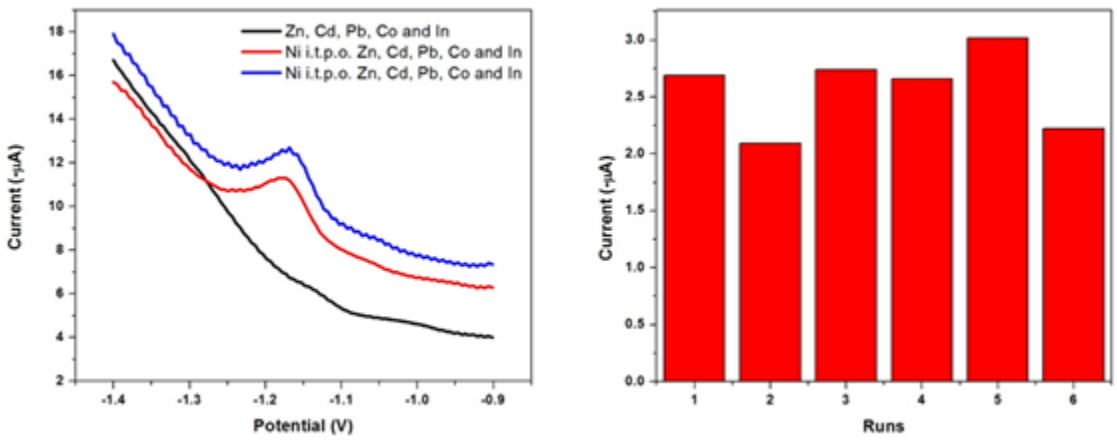

Figure 7.13: (a) Square-wave adsorptive cathodic stripping voltammograms (SW-AdCSV) and (b) corresponding $[Ni(dmgH)_2]$ stripping peak current vs. consecutive runs of 20 µL 30 µg L^{-1} Ni^{2+} in the presence of 100 µg L^{-1} Zn^{2+}, Cd^{2+}, Pb^{2+}, Co^{2+} and In^{2+} at PPECs in conjunction with commercial SPCEs.

7.3.11. Quantitative Analytical Performance of the fabricated PPECs

The favorable adsorptive stripping voltammetric performance of the pre-stored PEC is demonstrated in *Figure 7.14*. A set of square-wave voltammograms and calculated calibration plots recorded in three concentration ranges: (a) 300 – 2100, (b) 30 – 210 and (c) 15 – 120 µg L^{-1} Ni^{2+} ions, at optimum conditions were performed in deaerated samples. The voltammograms were recorded between – 0.7 and – 1.3 V. PPECs were used as disposable electrochemical cells for each Ni(II) cation concentration. To verify a linear relationship of the $[Ni(dmgH)_2]$ peak current on Ni(II) concentration, calibration plots were analyzed. A concentration dependence was observed over all concentration ranges under investigation. The linearity of the of the calibration plots improved as the concentration range was lowered by factors of 10. A linear relationship was established between 15 – 90 µg L^{-1} $[Ni(dmgH)_2]$ concentration (*Figure 7.14, (c)*). Electrode saturation occurs at concentrations greater than 90 µg L^{-1} $[Ni(dmgH)_2]$ and a plateau is observed in the obtained calibration curve due to pre-concentration of the electrode surface with $[Ni(dmgH)_2]$ at accumulation times of 90 s blocking the electron transfer rate and diminishing the increase in peak current as a result of increased Ni^{2+} cations.

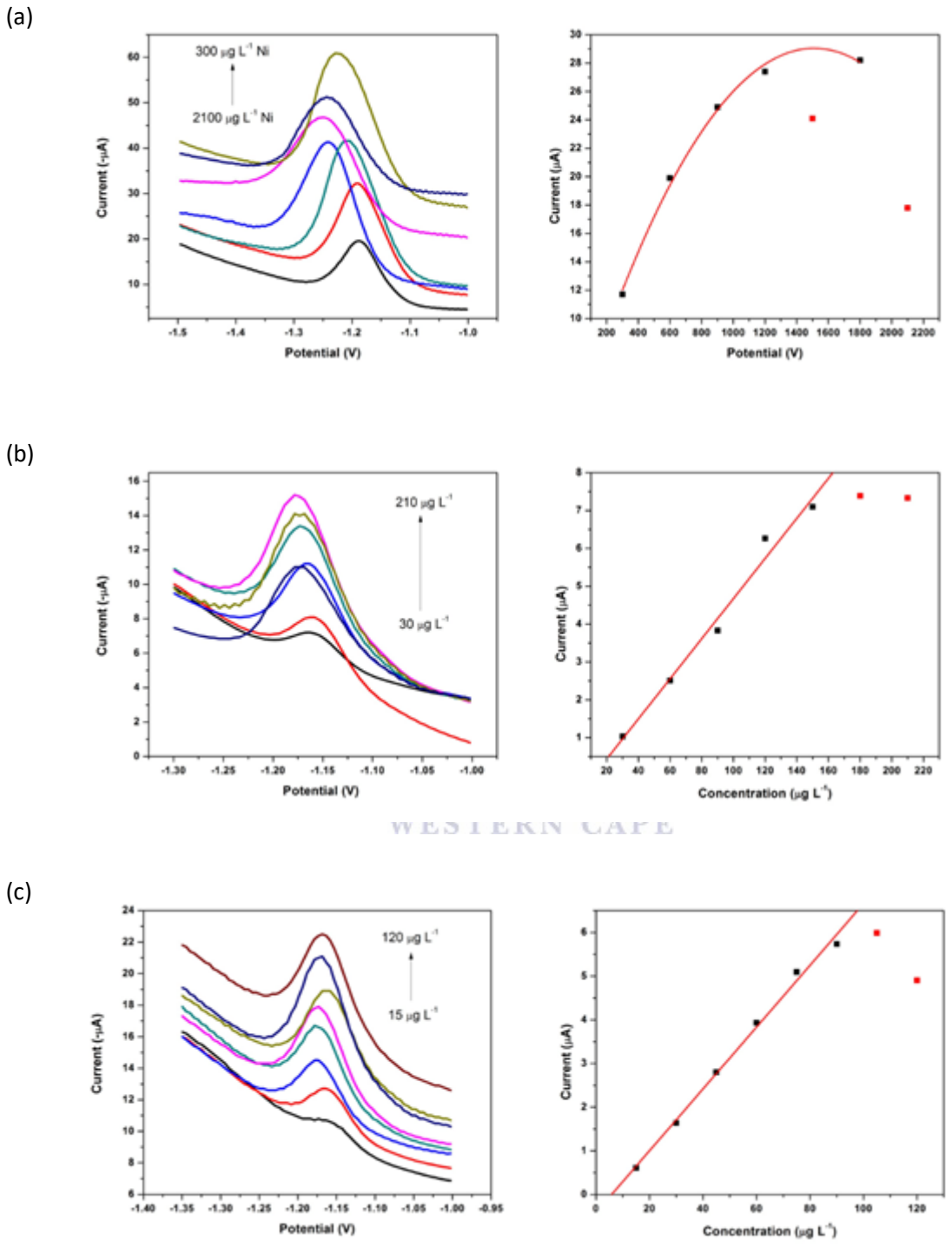

Figure 7.14: Square-wave adsorptive cathodic stripping voltammograms of PPECs in conjunction with SPCEs and corresponding calibration plots recorded with 20 µL volumes of (a) 300 – 2100, (b) 30 – 210 and (c) 15 - 120 µg L^{-1} [$Ni(dmgH)_2$] in 0.1 M NH_3/NH_4Cl buffer. SWV parameters: E_{acc} = - 0.7 V, t_{acc} = 90 s, amplitude = 35 mV and f = 20 Hz, (n = 3).

The detection limit of the PPEC at a SPCE was estimated from three-times the standard deviation of five replications of square wave voltammograms recorded in the absence of $[Ni(dmgH)_2]$ (3σ), divided by the slope of the calibration curve between 15 – 90 µg L^{-1} (3σ/slope) according to *Equation 7.7*. The calculated limit of detection (L.O.D.), limit of quantitation (L.O.Q), sensitivity and recorded correlation coefficient obtained from the calibration curve is recorded in *Table 7.1*. The calculated detection limit for $[Ni(dmgH)_2]$ detection was 6.27 µg L^{-1}. A linear regression of $R^2 = 0.995$ was indicated and a sensitivity of 7.08 µA L μg^{-1} determined. Three replications were performed for all calibration curves. The high sensitivity and good linearity of the dimethylglyoxime-PPEC in the concentration range between 15 – 90 µg L^{-1} indicates the possibility for high accuracy quantitation of the developed system.

$$\text{LOD/LOQ} = \frac{F \times \sigma}{b} \qquad \textit{(Equation 7.7)}$$

Where

LOD: Limit of Detection

LOQ: Limit of Quantitation

F: Factor of 3.3 and 10 for LOD and LOQ, respectively

σ: Standard deviation of the blank, standard deviation of the ordinate intercept, or residual standard deviation of the linear regression

b: Slope of the regression line

Table 7.1: Analytical performance of the fabricated PPECs (n = 3) in the 15 – 120 µg L^{-1} Ni^{2+} concentration.

Analytical Parameter	*Individual Analysis of Ni^{2+}*
Sensitivity (µA L $µg^{-1}$)	*7.08×10^{-8}*
Correlation Co-efficient (R^2)	*0.995*
Detection Limit (µg L^{-1})	*6.27 ± 1.32*
Quantitation Limit (µg L^{-1})	*18.8 ± 4.2*

The effectiveness of the developed DMG-Hg-PPEC, to quantitatively detect Ni^{2+} metal cations in water samples was investigated by comparing the determined limits of detection (LOD) with recently reported literature values. *Table 7.2*, illustrates a summary of previously reported Ni^{2+} sensing techniques and its analytical performance. The developed sensor shows comparable results to other reported sensor technologies based on the adsorptive stripping voltammetric technique in the low µg L^{-1} range under short evaluation times. Slightly higher limits of detection were achieved for the paper-based sensor over other solid electrode materials with low analysis times. This is attributed to lower sensitivity and lower sample volumes utilized in the DMG-Hg-PPEC. Larger concentration additions were required for adequate change in stripping peak current attributed to lower electrode sensitivity.

Table 7.2: A summary of previously reported detection limits for in-situ Ni^{2+} detection in water samples.

Metal Ions	*Substrate*	*Technique*	*Accumulation Time (s)*	*Dynamic Linear Range (µg L^{-1})*	*Detection Limit (µg L^{-1})*	*Reference*
Ni^{2+}	mpBiF-SPCE	AdCSV	180	1 - 10	0.027	[8]
Co^{2+}				1 - 10	0.094	
Ni^{2+}	RBiABE	DPAdSV	30	0.6 - 41	0.18	[9]
Co^{2+}				0.06 – 4.1	0.018	
Ni^{2+}	PbF-SPE	SWV	60	0.6 – 2.9	0.2	[10]
Co^{2+}				0.6 – 5.9	0.3	
Ni^{2+}	SBVE	SWAdCSV	30	0 - 10	0.6	[11]
Ni^{2+}	DMG-CPE	DPAdSV	120	80 - 600	27	[12]
Ni^{2+}	DMG-N-SPE	DPAdSV	120	60 - 500	30	[13]
Ni^{2+}	ERGO-PG-MFE	SWAdCSV	210	2 - 16	0.12	Chapter 5
Ni^{2+} with Co^{2+} and Zn^{2+}	NGr-DMG-GCE	SWAdCSV	120	2 - 20	1.5	Chapter 6
Ni^{2+}	DMG-Hg-µPPEC	SWAdCSV	90	15 - 90	6.27	This Work

7.3.12. Recovery studies of PPECs

Recovery studies in (a) test solutions in the presence of possible metallic interferents, (b) test solutions in the presence of dirt and (c) in real tap water samples were performed by simple calibration techniques, since standard addition methods could not be employed. No Ni^{2+} was detected in any samples prior to spiking with known concentrations. As previously stated this may be attribute to low concentration present below the LOD. Accurate recovery data was obtained for the test sample and real water sample within 10 % error. Contaminated dirt samples however reduced the ability to accurately detect metal cations.

Table 7.3: Recovery studies for in-situ Ni^{2+} detection in test, contaminated and water samples*.

Ni^{2+} Sample	*Original ($\mu g\ L^{-1}$)*	*Added ($\mu g\ L^{-1}$)*	*Found ($\mu g\ L^{-1}$)*	*Recovery (%)*
Test Sample	*N/D*	*45*	*45.61*	*101.34*
Test Sample with added Dirt	*N/D*	*45*	*53.45*	*118.77*
Real Water Sample	*N/D*	*45*	*41.46*	*93.12*

* where, n = 3

7.3.13. Effect of Chelating Agent on Ni^{2+} Detection at PPECs

A variety of chelating agents have previously been reported for the AdSV detection of Ni^{2+}. Ni-chelate complexes formed with dimethylglyoxime, nioxime and morin hydrate have been studied. The probable structures of (a) dimethylglyoxime, (b) nioxime and (c) morin hydrate with Ni^{2+} are illustrated in *Figure 7.15*.

Figure 7.15: Probable Ni(II)-chelate structures formed with (a) dimethylglyoxime, (b) nioxime and (c) morin hydrate

Figure 7.16 represents the square-wave adsorptive cathodic stripping voltammograms (SW-AdCSV) obtained from reduction of 30 µg L^{-1} Ni^{2+} at PPEC, pre-stored with 10 mg L^{-1} Hg and 2 mM (a) dimethylglyoxime, (b) nioxime and (c) morin hydrate. Single, well-defined stripping peaks are obtained for all three chelating agents. The stripping reduction peak attribute to the Ni(II)-dmg complex, Ni(II)-nioxime and Ni(II)-MR showed cathodic stripping reduction peaks at -1.13 V, -1.16 V, - 1.08 V respectively. The nioxime complex showed the largest peak current response over all three Ni-ligand complexes, a minimum of 3 and 2.5 times response of Ni(II)-dmg and Ni(II)-MR complexes. This increased stripping peak current may be attributed to the affinity of Ni^{2+} to form the Ni-nioxime complex and its affinity towards the electroplated Hg film. The results demonstrate future applications of the chelating agents towards Ni^{2+} detection.

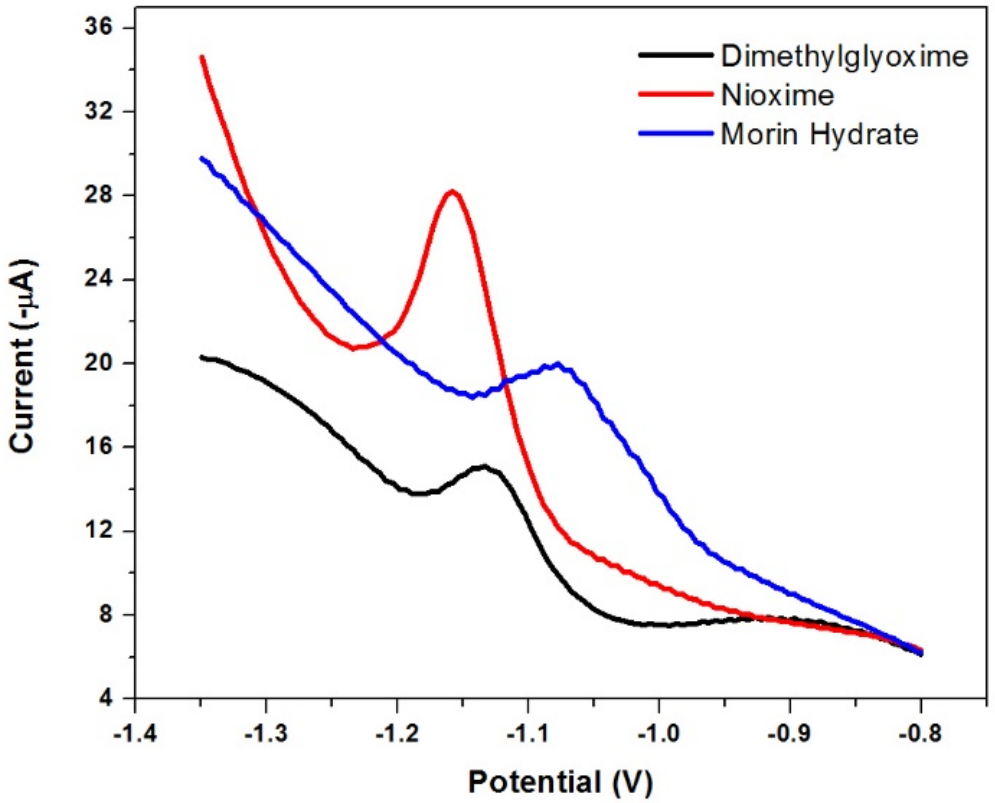

Figure 7.16: Square wave adsorptive cathodic stripping voltammograms (SW-AdCSVs) obtained from 20 µL sample of 50 µg L^{-1} Ni^{2+} at (a) SPCE with PEC pre-stored with a 20 µL solution containing 2 mM DMG and 10 mg L^{-1} Hg, (b) SPCE with PEC pre-stored with a 20 µL solution containing 2 mM Nioxime and 10 mg L^{-1} Hg and (c) SPCE with PEC pre-stored with a 20 µL solution containing 2 mM Morin hydrate and 10 mg L^{-1} Hg. 0.1 M NH_3/NH_4Cl buffer was used as supporting electrolyte. SWV parameters: E_{acc} = - 0.7 V, t_{acc} = 90 s, amplitude = 35 mV and f = 20 Hz.

7.3.14. Graphene infused pre-stored paper-based electrochemical cells

A major drawback in the development and commercialization of micro-volume paper-based electrochemical devices is the low-sensitivity associated with the use of paper substrates. Electron transfer through the cellulose fiber structure is limited. It was theorized that infusion of highly conductive graphene-derivatives within the cellulose structure of the PPEC may facilitate electron

transfer from analyte within in the porous substrate to the SPCE surface. In *Chapter 5*, an electrochemical reduction approach was developed to form an electrochemically reduced graphene oxide modified pencil graphite electrode (ERGO-PGE) for the detection of Ni^{2+} in the presence of a Hg-film and dimethylglyoxime. A similar technique was utilized for ERGO infused PEC as described previously. The electrochemical activity of the ERGO-infused PECs was investigated in 5 mM $Fe(CN)_6^{3-/4}$ redox couple with 1 M KCl as supporting electrolyte by cyclic voltammetry. The recorded cyclic voltammograms of (a) unmodified PEC, (b) GO-infused PEC and (c) ERGO-PEC at SPCE is shown in *Figure 7.17* between -1.0 and 1.0 V. A single redox couple is observed for all three PEC variations. An enhancement in peak currents of both anodic and cathodic peaks and reduction in peak separation are seen upon infusion of GO within the PEC over unmodified PECs. This increase could be attributed to the increased surface-area-to-volume ratio of the PEC with nanomaterial modification or the inclusion of oxygen functional groups. A slight decrease in peak currents is seen upon reduction to ERGO and could be attributed to PEC washing in buffer upon reduction. The graphene-infused PECs were further applied to the detection of $[Ni(dmgH)_2]$ complexes. Here, inhibition of stripping peak currents was observed due to blocking of pores in the paper substrate and lack of conduction due to separation of graphene sheets within the cellulose structure limiting electron transfer through the 3D material. Adequate loading of graphene within the PEC was not achieved to allow for electron conduction. *Figure 7.17, inset* shows an image of the GO-infused PEC prior to electrochemical reduction.

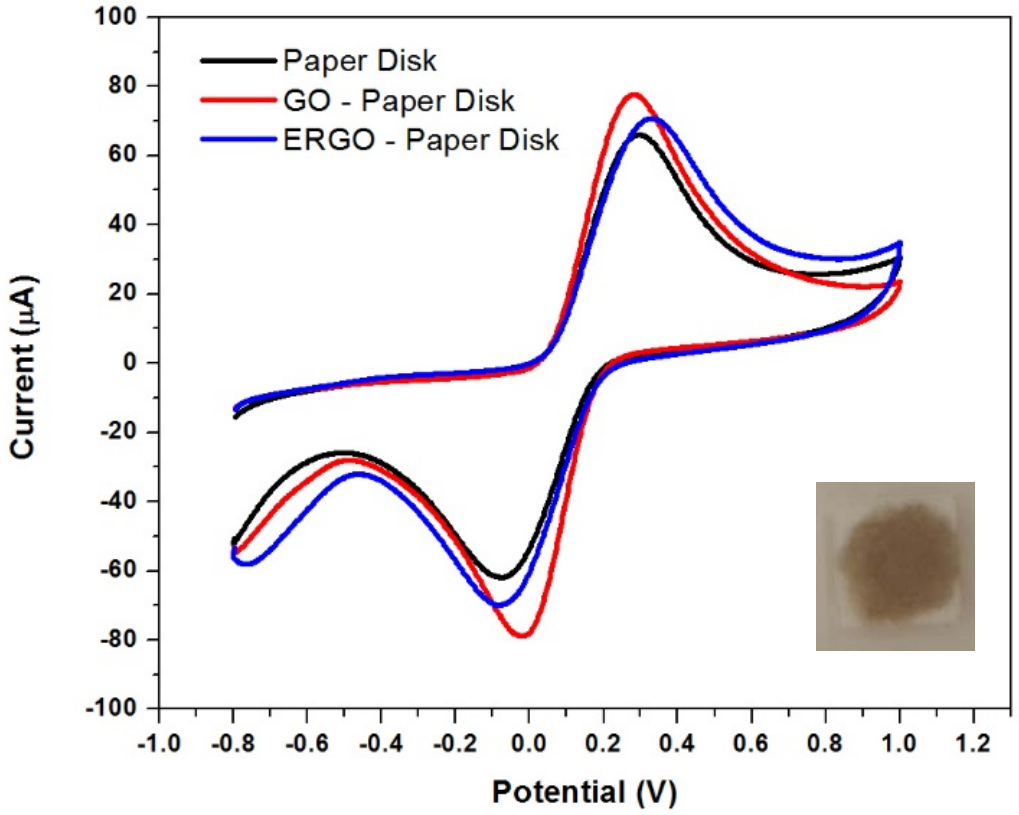

Figure 7.17: CVs of (a) unmodified, (b) GO-infused and (c) ERGO PEC with 20 µL 5 mM $Fe(CN)_6^{3-/4}$ and 1 M KCl as supporting electrolyte at a SPCE and a scan rate of 100 mV s^{-1}. Inset: GO-infused PEC prior to electrochemical reduction.

Similar to *Chapter 6*, infusion of PECs with NGr nanocomposites were investigated for their ability to enhance electron transfer of the PECs and as a result improve electrode sensitivity in Ni^{2+} detection. *Figure 7.18* shows cyclic voltammograms of (a) unmodified and (b) NGr-infused PECs recorded in 5 mM $Fe(CN)_6^{3-/4}$ with 1 M KCl as supporting electrolyte at SPCEs. The voltammograms show no change in sensitivity of the modified PEC and as such shows no noticeable enhancement in electron transfer rate. To our best guess this shows that graphene loading is not adequate to allow for contact of individual graphene sheets within the PEC to allow flow of electrons or electrical conduction.

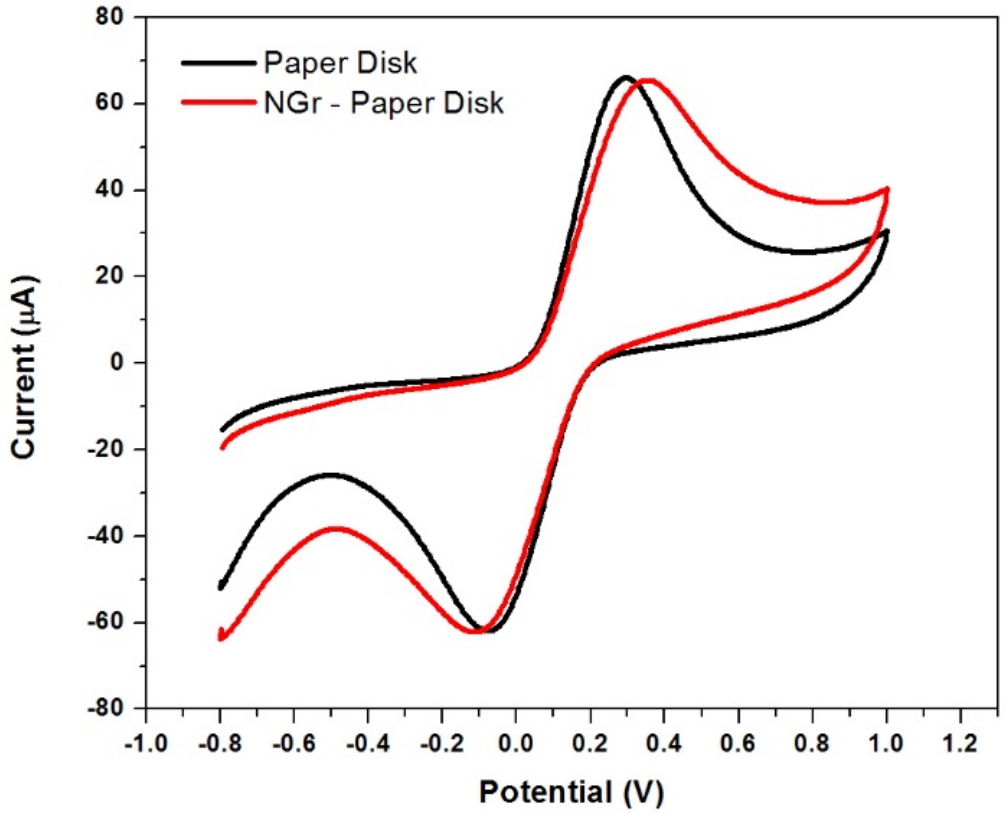

Figure 7.18: CVs of (a) unmodified and (b) NGr-infused with 20 µL 5 mM $Fe(CN)_6^{3-/4}$ and 1 M KCl as supporting electrolyte at a SPCE and a scan rate of 100 mV s^{-1}. Inset: GO-infused PEC prior to electrochemical reduction.

The application of the NGr-infused PPECs towards 30 µg L^{-1} Ni^{2+} detection in the presence of 2 mM DMG, 10 mg L^{-1} Hg^{2+} was studied and the recorded square-wave voltammograms are shown in *Figure 7.19*. The unmodified PPECs, as stated above showed a single reproducible peak attributed to the reduction of Ni^{2+}. Similar to the ERGO-PEC, a distinct weakening in stripping peak currents for Ni^{2+} detection is observed upon infusion of graphene within the cellulose structure. The graphene material blocks pores of the paper-based cellulose fibers stocking the flow of metal cations to the electrode surface. Further, as demonstrated in *Figure 7.18*, no enhancement in electron transfer is observed due to graphene infusion. The formation of a second, broad cathodic peak at ~ - 0.9 V is observed with inclusion of the NGr nanocomposite. The exact nature

of this peak was not known and was thought to perhaps be a new complex of Ni with graphene. The second reduction peak increases with inclusion of Hg in the PEC, while the Ni^{2+} remains unchanged.

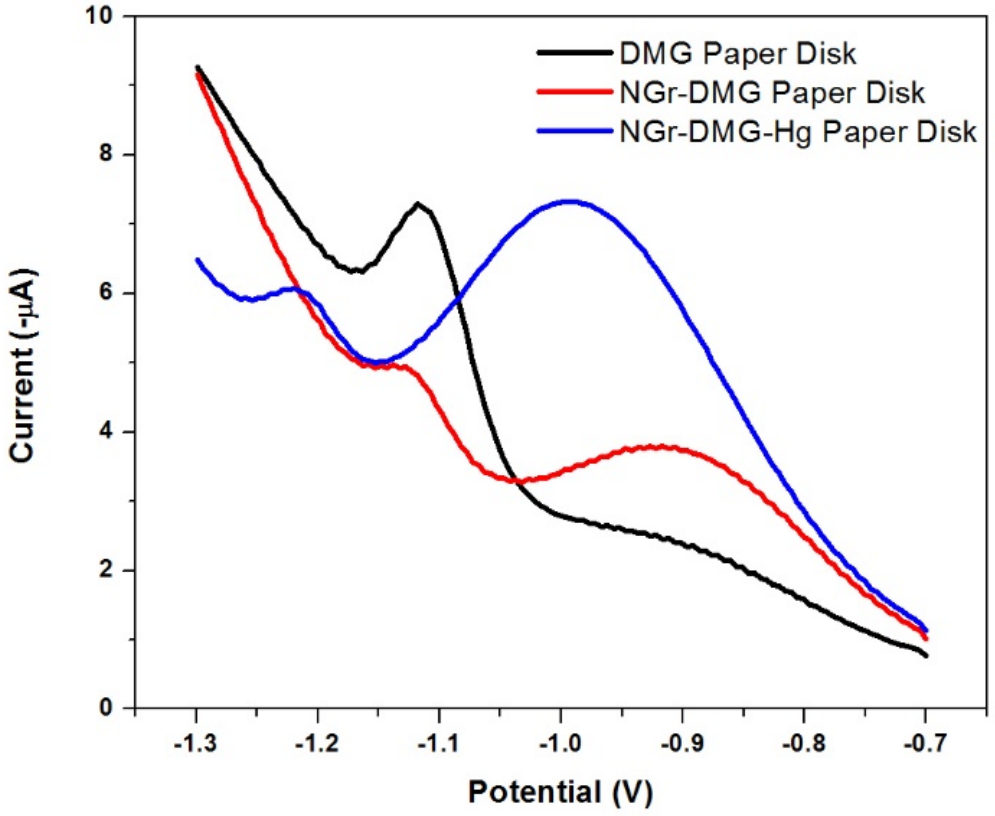

Figure 7.19: Square-wave voltammograms (SWV) obtained from (a) unmodified and (b) NGr-infused PPEC in conjunction with SPCE in solution containing 30 μg L^{-1} Ni, 2 mM DMG, 10 mg L^{-1} Hg^{2+}, 0.1 M NH_3/NH_4Cl buffer, indicating the reproducibility of the PPECs. Inset: Ni^{2+} peak currents vs. consecutive runs. SWV parameters: E_{acc} = - 0.7 V, t_{acc} = 90 s, amplitude = 35 mV and f = 20 Hz.

The nature of the second cathodic reduction peak was studied by investigating its dependence on Ni^{2+} concentration. The recorded square-wave voltammograms for 0 – 100 μg L^{-1} Ni^{2+} at the NGr-PEC in conjunction with SPCEs are shown in *Figure 7.20*. A slight increase in peak currents of the 2nd reduction peak at – 0.9 V is observed with increasing Ni^{2+} concentration.

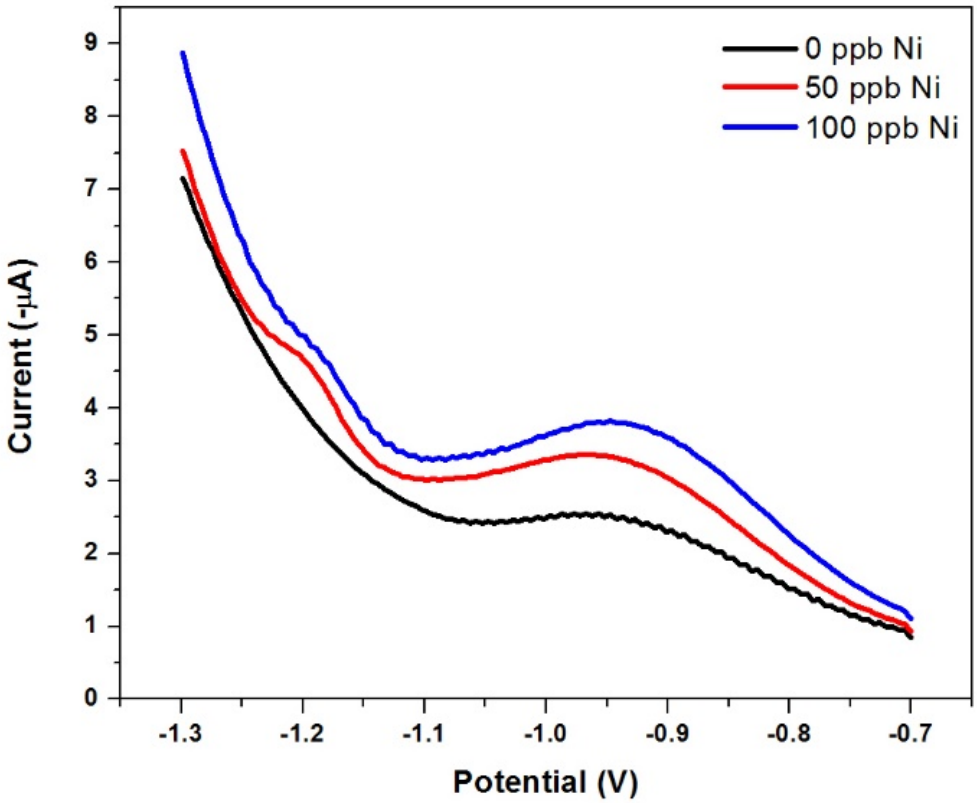

Figure 7.20: Square-wave voltammograms (SWV) of NGr-infused PPEC in conjunction with SPCE for 0 - 100 µg L^{-1} Ni^{2+}, 2 mM DMG, 10 mg L^{-1} Hg^{2+}, 0.1 M NH_3/NH_4Cl buffer, indicating the reproducibility of the PPECs. Inset: Ni^{2+} peak currents vs. consecutive runs. SWV parameters: E_{acc} = - 0.7 V, t_{acc} = 90 s, amplitude = 35 mV and f = 20 Hz.

7.3.15. µPECs with Integrated Graphene WE

As previously discussed, µPECs have showed good ability to be applied as sensing device for the adsorptive stripping voltammetric detection of Ni^{2+}. However, the lower sensitivities of the PPECs over commonly used solid electrodes is a considerable drawback of the paper devices. Employing common techniques to improve electrode sensitivity such as graphene modification was shown in *Section 7.3.14*, making use of an infusion technique. The low loading of the conductive graphene within the cellulose fibre structure using only 20 µL of GO and RGO solutions made it unusable in electrochemical applications. As such, a filtration method to prepare

integrated graphene working electrodes in conjunction with screen printing techniques to prepare CE and RE was suggested. Typically, 10 mL samples of 2 mg mL^{-1} GO and RGO dispersions prepared in water and NMP respectively following 2 hr ultrasonication was filtered through the chromatography paper by successive 3 μL additions. A conductive graphene WE was created. *Figure 7.21*, shows HRSEM images of (a) unmodified PEC, (b) GO-PEC and (c) RGO-PEC at 100 X magnification. *Figure 7.21 (a)* shows the fibrous structure of the PEC before modification. The interwoven nature creates pores creating the permittivity as discussed previously. Upon, modification with 2 mg mL^{-1} GO, pores in the PEC are filled and GO is further deposited on the surface of the PEC (*Figure 7.21 (b)*). This is indicative of high loading capacity of the chromatography paper. Crumpled, flake-like features are observed which corresponds with SEM imaging for GO in *Chapter 4*. The morphology of RGO-PEC differs significantly from that of GO-PEC, as expected. *Figure 7.21 (c)* shows a smooth surface morphology with slight fold in between cellulose fibers. Showing the ability of small particle sizes to effectively penetrate the paper pores. The RGO binds to the cellulose fibers due to strong electrostatic interaction between functional groups of the chromatography paper and negatively charged RGO. Uniform penetration and deposition on the surface is achieved. A measured resistance of 324 Ω was recorded. Similar results were shown in the work by Weng *et al*. [14].

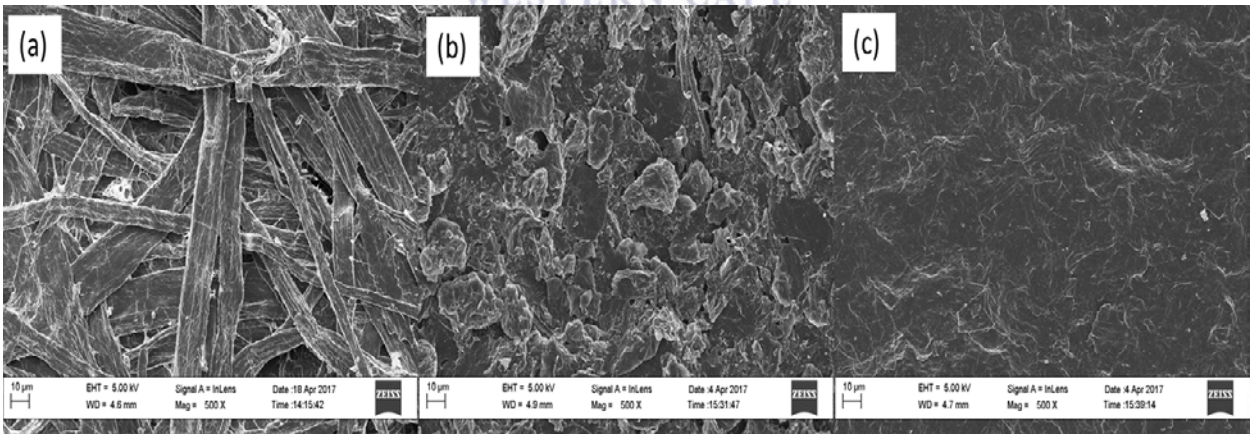

Figure 7.21: HRSEM image of the (a) unmodified PEC, (b) GO-PEC and (c) RGO-PEC at 100 X magnification

The filtered RGO working electrode PEC was applied to the analysis of 5 mM $Fe(CN)_6^{3-/4}$ by cyclic voltammetry and shown in *Figure 7.22*. A single redox couple was seen for the oxidation

and reduction of the $Fe(CN)_6^{3-/4}$ probe between – 1.0 and 1.3 V. A lower sensitivity compared to the PECs in conjunction with SPCEs can be seen due to the considerably lower conductivity of the filtered graphene working electrodes. The result however offers exciting possibilities for its use in electrochemical sensing applications. Folded or origami paper-based devices may be developed for metal detection to provide contact of the working electrode with a prestored reagent zone.

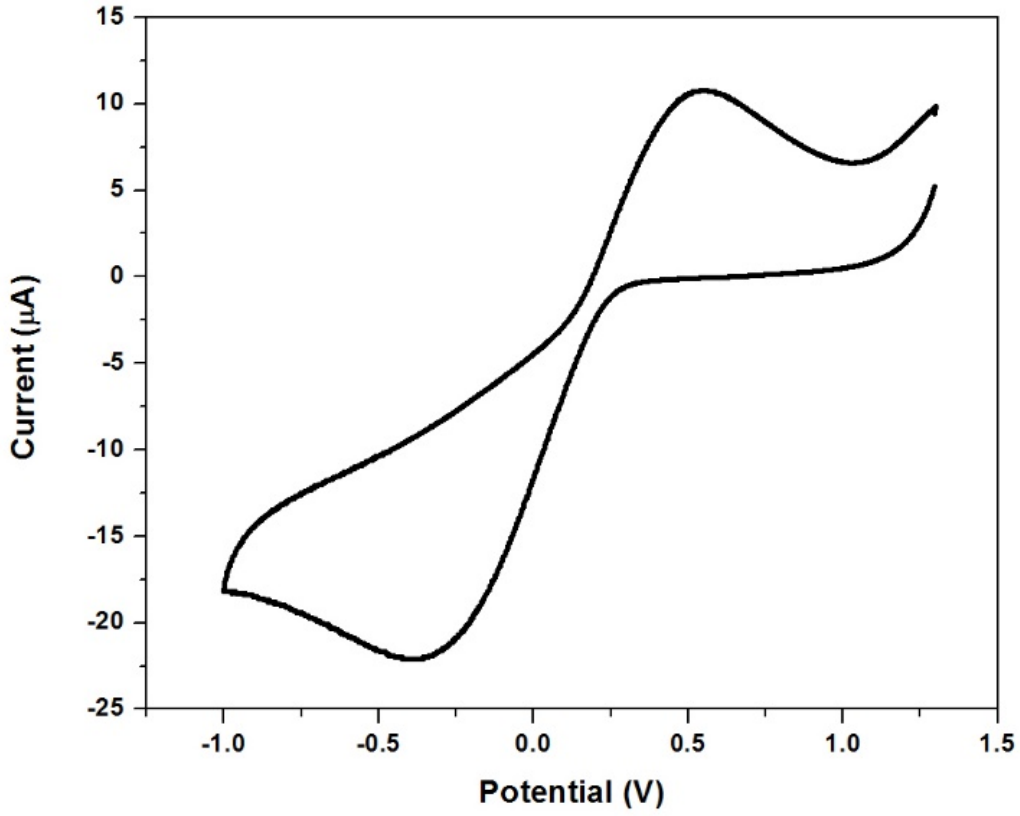

Figure 7.22: CV of filtered Gr-paper electrode with 20 µL 5 mM $Fe(CN)_6^{3-/4}$ and 1 M KCl as supporting electrolyte at a scan rate of 100 mV s^{-1}.

7.4. Conclusions and Future Work

A paper-based electrochemical device was for the first time applied to the detection of metal cations in water samples making use of an adsorptive cathodic stripping voltammetry technique. To the best of our knowledge, this was the first work reported on the use of AdCSV for metal

detection in microfluidic paper-based electrochemical cells (µPECs), building on the work performed by Tan *et al*. [4] for the detection of Pb^{2+} by ASV using prestored paper disks. The µPECs make use of microliter sample volumes along with dry storage of reagents within the paper structure. The cellulose structure acts as a 3D scaffold and cell for reaction of dimethylglyoxime, Hg and electrolyte solution with Ni^{2+}. The µPECs showed good sensitivity and reproducibility towards Ni^{2+} detection in water samples with excellent selectivity in the presence of Zn^{2+}, Cd^{2+}, Pb^{2+}, Co^{2+} and In^{2+}. In addition, morin hydrate and nioxime were compared to its DMG counterpart and showed possibility for future studies in the field, particularly due to the excellent response of Ni(II)-nioxime complexes. Building on the developed techniques in *Chapter 5 and 6* respectively, the ability to infuse the paper substrate with graphene to improve electron transfer kinetics within the cellulose structure was investigated. It was found that low-volume storage of graphene and graphene oxide within the prestored paper disks resulted in graphene sheets randomly scattered within the paper substrate with no real conduction achieved due to the low loading. No significant variations in electron transfer rates or sensitivity towards Ni^{2+} was found. Creating working electrodes solely comprised on filtered graphene sheets immobilised within the cellulose fibre structure showed promise as working electrode material and opens up an exciting avenue for future work on integrated paper electrodes.

References

[1] V. Linder, S.K. Sia, G.M. Whitesides, Reagent-loaded cartridges for valveless and automated fluid delivery in microfluidic devices, Anal. Chem. 77 (2005) 64–71. doi:10.1021/ac049071x.

[2] J. Hoffmann, D. Mark, S. Lutz, R. Zengerle, F. von Stetten, Pre-storage of liquid reagents in glass ampoules for DNA extraction on a fully integrated lab-on-a-chip cartridge, Lab Chip. 10 (2010) 1480–1484. doi:10.1039/b926139g.

[3] S. Ge, L. Zhang, Y. Zhang, F. Lan, M. Yan, J. Yu, A. Furchner, K. Hinrichs, V. Syritski, N. Wu, L.M. Liz-Marzán, I. Pastoriza-Santos, J. Pérez-Juste, Nanomaterials-modified cellulose paper as a platform for biosensing applications, Nanoscale. 31 (2017) 174–182. doi:10.1039/C6NR08846E.

[4] S.N. Tan, L. Ge, W. Wang, Paper disk on screen printed electrode for one-step sensing

with an internal standard, Anal. Chem. 82 (2010) 8844–8847. doi:10.1021/ac1015062.

[5] D.D. Liana, B. Raguse, J. Justin Gooding, E. Chow, J.J. Gooding, E. Chow, Recent advances in paper-based sensors, Sensors (Switzerland). 12 (2012) 11505–11526. doi:10.3390/s120911505.

[6] L. Baxter, A. Bobrowski, M. Bond, G. Heath, R.L. Paul, R. Mrzljak, J. Zarebski, Electrochemical and spectroscopic investigation of the reduction of dimethylglyoxime at mercury electrodes in the presence of cobalt and nickel., Anal. Chem. 70 (1998) 1312–23. doi:10.1021/ac9703616.

[7] J. Zen, N. Chi, F. Hsu, M. Chung, Sq uare-wave Voltam metric Determination of Copper(ii) With a Nafion-Dimethylglyoxime Mercu ry-f il m Electrode, Analyst. 120 (1995) 0–4.

[8] S. Dal Borgo, H. Sopha, S. Smarzewska, S.B. Hočevar, I. Švancara, R. Metelka, Macroporous Bismuth Film Screen-Printed Carbon Electrode for Simultaneous Determination of Ni(II) and Co(II), Electroanalysis. 27 (2015) 209–216. doi:10.1002/elan.201400422.

[9] B. Bas, K. Wegiel, K. Jedlinska, The renewable bismuth bulk annular band working electrode: Fabrication and application in the adsorptive stripping voltammetric determination of nickel(II) and cobalt(II), Anal. Chim. Acta. 881 (2015) 44–53. doi:10.1016/j.aca.2015.05.005.

[10] A. Bobrowski, A. Królicka, M. Maczuga, J. Zarębski, A novel screen-printed electrode modified with lead film for adsorptive stripping voltammetric determination of cobalt and nickel, Sensors Actuators, B Chem. 191 (2014) 291–297. doi:10.1016/j.snb.2013.10.006.

[11] G.M.S. Alves, J.M.C.S. Magalhães, H.M.V.M. Soares, Simultaneous Determination of Nickel and Cobalt Using a Solid Bismuth Vibrating Electrode by Adsorptive Cathodic Stripping Voltammetry, Electroanalysis. 25 (2013) 1247–1255. doi:10.1002/elan.201200643.

[12] A. Ferancová, M.K. Hattuniemi, A.M. Sesay, J.P. Räty, V.T. Virtanen, Electrochemical Monitoring of Nickel(II) in Mine Water, Mine Water Environ. (2015).

doi:10.1007/s10230-015-0357-1.

[13] A. Ferancová, M.K. Hattuniemi, A.M. Sesay, J.P. Räty, V.T. Virtanen, Rapid and direct electrochemical determination of Ni(II) in industrial discharge water, J. Hazard. Mater. 306 (2016) 50–57. doi:http://dx.doi.org/10.1016/j.jhazmat.2015.11.057.

[14] Z. Weng, Y. Su, D.W. Wang, F. Li, J. Du, H.M. Cheng, Graphene-cellulose paper flexible supercapacitors, Adv. Energy Mater. 1 (2011) 917–922. doi:10.1002/aenm.201100312.

Chapter 8 :

Fabrication of Gold Nanoparticle, Ionic liquid (1-Methylimidazole) enhanced Microfluidic Paper-based Electroanalytical Devices (µPEDs) towards the detection of Cu(II) and Ni(II) by Stripping Voltammetric Techniques

Abstract

Accurate detection of environmental pollutants at low-cost, disposable devices has improved the ability for monitoring of real water samples in recent times. Combining quantitative analytical procedures with portable devices significantly improves detection capabilities in resource limited settings. In this work, a simple method for fabricating microfluidic paper-based electroanalytical devices (µPEDs) for Cu^{2+} and Ni^{2+} detection in water samples is described. Electrochemical stripping analysis techniques are coupled to low volume, disposable µPEDs for use in adsorptive stripping voltammetry (AdSV) and anodic stripping voltammetry (ASV). Further, for the first time commercial gold nanoparticles and 1-Methylimidazole ionic liquids integrated within the cellulose fiber structure were utilized to improve electron transfer rates and low sensitivities associated with quantitative electrochemical detection in paper-based devices. Improved sensitivities were achieved at the gold nanoparticle, ionic liquid infused microfluidic paper-based electroanalytical devices (AuNP-IL-µPEDs) for Cu^{2+} and Ni^{2+}. Instrumental parameters including deposition/accumulation time, deposition/accumulation potential, etc. was optimised. Limits of detection (LOD) of 3.78 µM and 5.13 µg L^{-1} was recorded for Cu^{2+} and Ni^{2+} was achieved. Accurate detection, well below the WHO maximum contamination level was achieved.

Keywords

Microfluidic paper-based devices, stripping voltammetry, heavy metals, copper, nickel, chelating agent, gold nanoparticles, ionic liquid

Highlights

- Microfluidic paper-based electrochemical devices are for the first time applied to the detection of Cu^{2+} and Ni^{2+} by electrochemical anodic and adsorptive stripping analysis respectively,
- A simple wax stamping method is applied to the fabrication of hydrophilic channels and designated reaction zones,
- Improved sensitivity towards Cu^{2+} and Ni^{2+} detection is for the first time achieved by impregnation of the cellulose structure of µPEDs with gold nanoparticles and conductive ionic liquids (1-methylimidazole)
- The fabricated AuNP-IL-µPED showed accurate detection of Cu^{2+} and Ni^{2+} in real tap water samples

Graphical Abstract

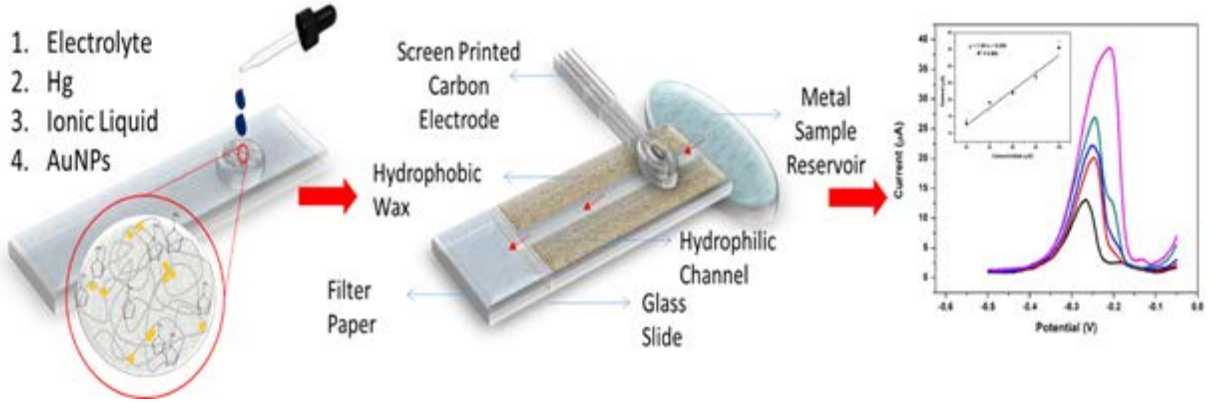

8.1. Introduction

The desire to create low-cost and portable devices for accurate monitoring of environmental pollutants and medical diagnostics has spurred the development of point-of-care (POC) devices over the last two decades. Here, simple sample introduction methods without the need for pre-treatment are utilised in providing information as early as possible in the absence of expensive instrumentation. To date, microfluidic devices fabricated from traditional glass and polymer based substrates have lead the charge in this field [1]. More recently however, "lab-on-paper" has

provided an attractive alternative in both biological and environmental monitoring applications [2]. Applications of paper-based analytical devices (PADs) have steadily increased in recent times due to their biodegradable nature and simple wicking mechanisms allowing liquid transport without the need for external pumps. Low sample volumes, ease of modification, low cost, portability and ease of use characterize the fabricated PADs. Colorimetric sensing at paper devices has been the most utilized technique to date and remains widely used in commercial applications. In this technique, analyte flow by capillary action over a dye or label resulting in colour changes provides semi-quantitative analytical information [3]. A drive to provide more accurate and quantitative analysis in paper-based sensing led to the development of PADs coupled to electrochemical monitoring by Dungchai *et al*. [1] in 2009. In this work, patterned hydrophilic channels and screen printed electrodes were used for the detection of glucose, lactate and uric acid by cyclic voltammetry. Since then, microfluidic paper-based electrochemical devices (μPEDs) have flourished and have been applied to the detection of organic materials [4] and heavy metals in water samples. Among others, Au^{3+} [2], Cd^{2+} [5–7], Pb^{2+} [5–8] and Zn^{2+} [7] have all been investigated by cyclic voltammetry and anodic stripping voltammetric (ASV) techniques. To the best of our knowledge, no work has been conducted for the detection of Cu^{2+} by ASV or Ni^{2+} and other metal cations on μPEDs by adsorptive stripping voltammetric (AdSV) methods.

Patterning of paper substrates with hydrophobic materials provides the basis for fabrication of microfluidic channels in paper-based substrates. Paper as substrate material in paper microfluidics was first introduced by the Whiteside's research group for rapid diagnostics [9] using a photoresist and organic polymer. While photolithography is widely used in the fabrication of devices on a large scale [9,10], the technique is characterized by expensive instrumentation and skilled labour. Alternative methods have been developed based on commercial molten paraffin (PF) wax and hydrophobic polymethylsiloxane (PDMS) to alleviate costs and time required in fabrication steps. Wax printing using Xerox wax printers have made tremendous strides in the field of paper-based microfluidics due to its ability to easily pattern a wide range of patterns with little modification. However, this technique still makes use of designated instrumentation. Simpler methods have been developed. These techniques include: crayon or wax screen printing [10–12], one-step plotting using permanent markers [13], wax-dipping relying on a magnetic field [14] and vinyl templates, contact printing using rubber [15] and metallic [16,17] stamps, soldering iron, Parafilm pressing [18], embossing and simple cut-and-stick methods [19,20].

The use of organic binders (e.g. chitosan and nafion) in electrochemical sensors to improve electrode stability and limit the effect of added surfactants is well documented in literature [21–23]. Ionic surfactants have shown ability in improving the adsorptive stripping technique. Their ability to form stable complexes and adsorb onto electroplated metal films by electrostatic attraction have been studied [21]. Ionic liquids (IL) with similar structures to surfactants offer the possibility of increasing stripping peak currents. To date, ILs based on imidazole and fluorophosphate derivatives have been used as electrochemical solvent and electrode modifier in the fabrication of electrochemical sensors for metal analysis [21,24–28]. High conductivity, fast electron transfer, improved sensitivity, antifouling behaviour and wide potential window are achieved by IL modified electrodes [21,27,28].

Metallic nanoparticles have been incorporated in electrochemical sensing applications since the discovery of their electronic properties became aware. Improved electron transfer kinetics associated with the conductive nanoparticles and increased surface-area-to-volume ratio are exploited. To date, uses of nanoparticles in paper-based sensors have been limited to (i) their intrinsic physical properties to adsorb biological materials and (ii) their optical properties in colorimetric devices. To the best of our knowledge no work has been performed on metallic nanoparticle impregnated paper-devices for enhanced electrochemical sensing for metal detection.

This work describes the development of a simple, low-volume disposable microfluidic paper-based electrochemical device (µPED) with improved sensing capabilities towards the detection of metal cations in water samples by electrochemical stripping analysis. Patterned hydrophilic channels and reaction zones are formed by low-cost hand stamping techniques with commercial paraffin wax on chromatographic paper to develop simple µPEDs in conjunction with commercial screen printed carbon electrodes (SPCEs). Reaction zones, with impregnated gold nanoparticles, ionic liquids, metallic films, chelating agents and electrolyte solution offer the ability for selective and sensitive low-volume detection of metal ions. Herein, the applicability of AuNP-IL-µPEDs towards both anodic and adsorptive stripping voltammetric techniques are investigated by detection of Cu^{2+} and Ni^{2+} in tap water samples. The sensors are based on the deposition/accumulation of Cu^{2+} or $[Ni(dmgH)_2]$ complexes at electroplated mercury films. Capillary action by a wicking mechanism transports analyte across the reaction zone, where amalgamation and complex formation takes place prior to electrochemical detection, mimicking

stirring in traditional sensors. Further, species separation and filtration of contaminants is achieved in the microfluidic channel.

8.2. Experimental Section

8.2.1. Chemicals and Reagents

All chemicals used in the study were of analytical reagent grade. Ultra-pure distilled water (Millipore) was used to prepare all solutions. Gold (III) chloride, 3,4-Dihydroxy-3-cyclobutene-1,2-dione (Squaric acid), 1-Methylimidazole and 2, 3-Butanedione-dioxime (Dimethylglyoxime) were purchased from Aldrich. Cu^{2+}, Ni^{2+} and Hg^{3+} standard stock solutions (1 000 mg L-1, atomic absorption standard solution) and all other metal standards were obtained from Sigma-Aldrich and diluted as required. Acetate (0.1 M, pH 4.6) and Ammonia/Ammonium Chloride (NH_3/NH_4Cl) buffer solution (0.1 M, pH 9.3) was used as supporting electrolyte and prepared by mixing appropriate quantities of glacial acetic acid (CH_3COOH, 99%) and sodium acetate (CH_3COONa) and ammonia (NH_3) and ammonium chloride (NH_4Cl). A Metrohm 827 pH lab pH meter was calibrated using pH 4 and 7 calibration buffer solutions and then used to verify the pH of the prepared buffer solutions. All stock solutions were prepared in water unless stated otherwise.

8.2.2. Apparatus

All voltammetric experiments were performed using a computer-controlled Nova 1.1 software on an Autolab PGSTAT101 potentiostat (Metrohm Autolab, The Netherlands). A three-electrode SPCE system with carbon working electrode (4 mm diameter), carbon auxiliary electrode and Ag/AgCl reference electrode (DRP-C101), purchased from Dropsens, was employed without further modification or pre-treatment. Conventional 20 mL voltammetric cells were replaced with AuNP-IL-µPED for all analysis unless stated otherwise. All experiments were carried out at room temperature.

8.2.3. Gold Nanoparticle, Ionic Liquid, Microfluidic Paper-based Electrochemical Device (AuNP-IL-µPED) Fabrication

Microfluidic paper-based electroanalytical devices (µPEDs*)* were assembled using commercial chromatography paper strip Whatman filter paper grade 1 by a simple contact printing

method using rubber and PDMS stamps and wax printing using a Xerox wax printer. Typically, elastomeric stamps with custom patterns were immersed into molten paraffin wax or PDMS and gently pressed onto 10 x 2 cm chromatographic strips for 30 s periods. Upon contact for 30 s, molten wax or PDMS penetrates the depth of the cellulose structure under simple hand-applied pressure. The stamp is removed and the chromatographic paper is patterned with hydrophobic material. To ensure penetration along the depth of the substrate material, a 30 s melting step is performed on a hot-plate at 100 ^{o}C. Similarly, in wax printing custom designs are printed onto chromatography paper sheets creating a surface layer of wax in the desired pattern. A melting step is allowed for penetration through the entire paper substrate. Areas covered in hydrophobic wax will remain hydrophobic while areas without the printed material will be hydrophilic. As such, 10 mm diameter reaction zones, 6 cm x 100 µm microfluidic channels and 4 mm inlets are created.

A two-step approach was employed for impregnation of the fabricated µPED reaction zones to prepare AuNP-IL-µPED. Successive additions of: (i) aliquots (10 µL) of desired gold nanoparticles and ionic liquid concentrations and (ii) 10 µL portions of reagents (electrolyte, Hg, dimethylglyoxime, etc.) are drop cast onto reaction zones and spreading in the hydrophilic region took place. The modified paper-substrates were allowed to dry at room temperature for 30 min.

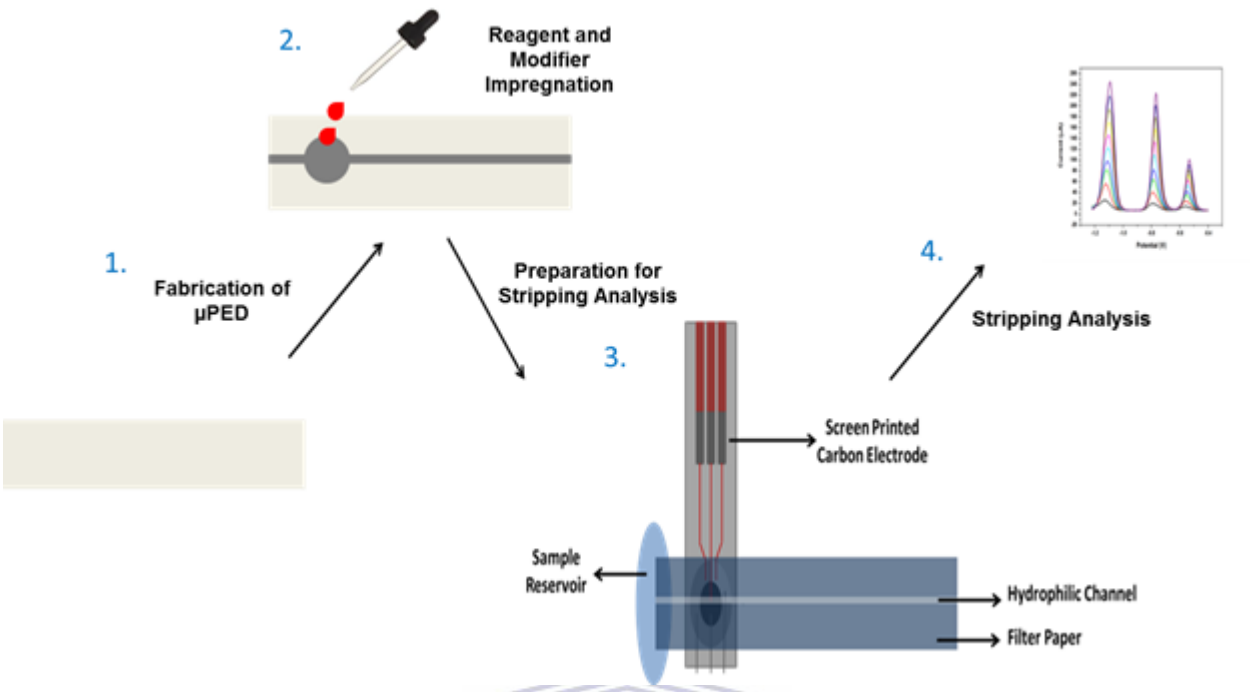

Figure 8.1: Schematic illustration of the AuNP-IL-μPED preparation and its subsequent application towards metal analysis in water samples by electrochemical stripping analysis

8.2.4. Procedure for Square-wave Anodic Stripping Voltammetry (SW-ASV)

Firstly, conventional glass slides used as substrate support was cleaned with 6 M nitric acid, rinsed with distilled water and allowed to dry at room temperature. A fresh, fabricated AuNP-IL-μPED was sandwiched between two glass slides with reaction zone on top of commercial SPCE and the inlet zone remaining uncovered. 100 μL portions of the metal cation analyte (Cu^{2+}) prepared in appropriate electrolyte solution (0.1 M acetate buffer, pH 4.6) was added to the inlet and allowed to flow through the microfluidic channel by capillary action. The wicking mimics stirring in conventional systems, bringing fresh analyte to the electrode surface. A deposition potential (E_{dep}) of – 1.4 V was applied for 120 s. The voltammogram was then recorded by applying a potential from -1.4 V to 0.6 V using SWASV with voltage step 0.005 V and frequency 50 Hz. No further pre-treatment or cleaning steps were carried out.

8.2.5. Procedure for Square-wave Adsorptive Cathodic Stripping Voltammetry (SW-AdCSV)

Similar to the procedure for SW-ASV, the developed AuNP-IL-µPED was sandwiched between cleaned glass slides along with a SPCE. Adequate concentrations of Ni^{2+}, prepared in 0.1 M NH_3/NH_4Cl buffer (pH 9.4) was added to the inlet prior to analysis and allowed to flow along the hydrophilic channel over the reaction zone impregnated with electrolyte, Hg and dimethylglyoxime. An accumulation potential (E_{acc}) of - 0.7 V will be applied for 120 s (t_{acc}) using a pulse height of 20 mV and a frequency of 50 Hz. After an equilibration time of 10 s a square-wave waveform will be applied between - 0.7 V and - 1.4 V.

8.2.6. Real Tap Water Sample Preparation

Real tap water samples collected from our laboratory after running for 2 min were pre-treated with the appropriate buffer solutions (2 M) in an 8:2 ratios. The prepared water sample was applied to the detection of Cu^{2+} and Ni^{2+} by ASV and AdCSV as described in *Sections 8.2.4 and 8.2.5.*

8.3. Results and Discussion

8.3.1. Wax Patterning of Hydrophobic Barriers

8.3.1.1. Visual Analysis of Wax Melting

Evaluation of the wax barriers was performed using arrays of varying line thicknesses between 0.1 – 1 mm after melting. The extent of melting was interrogated both visually and by Grey scale testing using image analysis software, Image J. *Figure 8.2* below, shows a visual analysis of the front and back of patterned Whatman No. 1 chromatography paper before and after melting. Before heating, perfect lines with straight edges was observed on the front of the chromatography paper with accurate dimensions due to patterning precision. The back shows very faint lines as black wax colour is seen through the paper, with thicker lines more easily observed. Following a 3 min heating on a hot plate at 200 ^oC clear lateral spreading of the melted ink can be seen at the front side of the chromatographic paper with a slight lightening of the black intensity. The back side however demonstrates the most significant change as a result of melting. Clear lines may be seen through the chromatographic paper for all line widths. Increasing the line width also

increases the black intensity, although not very dramatic changes are observed. The back side resembles the front very closely after melting, which is not the case before. This is a clear demonstration that both lateral and vertical spreading of the wax took place. Vertical spreading through the paper is almost complete, however this is only a qualitative test and is highly subjective.

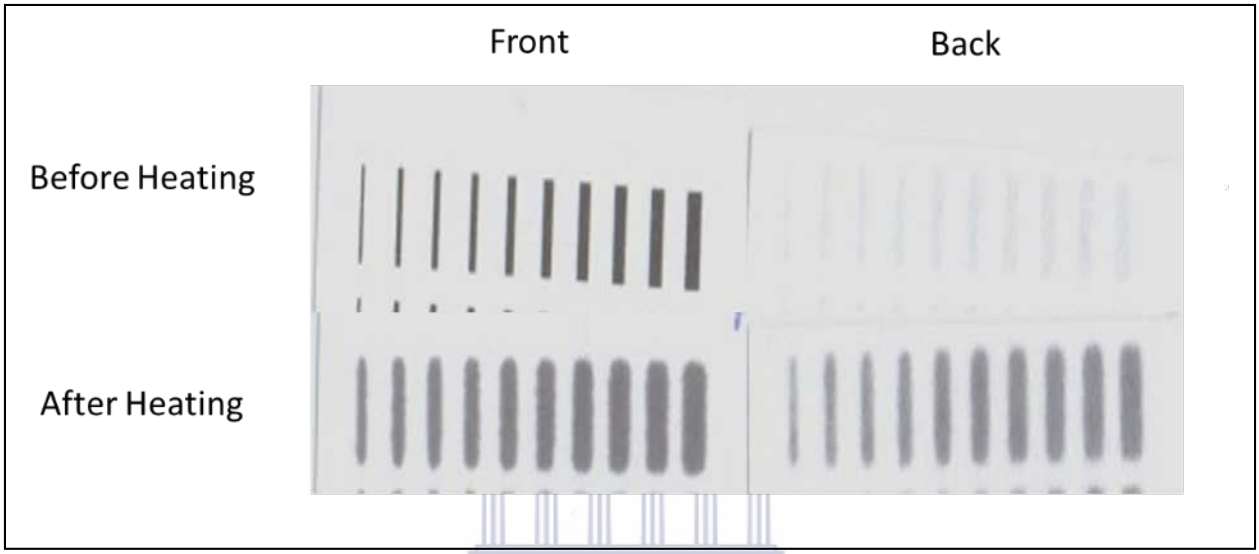

Figure 8.2: Array of wax lines (0.1 – 1 mm) patterned on Whatman No.1 chromatographic paper, before and after heating on a hot plate.

8.3.1.2. Greyscale Testing of Hydrophobic Barriers

Further analysis of the depth of vertical wax spreading was performed using Image J image analysis software. Grey scale analysis measures the depth of wax spreading through the paper substrate by measuring its black, white and grey colour intensities. Low and high grey scale values are observed for black and white colours respectively. *Figure 8.3* shows a typical 8-bit greyscale test as a function of line width for the melted wax line array. 8-bit grey scale values between 178 and 142 are observed for line widths between 0.1 and 1 mm. A general decrease in 8-bit grey scale value can be seen with increasing line width between 0.1 – 0.5 mm before a plateau is noticed. This indicates that line widths greater than 0.4 mm is ideal for creating hydrophobic barriers as the melted wax is able to penetrate the extent of the chromatographic paper under optimum conditions.

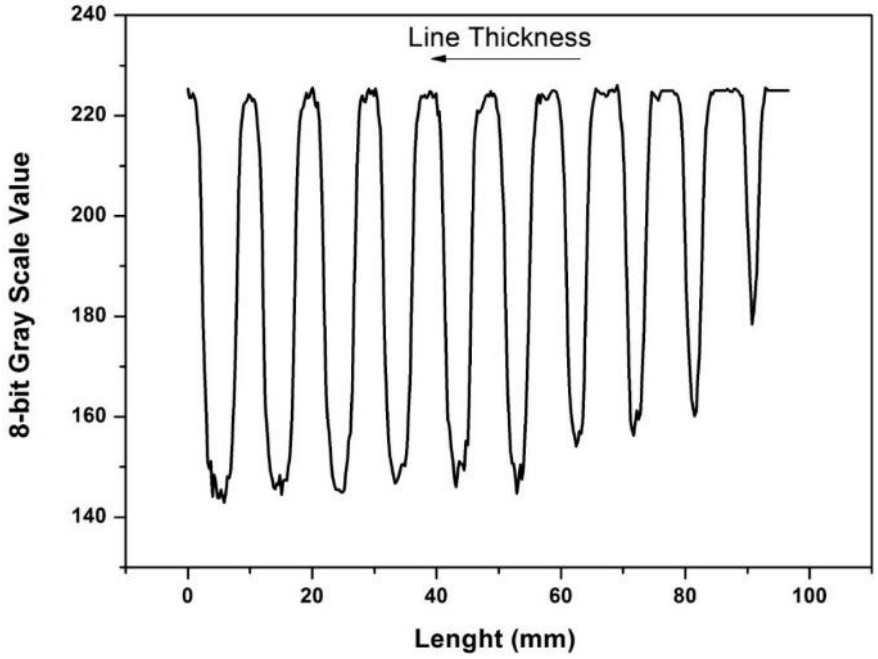

Figure 8.3: 8-bit Grey scale test studying the effect of wax line width on melting effectiveness.

8.3.1.3. Optimisation of Melting Parameters

The influence of melting temperature on effective boundary formation was investigated in *Figure 8.4* between 50 and 250 ^{o}C for 2 min at varying line thicknesses. For temperatures below 100 ^{o}C, very high, constant 8-bit grey scale values for all line widths between 0.1 – 1.0 mm. No significant changes in greyscale value are noted. The high 8-bit grey scale value is indicative of little wax penetration through the depth of the chromatographic paper due to inefficient melting of wax and are therefore not ideal temperatures for the development of effective hydrophobic barriers as liquid will travel under the printed boundaries. At temperatures greater than or equal to 100 ^{o}C effective melting is observed as shown by the considerable decrease in 8-bit greyscale values. Effective melting of the solid wax allows for the molten wax to penetrate the depth of the chromatographic paper. Similar trends are observed between 100 – 250 ^{o}C for varying line widths. A general gradual decrease in 8-bit grey scale value is demonstrated for increasing line widths. This may be attributed to the increase in molten wax volumes present for spreading in the paper

substrate. 200 ^{o}C was selected for all further experiments as it produces effective barriers without damaging the paper substrate.

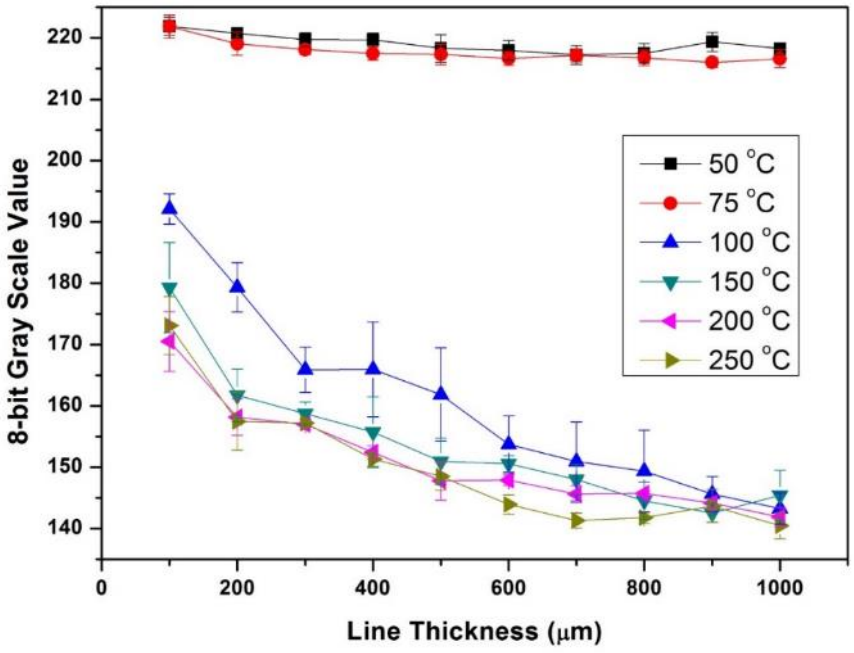

Figure 8.4: Influence of melting temperature (50 – 250 ^{o}C) on effective boundary formation.

The effect of melting time on the development of effective hydrophobic barriers in the chromatographic paper substrate was investigated and recorded in *Figure 8.5*. The effective barrier tests were performed using an 8-bit grey scale test on the reverse side of the paper after melting at 200 ^{o}C. The intensity of the of black colour after melting indicates the penetration of black wax through the depth of the paper. A low 8-bit grey scale value is indicative of adequate melting. A clear decrease in 8-bit grey scale value is seen with increasing line thickness from 100 – 1000 μm. Larger amounts of molten wax are therefore available allowing for wax to penetrate all the way through the pores in the cellulose structure. Effectiveness in hydrophobic barrier preparation is therefore observed. The trend in effective barrier construction as a function of melting time is not as evident. It is observed that 3 min melting times however does show the lowest 8-bit grey scale value across all line thicknesses. This time was used for melting.

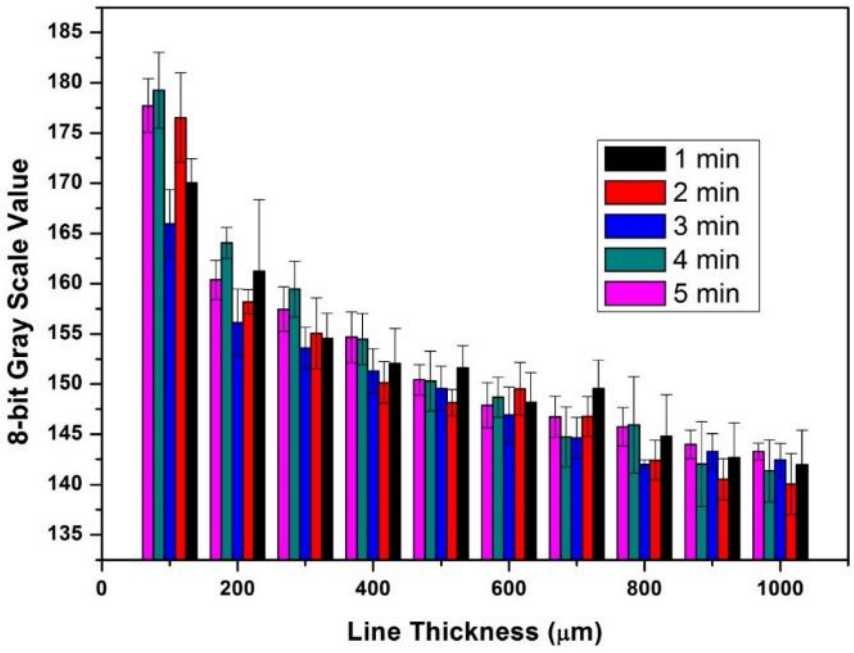

Figure 8.5: Influence of melting time on melting effectiveness at 200 °C.

8.3.1.4. Leak Tests of Printed Hydrophobic Barriers

Rectangles with 15 x 23 mm dimensions with a 12 mm circular cut-out were printed using a wax printer and a contact printing method using custom rubber stamps were developed for further testing. The printed hydrophobic barriers were investigated by visual image analysis before and after heating on a hot plate at 200 °C for 2 min. The recorded images are shown in *Figure 8.6*. Before heating, the front of the printed wax patterns demonstrates neat, precise patterns with no spreading of the printed wax. The back shows no significant wax penetration confirming the wax is printed only on the surface of the chromatography paper. After 2 min heating slight discoloration and spreading of the wax is seen. The printed pattern is now seen on the reverse side of the chromatography paper indicating significant melting of the wax printed pattern.

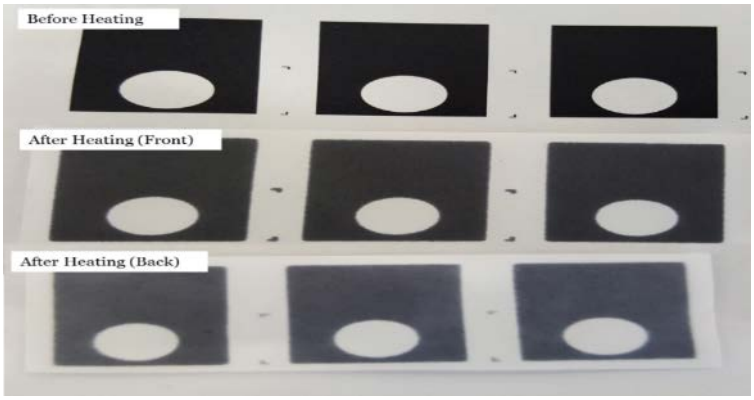

Figure 8.6: Wax printed hydrophobic designs, before and after melting under optimised conditions: 3 min at 200 ^{o}C.

Evaluation of both printed and stamped hydrophobic barriers was performed by measuring the extent of leaking once a fixed volume of diluted food dye was pipetted into the melted barriers, as seen in *Figure 8.7*. Perfectly formed droplets of the aqueous dye can be seen on the printed wax confirming the hydrophobicity of the printed patterns. However, placing the dye within the hydrophilic 12 mm circular cut-out allows for spreading within the circle and trapping by the hydrophobic wax barriers. The leak test was repeated three times to ensure good reproducibility of the printing. The leak test confirms that the melting parameters are adequate for creating hydrophobic barriers. Similarly, stamped patterns showed no leakage indicate adequate penetration of hydrophobic wax through the depth of the paper under the described conditions (*Figure 8.7 (b)*). Patterned stamps created using a CNC cutter created from soft linoleum and PDMS are shown in *Figure 8.7 (c and d)* respectively.

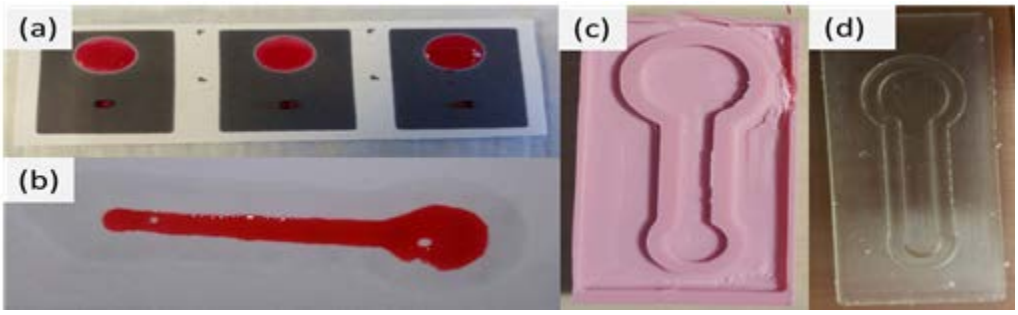

Figure 8.7: Effective leak test of (a) wax printed hydrophobic barriers and (b) µPED. Patterned stamps for contact printing made from (c) linoleum and (d) PDMS.

8.3.2. Characterization of Prepared AuNP-IL-µPED

8.3.2.1. High Resolution Electron Microscopy (HRSEM) of Modified µPEDs

High resolution electron microscopy (HRSEM) provides a powerful technique for the structural or surface characterization of materials and substrates. The structural changes in chromatography paper upon modification with hydrophobic paraffin wax by a simple contact printing (stamping) method is shown in *Figure 8.8 (a)*. Cellulose fibres are observed in both modified (white colour) and unmodified (dark colour) regions with a clear boundary established between the two at low magnifications (30 X). The straight line boundary present is indicative of minimal lateral spreading of the wax upon heating. The molten wax covers the surface and fills the pores of the cellulose structure. HRSEM however, provides only a surface characterization technique. As such, the extent of gravimetric movement of the ink cannot be measured here. Upon further increasing magnification, up to 1000 X within the hydrophilic region (dark colour), the interwoven nature of cellulose fibres of chromatographic paper is shown (*Figure 8.8 (b)*).

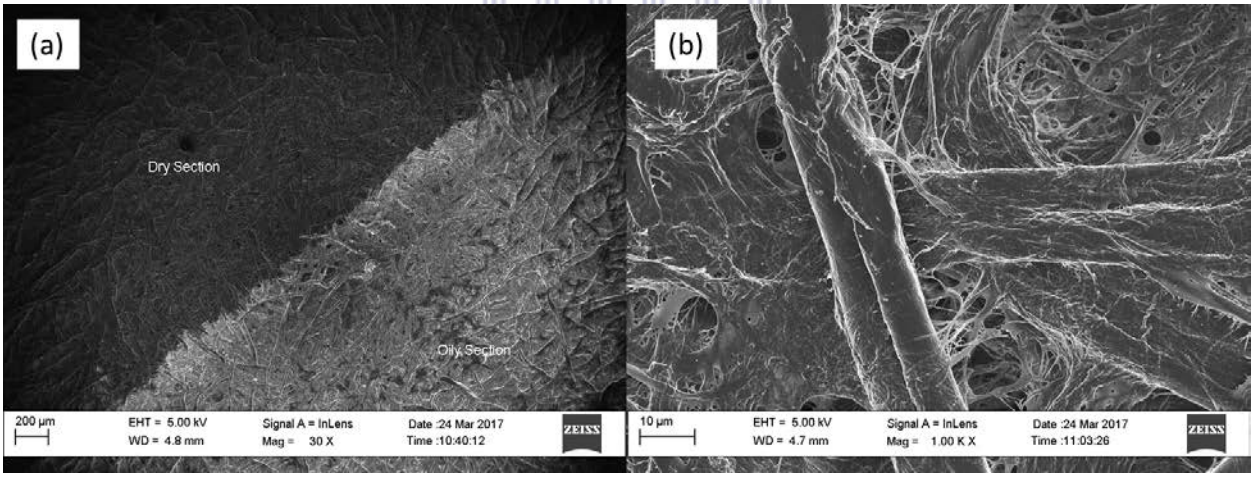

Figure 8.8: HRSEM image of (a) patterned chromatography paper showing clear distinction between hydrophobic and hydrophilic regions (20 X magnification) and (b) magnified image of unmodified cellulose structure (1000 X magnification).

Chromatographic paper decorated with gold nanoparticles was studied by HRSEM analysis (*Figure 8.9*). The dispersion of prepared gold nanoparticles within the cellulose fibre structure is shown in *Figure 8.9 (a)*. Gold nanoparticles are not clearly seen between the cellulose fibres of

chromatographic paper, upon visual investigation of HRSEM images at low magnifications (5 kX). Spherical particles may be confused as metallic nanoparticles. However, contrast between the cellulose fibres and metallic gold nanoparticles was established using a conventional back scattering method. Here, reflected electrons from metallic species with high energy are seen as bright spots. The small bright spots observed in the back-scattered image are indicative of gold nanoparticles decorated within the cellulose structure. A relatively uniform distribution of gold nanoparticles is shown throughout the area under investigation as hoped for. Few areas of agglomeration (not shown here) however were also observed. The size and shape of dispersed gold nanoparticles were studied at increased magnifications up to 100 kX in *Figure 8.9 (b)*. Uniformly shaped spherical particles were observed with an average particle size of ~ 90 nm. This is in agreement with SEM imaging of gold nanoparticles in *Chapter 4*.

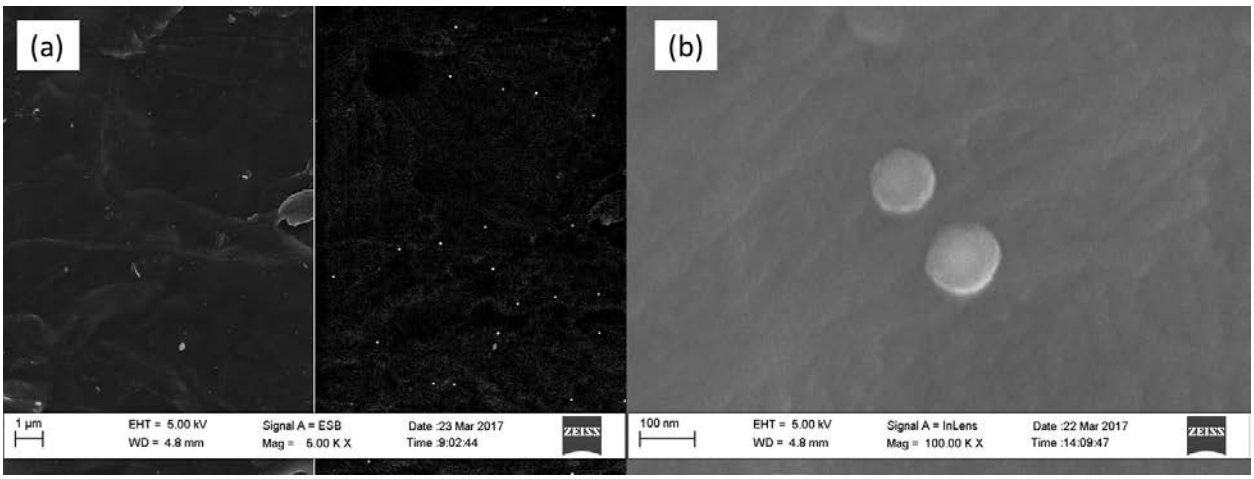

Figure 8.9: HRSEM images of AuNP-µPED created from chromatography paper showing (a) back-scattered image of gold nanoparticle distribution in cellulose structure (5000 X magnification) and (b) magnified images of individual gold nanoparticles (100 kX magnification).

Energy dispersive spectra (EDS) was utilised to interrogate the nature of the nanoparticles embedded within the interwoven cellulose structure. EDS spectra of unmodified and modified chromatographic paper are shown in *Figure 8.10*. Chromatography paper in the absence of gold nanoparticles (*Figure 8.10 (b)*) showed the presence of only carbon and oxygen as expected. No other elements were observed within the elemental composition of the paper substrate. Upon inclusion of gold nanoparticles within the reaction zone by simple drop casting techniques,

elemental gold peaks were demonstrated (*Figure 8.10 (b)*). The gold contributed between 30 and 45 % of elemental composition of the AuNP-µPED. This confirmed the characterization of nanoparticles within the cellulose structure as gold nanoparticles as previously assumed.

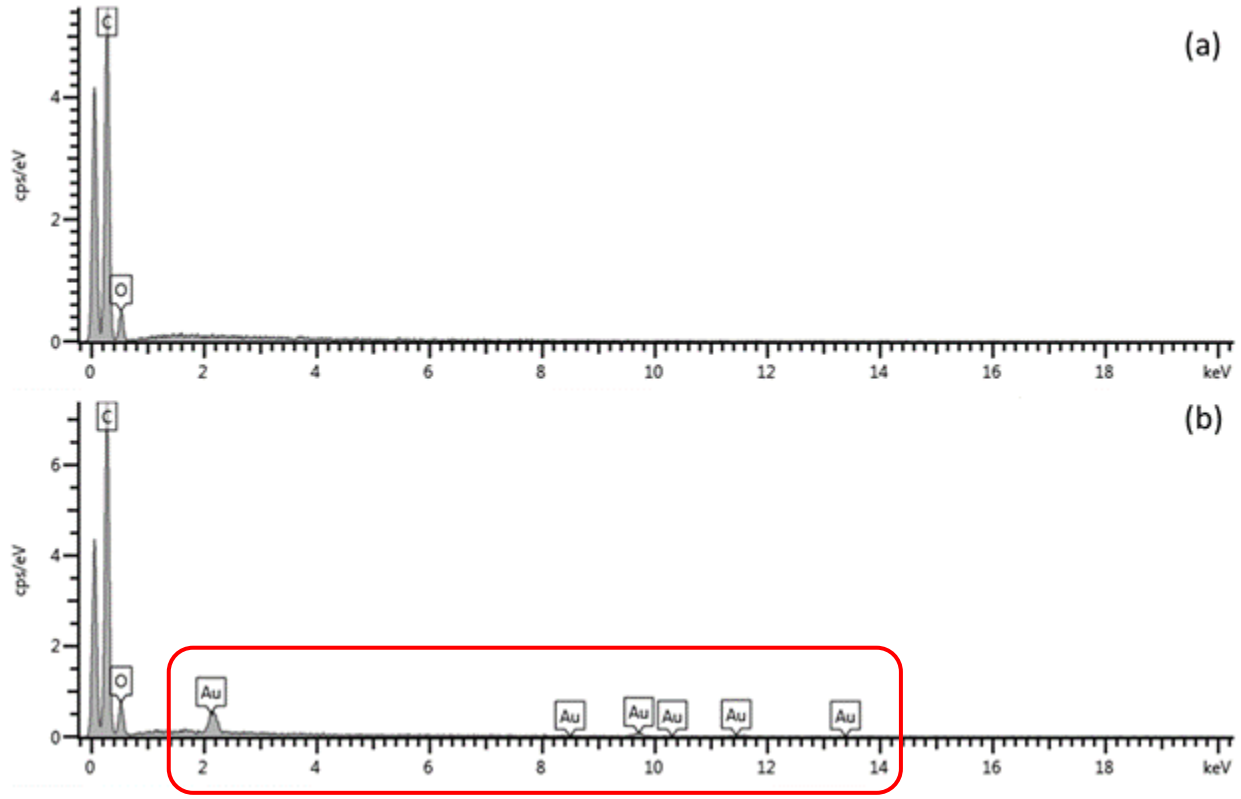

Figure 8.10: Energy dispersive spectra (EDS) of (a) chromatography paper and (b) AuNP-modified chromatography paper

8.3.3. Electrochemical application of AuNP-IL-µPED towards Cu^{2+} detection by ASV

8.3.3.1. Characteristic oxidation potential of Cu^{2+} at AuNP-IL- µPED

The characteristic oxidation potential of Cu^{2+} conversion to Cu^{0} in the presence of an electroplated Hg-film at the AuNP-IL-µPED in 0.1 M acetate buffer solution (pH 4.6) is shown in *Figure 8.11*. The square-wave anodic stripping voltammogram was studied between – 1.0 and 0.3 V. A well-resolved and completely symmetrical characteristic stripping peak for Cu^{2+} appears at – 0.255 V arising from redox reactions attributed to the anodic stripping voltammetric technique with a shoulder which may be attributed to the Cu^{1+} oxidation state. This in accordance with

literature values for Cu detection. Further, a large, sharp completely symmetrical peak is attributed observed at 0.035 V arising from the oxidation of Hg^0 to Hg^{3+}. The exact mechanism for Cu^{2+} detection occurs via a three-step process illustrated below:

$(Hg^{3+})_{solution} + 3\ e^- \rightarrow (Hg^0)_{adsorbed}$ Electroplating (8.1)

$Cu^{2+} + 2\ e^- + (Hg^0)_{adsorbed} \rightarrow Cu(Hg)_{adsorbed}$ Deposition Step (8.2)

$Cu(Hg)_{adsorbed} \rightarrow Cu^{2+} + 2\ e^- + Hg^{3+}$ Stripping Step (8.3)

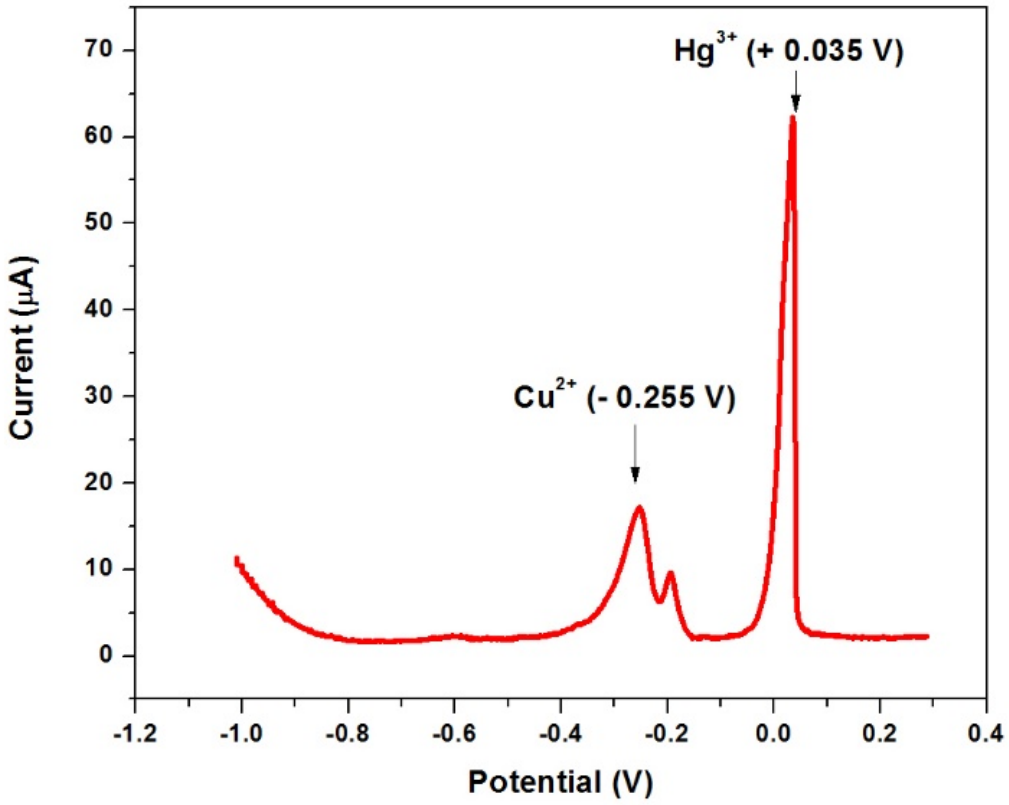

Figure 8.11: Square-wave anodic stripping voltammogram (SW-ASV) of 40 µM Cu^{2+} detection in the presence of 2000 µM Hg^{3+} at the AuNP-IL-µPED. Supporting electrolyte: 0.1 M acetate buffer solution (pH 4.6), scan rate (10 mV s^{-1}), deposition time (120 s), frequency (50 Hz), amplitude (0.04 V) and voltage step (0.004 V).

8.3.3.2. Current responses of Cu^{2+} at AuNP-IL-µPED

The influence of µPED modification on the stripping peak current of Cu^{2+} by anodic stripping voltammetry (ASV) was investigated and recorded in *Figure 8.12*. Square-wave voltammograms recorded for 40 µM Cu^{2+} at SPCE in conjunction with µPEDs modified with 20 µL (a) electrolyte, (b) 1000 µM Hg^{3+} in electrolyte, (c) 1-methylimidazole and 1000 µM Hg^{3+} in electrolyte and (d) 0.05 µM AuNP, 1-methylimidazole and 1000 µM Hg^{3+} in electrolyte are shown. Detection of Cu^{2+} at µPEDs modified with only 0.1 M acetate buffer (pH 4.6) showed a symmetrical, broad peak at – 0.22 V. An increase in stripping peak current is seen due to the formation of an electroplated Hg-film. Here, amalgam formation of Hg with electrochemically reduced Cu^{2+} is possible resulting in enhanced electrode preconcentration. Further, incorporation of the conductive ionic binder, 1-methlyimidazole facilitates the electrostatic attraction of metal cations onto the electrode surface increasing the stripping peak current. A slight shift to more negative potentials is observed due to slower electron transfer processes. Decoration of the µPED reaction zone with 0.05 mM AuNPs promotes the electron transfer kinetics and improved surface-area-to-volume ratio at the electrode surface. Improved stripping peak current and a shift to more positive electrode potentials (- 0.209 V). The AuNP-IL-µPED with incorporated Hg-film could therefore be used for sensitive detection of Cu^{2+} in water samples.

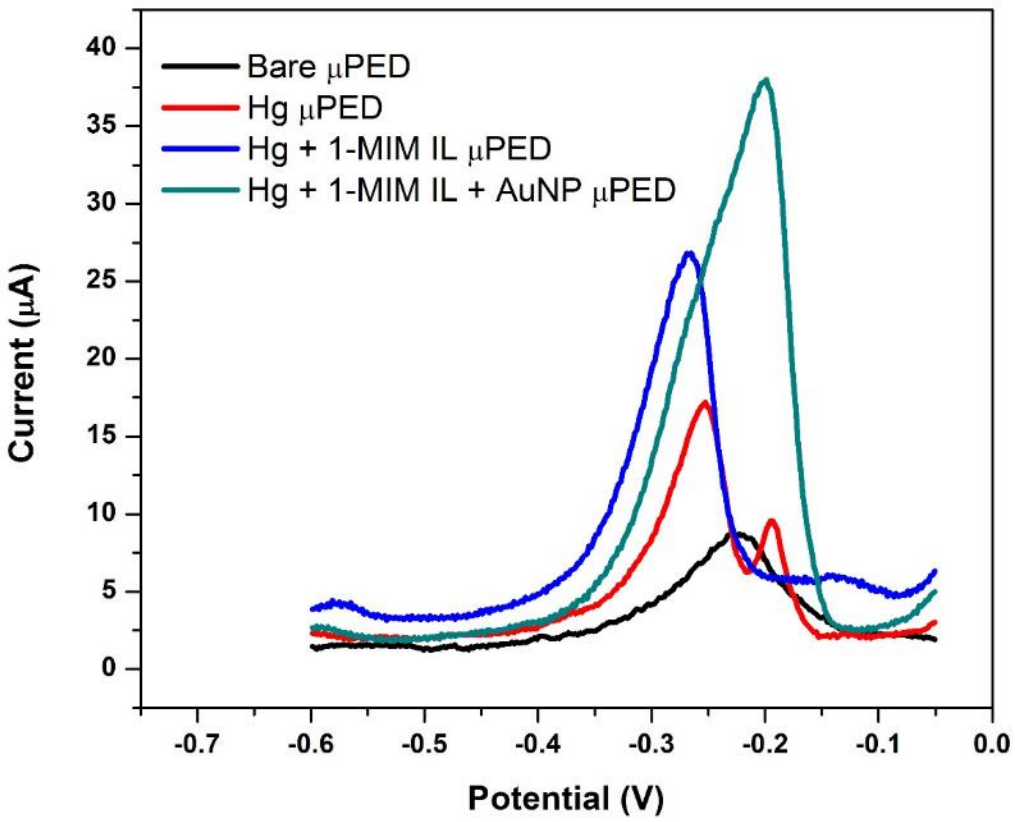

Figure 8.12: Square-wave voltammograms recorded for 40 μM Cu^{2+} at SPCE in conjunction with μPEDs modified with 20 μL (a) electrolyte, (b) 1000 μM Hg^{3+} in electrolyte, (c) 1-methylimidazole and 1000 μM Hg^{3+} in electrolyte and (d) 0.05 μM AuNP, 1-methylimidazole and 1000 μM Hg^{3+} in electrolyte. Supporting electrolyte: 0.1 M acetate buffer solution (pH 4.6), scan rate (10 mV s^{-1}), deposition time (120 s), frequency (50 Hz), amplitude (0.04 V) and voltage step (0.004 V).

8.3.3.3. Influence of Hg ion concentration

The ability to sensitively detect metal cations at carbon-based electrodes by electrocatalytic stripping voltammetric methods is highly dependent on its ability to form stable complexes i.e. amalgams and fused alloys at the electrode surface. The Hg ion concentration of the electroplated Hg-film significantly affects the preconcentration of Cu^{2+}. The influence of Hg ion concentration

of the impregnated AuNP-IL-μPED on the Cu^{2+} stripping peak current was investigated between 0 and 2000 μM (*Figure 8.13*). A linear increase in stripping peak current is observed with increasing Hg ion concentration over the range under investigation. As such faster electron transfer was achieved as well as increased Cu^{2+} preconcentration.

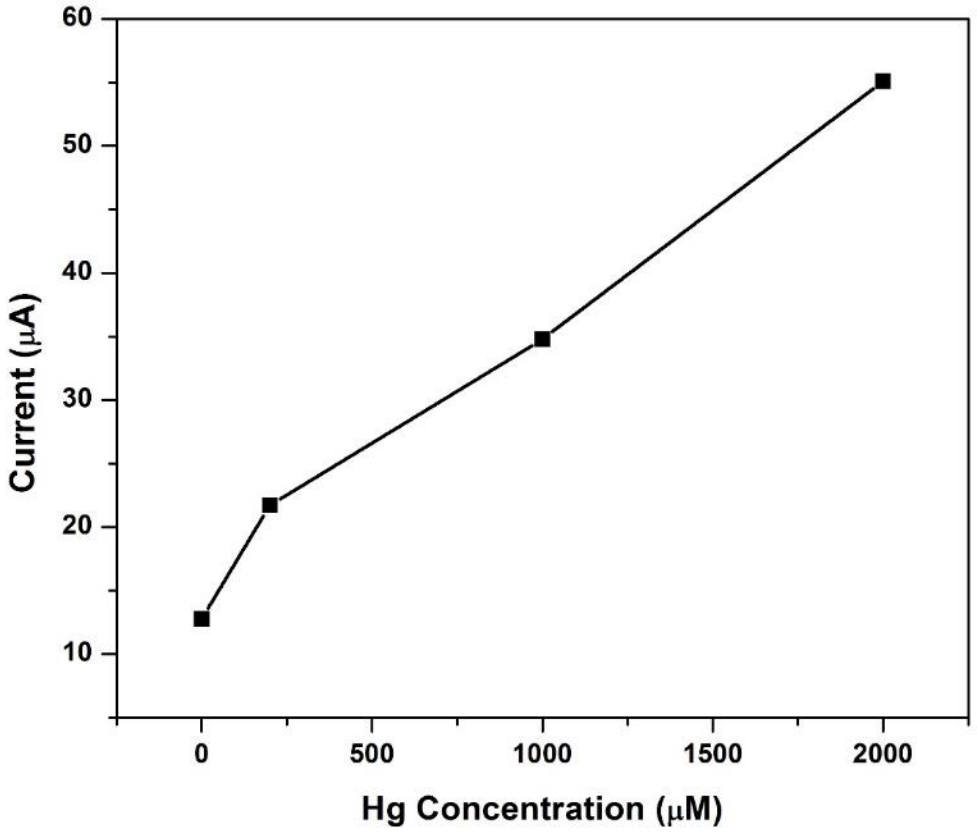

Figure 8.13: Influence of Hg ion concentration on the stripping peak current of 40 μM Cu^{2+} at AuNP-IL-μPEDs.

8.3.3.4. Optimisation of Instrumental Parameters

The accumulation of metal cations at the electrode surface is the determining step in all stripping voltammetric techniques. Instrumental parameters controlling the amount of analyte deposited on the electrode surface is fundamental in the stripping response. As such, instrumental parameter affecting the electrode preconcentration, namely deposition potential and deposition

time were optimised for their response towards 40 µM Cu^{2+} in 0.1 M acetate buffer solution (pH 4.6) at the developed AuNP-IL-µPED and shown in *Figure 8.14*.

Figure 8.14 (a), represents the effect of deposition potential on the stripping peak currents of Cu^{2+} in the range of + 0.2 V to – 1.2 V. As the deposition potential approaches the oxidation potential of Cu^{2+} at the AuNP-IL-µPED in conjunction with a SPCE (0.2 V to – 0.2 V), the peak current increases. At potentials greater than – 0.2 V, the stripping peak current increases drastically. Cu^{2+} ions are reduced to Cu^{0} and deposited at the electrode surface. A deposition potential of – 1.2 V was selected for all further experiments.

The influence of deposition time was studied between 0 and 180 s (*Figure 8.14 (b)*). Low deposition times (0 and 30 s) limits the amount of metal cations which can be deposited on the electrode surface and therefore low stripping peak currents are observed. Stripping peak currents dramatically increase at a 60 s deposition time. At deposition times greater than 60 s a plateau in stripping peak currents is observed. Saturation of the electrode surface with deposited metal cations impedes the flow of electrons and diminishes peak responses.

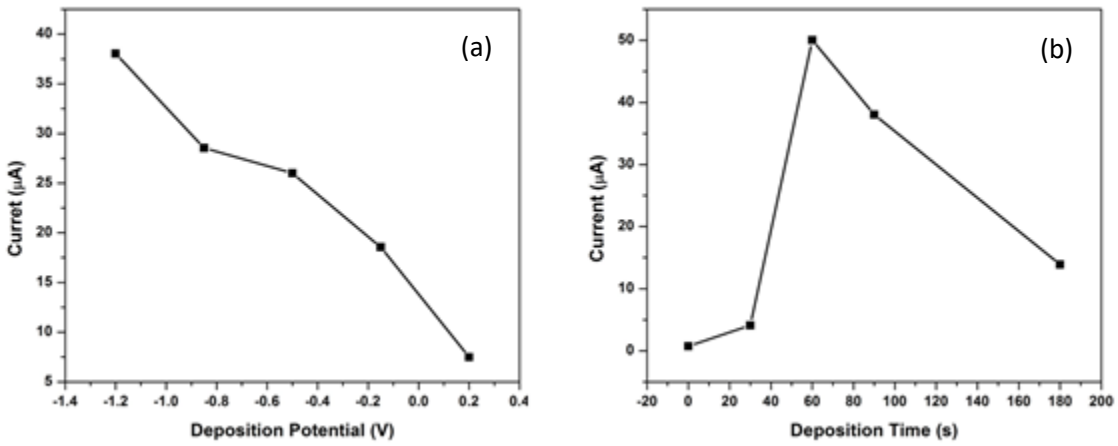

Figure 8.14: Influence of instrumental parameters: (a) deposition potential and (b) deposition time on the stripping peak response of 40 µM Cu^{2+} at AuNP-IL-µPEDs.

8.3.3.5. Quantitative Analytical Detection of Cu^{2+} at AuNP-IL- µPED

Metallic cations of Cu^{2+} were determined individually at the AuNP-IL-µPEDs in the presence of an electroplated Hg-film by SW-ASV. Square-wave voltammograms and corresponding calibration plots (*Figure 8.15 and Figure 8.15, inset*) were recorded for 20 – 100 µM Cu^{2+} in 0.1 M acetate buffer solution (pH 4.6). The recorded sensitivity and detection limits calculated from 5 replications (3σ/slope) are recorded in *Table 8.1*. A linear increase in stripping peak current is observed with increasing metal concentration with correlation coefficient of 0.969. A slight shift in peak potentials to more positive values with increasing metal ion concentration was observed. This shift suggests a resultant IR-drop effect. A calculated limit of detection and quantitation was determined to be 3.78 ± 2.1 and 11.3 ± 3.76 µM respectively according to *Equation 8.4*.

$$\text{LOD/LOQ} = \frac{F \times \sigma}{b} \quad \text{(Equation 8.4)}$$

Where

LOD: Limit of Detection

LOQ: Limit of Quantitation

F: Factor of 3.3 and 10 for LOD and LOQ, respectively

σ: Standard deviation of the blank, standard deviation of the ordinate intercept, or residual standard deviation of the linear regression

b: Slope of the regression line

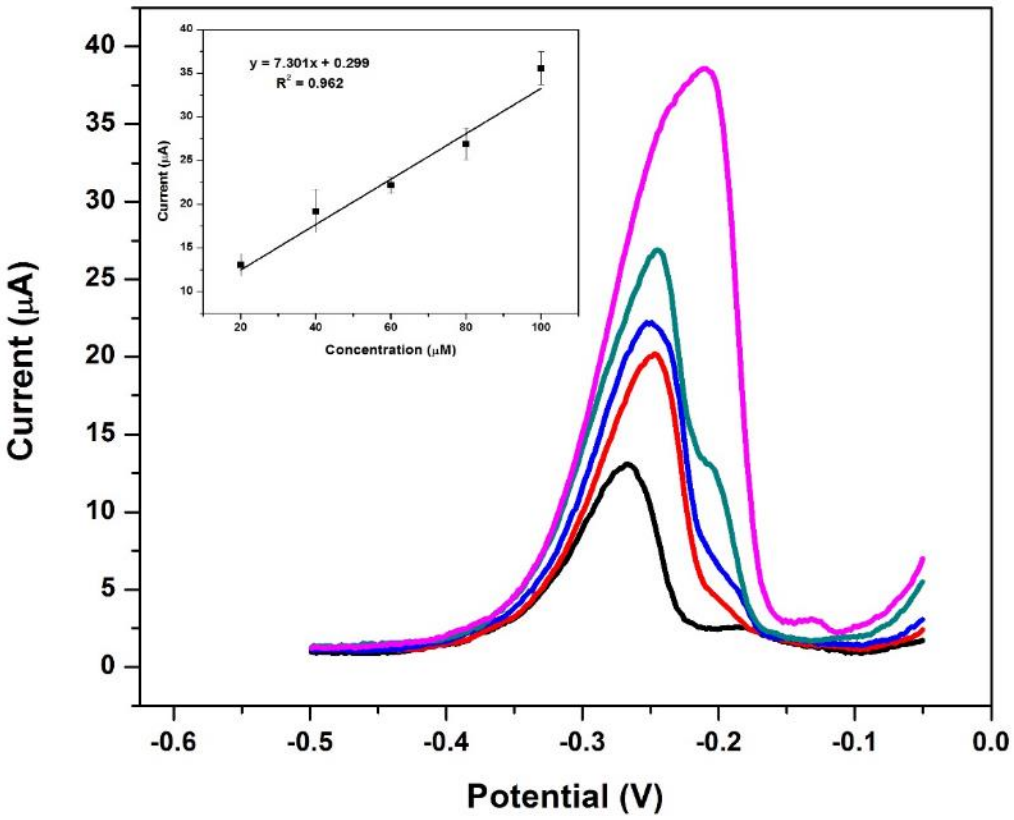

Figure 8.15: SW-ASVs of 20 – 100 µM Cu^{2+} at AuNP-IL-µPED in conjunction with SPCE. Inset: Corresponding calibration plot. Supporting electrolyte: 0.1 M acetate buffer solution (pH 4.6), scan rate (10 mV s^{-1}), deposition time (120 s), frequency (50 Hz), amplitude (0.04 V) and voltage step (0.004 V).

Table 8.1: Sensitivity, correlation coefficient (R^2), detection limit (LOD) and limit of quantitation (LOQ) recorded at AuNP-IL-µPED (n = 3)

Analytical Parameter	*Analysis of Cu^{2+}*
Sensitivity (µA L µg^{-1})	7.301 x 10^{-6}
Correlation Coefficient (R^2)	0.962
Detection Limits (µg L^{-1})	3.78 ± 2.11
Limit of Quantification (µg L^{-1})	11.3 ± 3.76

A comparison of the calculated limit of detection of the AuNP-IL-µPED towards Cu^{2+} detection by square-wave anodic stripping voltammetry (SW-ASV) with other sensors reported in literature is summarized in *Table 8.2*. To date, the detection of Copper by stripping voltammetric techniques has been limited to solid and paste electrodes modified with a variety of materials to improve electrode sensitivity. Typically, calculated limits of detection were found to be below 1.0 µg L^{-1} with relatively short analysis times. The reported LOD for the AuNP-IL-µPED in the presence of Hg was found to be 3.78 ± 2.1 µg L^{-1} at 120 s analysis time. This is in agreement with expected results due to lower sensitivity and sample volumes utilised at the paper-based sensors.

Table 8.2: A summary of previously reported sensors and limits of detection (LOD) for Cu^{2+} detection by stripping voltammetric techniques

Metal Ions	*Substrate*	*Technique*	*Accumulation Time (s)*	*Dynamic Linear Range ($\mu g\ L^{-1}$)*	*Detection Limit ($\mu g\ L^{-1}$)*	*Reference*
Cu^{2+}	*Nafion-G-HgFE*	*SWASV*	*120*	*20 - 180*	*0.12*	[22]
Cu^{2+}	*NH_2-rGO/β-CD-GCE*	*SWASV*	*300*	*3.2 – 63.5*	*0.57*	[29]
Cu^{2+}	*Tetracarbonylmolybdenum-MWCNT-PE*	*SWASV*	*60*	*0.0064 – 63.5*	*0.0051*	[30]
Cu^{2+}	*Sb_2O_3/CNTPE*	*SWASV*	*90*	*2 - 100*	*0.39*	[31]
Cu^{2+}	*GCE*	*DPASV*	*N/D*	*75 - 960*	*24*	[32]
Cu^{2+}	*SPGE*	*SWASV*	*240*	*5 - 300*	*1.0*	[33]
Cu^{2+}	*Hg-AuNP-IL-µPED*	*SWASV*	*120*	*20 - 100*	*3.78*	*This Work*

8.3.3.6. Real Sample analysis of Cu^{2+} at AuNP-IL- µPED

The AuNP-IL-µPED was applied to the detection of a known concentration of Ni^{2+} in test (0.1 M acetate buffer solution) and real (tap water) samples according to the developed procedure. The accuracy of the fabricated device was tested using a conventional calibration curve method. Here, 50 µM Cu^{2+} test solution was analysed at the AuNP-IL-µPED and compared to the linear equation of the calibration curve recorded for 3 successive replications. A recovery percentage of 96.2 % was found. The AuNP-IL-µPED was further used to analyse real tap water samples collected from our laboratory. It was found that the tap water contained Cu^{2+} concentrations below the calculated LOD and no signal was observed. In order to account for the influence of matrix effects, tap water samples were spiked with 50 µM Cu^{2+} and analysed by SW-AdCSV. The sensor achieved an accuracy of 91.73 %. The lower observed recovery occurred as a result of weakened conductivity in the tap water sample.

8.3.4. Detection of Ni^{2+} by AdCSV at AuNP-IL-µPED

8.3.4.1. Characteristic reduction potential of Ni^{2+} at AuNP-IL- µPED

The characteristic reduction of Ni^{2+} to Ni^0 in the presence of an electroplated Hg-film and dimethylglyoxime as complexing agent at the AuNP-IL- µPED with commercial SPCE is shown in *Figure 8.16*. A single, symmetrical stripping peak is shown for the reduction of Ni^{2+} from the $Ni(dmgH)_2$ complex at – 1.17 V is observed in 0.1 M NH_3/NH_4Cl buffer (pH 9.4) as supporting electrolyte. The adsorptive cathodic stripping voltammetric detection of Ni^{2+} occurs via an overall 10 electron transfer reduction proves and is summarized below:

$$Ni^{2+} + 2\ dmgH \rightarrow [Ni(dmgH)_2] + 2\ H^+ \qquad \text{Complex Formation} \qquad (8.5)$$

$$[Ni(dmgH)_2]_{sol} + Hg_{sol} \rightarrow Hg[Ni(dmgH)_2]_{ads} \qquad \text{Accumulation} \qquad (8.6)$$

$$Hg[Ni(dmgH)_2]_{ads} + 10\ e^- + 10\ H^+ \rightarrow Ni^0 + Hg + 2\ DHAB \qquad \text{Stripping} \qquad (8.7)$$

The exact mechanism of the adsorptive cathodic stripping technique is not well known. Typically, complex formation of metal cations with suitable chelating agents to form stable complexes is the initial step. Complex formation precedes a non-electrolytic accumulation of the formed complex onto an electroplated Hg-film by simple adsorption mechanism. Upon application of a reduction potential, metal cations are reduced from metal-chelate complexes from the electrode surface back into solution. Conversion of the chelating agent to a stable DHAB also occurs.

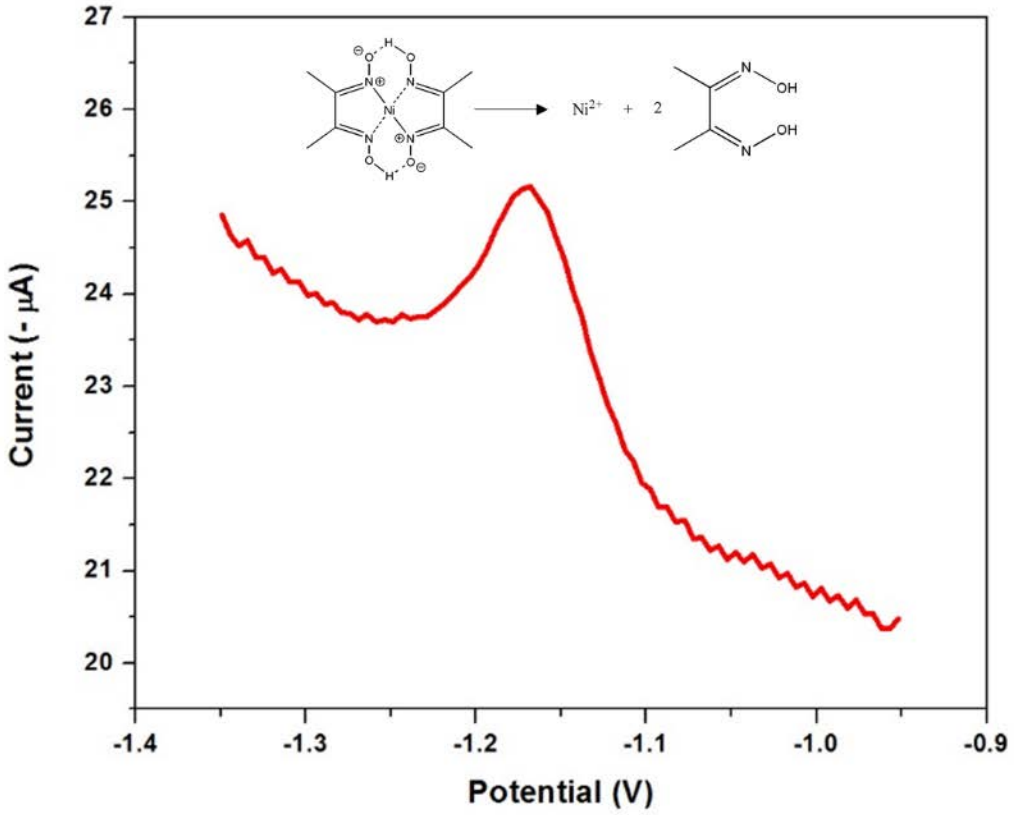

Figure 8.16: SW-AdCSV of 60 µg L^{-1} Ni^{2+} in 0.1 M NH_3/NH_4Cl buffer (pH 9.4) as supporting electrolyte containing 2 mM DMG and 15 mg L^{-1} Hg at AuNP-IL-µPED in conjunction with SPCE. E_{acc} = - 0.7 V, t_{acc} = 90 s.

8.3.4.2. Current responses of Ni^{2+} at AuNP-IL-µPED

The ability of AuNPs and 1-Methylimidazole, ionic liquid to enhance µPED sensitivity in conjunction with SPCEs towards $Ni(dmgH)_2$ complex detection is illustrated in *Figure 8.17*. Accurate and sensitive detection of Ni^{2+} in the presence of dimethylglyoxime and Hg at µPEDs is observed by a sharp, semi-symmetrical stripping reduction peak at – 1.17 V. This result corresponds with results found for AdCSV detection of Ni^{2+} at DMG-Hg-µPPECs in *Chapter 7*. A 36 % increase in stripping peak currents is observed for µPEDs modified with 1-methylimidazole (IL) over the unmodified µPED. The increase is attributed to electrostatic attraction of the $Ni(dmgH)_2$ complex at the electrode surface. A further increase in stripping

response is shown for µPEDs decorated with AuNPs and 1-methylimidazole. An increase of 35.9 % is recorded. Metallic nanoparticles in contact with the SPCE surface improved the electron transfer rate and also improved the surface-area-to-volume ratio, as previously discussed. No observable stripping peak shift is seen.

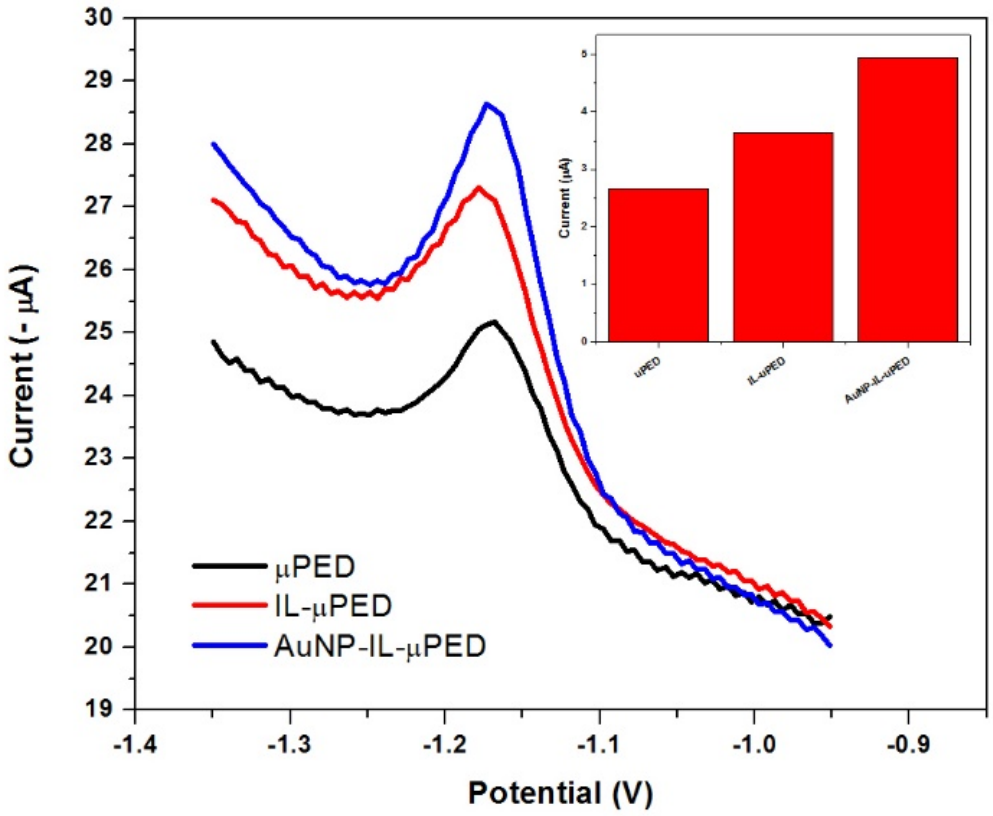

Figure 8.17: SW-AdCSVs of 60 µg L^{-1} Ni^{2+} in 0.1 M NH_3/NH_4Cl buffer (pH 9.4) as supporting electrolyte containing 2 mM DMG and 15 mg L^{-1} Hg at (a) µPED, (b) IL-µPED and (c) AuNP-IL-µPED in conjunction with SPCE. E_{acc} = - 0.7 V, t_{acc} = 90 s.

8.3.4.3. Influence of DMG concentration on Ni^{2+} detection at AuNP-IL-µPED

The effect of chelating agent concentration on the metal-chelate complex formation and its observed current response was studied from 0 – 3 mM DMG and demonstrated in *Figure 8.18*. A low sensitivity of the AuNP-IL-µPED towards Ni^{2+} is observed in the absence of chelating agent

(0 mM DMG). Impregnation of dimethylglyoxime within the cellulose structure by a dry storage method results in complex formation within the paper-substrate reaction zone as Ni^{2+} cations are driven across the microfluidic channel by capillary action. An increase in stripping peak currents is seen between 0.5 and 2.0 mM DMG as preconcentration of the electrode surface with formed stable complexes is achieved. A maximum stripping peak current was obtained for 2 mM DMG concentrations. Electrode saturation at higher concentrations inhibits electron transfer, effectively blocking the signal. A plateau in cathodic stripping peak currents is observed. *Figure 8.18, inset* shows recorded square-wave adsorptive cathodic stripping voltammograms (SW-AdCSV) of 60 µg L^{-1} Ni^{2+} in 0.1 M NH_3/NH_4Cl buffer (pH 9.4), at DMG-Hg-AuNP-IL-µPEDs in conjunction with SPCEs with (a) 0.5 mM and (b) 2 mM DMG. High capacitive (background) current is seen for the µPED with SPCE at higher chelating agent concentrations, while the peak current doubles.

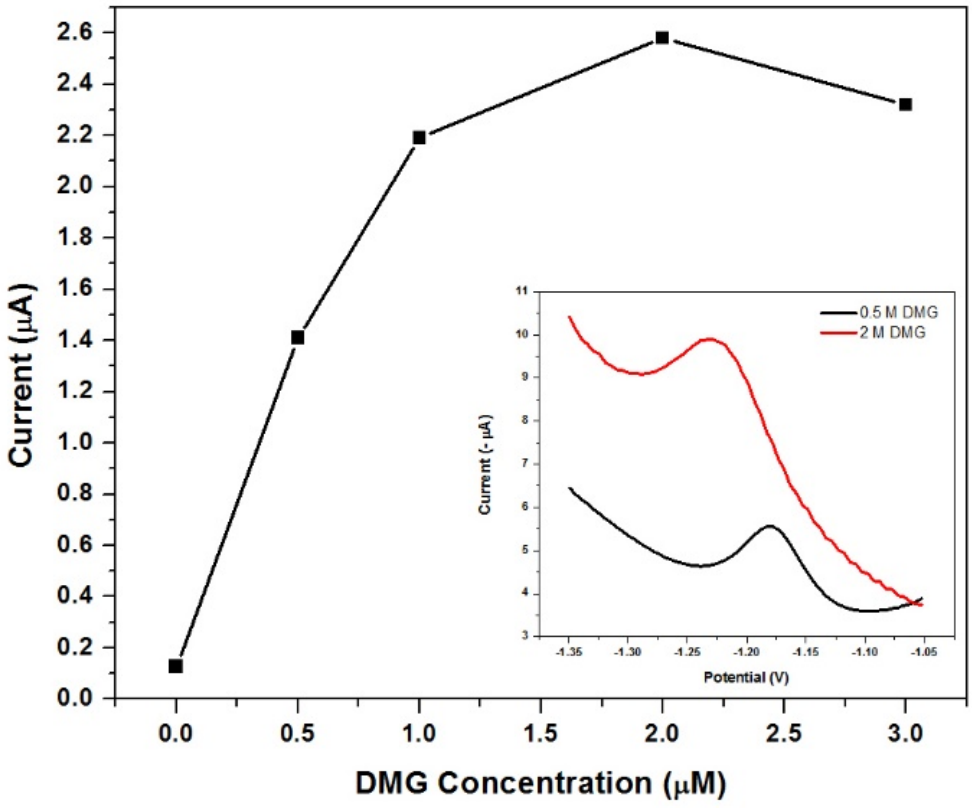

Figure 8.18: Influence of dimethylglyoxime concentration on the [Ni(dmgH)$_2$] complex stripping response.

8.3.4.5. Effect of Hg ion concentration on Ni^{2+} stripping response

Adsorption of formed stable complexes onto an electroplated metallic film is crucial in the development of sensitive adsorptive stripping voltammetric sensors. The effect of Hg ion concentration between 0 and 30 mg L^{-1} Hg, on the stripping response of Ni^{2+} reduction is shown in *Figure 8.19*. A linear increase in cathodic peak current to a maximum is observed for Hg ion concentrations between 0 and 15 mg L^{-1}. Further increases in metal cation concentration increases the thickness of the electrodeposited metallic film layer blocking flow of electrons. A resultant saturation of the electrode takes place and peak currents decrease. A Hg ion concentration of 15 mg L^{-1} was selected for further experimentation.

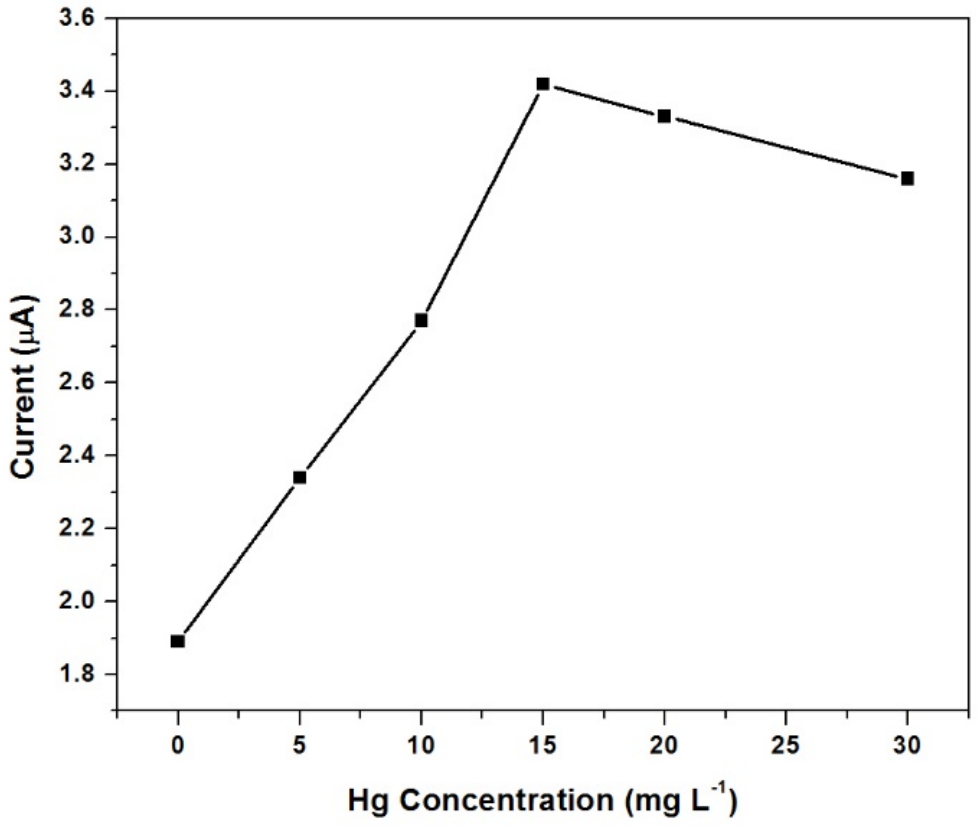

Figure 8.19: Influence of Hg ion concentration on the $[Ni(dmgH)_2]$ complex stripping response.

8.3.4.6. Instrumental parameter optimisation

Instrumental parameters controlling the preconcentration of $[Ni(dmgH)_2]$ complexes at the SPCE surface was optimised in *Figure 8.20*. Deposition/accumulation potential (*Figure 8.20 (a)*) and deposition/accumulation time (*Figure 8.20 (b)*) was studied for their response to 60 μg L^{-1} Ni^{2+} at AuNP-IL-μPEDs in the presence of 2 mM DMG and 15 mg L^{-1} Hg.

The effect of accumulation potential was studied between 0 and – 1.4 V. The stripping response towards Ni^{2+} increased as accumulation potentials approached – 0.7 V. Here, optimum electroplating of metal films and the non-electrolytic adsorption of $[Ni(dmgH)_2]$ complexes onto the electrode surface is achieved. As the reduction potential of Ni^{2+} is approached and surpassed,

reduction of metal cations is performed prior to analysis and is therefore not available for reduction in the cathodic stripping step. An accumulation/deposition potential (E_{acc}) of – 0.7 V was selected.

Optimising the time allowed for accumulation of metal-chelate complexes and deposition of metallic films controls the amount of analyte available for reduction. The accumulation time was investigated between 0 and 180 s. Increasing the accumulation time from 0 to 90 s, showed an increase in cathodic stripping peak current attributed to Ni^{2+} reduction. Changes in stripping response with longer analysis times were minimised due to saturation of the electrode surface. An accumulation time (t_{acc}) of 90 s was selected for all experiments.

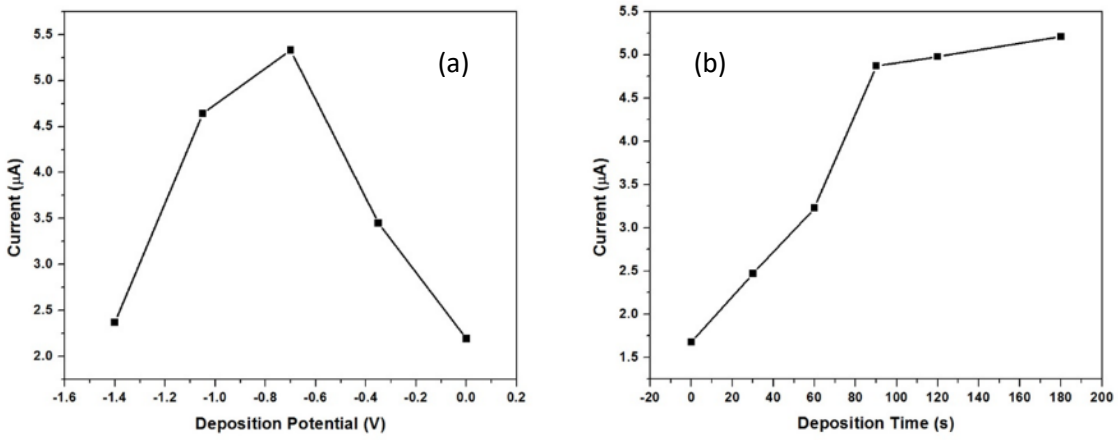

Figure 8.20: Influence of instrumental parameters: (a) deposition potential and (b) deposition time on the stripping peak response of 60 µg L^{-1} Ni^{2+} at AuNP-IL-µPEDs in the presence of 2 mM DMG and 15 mg L^{-1} Hg.

8.3.4.7. Analytical performance of the AuNP-IL-µPED

The AuNP-IL-µPED with impregnated 2 mM DMG and 15 mg L^{-1} Hg, was applied to the quantitative analytical detection of Ni^{2+} by adsorptive cathodic stripping voltammetry (AdCSV). The recorded square-wave voltammograms and corresponding calibration curve for Ni^{2+} ions between 30 – 150 µg L^{-1} in 0.1 M NH_3/NH_4Cl buffer (pH 9.4) as supporting electrolyte is shown in *Figure 8.21*. Well-solved stripping peak currents for Ni^{2+} reduction from the adsorbed $[Ni(dmgH)_2]$ complex is seen at ~ - 1.17 V. An increase in stripping peak current is observed with an increase in Ni^{2+} concentration, as expected for the disposable paper sensors. No shift in

reduction peak potential is observed. A sensitivity of 5.82 x 10^{-8} µA L $µg^{-1}$ was measured over the concentration range under investigation. This value is in the same order of magnitude and in keeping with those calculated in *Chapter 7*. The low correlation coefficient of 0.92 could be improved with improved reproducibility of the sensor. Limits of detection (LOD) were calculated by interrogating the standard deviation of 5 blanks, and dividing it by the slope of the calibration curve (3σ/slope). The calculated limit of detection of the DMG-Hg-AuNP-IL-µPED towards Ni^{2+} analysis was found to be 5.13 µg L^{-1}. The sensitivity, correlation coefficient, limit of detection and limit of quantitation are recorded in *Table 8.3*.

$$\text{LOD/LOQ} = \frac{F \times \sigma}{b} \qquad (\textit{Equation 8.8})$$

Where

LOD: Limit of Detection

LOQ: Limit of Quantitation

F: Factor of 3.3 and 10 for LOD and LOQ, respectively

σ: Standard deviation of the blank, standard deviation of the ordinate intercept, or residual standard deviation of the linear regression

b: Slope of the regression line

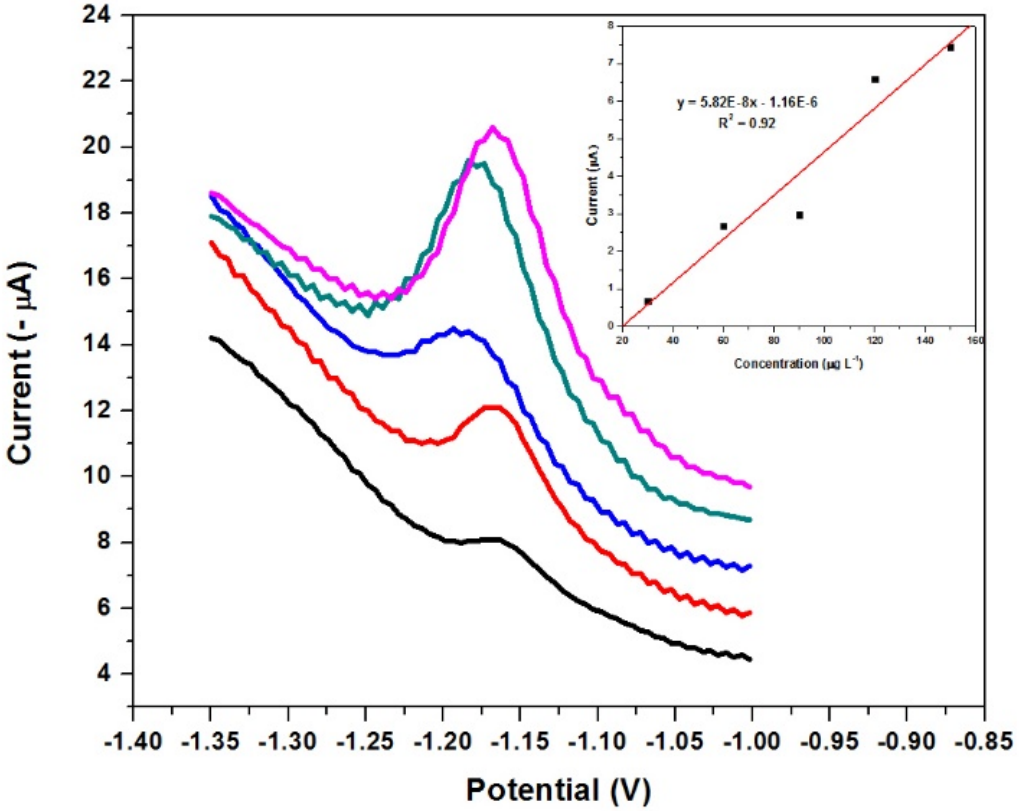

Figure 8.21: SW-AdCSVs of 30 - 150 µg L^{-1} Ni^{2+} in 0.1 M NH_3/NH_4Cl buffer (pH 9.4) as supporting electrolyte containing 2 mM DMG and 15 mg L^{-1} Hg at AuNP-IL-µPED in conjunction with SPCE. E_{acc} = - 0.7 V, t_{acc} = 90 s.

Table 8.3: Sensitivity, correlation coefficient (R^2), detection limit (LOD) and limit of quantitation (LOQ) recorded at AuNP-IL-µPED for Ni^{2+} detection*.

Analytical Parameter	*Analysis of Cu^{2+}*
Sensitivity (µA L $µg^{-1}$)	5.82×10^{-8}
Correlation Coefficient (R^2)	0.92
Detection Limits (µg L^{-1})	5.13 ± 3.74
Limit of Quantification (µg L^{-1})	15.39 ± 8.92

* where, n = 3

The AuNP-IL-µPED in the presence of 2 mM DMG and 15 mg L^{-1} Hg showed accurate limits of detection comparable to those found in literature as seen in *Table 8.4*. The limits of detection were found to be in the same range as those determined in *Chapter 7* at paper based sensors, while approximately 5 – 10 times higher than those conducted at solid electrodes with large volume samples, as expected. The result shows that the AuNP-IL-µPED may be used for Ni^{2+} detection at short analysis times.

Table 8.4: A summary of previously reported sensors and limits of detection (LOD) for Ni^{2+} detection by stripping voltammetric techniques

Metal Ions	Substrate	Technique	Accumulation Time (s)	Dynamic Linear Range ($\mu g\ L^{-1}$)	Detection Limit ($\mu g\ L^{-1}$)	Reference
Ni^{2+}	mpBiF-SPCE	AdCSV	180	1 - 10	0.027	[34]
Co^{2+}				1 - 10	0.094	
Ni^{2+}	RBiABE	DPAdSV	30	0.6 - 41	0.18	[35]
Co^{2+}				0.06 – 4.1	0.018	
Ni^{2+}	PbF-SPE	SWV	60	0.6 – 2.9	0.2	[36]
Co^{2+}				0.6 – 5.9	0.3	
Ni^{2+}	SBVE	SWAdCSV	30	0 - 10	0.6	[37]
Ni^{2+}	DMG-CPE	DPAdSV	120	80 - 600	27	[38]
Ni^{2+}	DMG-N-SPE	DPAdSV	120	60 - 500	30	[39]
Ni^{2+}	ERGO-PG-MFE	SWAdCSV	210	2 - 16	0.12	Chapter 5
Ni^{2+} with Co^{2+} and Zn^{2+}	NGr-DMG-GCE	SWAdCSV	120	2 - 20	1.5	Chapter 6
Ni^{2+}	DMG-Hg-μPPEC	SWAdCSV	90	15 - 90	6.27	Chapter 7
Ni^{2+}	DMG-Hg-AuNP-IL-μPED	SWAdCSV	90	30 - 150	5.13	This Work

8.3.4.8. Real Sample analysis of Ni^{2+} at AuNP-IL- μPED

The accuracy of the developed Ni^{2+} paper-based sensor was investigated by recovery studies. Recoveries of 102.1 % and 94.26 % were calculated in test samples and real tap water samples respectively. Recovery percentages with observed error below 7 % demonstrates the impeccable

accuracy of the AuNP-IL- µPED for 60 µg L^{-1} Ni^{2+}, which is well below the WHO maximum contamination limits.

8.4. Conclusions and Future Work

A novel microfluidic paper-based electroanalytical device (µPED) was developed and applied to the low-volume, accurate and sensitive quantitative analysis of Cu^{2+} and Ni^{2+} by anodic and adsorptive stripping voltammetry respectively. In conjunction with *Chapter 7*, this was the first work performed on the adsorptive stripping voltammetric detection of metal ions at paper-based analytical devices. In addition, formed nanocomposites based on gold nanoparticles and ionic liquids were for the first time used for enhancement of electron transfer kinetics in paper-based electroanalytical devices and presents an exciting possibility for future applications. Typically, dry reagent storage of AuNP, IL, reagents and electrolyte were used. Low limits of detection with good reproducibility and accuracy were found for the AuNP-IL- µPEDs.

References

[1] W. Dungchai, O. Chailapakul, C.S. Henry, Electrochemical detection for paper-based microfluidics, Anal. Chem. 81 (2009) 5821–5826. doi:10.1021/ac9007573.

[2] A. Apilux, W. Dungchai, W. Siangproh, N. Praphairaksit, C.S. Henry, O. Chailapakul, Lab-on-paper with dual electrochemical/ colorimetric detection for simultaneous determination of gold and iron, Anal. Chem. 82 (2010) 1727–1732. doi:10.1021/ac9022555.

[3] N. Ratnarathorn, O. Chailapakul, C.S. Henry, W. Dungchai, Simple silver nanoparticle colorimetric sensing for copper by paper-based devices, Talanta. 99 (2012) 552–557. doi:10.1016/j.talanta.2012.06.033.

[4] N. Dossi, R. Toniolo, A. Pizzariello, F. Impellizzieri, E. Piccin, G. Bontempelli, Pencil-drawn paper supported electrodes as simple electrochemical detectors for paper-based fluidic devices, Electrophoresis. 34 (2013) 2085–2091. doi:10.1002/elps.201200425.

[5] P. Rattanarat, W. Dungchai, D. Cate, J. Volckens, O. Chailapakul, C.S. Henry, Multilayer paper-based device for colorimetric and electrochemical quantification of metals, Anal. Chem. 86 (2014) 3555–3562. doi:10.1021/ac5000224.

[6] J. Shi, F. Tang, H. Xing, H. Zheng, L. Bi, W. Wang, Electrochemical detection of Pb and Cd in paper-based microfluidic devices, J. Braz. Chem. Soc. 23 (2012) 1124–1130. doi:10.1590/S0103-50532012000600018.

[7] Q.-M. Feng, Q. Zhang, C.-G. Shi, J.-J. Xu, N. Bao, H.-Y. Gu, Using nanostructured conductive carbon tape modified with bismuth as the disposable working electrode for stripping analysis in paper-based analytical devices, Talanta. 115 (2013) 235–240. doi:10.1016/j.talanta.2013.04.071.

[8] Z. Nie, C. a Nijhuis, J. Gong, X. Chen, A. Kumachev, A.W. Martinez, M. Narovlyansky, G.M. Whitesides, Electrochemical sensing in paper-based microfluidic devices., Lab Chip. 10 (2010) 477–483. doi:10.1039/b917150a.

[9] A.W. Martinez, S.T. Phillips, M.J. Butte, G.M. Whitesides, Patterned Paper as a Platform for Inexpensive, Low-Volume, Portable Bioassays, Angew. Chemie Int. Ed. 46 (2007) 1318–1320. doi:10.1002/anie.200603817.

[10] W. Dungchai, O. Chailapakul, C.S. Henry, A low-cost, simple, and rapid fabrication method for paper-based microfluidics using wax screen-printing., Analyst. 136 (2011) 77–82. doi:10.1039/c0an00406e.

[11] R. Lu, W. Shi, L. Jiang, J. Qin, B. Lin, Rapid prototyping of paper-based microfluidics with wax for low-cost, portable bioassay, Electrophoresis. 30 (2009) 1497–1500. doi:10.1002/elps.200800563.

[12] M. Liu, C. Zhang, F. Liu, Understanding wax screen-printing: A novel patterning process for microfluidic cloth-based analytical devices, Anal. Chim. Acta. 891 (2015) 234–246. doi:10.1016/j.aca.2015.06.034.

[13] J. Nie, Y. Zhang, L. Lin, C. Zhou, S. Li, L. Zhang, J. Li, Low-Cost Fabrication of Paper-Based Micro fl uidic Devices by One- Step Plotting, Anal. Chem. 84 (2012) 6331–6335.

[14] T. Songjaroen, J. Noiphung, I. Hongwarittorrn, K. Talalak, W. Laiwattanapaisal, Assay time reduction and thermal stability improvement of a low- cost , wax-dipping paper-based microfluidic device, J. Chem. Pharm. Res. 6 (2014) 2895–2903.

[15] K.L. Dornelas, N. Dossi, E. Piccin, A simple method for patterning poly(dimethylsiloxane) barriers in paper using contact-printing with low-cost rubber

stamps, Anal. Chim. Acta. 858 (2015) 82–90. doi:10.1016/j.aca.2014.11.025.

[16] P. de T. Garcia, T.M.G. Cardoso, C.D. Garcia, E. Carrilho, W.K.T. Coltro, A handheld stamping process to fabricate microfluidic paper-based analytical devices with chemically modified surface for clinical assays, RSC Adv. 4 (2014) 37637–37644. doi:10.1039/C4RA07112C.

[17] R.H. Muller, D.L. Clegg, Automatic Paper Chromatography, Anal. Chem. 21 (1949) 1123–1125. doi:10.1111/j.1749-6632.1951.tb48886.x.

[18] D. Delivery, P. Tip, P.M. Device, Chips and Tips, (2016) 3–6.

[19] M.M. Thuo, R. V Martinez, W. Lan, X. Liu, J. Barber, Fabrication of Low-Cost Paper-Based Micro fl uidic Devices by Embossing or Cut-and-Stack Methods, Chem. Mater. 26 (2014) 4230–4237.

[20] X. Fang, S. Wei, J. Kong, Paper-based microfluidics with high resolution, cut on a glass fiber membrane for bioassays., Lab Chip. 14 (2014) 911–5. doi:10.1039/c3lc51246k.

[21] E. Nagles, V. Arancibia, R. Ríos, C. Rojas, Simultaneous Determination of Lead and Cadmium in the Presence of Morin by Adsorptive Stripping Voltammetry with a Nafion – Ionic Liquid – coated Mercury Film Electrode, 7 (2012) 5521–5533.

[22] C.M. Willemse, K. Tlhomelang, N. Jahed, P.G. Baker, E.I. Iwuoha, Metallo-Graphene nanocomposite electrocatalytic platform for the determination of toxic metal ions, Sensors. 11 (2011) 3970–3987. doi:10.3390/s110403970.

[23] K. Pokpas, N. Jahed, O. Tovide, P.G. Baker, E.I. Iwuoha, Nafion-graphene nanocomposite in situ plated bismuth-film electrodes on pencil graphite substrates for the determination of trace heavy metals by anodic stripping voltammetry, Int. J. Electrochem. Sci. 9 (2014) 5092–5115.

[24] G. Zhao, Y. Si, H. Wang, G. Liu, A Portable Electrochemical Detection System based on Graphene/Ionic Liquid Modified Screen-printed Electrode for the Detection of Cadmium in Soil by Square Wave Anodic Stripping Voltammetry, Int. J. Electrochem. Sci. Int. J. Electrochem. Sci. 11 (2016) 54–64. www.electrochemsci.org (accessed April 3, 2017).

[25] H. Bagheri, A. Afkhami, H. Khoshsafar, M. Rezaei, A. Shirzadmehr, Simultaneous electrochemical determination of heavy metals using a triphenylphosphine/MWCNTs

composite carbon ionic liquid electrode, Sensors Actuators, B Chem. 186 (2013) 451–460. doi:10.1016/j.snb.2013.06.051.

[26] R. Liu, C. Lei, T. Zhong, L. Long, Z. Wu, S. Huan, Q. Zhang, A graphene/ionic liquid modified selenium-doped carbon paste electrode for determination of copper and antimony, Anal. Methods. 8 (2016) 1120–1126. doi:10.1039/C5AY02945G.

[27] S. Chaiyo, E. Mehmeti, K. Žagar, W. Siangproh, O. Chailapakul, K. Kalcher, Electrochemical sensors for the simultaneous determination of zinc, cadmium and lead using a Nafion/ionic liquid/graphene composite modified screen-printed carbon electrode, Anal. Chim. Acta. 918 (2016) 26–34. doi:10.1016/j.aca.2016.03.026.

[28] H. Bagheri, A. Afkhami, H. Khoshsafar, M. Rezaei, S.J. Sabounchei, M. Sarlakifar, Simultaneous electrochemical sensing of thallium, lead and mercury using a novel ionic liquid/graphene modified electrode, Anal. Chim. Acta. 870 (2014) 56–66. doi:10.1016/j.aca.2015.03.004.

[29] S. Huang, S. Lu, C. Huang, J. Sheng, W. Su, L. Zhang, Q. Xiao, Sensitive and selective stripping voltammetric determination of copper(II) using a glassy carbon electrode modified with amino-reduced graphene oxide and β-cyclodextrin, (n.d.). http://download.springer.com/static/pdf/243/art%253A10.1007%252Fs00604-015-1627-0.pdf?originUrl=http%3A%2F%2Flink.springer.com%2Farticle%2F10.1007%2Fs00604-015-1627-0&token2=exp=1491222688~acl=%2Fstatic%2Fpdf%2F243%2Fart%25253A10.1007%25252Fs00604-015-1627-0.pdf%3ForiginUrl%3Dhttp%253A%252F%252Flink.springer.com%252Farticle%252F10.1007%252Fs00604-015-1627-0*~hmac=4147fafd5ca100d81220950358c3f0fbaacce8c21f492d3ab50a84cec28fca17 (accessed April 3, 2017).

[30] M.I. Saidin, I. Md Isa, M. Ahmad, N. Hashim, A. Kamari, S.A. Ghani, S.M. Si, Square wave anodic stripping voltammetry of copper(II) at a MWCNT paste electrode modified with a tetracarbonylmolybdenum(0) nanocomposite, Microchim. Acta. 183 (2016) 1441–1448. doi:10.1007/s00604-016-1771-1.

[31] M. Majidian, J.B. Raoof, S.R. Hosseini, R. Ojani, Determination of copper ion by square

wave anodic stripping voltammetry at antimony trioxide-modified carbon nanotube paste electrode, J. Iran. Chem. Soc. (2017). doi:10.1007/s13738-017-1077-1.

[32] P. Markowski, G. Dzido, I. Baranowska, A.B. Jarzębski, Determination of Ag^{+} and Cu^{2+} ions in mixture samples obtained in the microwave assisted polyol process by differential pulse anodic stripping voltammetry (DPASV) method, Open Chem. 13 (2015) 444–450. doi:10.1515/chem-2015-0032.

[33] E.S. Almeida, E.M. Richter, R.A.A. Munoz, On-site fuel electroanalysis: Determination of lead, copper and mercury in fuel bioethanol by anodic stripping voltammetry using screen-printed gold electrodes, Anal. Chim. Acta. 837 (2014) 38–43. doi:10.1016/j.aca.2014.05.031.

[34] S. Dal Borgo, H. Sopha, S. Smarzewska, S.B. Hočevar, I. Švancara, R. Metelka, Macroporous Bismuth Film Screen-Printed Carbon Electrode for Simultaneous Determination of Ni(II) and Co(II), Electroanalysis. 27 (2015) 209–216. doi:10.1002/elan.201400422.

[35] B. Bas, K. Wegiel, K. Jedlinska, The renewable bismuth bulk annular band working electrode: Fabrication and application in the adsorptive stripping voltammetric determination of nickel(II) and cobalt(II), Anal. Chim. Acta. 881 (2015) 44–53. doi:10.1016/j.aca.2015.05.005.

[36] A. Bobrowski, A. Królicka, M. Maczuga, J. Zarębski, A novel screen-printed electrode modified with lead film for adsorptive stripping voltammetric determination of cobalt and nickel, Sensors Actuators, B Chem. 191 (2014) 291–297. doi:10.1016/j.snb.2013.10.006.

[37] G.M.S. Alves, J.M.C.S. Magalhães, H.M.V.M. Soares, Simultaneous Determination of Nickel and Cobalt Using a Solid Bismuth Vibrating Electrode by Adsorptive Cathodic Stripping Voltammetry, Electroanalysis. 25 (2013) 1247–1255. doi:10.1002/elan.201200643.

[38] A. Ferancová, M.K. Hattuniemi, A.M. Sesay, J.P. Räty, V.T. Virtanen, Electrochemical Monitoring of Nickel(II) in Mine Water, Mine Water Environ. (2015). doi:10.1007/s10230-015-0357-1.

[39] A. Ferancová, M.K. Hattuniemi, A.M. Sesay, J.P. Räty, V.T. Virtanen, Rapid and direct

electrochemical determination of Ni(II) in industrial discharge water, J. Hazard. Mater. 306 (2016) 50–57. doi:http://dx.doi.org/10.1016/j.jhazmat.2015.11.057.

Chapter 9 :

Graphene-enhanced Inkjet-printed Silver and Graphene Electrodes for the Detection of Nickel(II)-dimethylglyoxime [Ni(dmgH$_2$)] complexes by Adsorptive Cathodic Stripping Voltammetry (AdCSV)

Abstract:

The development of low-cost and disposable electrode materials has been at the forefront of sensor technologies in recent decades. Paper, offering the possibility for multi-functional, reagent storage, disposable and economically friendly sensing capabilities has proved to be suitable substrate material in paper-based analytical devices (PADs). In this work, we report a simple inkjet printing procedure for the fabrication of single analyte electrochemical sensors on both photographic and chromatographic paper substrates. Three-electrode systems, consisting of a 4 mm diameter working electrode (WE), counter electrode (CE) and reference electrode (RE) were prepared by inkjet printing of silver and graphene inks. In a second step, modification of the working electrode surface with (a) an electrochemically reduced graphene oxide, gold nanoparticle (ERGO-AuNP) film, to improve electrode sensitivity and (b) a nafion dimethylglyoxime carbon black (N-DMG-CB) ink, as an environmentally friendly approach was employed. Electrical and topographical characterization of the printing layers were performed in the fabrication process. Printing of Ag-NP ink showed good resistivity (15 – 25 Ω) on photographic paper and (20 – 30 Ω) for three printed layers on chromatographic paper. The prepared printed paper-based electrodes (PPE) offer quantitative analysis of Ni(II), based on the accumulation of Ni(dmgH)$_2$ complexes at the modified electrode surfaces by square-wave adsorptive cathodic stripping voltammetry (SW-AdCSV). Instrumental parameters including deposition potential and deposition time were optimized for both electrochemical sensors. Improved sensitivities were achieved at the modified integrated electrodes with limits of detection (LOD) of 32.19 and 48.01 μg L^{-1} for the ERGO-AuNP-CC-Ag-PPE and N-CB-DMG-Ag-PPE respectively. This is well below the EPA and WHO standards of 0.1 mg L^{-1} or 0.1 ppm for Ni^{2+} in drinking water.

Keywords:

Inkjet-printing, paper-based microfluidics, metal analysis, adsorptive cathodic stripping voltammetry, graphene, silver nanoparticle, dimethylglyoxime, Nickel, carbon black

Highlights:

- Inkjet printing in conjunction with screen printing techniques was employed towards the development of integrated three-electrode systems on paper substrates
- Simultaneous electrochemical reduction of graphene oxide with gold nanoparticles and a carbon black, dimethylglyoxime complex was employed to enhance electrode sensitivity
- The fabricated, modified paper-based sensors were for the first time successfully applied towards adsorptive cathodic stripping voltammetric (AdCSV) detection of metal ions in water
- Electrodes modified with (a) ERGO-AuNP and (b) N-DMG-CB showed improved sensitivity and detection towards Ni^{2+}
- Sensitive, accurate, disposable and cost effective sensors based on paper substrates were developed with great potential in the field of electrochemical sensing

Graphical Abstract:

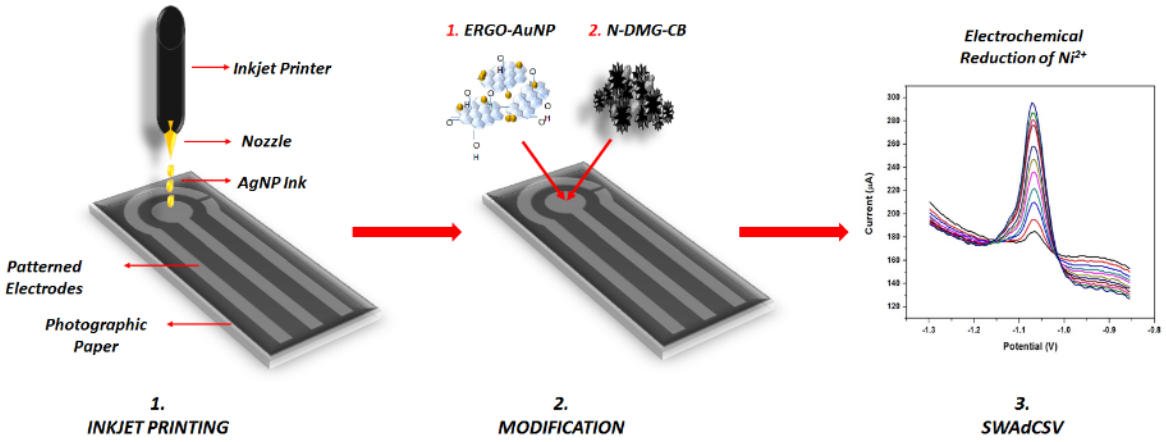

9.1. Introduction

Paper is inexpensive, easily modified, a good filter, biodegradable/disposable, porous and biocompatible, making it the ideal material for analytical applications. Paper-based electroanalytical devices (PEDs) have made tremendous strides in recent times due to their ability to combine the advantageous properties of electrochemical sensing with paper substrates. On-site monitoring of biological and environmental pollutants at PEDs. Although there is great potential for paper substrates as electrochemical sensor devices, improvements in fabrication, analysis techniques, sensitivity and reproducibility are still required to meet the standards set by other known substrates.

A variety of fabrication methods have been studied to develop integrated electrode systems on flexible and paper substrates. Photolithography [1–5], sputtering [6–8], screen printing [9–15], inkjet printing [16–23], hand-drawing [24] etc. have all been investigated to date. Drop on demand inkjet printing has proven to be a low-cost and time-saving alternative to commonly used photolithography [18] due to its ability to accurately pattern substrates by delivering low volume of material without the use of masks.

Carbon nanomaterials have been extensively studied to improve electrode sensitivty due to enhanced electron transfer kinetics and improved surface area-to-volume ratio. Graphene, graphene oxide, carbon nanotubes, carbon black, onion-like carbon and carbon dots have all been incorporated into electrochemical sensing applications.

In this work, inkjet printing of silver and graphene based inks were employed for the development of paper-based three-electrode systems for use in electrochemical metal analysis. A variety of commercial paper substrates, including photographic paper, chromatographic paper and transparency paper were investigated as electrode materials. The fabricated inkjet-printed paper-based sensors were studied for the electrochemical detection of metal ions in water by adsorptive stripping voltammetry. The system is based on the accumulative adsorption of metal-chelate complexes at the surface of an inkjet printed working electrode in conjunction with an in-situ plated metal film.

9.2. Materials and Apparatus

9.2.1. Apparatus

Conventional, low-cost three-electrode electrochemical systems were fabricated by Inkjet-printing of silver and graphene conductive inks. A Fujifilm Dimatix DMP-3281 materials deposition printer was employed for all inkjet printing at the CSIR. All designs were created using eMachineShop free design software in conjunction with DesignCAD. Readily available chromatography paper (Whatman's No. 1, 20 x 20 cm sheets) was purchased from Sigma-Aldrich. Penguin transparencies for mono laser printers (A4, 29.7 x 21.0 cm) and Penguin photo paper, premium hi gloss (A4, 21.0 x 29.7 cm) was obtained from the CSIR. Grey scale tests were performed using an image analysis software, Image J.

All electrochemical voltammetric experiments were performed with a Metrohm Autolab PGSTAT101 instrument, in combination with the Nova 1.11 Software and controlled by a personal computer. All electrochemical experiments were performed in a one compartment 20 mL voltammetric cell at room temperature, unless stated otherwise. A conventional hotplate and vacuum oven, obtained from Labotec was utilised for wax melting and sintering of conductive inks respectively.

9.2.2. Chemicals and Reagents

All chemicals used in the study were of analytical reagent grade. Ultra-pure distilled water (Millipore) was used to prepare all solutions. Harima NPS-JL-nano-silver ink, for low temperature curing was purchased from Harima Chemicals Group. Graphene dispersion, with ethyl cellulose in cyclohexanone and terpineol, inkjet printable was purchased from Sigma-Aldrich. Carbon conductive ink for screen printing was found in our lab. Nafion perfluorinated resin solution 5 wt. % in lower aliphatic alcohols and water and 2,3-Butanedione-dioxime (Dimethylglyoxime) were purchased from Aldrich. Nickel(II), Cobalt(II), Mercury(III) and Gold(III) standard stock solutions (1 000 mg L^{-1}, atomic absorption standard solution) and all other metal standards were obtained from Sigma-Aldrich and diluted as required. Natural graphite powder (microcrystal grade, 99.9995%) (Metal base) UCP1-M grade, Ultra "F" purity was purchased from Alfa Aesar and used for the preparation of graphene oxide (GO) by a modified Hummers method. Carbon

black was obtained from our laboratory. Standard red food colouring, diluted in DI water in a 1:4 ratio was used to test boundary effectiveness. Ammonia/Ammonium Chloride (NH_3/NH_4Cl) buffer solution (0.1 M, pH 9.3) was used as supporting electrolyte and prepared by mixing appropriate quantities of ammonia (NH_3) and ammonium chloride (NH_4Cl). A Metrohm 827 pH lab pH meter was calibrated using pH 4 and 7 calibration buffer solutions and then used to verify the pH of the prepared NH_3/NH_4Cl buffer solution.

9.3. Experimental Methods

9.3.1. Fabrication of Inkjet-Printed Electrodes

Inkjet printing was carried out on a Fujifilm Dimatix materials printer (DMP 3281) at 30 ^oC with a 10 pL drop volume cartridge on a variety of paper substrates. The Dimatix materials printer is a drop-on-demand piezoelectric inkjet printer designed for accurate multi-layer printing. Silver nanoparticle ink, graphene ink and graphene onto silver nanoparticle inks were investigated under optimised printing parameters. *Figure 9.1* shows the patterned three electrode systems, with (a) small and (b) large contacts fabricated by inkjet printing for use with a typical screen printed electrode cable or crocodile clamps respectively. Typically, a 4 mm working electrode, counter and reference electrode, electrical tracks and electrical contacts are illustrated. A variety of line thicknesses and printed layers were studied to achieve the optimum printing results. Post printing sintering at 160 ^oC was conducted to evaporate carrier solvent and additional non-conductive binding materials present in the ink to allow for optimal conductivity due to contact between the metal and carbon materials. Further, screen-printing of conductive carbon ink onto working and counter electrodes was performed in our lab. Carbon ink was diluted to appropriate viscosity and hand-brushed onto working and counter electrodes. The coated electrodes were allowed to dry in a vacuum oven at 85 ^oC for 1 hr. Commercial nail-polish was employed and brushed over electrical tracks on photographic paper to prevent solution flow to electrical contacts. In the case of chromatographic paper, wax printing or simple drawing of hydrophobic barriers by wax crayons was employed.

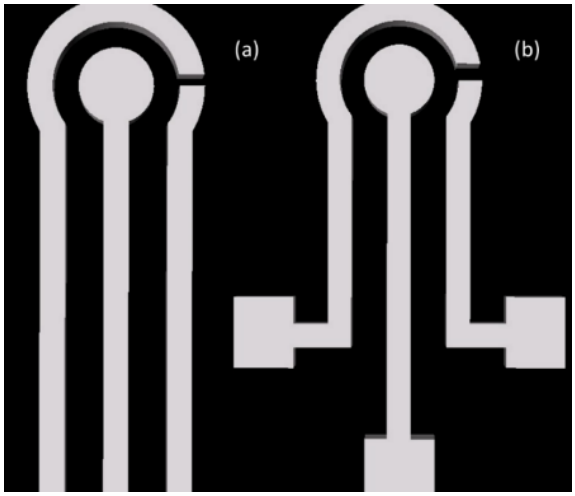

Figure 9.1: Schematic representation of Inkjet-printed three-electrode system designs with (a) small and (b) large contacts for printing on a variety of paper substrates

Scanning electron microscopy was used to study the accuracy of the printing procedure. *Figure 9.2 (a)* demonstrates the HRSEM image of the inkjet printed AgNP working electrode on photographic paper. A clear boundary is developed between the AgNP printed WE and the photographic paper. This finding confirms little spreading of the ink on the hydrophobic paper surface. Distinct patterns with sharp edges and dimensions can thus be achieved. The metallic AgNP appears as clear bright region on the microscope image due to large number of electrons associated with its metallic structure. The AgNPs are coated as a film on the surface of the paper and does not penetrate the substrate material. A smooth, uniform film is patterned on the photographic paper substrate. Small areas of oxidation of the AgNPs is further demonstrated. *Figure 9.2 (b and c)*, shows images of the three-electrode AgNP printed paper electrodes on photographic paper as designed above. Reproducible electrode designs were created by the developed printing procedure. Further, carbon coating of (b) the counter electrode and (c) working and counter electrodes with commercial carbon ink is illustrated.

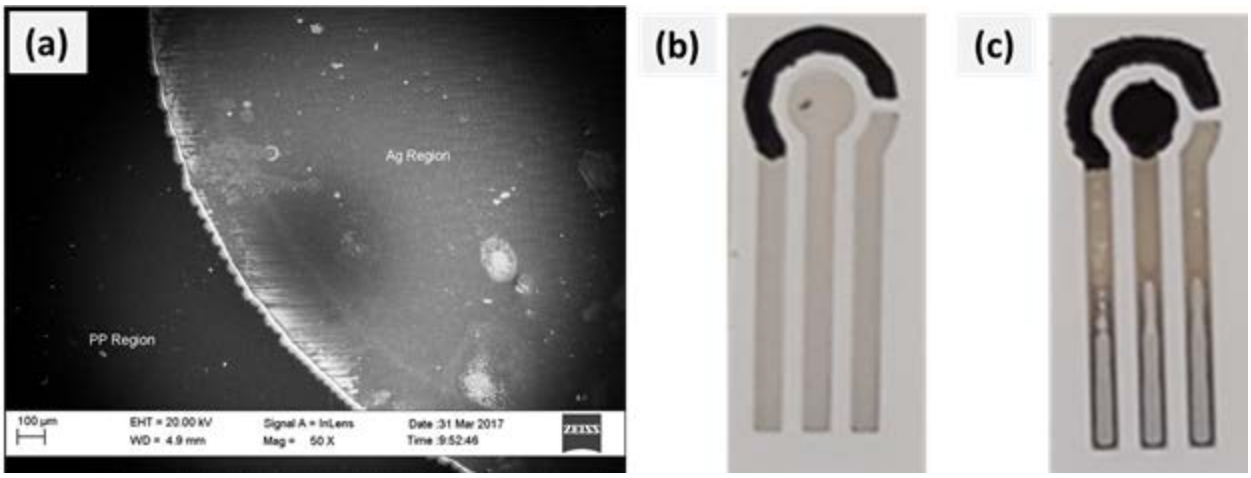

Figure 9.2: HRSEM image of Inkjet printed silver WE on photographic paper and the three electrode system electrodes with carbon coated (b) CE and (c) WE and CE

9.3.2. Preparation of Electrochemically Reduced Graphene Oxide, Gold Nanoparticle, Carbon-coated Silver Printed Paper-based Electrodes (ERGO-AuNP-CC-Ag-PPE)

A modified Hummer's method [25] was employed for the synthesis of graphene oxide (GO) [26] by mixing appropriate quantities of graphite powder, sodium nitrate and potassium permanganate in sulfuric acid. The prepared GO (5 mg) was exfoliated in 10 mL 0.1 M acetate buffer solution (pH 4.6) with 15 ppm Au solutions by ultra-sonication for 1.0 h, prior to use. Prepared carbon coated silver printed paper-based electrodes (CC-Ag-PPE) were immersed in 10 mL of GO-Au solutions (0.5 mg mL^{-1} GO and 15 ppm Au) and cyclic voltammetric reduction was performed under hydrodynamic conditions between -1.4 and 0.5 V [26]. CV parameters: E_{acc} = -1.4 V, t_{acc} = 120 s, f = 50 Hz, *Ampl.* = 40 mV and E_{step} = 4 mV. ERGO-AuNP-CC-Ag-PPEs were dried at room temperature for 30 min prior to use.

9.3.3. Preparation of Nafion, Dimethylglyoxime, Carbon Black, Silver Printed Paper-based Electrodes (N-DMG-CB-Ag-PPE)

Appropriate quantities of carbon black (0.8 g) and dimethylglyoxime (0.2 g) were mixed in a nafion solution (0.2 wt. %, in EtOH) to prepare the nafion-dimethylglyoxime-carbon black (N-DMG-CB) ink. The viscosity of the prepared ink was adjusted using EtOH, if needed. A variety of CB:DMG ratios were prepared as needed. Consecutive, 5 µL aliquots of as prepared N-DMG-

CB ink was drop-cast and screen printed onto the working electrode. N-DMG-CB-Ag-PPEs were dried at 85 ^{o}C for 1.0 h.

9.3.4. Procedure for SW-AdCSV analysis of Ni^{2+}

The N-DMG-CB-Ag-PPE and ERGO-AuNP-CC-Ag-PPE were immersed in a 20 mL electrochemical cell containing 10 mL of (a) appropriate concentrations of Ni^{2+} and (b) appropriate concentrations of Ni^{2+} in the presence of 2 mM DMG and 10 mg L^{-1} Hg^{3+} respectively. *In-situ* simultaneous accumulation of $Ni(dmgH)_2$ onto the working electrode was performed at E_{acc} = -0.7 V and t_{acc} = 120 s. Ammonia (NH_3/NH_4Cl) buffer (0.1 M, pH 9.4) was used as supporting electrolyte. The SWV parameters were as follows: E_{begin} = -0.7 V, E_{end} = -1.35 V, f = 5 Hz and *Ampl* = 10 mV.

9.4. Results and Discussion

9.4.1. Inkjet Printing of Paper-based Electrodes

9.4.1.1. Droplet Formation of Commercial Graphene Ink

Optimisation of printing parameters is an important step in the development of accurate features at the low micron scale. In inkjet printing, the formation of spherical droplets, along with numerous other factors including plating temperature, substrate type, etc. governs the accuracy of the printed tracks. *Figure 9.3*, shows the droplet formation sequence of graphene ink, recorded with the Fujifilm Dimatix Materials Printer camera in a typical deposition sequence. Spherical droplet formation, with a slight tail was achieved at approximately 500 µm from the cartridge nozzle. This allows for the substrate to be placed at a minimum distance of 500 µm from the printer cartridge. Further optimisation of the printing process is required to reduce imperfections such as stray droplets due to the presence of the tail.

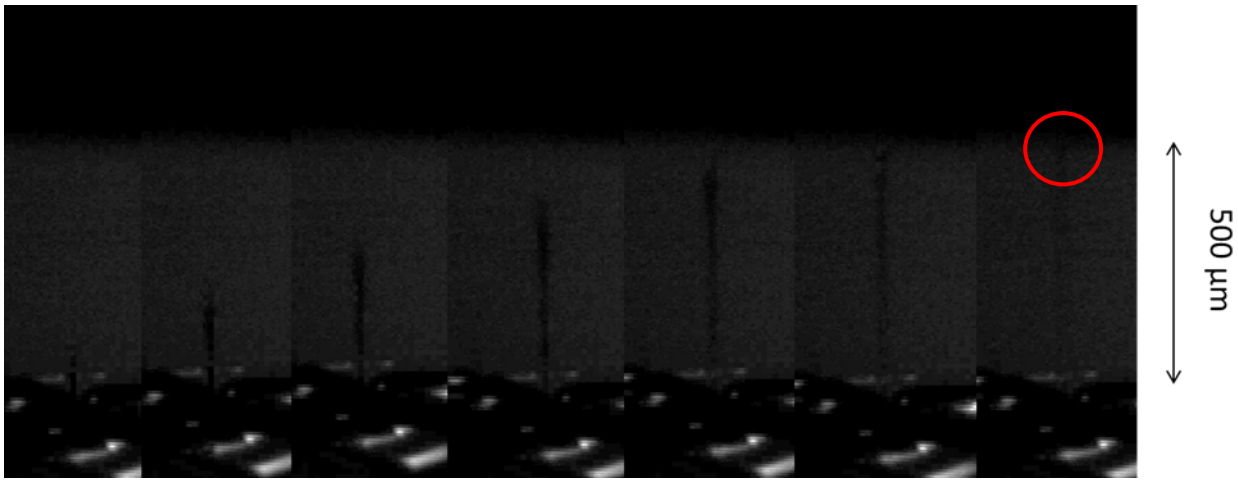

Figure 9.3: Droplet formation sequence of inkjet printing of commercial graphene ink

9.4.1.2. Electrical Characterization of Printed Inks

Thermal sintering processes are an important part of printing of conductive inks. In sintering procedures, printed materials are compacted by thermal processes to form a solid mass. This is achieved by evaporating all non-conductive solvent and additional binder additives resulting in a stacking and contact of conductive particles. A major limiting factor in the use of paper-based substrates however is the maximum temperature the paper can withstand before deterioration. Optimisation of the thermal processes is therefore of great importance.

The effect of sintering temperature of silver and graphene ink on the resistance of single layer printed tracks was investigated between 120 – 200 ^{o}C for penguin photographic paper and the results are recorded in *Figure 9.4* below. Silver ink demonstrated favourable resistance values in the low ohms range for all printed line widths (0.1 – 1.5 mm). The measured resistance decreases with increasing line width for 120, 160 and 200 ^{o}C respectively. Further, a relative levelling of the measured resistance is noted for line widths between 0.5 – 1.5 mm. 0.1 mm line width shows a considerable increase in resistance for all sintering temperatures. This may be attributed to the lack of conductive particles in tracks with small dimensions. Temperatures of 120 and 160 ^{o}C proved to be ideal for thermal sintering with similar measured resistance in the 20 – 35 Ω range. In contrast, a considerable increase in measured resistance is noted for sintering temperatures of 200 ^{o}C as warping and burning of the hydrophobic resin took place. While the recommended sintering temperature for commercial graphene ink is 250 ^{o}C, this was not an appropriate temperature for

any form of paper. Sintering temperatures under 200 ^{o}C were selected for interrogation. Commercial graphene ink used in the study exhibited extremely high resistance (MΩ) for all sintering temperatures under investigation with no discernible trend. This is an unacceptable value for inkjet printing of conductive inks.

Due to the absorbance and spreading properties of chromatography paper, three printed layers were required to demonstrate conductive printed tracks. *Figure 9.5* demonstrates the measured resistance for three layers of printed (a) Ag and (b) graphene as a function of sintering temperature. Silver ink showed measured resistance between 30 and 80 Ω. Comparable trends are observed to photographic paper. 120 ^{o}C provided the lowest resistance values and 0.1 mm line widths were not adequate for printing of conductive tracks. Three printed layers of graphene exhibited resistance values in the MΩ range.

Silver nanoparticle ink proved to be highly conductive on both photographic and chromatographic paper after thermal sintering processes for line widths between 0.5 and 1.5 mm. 120 ^{o}C proved to be a suitable temperature for sintering on both photo and chromatography paper with no deterioration of the paper substrate. Temperatures greater than 160 ^{o}C showed a significant increase in measured resistance. Commercial graphene ink did not show suitable measured resistance for any thermal sintering temperature. This is attributed to the inability to decompose the ethyl cellulose binder present in the graphene ink at temperatures lower than 250 ^{o}C and is therefore not suitable for inkjet printing on paper substrates.

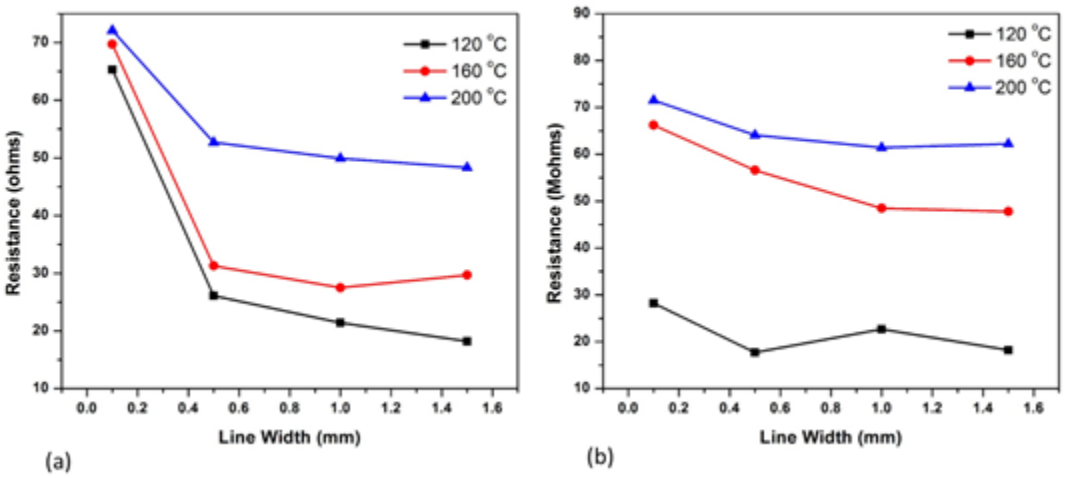

Figure 9.4: Measured resistance of (a) Ag and (b) graphene ink tracks as a function of sintering temperature on photography paper

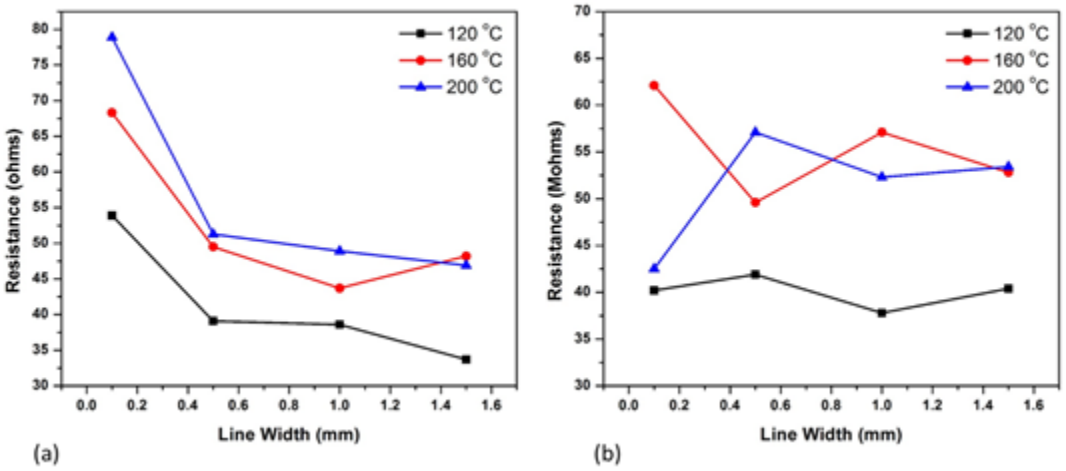

Figure 9.5: Measured resistance of three printed layers of (a) Ag and (b) graphene ink tracks as a function of sintering temperature on chromatography paper

The number of printed layers of silver ink on chromatography paper was investigated between 1 – 3 printed layers. Its effect on the measured resistance before and after curing at 120 ^{o}C for 1 h was recorded in *Figure 9.6*. A single printed layer of silver on chromatography ink shows unacceptable resistance values in the 10- 30 MΩ range when tested directly after printing. Simple room temperature curing however allows the solvent present in the Ag nanoparticle ink to

evaporate allowing conductivity of the single layer Ag ink before curing at approximately 500 Ω. Considerable lowering in measured resistance is further noted due to thermal curing at 120 ºC for 1 h allowing adequate removal of solvent and binding agent present under optimised conditions. A decrease in measured resistance (10 times) can be seen when comparing 1 printed layer to 3 successive printed layers. Three printed layers with curing at 120 ºC for 1 h is therefore ideal for development of Ag NPS-JL printed electrodes.

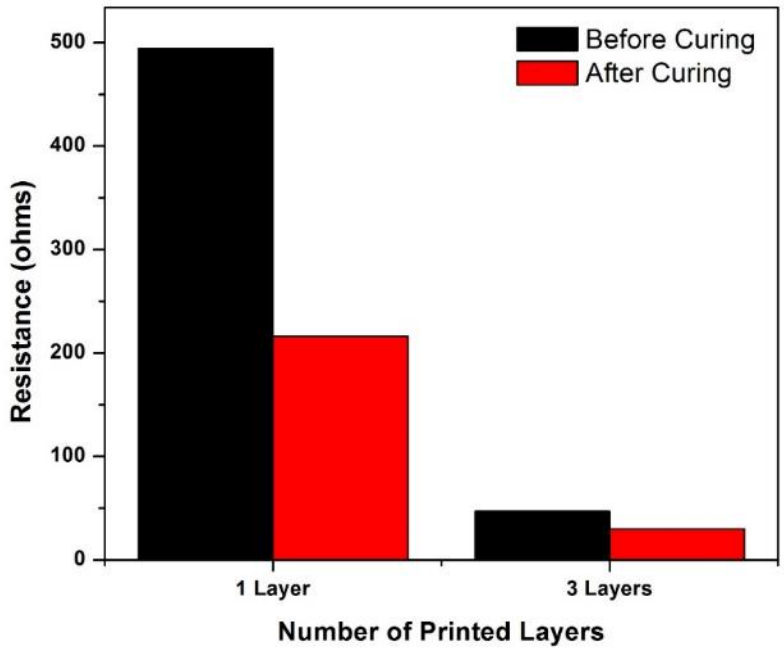

Figure 9.6: Measured resistance as a function of curing at 1 and 3 printed layers on chromatography paper. Curing at 120 ºC for 1 h.

9.4.1.3. Topographical Characterization of Printed Patterns

Microscope images of printed features on photographic paper for (a) silver and (b) graphene after thermal curing are shown in *Figure 9.7* below. Photo paper is commonly used in the development of printed electrodes on paper substrates due to the presence of a hydrophobic resin at its surface. The hydrophobic surface reduces the spreading of ink allowing for more precise droplet formation at the paper surface. As expected, precise and accurate tracks are demonstrated for silver on photographic paper (*Figure 9.7 (a)*), with sharp edges at printed boundaries and few

defects in the printed surface. Some residual ink spatter can be observed at the right edge which may be attributed to non-spherical droplet formation. Striations in the printed pattern occur as a result of printing progression, which is to be expected. In comparison, printing of commercial graphene ink on photo paper (*Figure 9.7 (b)*), demonstrates less accurate edges with an increase in stray droplet formation. In addition, residue of aggregated graphene sheets (black spots) are decorated on the printed surface. Discoloration of the non-printed photo paper was observed for graphene ink. This may indicate spreading of graphene ink within the paper not observed for silver.

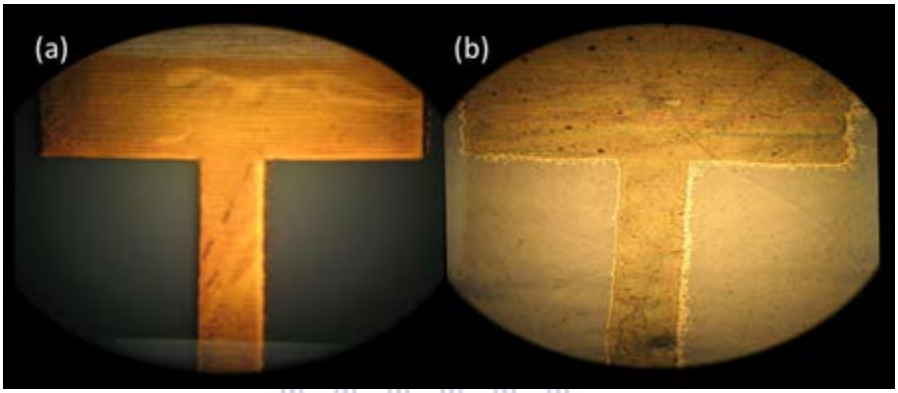

Figure 9.7: Laser images of 0.5 mm (a) silver and (b) graphene features on photographic paper

The topography of the printed layers was further investigated by laser profilometry. Here, cross sections of the recorded laser micrographs provide information on the printed features including surface morphology, topography and printed dimensions. Graphene, and silver tracks were studied and recorded in *Figure 9.8*. Both printed tracks demonstrated clear, distinct and reproducible dogbone patterns with straight lines and hard edges for a single printed layer on photographic paper. Silver (*Figure 9.8 (b)*) provided the best contrast between the substrate surface and printed ink compared to graphene (*Figure 9.8 (a)*) features, attributed to the optimised printing parameters allowing for minimum droplet spreading on the hydrophobic surface. Although graphene too shows clear printed designs on the photographic paper, the low resolution and excessive spreading as indicated by the thick printed channels is a considerable drawback. The well-defined features observed for silver ink is ideal for printing of electronic tracks on paper surfaces.

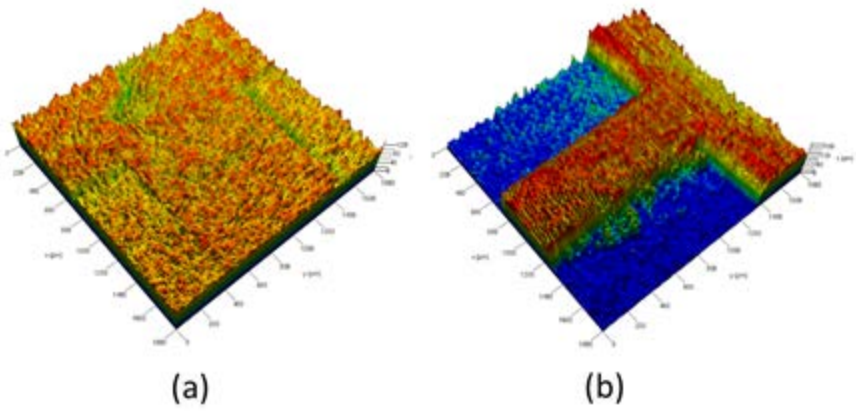

Figure 9.8: Laser micrographs illustrating topography of 0.5 mm printed (a) graphene and (b) Ag features on photographic paper

In the field of paper-based microfluidics, paper with the ability to allow liquid transport by simple wicking or capillary action is an ideal candidate. Whatman No. 1 chromatography paper with a cellulose fibre matrix has been extensively studied in this regard. Laser microscope images of (a) graphene, (b) graphene on Ag and (c) silver on chromatography paper were recorded and compared in *Figure 8* below. Here, clear dogbone patterned structures for 0.5 mm tracks can be seen for all three inks under investigation. Chromatography paper exhibited a porous, woven structure under microscope for all three printed inks with good wetting of the substrate surface compared to photo paper as shown in *Figure 8*. Graphene ink (*Figure 9.9 (a)*) appears black in colour with relatively sharp edges and straight lines for a single printed layer. Ag ink (*Figure 9.9 (c)*), appearing brown or somewhat gold in colour demonstrated similar results to graphene with slightly rounded edges as a result of spreading in the paper substrate. The hydrophilic nature and absorbent properties of the chromatographic paper is in direct opposition to the development of conductive patterns. Printing of graphene onto silver in order to enhance the conductivity of printed graphene electrodes demonstrated two distinct layers on top of one another. Significant spreading is observed due to an excess of ink in the paper resulting in less accurate, larger tracks compared to the graphene and Ag respectively.

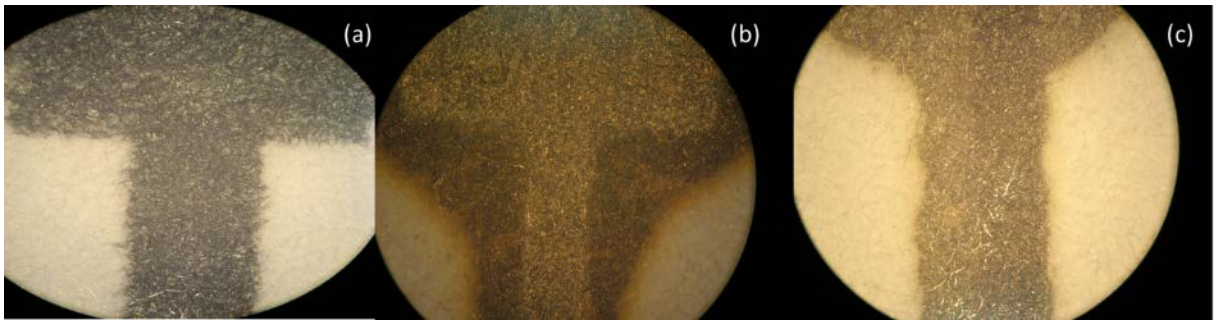

Figure 9.9: Laser images of 0.5 mm (a) graphene, (b) Ag + graphene and (c) Ag features on chromatographic paper

Laser profilometry was utilised for morphological and topographical characterisation of the printed layers on chromatographic paper. Cross sections of the recorded laser micrographs of (a) graphene, (b) graphene on silver and (c) silver single layer printed features of 0.5 mm dimensions are shown in *Figure 9.10*. Similar to printed features on photographic paper, clear distinctions between printed tracks and chromatographic substrates is observed. Relatively straight edges are recorded but slight spreading of inks in the porous hydrophilic cellulose structure is seen. A topographical investigation showed an increase in printed feature height for the two printed layers exhibited from graphene printed on silver compared to single printed tracks. Resolution can thus be improved with increasing printed layers. Small spaces in the printed features of single layers is observed.

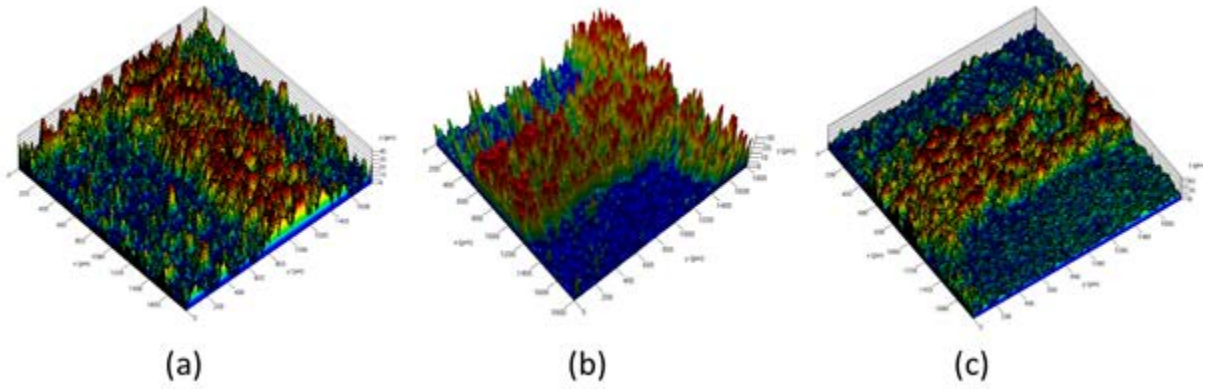

Figure 9.10: Laser micrographs illustrating the topography of 0.5 mm printed (a) graphene, (b) Graphene on Ag and (c) Ag features on chromatography paper

9.4.2. Preliminary Testing of Ag-printed Electrodes

Preliminary electrochemical testing of the inkjet printed photographic paper electrodes (PPPEs) were performed by cyclic voltammetric (CV) analysis in a 5 mM $Fe(CN)_6^{3-/4-}$ solution. The voltammograms, recorded at (a) Ag-PPPE and (b) carbon-coated Ag-PPPE between -1.0 V and 1.0 V at a scan rate of 100 mV s^{-1} are illustrated in *Figure 9.11* below. Electrodes comprised entirely of the Ag-NP three-electrode system demonstrates a large charging or capacitive current (8 and – 10 mA). A single, broad anodic peak is observed at 0.5 V, due to the oxidation of the $Fe(CN)_6^{3-/4-}$ analyte in 0.1 M KCl solution as supporting electrolyte. An absence of the cathodic peak, characterised by the reversible $Fe(CN)_6^{3-/4-}$ redox couple occurs as a result of a current overload experienced at very negative potentials. Further, oxidation and discoloration of the working electrode (WE) surface was discovered (*Figure 9.11, inset*). Carbon coating of the working and counter electrodes (WE and CE) by simple screen printing, significantly lowers the IR difference between the two electrodes. A resultant decrease in capacitive current is experienced compared to the AgNP printed electrodes. A discernible redox couple is observed.

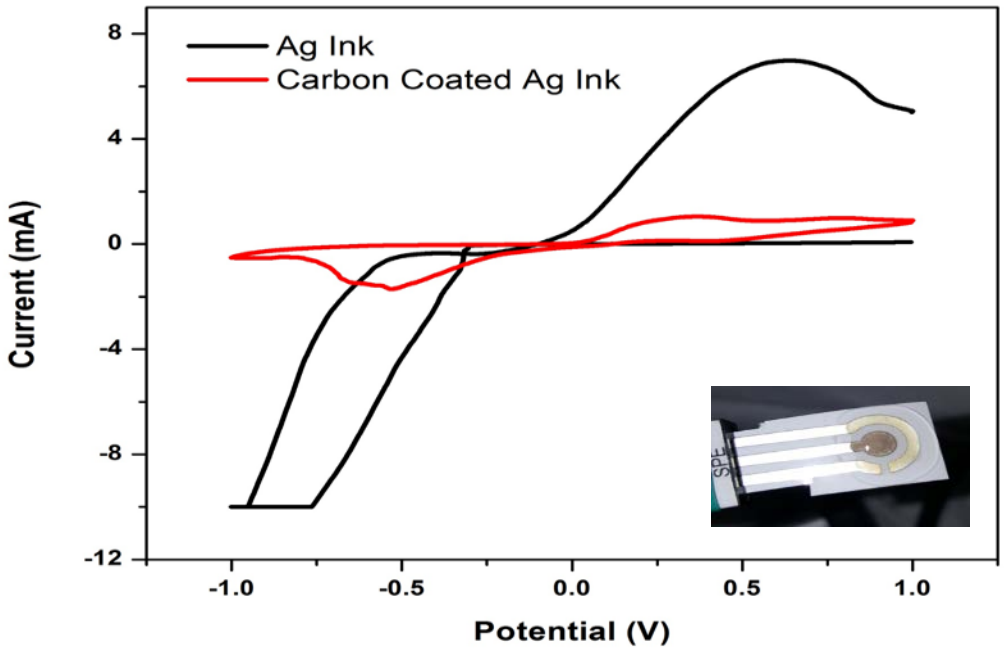

Figure 9.11: Cyclic voltammograms Electrochemical Characterisation of (a) Ag-printed photo-paper electrode and (b) CC-Ag-printed photo-paper electrode in 5 mM $Fe(CN)_6^{3-/4-}$ at scan rate of 10-100 mV s^{-1} in supporting electrolyte (1 M KCl).

9.4.3. Electrochemically Reduced Graphene Oxide – Gold Nanoparticle, Silver Printed Paper-based Electrodes (ERGO-AuNP-CC-Ag-PPE)

The electrochemical deposition and synthesis of electrochemically reduced graphene oxide and gold nanoparticles, followed by its subsequent deposition on the CC-Ag-PPE, by cyclic voltammetry is described in this section. Optimization of electrochemical deposition steps is further studied.

9.4.3.1. Electrochemical reduction of Graphene oxide and gold nanoparticles

Here, a direct electrochemical cyclic voltammetric reduction approach, following a constant potential reduction at – 1.4 V for 30 s was adopted for the preparation of electrochemically reduced graphene oxide, gold nanoparticle (ERGO-AuNP) composite paper-based electrodes. The control attributed to the deposition of graphene sheets on the electrode surface is crucial in the

development of the sensor. *Figure 9.12*, depicts the repetitive (5 cycles) cyclic voltammograms of (a) 0.5 mg mL^{-1} GO suspensions and (b) simultaneous reduction of 0.5 mg mL^{-1} GO colloidal suspensions with 15 ppm Au^{3+} onto carbon-coated silver nanoparticle printed photographic paper electrodes (CC-AgNP-PPPE). The CVs were recorded in the potential window between – 1.5 and 0.5 V. Two anodic (A and B) and three cathodic (A_1, B_1 and C_1) peaks are demonstrated. The redox couple with E_{pa} = 0.136 V and E_{pc} = 0.117 V, denoted by A and A_1 respectively is attributed to the reversible oxidation and reduction of the AgNP WE surface. A reduction in their associated peak currents is observed with an increasing number of scans as graphene sheets are deposited at the electrode surface. The redox couple B and B_1 at E_{pa} = - 0.49 V and E_{pc} = - 0.72 V confirms the deposition of graphene sheets at the electrode surface due to reduction of GO in direct contact with the electrode surface. Electrostatic adsorption binds the formed graphene to the electrode surface. A persistent increase in redox peak current with increasing successive potential cycles. The electrochemical reduction of graphene oxide could be attributed to the negative potentials. The electrochemical reduction of graphene oxide could be attributed to reduction of the functional groups such as – OH and – COOH on the graphene oxide surface. A third reduction peak show at C_1 (- 0.427 V) as a result of reduction of oxygen moieties at the electrode surface is seen. Similar results were obtained in the work by Wu *et al.* [27]. Gold nanoparticles formed within and on top of deposited graphene sheets in order to facilitate the desire reaction. Further studies have been based on the electrochemical reduction of AuNPs in the presence of ERGO [28–32]. An increase in the anodic and cathodic electrode peaks are observed upon inclusion of AuNPs within the ERGO coating in light of enhanced electron transfer of conductive metallic nanoparticles.

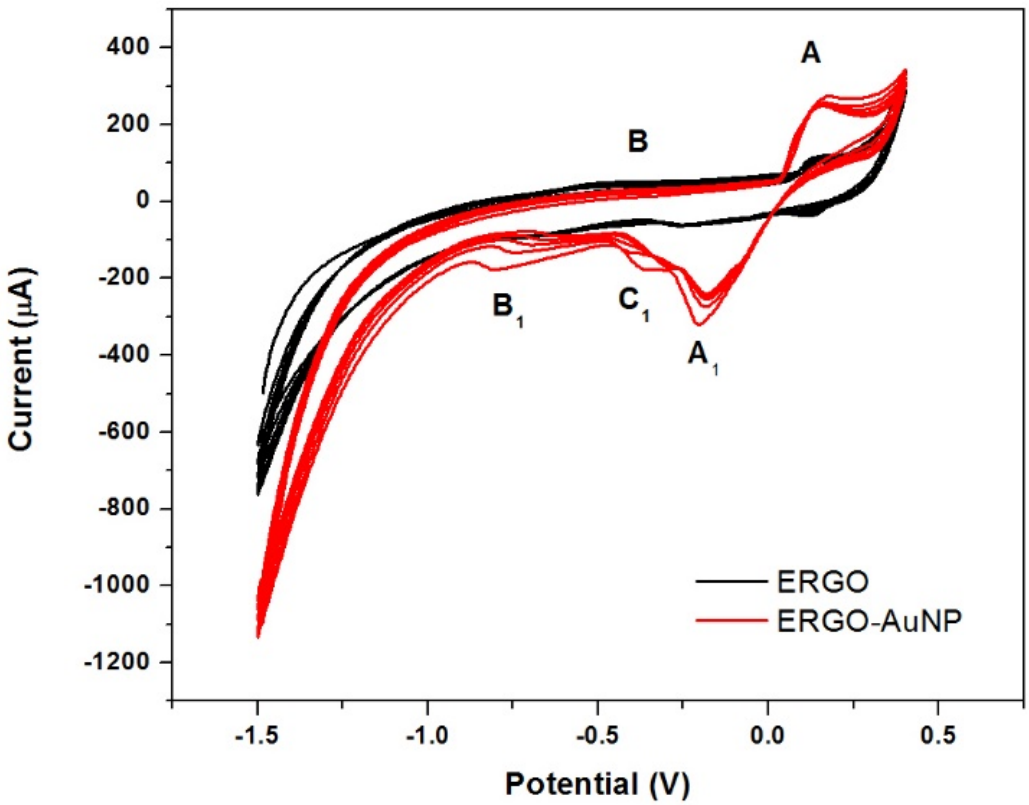

Figure 9.12: Cyclic voltammograms depicting the electrochemical reduction of 0.5 mg mL^{-1} GO and 15 mg L^{-1} Au^{3+} in acetate buffer solution (0.1 M, pH 4.6) at the CC-Ag-PPE under the following instrumental parameters: scan rate (10 mV s^{-1}), deposition time (120 s); frequency (50 Hz); amplitude (0.04 V) and voltage step (0.004 V).

Comparative cyclic voltammograms recorded at the *(a) CC-Ag-PPE, (b) ERGO-CC-Ag-PPE* and *(c) ERGO-AuNP-CC-Ag-PPE* in acetate buffer solution (0.1 M, pH 4.6) are shown in *Figure 9.13*. Carbon coated Ag-PPEs show characteristic voltammograms in the recorded potential window between – 1.5 and 0.3 V. A single oxidation and two reduction peaks are observed between 0.1 and 0.25 V attributed to the redox processes of the AgNP working electrode surface as expected. An increase in peak current as well as an increase in capacitive current is seen upon the formation of a formed graphene film at the electrode surface. Improved electron transfer kinetics and an increase in effective surface area is demonstrated for the ERGO-Ag-PPE. A

dramatic increase in background and AgNP redox peak is shown for incorporation of AuNPs within the reduced graphene oxide sheets as previously discussed. The gold nanoparticles further improved the electron transfer due to its highly conductive nature. The nanocomposite material may therefore be used as an effective means of improving electrode sensitivity.

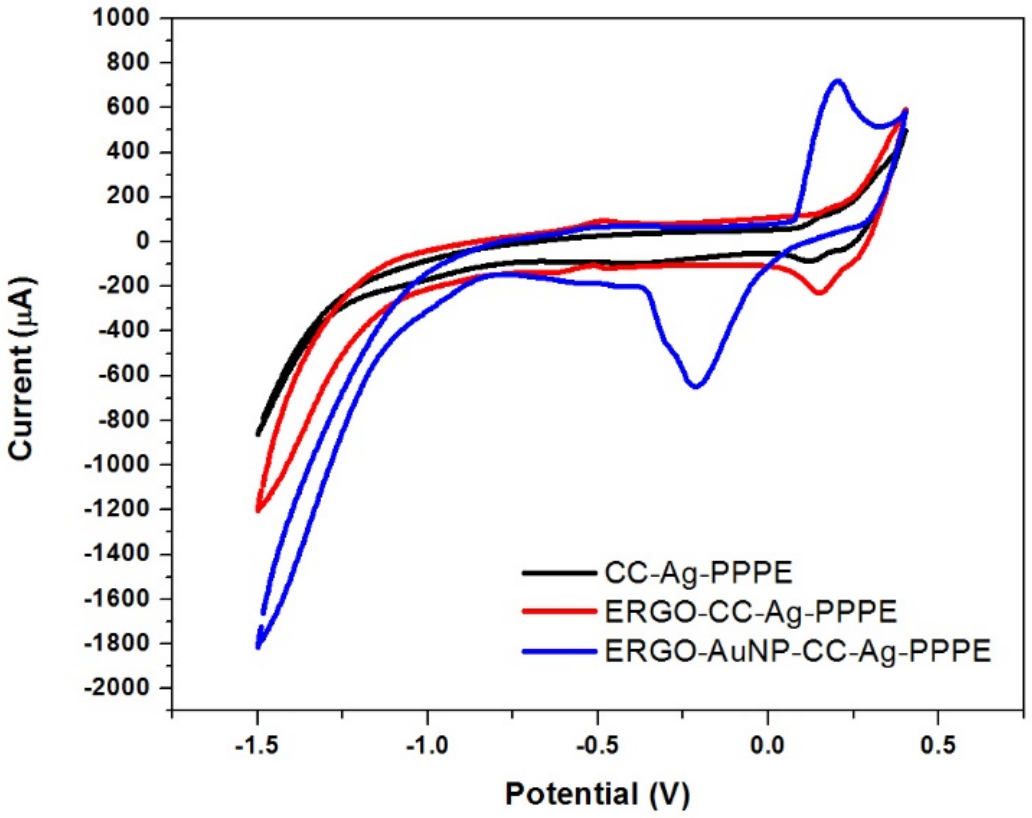

Figure 9.13: Cyclic voltammograms recorded at the (a) CC-Ag-PPE, (b) ERGO-CC-Ag-PPE and (c) ERGO-AuNP-CC-Ag-PPE in acetate buffer solution (0.1 M, pH 4.6) under the following instrumental parameters: scan rate (10 mV s^{-1}), deposition time (120 s); frequency (50 Hz); amplitude (0.04 V) and voltage step (0.004 V).

9.4.3.2. Electrochemical stripping performance of ERGO-AuNP-CC-Ag-PPE towards Ni^{2+} detection

The electrochemical performance of the graphene and gold nanoparticle modified electrodes were investigated towards the detection of [Ni(dmgH_2)] complexes by adsorptive cathodic stripping voltammetry. *Figure 9.14*, depicts the recorded square-wave voltammograms (SWV) of 300 μg L^{-1} Ni^{2+} in the presence of 2 mM DMG and 10 mg L^{-1} Hg^{3+} at (a) CC-Ag-PPPE, (b) ERGO-CC-Ag-PPPE (5 cycles), (c) ERGO-CC-Ag-PPPE (30 cycles), (d) ERGO-CC-Ag-PPPE (50 cycles) and (e) ERGO-AuNP-CC-Ag-PPPE (30 cycles). Reduction of the formed [Ni(dmgH_2)] complex is observed between – 1.0 and – 1.2 V for all modified paper-based sensors. This result correlates well with reported literature values and those recorded in previous chapters for Nickel detection at carbon electrodes and further demonstrates the ability for adsorptive cathodic stripping analysis at printed paper sensors. A small, broad cathodic stripping peak is observed at – 1.14 V for CC-Ag-PPPEs. Modification of the printed sensors with electrochemically reduced graphene oxide with 5 deposition cycles at the reported voltammetric conditions shows little to no variation in peak currents or electrochemical redox potential compared to the carbon coated sensor. Insufficient coating of the carbon surface with graphene is thus achieved, limiting contact between particles to effectively improve electron conduction. An increase in the number of voltammetric cycles up to 30 and 50 deposition cycles, respectively improved the graphene loading at the electrode surface. A 250 % increase in the Ni^{2+} stripping reduction peak was observed with a shift to more positive redox potentials (- 1.08 V) at the ERGO-CC-Ag-PPPE with 30 deposition cycles. Favourable enhancement of electron transfer kinetics and improved electroactive surface area for graphene modification with 30 cycles can be assumed. For graphene loading > 30 cycles, a slight plateau in stripping response is shown and can be seen in *Figure 9.15*. Here, multi-layer graphene sheets are formed and dominate over single- or few-layer graphene flakes inhibiting transfer of electrons responsible for reduction of metal cations. Thirty deposition cycles was therefore chosen as optimum conditions towards [Ni(dmgH_2)] complex detection by AdCSV. Simultaneous electrochemical deposition of ERGO and AuNPs onto the CC-Ag-PPPE surface further improved the peak current response towards Ni^{2+} detection. This outcome was in agreement with hypothesised capabilities of the AuNPs to further improve electron transfer at the electrode surface.

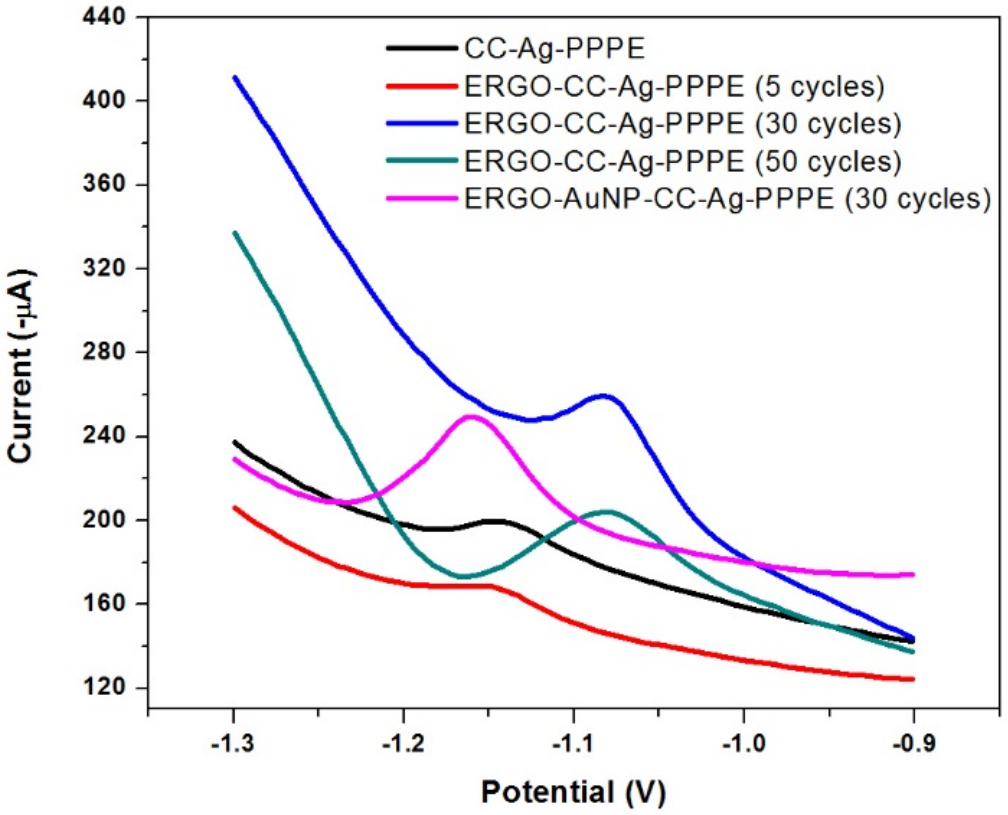

Figure 9.14: SW-AdCSVs of 300 µg L^{-1} Ni^{2+} in the presence of 2 mM DMG and 10 mg L^{-1} Hg^{3+} at (a) CC-Ag-PPPE, (b) ERGO-CC-Ag-PPPE (5 cycles), (c) ERGO-CC-Ag-PPPE (30 cycles), (d) ERGO-CC-Ag-PPPE (50 cycles) and (e) ERGO-AuNP-CC-Ag-PPPE (30 cycles). Supporting electrolyte: 0.1 M NH_3/NH_4Cl buffer (pH 9.4). SWV instrumental parameters: E_{acc} = -0.7 V, t_{acc} = 120 s, f = 5 Hz and *Ampl* = 10 mV.

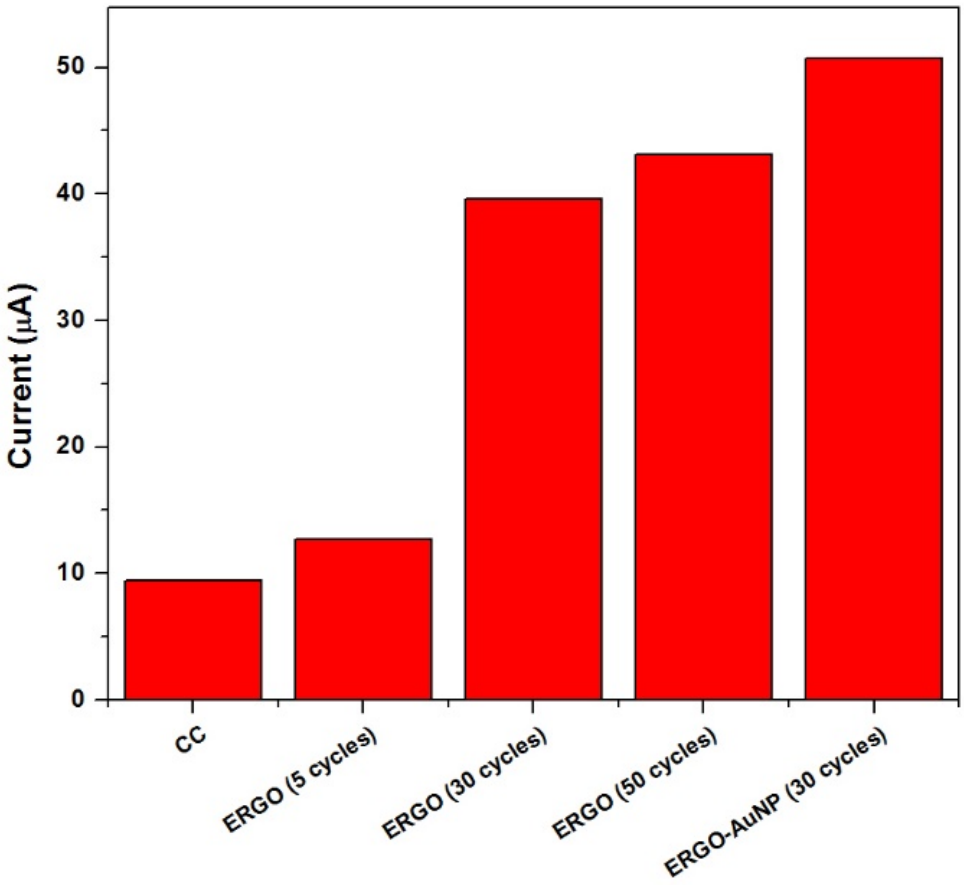

Figure 9.15: A comparison of stripping responses of 300 µg L^{-1} Ni^{2+} in the presence of 2 mM DMG and 10 mg L^{-1} Hg^{3+} at (a) CC-Ag-PPPE, (b) ERGO-CC-Ag-PPPE (5 cycles), (c) ERGO-CC-Ag-PPPE (30 cycles), (d) ERGO-CC-Ag-PPPE (50 cycles) and (e) ERGO-AuNP-CC-Ag-PPPE (30 cycles).

9.4.3.3. Morphological Characterization of ERGO-AuNP-CC-Ag-PPPE

Scanning electron microscopy was utilized to probe the surface morphological changes of the photographic paper along the fabrication routes of the ERGO-AuNP-CC-Ag-PPPE. *Figure 15*, shows the HRSEM images of (a) inkjet printed AgNP, (b) CC-AgNP, (c) ERGO-CC-AgNP and (d) AuNP-ERGO-CC-AgNP working electrodes on photographic paper at 5 kX magnification. The HRSEM image of patterned AgNP features on photographic paper by inkjet printing is shown in *Figure 9.16 (a)*. A smooth, uniform film is observed on the photo-paper substrate. Relative, spherical particles are observed with no defects in the surface morphology. *Figure 9.16 (b)*, shows

flake-like features deposited on the surface of the printed AgNP film. A rough, non-uniform topography is demonstrated. This is attributed to the homemade screen printing technique. Upon electrochemical reduction of 0.5 mg mL^{-1} suspensions of GO in 0.1 M acetate buffer solution (pH 4.6) for 5 cycles, wavy, few-layer sheets of graphene are deposited on the carbon electrode surface (*Figure 9.16 (c)*). The ERGO sheets are decorated across the electrode surface and resemble graphene sheets found in *Chapter 4*. Reduced graphene oxide is bound to the electrode surface by electrostatic attraction. The electrochemical reduction process was repeated in the presence of 15 ppm Au^{3+} and the formed ERGO-AuNP-CC-Ag-PPPE is shown in *Figure 9.16 (d)*. Graphene sheets are deposited on the electrode surface and decorated with AuNPs trapped between graphene sheets.

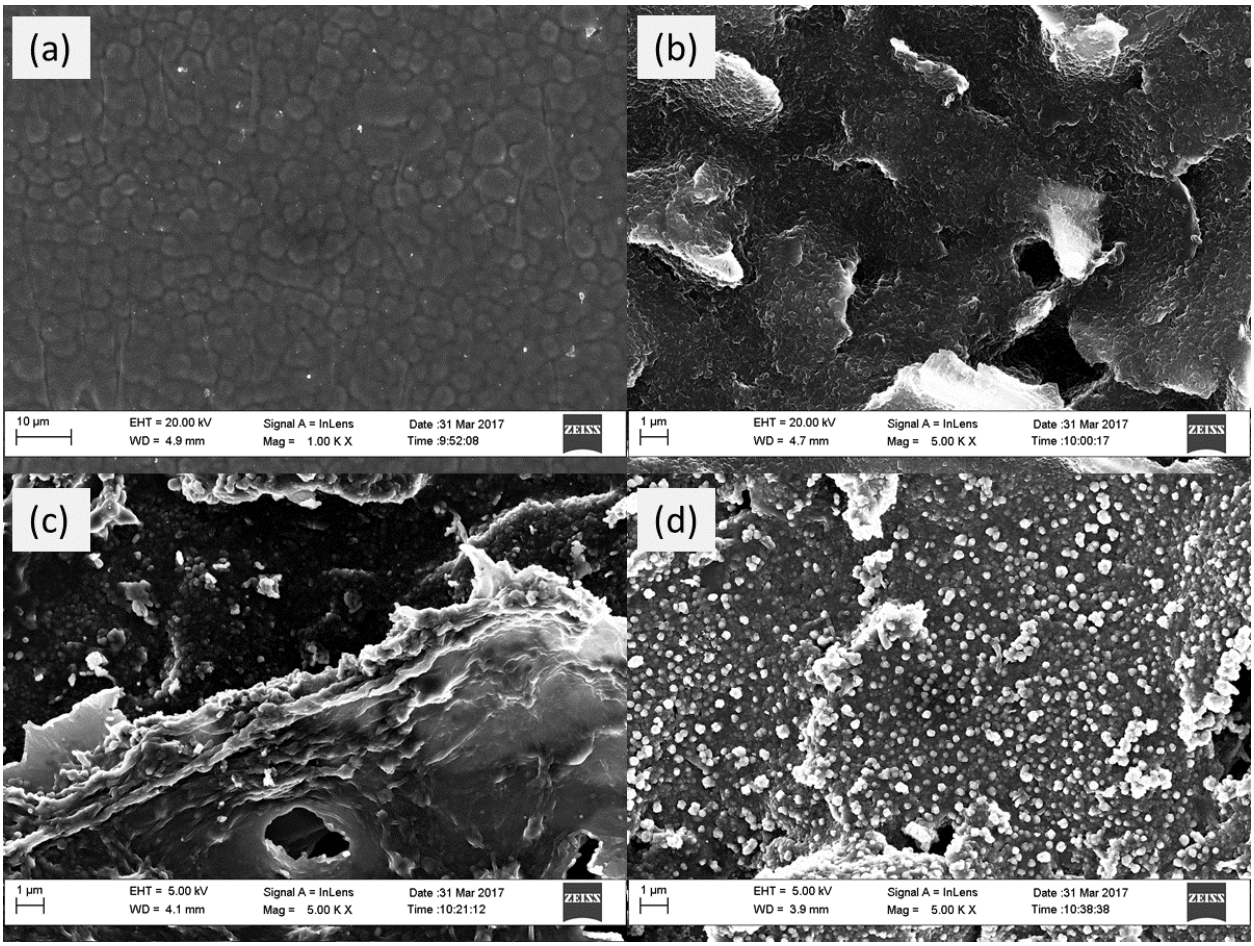

Figure 9.16: High resolution scanning electron microscope (HRSEM) images of (a) inkjet printed AgNP, (b) CC-AgNP, (c) ERGO-CC-AgNP and (d) AuNP-ERGO-CC-AgNP working electrodes on photographic paper at 5 kX magnification.

9.4.3.4. Analytical performance of ERGO-AuNP-CC-Ag-PPPE

Figure 9.17, illustrates the dependence of adsorptive stripping voltammetric (AdSV) peak current response on the incorporation of chelating agent and metallic films at the electrode surface. Square-wave voltammetric responses of 300 μg L^{-1} Ni^{2+} recorded at the ERGO-AuNP-CC-Ag-PPPE in the presence of (a) 0.1 M NH_3/NH_4Cl buffer, (b) 2 mM DMG, (c) 10 mg L^{-1} Hg^{3+} and (d) 2 mM DMG and 10 mg L^{-1} Hg^{3+} are shown. The absence of reduction peaks for buffer and Hg film electrodes, highlight the low sensitivity reduction of Ni^{2+} and its low-solubility in electroplated Hg-films. The inclusion of dimethylglyoxime as chelating agent allows for soluble metal-ligand complex formation and its subsequent adsorption at the electrode surface. A single, reversible, well-defined cathodic peak can be seen at – 1.15 V attributed to the reduction of the [Ni($dmgH_2$)] complex. Further, accumulation of the [Ni($dmgH_2$)] complex at an electroplated Hg-film results in a two-fold increase in the electrolytic Ni^{2+} stripping peak current.

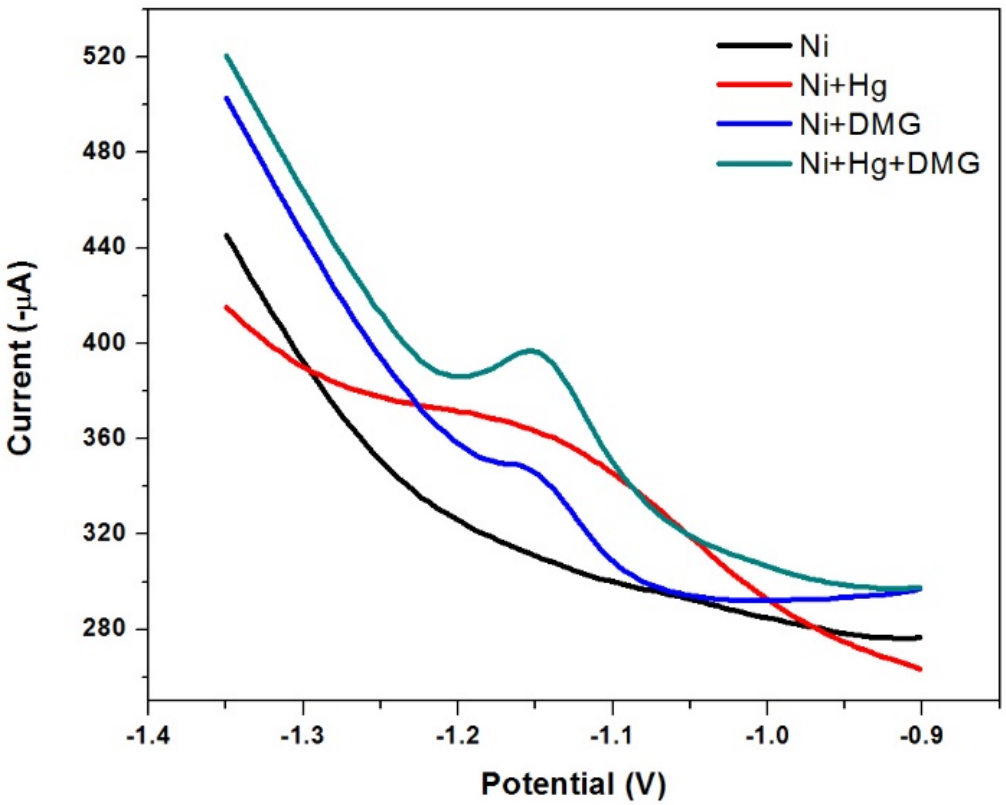

Figure 9.17: SW-AdCSVs of 300 µg L^{-1} Ni^{2+} at the ERGO-AuNP-CC-Ag-PPPE in the presence of (a) 0.1 M NH_3/NH_4Cl buffer, (b) 2 mM DMG, (c) 10 mg L^{-1} Hg^{3+} and (d) 2 mM DMG and 10 mg L^{-1} Hg^{3+}. Supporting electrolyte: 0.1 M NH_3/NH_4Cl buffer (pH 9.4). SWV instrumental parameters: E_{acc} = -0.7 V, t_{acc} = 120 s, f = 5 Hz and *Ampl* = 10 mV.

9.4.3.5. Effect of Chelating Agent Concentration at ERGO-AuNP-CC-Ag-PPPE

Section 9.4.3.5. highlights a clear dependence of metallo-chelate complex formation and its subsequent adsorption onto the working electrode, towards the stripping voltammetric response of Ni^{2+}. The dimethylglyoxime concentration was investigated between 0 and 3 mM and its effect on the stripping peak currents of [Ni($dmgH_2$)] complex reduction recorded in *Figure 9.18*. The absence of DMG prevents the formation of metal-complexes and limits the solubility of the metal cation within the electroplated Hg-film. No stripping response can be seen. Increasing the DMG concentration between 0 and 1 mM, shows a dramatic increase in stripping peak currents up to 90

μA. Adequate ligand is present for complexation to take place and electrode preconcentration improves. Electrode saturation with non-conductive ligand inhibits electron transport through the adsorbed layer and as a result a maximum stripping reduction peak current is achieved at DMG concentrations greater than 1 mM. An increase in DMG concentration no longer affects the observed stripping response. A 2 mM DMG concentration was chosen for all further experiments.

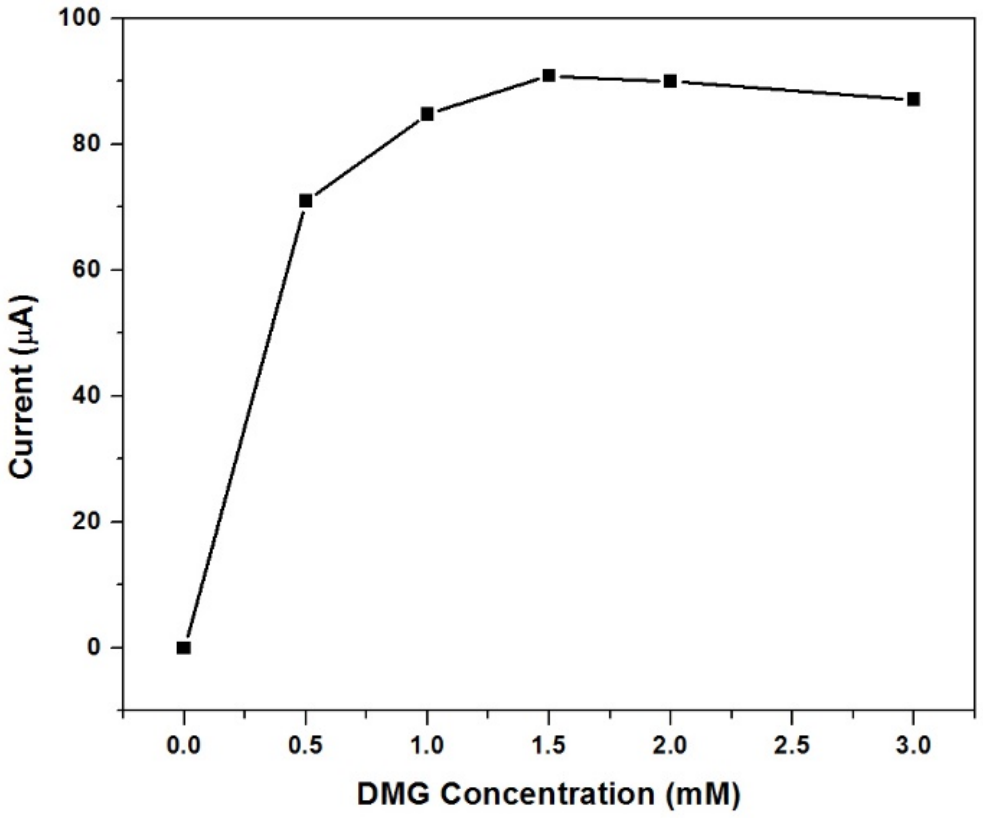

Figure 9.18: Effect of 0 – 3 mM DMG concentration on the stripping peak current response of 300 μg L^{-1} Ni^{2+} at the ERGO-AuNP-CC-Ag-PPPE in the presence of 10 mg L^{-1} Hg^{3+}. Supporting electrolyte: 0.1 M NH_3/NH_4Cl buffer (pH 9.4).

9.4.3.6. Effect of Hg Ion Concentration at ERGO-AuNP-CC-Ag-PPPE

Electroplating of metallic Hg-films at the ERGO-AuNP-CC-Ag-PPPE under constant – 0.7 V accumulation potentials significantly improves the solubility of the formed [Ni($dmgH_2$)]

complex, allowing for enhanced pre-concentration of Ni^{2+} ions at the electrode surface. The effect of Hg ion concentration on the stripping peak current of 300 µg L^{-1} Ni^{2+} at the ERGO-AuNP-CC-Ag-PPPE in the presence of 2 mM DMG, was investigated in the range of 0 – 30 mg L^{-1} Hg concentration. The results are illustrated in *Figure 9.19*. Stripping peak responses increase between 0 and 20 mg L^{-1} Hg concentration, after which saturation of the electrode surface takes place causing a decrease in response. 10 mg L^{-1} Hg concentration was chosen for further experiments.

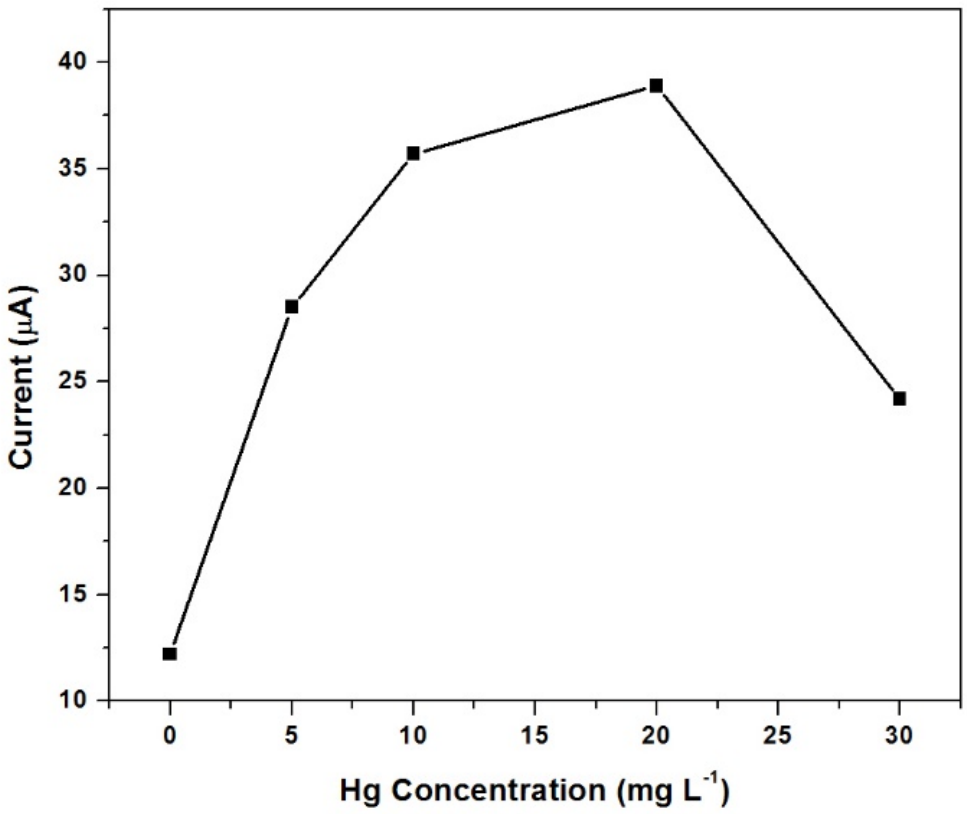

Figure 9.19: Effect of Hg concentration (0 – 30 mg L^{-1}) on the stripping peak current response of 300 µg L^{-1} Ni^{2+} at the ERGO-AuNP-CC-Ag-PPPE in the presence of 2 mM DMG. Supporting electrolyte: 0.1 M NH_3/NH_4Cl buffer (pH 9.4).

9.4.3.7. Optimization of ERGO-AuNP-CC-Ag-PPPE Instrumental Parameters

The effect of deposition potential on the stripping peak current for Ni^{2+} reduction was conducted between 0 and – 1 V and shown in *Figure 9.20, (a)*. Potentials more negative than the reduction potential of Ni^{2+} allowed for best accumulation and pre-concentration of the analyte ions at the electrode surface. A significant independence on metal pre-concentration is observed between 0 and – 0.8 V as indicated by low changes in stripping response. Increasing the deposition potential to more negative potentials (- 1 V), results in reduction of Ni^{2+} to Ni^0 prior to electrode preconcentration. An accumulation potential (E_{acc}) of – 0.7 V was chosen for further studies.

Figure 9.20, (b), depicts the optimisation of accumulation time towards [$Ni(dmgH_2)$] complex detection. A linear increase in stripping peak currents, attributed to Ni^{2+} reduction, is seen over the 0 to 240 s accumulation time range. As expected, increasing the accumulation time increases the amount of [$Ni(dmgH_2)$] complex able to be adsorbed onto the ERGO-AuNP-CC-Ag-PPPE surface. As such, more Ni^{2+} is available for reduction. This increase in pre-concentration improves electrode sensitivity. An accumulation time (t_{acc}) of 90 s was chosen for all further experiments, unless stated otherwise.

Instrumental parameter optimization is crucial in obtaining excellent stripping signals. The effect of stripping reduction peak currents on frequency changes between 0 and 30 Hz is shown in *Figure 9.20, (c)*. A general decrease in stripping response is observed with increasing frequency over the frequency range under investigation. Variations in frequency affect the scan rate in the square-wave stripping voltammograms. A frequency of 5 Hz was selected for further experimentation.

The influence of instrumental amplitude was studied between 0 and 20 mV at the ERGO-AuNP-CC-Ag-PPPE. A linear increase in stripping peak current attributed to reduction of the [$Ni(dmgH_2)$] complex is observed up to 10 mV. At amplitude values greater than 10 mV, a maximum peak current is achieved. An amplitude of 10 mV was selected.

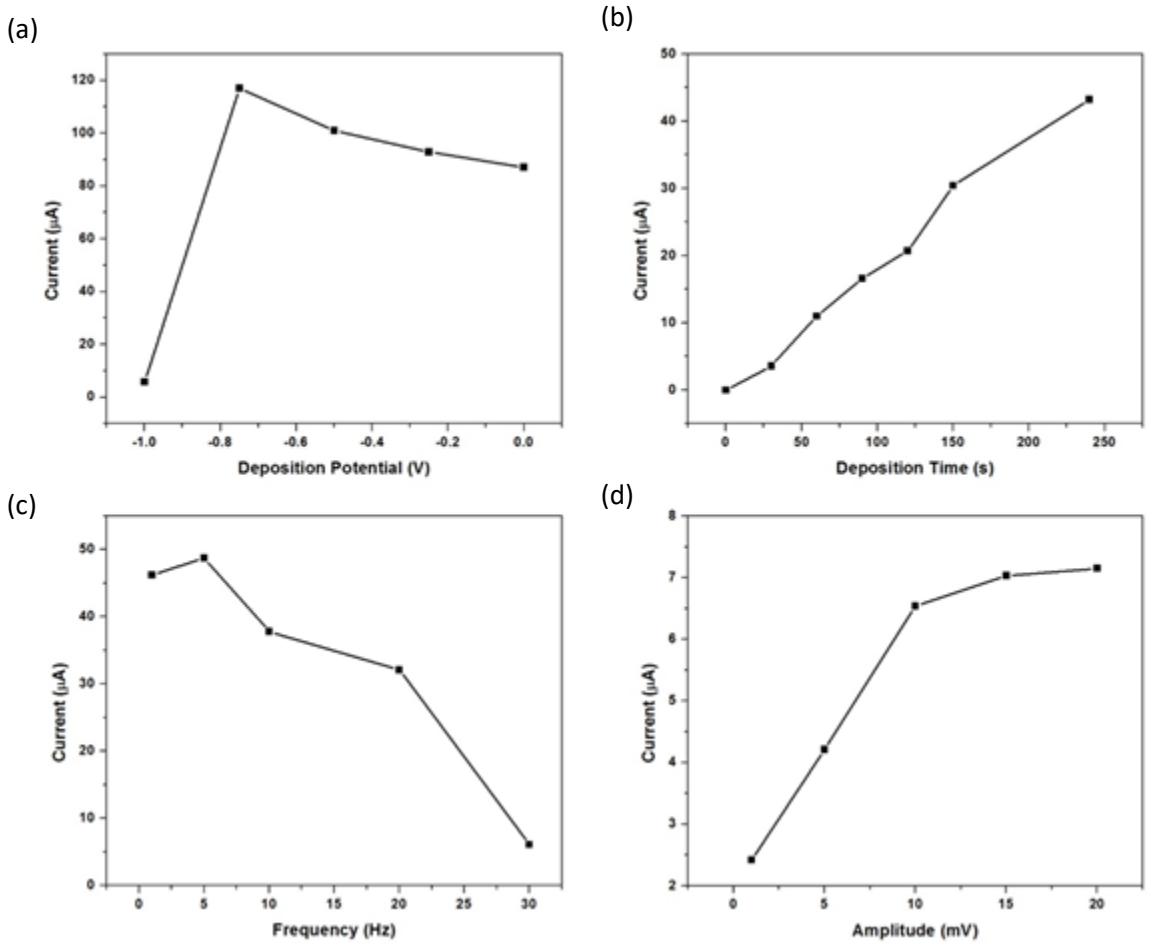

Figure 9.20: The influence of (a) accumulation potential (E_{acc}), (b) accumulation time (t_{acc}), (c) amplitude and (d) frequency on Ni^{2+} peak currents. Sample composition: 300 µg L^{-1} Ni, 2 mM DMG, 10 mg L^{-1} Hg(II), 0.1 M NH_3/NH_4Cl buffer.

9.4.3.8. Calibration Studies at ERGO-AuNP-CC-Ag-PPPE

The analytical performance of the printed paper sensor, modified with electrochemically reduced graphene oxide and gold nanoparticles in the presence of dimethylglyoxime chelating agent and an electroplated metal film was evaluated for Nickel detection in test samples under optimum conditions. The recorded square-wave stripping voltammograms and corresponding calibration plot for the analysis of Ni^{2+} in 0.1 M NH_3/NH_4Cl buffer solution (pH 9.4) containing at a ERGO-AuNP-CC-Ag-PPPE for 90 s are shown in *Figure 9.21*. The performance of the sensor

was investigated in the 50-500 µg L^{-1} range. A linear increase in the Ni^{2+} reduction stripping peak current is observed with increasing concentration of Ni^{2+}. The concentration range under investigation is 10 times higher than those reported in previous chapters and may be attributed to a lack in sensitivity of the printed paper devices compared to that of solid carbon electrodes. A shift to more positive reduction potentials is observed with increasing metal cation concentration. The increase in metal ions in the presence of excess DMG allows for improved [$Ni(dmgH_2)$] complex formation and its subsequent adsorption at the electrode surface. A resultant lowering in IR drop effect is observed and reduction of the adsorbed complex is simplified. Calibration plots were constructed from the recorded square-wave voltammetric data and plotted in *Figure 9.21*. A linear regression of 0.996 was found with good sensitivity (1.38 x 10^{-7} µA L μg^{-1}) over the concentration range under investigation. A dynamic linear range over the 100 – 500 µg L^{-1} Ni^{2+} range was indicated. The detection limit (LOD) of the Ni^{2+} sensor in the presence was determined according to *Equation 9.1*:

$$LOD/LOQ = \frac{F \times \sigma}{b} \quad (Equation\ 9.1)$$

Where

LOD: Limit of Detection

LOQ: Limit of Quantitation

F: Factor of 3.3 and 10 for LOD and LOQ, respectively

σ: Standard deviation of the blank, standard deviation of the ordinate intercept, or residual standard deviation of the linear regression

b: Slope of the regression line

The standard deviation of the blanks was determined from 5 replications of the ERGO-AuNP-CC-Ag-PPPE in 0.1 M NH_3/NH_4Cl Buffer (pH 9.4). Calculated standard deviations were larger than hoped for due to an increase in background current with consecutive runs as previously

stated due to charge build up at the electrode surface. Determined limits of detection were found to be 32.19 µg L^{-1} at an analysis time of 120 s. The results are summarized in *Table 9.1*.

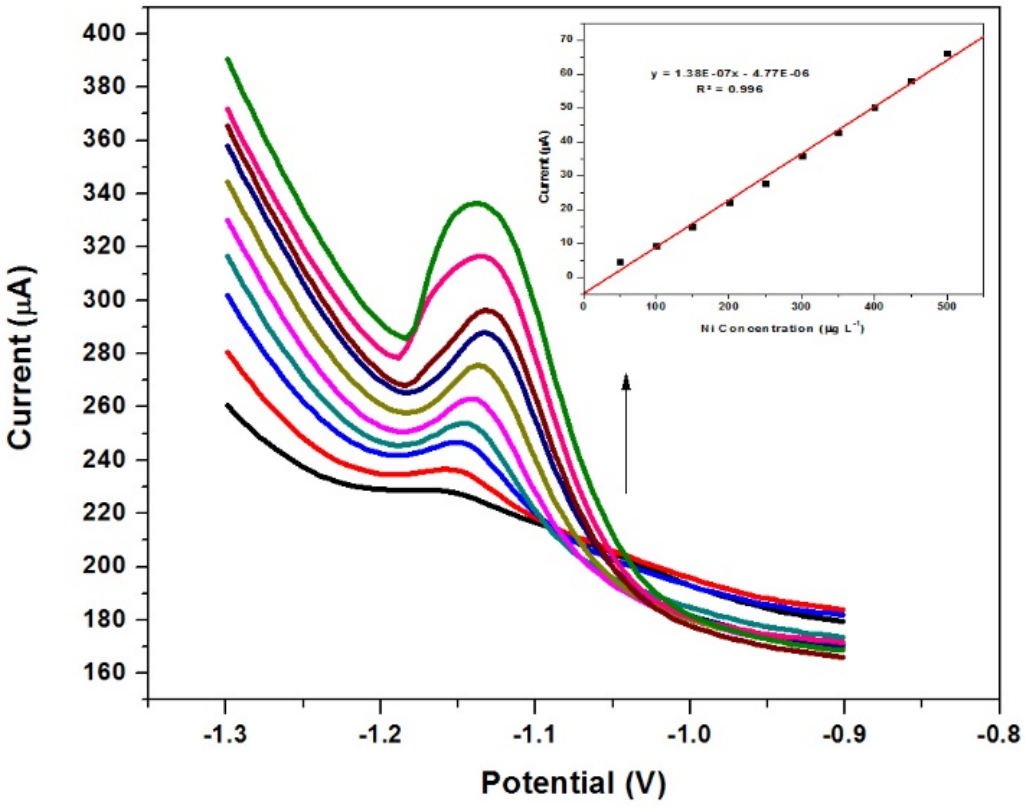

Figure 9.21: SWASV and corresponding calibration plot of individual analysis of Ni^{2+} obtained at ERGO-AuNP-CC-Ag-PPE over 50 – 500 µg L^{-1} range. Supporting electrolyte (0.1 NH_3/NH_4Cl Buffer, pH 9.4), deposition time (90 s), deposition potential (- 0.7 V), rotation speed (1000 rpm), frequency (5 Hz), amplitude (0.01 V).

Table 9.1: A summary of recorded analytical data for the ERGO-AuNP-CC-Ag-PPE over the 50 – 500 µg L^{-1} range*.

Analytical Parameter	*Analysis of Ni^{2+}*
Sensitivity (µA L $µg^{-1}$)	*1.38×10^{-7}*
Correlation Coefficient (R^2)	*0.996*
Detection Limits (µg L^{-1})	*32.19 ± 9.61*
Limit of Quantification (µg L^{-1})	*98.57 ± 26.2*

* where, n = 3

9.4.3.9. Application to Tap Water Samples of the ERGO-AuNP-CC-Ag-PPPE

Tap water samples, collected in our laboratory were applied to the detection of Ni^{2+} ions using the electrochemically reduced graphene oxide, gold nanoparticle modified carbon coated, inkjet printed silver photographic paper electrode (ERGO-AuNP-CC-Ag-PPE) in the presence of chelating agent and electroplated Hg film. A standard addition method was utilised to (a) detect the presence of Ni^{2+} contaminants in the water sample and (b) show that the developed sensor could be applied in the new sample matrix. No metal cations were detected within the working potential window in the tap water sample under the developed sensor conditions. This may be attributed to trace concentrations present below the sensor limits of detection. Upon spiking tap water samples with 150 µg L^{-1} of Ni^{2+} metal cation yielded good recovery percentages for the individual analysis of all three metals ions. The recovery percentages were determined using an extrapolation technique to determine the x-intercept. Spike concentrations were chosen to bring the metal ion concentration into the dynamic linear range of the sensor. A typical standard addition square-wave voltammogram and constructed calibration plot is shown in *Figure 9.22*.

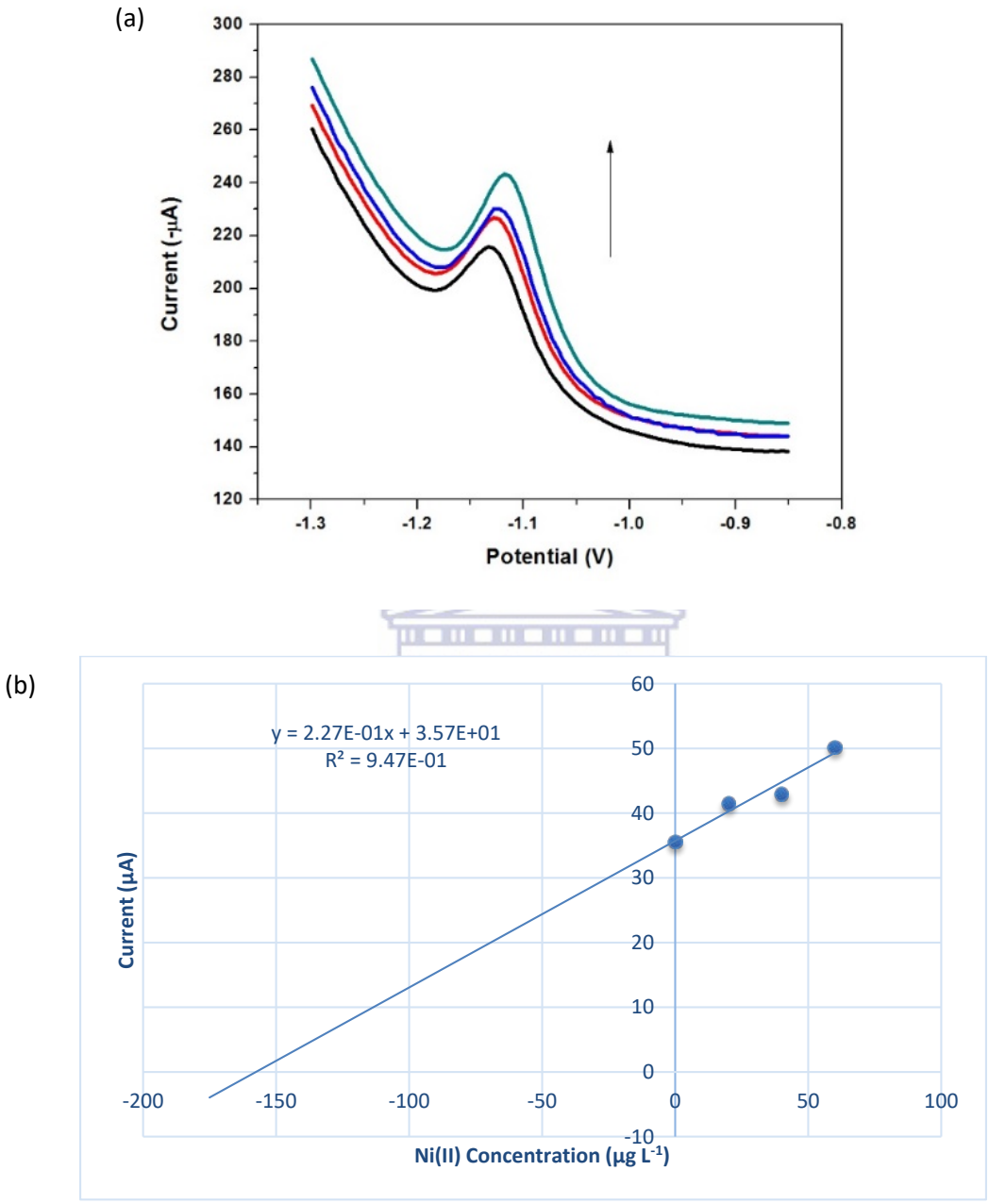

Figure 9.22: Analysis of tap water (pH 9.4) spiked with 150 µg L^{-1} of metal ion in the presence of 2 mM DMG and 10 mg L^{-1} Hg^{3+}. (a) SW-AdSV and (b) Calibration plot. Supporting electrolyte: 0.1 M NH_3/NH_4Cl buffer (pH 9.4). SWV instrumental parameters: E_{acc} = -0.7 V, t_{acc} = 120 s, f = 5 Hz and Ampl = 10 mV.

Table 9.2: Recorded recovery percentages in both test and water samples*.

Ni^{2+} Sample	Original ($\mu g\ L^{-1}$)	Added ($\mu g\ L^{-1}$)	Found ($\mu g\ L^{-1}$)	Recovery (%)
Test Sample	N/D	150	156.48	104.32 ± 7.68
Real Water Sample	N/D	150	138.86	92.57 9.32

* where, n = 3

9.4.3.10. Application of the ERGO-AuNP-CC-Ag-PPPE Towards Co^{2+} Detection

The developed ERGO-AuNP-CC-Ag-PPE sensor was applied towards the detection of Co^{2+} in 0.1 NH_3/NH_4Cl Buffer, pH 9.4 under similar conditions to those proposed for Ni^{2+} detection. As reported in literature and also in the results obtained from *Chapter 5*, the sensitivity of the $[Co(dmgH_2)]$ complex is significantly lower than those obtained for the $[Ni(dmgH_2)]$ above. Amalgam formation of the Co-Hg-complex is limited to its low solubility in the Hg-film, as such a higher concentration was investigated. *Figure 9.23*, shows the recorded voltammograms for $[Co(dmgH_2)]$ complex with Co concentration between 300 – 600 µg L^{-1}. Broad, irreversible peaks are observed between – 1 and -1.25 V, while a slight increase in stripping peak current is achieved before saturation at 500 µg L^{-1}. The paper-based sensor shows low sensitivity and selectivity towards Co detection.

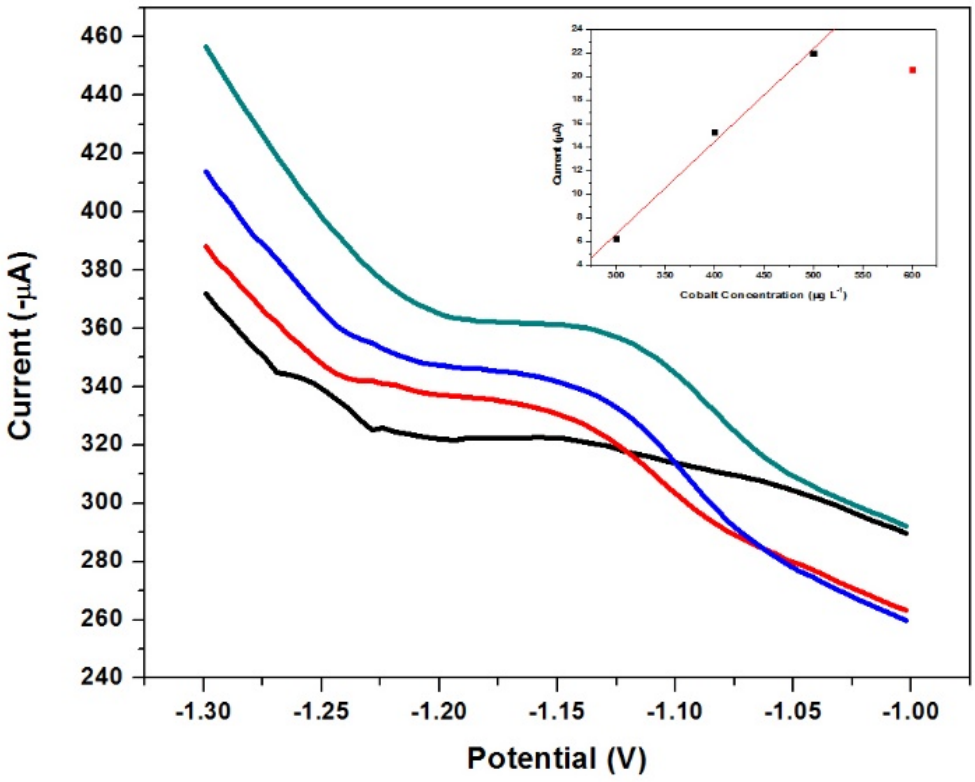

Figure 9.23: SW-AdCSV and corresponding calibration plot of Co^{2+} obtained at ERGO-AuNP-CC-Ag-PPE over 300 – 600 µg L^{-1} range. Supporting electrolyte (0.1 NH_3/NH_4Cl Buffer, pH 9.4), deposition time (90 s), deposition potential (- 0.7 V), rotation speed (1000 rpm), frequency (5 Hz), amplitude (0.01 V).

9.4.4. Carbon Black, Dimethylglyoxime Silver Printed Paper-based Electrodes (CB-DMG-CC-Ag-PPE)

9.4.4.1. Ni^{2+} Detection at the CB-DMG-Ag-PPPE

Silver printed working electrodes have shown low sensitivity towards [Ni($dmgH_2$)] complex detection and a narrow active potential window, as discussed in previous sections. Carbon inks have shown to significantly improve the active potential window and have shown a clear affinity towards the desired application. Carbon black ink, formed from the nanoparticle form of carbon was proposed as ultrasensitive carbon coating material to further improve the electrode

sensitivity of inkjet-printed paper-based sensors in the absence of an electroplated metallic film. *Figure 9.24*, represents typical square-wave adsorptive cathodic stripping voltammograms (SW-AdCSV) for 300 µg L^{-1} Ni^{2+} at the CB-Ag-PPPE and CB-DMG-Ag-PPPE respectively. The CB-Ag-PPPE shows no cathodic stripping peaks in the active potential window between – 0.7 and – 1.3 V in 0.1 M NH_3/NH_4Cl Buffer (pH 9.4) with deposition potential (- 0.7 V), deposition time (120 s), frequency (5 Hz), amplitude (0.1 V) and voltage step (0.005 V). In contrast, the CB-DMG-Ag-PPPE shows a sharp, well-resolved stripping peak at -1.14 V for Ni^{2+} reduction from the formed $[Ni(dmgH_2)]$ adsorption complex at the electrode surface. Immobilisation of the chelating agent at the electrode surface in conjunction with high active surface area and conductive carbon nanoparticles provides sensitive and selective detection of Ni^{2+} cations as previously shown in *Chapter 6*. The overall electrolytic reaction may be described in the two-step process below, as previously discussed:

$$Ni^{2+} + 2\ dmgH_2 + 2\ OH^- \rightarrow [Ni(dmgH)_2] + 2\ H_2O \quad \text{Pre-concentration Step} \quad (9.2)$$

$$[Ni(dmgH)_2] + 10\ e^- + 10\ H^+ \rightarrow Ni^{2+} + 2\ DHAB \quad \text{Stripping/reduction step} \quad (9.3)$$

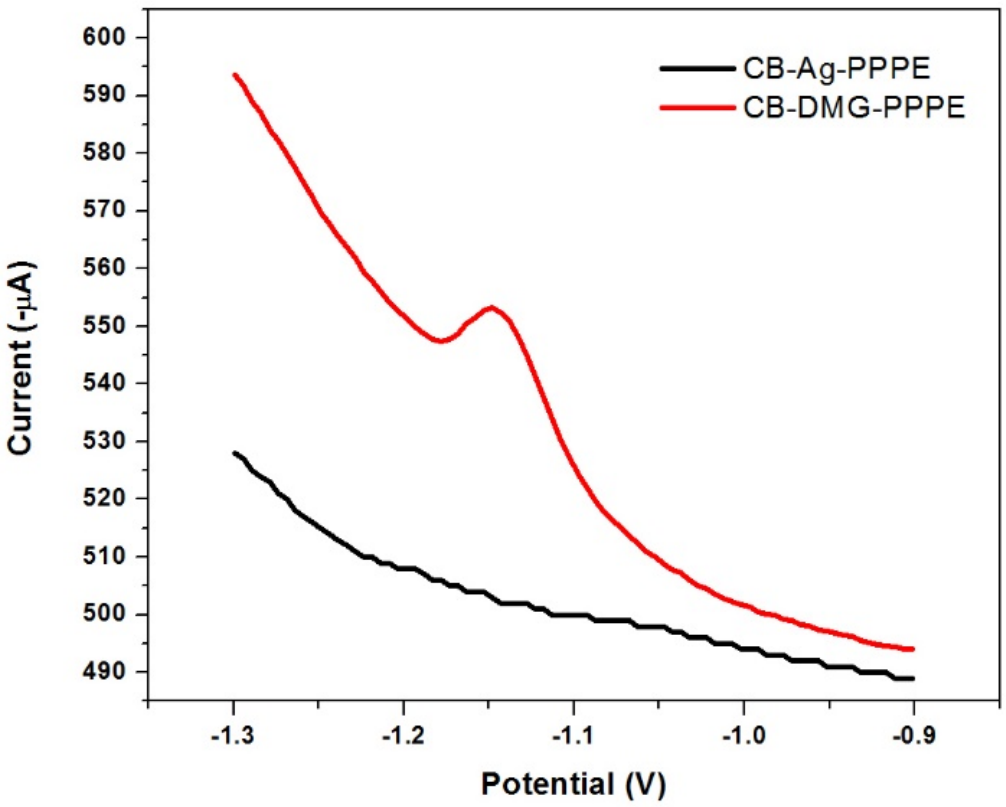

Figure 9.24: SW-AdCSV of 300 µg L^{-1} Ni^{2+}, obtained at the (a) CB-Ag-PPPE and (b) CB-DMG-Ag-PPPE. Supporting electrolyte (0.1 NH_3/NH_4Cl Buffer, pH 9.4), deposition time (90 s), deposition potential (- 0.7 V), rotation speed (1000 rpm), frequency (5 Hz), amplitude (0.1 V).

9.4.4.2. Influence of Chelating Agent Concentration in CB-DMG Ink

It has been shown in previous sections that the detection of Ni^{2+} is highly dependent on the formation of the [$Ni(dmgH_2)$] and its subsequent adsorption onto the working electrode surface. From *Chapter 6*, a sensitive technique could be established by immobilisation of the chelating agent at the electrode surface, simplifying the stripping voltammetric mechanism. Here, its application at printed paper electrodes was achieved. Optimisation of the dimethylglyoxime loading within the prepared carbon black ink (CB:DMG) are illustrated in *Figure 9.25* below. The CB:DMG ratios were varied between 1:0, 1:4, 1:2 and 1:1 and its effect on the stripping voltammetric peak currents were investigated towards 300 µg L^{-1} Ni^{2+} detection by AdCSV. The

absence of chelating agent (CB:DMG, 1:0) prevents adequate pre-concentration of Ni^{2+} at the electrode surface and no cathodic stripping peak is observed, as previously stated. Addition of DMG chelating agent at the working electrode facilitates adsorption of metal cations onto the electrode surface and the subsequent formation of metallo-chelate complexes. Ni^{2+}, present in larger concentrations can now be reduced and a stripping peak current achieved. The inclusion of more non-conductive DMG inhibits electron flow and a decrease in the measured peak current is seen. A 1:4 ratio of CB:DMG yielded the optimum stripping peak currents and was therefore selected for all further experiments.

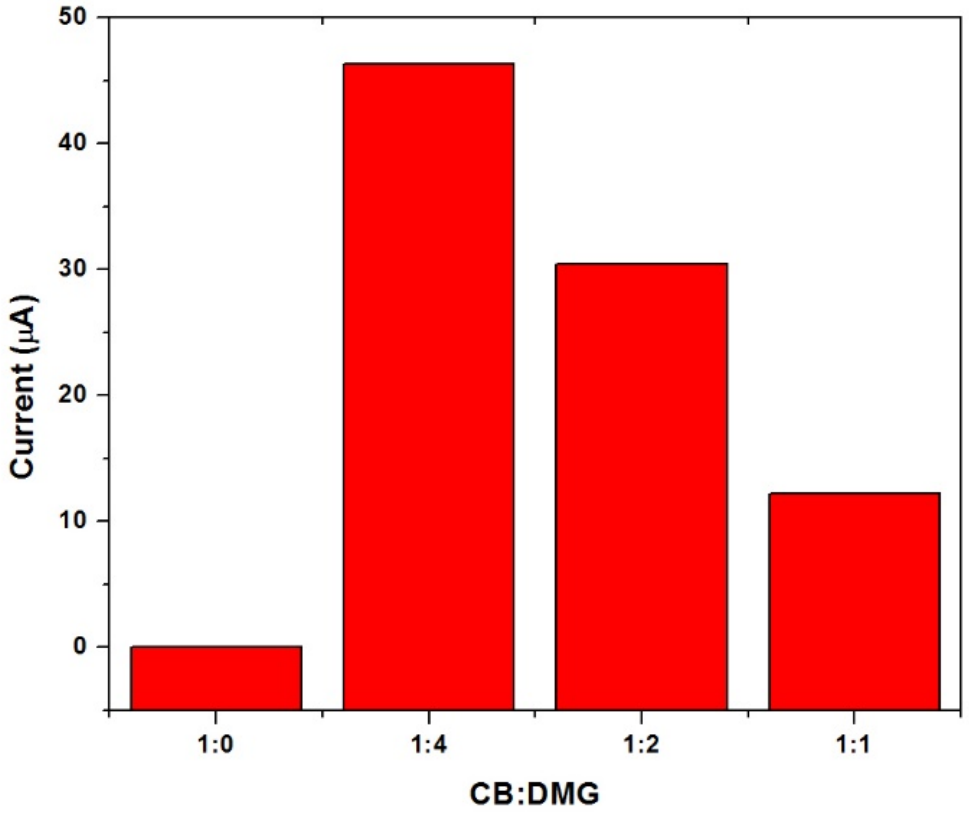

Figure 9.25: Influence of DMG loading within carbon black inks on the stripping peak current of 300 μg L^{-1} Ni^{2+}.

9.4.4.3. *Morphological Characterization of CB-DMG-Ag-PPPE*

The morphological characterization of the prepared electrodes was studied by scanning electron microscopy. *Figure 9.26,* shows the HRSEM images of (a) unmodified inkjet printed AgNP electrode, (b) carbon black modified Ag-electrode and (c) dimethylglyoxime, carbon black Ag-electrode. The HRSEM image of the unmodified AgNP electrode shows a uniform film of spherical Ag nanoparticles deposited on the photographic paper substrate. An even coating with no distinct defects in the printing process is observed. *Figure 9.26 (b),* demonstrates 'bushy' aggregates of carbon black particles deposited on the silver WE surface. Carbon black particles with an average particle size of ~ 80 nm are observed. Upon inclusion of dimethylglyoxime chelating agent in a 1:4 ratio, crystalline deposits can be seen within the carbon black film as indicated in *Figure 9.26 (c)* and confirms the formation of the CB-DMG composited electrode.

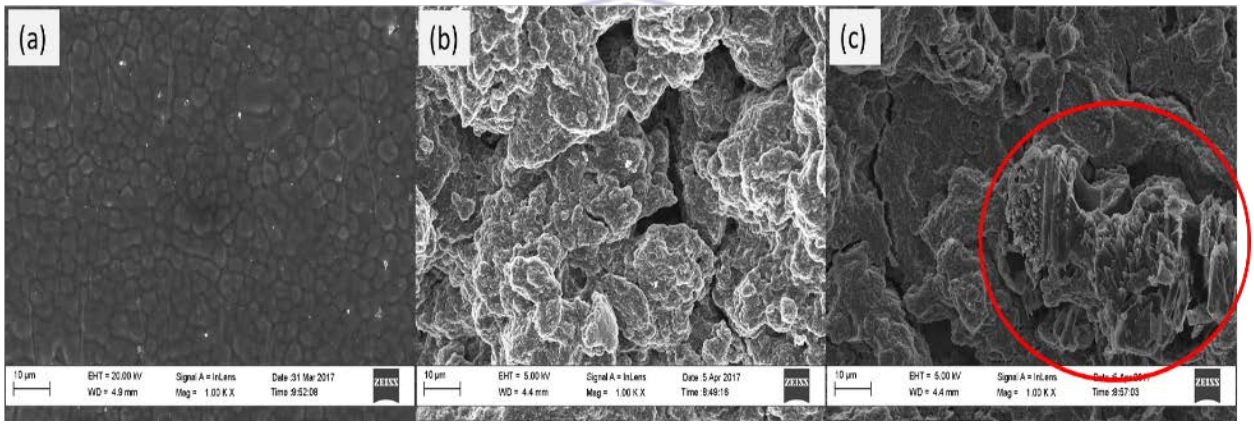

Figure 9.26: High resolution scanning electron microscope images of (a) inkjet printed AgNPs, (b) CB-AgNP and (c) DMG-CB-AgNP working electrodes on photographic paper at 1 kX magnification.

9.4.4.4. *CB-DMG-Ag-PPPE Instrumental Parameter Optimization*

The square wave instrumental parameters affecting the analytical response of the CB-DMG-Ag-PPPE; namely deposition potential, deposition time, frequency and amplitude were optimized and illustrated in *Figure 9.27.*

The influence of deposition potential on the stripping response of Ni^{2+} at the CB-DMG-Ag-PPPE was interrogated in the potential range between 0.0 and – 1.0 V (*Figure 9.27, (a)*).

Variations is the accumulation potential towards the established reduction potential of Ni^{2+} into Ni^{0} (0 V to -0.8), showed a gradual decrease in recorded peak currents achieved from Ni^{2+} detection. Reduction of the metal cations present in solution converts metal cations to their neutral state lowering the overall concentrations of cations available for reduction in the cathodic sweep. A further move to – 1.0 V, sharply decreases the stripping peak currents. E_{acc} of -0.75 V was selected.

The effect of accumulation time on the Ni^{2+} stripping response was studied between 30 and 300 s. *Figure 9.27, (b)*, shows a rapid increase in the Ni^{2+} peak current with increasing accumulation time between 0 and 180 s confirming the increase in adsorption of the Ni^{2+} on the CB-DMG-Ag-PPPE surface. Saturation of the electrode surface takes place at accumulation times greater than 180 s and results in a gradual stabilisation in stripping peak current. A deposition time of 120 s was selected for all analysis.

Figure 9.27, (c), shows the dependence of peak currents on the square wave frequency over the 0 to 30 Hz range. Maximum stripping voltammetric peak currents are achieved at low frequency values indicating longer analysis times are required to improve resolution and sensitivity of the paper-based sensors. A steady decline in reduction peak currents between 5 and 30 Hz can be seen due to slower electron transfer processes through the DMG film. A frequency of 5 Hz was selected for the square-wave waveform.

The influence of amplitude on the stripping peak current of Ni^{2+} was studied between 0 and 20 mV and shown in *Figure 9.27, (d)*. A steady increase in recorded stripping cathodic peak currents is observed.

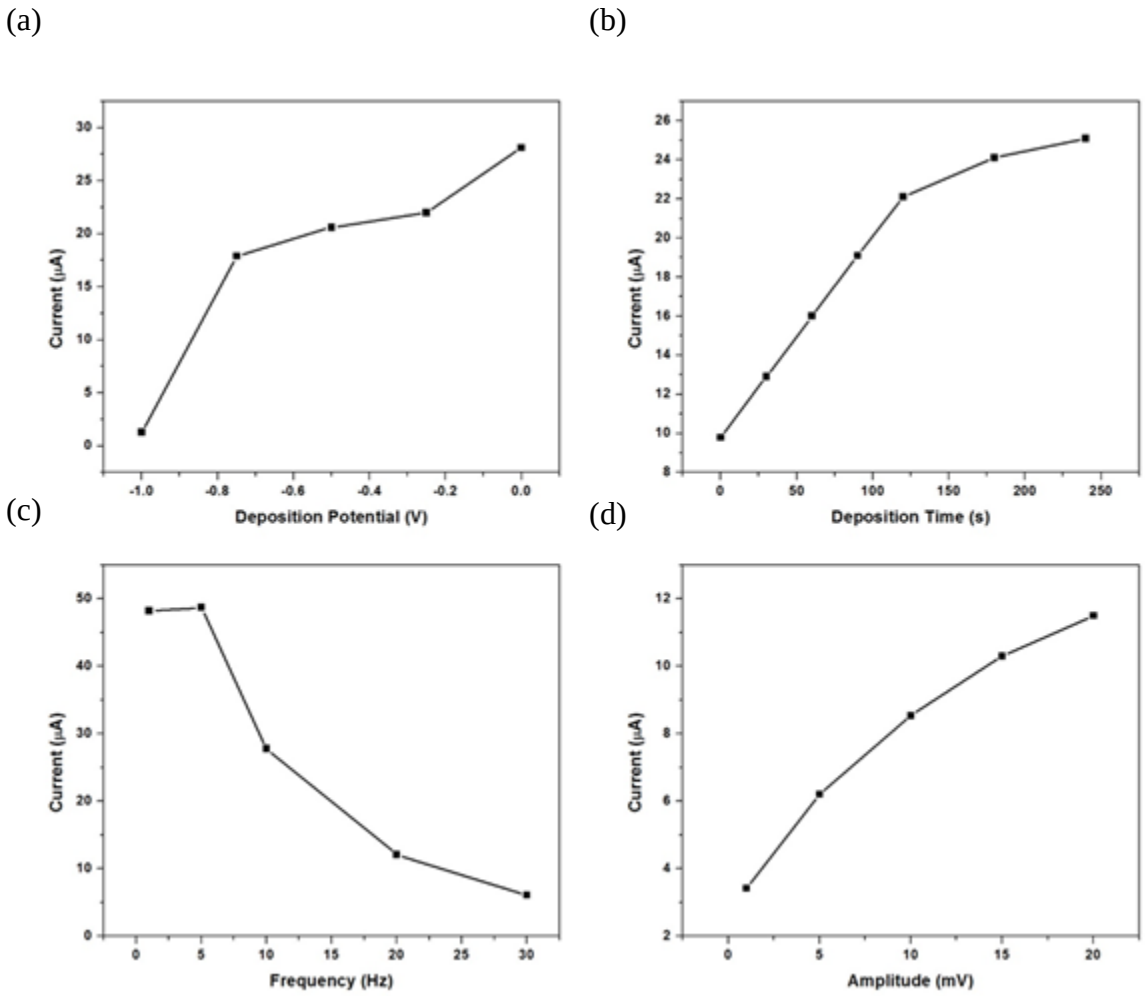

Figure 9.27: The influence of (a) accumulation potential (E_{acc}), (b) accumulation time (t_{acc}), (c) frequency and (d) amplitude on Ni^{2+} peak currents at CB-DMG-Ag-PPPE. Sample composition: 300 µg L^{-1} Ni, 0.1 M NH_3/NH_4Cl buffer.

9.4.4.5. Quantitative Analytical Performance of the CB-DMG-Ag-PPPE

The favorable adsorptive stripping voltammetric performance of the CB-DMG-Ag-PPPE is demonstrated in *Figure 9.28*. Square-wave voltammograms and the calculated calibration plot recorded over 50 – 500 µg L^{-1} Ni^{2+} ions, at optimum conditions were performed in deaerated samples. The voltammograms were recorded between – 0.9 and – 1.3 V. Voltammograms show a single, broad, reversible cathodic stripping peak at ~ - 1.18 V. Peak currents, credited to the reduction of Ni^{2+} cations from the $[Ni(dmgH)_2]$ complex increase with increasing Ni^{2+}

concentration. Positive peak potential shifts are indicated at higher metal ion concentration. The amount of energy to convert the cation into its neutral state is therefore decreased. *Figure 9.28, inset* represents the noted calibration plot obtained from the corresponding voltammograms. A constant, linear increase in peak currents is observed between 0 and 350 µg L^{-1} [$Ni(dmgH)_2$] concentration. At Ni^{2+} concentrations greater than 350 µg L^{-1} saturation of the electrode surface with adsorbed metal-complex is experienced and a deviation from linear concentration is observed. A plateau is evident in the calibration curve. A dynamic linear range between 50 and 350 µg L^{-1} [$Ni(dmgH)_2$] concentration is established with correlation coefficient of 0.989 indicating good linearity in the recorded region at an accumulation time of 90 s.

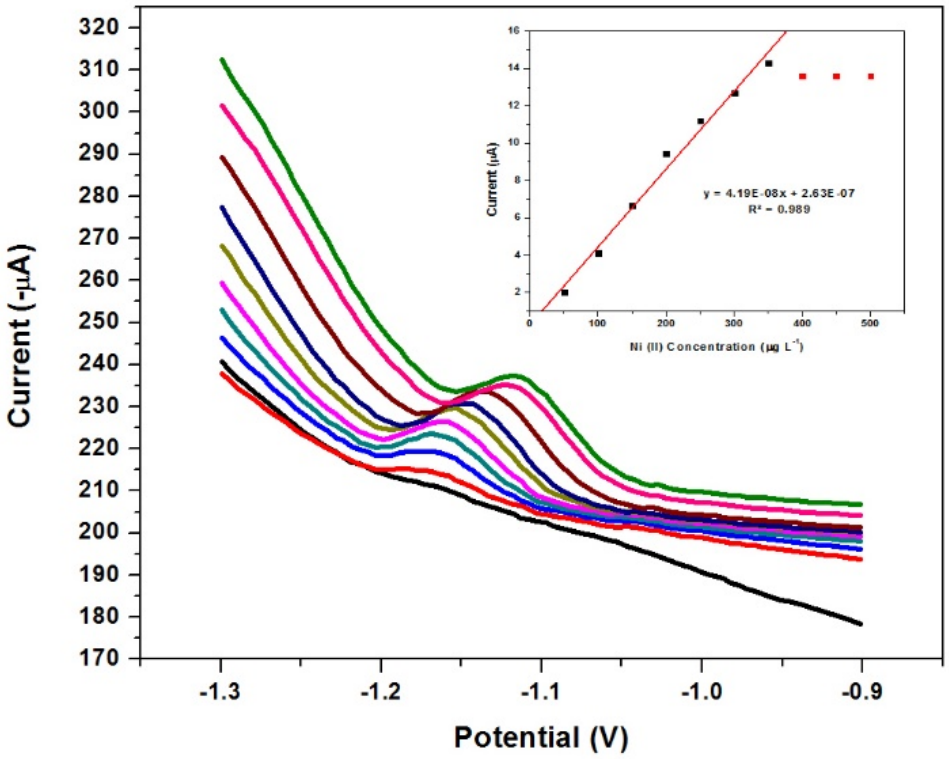

Figure 9.28: SW-AdCSVs and corresponding calibration plot of individual analysis of Ni^{2+} obtained at CB-DMG-CC-Ag-PPE over a 50 – 500 µg L^{-1} range. Supporting electrolyte (0.1 NH_3/NH_4Cl Buffer, pH 9.4), deposition time (90 s), deposition potential (- 0.7 V), rotation speed (1000 rpm), frequency (5 Hz), amplitude (0.01 V).

$$\text{LOD/LOQ} = \frac{F \times \sigma}{b} \qquad \textit{(Equation 9.2)}$$

Where

LOD: Limit of Detection

LOQ: Limit of Quantitation

F: Factor of 3.3 and 10 for LOD and LOQ, respectively

σ: Standard deviation of the blank, standard deviation of the ordinate intercept, or residual standard deviation of the linear regression

b: Slope of the regression line

Table 9.3: A summary of recorded analytical data for the CB-DMG-Ag-PPE over the 50 – 500 µg L^{-1} range.

Analytical Parameter	*Analysis of Ni^{2+}*
Sensitivity (µA L μg^{-1})	4.19×10^{-8}
Correlation Coefficient (R^2)	0.989
Detection Limits (µg L^{-1})	48.01 ± 12.24
Limit of Quantification (µg L^{-1})	144.03 51.92

9.4.4.6. Analysis of Tap Water Samples at the CB-DMG-Ag-PPPE

Similar to *Section 9.4.3*, the carbon black, dimethylglyoxime paper-based sensor (CB-DMG-Ag-PPPE) was applied to the quantitative analysis of Ni^{2+} ions in tap water samples collected in our laboratory. Water samples were prepared according to the procedure discussed in *Section 3.5.* Quantitative analysis of tap water was performed by means of a simple standard addition technique whereby successive additions of know sample concentration was added to the sample under

analysis to determine its concentration by extrapolation methods. It was found that the Ni^{2+} ion concentration in tap water samples could not be determined as it was below the sensor limits of detection or was not present in the sample at all. Spiked samples allowed for accurate recovery studies in the new sample matrix when studied within the linear dynamic range found previously. Good recovery percentages were determined for Ni^{2+} detection in both test (buffer) and real tap water samples respectively with an error below 5 %. The reported values from analysis are shown in *Table 9.4*, below.

(a)

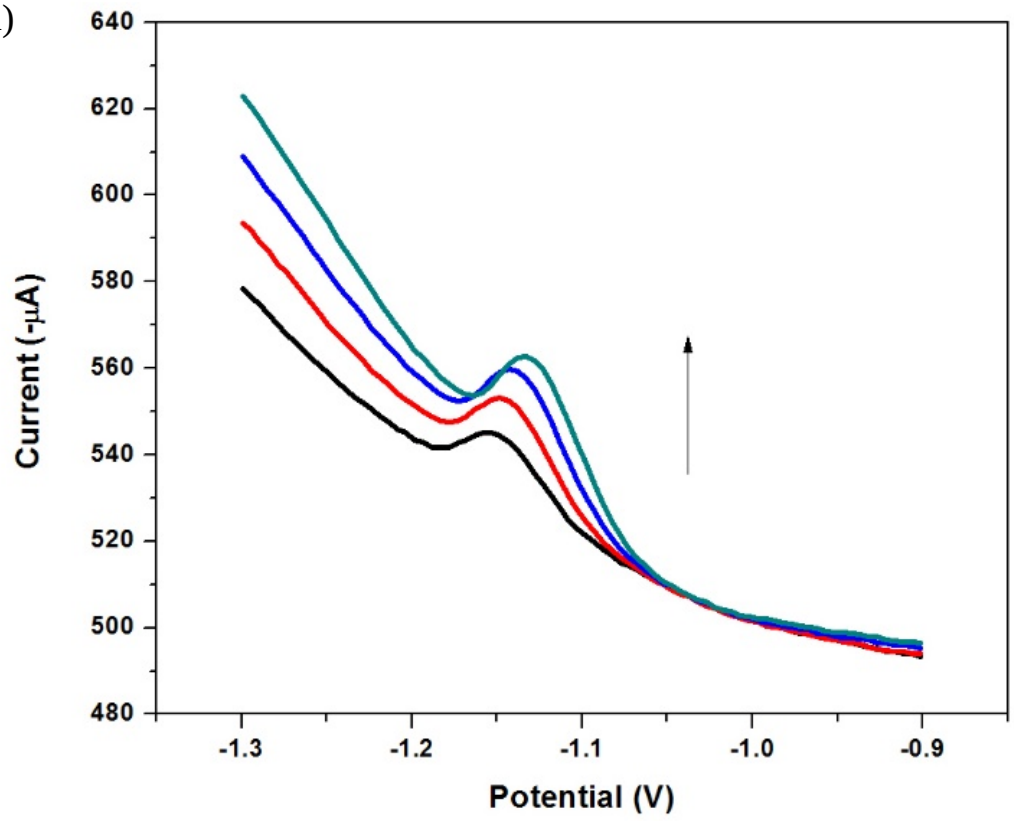

(b)

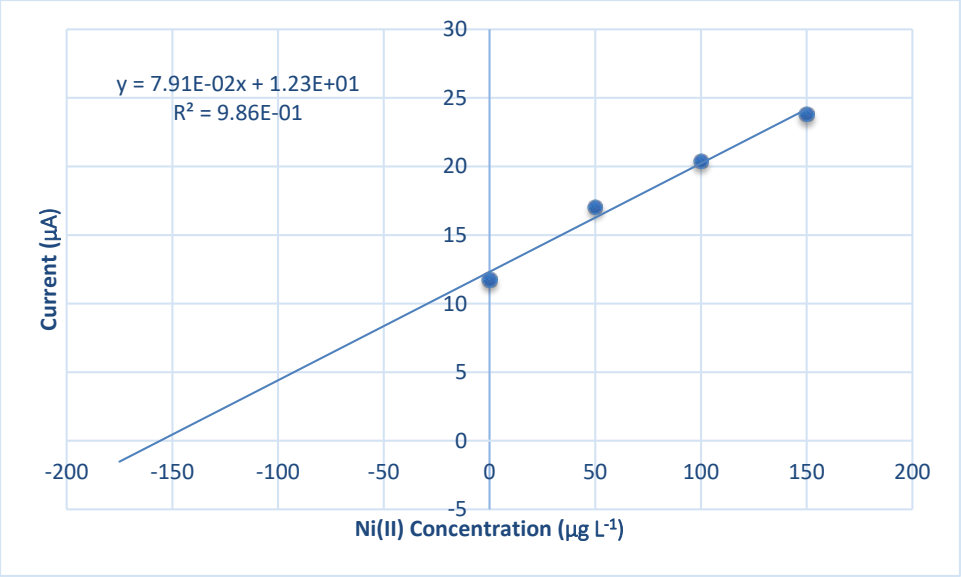

Figure 9.29: Analysis of tap water (pH 9.4) spiked with 150 µg L^{-1} of metal ion in the presence of 2 mM DMG and 10 mg L^{-1} Hg^{3+}. (a) SW-AdSV and (b) Calibration plot. Supporting electrolyte: 0.1 M NH_3/NH_4Cl buffer (pH 9.4). SWV instrumental parameters: E_{acc} = -0.7 V, t_{acc} = 120 s, f = 5 Hz and $Ampl$ = 10 mV.

Table 9.4: Recorded recovery percentages in both test and water samples

Ni^{2+} Sample	*Original ($\mu g\ L^{-1}$)*	*Added ($\mu g\ L^{-1}$)*	*Found ($\mu g\ L^{-1}$)*	*Recovery (%)*
Test Sample	*N/D*	*150*	*148.15*	*98.77 ± 7.41*
Real Water Sample	*N/D*	*150*	*155.49*	*103.66 ± 5.34*

A comparison of the calculated electrode sensitivities is shown in *Figure 9.30* below. As predicted, due to the presence of the electroplated Hg-film the ERGO-AuNP-CC-Ag-PPE exhibited improved sensitivity (10 times) over the CB-DMG-Ag-PPE. Further it could be surmised that improved electroactive surface area is achieved due to incorporation of graphene at the electrode surface. Most significantly though the immobilisation of non-conductive chelating agents at the electrode surface significantly diminishes electron transfer through the coated electrode. Both sensors showed accurate detection of Ni^{2+}. The ERGO-AuNP-CC-Ag-PPE showed

a significantly wider linear range over the CB-DMG-Ag-PPE as a direct result of its improved sensitivity towards metal cations.

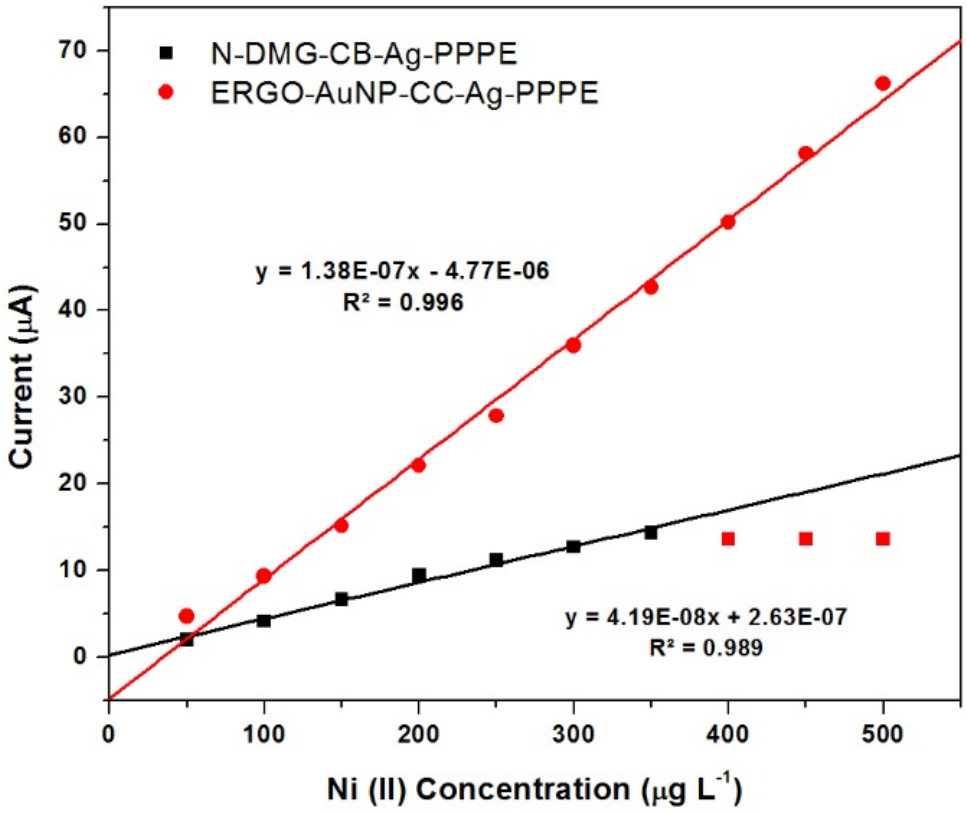

Figure 9.30: A comparison of calibration plots of 50 – 500 µg L^{-1} Ni^{2+} at (a) ERGO-AuNP-CC-Ag-PPE and (b) CB-DMG-Ag-PPE

The observed limits of detection recorded at the ERGO-AuNP-CC-Ag-PPE and CB-DMG-Ag-PPE are shown in *Table 9.5*, along with a summary of previously reported sensors for the detection of Ni^{2+} in water samples by AdSV. It can be seen that conventional solid electrode provided the best sensitivity towards nickel detection due to the low limits of detection obtained. This is in agreement with the expected findings due to conductive electrode materials. Lower limits of detection are obtained in the presence of an electroplated Hg-films due to amalgam formation with excess $[Ni(dmgH)_2]$ complexes even at short analysis times. The paper-based sensors based on chromatography paper provided sensitive responses (LODs) in an order of magnitude 10 times

greater than the observed solid electrodes. The integrated paper electrodes showed reduced sensitivities towards $[Ni(dmgH)_2]$ complex detection.

Table 9.5: A summary of previously reported sensors and limits of detection (LOD) for Ni^{2+} detection by stripping voltammetric techniques

Metal Ions	*Substrate*	*Technique*	*Accumulation Time (s)*	*Dynamic Linear Range ($\mu g\ L^{-1}$)*	*Detection Limit ($\mu g\ L^{-1}$)*	*Reference*
Ni^{2+}	*mpBiF-SPCE*	*AdCSV*	*180*	*1 - 10*	*0.027*	[33]
Co^{2+}				*1 - 10*	*0.094*	
Ni^{2+}	*RBiABE*	*DPAdSV*	*30*	*0.6 - 41*	*0.18*	[34]
Co^{2+}				*0.06 – 4.1*	*0.018*	
Ni^{2+}	*PbF-SPE*	*SWV*	*60*	*0.6 – 2.9*	*0.2*	[35]
Co^{2+}				*0.6 – 5.9*	*0.3*	
Ni^{2+}	*SBVE*	*SWAdCSV*	*30*	*0 - 10*	*0.6*	[36]
Ni^{2+}	*DMG-CPE*	*DPAdSV*	*120*	*80 - 600*	*27*	[37]
Ni^{2+}	*DMG-N-SPE*	*DPAdSV*	*120*	*60 - 500*	*30*	[38]
Ni^{2+}	*ERGO-PG-MFE*	*SWAdCSV*	*210*	*2 - 16*	*0.12*	*Chapter 5*
Ni^{2+} with Co^{2+} and Zn^{2+}	*NGr-DMG-GCE*	*SWAdCSV*	*120*	*2 - 20*	*1.5*	*Chapter 6*
Ni^{2+}	*DMG-Hg-μPPEC*	*SWAdCSV*	*90*	*15 - 90*	*6.27*	*Chapter 7*
Ni^{2+}	*AuNP-IL-μPED*	*SWAdCSV*	*90*	*30 - 150*	*5.13*	*Chapter 8*
Ni^{2+}	*ERGO-AuNP-CC-Ag-PPPE*	*SWAdCSV*	*120*	*50 – 500*	*32.19*	*This Work*
Ni^{2+}	*CB-DMG-Ag-PPPE*	*SWAdCSV*	*120*	*50 - 350*	*48.01*	*This Work*

9.5. Conclusions and Future Work

This chapter describes a simple inkjet printing process for the production of patterned three-electrode systems based on silver nanoparticles (AgNPs) deposited on commercial photographic paper. The fabricated Ag-PPE showed good conductivity in the low ohm range. Further, modification of the Ag-PPE with and electrochemical reduced graphene oxide gold nanoparticle (ERGO-AuNP) composite material and a nafion carbon black dimethylglyoxime film respectively, demonstrated improved sensitivity and provided an accurate and simple quantitative analytical approach towards the detection of Ni^{2+} in drinking water samples by adsorptive cathodic stripping voltammetry (AdCSV). The sensors provided good sensitivities and low limits of detection at short analysis times.

References

[1] X. Fang, S. Wei, J. Kong, Paper-based microfluidics with high resolution, cut on a glass fiber membrane for bioassays., Lab Chip. 14 (2014) 911–5. doi:10.1039/c3lc51246k.

[2] Z. Nie, C. a Nijhuis, J. Gong, X. Chen, A. Kumachev, A.W. Martinez, M. Narovlyansky, G.M. Whitesides, Electrochemical sensing in paper-based microfluidic devices., Lab Chip. 10 (2010) 477–483. doi:10.1039/b917150a.

[3] A.W. Martinez, S.T. Phillips, E. Carrilho, S.W. Thomas, H. Sindi, G.M. Whitesides, Simple telemedicine for developing regions: Camera phones and paper-based microfluidic devices for real-time, off-site diagnosis, Anal. Chem. 80 (2008) 3699–3707. doi:10.1021/ac800112r.

[4] W. Dungchai, O. Chailapakul, C.S. Henry, Electrochemical detection for paper-based microfluidics, Anal. Chem. 81 (2009) 5821–5826. doi:10.1021/ac9007573.

[5] J. Noiphung, T. Songjaroen, W. Dungchai, C.S. Henry, O. Chailapakul, W. Laiwattanapaisal, Electrochemical detection of glucose from whole blood using paper-based microfluidic devices, Anal. Chim. Acta. 788 (2013). doi:10.1016/j.aca.2013.06.021.

[6] A. Brett, F. Matysik, M. Vieira, Thin-film gold electrodes produced by magnetron sputtering. Voltammetric characteristics and application in batch injection analysis with amperometric detection, Electroanalysis. 9 (1997) 209–12.

http://onlinelibrary.wiley.com/doi/10.1002/elan.1140090304/abstract.

[7] H. Li, W. Wang, Q. Lv, G. Xi, H. Bai, Q. Zhang, Disposable paper-based electrochemical sensor based on stacked gold nanoparticles supported carbon nanotubes for the determination of bisphenol A, (2016). doi:10.1016/j.elecom.2016.05.010.

[8] L.Y. Shiroma, M. Santhiago, A.L. Gobbi, L.T. Kubota, Separation and electrochemical detection of paracetamol and 4-aminophenol in a paper-based microfluidic device, Anal. Chim. Acta. 725 (2012) 44–50. doi:10.1016/j.aca.2012.03.011.

[9] W. Dungchai, O. Chailapakul, C.S. Henry, A low-cost, simple, and rapid fabrication method for paper-based microfluidics using wax screen-printing., Analyst. 136 (2011) 77–82. doi:10.1039/c0an00406e.

[10] S. Cinti, D. Talarico, G. Palleschi, D. Moscone, F. Arduini, Novel reagentless paper-based screen-printed electrochemical sensor to detect phosphate, (2016). doi:10.1016/j.aca.2016.03.011.

[11] S. Cinti, F. Arduini, Graphene-based screen-printed electrochemical (bio)sensors and their applications: Efforts and criticisms, Biosens. Bioelectron. 89 (2017) 107–122. doi:10.1016/j.bios.2016.07.005.

[12] W. Kit-Anan, A. Olarnwanich, C. Sriprachuabwong, C. Karuwan, A. Tuantranont, A. Wisitsoraat, W. Srituravanich, A. Pimpin, Disposable paper-based electrochemical sensor utilizing inkjet-printed Polyaniline modified screen-printed carbon electrode for Ascorbic acid detection, J. Electroanal. Chem. 685 (2012) 72–78. doi:10.1016/j.jelechem.2012.08.039.

[13] N.J. Walch, F. Davis, N. Langford, J.L. Holmes, S.D. Collyer, S.P.J. Higson, Enhancement of Electrode Performance by a Simple Casting Method Using Sonochemically Exfoliated Graphene, Anal. Chem. 87 (2015) 9273–9279. doi:10.1021/acs.analchem.5b01829.

[14] M.Á.G. Rico, M. Olivares-Marín, E.P. Gil, Modification of carbon screen-printed electrodes by adsorption of chemically synthesized Bi nanoparticles for the voltammetric stripping detection of Zn(II), Cd(II) and Pb(II), Talanta. 80 (2009) 631–635. doi:10.1016/j.talanta.2009.07.039.

[15] J.A. Adkins, C.S. Henry, Electrochemical detection in paper-based analytical devices using microwire electrodes, Anal. Chim. Acta. 891 (2015) 247–254. doi:10.1016/j.aca.2015.07.019.

[16] A. Määttänen, U. Vanamo, P. Ihalainen, P. Pulkkinen, H. Tenhu, J. Bobacka, J. Peltonen, A low-cost paper-based inkjet-printed platform for electrochemical analyses, Sensors Actuators, B Chem. 177 (2013) 153–162. doi:10.1016/j.snb.2012.10.113.

[17] Y.H. Kahng, M.K. Kim, J.H. Lee, Y.J. Kim, N. Kim, D.W. Park, K. Lee, Highly conductive flexible transparent electrodes fabricated by combining graphene films and inkjet-printed silver grids, Sol. Energy Mater. Sol. Cells. 124 (2014) 86–91. doi:10.1016/j.solmat.2014.01.040.

[18] K. Abe, K. Suzuki, D. Citterio, Inkjet-printed microfluidic multianalyte chemical sensing paper, Anal. Chem. 80 (2008) 6928–6934. doi:10.1021/ac800604v.

[19] K. Abe, K. Kotera, K. Suzuki, D. Citterio, Inkjet-printed paperfluidic immuno-chemical sensing device, Anal. Bioanal. Chem. 398 (2010) 885–893. doi:10.1007/s00216-010-4011-2.

[20] K. Kim, S. Il Ahn, K.C. Choi, Simultaneous synthesis and patterning of graphene electrodes by reactive inkjet printing, Carbon N. Y. 66 (2014) 172–177. doi:10.1016/j.carbon.2013.08.055.

[21] F. Molina-Lopez, D. Briand, N.F. De Rooij, All additive inkjet printed humidity sensors on plastic substrate, Sensors Actuators, B Chem. 166–167 (2012) 212–222. doi:10.1016/j.snb.2012.02.042.

[22] T. Öhlund, J. Örtegren, S. Forsberg, H.E. Nilsson, Paper surfaces for metal nanoparticle inkjet printing, Appl. Surf. Sci. 259 (2012) 731–739. doi:10.1016/j.apsusc.2012.07.112.

[23] T. Hibbard, K. Crowley, A.J. Killard, Direct measurement of ammonia in simulated human breath using an inkjet-printed polyaniline nanoparticle sensor, Anal. Chim. Acta. 779 (2013) 56–63. doi:10.1016/j.aca.2013.03.051.

[24] N. Dossi, R. Toniolo, A. Pizzariello, F. Impellizzieri, E. Piccin, G. Bontempelli, Pencil-drawn paper supported electrodes as simple electrochemical detectors for paper-based fluidic devices, Electrophoresis. 34 (2013) 2085–2091. doi:10.1002/elps.201200425.

[25] J. William S. Hummers, R.E. Offeman, Preparation of Graphitic Oxide, J. Am. Chem. Soc. 80 (1958) 1339. doi:10.1021/ja01539a017.

[26] K. Pokpas, S. Zbeda, N. Jahed, N. Mohamed, P.G. Baker, E.I. Iwuoha, E.I.I. Sensorlab, Electrochemically reduced graphene oxide pencil-graphite in situ plated bismuth-film electrode for the determination of trace metals by anodic stripping voltammetry, Int. J. Electrochem. Sci. 9 (2014) 736–759. www.electrochemsci.org (accessed April 3, 2017).

[27] B. Wu, N. Zhao, S. Hou, C. Zhang, Electrochemical Synthesis of Polypyrrole, Reduced Graphene Oxide, and Gold Nanoparticles Composite and Its Application to Hydrogen Peroxide Biosensor, Nanomaterials. 6 (2016) 220. doi:10.3390/nano6110220.

[28] C. Rajkumar, B. Thirumalraj, S.-M. Chen, S. Palanisamy, Novel electrochemical preparation of gold nanoparticles decorated on a reduced graphene oxide–fullerene composite for the highly sensitive electrochemical detection of nitrite, RSC Adv. 6 (2016) 68798–68805. doi:10.1039/C6RA10690K.

[29] G. Gotti, K. Fajerwerg, D. Evrard, P. Gros, Electrodeposited gold nanoparticles on glassy carbon: Correlation between nanoparticles characteristics and oxygen reduction kinetics in neutral media, Electrochim. Acta. 128 (2014) 412–419. doi:10.1016/j.electacta.2013.10.172.

[30] Z. Zhao, M. Zhang, Y. Li, S. Cheng, X. Chen, J. Wang, Evaluation of Electrochemically Reduced Gold Nanoparticle—Graphene Nanocomposites for the Determination of Dopamine, Anal. Lett. 48 (2015) 1437–1453. doi:10.1080/00032719.2014.984189.

[31] A. Benvidi, A. Dehghani-Firouzabadi, M. Mazloum-Ardakani, B.-B.F. Mirjalili, R. Zare, Electrochemical deposition of gold nanoparticles on reduced graphene oxide modified glassy carbon electrode for simultaneous determination of levodopa, uric acid and folic acid, J. Electroanal. Chem. 736 (2015) 22–29. doi:10.1016/j.jelechem.2014.10.020.

[32] I. Khalil, N.M. Julkapli, W.A. Yehye, W.J. Basirun, S.K. Bhargava, Graphene-gold nanoparticles hybrid-synthesis, functionalization, and application in a electrochemical and surface-enhanced raman scattering biosensor, 2016. doi:10.3390/ma9060406.

[33] S. Dal Borgo, H. Sopha, S. Smarzewska, S.B. Hočevar, I. Švancara, R. Metelka, Macroporous Bismuth Film Screen-Printed Carbon Electrode for Simultaneous

Determination of Ni(II) and Co(II), Electroanalysis. 27 (2015) 209–216. doi:10.1002/elan.201400422.

[34] B. Bas, K. Wegiel, K. Jedlinska, The renewable bismuth bulk annular band working electrode: Fabrication and application in the adsorptive stripping voltammetric determination of nickel(II) and cobalt(II), Anal. Chim. Acta. 881 (2015) 44–53. doi:10.1016/j.aca.2015.05.005.

[35] A. Bobrowski, A. Królicka, M. Maczuga, J. Zarębski, A novel screen-printed electrode modified with lead film for adsorptive stripping voltammetric determination of cobalt and nickel, Sensors Actuators, B Chem. 191 (2014) 291–297. doi:10.1016/j.snb.2013.10.006.

[36] G.M.S. Alves, J.M.C.S. Magalhães, H.M.V.M. Soares, Simultaneous Determination of Nickel and Cobalt Using a Solid Bismuth Vibrating Electrode by Adsorptive Cathodic Stripping Voltammetry, Electroanalysis. 25 (2013) 1247–1255. doi:10.1002/elan.201200643.

[37] A. Ferancová, M.K. Hattuniemi, A.M. Sesay, J.P. Räty, V.T. Virtanen, Electrochemical Monitoring of Nickel(II) in Mine Water, Mine Water Environ. (2015). doi:10.1007/s10230-015-0357-1.

[38] A. Ferancová, M.K. Hattuniemi, A.M. Sesay, J.P. Räty, V.T. Virtanen, Rapid and direct electrochemical determination of Ni(II) in industrial discharge water, J. Hazard. Mater. 306 (2016) 50–57. doi:http://dx.doi.org/10.1016/j.jhazmat.2015.11.057.

Chapter 10 :

Microfluidic graphenised-paper electroanalytical devices (µGPED) for adsorptive cathodic stripping voltammetric detection of metal contaminants.

Conclusions and Future Work

The overriding aim of the study, to develop low-volume, cost efficient, accurate, sensitive and highly reproducible microfluidic graphenised paper-based electroanalytical devices (µGPEDs) for the detection of heavy metal contaminants in water samples by adsorptive cathodic stripping voltammetry (AdCSV) was achieved. The novel paper-based sensor, relying on complex formation of Ni^{2+} with dimethylglyoxime was the first approach of its kind in paper-based sensing devices where only anodic stripping voltammetric techniques have been performed to date. *Chapter One* outlines the main objectives and rationale employed for the sensor development and highlights steps and objectives employed to realize its full potential. Briefly, it was important to initially investigate the AdCSV procedure for metal analysis in water samples and develop strategies to enhance its sensitivity at conventional solid electrodes using graphene-based materials and nanocomposites. The developed technique was then employed in paper-based sensors created with chromatographic and photographic paper substrates for low-volume and low-cost detection. Related to this application patterning methods, reagent storage, nanoparticle enhancement, interference studies etc. were all required to be further investigated for its use in sensor development. Upon completion of a culmination of these steps, the research was able to be completed and the novel sensors developed. This chapter outlines the main conclusions of the study and provides and overview of the success and shortcomings achieved herein. It further highlights any recommendations for future work which may have arisen from the study.

The objectives of this work were to:

- Explore the synthesis and characterization of reagents used in the study:
    - Investigate the synthesis and characterisation of graphene oxide (GO) by a modified Hummers method and its subsequent reduction to graphene as well as characterization of commercial gold nanoparticles. Structural and morphological characterisation were performed using HRSEM, HRTEM, FTIR, AFM, XRD, Raman and UV-Vis.
    - Investigate the development of graphene-chelate nanocomposites and electrochemically reduced platforms for surface modification to improve electrode sensitivity.
- Develop a method for the adsorptive stripping voltammetric detection of metal cations in water based on a single accumulation and deposition step in the presence of suitable chelating agents and metallic films
- Investigate the ability to improve electrode sensitivity by electrode modification with graphene and gold nanoparticles
- Fabricate low-volume paper-based electroanalytical devices for the detection of Ni^{2+} by AdCSV
- Improve sensitivity of paper-based sensors by reagent storage with electrolyte, chelating agent and metallic films
- Further enhance sensitivity of the developed devices by modification with graphene, gold nanoparticles and ionic liquids
- Develop paper-based flow-systems based on patterning with hydrophobic materials
- Investigate the filtration, inkjet and screen printing techniques to create integrated electrode systems on paper substrates and apply them to the detection of metal ions by AdCSV
- Develop a method for the quantitative detection of metal ions in water based on the aforementioned devices.

The background of the study was performed by surveying relevant literature on metal contamination in water samples worldwide and in South Africa. The impact and toxicology of metal contamination on the environment and specifically human beings was investigated. Health concerns associated with prolonged exposure was addressed and specific maximum contamination levels set by WHO, EPA and South African drinking water guidelines investigated as measure of sensor effectiveness.

Literature studies were performed in two separate reviews in order to identify previously reported research pertaining to the study. Particularly, work performed on graphene-derivatives in stripping voltammetric applications were investigated with special interest in metal analysis. Methods of graphene preparation and the unique electrochemical properties associated with the preparation techniques were highlighted. In addition, techniques used for the detection of heavy metals in paper-based analytical devices was studied. A comparison of advantageous and disadvantageous properties of colorimetric, fluorescence, electrochemical and other techniques was performed. Gaps in the research conducted to date and possible improvements were identified.

The study made use of a quantitative analytical approach based on unique experimental strategies performed in our laboratory to investigate particular areas of interest in the fabrication of the appropriate paper-based sensors.

A review of the relevant literature in *Chapter Two* found that chemical synthesis approaches based on a modified Hummer's method provided the most plausible strategy for large scale graphene preparation with minimal structural defects and unique properties ideal for electrochemical applications. Electrochemical approaches are also ideal for modification of non-uniform surfaces where simple drop-casting is not possible. From the relevant literature, a few unique electrochemical properties of graphene use in stripping voltammetry was addressed: a large surface area, improved electron transfer rates, synergistic effects, wide potential window etc. were highlighted. It was further found that stripping voltammetric applications in recent times very rarely made use of graphene-based materials by themselves, but in conjunction with additional materials in the form of composites. Further, it was found that metal analysis by SV at graphene derived materials relied solely on anodic stripping voltammetry (ASV) where electrolytic conversion of analyte materials was performed prior to detection. Only one study to date has made

use an adsorptive stripping voltammetry (AdSV) approach for Pb^{2+} detection in the presence of β-cyclodextrin. However, while adsorption was used in the detection mechanism electrolytic conversion of the Pb cation to its zero oxidation state was achieved prior to analysis and therefore is a variation on ASV instead of AdSV. More conventional AdCSV approaches could therefore be investigated for metal analysis.

Chapter Three highlights the recent applications of metal analysis at paper-based analytical devices. It was found that not much work has been conducted on trace metal analysis at paper-based sensors to date. Optical detection methods such as colorimetric, fluorescence and chemiluminescence approaches are common place. Electrochemical approaches however offer the possibility of speciation and also application to a wider range of analytes. Similar to the graphene-derivatives found in *Chapter Two* no work on the AdCSV of metal ions has been studied as yet. An interesting finding was that no work on nanoparticle enhancement in electrochemical paper-based sensors has been utilized, opening an interesting sphere of research to be further investigated.

A discussion on the preparation and characterization of graphene and commercial gold nanoparticles by HRSEM, HRTEM, FTIR, AFM, XRD, Raman and UV-Vis analysis techniques was shown in *Chapter Four*. A modified Hummer's method was reported for the preparation of graphene oxide from pristine graphite powder. The inclusion of oxygen moieties in the graphitic structure yielded a brown suspension when dispersed in water as a direct result of the hydrophilic nature of GO. Hydroxyl, carboxyl and epoxy functional groups were confirmed by FTIR analysis between 400 and 4000 cm^{-1}, in agreement with literature. These could further be established by the $\pi \rightarrow \pi^*$ (C-C) and $n \rightarrow \pi^*$ (C-O) electronic transitions shown at UV-vis analysis. Upon subsequent reduction in the presence of $NaBH_4$, high quality few-layer reduced graphene oxide was obtained consisting of 5 stacked layers with flake thickness of 1.6 nm, obtained from AFM analysis, diffraction in the 002 plane from XRD analysis and an I_D/I_G ratio of 1.19 found from Raman spectrometry. It was further noted that incomplete reduction of oxygen moieties in the chemical reduction step was observed producing a reduced graphene oxide. Commercial, spherical gold nanoparticles with an average particle size of ~ 57 nm were observed from HRSEM and HRTEM analysis. This was confirmed by UV-vis analysis where an absorption band at 536 nm was detected corresponding to gold nanoparticles of ~ 50 nm.

Furthermore, a novel single step accumulation and deposition approach for Ni^{2+} detection was performed for the first time (*Chapter Five*). An accumulation potential of – 0.7 V was found to be adequate for the reduction of Hg^{2+} as well as allow for $[Ni(dmgH)_2]$ complex formation and its subsequent adsorption onto the electroplated metal film. This is contrary to previously reported studies whereby deposition/electroplating of a metallic film and adsorption of formed complexes onto the electrode surface was performed in two successive steps. More significantly however, the catalytic effects of graphene-modified electrodes, prepared by electrochemical reduction and deposition of graphene from graphene oxide suspensions onto pencil graphite electrodes, towards the reduction of Ni^{2+} from $[Ni(dmgH)_2]$ complexes in the presence of Hg were achieved for the first time. As previously stated, this is a significant finding as it is the first AdSV application of graphene towards metal analysis. HRSEM analysis of the modified PGE confirmed graphene deposition at the electrode surface. A 3 times enhancement in stripping response towards Ni^{2+} reduction was found in the presence of ERGO. The ERGO-PG-MFE showed excellent sensitivity (9.71×10^{-7} µA L μg^{-1}) and also highlighted the selectivity of the graphene materials towards Ni^{2+}. Low limits of detection of 0.12 ± 0.002 µg L^{-1} were achieved for Ni^{2+} analysis in the 2 – 20 µg L^{-1} range at 120 s analysis times for 3 replications. This result was comparable values to reported literature values at shorter analysis times.

The toxicity of Hg-films required for sensitive detection of Ni^{2+} as developed in *Chapter Five* is a major drawback of the analytical technique. An environmentally friendly approach was therefore developed for Ni^{2+} detection by AdCSV in *Chapter Six*. Graphene-dimethylglyoxime nanocomposites were prepared and modified onto glassy carbon electrodes. HRSEM analysis showed a smooth uniform surface with randomly dispersed graphene flakes at the chemically modified electrode (CME) surface upon modification with the composite material (NGr-DMG). The presence of nitrogen and fluorine in the energy dispersive x-ray spectra confirms the inclusion of DMG at the electrode surface. Electrochemical characterization of the CME showed an increase in peak current and a distinct narrowing in peak-to-peak separation for the $Fe(CN)_6^{3-/4-}$ redox couple as well as a dramatic decrease in R_{ct} from 400 000 to 70 000 Ω from the Nyquist impedance plot. The low sensitivity of the chemically modified electrode was improved by means of enhanced electron transfer kinetics and improved surface-area-to-volume ratio of graphene. Application of the NGr-DMG-GCE towards Ni^{2+} detection demonstrated a distinct enhancement in reduction peak current (9 times) over the N-DMG-GCE. Further, a low limit of detection of 1.5 ± 0.27 µg L^{-1}

[1] was observed for 3 replications over the 2 – 20 µg L^{-1} range at a 120 s analysis time. This was ten times less sensitive than the PGE counterpart due to the absence of a Hg-film. In addition, the sensor showed highly selective and reproducible detection of Ni^{2+} in the presence of Co^{2+} and Zn^{2+} for the first time with a RSD of 3.94 %.

Building on the work developed in *Chapter Five* and *Six* at solid carbon electrodes, the first approach for Ni^{2+} detection by AdCSV at paper-based sensors was achieved in *Chapter Seven*. A dry reagent storage method was developed to create prestored paper-based electrochemical cells (PPECs) infused with electrolyte, chelating agent and metallic films. The PPECs showed sensitive and selective detection of Ni^{2+} at sample volumes < 20 µL. Accurate, selective and reproducible detection in the presence of 100 µg L^{-1} Zn^{2+}, Cd^{2+}, Pb^{2+}, Co^{2+} and In^{2+} was achieved with an RSD of 4.36 % (n = 4). Comparison of three concentration ranges (300 – 2100 µg L^{-1}, 30 – 210 µg L^{-1} and 15 - 120 µg L^{-1} Ni^{2+}) indicated that linearity could be improved at lower Ni^{2+} concentrations (R^2 = 0.995) for 90 s analysis time. Detection limits of 6.27 ± 1.32 µg L^{-1} were calculated. This value was comparable to literature values but demonstrated a lower sensitivity over solid electrodes at bulk volumes. Recoveries of 101.34 and 93.12 % were recorded in test and real water samples respectively. Further, it was found that accurate detection could still be achieved in water samples littered with dirt etc. A comparison of chelating agents used in literature such as nioxime and morin hydrate were compared to the dimethylglyoxime method developed and nioxime showed outstanding possibility for future applications. Infusion of µPECs with graphene to improve electron transfer kinetics was further investigated. This was the first reported work on graphene infused paper devices for electrochemical detection of metal ions. The novel sensing technique showed little-to-no improvement in electron transfer kinetics due to low loading of graphene within the cellulose structure and effectively not improving conductivity of the device. Similar findings were reported for both ERGO and NGr infused paper disks. To overcome the low conductivity of the infused paper-based electrochemical cells, higher loading wt. % were studied by simple filtration techniques. Conductive working electrodes (324 Ω) were thus achieved and in conjunction with screen printed reference and counter electrodes created integrated three-electrode systems for use as electrochemical sensors fabricated from paper.

Infusion of graphene in paper-based electrochemical cells was not completely successful as hypothesized in *Chapter One*. As such, additional means of improving paper-based senor

sensitivity was investigated. A simple method for fabricating microfluidic paper-based electroanalytical devices (µPEDs) for Cu^{2+} and Ni^{2+} detection in water samples is described in *Chapter Eight*. Electrochemical stripping analysis techniques are coupled to low volume (< 100 µL), disposable µPEDs for use in adsorptive stripping voltammetry (AdSV) and anodic stripping voltammetry (ASV). A contact printing technique based on paraffin wax and rubber stamps created effective hydrophobic barriers in the chromatography paper under an applied hand-pressure, melting temperature of 120 ^{o}C and melting time of 2 min. This was confirmed by leak tests. A dry storage method created the reaction zones with gold nanoparticles and ionic liquids. A uniform distribution of AuNPs within the cellulose fiber structure was confirmed by HRSEM analysis and EDS and an average particle size of ~ 90 nm. Agglomeration of the AuNPs within the cellulose structure is therefore confirmed. The AuNP-IL-µPED was applied to Cu^{2+} and Ni^{2+} detection. Further, for the first time commercial gold nanoparticles and 1-Methylimidazole ionic liquids integrated within the cellulose fiber structure were utilized to improve electron transfer rates and low sensitivities associated with quantitative electrochemical detection in paper-based devices. A 2 and 3 times enhancement in stripping peak current for Cu^{2+} detection is observed for 1-methylimidazole and gold nanoparticle inclusion. The IL improves binding ability of the metal cations at the electrode surface while the conductive nanoparticles improve electron transfer kinetics. Similarly, a 1.3 and 2 times in enhancement is observed for Ni^{2+} detection by AdCSV. The paper-based microfluidic device with microliter sized channels created beneficial properties such as filtration, mixing, mimicking stirring and speciation by varying retention times in the channel. Improved sensitivities were achieved at the gold nanoparticle, ionic liquid infused microfluidic paper-based electroanalytical devices (AuNP-IL-µPEDs) for Cu^{2+} and Ni^{2+}. Detection limits of 3.78 µM and 5.13 µg L^{-1} was recorded for Cu^{2+} and Ni^{2+} detection. These were in agreement with literature reported values.

Chapter Nine describes the production of integrated three-electrode paper-based sensors on photographic and chromatographic paper substrates for the detection of Ni^{2+} by AdCSV. The integrated paper sensor was highly conductive (low ohms range) due to AgNP printing at a curing temperature of 120 ^{o}C for 1 hr. Curing dramatically improved the conductivity of the printed electrodes by 2.5 times. Further, increased numbers of printed layers further enhanced electrode conductivity in chromatography paper. The inkjet printing technique was able to fabricate accurate features with precise dimensions. Working electrodes were further modified by electrochemically

reduced graphene oxide and gold nanoparticle composites using an electrochemical deposition approach and a formed carbon black dimethylglyoxime nanocomposite. The modified electrode surfaces were confirmed by HRSEM analysis. AuNPs are seen to form within graphene sheets in the electrodeposition process and represented as spherical spots within the transparent sheets. Particle sizes of ± 100 nm were achieved. The application of the ERGO-AuNP-CC-Ag-PPE demonstrated the best sensitivity (5 times) towards Ni^{2+} detection at 30 cycles over the CC-Ag-PPE. The CB-DMG-Ag-PPE also demonstrated improved sensing capability over the CB-Ag-PPE Both sensors showed good sensitivity and detection towards Ni^{2+} detection with detection limits of 32.19 ± 9.61 and 48.01 ± 12.24 µg L^{-1} achieved at 90 s accumulation times over the 50 – 500 µg L^{-1} Ni^{2+} range.

The results obtained in the study show promising results in the field of paper-based microfluidics by combining low-volume, disposable paper-based substrates with electrochemical detection for accurate and sensitive quantitative analysis. To date, trace-metal analysis at paper-based electroanalytical devices (µPEDs) have been limited to metal cations suitable for detection by anodic stripping voltammetric detection (ASV). As such, only limited applications and low selectivity has been observed. The ability to perform adsorptive stripping voltammetry at the paper-based electrodes is unique and could open the door for improved and selective detection of metal ions but also organic materials in paper-based sensing. Further, reagent storage with chelating agents, electrolyte, metallic films etc. offers the capability of easily modifying µPEDs for a variety of applications with minimal effort and labor. In addition, the ability to use graphene, gold nanoparticles and ionic liquids to improve electrode sensitivity in paper-based sensing is an exciting finding. Numerous nanoparticles could further be investigated for this purpose. In addition, the ability to immobilize biological materials at the infused nanoparticles results in biosensing capabilities. The infusion of graphene within the paper reaction zone requires further exploration as this is an exciting prospect in sensing capabilities. Filtered graphene electrodes further expand the work for origami devices in paper sensing.